FUNDAMENTALS OF LIGHT MICROSCOPY AND ELECTRONIC IMAGING

FUNDAMENTALS OF LIGHT MICROSCOPY AND ELECTRONIC IMAGING

Second Edition

Douglas B. Murphy
Michael W. Davidson

WILEY-BLACKWELL
A JOHN WILEY & SONS, INC., PUBLICATION

Cover Image: Courtesy of Michael W. Davidson

Published by John Wiley & Sons, Inc., Hoboken, New Jersey
Published simultaneously in Canada

Library of Congress Cataloging-in-Publication Data:

Murphy, Douglas B.
Fundamentals of light microscopy and electronic imaging / Douglas B. Murphy, Michael W. Davidson. – 2nd ed.
p. ; cm.
Includes bibliographical references and index.
ISBN 978-0-471-69214-0 (cloth)
1. Microscopy. I. Davidson, Michael W. (Michael Wesley), 1950- II. Title.
[DNLM: 1. Microscopy. 2. Image Processing, Computer-Assisted. QH 211]
QH205.2.M87 2013
502.8'2–dc23
2012009798

Printed in Singapore

10 9 8 7 6 5 4 3 2 1

CONTENTS

PREFACE

In the 10 years since this book first appeared, much has happened to catapult light microscopy into the forefront of biomedical research methodologies. The advances include: fundamentally new optical methods and imaging technologies for "superresolution" imaging; an explosion of new fluorescent dyes and fluorescent protein probes; new designs for objectives and thin-film interference filters; new designs of illuminators, including LED illuminators used in fluorescence imaging; new generations of silicon-based detectors, such as EMCCD cameras and scientific CMOS cameras, and many other developments. We have modified many of the chapters to include these topics, and we have added new chapters to cover essential new areas in fluorescence microscopy: fluorescence dynamics with FRET, FRAP, and TIRF; two-photon microscopy and second harmonic generation imaging; superresolution imaging including methods for single-molecule localization imaging, structured illumination imaging, and stimulated emission depletion microscopy; and a new chapter on live-cell imaging methods. But we removed a chapter on video microscopy, in keeping with the technology of the new digital age. We have also kept: demonstrations and laboratory exercises to help master new principles; a glossary of terms, appendices that supplement the exercises; and a new Webliography of basic resources on the internet.

We hope the new will help promote interest in microscopy and provide investigators with the information necessary to get the best performance from their imaging equipment.

Douglas B. Murphy
Manager of Light Microscope Imaging,
HHMI Janelia Farm Research Campus, Ashburn, VA
Adjunct Professor of Cell Biology
Johns Hopkins Medical School, Baltimore, MD

Michael W. Davidson
Optical Microscopy Facility,
National High Magnetic Field Laboratory
Florida State University, Tallahassee, FL

ACKNOWLEDGMENTS

We wish to thank our many friends and colleagues who made this work possible, foremost our spouses, Christine Murphy and Pamela Davidson, for their great patience and encouragement throughout the project. Without their cooperation and understanding, the book could not have been written. We thank Christine Murphy, Tadja Dragoo, and Erin Wilson for help with the writing and for proofreading the text.

Special thanks are due to many individuals who made this work possible.

I (DBM) would like to thank the many students who have taken my microscope courses over the years at Johns Hopkins and Janelia Farm, who inspired me to write the book and gave valuable advice. In particular, I would like to thank my colleagues at Johns Hopkins and others who helped me with the first edition: Drs. Bill Earnshaw (University of Edinburgh), Gordon Ellis (University of Pennsylvania), Joe Gall (Carnegie Institution, Department of Embryology), Shinya Inoue (Marine Biological Laboratory), Ernst Keller (Carl Zeiss, Inc.), John Russ (North Carolina State University), Kip Sluder (University of Massachusetts Medical School), and Ken Spring (National Institutes of Health). For help with the second edition, I am deeply indebted to Eric Betzig, Mats Gustafsson, Harald Hess, Na Jie, and Karel Svoboda at Janelia Farm, as well as many Janelia Farm fellows and colleagues, including: Alma Arnold, Tim Brown, Reto Fiolka, Margaret Jefferies, Gleb Shtengel, Johannes Seelig, and Lin Shao. Rebecca Williams (Cornell University) and Jerome Mertz (Boston University) also helped in important ways. I especially want to give special thanks to Reed George and Gerry Rubin at Janelia Farm whose cooperation made it possible for me to work on this project, and Peter Devreotes at Johns Hopkins Medical School for encouragement and support.

I (MWD) would like to thank (in addition to most of the folks listed above) the many graphics artists, laboratory technicians, graduate students, and programmers who have worked so diligently on the Molecular Expressions, Nikon MicroscopyU, Zeiss Campus, and Olympus Resource Center websites over the past decade and assisted in the creation of figures and images in the second edition. These include: Adam Rainey, Tony Gines, Chris Burdette, Aaron Baillie, Nathan Kennedy, Kevin John, Rich Ludlow, John Childs, Chris Steenerson, Lane Henderson, Pablo Montoya, Steve Price, David Howard, John Bouma, Sean Fink, Shane Hewett, Stephanie Corn, Matt Parry-Hill, John Long, Matt De Marco, Lionel Parsons, Nate Bibler, Bo Flynn, Nathan Claxton, Korey

Wilson, Ericka Ramko, Michelle Baird, Paula Cranfill, John Allen, Sarah Gilbert, Patrick Roche, John Griffin, Tom Fellers, Shannon Neaves, Riley Evans, Brittany Sell, and David Homan. I would also like to thank my colleagues at Florida State University and the National High Magnetic Field Laboratory who have provided help in all phases of the development of our Optical Microscopy facility: Jack Crow, Brian Fairhurst, Greg Boebinger, Clyde Rea, Alan Marshall, Dave Gilbert, Ross Ellington, Tim Cross, Lei Zhu, Tom Roberts, Kim Riddle, Steve Lenhert, Randy Rill, Dave van Winkle, Kirby Kemper, Bob Johnson, Ray Bye, Betty Southard, and John Fraser. Colleagues from other universities have also contributed by teaching us new tricks in microscopy and fluorescent probe development: Robert Campbell (University of Alberta), Dave Piston (Vanderbilt University), Jason Swedlow (University of Dundee), Jennifer Lippincott-Schwartz (NIH), George Patterson (NIH), Clare Waterman (NIH), Kurt Thorn (University of California, San Francisco), Rich Day (Indiana University), Dmitriy Chudakov (Russian Academy of Science), Vlad Verkhusha (Albert Einstein), and Tom Deerinck (University of California, San Diego).

We give special acknowledgment and thanks to our colleagues at Carl Zeiss, Leica Microsystems, Nikon USA, Olympus America, Molecular Probes (Life Technologies), Hamamatsu Photonics, and other companies for many years of support and for helpful information and details for many of the figures. We give special thanks and acknowledgment to: (Nikon) Stan Schwartz, Steve Ross, Nathan Claxton, Gary Laevsky, Joel Silfies, Eric Flem, Ed Lieser, Lee Shuett, Don Armstrong, Ric Villani, John Zentmeyer, Richard Gruskin, Allison Forlenza, Joe LoBiondo, Deborah Robbins, Tracey Webb, Jeff Larson, and Mike Davis. (Olympus) George Steares, Bill Fester (now at 3I), Nick George (now at Semrock), Ian Kirk, Ed Lachica (now at Lumen Dynamics), Monica Kirk (now at 3I), Kim Wicklund, Tim Randall, Chris Higgins, Stuart Shand, Kenji Matsuba, Richard Baucom, Brad Burklow, Laura Ferguson, Brendan Brinkman, Sam Tesfai, Thomas Geer, and Paul Jantzen. (Zeiss) Alex Söll, Jochen Tham, Maya Everett, Rudi Rottenfusser, Scott Olenych, Matthias Langhorst, Kenny Patterson, Elise Shumsky, Brian Crooks, and Klaus Weisshart. (Leica) Sebastian Tille, Bernd Sägmüller, Sean Garvey, Doug Reed, Anthony Santerelli, and Geoff Daniels.(Hamamatsu) Butch Moomaw, Ken Kaufmann, and Mark Hobson. (Semrock) Turan Erdogan, Nick George, and Prashant Prabhat. (Photometrics) Chris Murphy, Hilary Hicks, and David Barnes. (Chroma) Mike Stanley and Chris Bauman. (Omega) Dan Osborn. (Molecular Probes) Mike Ignatius, Mike O'Grady, Nick Dolman, Cathy Erickson, Jason Kilgore, Magnus Persmark, and Iain Johnson. (Hunt Optics and Imaging) Andrew Hunt and John Marchlenski. (BioVision) Ken Anderson, Fernando Delaville (now at Leica).

Finally, we thank our editors at John Wiley & Sons for their great patience in receiving the manuscript and managing the production of the book.

D.B.M.
M.W.D.

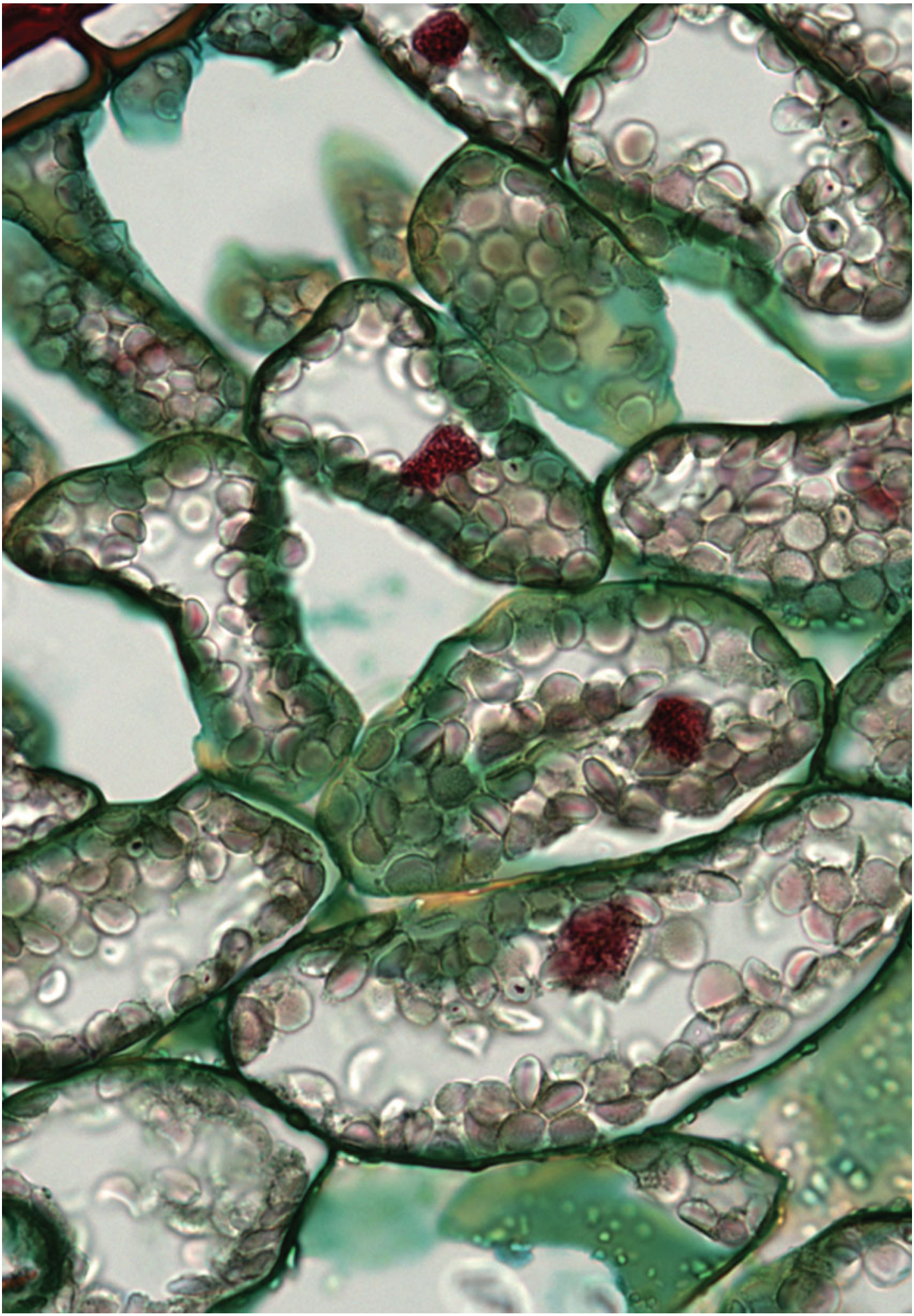

CHAPTER

1

FUNDAMENTALS OF LIGHT MICROSCOPY

OVERVIEW

In this chapter, we examine the optical design of the light microscope and review procedures for adjusting the microscope and its illumination to obtain the best optical performance. The light microscope contains two distinct sets of interlaced focal planes, eight planes in all, between the illuminator and the eye. All of these planes play an important role in image formation. As we will see, some planes are not fixed, but vary in their location depending on the focus position of the objective and condenser lenses. Therefore, an important first step is to adjust the microscope and its illuminator for Koehler illumination, a method of illumination introduced by August Koehler in 1893 that gives bright, uniform illumination of the specimen and simultaneously positions the sets of image and diffraction planes at their proper locations. We will refer to these locations frequently throughout the book. Indeed, microscope manufacturers build microscopes so that filters, prisms, and diaphragms are located at precise physical locations in the microscope body, assuming that certain focal planes will be precisely located after the user has adjusted the microscope for Koehler illumination. Finally, we will practice adjusting the microscope for examining a stained histological specimen, review the procedure for determining magnification, and measure the diameters of cells and nuclei in a tissue sample.

OPTICAL COMPONENTS OF THE LIGHT MICROSCOPE

A *compound light microscope* is an optical instrument that uses visible light to produce a magnified image of an object (or specimen) that is projected onto the retina of the

Brightfield microscopy of stained mesophyll cells in a leaf section.

Fundamentals of Light Microscopy and Electronic Imaging, Second Edition.
Douglas B. Murphy and Michael W. Davidson.

eye or onto the photosensitive surface of an imaging device. The word *compound* refers to the fact that two lenses, the objective and the eyepiece (or ocular), work together to produce the final magnification M of the image such that:

$$M_{\text{final}} = M_{\text{obj}} \times M_{\text{oc}}.$$

Two microscope components are of critical importance in forming the image: (1) the *objective*, which collects light diffracted by the specimen and forms a magnified real image at what is called the real intermediate image plane near the eyepieces or oculars, and (2) the *condenser*, which focuses light from the illuminator onto a small area of the specimen. (We define real vs. virtual images and examine the geometrical optics of lenses and magnification in Chapter 4; a real image can be viewed on a screen or exposed on a sheet of film, whereas a virtual image cannot.) The arrangement of these and other components in an upright stand research level microscope is shown in Figure 1.1, and for an inverted research microscope in Figure 1.2. Two lamps provide illumination for brightfield and interference (illumination from below: *diascopic*) and fluorescence (illumination from above: *episcopic*) modes of examination. Both the objective and condenser contain multiple lens elements that perform close to their theoretical limits and are therefore expensive. As these optics are handled frequently, they require careful attention. Other components less critical to image formation are no less deserving of care, including the tube lens and eyepieces, the lamp collector and lamp socket and its cord, filters, polarizers, retarders, and the microscope stage and stand with coarse and fine focus.

At this point, take time to examine Figure 1.3, which shows how an image becomes magnified and is perceived by the eye. The figure also points out the locations of important focal planes in relation to the objective, the ocular, and the eye. The specimen on the microscope stage is examined by the objective, which produces a magnified real image of the object in the image plane of the ocular. When looking in the microscope, the ocular acting together with the eye's cornea and lens projects a still more magnified real image onto the retina, where it is perceived and interpreted by the brain as a magnified virtual image about 25 cm (10 in) in front of the eye. For photography, the intermediate image is recorded directly or projected as a real image onto a camera.

Microscopes come in both inverted and upright designs (Figs. 1.1 and 1.2). In both designs the location of the real intermediate image plane at the eyepiece is fixed, and the focus dial of the microscope is used to position the image at precisely this location. In most conventional upright microscopes, the objectives are attached to a nosepiece turret on the microscope body, and the focus control moves the specimen stage up and down to bring the image to its proper location in the eyepiece. In inverted designs, the stage itself is fixed, being bolted to the microscope body, and the focus dials move the objective turret up and down to position the image in the eyepieces. Inverted microscopes are rapidly gaining in popularity because one can examine living cells in culture dishes filled with medium using standard objectives and avoid the use of sealed flow chambers, which can be awkward. One also has better access to the stage, which can serve as a rigid working platform for microinjection and physiological recording equipment. Inverted designs also have their center of mass closer to the lab bench and are therefore less sensitive to vibration. However, there is some risk of physical damage, as objectives may rub against the bottom surface of the stage during rotation of the objective turret. Oil immersion objectives are also at risk, because gravity can cause oil to drain down and enter the crevice between the nose and barrel, potentially

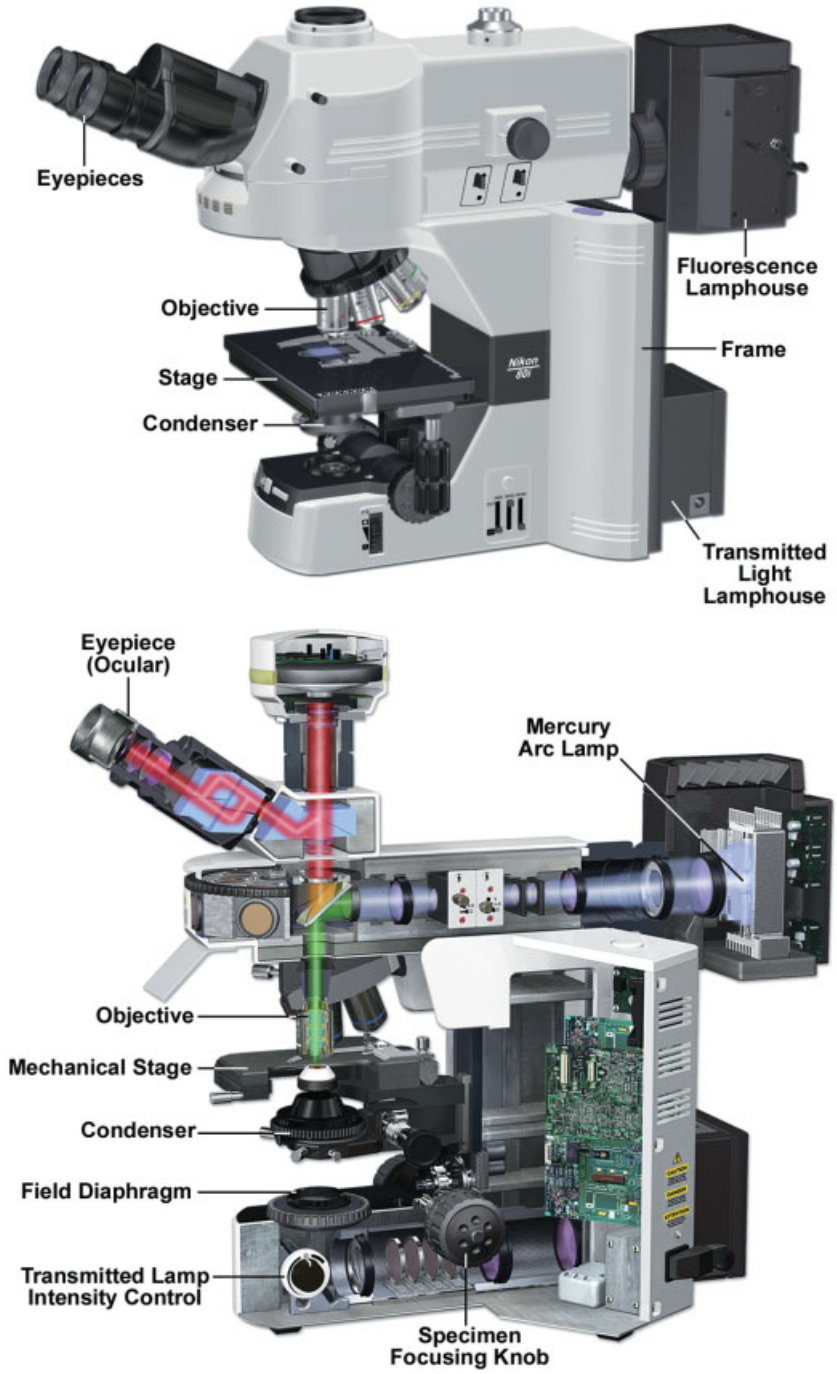

Figure 1.1

The research light microscope with upright stand. Two lamps provide transmitted and reflected light illumination. Note the locations of the knobs for the specimen and condenser lens focus adjustments. Also note the positions of two variable iris diaphragms: the field diaphragm near the illuminator, and the condenser diaphragm at the front aperture of the condenser. Each has an optimum setting in a properly adjusted microscope. Above: Nikon Eclipse 80i upright microscope; below: Olympus BX71 upright microscope.

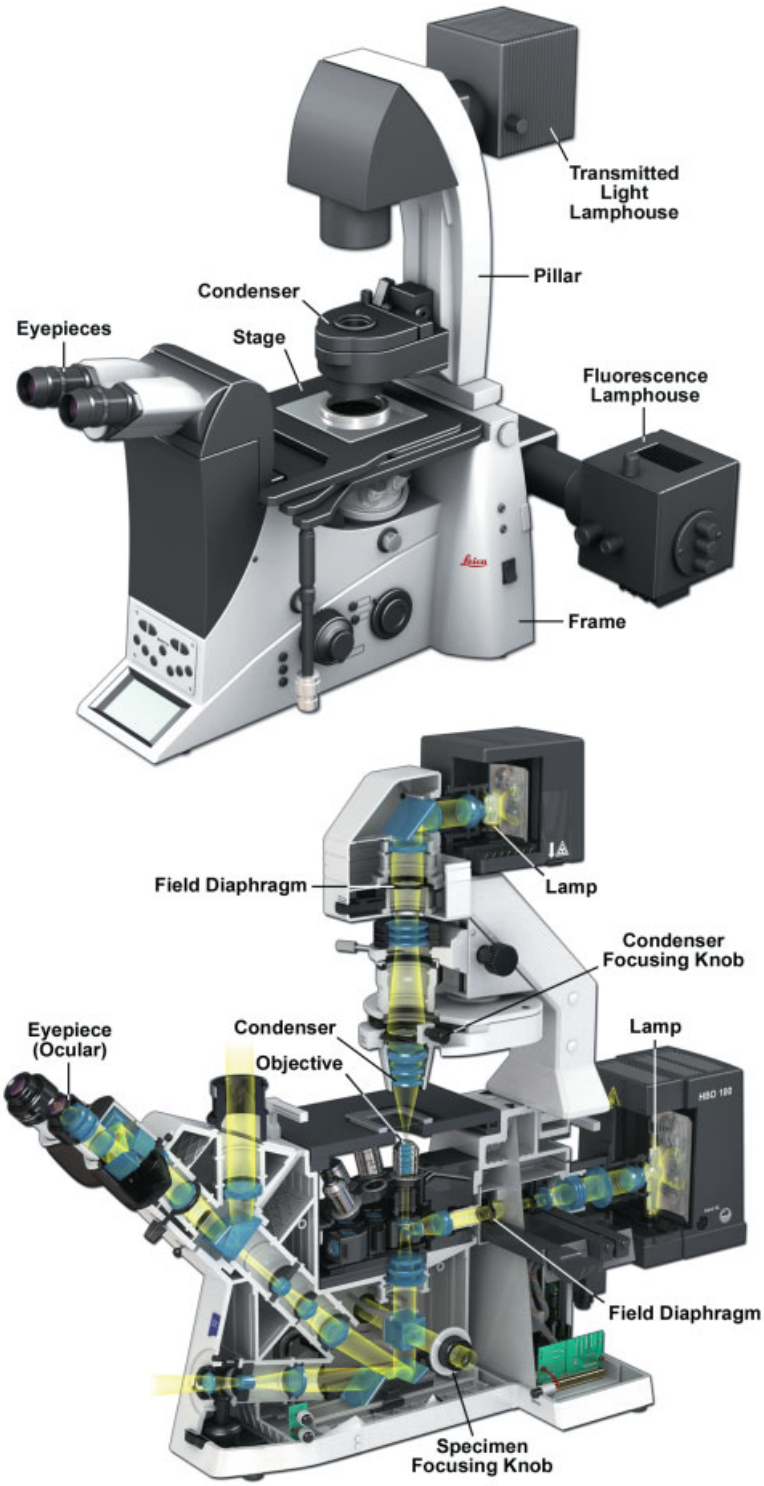

Figure 1.2

The research light microscope with inverted stand. As in upright designs, two lamps provide transmitted and reflected light illumination. Note the locations of the knobs for the specimen and condenser lens focus adjustments, which are often in different locations on inverted microscopes. Also note the positions of two variable iris diaphragms: the field diaphragm near the illuminator, and the condenser diaphragm at the front aperture of the condenser. Each has an optimum setting in a properly adjusted microscope. Above: Leica Microsystems DMI6000 B inverted microscope; below: Zeiss Axio Observer inverted microscope.

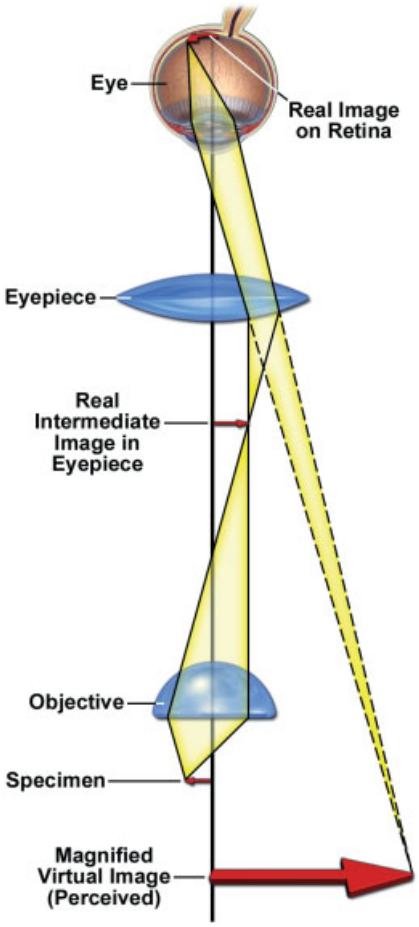

Figure 1.3
Perception of a magnified virtual image of a specimen in the microscope. The objective forms a magnified image of the object (called the real intermediate image) in the eyepiece; the intermediate image is examined by the eyepiece and eye, which together form a real image on the retina. Because of the perspective, the retina and brain interpret the scene as a magnified virtual image about 25 cm in front of the eye.

contaminating internal lens surfaces, ruining the optical performance and resulting in costly lens repair. This can be prevented by wrapping a pipe cleaner or hair band around the upper part of the lens to catch excess drips of oil. Therefore, despite many advantages, inverted research microscopes require a little more attention than do standard upright designs.

APERTURE AND IMAGE PLANES IN A FOCUSED, ADJUSTED MICROSCOPE

Principles of geometrical optics show that a microscope has two sets of interlaced conjugate focal planes, a set of four *object or field planes*, and a set of 4 *aperture or*

diffraction planes, that have fixed, defined locations with respect to the object, optical elements, the light source, and the eye or camera. Each plane within a set is *conjugate* with the other planes, with the consequence that all of the planes of a given set can be seen simultaneously when looking in the microscope. The field planes are observed in normal viewing mode using the eyepieces. This mode of viewing is called the normal, or object, or orthoscopic mode, and the real image of an object is called an *orthoscopic* image. Viewing the aperture or diffraction planes requires using an eyepiece telescope or Bertrand lens, which is focused on the rear aperture of the objective (see Note). This mode of viewing is called the aperture, or diffraction, or conoscopic mode, and the image of the diffraction plane viewed at this location is called the *conoscopic* image. In this text, we refer to the two viewing modes as the *normal* and *aperture viewing modes* and do not use the terms orthoscopic and conoscopic, although these terms are common in other texts.

Note: Objectives, Eyepieces, and Eyepiece Telescopes

An *aperture* is a hole or opening in an opaque mask designed to eliminate stray light from entering the light path, and most field and aperture planes of a microscope contain them. A fixed circular aperture is found at or near the rear focal plane of the objective (Fig. 1.4). (The precise location of the rear focal plane is a function of the focal length of the lens; for objectives with short focal lengths, the focal plane may be located inside the lens barrel.) The aperture mask is plainly visible at the back surface of the objective. This aperture marks one of the key aperture planes of the microscope, and we refer to this site frequently in the text.

The *eyepiece telescope* (not shown), sometimes called a phase or centering telescope, is a special focusable eyepiece that is used in place of an ocular to view the *rear aperture of the objective* and other aperture planes that are conjugate to it. To use the telescope, remove an eyepiece, insert the eyepiece telescope, and focus it on the circular edge of the objective rear aperture. Some microscopes contain a built-in focusable telescope lens called a *Bertrand lens* that can be conveniently rotated into and out of the light path as required.

The identities of the sets of conjugate focal planes are listed in Table 1.1, and their locations in the microscope under conditions of Koehler illumination are shown in Figure 1.5. The terms *front aperture* and *rear aperture* refer to the openings at the front and rear focal planes of a lens from the perspective of a light ray traveling from the lamp to the retina. Knowledge of the location of these planes is essential for adjusting the microscope and for understanding the principles involved in image formation. Indeed, the entire design of a microscope is based around these planes and the user's need to have access to them.

The *exit pupil* of the eyepiece, one of the microscope's aperture planes, is the disk of light that appears to hang in space a few millimeters above the back lens of the eyepiece; it is simply the image of the illuminated rear aperture of the objective. Normally, we are unaware that we are viewing four conjugate field planes when looking

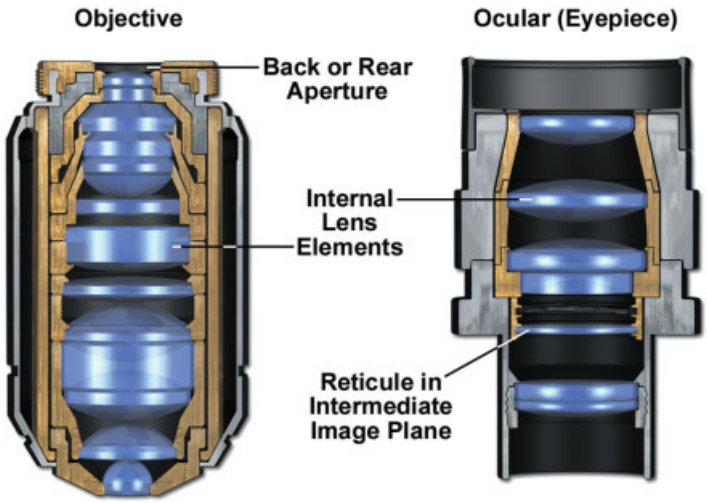

Figure 1.4

Objective and eyepiece diagrams. (a) Cross section of an objective showing the location of the back or rear aperture. (b) Cross sectional view of a focusable eyepiece, showing the location of the real intermediate image, in this case, containing an eyepiece reticule. Notice the many lens elements that make up these basic optics.

TABLE 1.1 Conjugate Planes in Optical Microscopy

Field Planes	Aperture Planes
(Normal view through the eyepieces)	(Aperture view through the eyepiece telescope)
Lamp (field) diaphragm	Lamp filament
Object (specimen) or field plane (diaphragm)	Front aperture of condenser
Real intermediate image plane (eyepiece field stop)	Rear aperture of objective
Retina or camera sensor face	Exit pupil of eyepiece (coincident with pupil of eye)

through the eyepieces of a microscope. As an example of the simultaneous visibility of conjugate focal planes, consider that the image of a piece of dirt on the focused specimen could lie in any one of the four field planes of the microscope: floaters near the retina, dirt on an eyepiece reticule, dirt on the specimen itself, and dirt on the glass plate covering the field diaphragm. With knowledge of the locations of the conjugate field planes, one can quickly determine the location of the dirt by rotating the eyepiece, moving the microscope slide, or wiping the cover plate of the field diaphragm. Before proceeding, you should take the time to identify the locations of the field and aperture planes on your microscope in the laboratory.

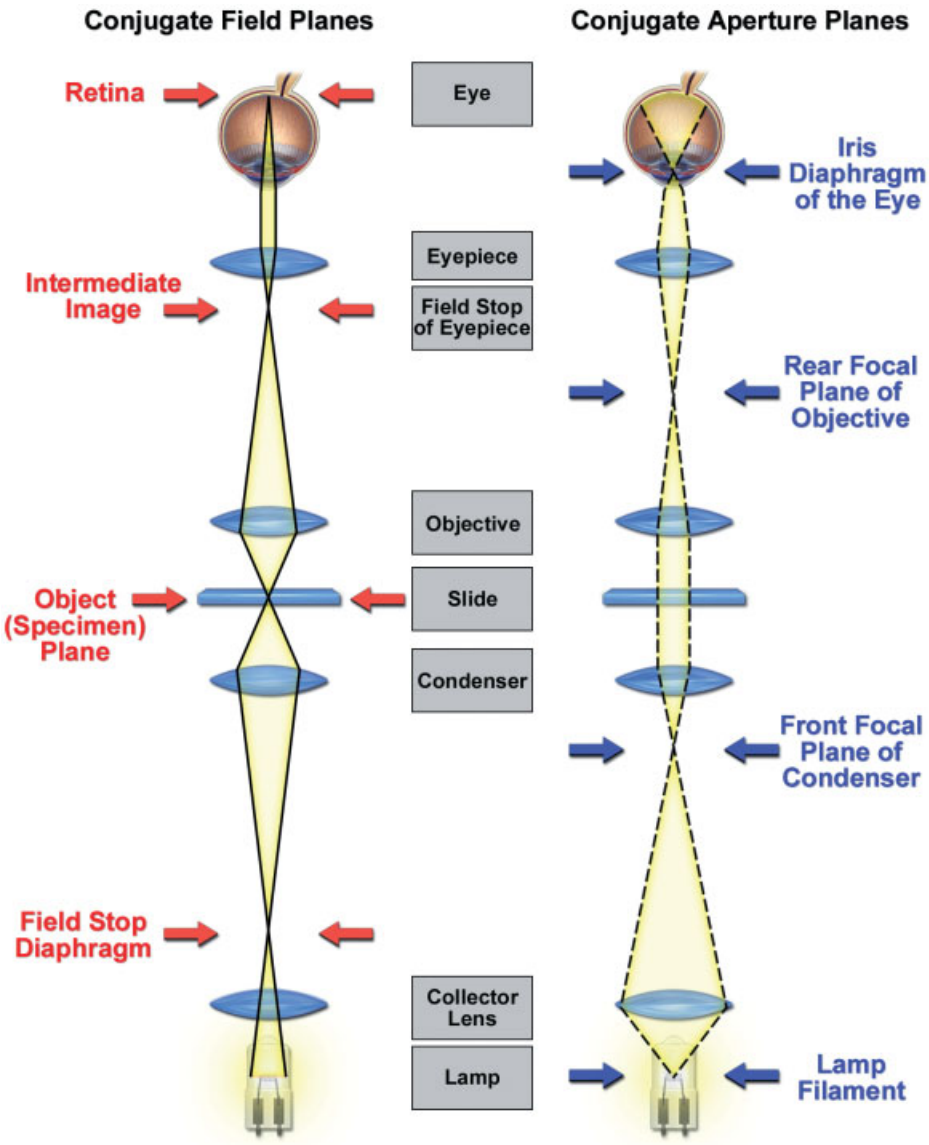

Figure 1.5

Conjugate and aperture planes in Koehler illumination. Arrows mark the conjugate focal planes. Note the locations of four conjugate field planes (red arrows; left) and four conjugate aperture planes (blue arrows; right) indicated by the crossover points of rays in the diagrams. The left-hand diagram shows that the specimen or object plane is conjugate with the real intermediate image plane in the eyepiece, the retina of the eye, and the field stop diaphragm between the lamp and the condenser. The right-hand drawing shows that the lamp filament is conjugate with aperture planes at the front focal plane of the condenser, the rear focal plane of the objective, and the pupil of the eye. The two sets of conjugate planes interdigitate with one another.

KOEHLER ILLUMINATION

Illumination is a critical determinant of optical performance in light microscopy. Apart from the intensity and wavelength range of the light source, it is important that a large cone of light emitted from each source point be collected by the lamp collector and that the source be imaged onto the front aperture of the condenser. From there, each point of the source image is projected through the specimen and to infinity as a parallel collimated pencil of light. The size of the illuminated field at the specimen is adjusted so that it matches the specimen field diameter of the objective being employed. Because each source point contributes equally to illumination in the specimen plane, variations in intensity in the image are attributed to the object and not to irregular illumination from the light source. The method of illumination introduced by August Koehler in the late nineteenth century fulfills these requirements and is the standard method of illumination used in light microscopy (Fig. 1.6). Under the conditions set forth by Koehler, a *collector lens* on the lamp housing is adjusted so that it focuses an image of the lamp filament at the front focal plane of the condenser while completely filling the aperture with light. Under this condition, illumination of the specimen plane is bright and even. Achieving this condition also requires focusing the condenser using the condenser focus knob, an adjustment that brings two sets of conjugate focal planes into precise physical locations in the microscope, a requirement for a wide range of image contrasting techniques that are discussed later in Chapters 7–11. The main advantages of Koehler illumination in image formation are:

- *Bright and even illumination in the specimen plane and in the conjugate image plane.* Even when illumination is provided by an irregular light source, such as a lamp filament, illumination of the object-specimen is remarkably uniform across an extended area. Under these conditions of illumination, a given point in the specimen is illuminated by every point in the light source, and conversely, a given point in the light source illuminates every point in the specimen.
- *Positioning of two different sets of conjugate focal planes at specific locations along the optical axis of the microscope*, a strict requirement for maximal spatial resolution and optimal image formation for a variety of optical modes. As we will see, stage focus and condenser focus and centration position the focal planes correctly, while correct settings of the field diaphragm and the condenser aperture diaphragm give control over resolution and contrast. Once properly adjusted, it is easier to locate and correct faults, such as dirt and bubbles that can degrade optical performance.

ADJUSTING THE MICROSCOPE FOR KOEHLER ILLUMINATION

Review Figure 1.5 again to familiarize yourself with the locations of the two sets of focal planes, one set of four field planes, and one set of four aperture planes. You will need an eyepiece telescope or Bertrand lens to examine the aperture planes and to make certain adjustments. In the absence of a telescope lens, one may simply remove an eyepiece and look straight down the optical axis at the objective aperture; however, without a telescope, the aperture diameter is small and difficult to see clearly. The adjustment procedure is given in detail below. You will need to check your alignment every time you change a lens to examine the specimen at a different magnification.

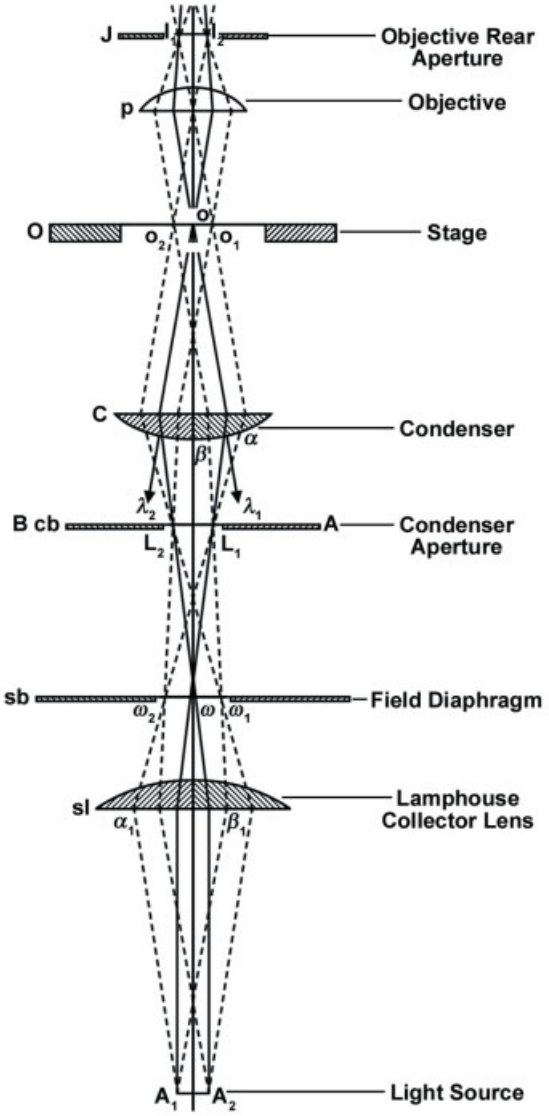

August Koehler
1866-1948

Figure 1.6

August Koehler introduced a new method of illumination that greatly improved image quality and revolutionized light microscope design. Koehler introduced the system in 1893 while he was a university student and instructor at the Zoological Institute in Giessen, Germany, where he performed photomicrography for taxonomic studies on limpets. Using the traditional methods of critical illumination, the glowing mantle of a gas lamp was focused directly on the specimen with the condenser, but the images were unevenly illuminated and dim, making them unsuitable for photography using slow-speed emulsions. Koehler's solution was to reinvent the illumination scheme. He introduced a collector lens for the lamp and used it to focus the image of the lamp on the front aperture of the condenser. A luminous field stop (the field diaphragm) was then focused on the specimen with the condenser focus control. The method provided bright, even illumination, and fixed the positions of the focal planes of the microscope optics. In later years, phase contrast microscopy, fluorescence microscopy with epi-illumination, differential interference contrast microscopy, and confocal optical systems would all utilize and be critically dependent on the action of the collector lens, the field diaphragm, and the presence of fixed conjugate focal planes that are inherent to Koehler's method of illumination. The interested reader should refer to the special centenary publication on Koehler by the Royal Microscopical Society (see Koehler, 1893).

Note: Summary of Steps for Koehler Illumination

1. Check that the lamp is focused on the front aperture of the condenser.
2. Focus the specimen.
3. Focus the condenser to see the field stop diaphragm.
4. Adjust the condenser diaphragm using the eyepiece telescope.

- *Preliminaries.* Place a specimen slide, such as a stained histological specimen, on the stage of the microscope. Adjust the condenser height with the condenser-focusing knob so that the front lens element of the condenser comes within ~1–2 mm of the specimen slide. Do the same for the objective. Be sure all diaphragms are open so that there is enough light (includes illuminator's field diaphragm, the condenser's front aperture diaphragm, and in some cases, a diaphragm in the objective itself). Adjust the lamp power supply so that the illumination is bright but comfortable when viewing the specimen through the eyepieces.
- *Check that the lamp fills the front aperture of the condenser.* Inspect the front aperture of the condenser by eye and ascertain that the illumination fills most of the aperture. It helps to hold a piece of lens tissue against the aperture to check the area of illumination (Fig. 1.7). Using an eyepiece telescope or Bertrand lens, examine the rear aperture of the objective and its conjugate planes, the front aperture of the condenser, and the lamp filament. Be sure the lamp filament is centered, using the adjustment screws on the lamp housing if necessary, and

Figure 1.7
Examining the area of illumination at the condenser front aperture.

confirm that the lamp filament is focused in the plane of the condenser diaphragm. This correction is made by adjusting the focus dial of the collector lens on the lamp housing. Once these adjustments are made, it is usually not necessary to repeat the inspection every time the microscope is used. Instructions for centering the lamp filament or arc are given in Chapter 3. Lamp alignment should be rechecked after the other steps have been completed.

- *Focus the specimen.* Bring a low power objective to within 1 mm of the specimen, and looking in the microscope, carefully focus the specimen using the microscope's coarse and fine focus dials. It is helpful to position the specimen with the stage controls so that a region of high contrast is centered on the optical axis before attempting to focus. It is also useful to use a low magnification "dry" objective (10–25×, used without immersion oil) first, since the *working distance*, the distance between the coverslip and the objective, is 2–5 mm for a low power lens. This reduces the risk of plunging the objective into the specimen slide and causing damage. Since the lenses on most microscopes are *parfocal* (see Chapter 4), higher magnification objectives will already be in focus or close to focus when rotated into position.
- *Focus and center the condenser.* With the specimen in focus, close down (stop down) the *field diaphragm* and then, while examining the specimen through the eyepieces, focus the angular outline of the diaphragm's periphery using the condenser's focusing knob (Fig. 1.8). If there is no light, turn up the power supply and bring the condenser closer to the microscope slide. If light is seen but seems to be far off axis, switch to a low power lens and move the condenser positioning knobs slowly to bring the center of the illumination into the center of the field of view. Focus the image of the field diaphragm and center it using the condenser's two centration adjustment screws (Fig. 1.9). The field diaphragm is then opened just enough to accommodate the object or the field of a given detector. This helps

Figure 1.8
Adjusting the field diaphragm opening size and focusing the condenser.

Figure 1.9
Adjusting the condenser centering knobs during alignment of the microscope for Koehler illumination.

reduce scattered or stray light and improves image contrast. The condenser is now properly adjusted. We are nearly there! The conjugate focal planes that define Koehler illumination are now at their proper locations in the microscope.

- *Adjust the condenser diaphragm while viewing the objective rear aperture with an eyepiece telescope or Bertrand lens.* Finally, the condenser diaphragm is adjusted to obtain the best resolution and contrast, but is not closed so far as to degrade the resolution. In viewing the condenser front aperture using a telescope, the small bright disc of light seen in the telescope represents the objective's rear aperture plus the superimposed image of the condenser's front aperture diaphragm. As you close down the condenser diaphragm, you will see its edges enter the aperture opening and limit the objective aperture's diameter. Focus the telescope so the edges of the diaphragm are seen clearly. Stop when ~3/4 of the maximum diameter of the aperture remains illuminated and use this setting as a starting position for subsequent examination of the specimen (Fig. 1.10). As pointed out in Chapter 6, the setting of this aperture is crucial, because it determines the resolution of the microscope, affects the contrast of the image, and establishes the depth of field. It is usually impossible to optimize for resolution and contrast at the same time, so the 3/4 open position indicated here is a good starting position. The final setting depends on the inherent contrast of the specimen.
- *Adjust the lamp brightness.* Image brightness is controlled by regulating the lamp voltage, or if the voltage is nonadjustable, by placing neutral density filters in the light path near the illuminator in specially designed filter holders. *The aperture diaphragms should never be closed down as a way to reduce light intensity,* because this action reduces the resolving power and may blur fine details in the image. We will return to this point in Chapter 6.

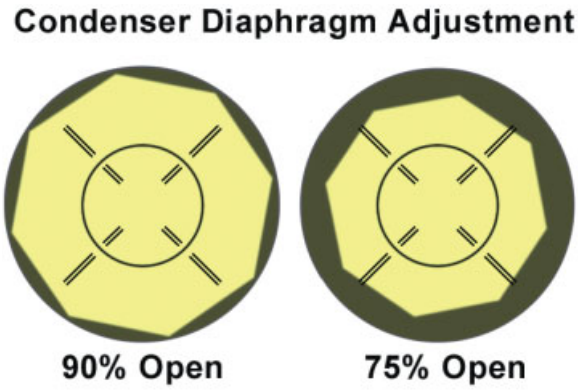

Figure 1.10
Adjusting the condenser diaphragm opening size to maximize contrast.

The procedure for adjusting the microscope for Koehler illumination seems invariably to stymie most newcomers. With so many planes and devices to think about, this is perhaps to be expected. To get you on your way, try to remember this simple two step guide: *Focus on a specimen and then focus and center the condenser*. Post this reminder near your microscope. If you do nothing else beyond this, you will have properly adjusted the image and aperture planes of the microscope, and the rest will come quickly enough after practicing the procedure a few times. Although the adjustments sound complex, they are simple to perform, and their significance for optical performance cannot be overstated. The advantages of Koehler illumination for a number of optical contrasting techniques will be revealed in the next several chapters.

Note: Focusing Oil Immersion Objectives

The *working distance*, the distance between the front lens element and the first surface of the coverslip of an oil immersion lens is so small (~60 μm for some oil immersion lenses) that the two optical surfaces nearly touch each other when the specimen is in focus. Since the focal plane at the specimen (the depth of field) is also very thin (0.1 μm for a 100×, 1.4 NA objective), focusing on a thin, transparent specimen can be a real challenge. Due to such close tolerances, it is unavoidable that the lens and coverslip will occasionally make contact, but this is usually of little consequence. The outermost lens elements are mounted in a spring-loaded cap, so that the lens can be compressed a bit by the specimen slide without damaging the optics. The lens surface is also recessed and not coplanar with the surface of the metal lens cap, which prevents accidental scratching and abrasion.

Begin focusing by bringing the lens in contact with the drop of oil on the coverslip. The drop of oil will expand as the lens is brought towards focus, and at contact (essentially the desired focus position), the oil drop stops expanding. If overfocused, the microscope slide is pushed up off the stage by a small amount on an inverted microscope; on an upright microscope the spring-loaded element of the objective compresses a bit. Retract the lens to the true focal position and then examine the

specimen. In normal viewing mode, it should only be necessary to change the focus by a very small amount to find the specimen. It can help to move the specimen stage controls with the other hand to identify the shadows or fluorescence of a conspicuous object, which may serve as a guide for final focus adjustment. Notice there is a risk, in cases where focus movements are too extreme, that the objective (of an upright microscope) or the condenser (on an inverted microscope) might break the microscope slide, or worse, induce permanent strain in the optics. Focusing with oil immersion optics always requires extra care and patience.

Before observing the specimen, examine the rear focal plane of the objective with an eyepiece telescope to check for lint and oil bubbles. Small bubbles and lint produce bright foci of scattered light whose identity can be confirmed by focusing the telescope. An insufficient amount of oil between the lens and coverslip can cause the entire rear aperture to be misshapen; if this is the case, focusing the telescope will bring the edge of the oil drop into sharp focus. These faults should be removed or corrected, as they will significantly degrade optical performance.

FIXED TUBE LENGTH VERSUS INFINITY OPTICAL SYSTEMS

Until the late 1980s, most microscopes had a fixed tube length with a specified distance between the nosepiece opening, where the objective is attached, and the eyepiece seat in the observation tubes. This distance is known as the *mechanical tube length* of the microscope. The design assumes that when the specimen is placed in focus, it is a few micrometers further away than the front focal plane of the objective (Fig. 1.11a). Finite tube lengths were standardized at 160 mm during the nineteenth century by the Royal Microscopical Society (RMS), and were in use for over 100 years. Objectives designed to be used with a microscope having the industry standard tube length of 160 mm are inscribed with "160" on the barrel.

Adding optical accessories into the light path (between the microscope frame and observation tube head) of a fixed tube length microscope increases the effective tube length to a value greater than 160 mm. Therefore, inserting auxiliary components, such as a reflected light or fluorescence illuminator, polarizers, filters, and DIC prisms, can introduce spherical aberration and "ghost images" into an otherwise perfectly corrected optical system. During the period when most microscopes had fixed tube lengths, manufacturers were forced to place additional optical elements into these accessories to reestablish the effective 160-mm tube length of the microscope. The optical cost was an increase in magnification and reduced light intensity in resulting images. To circumvent these artifacts, the German microscope manufacturer Reichert pioneered the concept of *infinity optics*. The company started experimenting with infinity-corrected optical systems as early as the 1930s, but this concept did not become standard equipment for most manufacturers until 50 years later.

Infinity optical systems have a different objective design that produces a flux of parallel light wavefronts imaged at infinity, which are then brought into focus at the intermediate image plane by a special optic termed a *telan* or *tube* lens. The region between the objective rear aperture and the tube lens is called *infinity space*, where auxiliary components can be introduced into the light path without producing focus artifacts or optical aberrations (Fig. 1.11b). Correction for optical aberration in infinity

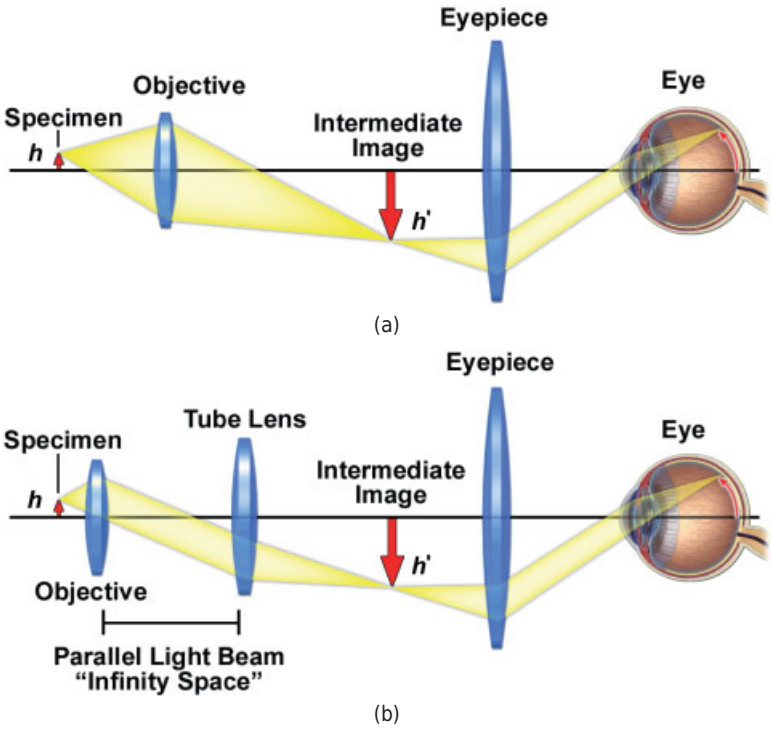

Figure 1.11

Finite and infinity corrected microscope optical configuration. (a) Finite microscope optical train showing focused light rays from the objective at the intermediate image plane. (b) Infinity-corrected microscope with a parallel light beam between the objective and tube lens. This is the region of the optical train that is designed for auxiliary components, such as DIC prisms, polarizers, and filters.

microscopes is accomplished by modifying either the tube lens or the objective, or both. Infinity microscopes can maintain parfocality between objectives even when auxiliary components are introduced, and these components are designed to produce exactly 1× magnification to enable comparison of specimens using a combination of several optical techniques, such as phase contrast and DIC with fluorescence. This is possible because optical accessories (such as DIC prisms) placed in the infinity space do not shift the location or focal point of the image. A note of caution: objectives designed for older 160-mm fixed tube length microscopes are not interchangeable with newer infinity-corrected microscopes.

PRECAUTIONS FOR HANDLING OPTICAL EQUIPMENT

- *Never strain, twist, or drop objectives or other optical components*. Optics for polarization microscopy are especially susceptible to failure due to mishandling.
- *Never force the focus controls* of the objective or condenser, and always watch lens surfaces as they approach the specimen. This is especially important for high power, oil-immersion lenses.

- *Never touch optical surfaces*. In some cases, just touching an optical surface can remove unprotected coatings and ruin filters costing hundreds of dollars. Carefully follow the procedures for cleaning lenses and optical devices.

CARE AND MAINTENANCE OF THE MICROSCOPE

Microscopes are sophisticated instruments that require periodic maintenance and cleaning to guarantee satisfactory performance. When neglected by continuous exposure to dust, lint, pollen, dirt, and failure to remove immersion oil after use, the optical performance can deteriorate to the point that images are negatively affected. Likewise, regular maintenance of the microscope's mechanical and electrical components is equally important to prevent a gradual degradation in the operation of the focusing rack, stage translation mechanism, adjustable diaphragms, filter sliders, and auxiliary electronics. Dust covers are usually provided with microscopes when they are purchased and should be installed whenever the instrument is not in use to prevent contamination from airborne particles drifting through the laboratory. However, even when the microscope is routinely covered during periods of inactivity, those instruments that are used on a daily basis are still likely to experience a slow buildup of contaminants over time.

Particulates, such as dust, lint, fibers, and general debris (collectively referred to as dirt), can seriously affect the quality of an image if they land on a glass surface in a plane near the specimen or the camera sensor. Critical areas to examine for dirt contamination are the objective front lens element, the surface of the camera sensor (and its protective glass cover), both surfaces of the cover slip, the surface of the microscope slide, camera adapter optical surfaces, the upper lens of the condenser, the eyepiece lenses, both surfaces of the reticule, and other glass surfaces in the light path, including lamps, filters, beamsplitters, collector lenses, and heat filters. Cleaning of the microscope optical components is discussed in Chapter 4. Problems with the focusing rack or mechanical stage controls should be left for qualified microscope technicians. External painted surfaces on most microscopes are extremely durable. However, they can be cleaned when needed using a lightly moistened microfiber cloth. Remove loose dust and dirt using a soft hairbrush or ear syringe (available in drugstores). Avoid using compressed air as the propellant can leave unwanted deposits on painted and glass surfaces.

Exercise: Calibration of Magnification

Examine a histological specimen to practice proper focusing of the condenser and setting of the field stop and condenser diaphragms. A 10-μm thick section of pancreas or other tissue stained with hematoxylin and eosin (H&E) is ideal. A typical histological specimen is a section of a tissue or organ that has been chemically fixed, embedded in epoxy resin or paraffin, sectioned, and stained with dyes specific for nucleic acids, proteins, carbohydrates, and so on. In H&E staining, hematoxylin stains the nucleus and cytoplasmic RNA a dark blue or purple color, while eosin stains proteins (and the pancreatic secretory granules) a bright orange-pink. When the specimen is illuminated with monochromatic light, the contrast perceived by the eye is largely due to these stains. For this

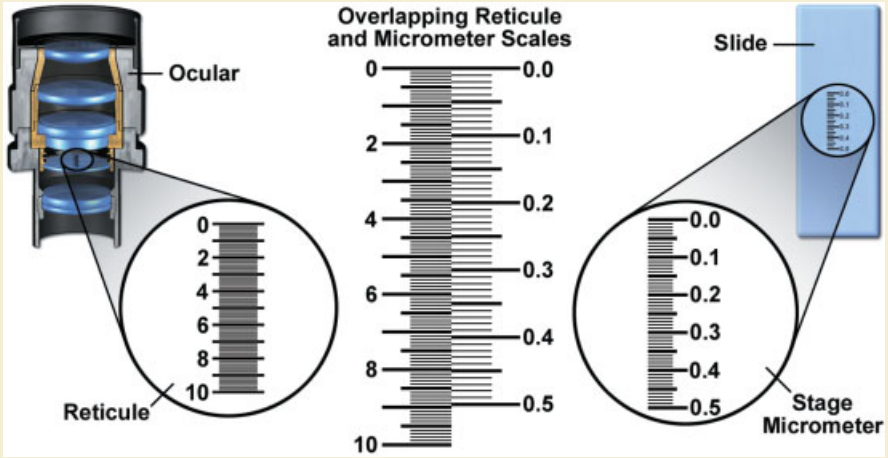

Figure 1.12

The eyepiece reticule and stage micrometer used for determining magnification. The typical eyepiece reticule is divided into 1/100 cm (100 μm unit) divisions, and the stage micrometer into 1/100 mm (10 μm unit) divisions. The appearance of the two overlapping scales is shown in the middle of the figure.

reason, a stained histological specimen is called an *amplitude specimen*, and is suitable for examination under the microscope using "brightfield" optics. A suitable magnification is 10–40×.

Equipment and procedure

Three items are required: a focusable eyepiece, an eyepiece reticule, and a stage micrometer (Fig. 1.12). The eyepiece reticule is a round glass disk usually containing a 10-mm scale divided into 0.1 mm (100 μm) units. The reticule is mounted in an eyepiece and is then calibrated using a stage micrometer to obtain a conversion factor (μm/reticule unit) that is used to determine the magnification obtained for each objective. The reason for using this calibration procedure is that the nominal magnification of an objective (found engraved on the lens barrel) is only correct to within ±5%. If precision is not of great concern, however, an approximate magnification can be obtained using the eyepiece reticule alone. In this case, simply measure the number of micrometers from the eyepiece reticule and divide by the nominal magnification of the objective. For a specimen covering 2 reticule units (200 μm), for example: 200 μm/10× Mag = 20 μm length.

The full procedure, using the stage micrometer, is performed as follows:

- To mount the eyepiece reticule, unscrew the lower barrel of the focusing eyepiece and place the reticule on the stop ring with the scale facing upwards. The stop-ring marks the position of the real intermediate image plane. Make sure the reticule size matches the internal diameter of the eyepiece and rests on the field stop. Reticules can be obtained from the microscope vendor or companies, such as Edmund Scientific Company or Klarmann Rulings.

Carefully reassemble the eyepiece and return it to the binocular head. Next, focus the reticule scale using the focus dial on the eyepiece and then focus on a specimen with the microscope focus dial. The images of the specimen and reticule are conjugate and should be simultaneously in sharp focus.

- Examine the stage micrometer slide, rotating the eyepiece so that the micrometer and reticule scales are lined up and partly overlapping. The stage micrometer consists of a 1- or 2-mm scale divided into 10-μm units, giving 100 units/mm. The micrometer slide is usually marked 1/100 mm. The conversion factor we need to determine is simply the number of μm/reticule units. This conversion factor can be calculated more accurately by counting the number of micrometers contained in several reticule units in the eyepiece. The procedure must be repeated for each objective, but only needs to be performed one time.
- Returning to the specimen slide, the number of eyepiece reticule units spanning the diameter of a structure is determined and multiplied by the conversion factor to obtain the distance in micrometers.

Exercise

1. Calibrate the magnification of the objective/eyepiece system using the stage micrometer and an eyepiece reticule. First determine how many micrometers are in each reticule unit.
2. Determine the mean diameter and standard deviation of a typical cell, a nucleus, and a cell organelle, where the sample size, *n*, is 10. Examination of cell organelles requires a magnification of 40–100×.
3. Why is it wrong to adjust the brightness of the image using either of the two diaphragms? How else (in fact, how should you) adjust the light intensity and produce an image of suitable brightness for viewing or photography?

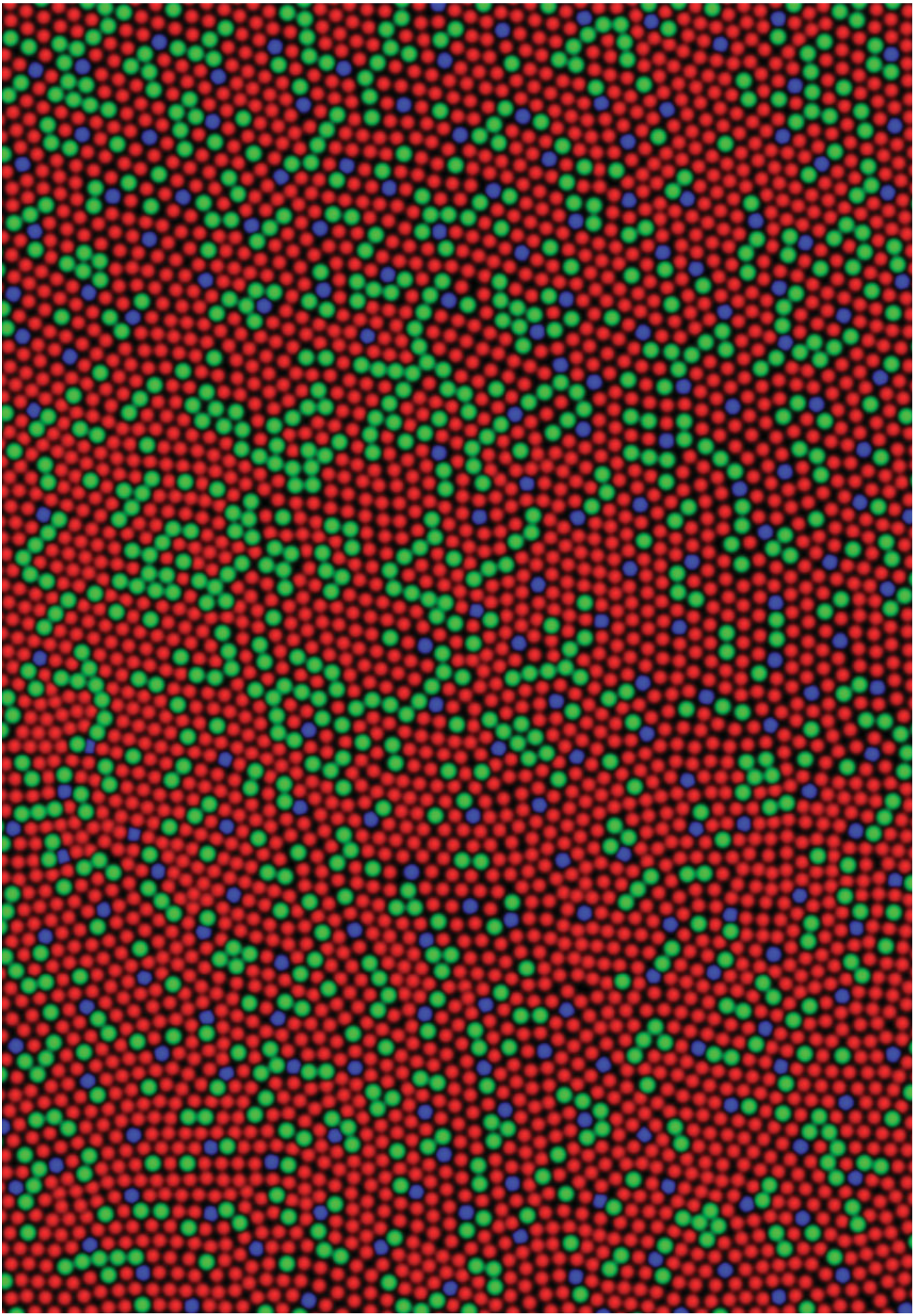

CHAPTER
2

LIGHT AND COLOR

OVERVIEW

In this chapter, we review the nature and action of light as a probe to examine objects in the light microscope. Knowledge of the wave nature of light is essential for understanding the physical basis of color, polarization, diffraction, image formation, and many other topics covered in this book. The eye–brain visual system is responsible for the detection of light, including the perception of color and differences in light intensity that we recognize as contrast. The eye is also a remarkably designed detector in an optical sense—the spacing of photoreceptor cells in the retina perfectly matches the requirement for resolving the finest image details formed by its lens (Fig. 2.1). Knowledge of the properties of light is important in selecting filters and objectives, interpreting colors, performing low-light imaging, and many other tasks.

LIGHT AS A PROBE OF MATTER

It is useful to think of light as a probe that can be used to determine the structure of objects viewed under a microscope. Generally, probes must have size dimensions that are similar to or smaller than the structures being examined. Fingers are excellent probes for determining the size and shape of keys on a computer keyboard, but fail in resolving wiring patterns on a computer's integrated circuit chip. Similarly, waves of light are effective in resolving object details with dimensions similar to the wavelength of light, but generally do not do well in resolving molecular and atomic structures that

Interpretive drawing of cone cells in the human fovea.

Fundamentals of Light Microscopy and Electronic Imaging, Second Edition.
Douglas B. Murphy and Michael W. Davidson.

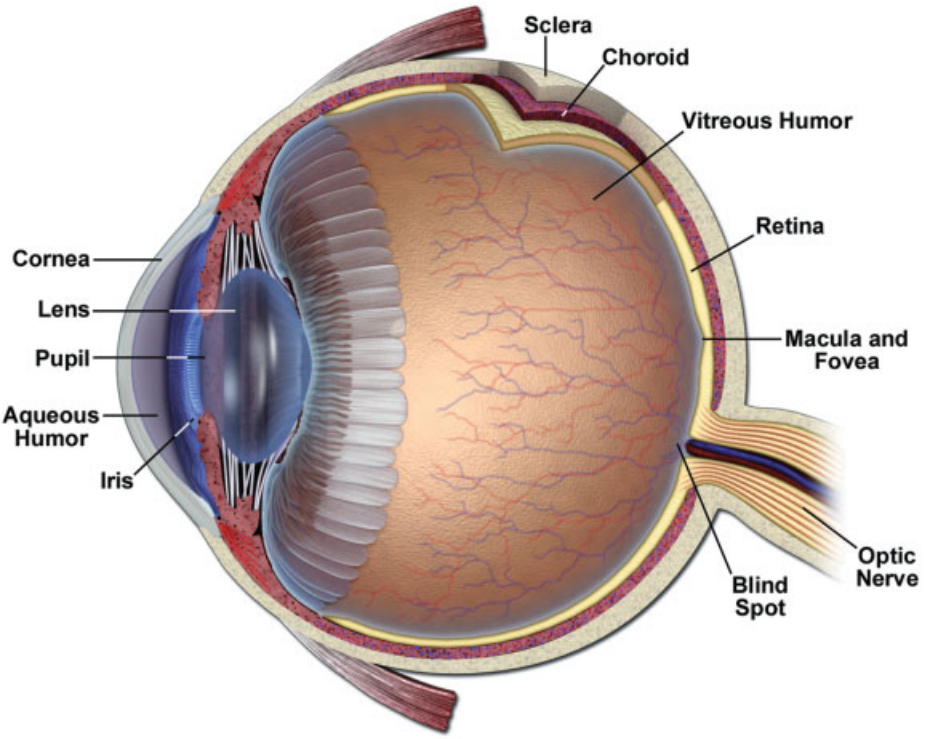

Figure 2.1

Structure of the human eye. The cornea and lens of the eye work together with the eyepiece to focus a real magnified image on the retina. The aperture plane of the eye-microscope system is located in front of the lens in the pupil of the eye, which functions as a variable diaphragm. A large number of rod cells cover the surface of the retina. The 3-mm macula, or yellow spot, contains a 0.5-mm diameter fovea, a depressed pit that contains the majority of the retina's cone cells that are responsible for color vision. The blind spot contains no photoreceptor cells and marks the site of exit of the optic nerve.

are much smaller than the wavelength. For example, details as small as 0.2 μm can be resolved visually in a microscope with an oil immersion objective. *As an approximation, the resolution limit of the light microscope with an oil immersion objective is about one-half of the wavelength of the light employed*.

Visible light, the agent used as the analytic probe in light microscopy, is a form of energy called electromagnetic radiation. This energy is contained in discrete units or quanta called photons that have the properties of both particles and waves. Photons as electromagnetic waves exhibit oscillating electric and magnetic fields, designated E and B, respectively, whose amplitudes and directions are represented by vectors that oscillate in phase as sinusoidal waves in two mutually perpendicular planes (Fig. 2.2). Photons are associated with a particular energy (ergs), which determines their wavelength (nm) and vibrational frequency (cycles/s). It is important to realize that the electromagnetic waves we perceive as light (400–750 nm or about 10^{-7} m) comprise just a small portion of the entire electromagnetic spectrum, which ranges from 10^{4} m (radio waves) to 10^{-10} m (γ-rays) (Fig. 2.3).

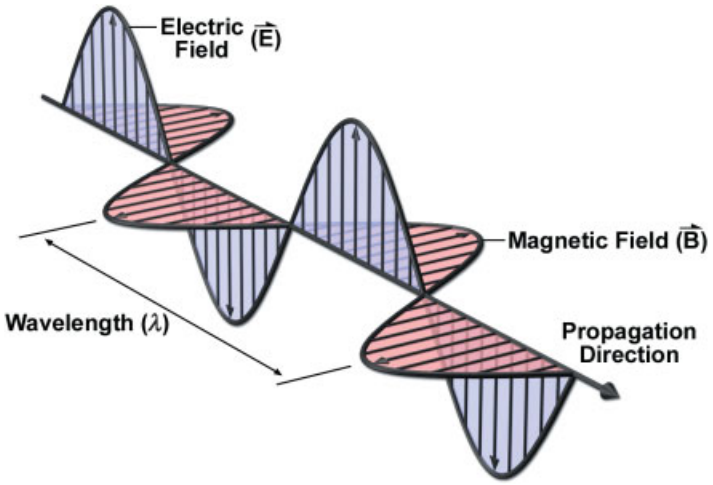

Figure 2.2

Light as an electromagnetic wave. The wave exhibits electric (E) and magnetic (B) fields whose amplitudes oscillate as a sine function over dimensions of space and time. The amplitudes of the electric and magnetic components at a particular instant or location are described as vectors that vibrate in two planes perpendicular to each other and perpendicular to the direction of propagation. However, at any given time or distance, the E and B vectors are equal in amplitude and phase. For convenience, it is common to show only the electric field vector (E vector) of a wave in graphs and diagrams and not specify it as such.

The figure also compares the sizes of cells, molecules, and atoms with the wavelengths of different radiations. See Hecht (2001) and Falk et al. (1986) for interesting discussions on the nature of light.

Although it is frustrating that light cannot be defined in terms of a single physical entity, it can be described through mathematical relationships that depict its dual particle- and wave-like properties. The properties of energy, frequency, and wavelength are related through the following equations, which can be used to determine the amount of energy associated with a photon of a specific wavelength:

$$c = \nu\lambda,$$
$$E = h\nu,$$

and combining,

$$E = hc/\lambda,$$

where c is the speed of light (3×10^{10} cm/s), ν is the frequency (cycles/s), λ is the wavelength (cm), E is energy (ergs), and h is Plank's constant (6.62×10^{-27} erg-seconds). The first equation defines the velocity of light as the product of its frequency and wavelength. We will encounter conditions where velocity and wavelength vary, such as when photons enter a glass lens. The second equation relates frequency and energy, which becomes important when we must choose a wavelength for examining live cells. The third equation relates the energy of a photon to its wavelength. Since $E \sim 1/\lambda$, 400-nm violet wavelengths are twice as energetic as 800-nm infrared wavelengths.

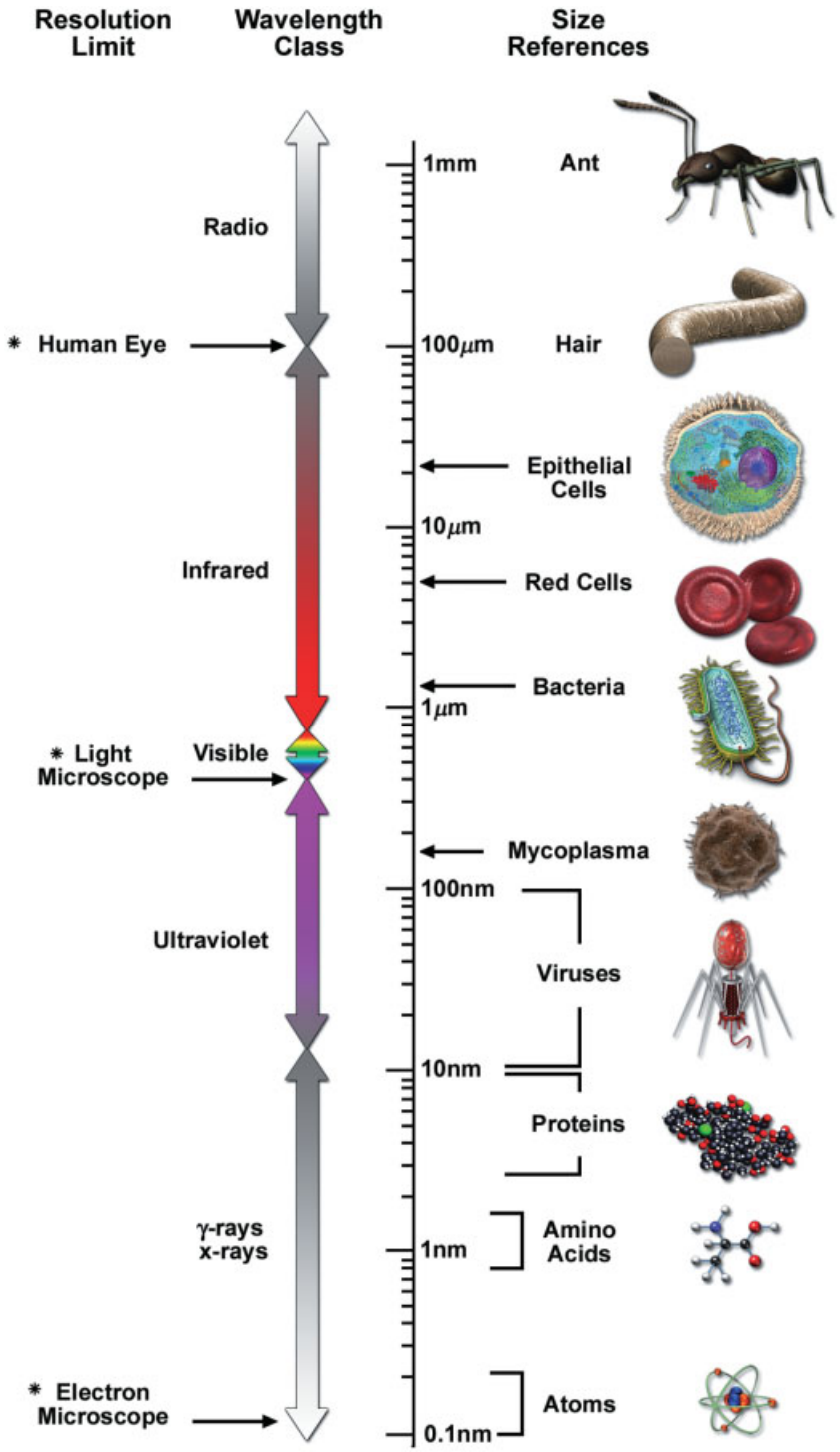

Figure 2.3

The electromagnetic spectrum. The figure shows a logarithmic distance scale (range 1 mm to 0.1 nm). One side shows the wavelength ranges of common classes of electromagnetic radiation; for reference, the other side indicates the sizes of various cells and macromolecules. Thus, a red blood cell (7.5 μm) is 15 times larger than a wavelength of visible green light (500 nm). The resolution limits of the eye, light microscope, and electron microscope are also indicated (*). For the eye, the resolution limit (0.1 mm) is taken as the smallest interval in an alternating pattern of black and white bars on a sheet of paper held 25 cm in front of the eye under conditions of bright illumination. Notice that the range of visible wavelengths spans just a small portion of the spectrum.

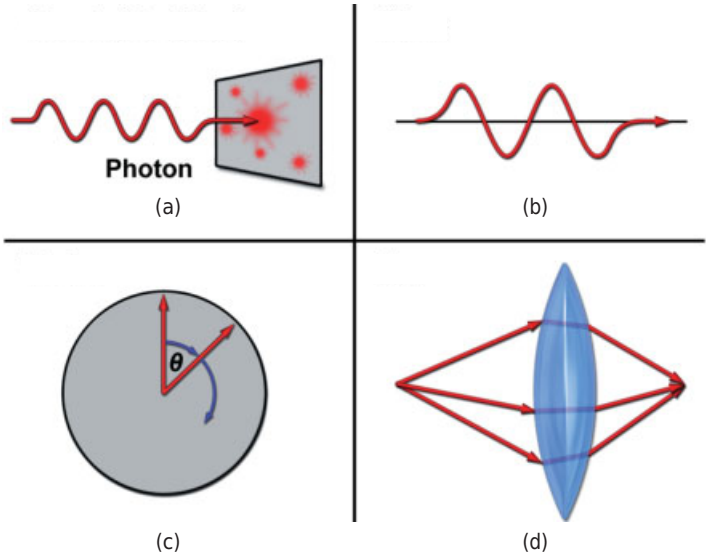

Figure 2.4
Light as (a) quanta, (b) waves, (c) vectors, and (d) rays.

THE DUAL PARTICLE- AND WAVE-LIKE NATURE OF LIGHT

For the most part, we will be referring to the wave nature of light and the propagation of electromagnetic radiation as the movement of planar wavefronts of a specific wavelength through space. The propagation vector is linear in a homogeneous medium like air or glass or in a vacuum. The relatively narrow spectrum of photon energies (and corresponding frequencies) we experience as light is capable of exciting the visual pigments in the rod and cone cells in the retina and corresponds to wavelengths ranging from 400 nm (violet) to 750 nm (red). As shown in Figure 2.4, we depict light in various ways depending on which features we wish to emphasize:

- As *quanta* (photons) of electromagnetic radiation, where photons are detected as individual quanta of energy (as photoelectrons) on the surfaces of quantitative measuring devices, such as charge-coupled device (CCD) cameras or photomultiplier tubes.
- As *waves*, where the propagation of a photon is depicted graphically as a pair of electric (E) and magnetic (B) fields that oscillate in phase and in two mutually perpendicular planes as functions of a sine wave. The vectors representing these fields vibrate in two planes that are both perpendicular to each other and perpendicular to the direction of propagation. For convenience, it is common to show only the wave's electric field vector (E-vector) in graphs and diagrams and not specify it as such. When shown as a sine wave on a plot with x and y coordinates, the amplitude of a wave on the y-axis represents the strength of the electric or magnetic field, whereas the x-axis depicts the time or distance of travel of the wave or its phase relative to some other reference wave. At any given time or distance, the E and B field vectors are equal in amplitude and phase. Looking

down the *x*-axis (the propagation axis), the plane of the E vector may vibrate in any orientation through 360° of rotation about the axis. The angular tilt of the E vector along its propagation axis and relative to some fixed reference is called the *azimuthal angle* of orientation. Commonly, the sine waves seen in drawings refer to the average amplitude and phase of a beam of light (a light train consisting of a stream of photons), not to the properties of a single electromagnetic wave.

- As *vectors*, where the vector length represents the amplitude, and the vector angle represents the advance or retardation of the wave relative to an imaginary reference. The vector angle is defined with respect to a perpendicular drawn through the focus of a circle, where 360° of rotation corresponds to one wavelength (2π radians).
- As *rays or beams*, where the linear path of a ray (a light train or stream of photons) in a homogeneous medium is shown as a straight line. This representation is commonly used in geometrical optics and ray tracing to show the pathways of rays passing through lenses of an imaging system.

THE QUALITY OF LIGHT

As an analytic probe used in light microscopy, we also describe the kind or quality of light according to the degree of uniformity of rays comprising an illuminating beam (Fig. 2.5). The kinds of light most frequently referred to in this text include:

- *Monochromatic.* Waves having the same wavelength or vibrational frequency (the same color).
- *Polarized.* Waves whose E vectors vibrate in planes that are parallel to one another. The E vectors of rays of sunlight reflected off a sheet of glass are plane parallel and are said to be linearly polarized.
- *Coherent.* Waves of a given wavelength that maintain the same phase relationship while traveling through space (laser light is coherent, monochromatic, and polarized).
- *Collimated.* Waves having coaxial paths of propagation through space—that is, without convergence or divergence, but not necessarily having the same wavelength, phase, or state of polarization. The surface wavefront at any point along a cross-section of a beam of collimated light is planar and perpendicular to the axis of propagation.

Light interacts with matter in a variety of ways. Light incident on an object might be absorbed, transmitted, reflected, or diffracted, and such objects are said to be opaque, transparent, reflective, or scattering. Light may be absorbed and then re-emitted as visible light or as heat, or it may be transformed into some other kind of energy, such as chemical energy. Objects or molecules that absorb light transiently and quickly re-emit it as longer wavelength light are described as being phosphorescent or fluorescent depending on the time required for re-emission. Absorbed light energy might also be reradiated slowly at long infrared wavelengths and may be perceived as heat. Light absorbed by cells may be damaging if the energy is sufficient to break covalent bonds within molecules or drive adverse chemical reactions, including those that form cytotoxic free radicals. Finally, a beam of light can be bent or deviated while passing

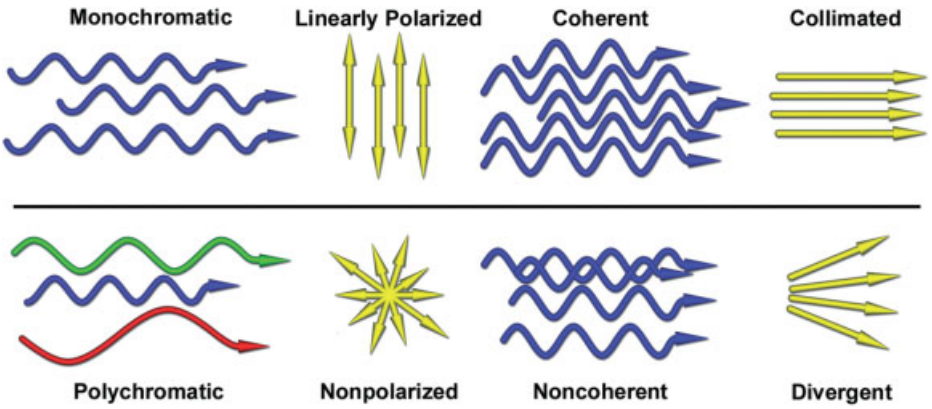

Figure 2.5
Eight waveforms depicting variations in the quality of light.

through a transparent object, such as a glass lens having a different refractive index (*refraction*), or may be bent uniformly around the edges of large opaque objects (*diffraction*), or even scattered by small particles and structures having dimensions similar to the wavelength of light itself (also known as diffraction). The diffraction of light by small structural elements in the specimen is the principal process governing image formation in the light microscope.

PROPERTIES OF LIGHT PERCEIVED BY THE EYE

The eye-brain system perceives differences in light intensity and wavelength (color) but does not see differences in the phase of light or its state of polarization. Thus, laser light, which is both coherent and polarized, cannot be distinguished from random light having the same wavelength (color). We will restrict our discussion here to the perception of light intensity, since the perception of color is treated separately in the following section.

The brightness of a light wave is described physically and optically in terms of the *amplitude* (A) of its E vector, as depicted in a graph of its sine function. Indeed, the amplitudes of sine waves are shown in many figures in the text. However, the nervous activity of photoreceptor cells in the retina is proportional to the light *intensity* (I), where intensity is defined as the rate of flow of light energy per unit area and per unit time across a detector surface. Amplitude (energy) and intensity (energy flux) are related such that the intensity of a wave is proportional to the square of its amplitude, where:

$$I \propto A^2.$$

For an object to be perceived, the light intensity corresponding to the object must be different from nearby flanking intensities and thereby exhibit contrast, where *contrast* (C) is defined as the ratio of intensities,

$$C = \Delta I / I_b,$$

ΔI is the difference in intensity between an object and its background, and I_b is the intensity of the background. If $I_{obj} \sim I_b$, as it is for many transparent microscope specimens, $C = 0$, and the object is invisible. More specifically, visibility requires that the object exceed a certain *contrast threshold*. In bright light, the contrast threshold required for visual detection may be as little as 2–5%, but should be many times that value for objects to be seen clearly. In dim lighting, the contrast threshold may be 200–300%, depending on the size of the object. The term *contrast* always refers to the ratio of two intensities and is a term commonly used throughout the text.

PHYSICAL BASIS FOR VISUAL PERCEPTION AND COLOR

As we will emphasize later, the eye sees differences in light intensity (contrast) and perceives different wavelengths as colors, but cannot discern differences in phase displacements between waves or detect differences in the state of polarization. The range of wavelengths perceived as color extends from 400 nm (violet) to 750 nm (red), while peak sensitivity in bright light occurs at 555 nm (yellow-green). The curves in Figure 2.6 show the response of the eye to light of different wavelengths for both dim light (night or rod vision) and bright light (day or cone vision) conditions. The eye itself is actually a *logarithmic* detector that allows us to see both bright and dim objects simultaneously in the same visual scene. Thus, the apparent difference in intensity between two objects I_1 and I_2 is perceived as the logarithm of the ratio of the intensities, that is, as $\log_{10}(I_1/I_2)$. It is interesting that this relationship is inherent to the scale used by Hipparchus (160–127 BC) to describe the magnitudes of stars in six steps with five equal intervals of brightness. Still using the scale today, we say that an intensity difference of 100 is covered by five steps of Hipparchus' stellar magnitude, such that

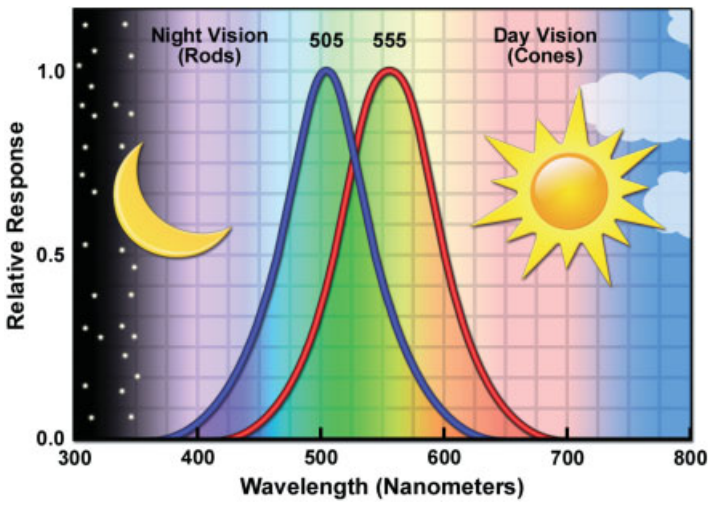

Figure 2.6

The spectral response of the eye in night and day vision. The two curves have been normalized to their peak sensitivity, which is designated 1.0; however, night (rod) vision is 40 times more sensitive than day (cone) vision. Rhodopsin contained in rod cells and color receptor pigments in cone cells have action spectra with different maxima and spectral ranges.

$2.512 \log_{10}100 = 5$. Thus, each step of the scale is 2.512 times as much as the preceding step, and $2.512^5 = 100$, demonstrating that what we perceive as equal steps in intensity is really the log of the ratio of intensities. The sensitivity of the eye in bright light conditions covers about three orders of magnitude within a field of view; however, if we allow time for physiological adaptation and consider both dim and bright lighting conditions, the sensitivity range of the eye is found to cover an incredible 10 orders of magnitude overall.

The shape and distribution of the light-sensitive rod and cone cells in the retina are adapted for maximum sensitivity and resolution in accordance with the physical parameters of light and the optics of the eye-lens system. Namely, the outer segments of cone cells, the cells responsible for color perception in the fovea, are packed together in the plane of the retina with an intercellular spacing of 1.0–1.5 μm, about one-half the radius of the minimum spot diameter (3 μm) of a focused point of light on the retina. The small 1.5-μm cone cell diameter allows the eye to resolve structural details down to the theoretical limit calculated for the eye–lens system. For an object held 25 cm in front of the eye, this corresponds to spacings of ~0.1 mm. It appears nature has allowed the light receptor cells to utilize the physics of light and the principles of lens optics as efficiently as possible!

Rod cell photoreceptors comprise 95% of the photoreceptors in the retina and are active in dim light but provide no color sense. Examine Figure 2.1 showing the structure of the eye and Figure 2.7 showing the distribution of rod cells in the retina. Rods contain the light-sensitive protein, *rhodopsin*, not the photovisual pigments required for color vision, and the dim light vision they provide is called *scotopic vision*. Rhodopsin, a photosensitive protein, is conjugated to a chromophore, 11-*cis*-retinal, a carotenoid that photoisomerizes from a *cis* to *trans* state upon stimulation and is responsible for electrical activity of the rod cell membranes. The peak sensitivity of the rod photoreceptor cells (510 nm) is in the blue-green region of the visual spectrum. Rod cell vision is approximately 40 times more sensitive to stimulation by light than the cone cell

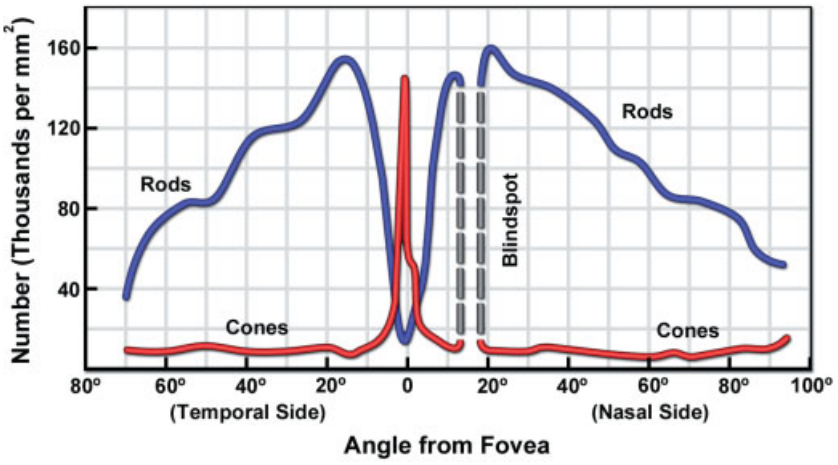

Figure 2.7

Distribution of rod and cone cells in the retina. The number of cells per mm^2 is plotted versus the angle from the fovea as seen from the lens. The fovea is distinct in having a paucity of rods and an abundance of cones. The blind spot lacks photoreceptor cells.

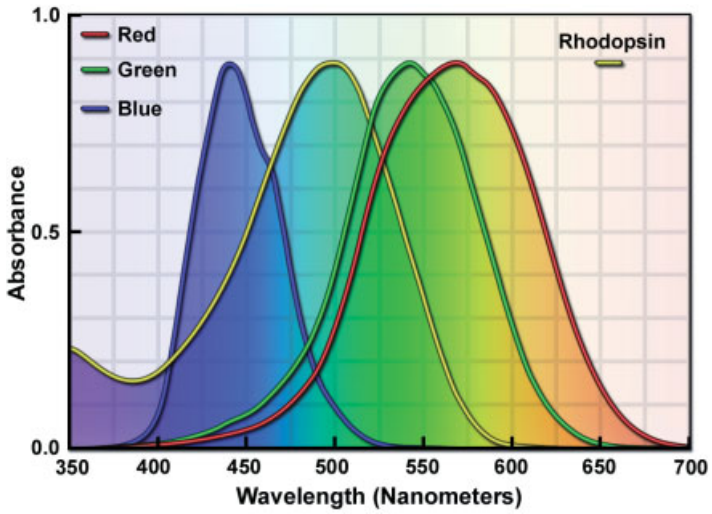

Figure 2.8

Absorption difference spectra of the four human visual pigments. The pigments show maxima in the red, green, and blue regions of the visual spectrum. The values are close to those measured for rod and cone cells *in vivo* and confirm Maxwell's theory for RGB-based color vision over a century ago.

receptors that mediate color vision. Bright light rapidly bleaches rhodopsin, causing temporary blindness in dim lighting conditions, but rhodopsin isomerizes gradually over a 20–30-minute period, after which rod receptor function is largely restored. Full recovery may require several hours or even days—ask any visual astronomer or microscopist! To avoid photobleaching your rhodopsin pigments and to maintain high visual sensitivity for dim specimens (common with polarized light or fluorescence optics), you should make observations in a darkened room. Red light illumination in the otherwise darkened microscope room is also commonly employed, because red wavelengths bleach the rhodopsin inefficiently (see Fig. 2.8 for differences in absorption spectra of visual pigments), yet allow you to see to operate equipment and take notes.

Cone cell photoreceptors comprise only 5% of the retinal photoreceptor cells and are contained nearly exclusively in the small central *fovea* of the retina, a 0.5-mm diameter spot that is responsible for color perception and visual acuity. Vision dominated by the function of cones under bright light conditions is called *photopic vision*. Cone cells contain red-, green-, or blue-sensitive pigment proteins that are also conjugated to 11-cis-retinal. The color photovisual pigments are highly homologous to each other and share about 40% amino acid sequence homology with rod cell rhodopsin (Nathans, 1984). Absorption difference spectra for purified rhodopsin and the three color pigments are shown in Figure 2.8.

ADDITION AND SUBTRACTION COLORS

As discussed in this section, color can be described as the addition or subtraction of specific wavelengths of light. Light is perceived as white when all three cone cell types (red, green, and blue) are stimulated equally as occurs when viewing a nonabsorbing

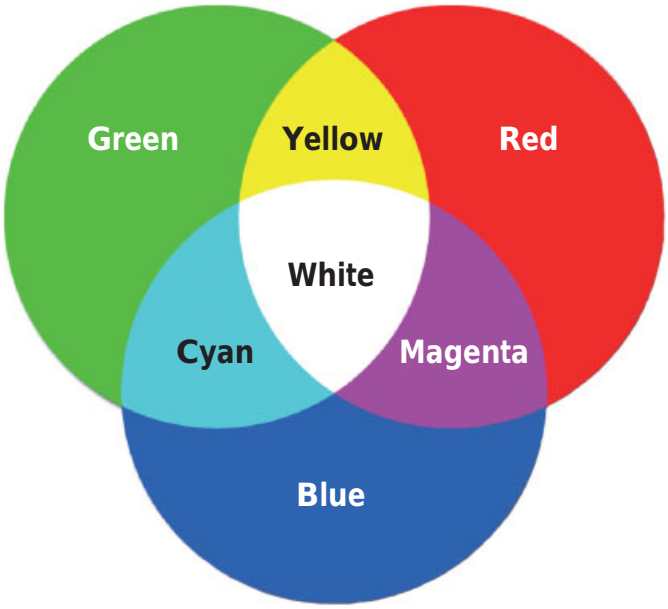

Figure 2.9
Addition colors of the red–green–blue tricolor system. This color display can be produced by projecting the light from RGB color filters with three separate projectors on a screen as described in the text.

white sheet of paper in sunlight. It was found over a century ago by James Clerk Maxwell (1831–1879) that color vision can be approximated by a simple tristimulus system involving red, green, and blue color stimulation. By varying the relative intensities of the three colors, all of the colors of the visual spectrum can be created, ranging from violet to red. *Addition colors* are created by combining different color wavelengths. A fine example of mixing wavelengths to create positive colors can be made using three focusable projector lamps, each equipped with monochromatic red, green, and blue cellophane filters (the kind used for RGB color analysis) from a scientific supply house.

Three color disks can be projected on a screen and made to overlap as shown in Figure 2.9. Try it and experience how mixing red and green gives yellow. *Subtraction colors*, in contrast, are generated by the subtraction (absorption) of light of a specific wavelength from white light composed of a mixture of wavelengths. This is the principle involved in determining the colors of paints and pigments. A pigment that looks red, for example, absorbs both blue and green wavelengths, but reflects red, so it is red by default. Thus, colors observed in pigments are generated by a process of subtraction. To appreciate this point, it is informative to examine colored objects (paints and pigments) with a handheld *spectroscope* under bright white light illumination. It is fascinating that yellow, cyan-blue, and magenta pigments are composed, respectively, of equal mixtures of red and green, green and blue, and blue and red wavelengths.

Thus, perception of the color yellow can arise in two ways: (1) by simultaneous stimulation of the red and green cone cells by a monochromatic yellow (580 nm) light source—the red and green photovisual pigments exhibit broad excitation spectra that

overlap significantly in the 580-nm band region and are both stimulated almost equally; or (2) by stimulating the red and green cones separately with a mixture of distinct red and green wavelengths, each wavelength selectively stimulating red and green cone cells in the retina. In either case, the color yellow is defined as the simultaneous stimulation of both red and green visual pigments. Perception of other colors requires stimulation of one, two, or all three cone cell types to varying degrees. The mixing of different colored paints to produce new colors, which is our common experience in producing colors, is actually a subtractive process. Consider why mixing yellow and blue paints produces a green color: yellow pigment (reflects red and green but absorbs blue) and blue pigment (reflects blue and green but absorbs red) gives green because green is the only wavelength that is reflected and not absorbed by the mixture of yellow and blue pigments.

Thus, combining blue and yellow wavelengths of light gives white, but mixing blue and yellow pigments gives green! Removal of a specific wavelength from the visual spectrum is also the mechanism for producing interference colors, and is discussed in Chapter 9. A useful overview on the perception of color when viewing natural phenomena is given by Minnaert (1954).

Exercise: Complementary Colors

A complementary color is a color that gives white light when mixed with its complement. Thus, yellow and cyan-blue are complementary colors, as are the color-pairs green with magenta and red with cyan. Our perception of complementary colors is due to the red, green, and blue photovisual pigments in the cone cells of the retina. Note that mixing wavelengths of different colors is distinct from mixing colored pigments.

Combining red, green, and blue light. To experience the relationships among complementary colors, prepare three light sources with red, blue, and green color filters and project images of three disks of red, green, and blue color on a projection screen. Move the disk images to partially overlap the colors so that it is possible to see that red plus green gives yellow, red plus blue gives magenta, and blue plus green gives cyan. The overlap of red, green, and blue gives white. Thus, when all three color types of cone cells in the retina are saturated, we see white light.

Mixing colored pigments. As is known, mixing yellow and blue pigments gives green. The reason for this is that blue and yellow pigments reflect green light; all other wavelengths are absorbed by the blue and yellow dyes in the mixture. To demonstrate this, prepare two beakers with 500-mL water and add eight drops of blue and yellow food coloring separately to each beaker. Display the beakers on a light box. The generation of green by mixing the yellow and blue pigments (a subtractive process) is different from the mixing of blue and yellow light, which gives white light (an additive process), as was demonstrated above.

Removing colors from a white light source. The relationship between complementary color and subtraction colors can be demonstrated using a bright white

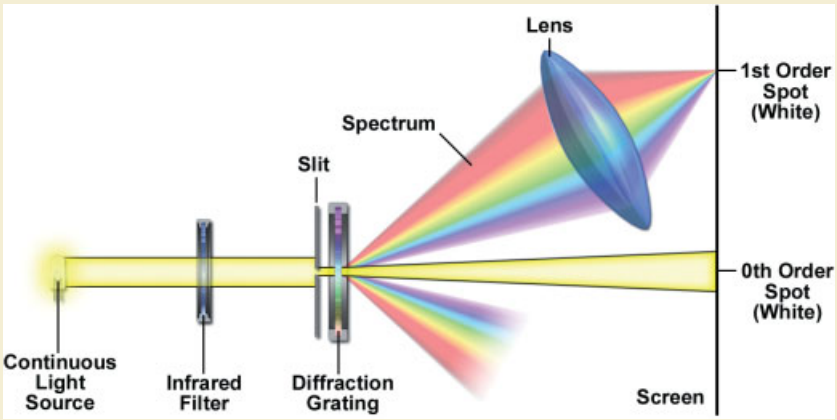

Figure 2.10
Optical bench setup for demonstrating complementary colors.

light source, a slit, a diffraction grating and a large diameter magnifying glass to form the image of the slit on a projection screen. Set up the optical bench apparatus with a bright xenon light source, a 1-mm wide slit made from razor blades, an IR blocking filter, and a holographic diffraction grating as described in Figure 2.10. Intercept the dispersed color spectrum with a white card and examine the spectral colors. With the help of a partner, examine the colors on the card with the spectroscope. Scan the spectroscope back and forth across the spectrum and confirm that each color is pure, monochromatic, and located in the spectrum according to its wavelength. Next, intercept the spectrum between the grating and the projection screen with a 4–6-in diameter magnifying glass and focus the image of the slit on a projection screen. Notice that the color of the focused image of the slit is white. It is clear that the individual spectral colors have been recombined to give white light. Next, insert an opaque 1-cm wide white paper strip into the light path to remove a band of wavelengths, such as red and orange from the spectrum. Note the corresponding color of the slit in the image plane. The color of the slit on the screen and the color of the blocked light are called complementary colors. What are the complementary colors for red, green, and blue?

Examine the colors of afterimages. Another way to examine complementary colors is to produce "after images" on the retina. Stare at a collection of large, brightly colored objects for 30–60 seconds in a brightly illuminated area. Do not let your eyes wander, but focus steadily on a central spot in the visual field. Then shift your vision to stare at a blank white sheet of paper or brightly illuminated white wall. Do you see an afterimage composed of complementary colors of the objects? The complementary colors are seen because the cones stimulated by certain colors become depleted and temporarily exhausted after prolonged viewing, so unstimulated cones in the same area of the retina provide the principal stimulus when you look at a white page. Cyan-blue, magenta-red, and yellow are the three complementary colors to red, green, and blue.


670
530
580
480
405
430
INTENSITY 480
58.36
ON/Off
Dim
Min
1
2
3
4
5
6

CHAPTER
3

ILLUMINATORS, FILTERS, AND THE ISOLATION OF SPECIFIC WAVELENGTHS

OVERVIEW

To obtain optimal imaging performance in the light microscope, the specimen must be properly illuminated. This requires proper selection of wavelength and intensity and correct alignment and focus of the lamp. The first objective is met by matching the particular application to the proper combination of illuminator and filters. Since research microscopes may be equipped with a variety of different lamps, including quartz halogen lamps and other tungsten filament lamps, and mercury, xenon, and metal halide arc lamps, we discuss the energy and spectral output of various illuminators. Filters that adjust light intensity and provide wavelengths of a particular color are also discussed. For example, if the microscope is equipped with a constant voltage power supply, the intensity must be controlled using neutral density filters; similarly, colored glass filters and interference filters are used to isolate specific color bandwidths. It is the combination of illuminator and filters that determines the quality of light directed to the condenser for illuminating the specimen. While all forms of light microscopy require selecting illuminators and filters, knowledge of their action and function becomes especially important in fluorescence and confocal fluorescence microscopy. We close the chapter by discussing how illuminators and filters must be carefully considered when examining living cells. An excellent review of noncoherent light sources for light microscopy is provided by Nolte et al. (2006).

ILLUMINATORS AND THEIR SPECTRA

Successful imaging requires delivery to the condenser of a focused beam of light that is bright, evenly distributed, constant in amplitude, and versatile with respect to the


LED illuminator with six LED modules and folded optical pathway.

Fundamentals of Light Microscopy and Electronic Imaging, Second Edition.
Douglas B. Murphy and Michael W. Davidson.

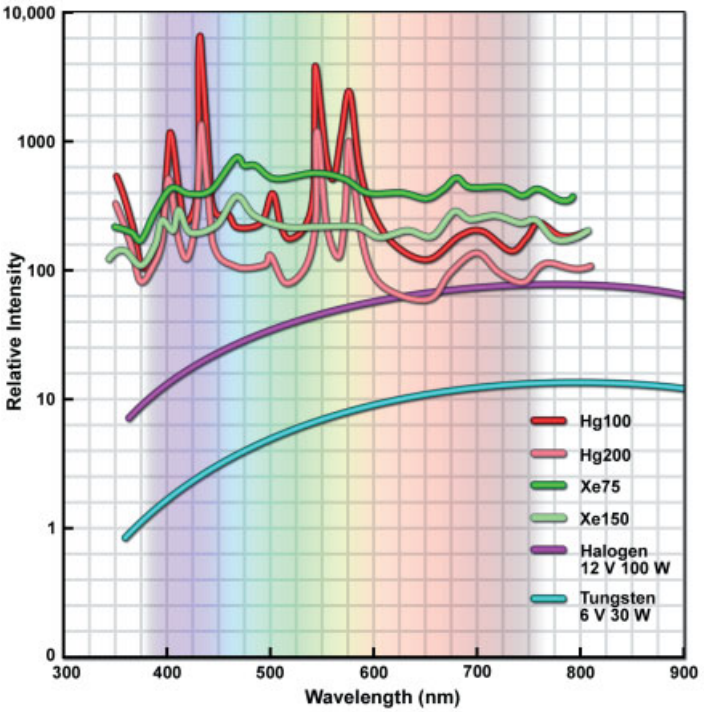

Figure 3.1

The spectra of various illuminators. Tungsten filament lamps give continuous emission, but their output is reduced at shorter wavelengths; mercury and xenon arc lamps are brighter, although mercury contains prominent emission lines in the visible range. Notice that over much of its range, the intensity of a 75-W xenon bulb (XBO) is several times greater than that of a 100-W mercury lamp (HBO). Although higher wattage arc lamps have a greater total output, the distance between their electrodes is greater, so that light intensity in the arc is more evenly distributed, but dimmer.

range of wavelengths, convenience, and cost. Alignment and focus of the illuminator are therefore essential and are the first steps in adjusting the illumination pathway in the microscope. A number of incandescent filament lamps and arc lamps are available to meet the needs of various applications. The spectra of the principal lamps used in microscopy are shown in Figures 3.1 and 3.2 and are described here.

Incandescent lamps with tungsten wire filaments and inert argon gas are frequently used for brightfield and phase contrast optics and are bright enough for certain applications requiring polarized light. Tungsten and quartz halogen lamps are convenient and inexpensive, easy to replace, and provide bright, even illumination when used together with a ground glass filter, hence their popularity in nearly all forms of light microscopy. These lamps produce a continuous spectrum of light across the visual range, with peak output occurring in the red and infrared (IR) range, and blue and ultraviolet (UV) output being the weakest. Excitation of the filament is regulated by a continuously variable power supply. As voltage and excitation are increased, brightness increases, and the spectrum shifts to increasingly higher-energy photons with shorter wavelengths. Therefore, color balance of the light from an incandescent lamp varies depending on the voltage applied to the lamp. When producing color micrographs, a specific voltage is selected in order to obtain a consistent and predictable spectrum of wavelengths.

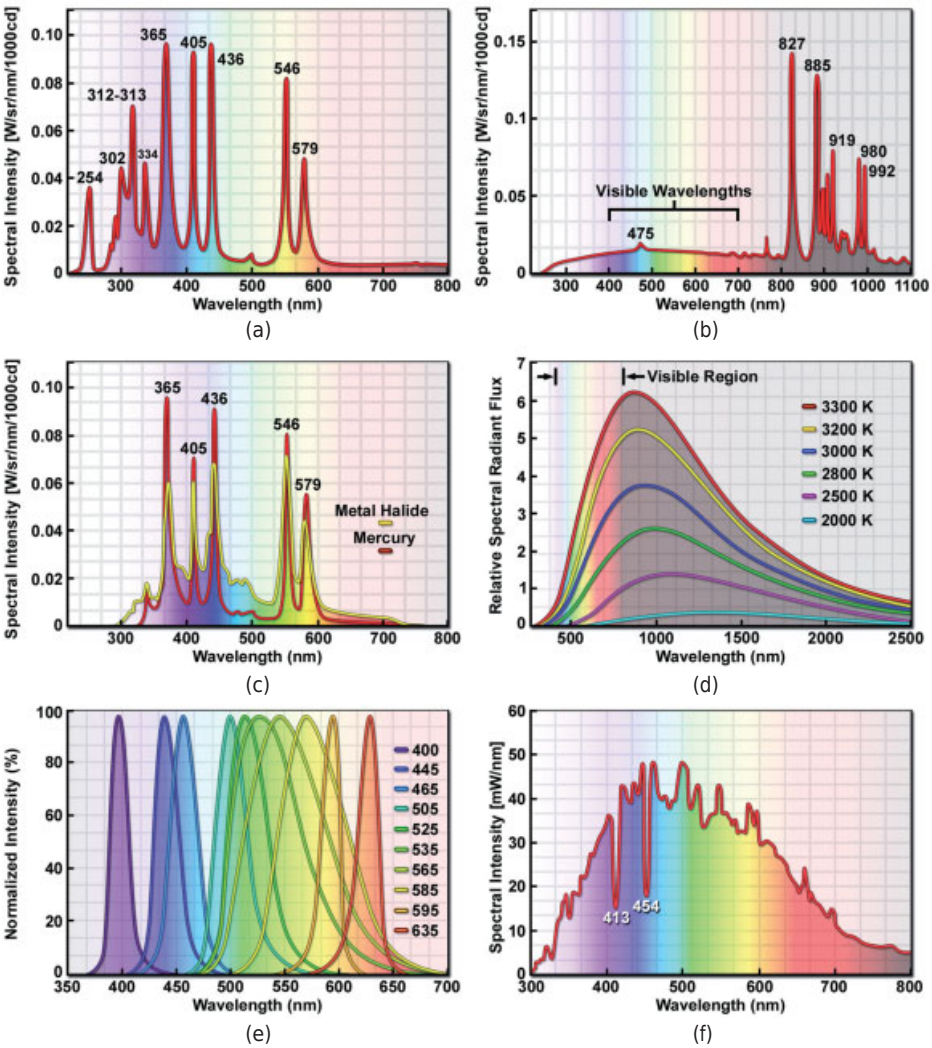

Figure 3.2

Detailed spectra of microscope lamps. (a) Mercury arc lamp with bright emission lines at 365, 405, 436, 546, and 579 nm. Significant emission occurs in the UV (below 400 nm) and IR portions of the spectrum (not shown). (b) Xenon arc lamp showing peaks in the infrared. (c) Metal halide arc lamp with emission lines similar to the mercury arc lamp. (d) Quartz halogen tungsten filament lamp. Much of the radiation is in the infrared range. (e) Emission spectra of common LEDs used in microscopy. Note the spectra of lamps emitting in the 535- to 585-nm region are broadened when compared to others. (f) LiFi™ plasma lamp spectrum with reabsorption peaks at 413 and 454 nm.

Special tungsten film and photographic filters are available to correct for the red-rich spectral output of these lamps. Readers can find more information on tungsten-based lamps in a comprehensive article published by OSRAM (2000).

Ion arc lamps are 10–100 times brighter than incandescent lamps and can provide brilliant monochromatic illumination when combined with an appropriate filter, but the increase in brightness comes with some inconveniences in mechanical alignment,

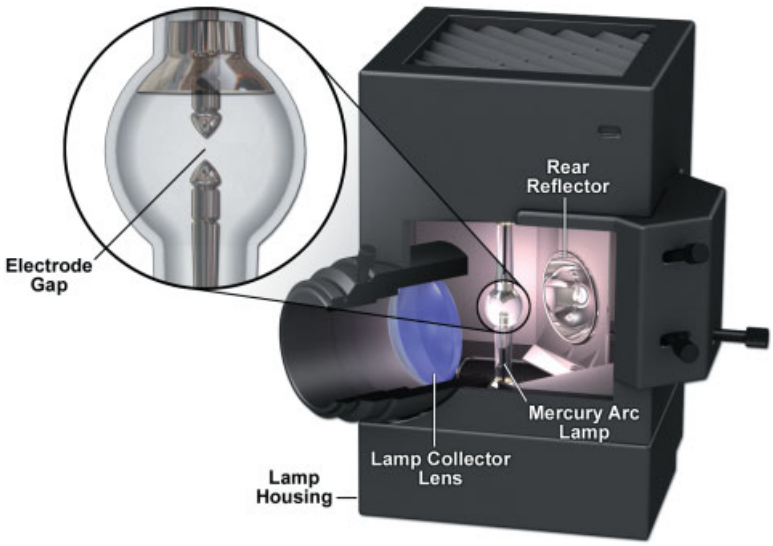

Figure 3.3

Arc lamp and illuminator housing. The bulb or lamp (also called a burner) is oriented vertically and contains a rear reflector to increase the output efficiency of the illuminator. The gap between the two electrodes contains a bright ionized plasma discharge. The collector lens produces a magnified image of the arc that fills the rear aperture of the objective. Uniform coverage of the objective rear aperture is required for optimal resolution and uniform illumination of the specimen.

shorter lifetime, and higher cost. Two types are commonly used: the 75-W xenon and 100-W mercury arc lamps (Fig. 3.3). Both lamps produce continuous spectra across the entire visible range from 400 to 750 nm and extending into the UV and IR. In fact, only about a fifth of the output of these arc lamps is in the visible portion of the spectrum, the remainder being in the UV and IR, so special blocking filters must be used when examining living cells, which are sensitive to UV and IR radiation. More information on arc-discharge lamps is available from Nakar et al. (2008), OSRAM (1999), and Thomson and Hageage (1975).

Arc lamps tend to flicker due to subtle variations in power. This can be annoying, especially during time-lapse recording, but stabilized power supplies are now available that minimize this problem. You should also avoid turning the lamp on and off frequently, as this poses a risk to nearby electronic equipment (if shielding is inadequate) and shortens the life of the bulb. When turning an arc lamp on or off, make it a practice to wait at least 30 minutes before reversing the action. If there is a 30- to 60-minute pause in the use of the microscope, it is better to leave the lamp on than to turn it off and reignite it again. There are, however, new lamp designs that use a variable transformer to control light intensity. As the bulb is turned down, a heating mechanism keeps the lamp hot so that brightness increases immediately when the power is turned up again. The lifetime of mercury and xenon lamps is generally rated at 200–300 hours; however, the UV output of a mercury lamp weakens (sometimes considerably) with prolonged use, since metal vapors from the electrodes become deposited on the glass envelope. In addition, the arc becomes unstable and begins to flicker. Although arc lamps are expensive, the actual cost works out to be about 50 cents per hour, so it is advisable to replace them after their nominal lifetime has expired even though they are still working.

The *mercury arc lamp* is distinct in emitting several prominent emission lines, some of which are up to 100 times brighter than the continuous background: 254 (far UV), 365 (near UV), 405 (violet), 436 (deep blue), 546 (yellow-green), 578, 579 (yellow doublet band), plus several lines in the IR (Fig. 3.2a). The 546-nm green line of the mercury arc lamp is a universal reference for calibrating wavelengths in a number of optical devices and is a favorite among biologists for examining living cells. UV emission accounts for about half of the output of the mercury lamp, so care must be taken to protect the eyes and living cells that are illuminated by it. When changing and aligning a new lamp, avoid staring at the unattenuated beam; when examining live cells, use a green bandpass filter plus a UV-blocking filter, such as a Schott GG420 glass filter. Since mercury lamps also emit in IR, heat-cut filters are desirable to block these wavelengths as well.

The spectrum of the *xenon arc lamp* is largely continuous and lacks prominent emission lines. Its advantage is bright, uniform output across the entire range of visual wavelengths (Fig. 3.2b). In blue-green and red wavelengths, it is significantly brighter than a 100-W mercury lamp, making it advantageous for certain applications in fluorescence microscopy. Since about half of the light emitted from a xenon lamp is in the IR, special IR-blocking filters, such as a Schott BG38 or BG39 glass filter and/or an IR-reflecting mirror, are used to attenuate and block these wavelengths and protect cells from excess heat. The detectors of electronic cameras, particularly those of CCD cameras, are also particularly sensitive to IR light, which can fog the image. Although the intensity of a 75-W xenon lamp is high, the distance between the lamp electrodes is small—only 0.75 mm—which can make it difficult to obtain an even distribution of the light across the front aperture of the condenser and therefore across the specimen in the object plane.

Metal halide lamps produce a spectrum with emission lines similar to mercury (Fig. 3.2c). They are popular because they are bright (150–250 W), have a long bulb life (2000 hours), and feature a large electrode gap (5 mm) that illuminates the specimen more homogeneously. They also exhibit a much higher level of continuous background illumination in between the emission peaks, which can make this lamp more suitable than mercury for exciting dyes such as fluorescein and green fluorescent protein (GFP). Unlike xenon and mercury arc lamps, the metal halide lamps used in microscopy are equipped with elliptical reflectors in which the bulb is embedded at the factory during manufacture. Metal halide lamps are housed in external units that are coupled to the microscope using a liquid light guide and a collimating lens system that spreads the illumination to fill the objective rear aperture. Liquid light guides serve to scramble or mix the light to decrease spatial and temporal coherence. Several companies now make metal halide illuminators. A disadvantage is the relatively high cost of both illuminator power supply and bulb.

LED light sources. Light-emitting diodes are semiconductor junctions that emit photons over a relatively narrow 20–50-nm bandwidth in the presence of an applied current (Fig. 3.2e). The light is distinct from the coherent, 1-nm bandwidth light of a laser. LEDs are becoming popular in microscopy because they do not produce heat, do not produce unwanted flanking wavelengths that must be removed by clean-up filters, last thousands of hours, produce narrowband spectra that remain true with ageing, and can be turned on and off rapidly, as described by Beacher (2008) and Albeanu et al. (2008).

LiFi™ is the trade name for a new continuous spectrum light source that is emerging as a potentially useful illumination strategy for microscopy (Fig. 3.2f). The lamp contains metal halide ions and a Noble gas sealed in a tiny quartz tube that is excited using high energy radio frequency waves rather than electrodes, as discussed by Wharmby (1997). The output is very stable, and the lamps feature a lifetime ranging up to 20,000 hours. Commercial units are available that are coupled to the microscope using a liquid light guide.

A Light-Emitting Diode Illuminator

Light-emitting diode (LED) illuminators represent a new frontier in microscope imaging. Because LEDs in the cyan and blue spectral regions emit a 20-nm wide spectral bandwidth, do not contain unwanted UV or IR radiation, are cool and small, can be turned on or off in under a millisecond, and are controlled by inexpensive power supplies, they have many desirable features lacking in arc lamps. One can fit a fluorescence microscope with LED light sources to provide UV, visible, and near-IR wavelengths for optimum illumination of fluorescent labels. The Zeiss Colibri illuminator illustrated in Figure 3.4 holds up to four swappable LED modules and three dichromatic mirrors that allow the investigator to add a new wavelength to the illumination system within just a few minutes. At 10–50 mW, LEDs now have sufficient power for fluorescence excitation in a microscope, including the examination of fixed cells and tissues, as well as live-cell imaging coupled to Förster resonance energy transfer (FRET) and fluorescence lifetime microscopy (FLIM) techniques. For these kinds of experiments the investigator can change between wavelengths within fractions of a millisecond, all under simple software control. Given the advantages of LEDs for imaging and the development of LEDs with ever increasing power, it is likely that they will become a popular device for microscope illumination.

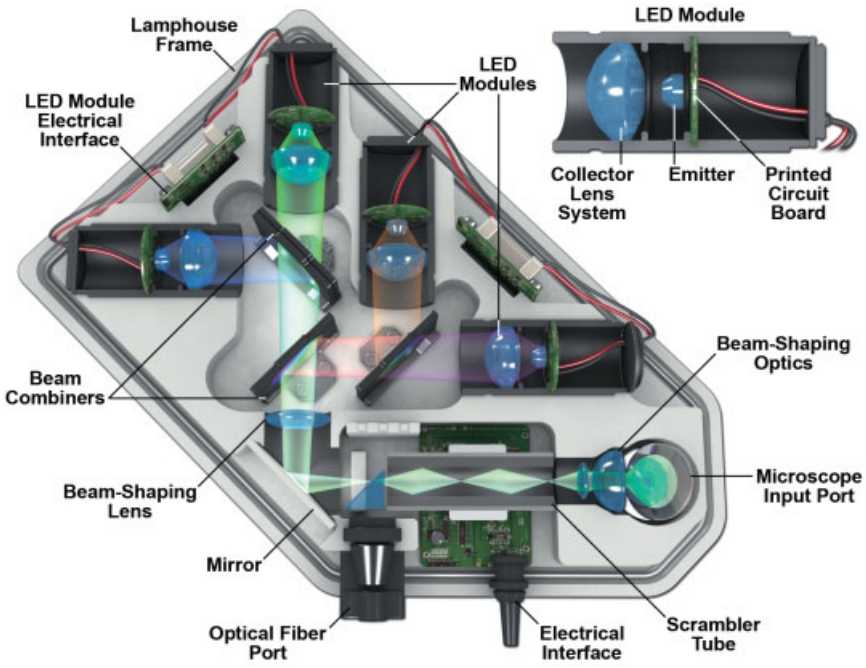

Figure 3.4
Example of an LED illuminator.

ILLUMINATOR ALIGNMENT AND BULB REPLACEMENT

Microscope illuminators consist of a lamp housing with a lamp and concave reflector, a focusable collector lens, an electrical socket for holding the bulb, and an external power supply. The socket and power cord, in particular, deserve attention. Oxidized metal surfaces of the socket electrodes and the copper conducting wire in an arc lamp should be cleaned with an emery cloth each time the lamp is changed to assure good electrical contact. The socket's power cord should never be crimped (as occurs when the illuminator is shoved up against a wall), as this action loosens wires, which can lead to inconvenient and expensive repair. The bulb, rear reflector, and front collector lens should be kept clean of all dirt, lint, and finger oils. At the time of changing a bulb and after the collector lens and metal housing have been removed, move the illuminator's adjustment screws with a screwdriver to observe their effect on the location of the bulb and the reflector. Some arc lamp housings only contain adjustment screws for the rear reflector, whereas others contain additional screws for adjusting the bulb itself. Arc lamp illuminators should be maintained in an upright position during use to preserve the life of the bulb. *Never ignite an arc lamp when it is outside its protective metal housing!*

Demonstration: Spectra of Common Light Sources

Please note: Never look directly at unattenuated mercury or xenon beams, because they are, respectively, extremely UV and IR rich and potentially damaging to the eye!

It is useful to become familiar with the spectra of common illuminators by indirect inspection with a spectroscope or a diffraction grating. There are several ways to do this:

- For display and discussion in a group, set up the I-beam/optical bench and project the spectra of illuminators on a screen using a diffraction grating, as shown in Figure 2.10.
- For individual study, wrap a piece of aluminum foil containing a slit aperture over the mouth of the illuminator and examine the slit at a distance of several feet with a handheld diffraction grating held close to the eye. A transparent holographic grating works best. To make a slit, cut a 1-cm long slit in the foil using a razor blade, while holding the foil placed against a sheet of stiff cardboard.
- An inexpensive, handheld spectroscope based on a sine-wave (holographic) diffraction grating is available from Learning Technologies, Cambridge, Massachusetts. Direct the unfiltered beam of the illuminator onto a white card or projection screen positioned several feet away and follow the instructions for using the spectroscope. The advantage of the spectroscope is that it permits one to determine the wavelengths of colors and emission lines from a built-in wavelength scale. You should perform these observations in a darkened room.

Examine the spectrum of a tungsten lamp or quartz halogen lamp first. The continuous smooth nature of the spectrum and the relative falloff in brightness at the blue end of the spectrum are characteristic. Examine the spectrum with the power supply adjusted at the minimum and maximum permissible settings to see the shift in the peak spectral output. As power increases, the intensity of shorter bluer wavelengths increases. (The peak emission wavelength in the IR also decreases, but this cannot be seen visually.)

Next, examine the spectrum of the xenon arc and notice the uniform intensity across the entire visible range. Careful inspection will show that the spectrum is not perfectly smooth, but rather has weak emission lines in the visible range near 470 nm (blue) and also at the red end of the spectrum near 680 nm. Fifty percent of the output of this lamp is in the IR, where prominent, though invisible, emission lines occur at >800 nm.

The spectrum of the mercury arc consists of several prominent emission lines (365, 406, 436, 546, and 578 nm) superimposed on a continuous background. Half of the output of this lamp is in the UV, with one of the most prominent (but invisible) emission lines being located at 365 nm. This wavelength is commonly used for photoactivation of caged fluorescent compounds, stimulation of UV-excitable fluorescent dyes, and conversion of colchicine to its photoisomer, lumicolchicine. This line and the 405-nm violet line can be visualized using the optical bench setup by holding a piece of fluorescent white paper in the proper location in the spectrum in a darkened room. A suitable piece of paper can be found using a handheld near-UV black light to select for sheets that exhibit brilliant bluish white fluorescence due to the presence of phenolic compounds in the paper. The 405-nm violet line and the 365-nm near-UV line suddenly become visible when the white card is inserted into the blue end of the spectrum.

Finally, examine the spectrum of an LED lamp and a laser (such as a green or red laser pointer), and compare the narrow widths of their spectra. Illumination from these light sources covers just a narrow band of the visible spectrum.

After a bulb is changed and aligned, the image of the arc or filament should be focused in the front aperture plane of the condenser using the illuminator's collector lens focusing dial, which is located on the illuminator housing. On some microscopes, it may be possible to place a lens tissue across the front of the condenser aperture or to stop down the condenser diaphragm in order to see the image of the focused filament. Alternatively, the focused image of the filament or arc may be viewed at its conjugate location at the objective rear aperture using an eyepiece telescope or Bertrand lens. In this case, the light should be turned down to a minimum or attenuated with appropriate neutral density filters. To see the image clearly, it may be necessary to remove a ground glass diffusing screen, whose function is to remove the pattern of the filament from the image of the specimen.

Alignment of a new bulb is especially critical for mercury or xenon arc lamps, such as those mounted in epi-illuminators used for fluorescence microscopy, because the arc in the lamp is small (~1 mm), and the arc's image at the condenser aperture

must be positioned on the optical axis of the microscope. Light from an arc lamp can be safely examined after attenuation with a fluorescence filter set plus additional neutral density filters. It is easier on the eye to examine the green excitation light provided by a rhodamine filter set. A similar procedure can be applied for arc lamps used in trans-illumination mode.

Demonstration: Aligning a 100-W Mercury Arc Lamp in an Epi-Illuminator

- Always turn off the power supply and allow the lamp to cool completely before changing a failed bulb. Since arc lamps are under moderately high pressure when they are hot, an applied mechanical force can cause them to explode, and therefore safety goggles should be worn during lamp replacement. After replacing a bulb, secure the lamp socket to the lamp housing and fasten the housing to the microscope before reigniting the lamp.
- Place neutral density filters in the light path sufficient to block ~97% of the light, and place a rhodamine fluorescence filter cube into position so that the 546-nm green line of the arc is reflected onto the specimen plane. Insert additional UV- and IR-blocking filters into the path to protect the eyes.
- Tape a white card or paper on the microscope stage, focus an objective until you see an intense, focused dot on the card, and mark the location with a pen. The dot defines the position of the optical axis of the microscope.
- Without disturbing the card, rotate the objective turret to an empty position and observe an intense, extended spot of light on the card. Focus the collector lens of the lamp until the bright primary image of the arc is sharply defined. If the arc's image does not coincide with the dot, you will need to adjust the bulb using the adjustment screws on the illuminator housing (Fig. 3.5).
- There should also be a dimmer reflection image of the arc, which is focused and aligned using the reflector's adjustment screws on the lamp housing. Position the reflection image so that it is on top of or next to the primary image of the arc.

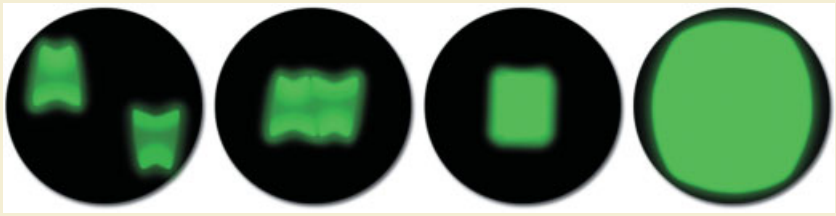

Figure 3.5
Alignment of an arc lamp. Direct image of an electrode arc and its reflection in a special observation window near the illuminator. (a)–(d): Adjustment screws are used to center and superimpose the two images.

- Slowly defocus the lamp collector lens and ascertain that the beam expands uniformly around the black dot on the card. This is an important test of alignment. If the arc's image does not expand symmetrically, you must make an additional round of adjustments. Sometimes, it helps to expand the image slightly with the collector lens before making additional adjustments.
- While looking in the microscope at a focused fluorescence specimen, adjust the collector lens of the illuminator until the image is bright and uniform from one edge of the field to the other and across all diameters of the field. At this position, the arc is focused on the objective's rear aperture. In epi-illumination, the objective functions as both a condenser and an objective.

For incandescent filament lamps, the procedure is easier. After remounting the bulb, turn on the power supply and examine the lamp filament in the microscope using a telescope eyepiece or Bertrand lens. Focus the telescope to view the edge of the condenser diaphragm at the front aperture of the condenser. In the absence of a diffuser screen, the filament should be sharply focused; if not, adjust the lamp's collector lens. Notice the pattern of vertical lines representing the filament. Center the image of the filament, and then center the image of reflection so that the vertical lines of the primary and reflection images are interdigitated (see Fig. 3.6). Some illuminators do not contain adjustable collector lenses for low-power lamps. If the filament image seems off-center, try remounting the bulb.

Note: For those using older arc lamps (prior to year 2000), it is very important to understand the potential hazard of turning on and off older arc lamps near functioning electronic equipment. These lamps should be turned on and allowed to stabilize for a

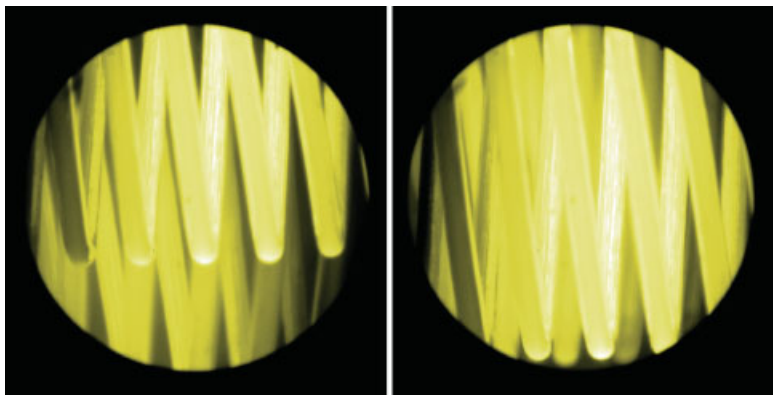

(a) (b)

Figure 3.6

Alignment of a filament lamp before (a) and after adjustment (b). In the absence of a diffuser screen, the image of the lamp can be seen in the rear aperture of the objective using an eyepiece telescope or Bertrand lens. The reflection image of the filament is adjusted to interdigitate with the filament loops seen in the direct image.

minute or two *before* turning on the other pieces of nearby electronic equipment. Although the power supply and cable are generally very well shielded, a momentary 20,000–50,000 V surge passing between the DC power supply and the arc lamp (or on some designs just within the lamp socket) generates magnetic fields that are strong enough to damage sensitive integrated circuits in nearby cameras, computers, and other electronic equipment. Upon turning the lamp off, the reverse procedure should be used.

FILTERS FOR ADJUSTING THE INTENSITY AND WAVELENGTH OF ILLUMINATION

Selecting and adjusting the lamp for a particular application are important, but the actual control of the wavelength and intensity of illumination in a microscope requires the use of filters, so it is important to understand the fundamentals of their action and performance. The microscopist needs to know how to interpret the transmission spectra of filters, select the best among several possible filters for a given application, and explain differences in image quality, fluorescence quality, and cell behavior obtained with different filter combinations. This is particularly true in fluorescence microscopy, where filters must match the excitation and emission requirements of fluorescent dyes. Fortunately, the task is manageable, and filtering light to select a band of wavelengths from the illuminating beam presents many challenges and rewards. For more information on filters for light microscopy, see Erdogan (2011) and Reichman (2000).

Neutral density filters regulate light intensity, whereas *colored glass filters* and *interference filters* are used to isolate specific colors or bands of wavelengths. There are two classes of filters that regulate the transmission wavelength: edge filters and bandpass filters (Fig. 3.7). Edge filters are classified as being either *longpass* (transmit

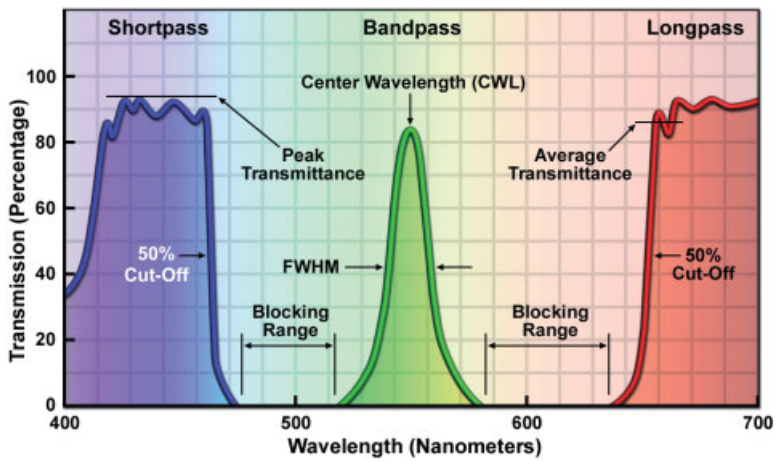

Figure 3.7

Filters for isolating the wavelength of illumination. Shortpass and longpass filters, sometimes called edge filters, block or transmit wavelengths at specific cut-off wavelengths. Bandpass filters exhibit broadband or short-band transmission centered on a particular band of wavelengths. Filter performance is defined by the central wavelength (CWL) and by the full width at half maximum (FWHM). Another term for FWHM is half-bandwidth (HBW). A bandpass filter can also be created from two overlapping shortpass and longpass filters.

long wavelengths, block short ones) or *shortpass* (transmit short wavelengths, block long ones), whereas bandpass filters transmit a band of wavelengths while blocking wavelengths above and below the specified range of transmission. Optical performance is defined in terms of the efficiency of transmission and blockage (% transmission), and by the steepness of the so-called cut-on and cut-off boundaries between adjacent domains of blocked and transmitted wavelengths. Edge filters are described by referring to the wavelength giving 50% of peak transmission; *bandpass* filters are described by citing the full width at half maximum (FWHM) and specifying the peak and central transmitted wavelengths. FWHM is the range of the transmitted band of wavelengths in nanometers and is measured as the distance between the edges of the bandpass peak where the transmission is 50% of its maximum value. For the high performance filters used in fluorescence microscopy, these boundaries are remarkably sharp, appearing on transmission spectra as nearly vertical lines.

In part, the resurgence of light microscopy as an analytic tool in research has been driven by the technologies used for depositing thin films of dielectric materials and metals on planar glass substrates. Companies now manufacture interference filters with transmission and blocking efficiencies approaching 100% and with bandwidths as narrow as 1 nm anywhere along the UV-visible-IR spectrum—a truly remarkable accomplishment. This achievement has stimulated development of new research applications involving laser-based illumination, new fluorescent dyes and molecules, and ratio imaging at multiple specific wavelengths.

Neutral Density Filters

Neutral density filters are used in microscopy to attenuate uniformly the intensity of light over the entire range of visible wavelengths. They are commonly employed in differential interference contrast (DIC), polarization, and fluorescence microscopy with high-intensity arc lamps that cannot be regulated with an adjustable power supply. In these circumstances, neutral density filters must be used. As discussed in Chapter 6, it is impermissible to reduce the intensity of illumination by closing down the condenser diaphragm, as this action affects resolution and contrast. A light-absorbing filter is the only solution.

Neutral density (ND) filters have a neutral gray color like smoked glass and are usually calibrated in units of *absorbance* or optical density (OD), where:

$$\mathrm{OD} = \log_{10}(1/T),$$

and T is the transmittance (intensity of transmitted light/intensity of incident light). Thus, a 0.1 OD neutral density filter gives 79% transmission and blocks 21% of the incident light. Other manufacturers indicate the transmittance directly. When stacking multiple ND filters, it is convenient to remember that the total optical density of the stack equals the sum of the individual filter optical densities.

ND filters are either absorbing or reflecting in design. Absorbing filters contain rare earth elements throughout the glass, so there is no reflective coating that can be scratched off, and their orientation in the beam is not critical. Reflecting ND filters contain an evaporated coating of metal on one of the surfaces, so care must be taken not to scratch them. These filters must be inserted into the beam with the reflective surface facing the light source. They can, however, be cheaper and thinner than absorbing filters, and are the filter of choice for use with lasers.

Colored Glass Filters

Colored glass filters are used for applications not requiring precise definition of transmitted wavelengths. They are commonly used to isolate a broad band of colors or as longpass filters to block short wavelengths and transmit long ones. Colored glass filters contain rare earth transition elements, or colloidal colorants, such as selenide or other substances to give reasonably sharp transmission-absorption transitions at a variety of wavelengths. Since colored glass filters work by absorbing quanta of nontransmitted wavelengths, they can be heat sensitive and subject to altered transmission properties or even breakage after prolonged use. However, as the absorbent atoms are contained throughout the glass and are not deposited on its surface, colored glass filters offer major advantages: They are less resistant to physical abrasion and chemical attack from agents contained in fingerprints and other sources, and their optical performance is not sensitive to the angle of incidence of incoming rays of light. Colored glass filters are also less expensive than interference filters and are generally more stable and long-lived.

Interference Filters

Interference filters often have steeper cut-in and cut-off transmission boundaries than colored glass filters and therefore are frequently encountered in fluorescence microscopy where sharply defined bandwidths are required. Interference filters are optically planar sheets of glass coated with dielectric substances in multiple layers, each $\lambda/2$ or $\lambda/4$ thick, which act by selectively reinforcing and blocking the transmission of specific wavelengths through constructive and destructive interference (Fig. 3.8). Bandpass filters transmit a limited range of wavelengths that experience reinforcement through constructive interference between transmitted and multiple reflected rays; wavelengths that do not reinforce each other destructively interfere and are eventually backreflected out of the filter.

Interference filters contain layers of *dielectric substances*, electrically nonconductive materials of specific refractive index, typically optically transparent metal salts such as zinc sulfide, sodium aluminum fluoride (cryolite), magnesium fluoride, and other substances. In some designs, semitransparent layers of metals are included as well. The interface between two dielectric materials of different refractive index partially reflects incident light backward and forward through the filter, and is essential for constructive interference and reinforcement. The wavelength that is reinforced and transmitted depends on the thickness and refractive index (the optical path) of the dielectric layers. The coatings are built up in units called cavities, with one cavity containing four to five alternating layers of dielectric salts separated by a spacer layer (Fig. 3.9).

The steepness of the transmission boundary and the definition of filter performance are increased by increasing the number of cavities. An 18-cavity filter may contain up to 90 separate dielectric layers. The deposition of salts is performed by evaporation of materials in a computer-controlled high-vacuum evaporator equipped with detectors for optical interference, which is used to monitor the thicknesses of the various layers. The final layer is covered with glass or overcoated with a scuff-resistant protective coating of silicon monoxide or silicon dioxide (referred to as quartz) to guard against abrasion. The availability of computers and programs to model the behavior of multiple dielectric cavities has stimulated a revolution in thin-film technology, allowing significant

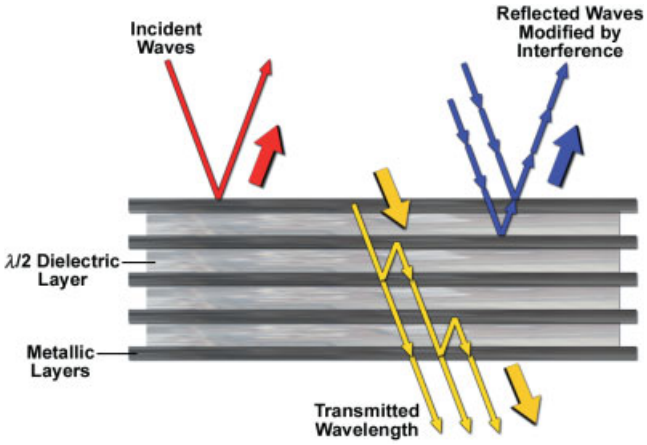

Figure 3.8

The action of an interference filter. An interference filter selectively transmits waves centered at a particular wavelength. For the filter shown, two thin films of metal cover a layer of dielectric material with an optical path of exactly $\lambda/2$ for a particular wavelength. The angle of the incident beam is usually perpendicular to the face of the filter, but is shown obliquely to reveal the behavior of transmitted waves. Since transmitted and multiply reflected waves of the designated wavelength are in phase, principles of constructive interference allow reinforcement and transmission through the filter. Shorter and longer wavelengths experience destructive interference and exit the filter as a backreflection.

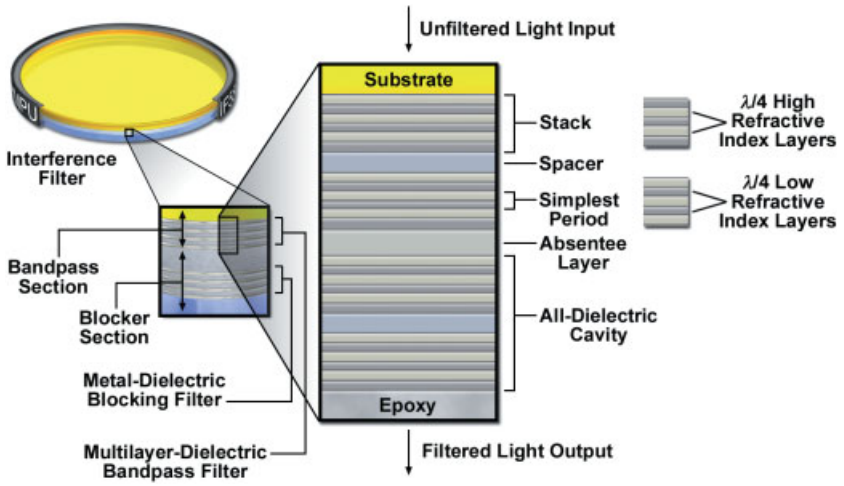

Figure 3.9

Structure of an all-dielectric interference filter. The revolution in thin film technology continues to drive the development of high-performance interference filters. The two-cavity filter shown contains alternate layers of high and low refractive index dielectric materials, each $\lambda/4$ and $\lambda/2$ thick, with five such layers defining a cavity. Computers control the deposition of layers of dielectric materials in a vacuum evaporator while film thickness is determined by interference optics. Dozens of such layers are deposited during a single run in the evaporator. Three cavities are the industry standard, but 18-cavity filters with 90 separate layers that can produce bandwidths of less than 1 nm are now routinely produced.

Hard Coating Interference Filters

In recent years, the company Semrock introduced hard coating-thin film technology from the communications industry to create new interference filters for microscopy. The new films are very uniform and homogeneous and have very sharp transitions in refractive index between the different layers, which allow many more alternating dielectric layers than with the earlier soft coating materials. Another benefit is the hard durable nature of the coating and its resistance to abrasion, heat, chemicals, and laser beams, making them ideal for use in the laboratory. The coatings are applied to glass substrates in a vacuum evaporator, where coating thickness is monitored by light transmission through the filter by a computer, which controls sets of electrodes responsible for depositing of dielectric salts during manufacture of the thin film. Evaporators and sophisticated computer programs are also an important part of the story. Several companies now use hard coating technology to create high performance filters. As mentioned in the text, the advantage of increasing the number of alternating dielectric layers is the ability to obtain extremely sharp cut-on and cut-off boundaries between transmitted and reflected wavelengths. The percent reflection and transmission of these filters can approach 0 and 100%. Filters of the type just described and shown in Figure 3.10 might have as many as 200 alternating dielectric layers. In the extreme, bandpass filters with up to 800 layers have been made with transmission bandwidths of just a few nanometers.

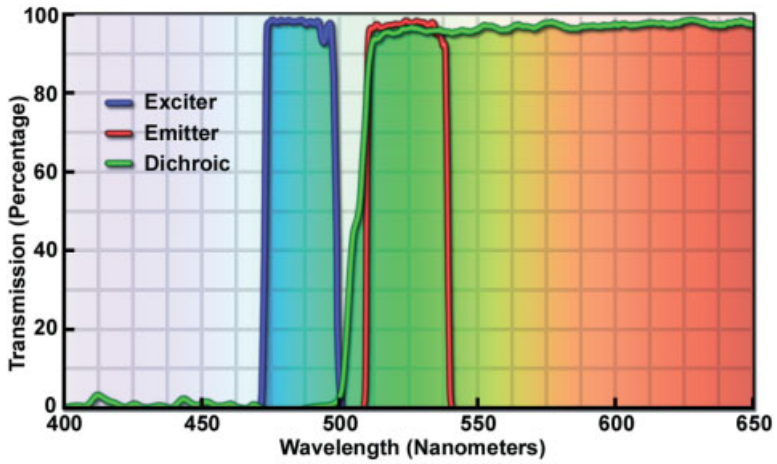

Figure 3.10

Hard-coating interference filter set for FITC, GFP, and Alexa Fluor 488 and other spectrally similar fluorophores.

improvements in the selection of specific wavelengths and in the intensity and contrast of fluorescence images. The technology has also stimulated research for the production of new fluorescent dyes, optical variants of GFP, fluorescent crystals (quantum dots) and other substances for use with a variety of illuminators and lasers. Because filter production is technology dependent and labor intensive, interference filters remain relatively expensive.

Interference bandpass filters for visible wavelengths frequently transmit wavelengths in the UV and IR range that may not be included in transmission spectra and documentation provided by the manufacturer. For microscopy involving live cell applications, it is safest to obtain the extended transmission spectra of all filters used and to employ efficient UV- and IR-blocking filters, particularly when UV- and IR-rich mercury or xenon arc lamps are used. Even with fixed fluorescent cells, an IR blocking filter, such as a KG-1, BG38, or BG39 glass filter, is frequently used as a heat-cut filter to protect optics and to prevent image fogging on IR-sensitive CCD cameras.

Interference filters gradually deteriorate upon exposure to light, heat, humidity, and especially exposure to abrasion, fingerprints, and harsh chemicals. Gently remove fingerprints and deposits from interference filters with a lens tissue and a neutral lens cleaner. Care must be taken not to rub interference coatings too hard, as this might scratch the surface, making the filter less efficient and shortening its life. Filters containing semitransparent metal coatings are usually mounted with the shiniest (silvery, nearly colorless) side of the filter facing the light source. The bindings at filter edges are usually inscribed with arrows to aid in the orientation and placement of filters in the light path of the microscope.

EFFECTS OF LIGHT ON LIVING CELLS

Since the energy per quantum is related to wavelength ($E = hc/\lambda$), short wavelengths are more energetic than long ones. UV wavelengths flanking the blue end of the visual spectrum (200–400 nm) are particularly damaging to cells, because photons of UV light are powerful enough to break covalent bonds, thereby creating reactive free radicals that chemically alter and denature macromolecules, such as proteins, nucleic acids, lipids, and small metabolites. Damage to DNA and membrane proteins, such as ion channels and gates, is a particular concern. Photons of near-IR radiation are less energetic than those of visible light, but are absorbed by carbon bonds in macromolecules, such as DNA, and by water (moderately in the range from 750 to 1000 nm, and strongly at wavelengths >1000 nm), leading to accumulation of kinetic energy (heat) and denaturation of molecules. Visible light itself is unique because it is absorbed relatively poorly by living cells, particularly at green and yellow wavelengths. For the most part, cellular absorption of visible light is considerably less than for the flanking UV and IR wavelengths. Since green light is relatively nontoxic and marks the peak sensitivity for human color vision, the 546-nm green line of the mercury arc lamp is commonly used for monochromatic illumination of living cells (Khodjakov and Rieder, 2006).

It is apparent that live cells must be protected from unwanted UV and IR radiation. IR- and UV-blocking filters, such as Schott filters BG38 (for IR) and GG420 (for UV), are especially useful, since the spectra generated by mercury, metal halide, and xenon arc lamps used in microscopy are rich in UV and IR radiation (for mercury, 30% UV, 40% IR, 30% visible; for metal halide, 15% UV, 45% IR, 40% visible; for xenon, 5% UV, 70% IR, and 25% visible). Phototoxicity in the microscope is recognized by the

cessation of cell motility and the arrest of organelle movement (see Chapter 16); within 3 seconds of exposure to the full spectrum of a 100-W mercury arc, amoebae retract filopodia and freeze, their cytoplasm appearing to have gelled. Upon further exposure, cells respond by blebbing and swelling, and particles contained in dilated vesicles begin to exhibit vibrational movements (Brownian movements) that are not as obvious in the living state. It is useful to observe cells without protective filters to become familiar with these effects.

Cells may require additional chemical protection from the buildup of high concentrations of damaging free radicals. For well chamber slides, the simplest measures are to increase the volume of medium in the chamber to dilute the radicals or to use anti-free radical reagents, such as 10-mM ascorbate or succinate in the culture medium to neutralize free radicals as they form. Alternatively, the rate of free radical formation can be slowed by reducing the concentration of dissolved oxygen in the culture medium using a mixture of oxygen-scavenging enzymes, such as catalase, glucose oxidase, and D-glucose, or supplementing the medium with Oxyrase (Oxyrase, Inc., Mansfield, OH), which is a commercial preparation of respiratory particles of bacterial cell membranes that contains oxygen-removing enzymes. To maintain low oxygen concentrations, cells must be enclosed in specially designed flow cells. If well chambers are used, the medium should be covered with a layer of lightweight nontoxic mineral oil to prevent recharging of the medium with atmospheric oxygen. The presence of these agents is usually harmless to vertebrate somatic cells, since cells in most tissues exist in a low-oxygen environment.

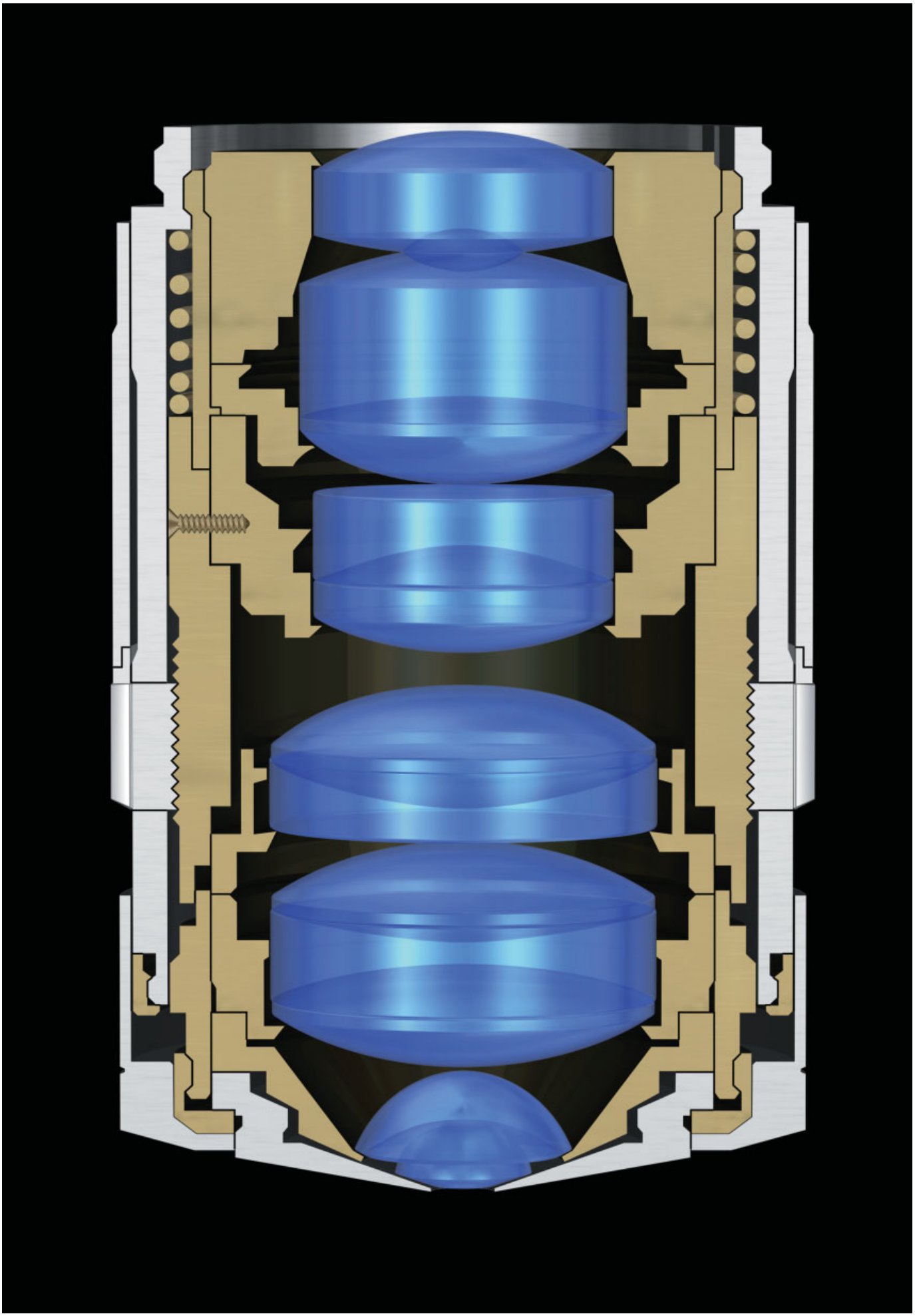

CHAPTER
4

LENSES AND GEOMETRICAL OPTICS

OVERVIEW

In this chapter, we discuss some essential principles of geometrical optics, the action of lenses on light as revealed by ray tracing and explained by principles of refraction and reflection (Fig. 4.1). With the help of a few simple rules and from studying examples, we can understand the process of magnification, the properties of real and virtual images, the aberrations of lenses, and other phenomena. We also examine the designs and specifications of condensers and objectives, review the nomenclature inscribed on the barrel of an objective that specifies its optical properties and conditions for use, and give some practical advice on the cleaning of optical components.

REFLECTION AND REFRACTION OF LIGHT

Objects are perceived by the eye through the wavelengths they reflect and absorb. In *reflection*, incident rays of light are bent back or returned by an object's surface, sometimes modified by other actions, such as absorption or refraction. If the object's surface is planar, the law of reflection may be observed, whereby *the angle of incidence equals the angle of reflection* (Fig. 4.2). Both angles are described by the angles subtended between the incident and reflected rays and the normal (an imaginary line perpendicular to the surface). It is interesting that reflection is not dependent on wavelength. For this reason, the objective mirrors of reflecting telescopes are free of chromatic error, a major aberration of lens-based optics.

Drawing of a Leica objective used for STED microscopy.

Fundamentals of Light Microscopy and Electronic Imaging, Second Edition.
Douglas B. Murphy and Michael W. Davidson.

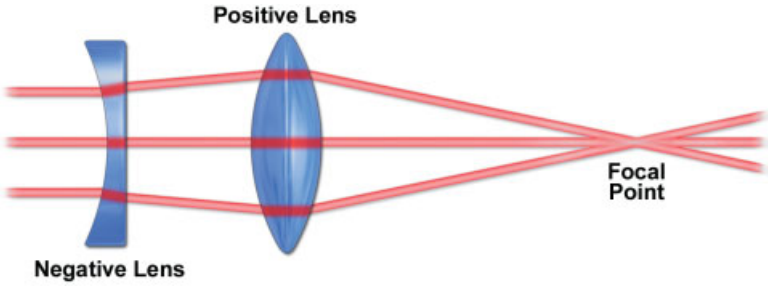

Figure 4.1
Geometrical optics of simple lenses. Negative lenses diverge and positive lenses converge incident beams of light.

Many objects, such as paper or clothing, reflect light in all directions, a condition called diffuse reflection. Microscopic structures (cellulose fibers) larger than the wavelength of light reflect rays by the law of reflection, only at a microscopic level, but because rays are reflected from minute domains in all directions, the reflection is called diffuse.

In *refraction*, as in the case of light entering a lens, light rays become bent (refracted) at the air-glass interface and follow a different path in the second medium. Refraction occurs because the velocities of light in transparent media like air and glass are different and distinct from its velocity in a vacuum. The speed of light in a vacuum (c) is 3×10^8 m/s, but during propagation through a medium such as glass, velocity and wavelength of light become reduced, although its frequency remains unchanged. The ratio of the velocities (or of the wavelengths) of light in a vacuum (c, λ) and in the medium (v_m, λ_m) define what is known as the *refractive index* n:

$$n = c/v_m = \lambda/\lambda_m.$$

Thus, given the refractive index of glass of 1.5, we can say that the velocity of light is 1.5 times as great in a vacuum as it is in glass, or conversely, that the velocity of light in glass is two-thirds of its velocity in a vacuum. Refractive index is an important term. It char-

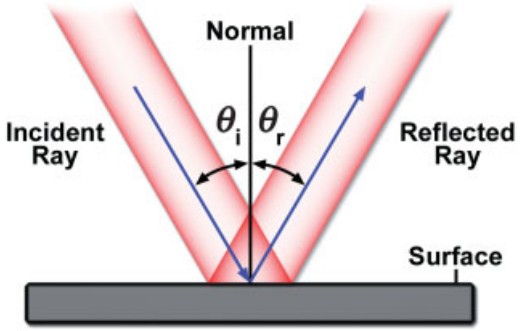

Figure 4.2
Reflection of light, showing $\theta_i = \theta_r$.

acterizes the velocity of light in a medium, and describes refraction of light and the ratio of refraction and reflection that occurs at the boundary to a transparent material.

We can consider refraction at a flat interface between two different transparent media. For light traveling from medium 1 into medium 2, the paths of the incident and transmitted rays and the refractive indices of the two media are related to each other through *Snell's law*, where the angles of the incident and transmitted rays are measured from the normal to the interface between the two media, thus:

$$n_1 \sin\theta_1 = n_2 \sin\theta_2,$$

or as:

$$\sin\theta_1 / \sin\theta_2 = n_2 / n_1 = v_2 / v_1.$$

When light rays pass from one medium through an interface into a second medium with a higher refractive index as in Figure 4.3a, the rays bend toward the normal. This is the usual case for light rays in air entering into a lens. On the other hand, if light rays enter a medium with a lower refractive index, such as rays exiting a lens and entering air, they bend away from the normal as shown in Figure 4.3b. It is the change in speed that occurs when light passes from one medium to another that is responsible for refraction at an optical interface.

Note: In the latter case of rays entering a lower refractive index medium, there is a unique angle, known as the critical angle, where rays are refracted at 90° to the normal and travel along the interface. At any incident angle larger than the critical angle, light rays will not pass through to the second medium at all. Instead, all rays are reflected back into the first medium, a process known as *total internal reflection*. The angle at which this change in refractive behavior occurs is called the *critical angle*, θ_c. A mode of light microscopy called total internal reflection fluorescence microscopy, or TIRF, that utilizes this principle is described in Chapter 12.

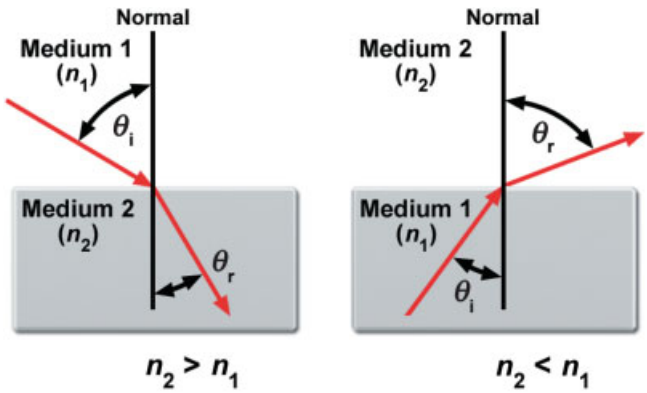

Figure 4.3

Refraction and Snell's law: $n_1 \sin\theta_1 = n_2 \sin\theta_2$. (a) When $n_2 > n_1$, light rays become bent in the direction of the normal. (b) When $n_2 < n_1$, light rays bend away from the normal. If θ_1 is adjusted so that $\theta_2 > 90°$ (greater than the critical angle), rays are totally reflected back into the first medium (total internal reflection).

IMAGE FORMATION BY A SIMPLE LENS

To understand microscope optics, we begin by describing some of the basic properties of a thin, simple lens. A thin lens has a thickness that is essentially negligible, and by simple we mean consisting of a single lens element with two refracting surfaces. The *principal plane* and *focal plane* of a lens are defined as those planes, within the lens and in the focused image, respectively, where rays or extensions of rays intersect and physically reunite. Thus, for a simple positive lens receiving a collimated beam of light, the plane in the lens in which extensions of incident and emergent rays intersect is called the principal plane, and the plane in which rays intersect to form an image is the focal plane. The *focal length* of a lens is the distance between the principal plane and the focal plane. Lenses can be either positive or negative. A *positive lens* converges parallel incident rays and forms a real image; such a lens is thicker in the middle than at the periphery and has at least one convex surface. (See the Note for definitions of real and virtual images.) Positive lenses magnify when held in front of the eye. A negative lens causes parallel incident rays to diverge; negative lenses are thinner in the middle than at the periphery, and have at least one concave surface. Negative lenses do not form a real image, and when held in front of the eye, they reduce or demagnify. The geometry of positive and negative simple lenses is shown in Figure 4.4.

For any given lens, there are two principal planes, one each for the front and back surface of the lens. For the special case of a thin biconvex lens, the two principal planes are coincident in the middle of the lens. Microscope objectives contain multiple lens elements, some of which may be united with transparent sealing compound to make a

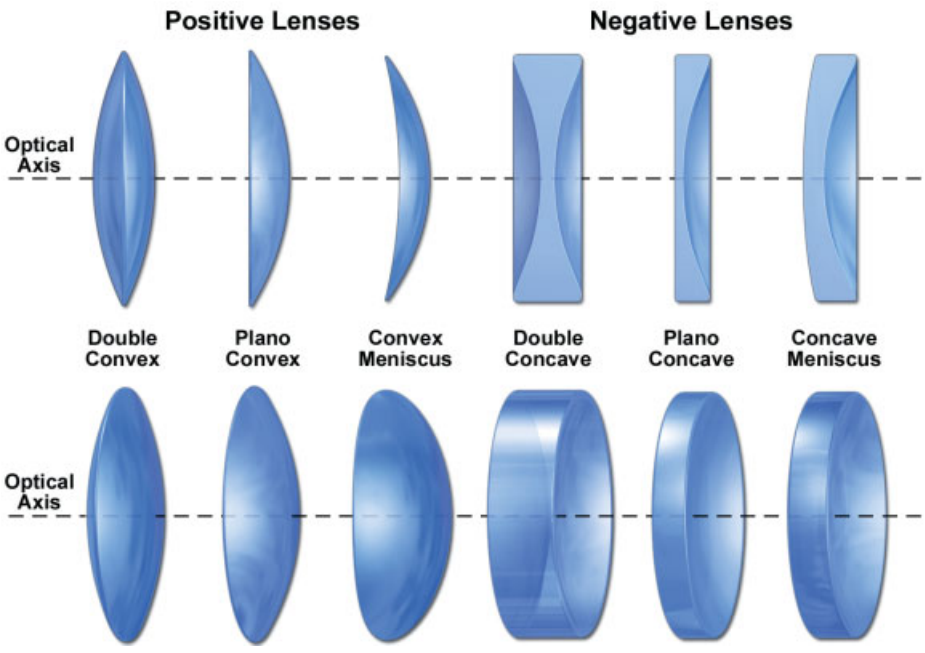

Figure 4.4
Examples of positive and negative lenses.

complex *thick lens*. The principal planes of thick lenses are physically separated, but their locations can be determined by ray tracing. Most lens elements used in microscope optics are ground and polished with spherical curvatures.

Note: Real and Virtual Images

Images can be defined as regions where rays, or the extensions of rays, become convergent as the result of refraction by a lens or reflection by a mirror. If the rays intersect and physically reunite, the image is said to be real. A *real image* can be seen on a viewing screen or recorded on a piece of film when a screen or film is placed in the image plane. If rays diverge, but the imaginary extensions of the rays become convergent and intersect, the image is said to be virtual. The plane occupied by a *virtual image* cannot be observed on a viewing screen or recorded on film. To be perceived, a real image must be formed on the retina of the eye. In the case of viewing an image in a microscope (Fig. 1.3), a real image is formed on the retina but is perceived as a virtual image located some 25 cm in front of the eye. Lens configurations giving real and virtual images are described in this chapter.

The geometric parameters of a *simple thin lens* are described in Figure 4.5, where the dashed vertical line represents the combined principal planes of a thin biconvex lens of focal length *f*. The object, an arrow on the left-hand side of the figure, is examined by the lens and imaged as a magnified real image (magnified inverted arrow) in the image plane on the right. The *focal length* is shown as the distance *f* from the principal plane of the lens to its *focal point F*, the front and rear focal lengths having the same value. The optical axis is shown by a horizontal line passing through the center of the lens and perpendicular to its principal plane. The *object distance*, *a* (distance from the object to the principal plane of the lens) and *image distance*, *b* (distance from the image to the principal plane of the lens) are also indicated.

The *focal length* of any simple lens can be determined by aiming the lens at a bright "infinitely distant" light source (>30 times the focal length), such as a lamp across

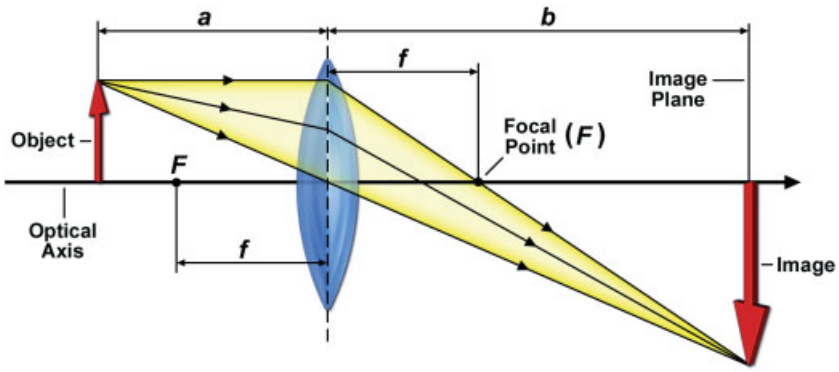

Figure 4.5

Geometrical optics of a simple lens. The focal length *f*, focal point *F*, object–lens distance *a*, and lens–image distance *b* are indicated.

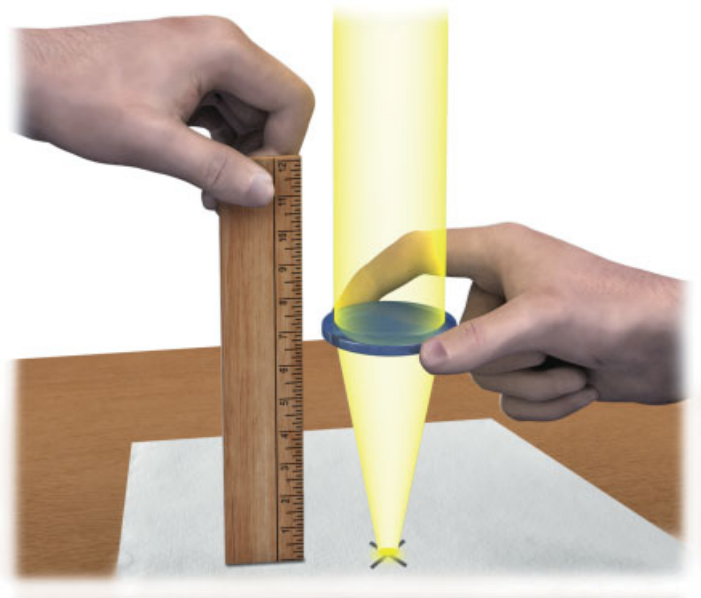

Figure 4.6
Determining the focal length of a simple lens. The image of a distant source is projected by the lens on a viewing surface; the focal length is the distance between the focal plane, and the lens as measured with a ruler.

the room or scene outdoors; by focusing the image on a sheet of paper held behind the lens, the focal length is readily determined (Fig. 4.6). We will now examine the basic rules that determine the action of a simple convex lens.

RULES OF RAY TRACING FOR A SIMPLE LENS

The three rules governing ray tracing for a simple lens are depicted in Figure 4.7 and are listed as follows:

1. A light ray passing through the center of a lens is not deviated.
2. A light ray travelling parallel with the optical axis will, after refraction, pass through the rear focal point.
3. A ray passing through the front focal point will be refracted in a direction parallel to the optical axis.

Notice that the intersection of any two of the three key rays just described identifies the location of the image plane.

OBJECT–IMAGE MATH

The well-known *lens equation* describes the relationship between focal length f and object and image distances, a and b:

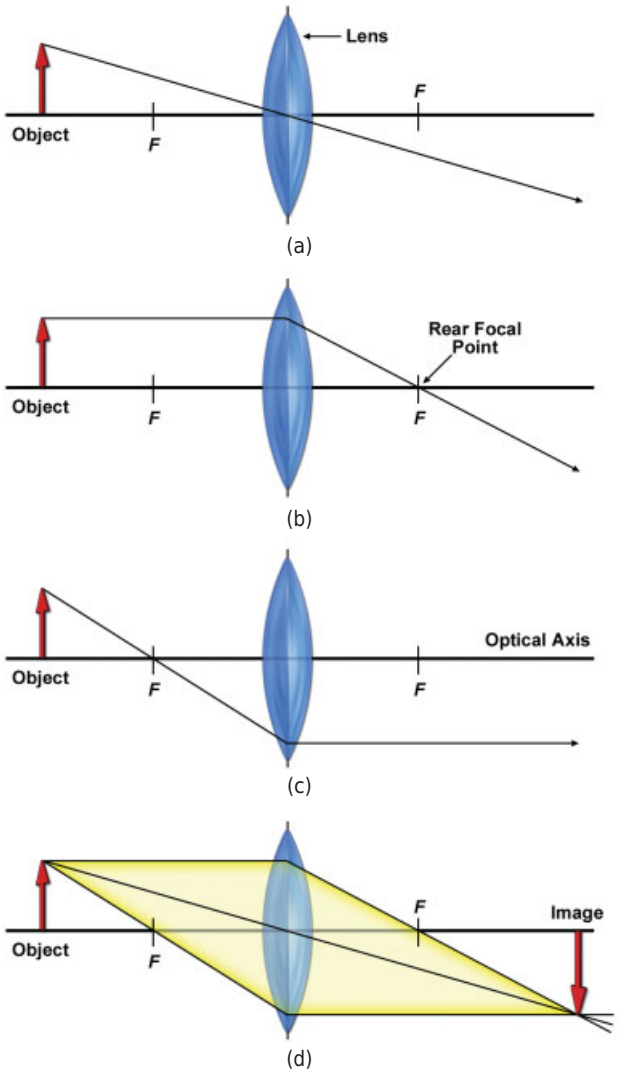

Figure 4.7

Principles governing ray tracing for a thin lens. (a) A ray, incident at any angle, which passes through the center of the lens remains undeviated from its original course on the other side of the lens. (b) Any ray traveling parallel to the optical axis and refracted by the lens always passes through the rear focal point *F*. (c) A ray passing through the front focal point of a lens at any angle is refracted and follows a path parallel to the optical axis. (d) The intersection of any two of the three rays described defines the location of the image plane.

$$1/f = 1/a + 1/b,$$

or

$$b = af/(a - f).$$

Further, the magnification factor M of an image is described as:

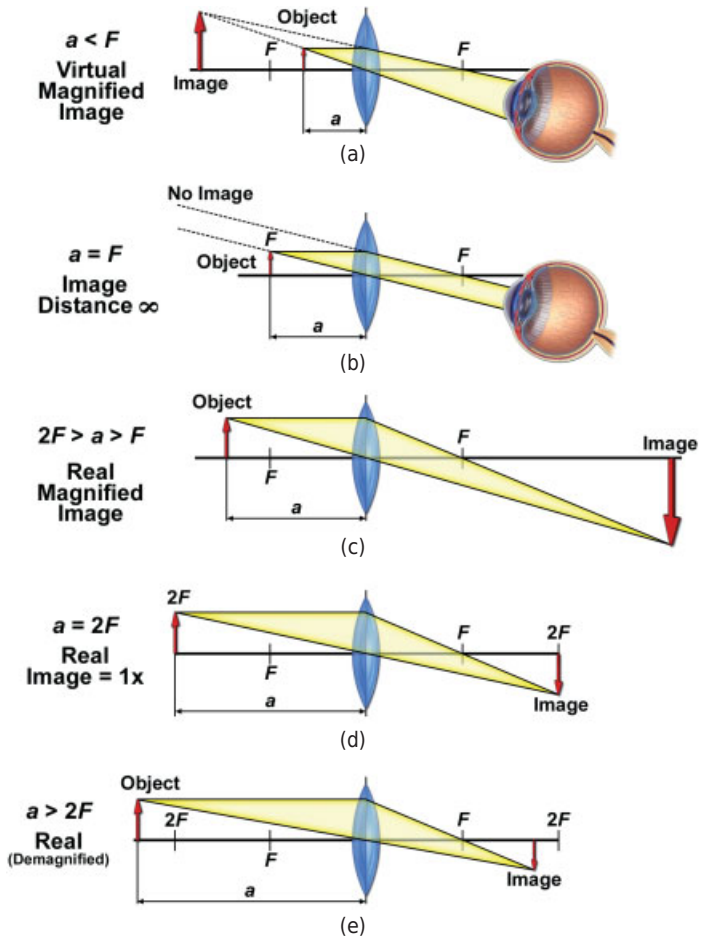

Figure 4.8

Object–image relationships. (a) $a < F$. (b) $a = F$. (c) $2F > a > F$. (d) $a = 2F$. (e) $a > 2F$.

$$M = b/a \text{ or } M = f/(a - f).$$

From these relationships, the action of a lens on image location and magnification can be deduced. Depending on the location of the object relative to the focal point of the lens, the image may be real or virtual, magnified or demagnified (Fig. 4.8; Spencer, 1982), and located on or away from the focal plane. In Figure 4.7, the image is located well outside the focal plane. It is good practice to work through the following relationships using any handheld magnifier or simple biconvex lens, such as the front lens of a binocular (10–50 mm is convenient), whose focal length has been determined by the procedure just described. The object should be self-luminous, moderately bright, and well defined. A 5–10-mm diameter hole cut in a large opaque cardboard sheet placed in front of a lamp works well as an object. Work in a partially darkened room.

It is useful to remember the principal conditions describing object–image relationships for a simple positive lens:

- $a < F$. No real image exists that can be projected on a screen. If the eye is placed behind the lens, a virtual image is perceived on the far side of the lens.
- $a = F$. The image distance b is infinite, so no image exists that can be projected on a screen. We used this condition above to determine the focal length of a lens only in reverse: parallel beams of light from an "infinitely distant" object converge at the focal length of the lens. This is the case for image formation in a telescope.

For the condition that $a > F$, a real image is always formed. The unique domains for this condition are as follows:

- $2F > a > F$. A real *magnified* image is formed. This arrangement is used for producing the first real image in a microscope.
- $a = 2F$. This is a specialized case. Under this condition, $b = 2F$ also. A real image is formed, but there is *no magnification* and $M = 1$.
- $a > 2F$. A real *demagnified* image is formed and $M < 1$.

In the case of a microscope objective focused on a specimen, the image is both real and magnified, meaning that the object is located at an *object distance* a between $1F$ and $2F$ ($2F > a > F$) (Figs. 4.5 and 4.9). Since the focused objective is very near the specimen, we deduce that the focal length of the objective must be very short, only a few millimeters. In the course of using the focusing dials of a microscope, the image comes into sharp focus when the correct object distance a has been obtained, and we obtain the correct adjustment without even thinking about object and image distances. In practice, focusing a microscope positions the image (the real intermediate image

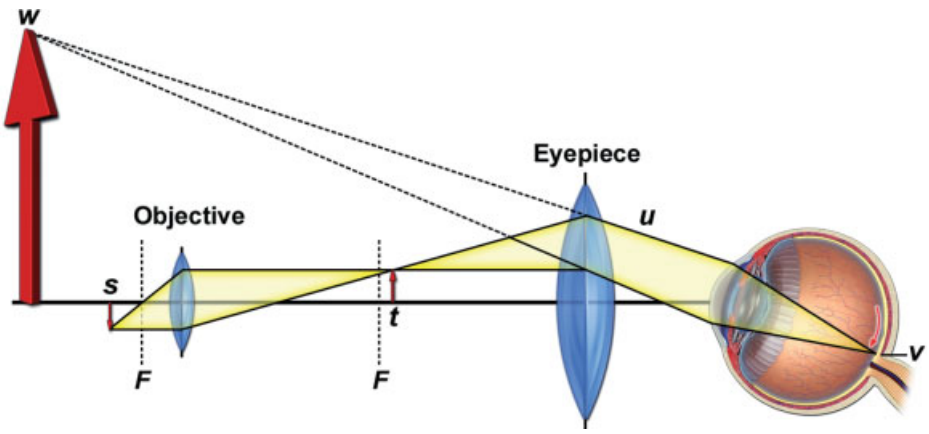

Figure 4.9

Location of real and virtual images in a light microscope marked *s* through *w*. Note that the specimen at *s* lies just outside the focus of the objective, resulting in a real, magnified image at *t* in the eyepiece. The primary image at *t* lies just inside the focus of the eyepiece, resulting in diverging rays at *u*. The cornea and lens of the eye form a real image of the object on the retina at *v*, which because of the diverging angle at *u* perceives the object as a magnified virtual image at *w*.

plane) at a fixed location in the front aperture of the eyepiece; when the microscope is defocused, there is still a real image nearby, but it is not in the proper location for the ocular and eye to form a focused image on the retina. Finally, notice that the *image distance b* is many centimeters long. The ratio *b/a* (the magnification *M*) usually ranges from <10 to 100.

Thus, when a microscope with finite focus objectives is focused on a specimen, the specimen lies just outside the front focal point of the objective, while the intermediate image is located at a distance 10–100 times the focal length of the objective in the eyepiece. For more detailed discussions on the topic, refer to Pluta (1988) or Hecht (2001).

Modern microscopes with *infinity focus objectives* follow the same optical principles already described for generating a magnified real image, only the optical design is somewhat different. For an objective with infinity focus design, the specimen is located at the focus of the lens, and parallel bundles of rays emerging from the rear aperture of the objective are focused to infinity and do not form an image; it is the job of the *tube lens* in the microscope body to receive the rays and form the real intermediate image at the eyepiece.

The advantage of this design is that it allows greater flexibility in microscope configuration while preserving the image contrast and resolution provided by the objective. Items such as waveplates, compensators, DIC prisms, reflectors, and fluorescence filter sets can be placed anywhere in the "infinity space" between the back of the objective and the tube lens. As long as these items have plane–parallel elements, their location in the infinity space region on the imaging path is not critical. If we consider the combination of objective plus tube lens as the effective objective lens, then the same optical rules pertain for generating a real magnified image, and we observe that the relationship $2F > a > F$ is still valid.

The function of the eyepiece or ocular is to magnify the primary image another 10-fold, and together with the lens components of the eye, to produce a real magnified image of the intermediate image on the retina. Thus, the object of the eyepiece is the intermediate image made by the objective. Note that in the case of the ocular, $0 < a < F$, so that the object distance is less than one focal length, resulting in a virtual image that cannot be focused on a screen or recorded on film with a camera. However, when the eye is placed behind the eyepiece to examine the image, the ocular-eye combination produces a real secondary image on the retina, which the brain perceives as a magnified virtual image located about 25 cm in front of the eye. The visual perception of virtual images is common in optical systems. For example, we also "see" virtual images when we employ a handheld magnifying glass to inspect small objects or when we look into a mirror.

THE PRINCIPAL ABERRATIONS OF LENSES

Simple lenses of the type discussed above have spherical surfaces, but a spherical lens is associated with many intrinsic optical faults called *aberrations* that distort the image in various ways. Of these faults, the major aberrations are chromatic aberration, spherical aberration, coma, astigmatism, curvature of field, and distortion (Fig. 4.10). Corrective measures include use of compound lens designs, use of glass elements with different refractive indexes and color dispersion, incorporation of aspherical lens curvatures, and other methods. The tube lens sometimes performs an additional important

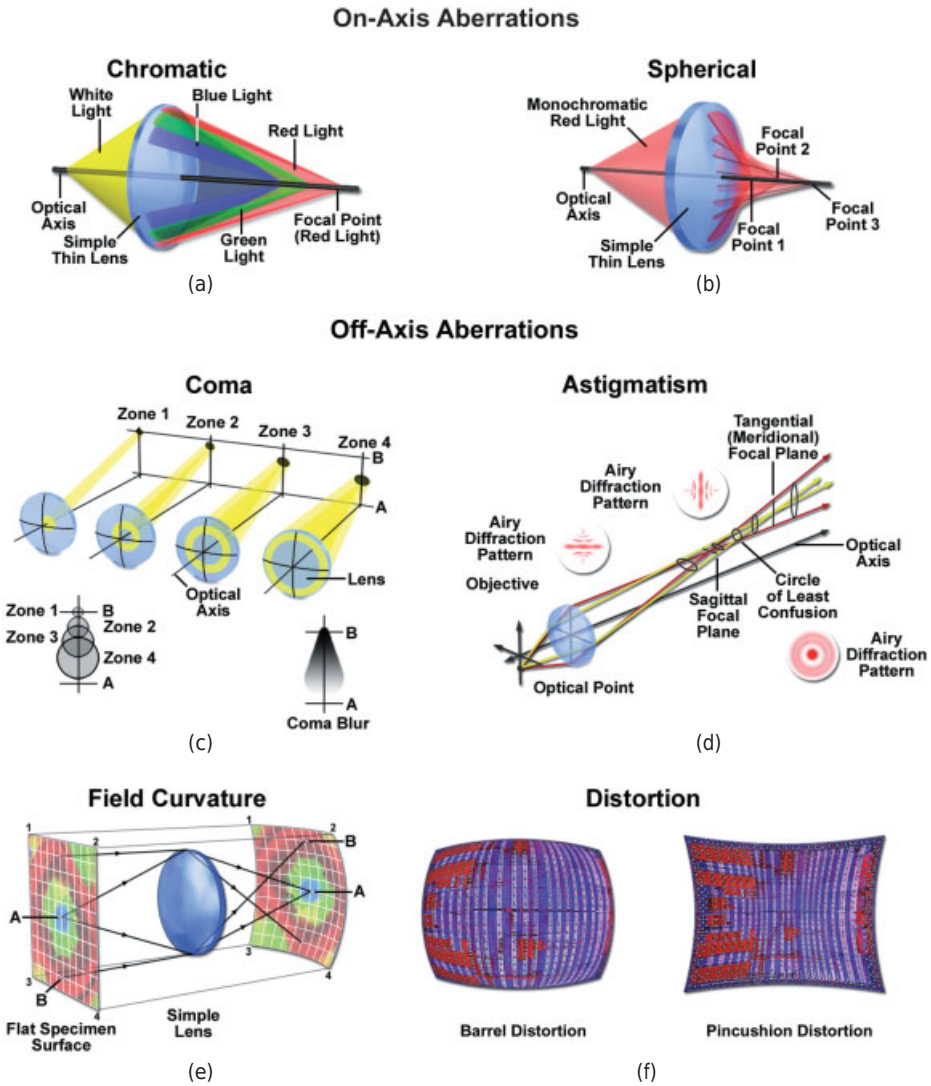

Figure 4.10

Aberrations of a simple lens. (a) Chromatic aberration: Parallel incident rays of different wavelength are focused at different locations. (b) Spherical aberration: Incident rays parallel to the optical axis and reaching the center and the periphery of the lens are focused at different locations. (c) Coma: Off-axis rays passing through the center and periphery of the lens are focused at different locations. (d) Astigmatism: An off-axis aberration causes waves passing through the vertical and horizontal diameters to focus an object point as a streak. (e) Field curvature: The image plane is curved and not planar. (f) Distortion: So-called barrel and pincushion distortions produce images that are not high in fidelity compared with the object.

function in removing residual aberrations of the objective. In some microscopes, the eyepieces also help perform this function. Objectives are designed to correct for aberrations, but can never completely remove them. It is common that a solution for correcting one fault worsens other faults, so the lens designer must prioritize goals for optical performance and then work toward the best compromise in correcting other aberrations. For these reasons, objectives vary considerably in their design, optical performance, and cost.

Chromatic aberration occurs because a lens refracts light differently, depending on the wavelength. Blue light is bent inward toward the optical axis more than red light. The result is disastrous: Blue wavelengths are focused in an image plane closer to the lens than the image plane for red wavelengths. Even at the best focus, point sources are surrounded by color halos, the color changing depending on the focus of the objective, the image never becoming sharp. Since each wavelength is focused at a different distance from the lens, there is also a difference in magnification for different colors (chromatic magnification difference). The solution is to make compound lenses made of glasses having different color-dispersing properties. For example, glass types known as crown and flint are paired together to make an achromatic doublet lens that focuses blue and red wavelengths in the same image plane.

Spherical aberration is the undesirable consequence of having lenses figured with spherical surfaces, the only practical approach for lens manufacture. Parallel rays incident at central and peripheral locations on the lens are focused at different axial locations, so that there is not a well-defined image plane, and a point source of light at best focus appears as a spot surrounded by a bright halo or series of rings. For an extended object, the entire image is blurred, especially at the periphery. One common solution is to use a combination of positive and negative lenses of different thicknesses in a compound lens design. Corrections for spherical aberration are made assuming a certain set of conditions: coverslip thickness, the assumption that the focal plane is at or near the coverslip surface, the refractive index of the medium between lens and coverslip, the wavelength of illumination, temperature, and others. Thus, users employing well-corrected objectives can unknowingly induce spherical aberration by using coverslips having the wrong thickness, by warming the objective, or by focusing on objects positioned away from the coverslip surface. Special objectives are now available with adjustable correction collars to minimize spherical aberration (Brenner, 1994).

Coma is an "off-axis aberration" that causes point objects to look like comets, focused spots with emanating comet tails, located at the periphery of an image. Coma affects the images of points located off the optical axis—that is, when object rays hit the lens obliquely. It is the most prominent off-axis aberration. Rays passing through the edge of the lens are focused farther away from the optical axis than are rays that pass through the center of the lens, causing a point object to look like a comet with the tail extending toward the periphery of the field. Coma is greater for lenses with wider apertures. Correction for this aberration is made to accommodate the diameter of the object field for a given objective.

Astigmatism, like coma, is an off-axis aberration. Rays from an object point passing through the horizontal and vertical diameters of a lens are focused as a short streak at two different focal planes. The streaks appear as ellipses drawn out in horizontal and vertical directions at either side of best focus, where the focused image of a point appears as an extended circular patch. Off-axis astigmatism increases with increasing displacement of the object from the optical axis. Astigmatism is also caused by asym-

metric lens curvature due to mistakes in manufacture or improper mounting of a lens in its barrel.

Curvature of field is another serious off-axis aberration. Field curvature indicates that the image plane is not flat, but has the shape of a concave spherical surface as seen from the objective. Different zones of the image can be brought into focus, but the whole image cannot be focused simultaneously on a flat surface as would be required for photography. Field curvature is corrected by the lens design of the objective and additionally by the tube or relay lens and sometimes the oculars.

Distortion is an aberration that causes the focus position of the object image to shift laterally in the image plane with increasing displacement of the object from the optical axis. The consequence of distortion is a nonlinear magnification in the image from the center to the periphery of the field. Depending on whether the gradient in magnification is increasing or decreasing, the aberration is termed pincushion or barrel distortion after the distorted appearance of a specimen with straight lines, such as a grid or reticule with a pattern of squares or rectangles. Corrections are made as described for field curvature.

DESIGNS AND SPECIFICATIONS OF OBJECTIVES

Achromats are red-blue corrected (meaning for wavelengths at 656 and 486 nm). Spherical correction is for mid-spectrum yellow-green light at 540 nm. These objectives give satisfactory performance in white light and excellent performance in monochromatic light and are quite suitable for low magnification work at 30–40× and lower. They are also much less expensive than more highly corrected objective designs (Fig. 4.11).

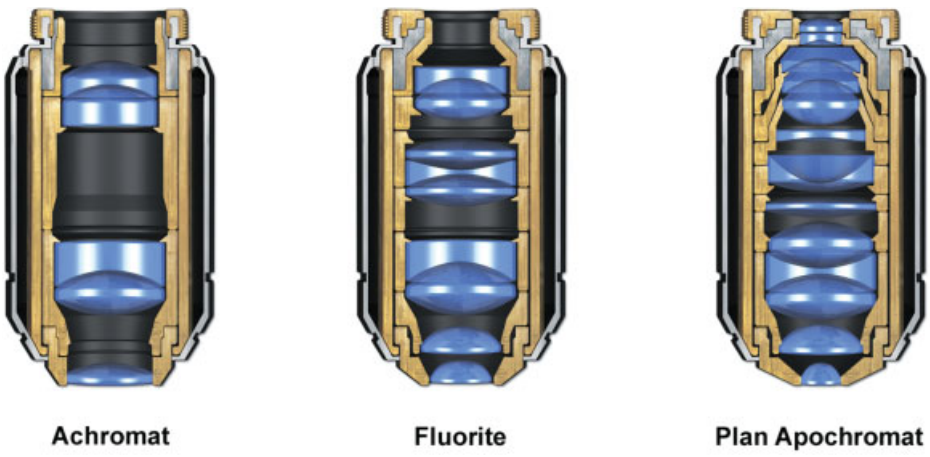

Figure 4.11

Objective designs. Apochromatic objectives may contain 12 or more lens elements to give bright, flat images with excellent color correction across the visual spectrum. Fluorite objectives have fewer lens components and produce sharp, bright images. These objectives exhibit excellent color correction and transmit UV light. Achromatic objectives are not as well corrected but are excellent for single color imaging.

Fluorite or *semiapochromat* objectives contain elements made of fluorite or fluorspar (CaF_2) or synthetic lanthanum fluorite—materials giving very high transmission and low color dispersion (Fig. 4.11). Corrections for color dispersion and curvature of field are easily applied. The combination of good color correction, extremely high transparency (including to near ultraviolet [UV] light) and high contrast makes them favorites for UV-excitable calcium dyes, activation of caged fluorescent molecules, immunofluorescence microscopy, polarization and differential interference contrast (DIC) microscopy, and other forms of light microscopy. The maximum obtainable numerical aperture (NA) is about 1.3.

Apochromats are expensive, highly color-corrected designs suitable for color photography using white light (Fig. 4.11). These objectives are red, green, blue, and dark blue corrected for color, and are corrected for spherical aberration at green and blue wavelengths. This design tends to suffer some curvature of field, but is corrected in *plan-apochromatic* objectives. The high degree of color correction makes them desirable for fluorescence microscopy and color brightfield imaging, since various fluorescence wavelengths emitted from a multiply stained specimen are accurately focused in the same image plane. It is also possible to obtain very large NAs (up to 1.49) with this objectives design, making them desirable for high resolution and low light applications, such as dim fluorescent specimens. Newer designs are now transparent to near-UV light, making them suitable for fluorescence microscopy involving UV-excitable dyes. The range of wavelengths used for *apochromatic correction* continues to get wider. Originally a three-color correction in red, green, and blue wavelengths, many apochromatic corrections are now based on a five-color spectrum ranging from near-UV to near-infrared (IR) (350–1000 nm). These modern objectives are particularly useful for photoactivation in the near-UV and for near-IR and multiphoton imaging, where excitation wavelengths are in the 800–1000 nm range.

A summary of the important characteristics of some commonly used objectives is provided in Table 4.1.

New Objective Designs

Many of the performance characteristics of today's objectives could not be achieved just 10 years ago and reflect advances in glass-making technology and lens fabrication methods. For example, objectives for TIRF imaging require large NAs of 1.45 or greater, some even requiring special immersion medium and coverslips. For TIRF imaging using conventional immersion oil, there are now objectives with NA values of 1.42–1.49 corresponding to effective half-angles of the acceptance light cone of 70–80°, an extraordinary technical achievement (see Table 4.2). Apochromatic objectives are another excellent example. Originally designed to bring red, green, and blue wavelengths to the same focus, today's apochromatic objectives are corrected for four or five wavelengths across the visible range. Objectives that are color corrected for UV, visible, and near-infrared wavelengths may be corrected for up to nine wavelengths; for example, for the Zeiss LD C-APO 40×/1.1 NA objective, light at 365-, 405-, 436-, 480-, 546-, 608-, 644-, 750-, and 850-nm wavelengths is focused within the central diffraction spot to within 80% of the theoretical maximum (100%). While much attention is given to axial and lateral chromatic aberration, there are equally demanding criteria for spherical aberration, coma, astigmatism, flatness of field, and distortion.

The procedure for creating a new objective design requires special lens design software and computer-aided design and computer-aided manufacturing (CAD-CAM) programs that model variables, such as the chromatic dispersion and refractive index of different glass types, the base curves given to the face of each lens element, the grouping and spacing of lens elements within a complex compound lens, and other parameters. The technology and effort applied to new lens design are of major importance in meeting new imaging challenges, such as TIRF in light microscopy. An example of objective performance as revealed by lens design software is shown in Figure 4.12.

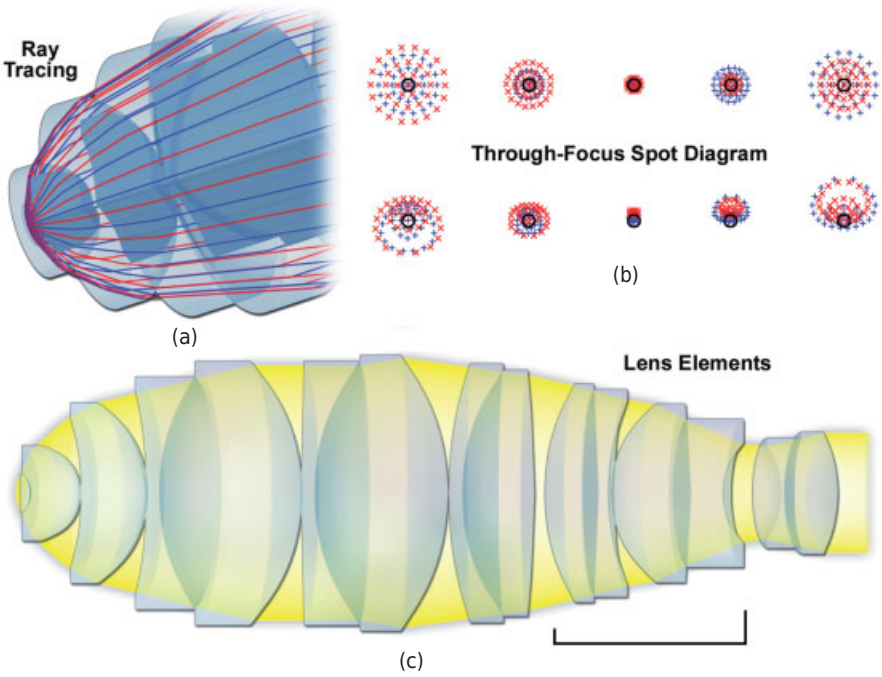

Figure 4.12

Modeling objective performance. New objective designs like the Nikon TIRF objective (apochromatic 60×/1.49 NA) shown here and described in Table 4.2 are examined in lens design programs such as ZEMAX. The goal in this case was to create an objective with NA > 1.45 that could be used with standard immersion oil for TIRF imaging. Chromatic aberration is well corrected axially, with both red (650 nm) and blue (435 nm) wavelengths focused largely within the Airy disk (31 μm radius for red) and is nearly as well corrected laterally at 50 μm off the optical axis. (a) The distribution of rays is shown at 10-mm intervals from the focal plane along the optical axis. (b) The through-focus spot diagram (on-axis, upper; off-axis, lower) of the objective. (c) A cross-sectional profile of the objective shows 15 lens elements (30 different base curves) with the majority in cemented doublets. The course of red and blue rays traveling through the objective is altered by lens designers by changing the types of glass and lens curvatures and spacings. The bracketed group of lenses in panel c is moved as a unit by adjusting a correction collar on the objective barrel to correct for spherical aberration. In this design, particular attention was given to both the refractive index and base curvature of the front lens element in order to achieve a numerical aperture of 1.49.

TABLE 4.1 Characteristics of Selected Objectives[a]

M (×)	Type	Medium (n)	WD (mm)	NA	d_{min} (μm)	DOF (μm)	B
5	Achromat	1	9.9	0.12	2.80	38.19	0.1
10	Achromat	1	4.4	0.25	1.34	8.80	0.4
20	Achromat	1	0.53	0.45	0.75	2.72	1.0
25	Fluorite	1.515	0.21	0.8	0.42	1.30	6.6
40	Fluorite	1	0.5	0.75	0.45	0.98	2.0
40	Fluorite	1.515	0.2	1.3	0.26	0.49	17.9
60	Apochromat	1	0.15	0.95	0.35	0.61	2.3
60	Apochromat	1.515	0.09	1.4	0.24	0.43	10.7
100	Apochromat	1.515	0.09	1.4	0.24	0.43	3.8

[a] The magnification (M), type of lens design, refractive index (n) of the intervening medium (air or immersion oil), working distance (WD), numerical aperture (NA), minimum resolvable distance (d), depth of field (DOF), and brightness (B) are indicated. Terms are calculated as: wave-optical depth of field, $n\lambda/NA^2$; brightness in epi-illumination mode, $10^4\ NA^4/M^2$. Resolution and depth of field are discussed in Chapter 6.

Special Objective Designs

Other performance characteristics, such as working distance, immersion design, and UV transparency are optimized in special objective designs:

- *Long working distance objectives* allow focusing over an extended range of up to several mm, for example: when looking at details in thick sections that may be a long distance from the coverslip; when imaging through thick substrates (microscope slides, culture dishes); or when introducing devices, such as micropipettes between the specimen and the objective. The *working distance* is the distance between the surface of the front lens element of the objective and the surface of the coverslip nearest to the objective (Fig. 4.13). Whereas a high resolution 40×/1.3 NA oil immersion objective might have a short working distance of just 0.2 mm, a 40×/1.0 LWD water immersion objective might have a working distance of over 2 mm.
- *Water immersion and dipping objectives* are used for examining cells and tissues in an aqueous medium, where specimen details are positioned several, even tens of micrometers, from the coverslip surface. Under these conditions where the object is not close to the coverslip surface, the spherical aberration with oil immersion objectives becomes significant, producing image blur and reducing the strength of fluorescence signals in confocal microscopes. Water-immersion objectives are corrected for imaging in an aqueous volume and minimize the problem, although their reduced NA reduces resolution somewhat. They are designed for use with a coverslip and use water as the immersion medium. There are also special immersion oils with a refractive index of 1.333 that do not evaporate that can be convenient. Another type of water-immersion objective, called a *dipping*

TABLE 4.2 New High Performance Objectives for Fluorescence Imaging

Company	Lens Type	Mag/NA	WD (mm)	FN (mm)	B	Notes
Leica	PL APO	5/0.15	12.1	N/A	0.2	Dry
Leica	PL APO	40/1.25–0.75	0.1	N/A	15.3	Oil, aperture control
Leica	PL APO	63/1.2	0.22	N/A	5.2	Oil, SA corr.
Leica	PL APO	100/1.46	0.09	N/A	4.5	Oil, confocal scanning
Nikon	PL APO	20/0.75	1.0	N/A	7.9	Dry
Nikon	PL APO	60/1.2	0.22	N/A	5.8	Water immersion, SA corr.
Nikon	APO TIRF	60/1.49	0.12	N/A	13.7	Oil with NA > 1.45, SA corr. (see Fig. 4.12)
Nikon	PL APO	100/1.4	0.17	N/A	3.8	Large W.D. at high NA
Nikon	PLAN	100/1.1	2.5	N/A	1.5	Dipping lens, SA corr, U-I-R
Nikon	FLUOR	100/0.5–1.3	0.2	N/A	2.9	U-I-R, Aperture control
Olympus	Super Hi NA	20/0.95	2.0	22	20.4	Dipping lens, U-V-I
Olympus	PL APO	60/1.42	0.15	26.5	11.3	Oil, U-V-I
Olympus	PL APO	100/1.4	0.13	26.5	3.8	Oil, U-V-I
Olympus	APO	100/1.65	0.1	22	7.4	Oil, TIRFM, U-V-I
Zeiss	PL APO	20/0.8	0.55	25	10.2	Dry
Zeiss	PL APO	25/0.8	0.57	25	6.6	Multi-imm., SA corr., therm-insul.
Zeiss	PL APO	40/1.4	0.13	25	24.0	Oil, U-V-I
Zeiss	C-APO	40/1.2	0.28	25	13.0	Water imm., SA corr., U-V-I
Zeiss	PL FLUOR	63/1.3	0.17	25	7.2	Multi-imm, SA corr, therm-insul.

Recent objective designs optimize one or more parameters for efficient fluorescence imaging, including brightness, contrast, spherical aberration, chromatic correction, working distance, water immersion, among others. Abbreviations are: magnification/numerical aperture (Mag/NA), working distance (WD), and field number (FN). Brightness (B) is calculated as $NA^4/M^2 \times 10^4$ for epi-illumination fluorescence imaging.

objective, can be mounted on an upright microscope and partially immersed into a Petri dish or chamber containing the specimen in aqueous medium. Dipping objectives frequently have a long working distance for use in physiology, a ceramic casing that acts as an insulator to minimize temperature changes in the medium, and a correction collar to correct for residual spherical aberration from differences in refractive index and temperature.

- *Multi-immersion objectives* are used in cases where it is necessary to image specimen details that are several micrometers away from the coverslip surface and where the refractive index of the tissue and/or the mounting medium causes blurring. Histological specimens are frequently mounted in aqueous media, glycerol,

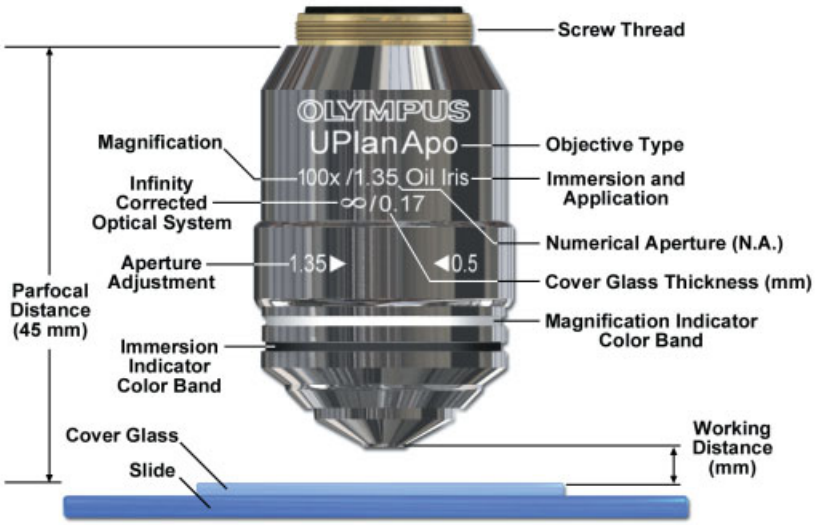

Mag.	1×	2×	4×	10×	20×	40×	50×	60×	100×
Code	Black	Gray	Red	Yellow	Green	Light Blue		Dark Blue	White
Imm. Med.	Oil		Water		Glycerin	Oil/Water/Glycerin			
Code	Black		White		Orange	Red			

Figure 4.13

Key for interpreting the markings on the decorative barrel of an objective. Markings on the objective barrel indicate the type of lenses and correction, initial magnification, immersion medium, numerical aperture, lens–image distance, and required coverslip thickness. For quick reference, the color-coded ring, farthest from the thread, denotes the type of immersion medium (black-immersion oil, white-water, orange-glycerin, yellow-methylene iodide, and red-multi-immersion).

or even Mowiol, Canada balsam or other solidifying media. With a multi-immersion objective, one can choose the appropriate immersion medium (oil, glycerol, water) and adjust the correction collar on the objective to get the best image definition.

- *UV objectives* made of quartz and other UV-transparent materials support imaging in the near-UV and visible range (240–700 nm) and are used for calcium imaging and in applications requiring uncaging and photoactivation.

Markings on the Barrel of an Objective

The engraved markings on the barrel of the objective describe the contrast type, magnification, NA, required coverslip thickness if applicable, and type of immersion medium (Fig. 4.13).

Image Brightness

Notice in Table 4.1 that the ratio of NA to magnification determines the light-gathering power of an objective and hence the image *brightness* (*B*). *B* is defined through relationships to NA and magnification (*M*) as:

$$B \propto (\mathrm{NA}/M)^2 \text{ (transillumination mode)},$$

and

$$B \propto (\mathrm{NA}^4/M^2) \text{ (epi-illumination mode)},$$

where *M* is the magnification, and NA is the numerical aperture, a geometric parameter related to the light-gathering power of an objective. NA as a primary determinant of the spatial resolution of an objective is discussed in Chapters 5 and 6. The values for magnification and NA are indicated on the lens barrel of the objective. A 60×/1.4 NA apochromatic objective gives among the brightest images, and because its image is color corrected across the entire visual spectrum and is flat and substantially free of common aberrations, it is popular in fluorescence microscopy. The 40×/1.3 NA fluorite objective is significantly brighter, but is less well corrected.

Objective Parfocality

In order to enable a set of microscope objectives to be interchanged with minimal refocusing, manufacturers build their instruments so that the objectives have a fixed dimension, called the *parfocal distance*, from the mounting hole in the nosepiece to the focal point on the specimen. Therefore, a set of parfocally matched objectives, such as 10–100× plan-achromats, project an image to approximately the same plane in the microscope body tube. When the nosepiece is rotated to change to a new parfocal objective, the operator can reestablish focus with only a minor adjustment to the fine focus knob. Most manufactures use a parfocal distance of 45 mm, but Nikon microscopes have a longer, 60-mm parfocal distance that is designed to achieve longer working distances with large NA objectives. Aside from the ease of operation with parfocal objectives, they should also be considered a safety feature to prevent collisions between the objective and the specimen slide when switching from a low to high magnification objective.

CONDENSERS

Imaging performance by a microscope depends not only on the objective but also on the light delivery system, which includes the illuminator and its collector lens, and of particular importance, the condenser. High-performance condensers are corrected for chromatic and spherical aberrations and curvature of the focal plane (field curvature). However, most of these aberrations are still apparent when using the Abbé condenser, a very common condenser that is based on a two-lens design (Fig. 4.14). The three-lens aplanatic condenser (indicating correction for spherical aberration and field curvature)

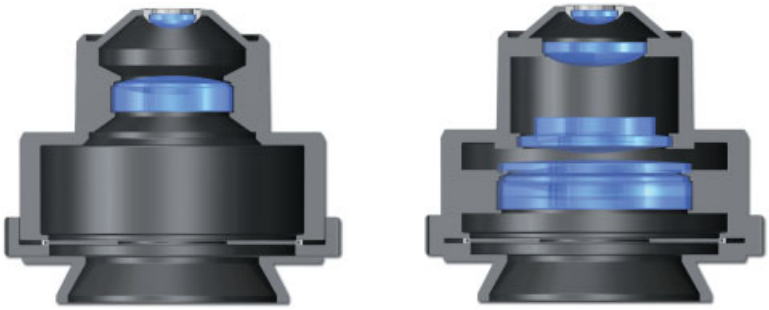

Figure 4.14
Two common microscope condensers. (a) The Abbé condenser contains two achromatic doublet lenses and gives very good performance for dry lenses of low to medium power. (b) The achromatic–aplanatic condenser is useful for lenses with NA > 0.5, and is essential for oil immersion lenses with high numerical apertures. For low NA performance, the top element on some condensers can be removed. This condenser focuses light in a flat focal plane and is highly corrected for the significant lens aberrations.

is superior but still exhibits chromatic aberration. The highly corrected achromatic–aplanatic condenser has five or six lenses including two achromatic doublet lenses, provides NAs up to 1.4, and is essential for imaging fine details using immersion-type objectives. These condensers are corrected for chromatic aberration at red and blue wavelengths, spherical aberration at 550 nm, and field curvature. Such a condenser can be used dry for NAs up to ~0.9, but requires immersion medium for higher NA values, although the condenser is commonly used dry even with oil immersion objectives. Note, however, that for maximal resolution in transmitted light mode, the NA of the condenser should be equal to the NA of the objective, which requires that both the condenser and the objective are oiled.

OCULARS

Oculars or eyepieces are needed to magnify and view the image produced by the objective. To make optimal use of the resolution afforded by the objective, an overall magnification equal to 500–1000 times the NA of the objective is required. More magnification than this produces "empty" magnification, a case where the image appears highly magnified, but blurry. For most applications, 10× eyepieces work well. When higher magnifications are required for a specific objective, a magnifying booster lens (in Zeiss microscopes, an Optovar lens magnification system) can be placed in the optical path. Alternatively, a different set of higher-magnification eyepieces can be employed. If the eyepiece is examined when the microscope is focused and the lamp turned on, a bright disk can be seen floating in space a few millimeters outside the eyepiece. The disk is called the *exit pupil* or *Ramsden disk* and represents the aperture at the rear focal plane of the objective. When viewing a focused specimen, the exit pupil of the eyepiece will be found to be coincident with the *entrance pupil* of the eye, an adjustment that occurs automatically as we focus the specimen.

Eyepiece specifications are engraved on the eyepiece barrel to indicate their magnifying power and field of view. An eyepiece engraved 10×/20 indicates a 10× magnification and 20-mm diameter field of view. The field of view marking also provides a quick reference for determining the diameter of the field in the specimen plane as seen with a given objective. For example, when combined with a 100× objective, this eyepiece would give 20 mm/100, or 200 μm for the diameter of the object field. Other special design features of the ocular are designated by letter codes, the most common of which indicate high eye point (distance between ocular surface and Ramsden disk) for eyeglass wearers, additional corrections for color and flatness of field, and widefield or wide angle of view. Eyepieces also come with focusable and nonfocusable eye lenses. At least one focusable eyepiece should be included on the microscope to allow parfocal adjustment of the optics, so that the same focal plane examined by the eye will be in focus on a camera mounted on the microscope. Oculars are based around a general design containing two achromatic doublet lenses (the field and eye lenses) and a *field stop*, a raised ridge or flange along the inside wall of the ocular that marks the site of the intermediate image plane. In oculars of so-called Huygenian design, the field stop and image plane are located between the field and eyepiece lenses; in Ramsden designs, the focal plane and field stop are located in front of the field lens below the eyepiece. To use an eyepiece reticule, the eyepiece is unscrewed and the reticule is placed in the image plane and rests on the flange comprising the field stop (see Fig. 1.12).

MICROSCOPE SLIDES AND COVERSLIPS

Many objectives are designed to be used with standard (1.1-mm thick) glass slides and coverslips of a certain thickness, usually 0.17 mm, which corresponds to thickness grade #1.5. Other coverslip thicknesses induce spherical aberration and give poorer performance, especially when used with high, dry objectives above 40×. For objectives with an NA < 0.4, coverslip thickness is not particularly important. *Remember the thickness of your slides and coverslips counts!* Refer to the following chart when ordering coverslips:

Grade Number	Thickness (μm)
0	83–130
1	130–160
1.5	160–190 (standard)
2	190–250

THE CARE AND CLEANING OF OPTICS

Maintenance and care are required to protect an expensive optical instrument and to guarantee that optimal high-contrast images will be obtained from it. Neglect, such as not removing immersion oil, forgetting to cover open ports and apertures, or accidental twisting or dropping of an objective can ruin optical performance. Even if the microscope is left unused but unprotected on the lab bench, image quality can deteriorate rapidly due to the accumulation of dust from the air. James and Tanke (1991) and Inoué and Spring (1997) provide detailed descriptions on the effect of dirt on the microscope

image and the cleaning of optical surfaces. The following are a few tips for maintaining the performance and image quality of your microscope.

Dust

Keep the microscope protected with a plastic or cloth cover. Wipe dust off the microscope body and stage with a damp cloth. Keep the objective turret spotless and free of dust, immersion oil, spilled culture medium, and salt solutions. Hardened thread grease, or, additionally, on inverted microscopes, dried immersion oil, buffers, and media, can weld objectives onto the rotating objective turret making them difficult to remove or exchange. If an objective is frozen fast, place a drop of water (if salts) or oil-penetrating agent (if oil) at the lens-turret interface to loosen the material before trying to remove the objective. Keep all openings covered with caps so that dust cannot enter the microscope and soil inaccessible lenses, mirrors, and prisms in the microscope body. Make use of the plastic caps designed to cover all objective ports, eyepiece sleeves, and camera ports that are unoccupied and empty. The internal optical pathway should always be completely protected from airborne dust. In routine use, the exposed lenses of the eyepieces usually accumulate dust, debris, and eyelashes very quickly. They can be cleaned easily using a chamois or cotton swabs moistened with lens cleaner (Fig. 4.15).

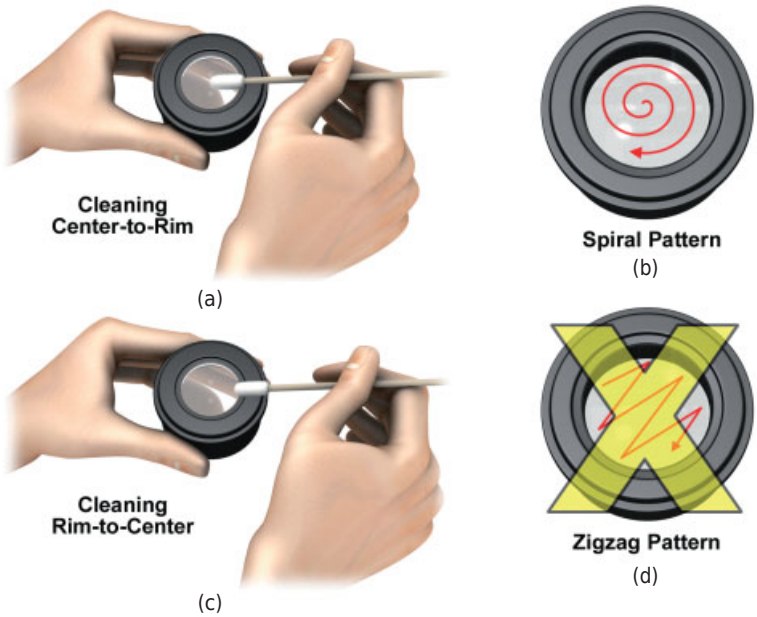

Figure 4.15

Cleaning eyepiece lenses. (a) Cleaning is achieved using a spiral motion of a moistened cotton swab from the center to the rim. (b) Correct spiral pattern used to clean lens surface. (c) Avoid cleaning the lens rim-to-center. (d) Never wipe using zigzag movements as this will only spread the dirt.

Immersion Oil

When finished with an observing session, gently wipe off and clean away excess oil with a high-quality lens tissue and then clean the lens surface with an agent designed for cleaning microscope optics. Immersion oil is a slow-acting solvent that can weaken the cementing compounds that act as a seal between the front lens element and the metal lens cap of the objective. Residual oil should be removed with a lens tissue wetted with a mild lens cleaner, such as the solution sold by Edmund Scientific Company (Barrington, NJ). Commercial glass cleaners, such as Sparkle and Windex, are also effective in removing immersion oil, but these generally contain an acid or base that has the potential to erode the antireflection coating on the front lens element and should be used only if a neutral cleaner is not available. For more tenacious deposits one can try, in order, ethanol or ethyl ether. However, solvents, such as toluene or benzene, should be used rarely, if at all, as these chemicals will eventually dissolve the front lens sealing compounds. Generally, it is advisable to remove immersion oil and contaminating liquids with the objective still mounted on the microscope, as this will avoid mishandling or dropping, the worst accidents that can befall a valuable objective.

Scratches and Abrasions

Never wipe the surfaces of objectives with papers or cloths that are not certified to be free of microscopic abrasives. All objectives contain an exposed optical surface that must be protected from abrasion. Strands of wood fibers in coarse paper, or worse, the stick end of a cotton swab applicator, are strong enough to place dozens of permanent scratch marks (sleeks) on the front lens element with a single swipe. Once present, scratches cannot be removed, and their effect (even if hardly visible) is to scatter light and permanently reduce image contrast. Further, most lenses contain an antireflection coating composed of layers of a dielectric material; each layer is just a few atoms thick. Although antireflection surfaces are protected with a layer of silicon monoxide, you should use only high-quality lens tissue and apply only a minimum of force to wipe off drops of excess oil.

Mechanical Force

Never apply strong physical force to an objective or other optical component. To bring another objective into position, move the rotating turret; do not grab and pull on an objective to bring it into position. Also, never remove a stuck objective with a vice-grips or a pipe wrench! If the threads of an objective become stuck to the rotating turret from dried culture medium, oil, or corrosion, apply a drop of water or lens cleaner or penetrating oil to loosen the objective and avoid using force. Likewise, never drop an objective onto the lab bench or floor. Also, do not allow an objective to strike exposed edges of the microscope stage or the condenser (easy to do on some inverted microscope designs). Impacts of this kind cause two forms of irreparable damage. (1) They can crack the compounds that seal the top lens element and metal lens cap, thus allowing immersion oil to penetrate into the lens and coat internal lens elements, causing permanent damage. (2) They can induce permanent stresses in the glass lens components of an objective and may severely degrade its performance in sensitive forms of light microscopy that use polarized light.

Exercise: Constructing and Testing an Optical Bench Microscope

Microscope construction and testing

- Determine the focal lengths of various simple lenses using the method described in the text and label them with pieces of lab tape applied to their edges. Use three 50-mm lenses for the objective, the ocular, and illuminator's collector lens to construct an optical bench microscope using a "meter stick optical bench".
- Mount in order of sequence on the optical bench: a tungsten lamp illuminator, 50-mm collector lens, specimen holder, objective, and ocular.
- Handwrite the letter *a* with a fine marker pen on a sheet of lens tissue or on a microscope slide, and tape it to the specimen holder, centering the letter on the optical axis.
- Position the collector lens about 75 mm away from the lamp filament. Position the specimen about 20 cm away from the collector lens. The light from the illuminator should be focused into a 1–2-cm diameter spot centered on the object (the letter *a*).
- Using the lens equation $1/f = 1/a + 1/b$, calculate the object-lens distance that gives an image-lens distance of ~30 cm, and mount the objective at the calculated position.
- Place a sheet of paper (a paper screen) at the 30-cm location to confirm that the intermediate image of the letter *a* is both real and magnified. Notice that the intermediate image is both inverted and upside-down. Confirm that it is necessary to position the objective between 1 and 2 focal lengths away from the object to obtain a magnified real intermediate image of the object as shown in Figure 4.8c.
- Place a paper screen in the plane of the virtual image to confirm that it is indeed virtual—that is, no image is produced on the screen. You have now created a compound light microscope!

Answer the following questions about your microscope:

1. Is the object located precisely at the focal length of the objective?
2. Is the real intermediate image located precisely at the focal length of the ocular?
3. Explain why the eye–brain perceives a magnified virtual image, while the retina receives a real image from the ocular lens.

Objective aberrations

Prepare a specimen consisting of a piece of aluminum foil with a dozen small pinholes contained within a 5-mm diameter circle, and mount it on the optical

bench microscope. The ideal specimen has some pinholes on or close to the axis and other pinholes near the periphery of the field of view. What lens aberrations do you observe while examining the pinhole images? Here are some tips:

- *Chromatic aberration.* Move the objective back and forth through focus and notice how the fringes around the points of light change color depending on the lens position.
- *Spherical aberration.* Pinholes at the periphery of the visual field look blurry. The blurriness can be reduced by creating a 5-mm hole in an opaque mask and placing it in the rear focal plane of the objective.
- *Coma and astigmatism.* At best focus, peripheral pinholes look like streaks with comet tails that radiate from the center of the field (coma). As the objective is moved back and forth through the plane of best focus, the streaks become drawn out into elliptical shapes that change their orientation by 90° on each side of focus (astigmatism).
- *Distortion and curvature of field.* At best focus, the focal plane is curved like the shape of a bowl, so only one zone of a certain radius can be focused at any one time (curvature of field). To view pincushion or barrel distortion, replace the pinhole specimen with a fine mesh copper grid used for electron microscopy and examine the pattern of the square mesh of the grid on the viewing screen (distortion).

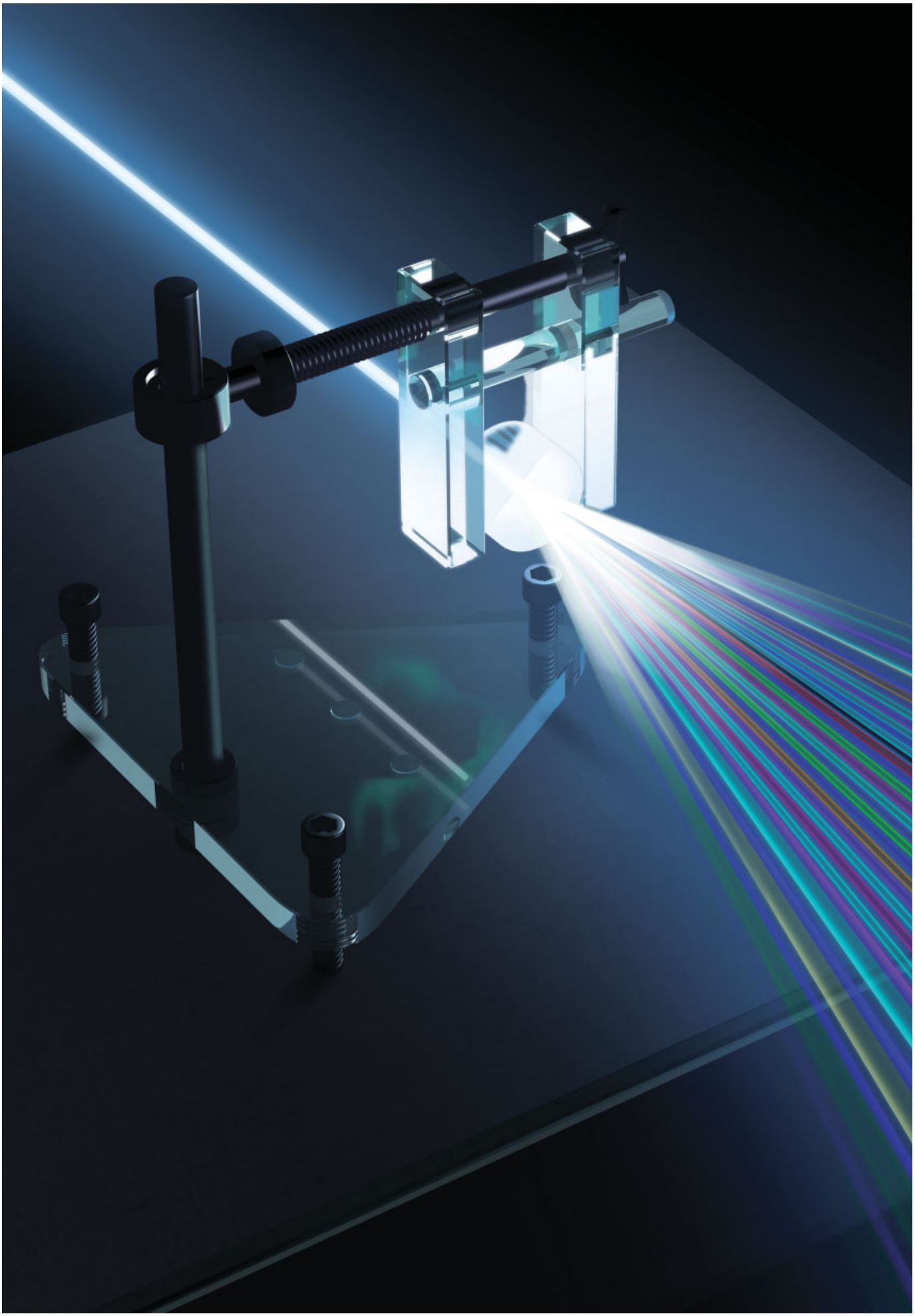

CHAPTER
5

DIFFRACTION AND INTERFERENCE IN IMAGE FORMATION

OVERVIEW

This chapter deals with diffraction and interference in the light microscope—the key principles that determine how a microscope forms an image. Having just concluded a section on geometrical optics where image locations and foci are treated as points, lines, and planes, it is surprising to learn that in the microscope the image of a point produced by a lens is actually an extended spot surrounded by a series of rings and that a focal plane is contained in a three-dimensional slab of finite thickness. These properties are due to the diffraction of light (Fig. 5.1). In the microscope, light from the illuminator is diffracted (literally broken up in the sense of being scattered or spread) by the specimen, collected by the objective (a second site for diffraction), and focused in the image plane, where waves constructively and destructively interfere to form a contrast image. In fluorescence imaging, waves of fluorescent light experience diffraction in the front aperture of the objective. The scattering of light (diffraction) and its recombination (interference) are phenomena of physical optics or wave optics. We study these processes because they demonstrate how light, carrying information from an object, is able to create an image in the focal plane of a lens. With a working knowledge of diffraction, we understand why adjusting the condenser aperture and using oil immersion techniques affect spatial resolution. Diffraction theory also teaches us that there is a limit beyond which a lens cannot resolve fine spatial features in an object. In studying diffraction, we see that complex optical phenomena can be understood in mathematically precise and simple terms, and we come to appreciate the microscope as a sophisticated optical instrument. Readers interested in the physical optics of diffraction and interference of light can refer to the excellent texts by Hecht (2001) and Pluta (1988).

Diffraction of light at a grating.

Fundamentals of Light Microscopy and Electronic Imaging, Second Edition.
Douglas B. Murphy and Michael W. Davidson.

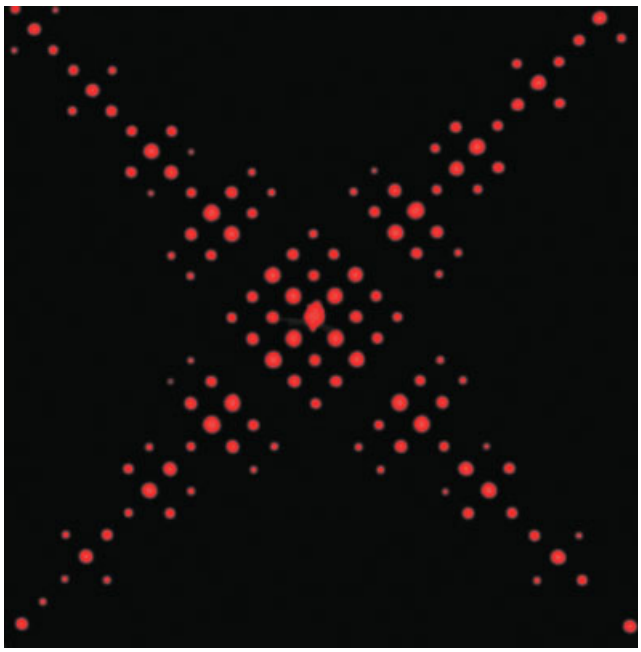

Figure 5.1
Diffraction image of a copper mesh grid. A 400-mesh grid was illuminated with a laser pointer, and its diffraction pattern was photographed on a projection screen. Multiple diffraction spots are observed due to the relatively large spacing between grid bars and the coherent laser light source.

DIFFRACTION AND INTERFERENCE

Diffraction is the spreading of light that occurs when a beam of light interacts with an object. Depending on the circumstances and type of specimen, diffracted light is perceived in different ways. For example, when a beam of light is directed at the edge of an object, light appears to bend around the object into its geometric shadow, a region not directly illuminated by the beam (Fig. 5.2a). The situation reminds us of the behavior of water waves incident on a log floating in a pond. The waves wrap around the ends of the log into the geometrical shadow; instead of reflecting away from the ends of the log, they seem to grab hold of the ends and swing themselves around into the sheltered zone.

The redirected component of diffracted light is easily observed when a tree or person is backlighted by a strong light source under conditions where the background behind the object is still dark; the bright line outlining the silhouette of the object is diffracted light. Of particular interest to us is the image of a point source of light in the microscope, since images are composed of a myriad of overlapping points. As we will see, waves emanating from a point in the object plane become diffracted at the margins of the objective (or at the edges of a circular aperture at the rear focal plane of the lens), causing the image of the point to look like an extended disk or spot. Thus, the image of a point in a microscope is not a point at all, but a diffraction pattern with a central

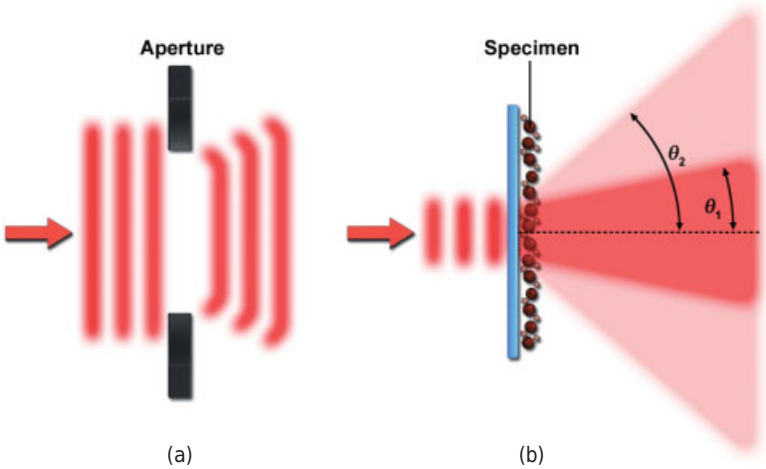

Figure 5.2

Diffraction at an aperture and at a specimen with fine particles. (a) The electric field of a planar wavefront becomes disturbed by diffraction upon passage through an aperture. The waves appear to grab hold of the aperture and swing around into its geometric shadow. The amplitude profile of a transmitted wavefront is also no longer uniform and remains permanently altered after passage through the aperture (not shown). (b) A substrate containing a layer of a mixture of fine particles (0.2- and 2-μm diameter) diffracts an incident planar wavefront into scattered beams that diverge at different angles. The angle of spreading (θ) is inversely proportional to the size of the particles, so θ_1 corresponds to light diffracted by the larger particles.

disk of finite diameter. Because of diffraction, an object's image never perfectly represents the real object, and there is a limit below which an optical system cannot resolve structural details.

Diffraction is also observed when a beam of light illuminates a microscope slide covered with fine dust or scratches (Fig. 5.2b). The spreading of an automobile's headlight beams on a foggy night is another good example of the phenomenon. In these cases, diffraction is defined as the scattering of light by small particles having physical dimensions similar to the wavelength of light. The amount of scattering and angle of spreading of the beam depend on the size and density of the light-diffracting particles. In the case of illuminated specimens in the microscope, there are therefore two primary sites of diffraction: one at the specimen itself and another in the aperture of the objective. Image formation by a lens is critically dependent on these events. If light passes through an object in a light microscope but does not become absorbed or diffracted, it remains invisible. It is the spreading action or diffraction of light at the specimen that allows objects to become visible, and the theory of image formation is based on this principle.

Just as diffraction describes the scattering of light by an object into divergent waves, *interference* describes the recombination and summation of two or more superimposed waves, the process responsible for creating the real intermediate image of an object in the focal plane of a microscope. In a physical sense, diffraction and interference are manifestations of the same process. The traditional way of describing interference is to show the recombination of waves graphically in a plot depicting their amplitude, wavelength, and relative phase displacement (Fig. 5.3). The addition of two

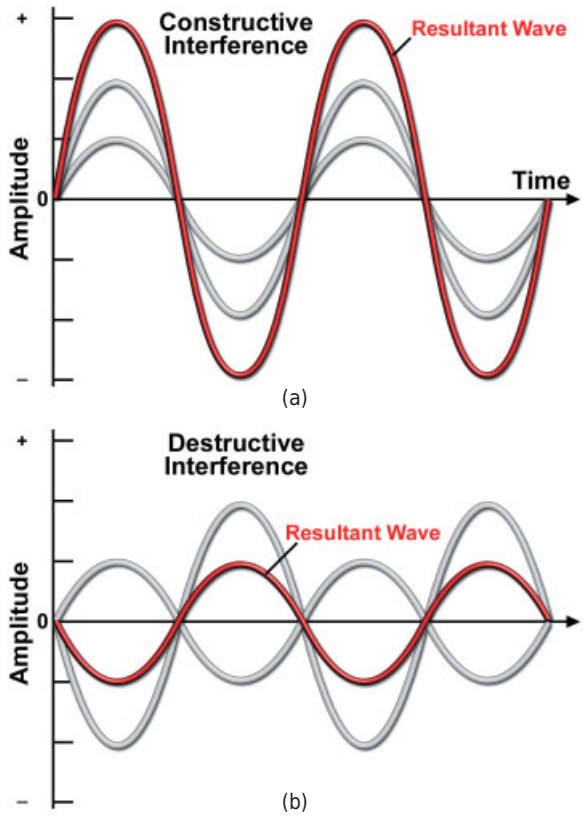

Figure 5.3

Two coincident waves can interfere if their E vectors vibrate in the same plane at their point of intersection. Two waves are shown that vibrate in the plane of the page. In these examples, both waves (tinted gray) have the same wavelength, but vary in amplitude. The amplitude of a resultant wave (red curve) is the arithmetic sum of the amplitudes of the two original waves. (a) Constructive interference occurs for two waves having the same phase. (b) Destructive interference occurs for waves shifted in phase; if the amplitudes of the waves are the same and the relative phase shift is $\lambda/2$, the wave is eliminated.

initial waves produces a resultant wave whose amplitude may be increased (*constructive interference*) or diminished (*destructive interference*).

The term *interference* is frequently taken to mean that waves annihilate each other if they are out of phase with each other by $\lambda/2$, and indeed a graphical depiction of interfering waves reinforces this idea. However, since it can be demonstrated that all of the photon energy delivered to a diffracting object, such as a diffraction grating, can be completely recovered (e.g., in a resultant diffraction pattern), it is clear that photons do not self-annihilate; rather, their energies become redistributed (channeled) during diffraction and interference in directions that permit constructive interference. Likewise, interference filters do not destroy the light they do not pass; they merely reflect or absorb it. It is therefore best to think of diffraction and interference as phenomena involving the redistribution of light waves and photon energy. Accordingly, wave constructions of the kind shown in Figure 5.3 are best thought of as devices

that help us calculate the energy traveling in a certain direction or reaching a certain point. The mechanism by which light energy becomes redistributed is still not understood, but we recognize the principle that diffraction and interference channel photon energy to regions where it can be constructive and away from regions where it is destructive. We referred to this property when describing the action of interference filters in Chapter 3.

THE DIFFRACTION IMAGE OF A POINT SOURCE OF LIGHT

The image of a self-luminous point object in a microscope, telescope, camera, or any other image-generating instrument is a diffraction pattern created by the action of interference in the image plane. The situation is directly related to the observation of fluorescent beads in a fluorescence microscope. When highly magnified, the image is observed to consist of a central spot or diffraction disk surrounded by a series of diffraction rings. In the nomenclature of diffraction, the bright central spot is called the 0th order diffraction spot, and the rings are called the 1st, 2nd, 3rd, ... order diffraction rings (see Fig. 5.4). When the objective is focused properly, the intensity of light

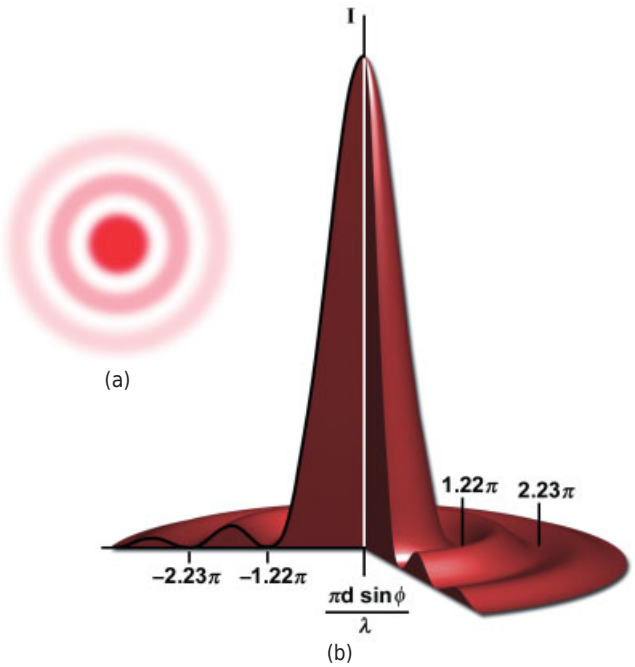

Figure 5.4

The diffraction pattern of a point source of light. (a) Diffraction pattern showing central diffraction disk surrounded by diffraction rings. (b) Intensity profile of a diffraction spot. The central spot and surrounding rings are evident. The separation distance between the center of the spot and the first minimum depends on the angular aperture of the lens. The units of distance (π) on the x-axis result from the formula used to calculate shape of the intensity profile.

at the minima between the rings is zero. As we will see, no lens-based imaging system can eliminate the rings or reduce the spot to a point. The central diffraction spot, which contains ~84% of the light from the point source, is also called the *Airy disk*, after Sir George Airy (1801–1892), who described some of its important properties.

The Airy disk pattern is due to diffraction, whose effect may be described as a disturbance to the electric field of the wavefront in the aperture of the lens—the consequence of passing an extended electromagnetic wavefront through a small aperture. The disturbance propagates with the wavefront and continues to alter the amplitude profile of the wavefront as the front converges to a focus in the image plane. Diffraction (the disturbance) constantly perturbs the incident wavefront, and since no one has invented a lens design to remove it, we must accept its alteration of points comprising the image. The size of the central disk in the Airy pattern is related to the wavelength λ and the aperture angle of the lens. For a telescope or camera lens receiving an incident planar wavefront from an infinitely distant source, such as a star, the aperture angle is given as the focal ratio f/D, where D is the lens diameter and f is the focal length. In this case, the *aperture angle* is the angular diameter of the lens as seen from a point in the image plane at focal length f. The size of the diffraction disk radius d is given by:

$$d = 1.22\lambda(f/D).$$

In a microscope, the aperture angle is described by the numerical aperture NA, which includes the term $\sin\theta$, the half-angle over which the objective can collect light coming from a nearby object. (NA is defined further in Chapter 6.) In the case of a microscope image, the radius d of the diffraction spot for a self-luminous point of light in the image plane is described by a related expression:

$$d = 1.22\lambda/2\text{NA}.$$

In both situations, the size of the spot decreases with decreasing wavelength and increasing numerical aperture, but always remains a disk of finite diameter. The spot size in the focal plane produced by a 25× oil immersion objective with NA = 1 is about 8 μm. An image in which resolution is limited by the size unit diffraction spot, rather than by scattered light or lens aberrations, is called *diffraction limited*. We examine the relationship between diffraction and resolution in Chapter 6.

In cameras and telescopes, the image of a star is likewise always a finite diffraction disk (not a point) with linear radius $r = 1.22\lambda(f/D)$, where f/D is called the *focal ratio* or *f*-number. Roughly, the diameter of the diffraction spot in micrometers is the focal ratio in millionths of a meter. Thus, the diameter of the diffraction spot in the primary focal plane of the 250-cm diameter, *f*/5 mirror of the Hubble Space Telescope is 5 μm. In the case of the human eye or photographic camera, the image of a point source on the retina or film has a diameter of about 3 μm. In all of these optical systems, the image of a point source corresponds to a diffraction disk, and the terms NA and f/D are measures of their effective aperture angle and light-gathering ability. As shown in this chapter, the spatial resolution of the microscope is limited by the smallest disk that it is possible to obtain by varying λ and NA. Only when the images of specimen details subtend diameters greater than this limit can you begin to obtain information regarding the size, shape, and periodicity in the object.

THE CONSTANCY OF OPTICAL PATH LENGTH BETWEEN OBJECT AND IMAGE

Before we examine the effect of lens diameter on diffraction spot size and spatial resolution, we need to consider the concept of optical path length for an imaging system containing a perfectly corrected lens. In practice, microscope objectives and other corrected lenses only approximate the condition of being perfectly corrected, and waves arrive at the conjugate image point somewhat out of place and out of phase. This is usually not a serious problem. Despite practical limitations in finishing lenses with spherical surfaces, most microscope lenses give diffraction-limited performance with an average error in phase displacement (wavefront error) of less than $\lambda/4$, and manufacturers strive to obtain corrections of $\lambda/10$ or better. As is known, light from a self-luminous point in an otherwise dark specimen plane radiates outward as an expanding spherical wavefront; waves collected by the objective are refracted toward the center line of the lens and progress as a converging spherical wavefront to a single point in the image plane. However, it also true—and this point is critical for image formation—that *the number of vibrations, as well as the transit time experienced by waves traveling between an object point to the conjugate image point, are the same regardless of whether a given wave passes through the middle or the periphery of the lens*.

Demonstration: Viewing the Airy Disk with a Pinhole Aperture

It is easy to observe the Airy disk by examining a point source of light through a pinhole (Fig. 5.5). This is best done in a darkened room using a bright lamp or microscope illuminator whose opening is covered with a small piece of aluminum foil containing a pinhole that will serve as a point source of light when viewed at a distance of several feet. The illuminator's opening should be completely covered so that the amount of stray light is minimal. A second piece of foil is prepared with a minute pinhole, 0.5-mm diameter or less, and is held up to the eye to examine the point source of light at the lamp. The pinhole-eye lens system (a pinhole camera) produces a diffraction pattern with a central Airy disk and surrounding diffraction rings. The same observation can be made outdoors at night examining distant point sources of light with just the pinhole held over the eye. This simple diffraction pattern is the basic unit of image formation. If the eye pinhole is made a little larger, the Airy disk becomes smaller, in accordance with the principle of angular aperture we have described. Now turn on the room lights and look though the pinhole at objects in the room, which look dim (not much light through the pinhole) and blurry (low resolution). The blurry image is caused by large overlapping diffraction spots of image components on the retina. When the pinhole is removed and the objects viewed directly, the image is clearer because the larger aperture size afforded by the eye's lens results in smaller diffraction spots and an increase in resolution and clarity. We begin to appreciate that an extended image can be viewed as the summation of a myriad of overlapping diffraction spots.

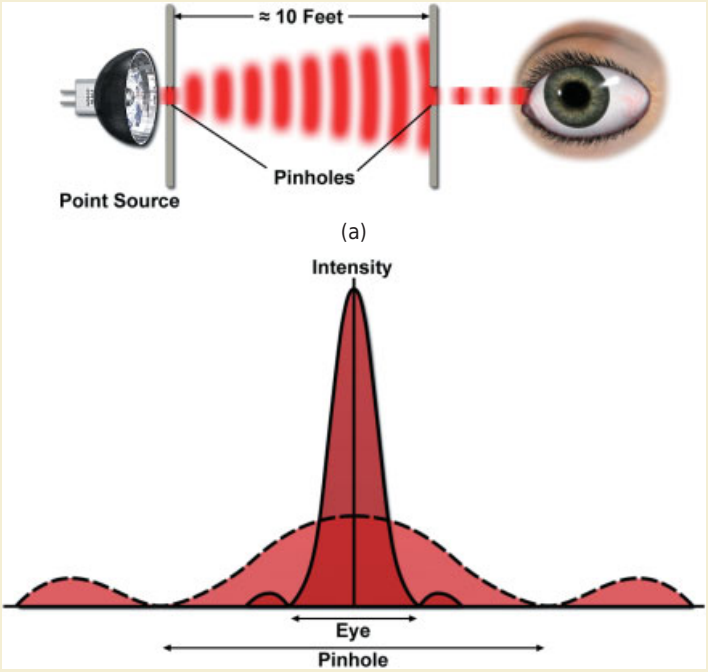

Figure 5.5

The image of a point source of light viewed through a pinhole is a perceptible disk. (a) Viewing a point source of light through a pinhole. (b) Relative sizes of the diffraction disk on the retina when a point source is viewed with unobstructed vision (solid line) and through a pinhole (dashed line). With a pinhole, the diffraction disk expands about 10-fold to 30–40 μm, covering a patch of hundreds of cone cells on the retina, thereby allowing perception of a visible diffraction disk and surrounding rings.

Ideally, all waves from an object point should arrive at the image point perfectly in phase with one another. Given the large differences in the spatial or geometric path lengths between central and peripheral waves, this seems improbable. The explanation is based on the concept of *optical path length*, a length distinct from the geometric path length. It can be used to calculate the number of vibrations experienced by a wave traveling between two points. As it turns out, variations in the thickness of the lens compensate for the differences in geometric paths, causing all waves to experience the same number of vibrations (Fig. 5.6). It can also be shown that the transit time required for light to travel between object and image points along different trajectories having the same optical path length is the same. These concepts become important when we discuss the spatial and temporal coherence of light later in the chapter.

In optics, the *optical path length* (OPL) through an object or space is the product of the refractive index n and thickness t of the object or intervening medium:

$$\text{OPL} = nt.$$

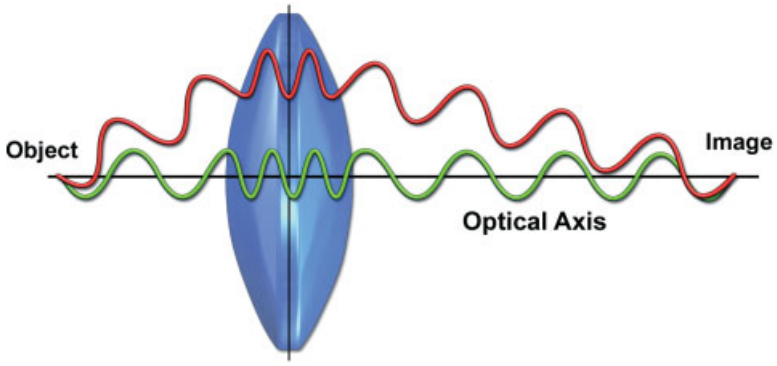

Figure 5.6

Preservation of the optical path length between the object and image. The optical path length may be regarded as the number of cycles of vibration experienced by a wave between two points. Two waves traveling in phase from a point in an object and entering the center and periphery of a lens cover different physical distances, but experience the same optical path length, and therefore arrive simultaneously and in phase at the conjugate point in the image plane. This occurs because the wave traveling the shorter geometric path through the middle of the lens is relatively more retarded in its overall velocity, owing to the longer distance of travel in a high-refractive-index medium (the glass lens). Note that the total number of cycles (the number of wavelengths) is the same for both waves.

If the propagation medium is homogeneous, the number of vibrations of a wave of wavelength λ contained in the optical path is determined as:

$$\text{Number of vibrations} = nt/\lambda.$$

Since the frequency of vibration remains constant and the velocity of light = c/n, when a wave traverses a lens of higher refractive index than the surrounding medium, *the wavelength and velocity decrease during transit through the lens*. Thus, the number of cycles of vibration per unit of geometrical distance in the lens is greater than the number of cycles generated over the equivalent distance in the surrounding medium. The overall optical path length expressed as the number of vibrations and including the portions in air and in glass is thus described as:

$$\text{Number of vibrations} = n_1 t_1/\lambda_1 + n_2 t_2/\lambda_2,$$

where the subscripts 1 and 2 refer to parameters of the surrounding medium and the lens. As we will encounter later on, the *optical path length difference*, Δ, between two rays passing through a medium alone versus through an object plus medium is given as:

$$\Delta = (n_2 - n_1)t.$$

EFFECT OF APERTURE ANGLE ON DIFFRACTION SPOT SIZE

Now let us examine the effect of the aperture angle of a lens on the radius of a focused diffraction spot. We consider a self-luminous point P that creates a spherical wavefront

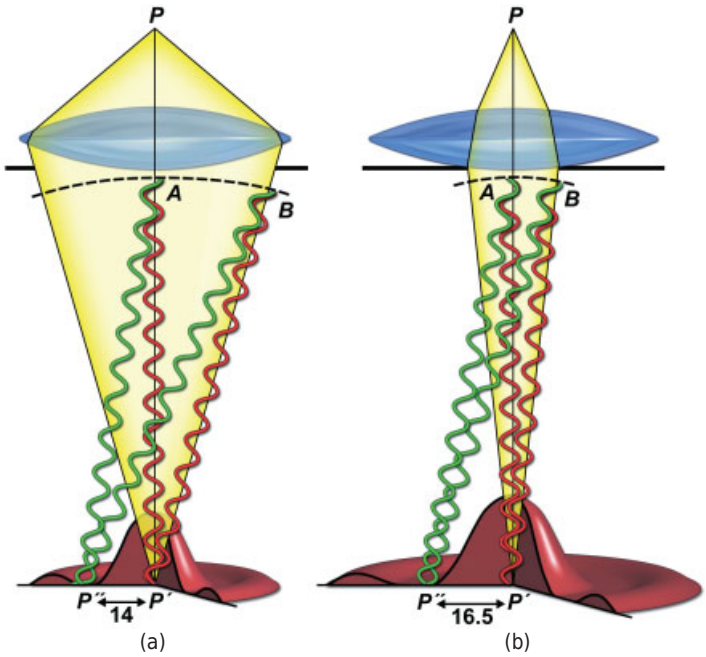

Figure 5.7

Aperture angle determines the size of the diffraction spot. Point source *P* and its conjugate image *P′* in the image plane. Point *P″* is moved laterally in the focal plane away from *P′* until destructive interference at a certain distance determines the location of the first diffraction minimum and thus the radius of the diffraction spot. (a) Points *A* and *B* in the wavefront with full lens aperture. (b) Points *A* and *B* in the wavefront with reduced aperture angle caused by partially stopping down the condenser iris diaphragm.

that is collected by the objective and focused to a spot *P′* in the image plane (Fig. 5.7a). In agreement with the principle of the constancy of optical path length, waves passing through points A and B at the middle and edge of the lens interfere constructively at *P′*. (The same result is observed if Huygens' wavelets [discussed in the next section] are constructed from points A and B in the spherical wavefront at the rear aperture of the lens.) If we now consider the phase relationship between the two waves arriving at another point *P″* displaced laterally from *P′* by a certain distance in the image plane, we see that a certain distance is reached where the waves from A and B are now 180° out of phase with each other and destructively interfere. The light intensity at this position (the first minimum in the diffraction pattern of the spot) is zero. Indeed, it can be shown that the *sum of contributions from all points in the aperture results in an amplitude of zero at this location and nearly so at all other locations in the image plane other than in the central diffraction spot and surrounding diffraction rings*. A geometrical explanation of the phenomenon is given by Texereau (1963).

In Figure 5.7b, we observe that a smaller aperture (closing down the condenser diaphragm in a conjugate focal plane) reduces the angular aperture of the optical system, which increases the size of the diffraction spot and the distance *P′P″* to the first diffraction minimum. Therefore, reducing the angular aperture decreases spatial resolution in the image. If we reexamine the optics of the pinhole camera, it now becomes clear why viewing a point source through a pinhole aperture held in front of the eye

allows perception of an observable diffraction disk (Fig. 5.5). For the fully dilated eye, the Airy disk of a point source covers ~2 cone cells on the retina, but with the reduced angular aperture using a pinhole, the disk diameter expands some 40-fold, stimulates dozens of receptor cells, and results in the perception of a disk.

DIFFRACTION BY A GRATING AND CALCULATION OF ITS LINE SPACING, *D*

We will now examine the diffraction of light by a specimen using a transparent diffraction grating as a model for demonstration and discussion. We should bear in mind that the principles of diffraction we observe at a grating on an optical bench resemble the phenomena that occur at specimens in the microscope. A *diffraction grating* is a planar substrate containing numerous parallel linear grooves or rulings, and like a biological specimen, light is strongly diffracted when the spacing between grooves is close to the wavelength of light (Fig. 5.8). If we illuminate the grating with a narrow beam from a

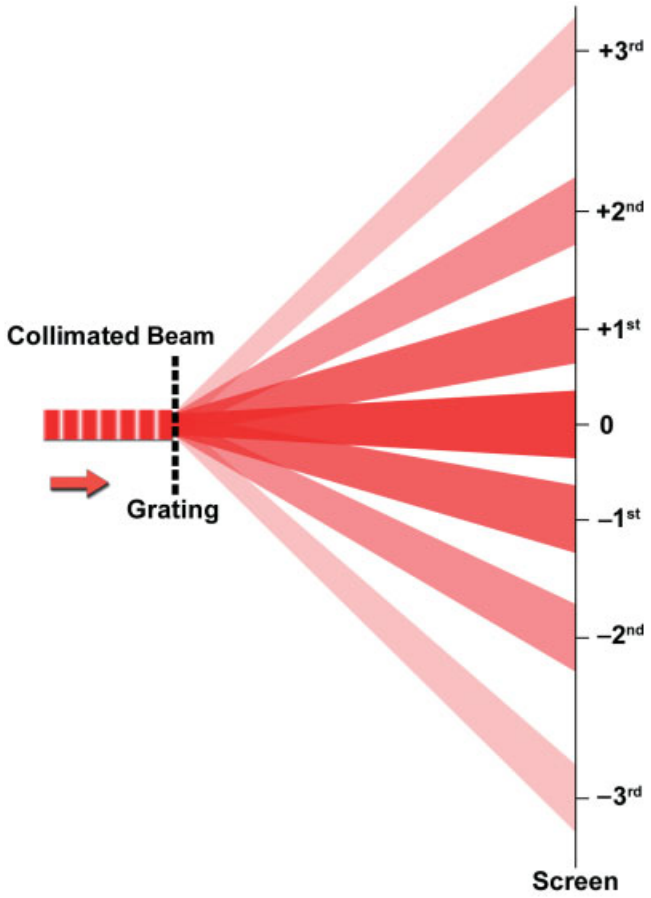

Figure 5.8
The action of a diffraction grating. Multiple orders of diffracted light are shown.

monochromatic light source, such as a laser pointer, and project the diffracted light onto a screen 1–2 m distant, a bright, central 0th order spot is observed, flanked by one or more higher order diffraction spots, the 1st, 2nd, 3rd, . . . order diffraction maxima. The 0th order spot is formed by waves that do not become diffracted during transmission through the grating. The spots are always arranged such that the orientation of an imaginary line containing them is perpendicular to the orientation of rulings in the grating. The diffraction spots identify unique directions (diffraction angles) along which waves emitted from the grating are in the same phase and become reinforced as bright spots due to constructive interference. In the regions between the spots, the waves are out of phase and destructively interfere.

The *diffraction angle* θ of a grating is the angle subtended by the 0th and 1st order spots on the screen as seen from the grating (Fig. 5.9). The right triangle containing θ at the screen is congruent with another triangle at the grating defined by the wavelength of illumination, λ, and the spacing between rulings in the grating, d. Thus, $\sin \theta = \lambda/d$, and reinforcement of diffraction spots occurs at locations having an integral number of wavelengths—that is, 1λ, 2λ, 3λ, and so on—because diffracted rays arriving at these unique locations are in phase, have optical path lengths that differ by an integral number of wavelengths, and interfere constructively, giving bright diffraction spots. If $\sin \theta$ is calculated from the distance between diffraction spots on the screen and between the screen and the grating, the spacing d of the rulings in the grating can be determined using the *grating equation*:

$$m\lambda = d \sin \theta,$$

where λ is the wavelength and m is an integral number of diffraction spots. (For calculations based on the distance between the 1st and 0th order spots, $m = 1$; if the distance between the 2nd and 0th order spots is used, $m = 2$, etc.). Notice that the diffraction angle θ *increases* as the grating spacing d *decreases* and as the wavelength λ *increases*.

The effect of wavelength can be demonstrated by illuminating the grating with white light. Under this condition, the 0th order spot appears white, while each higher order diffraction spot appears as an elongated spectrum of colors. Thus, the diffraction angle depends directly on the wavelength. Blue light, being most energetic, is scattered the least, so the blue ends of the spectra are always located closest to the 0th order central spot.

An alternate device, called *Huygens' principle*, can also be used to determine the location of the diffraction spots and diffraction angle θ of a grating. Christian Huygens, the Dutch physicist (1629–1692), used a geometrical construction for determining the location of a propagating wavefront, now known as the *construction of Huygens' wavelets* (Fig. 5.10). According to Huygens' principle, every point on a propagating wavefront serves as the source of *spherical secondary wavelets*, such that the wavefront at some later time is defined by the envelope covering these wavelets. Further, if wave propagation occurs in an isotropic medium, the secondary wavelets have the same frequency and velocity as the original reference wavefront. The geometrical construction of Huygens' wavelets is a useful device for predicting the locations of wavefronts as modified by both refraction and diffraction; however, Huygens' theory does not account for many wave-optical phenomena of diffraction, which require the application of newer approaches in physical optics.

When applied to the diffraction grating, we can use the construction of Huygens' wavelets to determine the location of the diffraction spots and the diffraction angle.

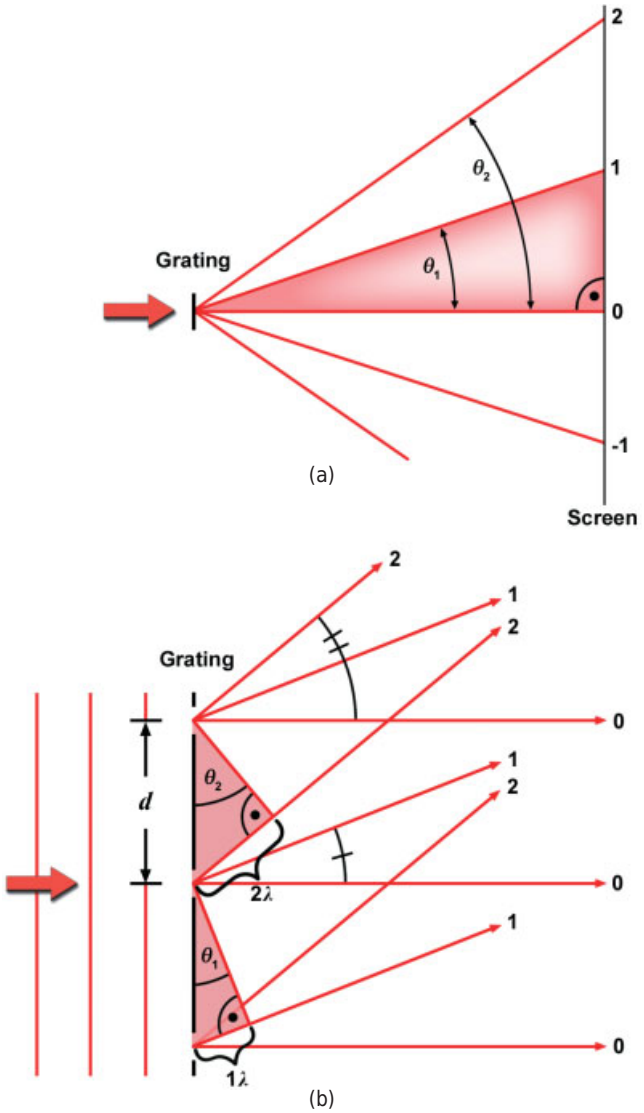

Figure 5.9

Dependence of scattering angle on grating spacing and wavelength. (a) Rays from a diffraction grating projected on a viewing screen. The angle of scattering of the 1st and 2nd order rays is shown as θ_1 and θ_2. The grating and 1st and 2nd order spots define a right triangle that includes θ_1 and is congruent with a triangle that can be delineated at the grating, as shown in panel b. (b) The diffracted rays at the grating define a right triangle that includes the diffraction angle θ. For the 1st and 2nd, . . . order diffracted rays, the base of the triangle is an integral number of wavelengths, 1λ, 2λ, and so on. Thus, the angle of diffraction depends on two parameters: the grating spacing d and wavelength λ.

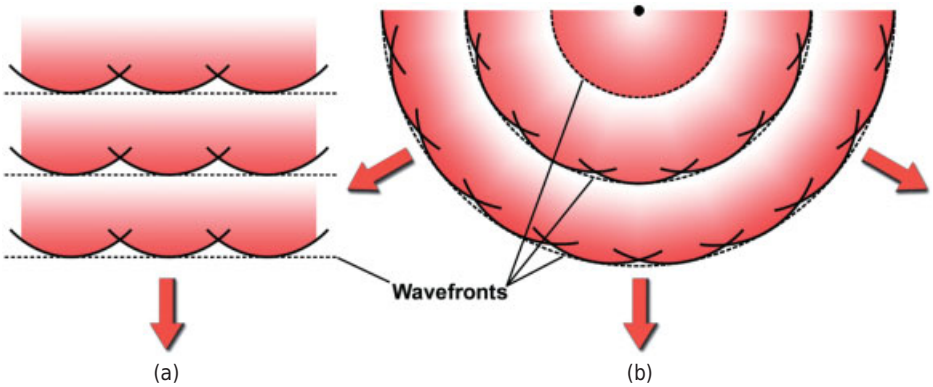

Figure 5.10
Constructions of Huygens' wavelets are used to describe the propagation of (a) planar and (b) spherical wavefronts.

Take a moment to study the construction for a diffraction grating with spacing d in Figure 5.11, which emphasizes the concept that the diffraction spots occur at angles where there is constructive interference. At locations between the diffraction spots, waves vary by a fraction of a wavelength and destructively interfere. Although Huygens' wavelet construction accounts for the locations of diffraction spots, it does not account for all aspects of the diffraction process. For example, the sum of all of the energy present in the luminous regions of the diffraction pattern is known to equal the energy incident on the grating. This is inconsistent with ray particle models and predictions from the geometrical construction of wavelets that photons are distributed uniformly on the diffraction screen, being annihilated where there is destructive interference. We enter here a murky area where the wave and particle natures of light are difficult to reconcile.

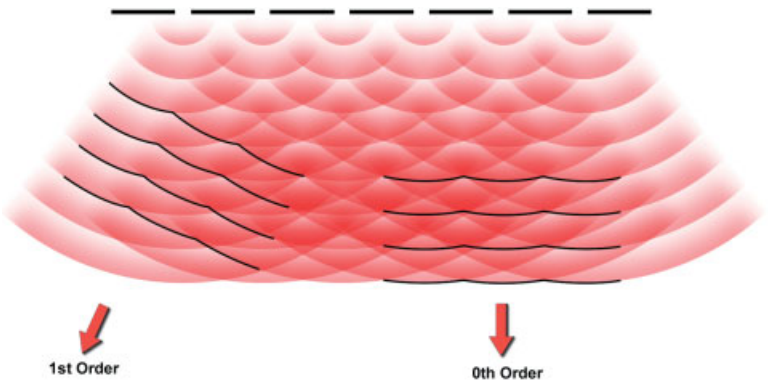

Figure 5.11
Geometrical determination of scattering angles in a diffraction grating using the construction of Huygens' wavelets. For simplicity, just two diffraction orders are shown.

Demonstration: The Diffraction Grating

It is possible to see the trajectories of diffracted rays by immersing a transparent diffraction grating replica in a dish of water. Fill a 9×12-in glass baking dish with water, add 1–2 mL of milk, and place the dish on a dark background. Place a small laser or laser pointer up against the dish and direct the beam at a diffraction grating immersed in the water. The rulings on the grating should be oriented vertically. The 0th order beam and higher order diffracted beams are made visible by the light-scattering properties of the micelles of lipid and protein in the milk. Notice that the diffracted rays are linear and sharply defined. Each point along a ray represents a location where overlapping spherical wavefronts emergent from each illuminated ruling in the grating give constructive interference, meaning that the waves are in phase with one another, differing precisely by an integral number of wavelengths. The dark spaces in between the rays represent regions where the wavefronts are out of phase and give destructive interference. The geometry supporting destructive interference does not mean, however, that light self-annihilates in the dark zones. For any given point located in the dark zone, it can be seen that there is no visible light between the point and the illuminated spot on the grating. Instead, diffraction results in the light energy being directed only along paths giving constructive interference. All of the light energy contained in the incident laser beam is contained in the 0th order and higher order diffracted rays. The diffraction angle θ that is subtended at the grating by the 0th order ray and a higher order diffracted ray depends on the refractive index of the medium and on the wavelength λ.

Illuminate a diffraction grating with a bright white light source and project the diffraction pattern on a wall or viewing screen (Fig. 5.12). It is convenient to use the I-beam optical bench so that the grating, filters, and masks can be stably mounted in holders clamped to the beam. If high-intensity xenon or mercury arc lamps are used, you should position a heat-absorbing filter (BG38 glass), or, better, a heat-reflecting mirror (hot mirror) between the lamp and the grating to keep the grating from melting. It is also useful to place a piece of aluminum foil with a 2–3-mm diameter hole immediately in front of the grating in order to block stray light (labeled "aperture" in drawing). On the viewing screen, notice the central 0th order spot, white and very bright, flanked on two sides by 1st, 2nd, and higher order diffraction spots, each of which appears as a bright spectrum of colors, with the blue ends of the spectra oriented toward the 0th order spot.

Higher-energy blue wavelengths are diffracted the least and are located closest to the 0th order spot within each diffraction-order spectrum and in accordance with the relation already given, showing that the diffraction angle $\theta \propto \theta/d$. It is easy to measure the angle θ by simple trigonometry, particularly when monochromatic light is used. When the grating is illuminated with monochromatic light from a red laser pointer, all of the diffraction spots appear as sharply defined points.

Using a white card as a screen, move the card closer to the grating. Observe that the diffraction angle defined by the grating and the 1st and 0th order diffraction spots remains constant and the spots move closer together as the card approaches the grating. It is easy to see the linear diffracted rays by darkening the room and introducing a cloud of chalk or talcum dust between the grating and the screen.

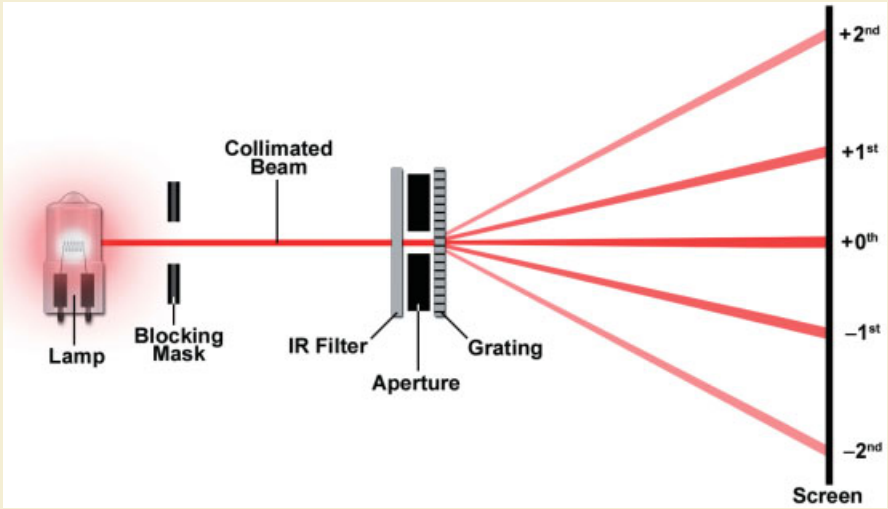

Figure 5.12

Demonstration of diffraction with a grating. An optical bench may be used to hold optical elements at fixed locations. A collimated bright white light source and a heat-cut filter are used to illuminate a diffraction grating covered by a closely apposed aperture mask containing a 2- to 3-mm hole or slit. If a slit is used instead of a hole, it should be perpendicular to the rulings in the grating.

Finally, examine the diffraction pattern of a sinusoidal (holographic) grating. The sinusoidal grating channels much of the incident light into the 1st order diffraction spots, which are much brighter than the spots produced by a conventional ruled grating. Such gratings are very useful for examining the spectra of filters and illuminators.

ABBÉ'S THEORY FOR IMAGE FORMATION IN THE MICROSCOPE

Ernst Abbé (1840–1905) developed the theory for image formation in the light microscope while working in the Carl Zeiss optical workshop in Jena, Germany (Fig. 5.13). Abbé observed that diffracted light from a periodic specimen produces a diffraction pattern of the object in the rear focal plane (the diffraction plane) of the objective. *According to Abbé's theory, interference between 0th and higher order diffracted rays in the image plane generates image contrast and determines the limit of spatial resolution that can be provided by an objective*. For a periodic object such as a diffraction grating, it is easy to demonstrate that light from at least two orders of diffraction must be captured by the objective in order to form an image (see Exercise, this chapter). In the minimal case, this could include light coming from two adjacent diffraction spots, such as the 0th and one 1st order spot generated by the grating. If light from only a single diffraction order is collected by the lens (only the 0th order is collected), there is no interference, and no image is formed. Put another way, there is no image if light diffracted at the specimen is excluded from the lens. Extending the concept further, the larger the number of diffraction orders collected by the objective, the sharper and better resolved (the greater the information content) are the details in the image.

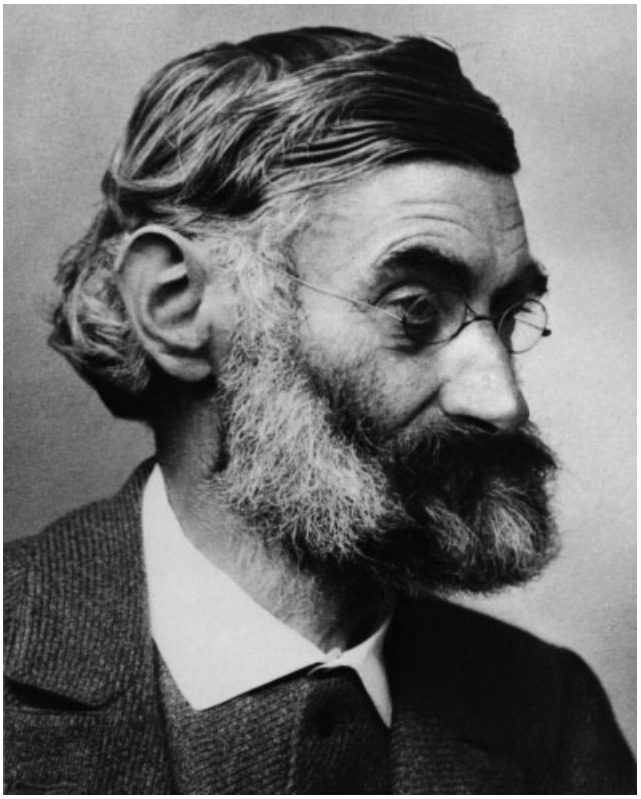

Figure 5.13

Ernst Abbé, 1840–1905. Principles of microscope and objective lens design, the theory of image formation in the microscope, and standardized lens manufacturing procedures all trace their beginnings to the work of Ernst Abbé and his collaborations with Carl Zeiss in Jena, Germany, in the 1860s. Until then, lens making was an art and a craft, but the new industrial philosophy demanded technical perfection, lens designs based on theory and research, and improvements in raw materials. At Abbé's initiative, lens curvatures were examined using an interference test with Newton's rings, and lens designs were based on Abbé's sine-squared condition to remove aberrations. He created the first plan achromatic lens, and after much research, the apochromatic lens, which was commercially sold in 1886. After many false starts over a 20-year period, the research theory-testing approach for manufacturing lenses proved to be successful. These improvements and new photographic lens designs required new types of glass with values of refractive index and color dispersion that were not then available. Abbé and Zeiss won grants and developed new glasses in collaborations with the industrialist, Otto Schott, owner of the Jena Glassworks. Other inventions were the Abbé achromatic condenser, compensating eyepieces for removing residual color aberration, and many other significant items of optical testing equipment. Abbé is perhaps most famous for his extensive research on microscope image formation and his diffraction theory, which was published in 1873 and 1877. Using a diffraction grating, he demonstrated that image formation requires the collection of diffracted specimen rays by the objective and interference of these rays in the image plane. By manipulating the diffraction pattern in the rear aperture, he could affect the appearance of the image. Abbé's theory has been summarized as follows: *The microscope image is the interference effect of a diffraction phenomenon*. Abbé also introduced the concept of numerical aperture ($n \sin\theta$) and demonstrated the importance of angular aperture on spatial resolution. It took 50 years for his theory to become universally accepted, and it has remained the foundation of microscope optical theory ever since. Ernst Abbé was also a quiet but active social reformer. At the Zeiss Optical Works, he introduced radical reforms, including the 8-hour day, sick benefits, and paid vacations. Upon his death, the company was handed over to the Carl Zeiss Foundation, of which the workers were part owners.

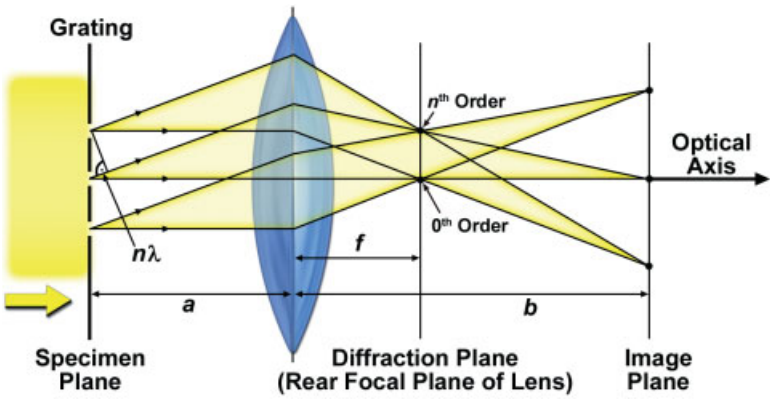

Figure 5.14

Abbé's theory for image formation in a light microscope. An objective focused on a grating ($2f > a > f$) in the object plane produces a magnified real image of the grating in the image plane. The diffraction plane is located at $1f$ in the rear aperture of the lens. An incident planar wavefront is shown. Diffracted *n*th order and nondiffracted 0th order rays are separated in the diffraction plane, but are combined in the image plane.

Objects that exhibit fine, periodic details (diffraction gratings, diatoms, and striated muscle) provide important insights about the roles of diffraction and interference in image formation. Figure 5.14 shows a diffraction grating with periodic rulings illuminated by a collimated beam of light having planar wavefronts. Light diffracted by the rulings is collected by a lens, and an image of the rulings is created in the primary image plane.

Note the following:

- A certain amount of incident light does not interact with the specimen and is transmitted as undeviated (nondiffracted) rays. These rays form the central 0th order diffraction spot in the diffraction plane and go on to evenly illuminate the entire image plane.
- Each ruling in the grating acts as an independent source of diffracted waves that radiate outwards as a series of spherical wavefronts (Huygens' wavelets) toward the objective. Note that the aperture of the lens is large enough to capture some of the diffracted light. The effective NA of the objective is critically dependent on the setting of the condenser aperture. The diffracted light forms higher order diffraction spots flanking the 0th order spot in the diffraction plane.
- The 0th and higher order diffraction spots in the diffraction plane correspond to locations where there is constructive interference of waves that differ in their path lengths by exactly 1, 2, 3 . . . wavelengths, respectively. The waves at each spot are exactly in phase and are diffracted at the slits in the specimen at the same unique angle of diffraction (θ). Note that each point in the diffraction plane corresponds to a certain angle of light leaving the specimen. The absence of light between the spots is due to interference between waves that are in or out of phase with each other. The 0th and higher order diffraction spots are most clearly focused and separated from one another in the diffraction plane (the rear focal plane of the objective).
- Image formation in the image plane is due to the interference of undeviated and deviated components that are now rejoined and interfere in the image plane, causing the resultant waves in the image plane to vary in amplitude and generate

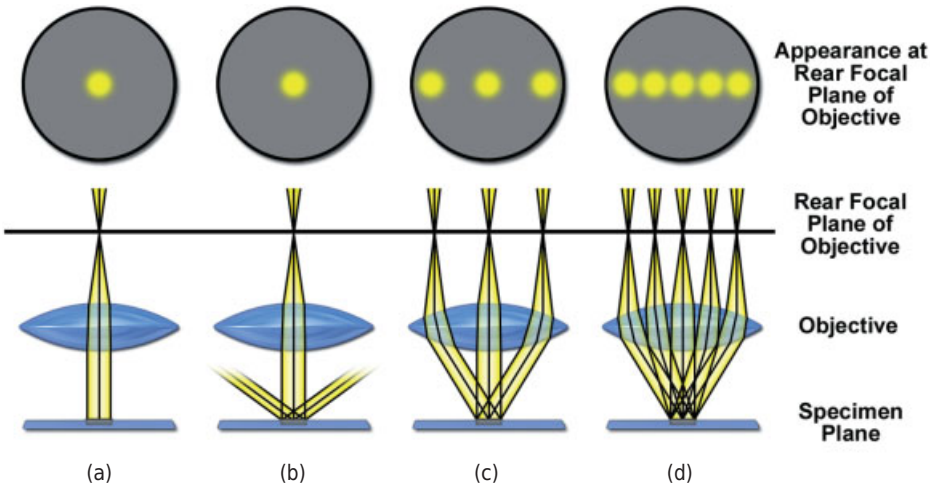

Figure 5.15

Generation of an image by interference requires collection of two adjacent orders of diffracted light by the objective. If diffraction at the specimen does not occur (a), or diffracted rays are not collected by the objective (b), no image is formed. In panel c, a minimum of two adjacent diffraction orders (0th and 1st) are collected, and an image is formed. In panel d, multiple diffracted orders are collected, leading to a high degree of definition in the image.

contrast. Abbé demonstrated that at least two different orders of light must be captured by a lens for interference to occur in the image plane (Fig. 5.15).

- A periodic specimen with an interperiod spacing d gives rise to a periodic pattern with spacing D in the diffraction plane, where $D \sim 1/d$. Therefore, the smaller the spacings in the object, the farther apart the spots are in the diffraction plane, and vice versa. The relationship is:

$$d \approx f\lambda/D\cos\theta,$$

where f is the focal length of the lens, λ is the wavelength, and θ is the acute angle at the principal plane in the objective from which the focal length is measured and which forms a right triangle together with the 0th and 1st order diffraction spots.

Abbé's theory of image formation explains the following important points: if a specimen does not diffract light or if the objective does not capture the diffracted light from an object, no image is formed in the image plane. If portions of two adjacent orders are captured, an image is formed, but the image may be barely resolved and indistinct. If multiple orders of diffracted light are captured, a sharply defined image is formed. The theory is also the basis for determining the spatial resolution of the light microscope, which is the subject of the next chapter.

A DIFFRACTION PATTERN IS FORMED IN THE REAR APERTURE OF THE OBJECTIVE

Let us now consider the diffraction pattern in the microscope's diffraction plane in the rear aperture (rear focal plane) of the objective. Under conditions of Koehler

illumination, a diffraction image of a specimen is formed just behind the objective in the objective's back (or rear) focal plane. You should take a moment to reinspect the figures in Chapter 1 and recall that this plane is conjugate with other aperture planes in the microscope—that is, the lamp filament, the front focal plane of the condenser, and the iris aperture of the eye. For specimens having periodic details (a diffraction grating) and under certain conditions of diaphragm adjustment, one can inspect the diffraction pattern of an object using a Bertrand lens. The diffraction pattern in the rear aperture and the image in the image plane are called *inverse transforms of each other*, since distance relations among objects seen in one plane are *reciprocally* related to spacings present in the other plane, as will now be explained.

Demonstration: Observing the Diffraction Image in the Rear Focal Plane of a Lens

It is easy to confirm the presence of a diffraction image of an object in the rear aperture of a lens using an electron microscope copper grid and an I-beam optical bench containing a bright light source, such as a 3-mW HeNe laser (Fig. 5.16). A 50 mm or shorter focal length lens is placed just in front of the laser to spread the beam so as to illuminate the full diameter of the grid. The EM grid taped to a glass microscope slide and mounted on a holder on the bench serves as an object. Position the grid at a distance that allows full illumination of its surface by the laser. Confirm that the grid generates a diffraction pattern by inserting a piece of paper into the beam at various locations behind the grid. Now position an optical bench demonstration lens of 50- to 100-mm focal length just over 1 focal length from the grid to create a sharply focused image (real intermediate image) of the grid on a projection screen some 2–3 m away from the lens. Adjust the lens position as required to obtain a focused image of the grid on the screen. The image reveals an orthogonal pattern of empty holes delimited by metal bars of the grid, which is a stamped piece of copper foil. To see the focused diffraction pattern of the grid, insert a white sheet of paper in the optical path at one focal length away from the lens. The diffraction pattern consists of an orthogonal pattern of bright points of light (see Fig. 5.1). Confirm that the focused diffraction image is located precisely in the rear focal plane at 1 focal length distance by moving the paper screen back and forth along the beam.

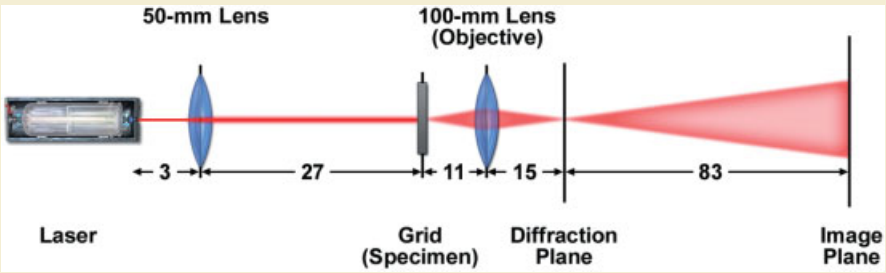

Figure 5.16

Demonstration of the diffraction image in the rear focal plane of a lens. Distances between optical components are given in centimeters.

Let us first consider the image of an object like a diffraction grating with lines spaced just a few micrometers or less apart. Light that passes through the grating (we might imagine any microscope specimen) and does not interact with it is called direct light, and forms a small central spot (the 0th order diffraction spot) in the middle of the diffraction pattern. Light that becomes diffracted (diffracted waves) forms a pattern of widely separated 1st, 2nd, 3rd, . . . order spots flanking the 0th order spot. The diffraction patterns of periodic objects like diatoms or striated muscle can be observed by closing the condenser diaphragm down to a minimum and inspecting the diffraction plane with a Bertrand lens. It is understood that the light contained in the diffraction pattern goes on to form the image of the grating through interference in the real intermediate image plane in the eyepieces of the microscope. Looking at the image through the eyepieces, we do not see the diffraction pattern, but the inverse transform that is derived from it. Thus, we say that the *object image is the inverse transform of the diffraction pattern in the rear aperture*. The reciprocal nature of the space relationships of the two images is described as follows: Fine periodic features separated by short distances in the object and image are seen as widely separated diffraction spots in the diffraction image; coarse features separated by relatively long distances in the object and real intermediate image take the form of closely separated diffraction spots near the central 0th order spot in the diffraction pattern.

Joseph Gall demonstrated this relationship by placing a transparent image (photographic negative) of a periodic polymer at the rear aperture and by providing illumination from a pinhole placed at the lamp's field stop. There was no specimen on the stage of the microscope. Looking in the eyepieces, the diffraction pattern (the inverse transform) of the polymer is observed. Used in this manner, the microscope functions as an optical diffractometer (Gall, 1967). Thus, images located in the diffraction plane and in the image plane are inverse transforms of one another, and the two images exhibit space relationships that are related as the reciprocal of the space relations in the other image. The exercise at the end of this chapter reinforces these points. We will revisit this concept throughout the book, particularly in the chapters on phase contrast microscopy and in the section on fast Fourier transforms in Chapter 18.

PRESERVATION OF COHERENCE: ESSENTIAL REQUIREMENT FOR IMAGE FORMATION

Our discussion of the role of diffraction and interference in image formation in the light microscope would not be complete without considering the requirement for coherent light in the microscope. Object illumination with rays that are partially coherent is required for all forms of interference light microscopy (phase contrast, polarization, and differential interference contrast) discussed in the following chapters.

Nearly all "incoherent" light sources, even incandescent filament lamps, are partially coherent—that is, the waves (wave bundle) comprising each minute ray emanating from a point on the filament vibrate in phase with each other. In reality, the degree of coherence within a given ray is only partial, since the photons vibrate slightly out of phase with each other. The distance over which the waves exhibit strong coherence is also limited—just a few dozen wavelengths or so—so that if you examined the amplitude of the ray along its length, you would see it alternate between high-amplitude states, where the waves vibrate coherently, and low-amplitude states, where waves are transiently out of phase with each other. In contrast, laser beams can be coherent over

meters of distance, whereas waves emitted from a fluorescence source are completely incoherent.

Coherence derives from the fact that atoms in a microscopic domain in the filament, excited to the point that they emit photons, mutually influence each other, which leads to synchronous photon emission. Thus, a tungsten filament or the ionized plasma in a mercury arc may each be considered as a large collection of minute atomic neighborhoods, each synchronously emitting photons. A discrete collection of coherent waves following the same trajectory is thus called a ray or pencil of light. The action of the collector lens of the illuminator is to form an image of the filament in the front aperture of the condenser, which then becomes the source of partially coherent rays that illuminate the object in the specimen plane (Fig. 5.17).

For a given incident ray, it is now possible to see that a coherence relationship exists between the diffracted and undiffracted (0th order) beams. This coherence relationship is maintained between the object and the image plane, where waves recombine and interfere. At that site, the myriad coherent wave partners add incoherently with other waves to produce the final image. This important concept underlies many forms of light microscopy.

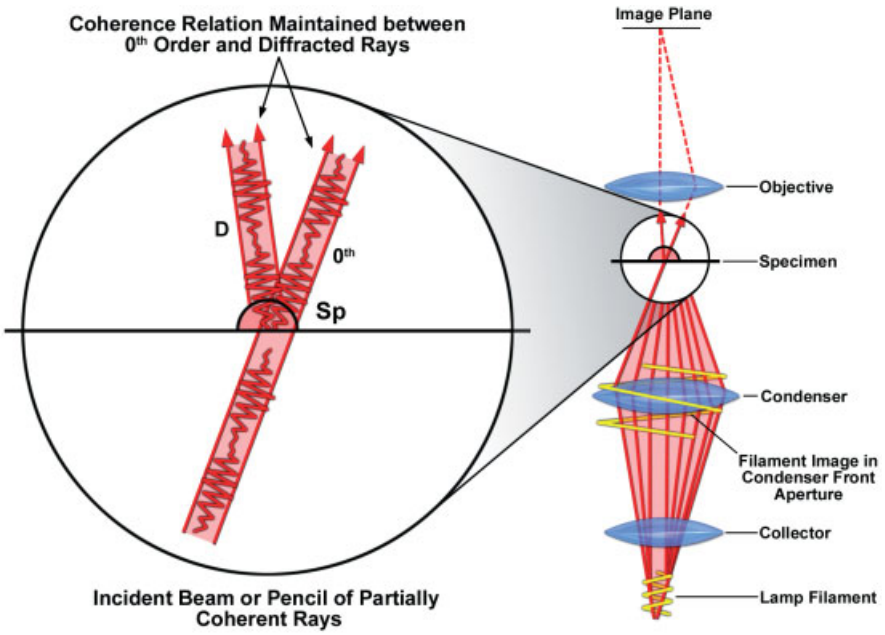

Figure 5.17

Partially coherent wave bundles in the light microscope. Small domains in the lamp filament emit partially coherent wave bundles that reform the image of the filament in the front aperture of the condenser. Rays (small beams or "pencils" of partially coherent photons) incident on a small particle in the specimen plane are broken up into diffracted and undeviated (0th order) waves that maintain their coherence relationship. Myriad ray pairs go on through the objective and combine incoherently with other rays in the image plane to form the image. The coherence relationship between undeviated and diffracted rays is essential for image formation in all forms of interference microscopy (phase contrast, polarization, and differential interference) described in the following chapters.

Exercise: Diffraction by Microscope Specimens

1. Determine the periodicity of unknown diffraction gratings using the diffraction equation, $m\lambda = d \sin\theta$. Measure the distances in centimeters between the 1st and 0th order spots on a projection screen and the distance between one of the spots and the grating to calculate $\sin\theta$ and the grating spacing, d. It is easiest to perform this measurement using a narrow, monochromatic beam, such as that provided by a laser pointer.
2. Review Koehler illumination and check the focus of the illuminator of your microscope. Focus on a piece of diffraction grating mounted on a glass microscope slide with a 40× dry objective, and calculate the spacing using the eyepiece reticule and calibration factor determined in the exercise for Chapter 1. For accuracy, measure the number of eyepiece units covering 10 or more spacings on the stage micrometer, repeat the procedure 10 times, and determine the mean value. How well do the two numbers agree?
3. Examine and compare the diffraction patterns of various other specimens on the projection screen and estimate their periods (suggestions: microscopic barbules on a bird feather, grooves on a semitransparent CD disk). If the CD is completely opaque, treat it as a reflection grating, tilting the CD at a 45° angle to form a right triangle between the 0th order spot, the CD, and the light source using the equation for a 90° reflection: $d = \checkmark 2\lambda / \sin\theta$. Use the laser pointer as a light source.
4. Focus the grating in monochromatic green light using a 10× objective with your microscope, stop down (maximally constrict) the condenser aperture diaphragm, and look to see if you can still resolve the grating in normal viewing mode. Examine the diffraction pattern of the grating with an eyepiece telescope under conditions where the image is not resolved, barely resolved, and fully resolved. Do you agree with Abbé's conclusion that a minimum of two adjacent diffraction orders is required for resolution?
5. Using the same condenser position, remove the green filter and examine the grating in red and blue light. For each color filter, examine the pattern of diffraction spots with the eyepiece telescope and note the corresponding changes in the spacing between the 1st order diffraction spots. Do your observations agree with the relationship between spatial resolution and wavelength?

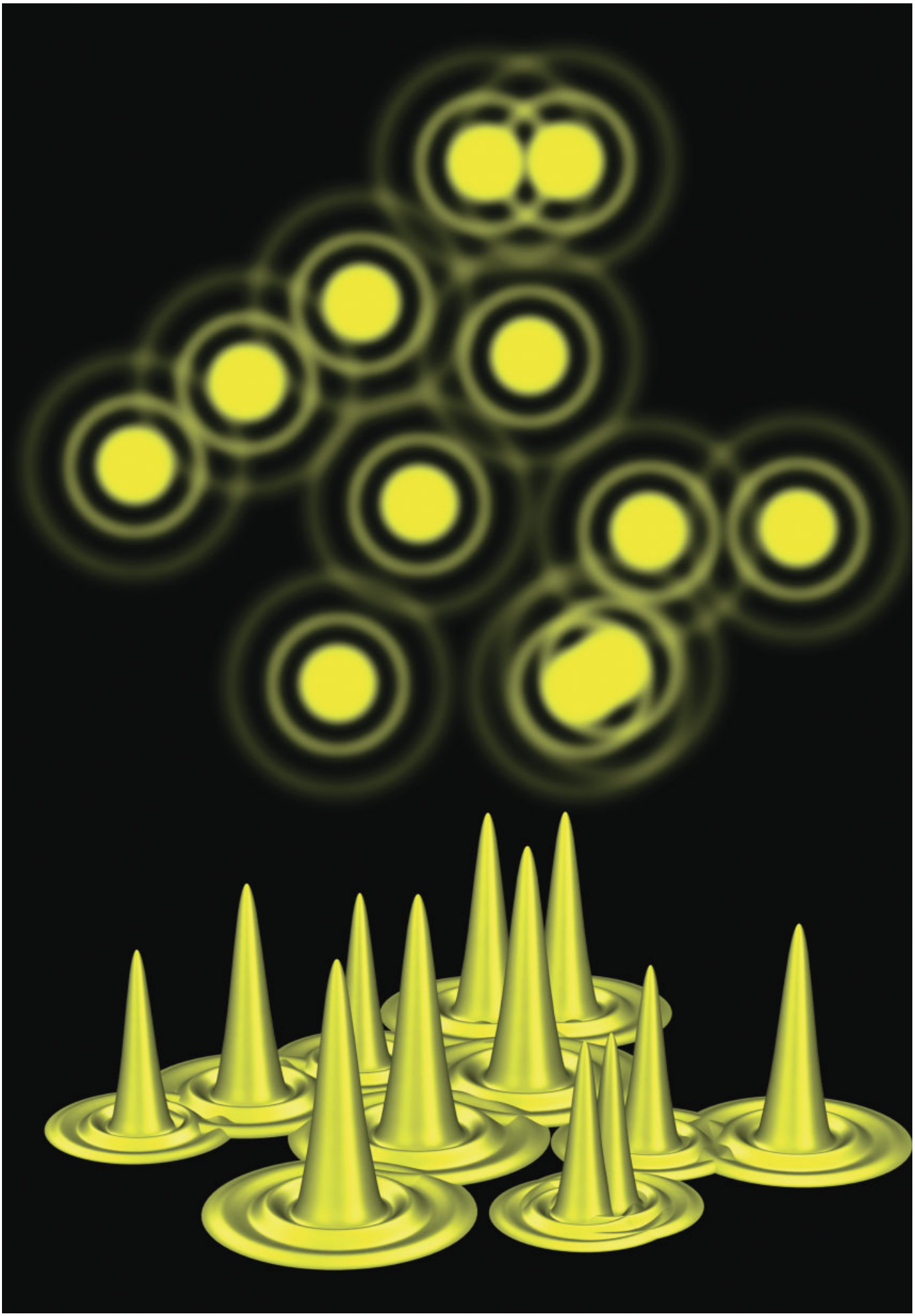

CHAPTER
6

DIFFRACTION AND SPATIAL RESOLUTION

OVERVIEW

In this chapter, we examine the role of diffraction in determining spatial resolution and image contrast in the light microscope. In the previous chapter, we emphasized that Abbé's theory of image formation in the light microscope is based on three fundamental actions: diffraction of light by the specimen, collection of diffracted rays by the objective, and interference of diffracted and nondiffracted rays in the image plane. The key element in the microscope's imaging system is the objective, which determines the precision with which these actions are effected. As an example, examine the remarkable resolution and contrast in the image of the diatom, *Pleurosigma*, made with an apochromatic objective designed by Abbé and introduced by Carl Zeiss over 100 years ago (Fig. 6.1). To understand how such high resolution images are obtained, we examine an important parameter of the objective, the numerical aperture (NA), the angle over which the objective can collect diffracted rays from the specimen and the key parameter determining spatial resolution. We also investigate the effect of NA on image contrast. In examining the requirements for optimizing resolution and contrast, we make an unsettling discovery: it is impossible to obtain maximal spatial resolution and optimal contrast using a single microscope setting. A compromise is required that forces us to give up some spatial resolution in return for an acceptable level of contrast.

NUMERICAL APERTURE

Implicit in the Overview is an understanding that the objective aperture must capture some of the diffracted rays from the specimen in order to form an image, and that lenses

Airy disks (above) and the corresponding point-spread functions (below).

Fundamentals of Light Microscopy and Electronic Imaging, Second Edition.
Douglas B. Murphy and Michael W. Davidson.

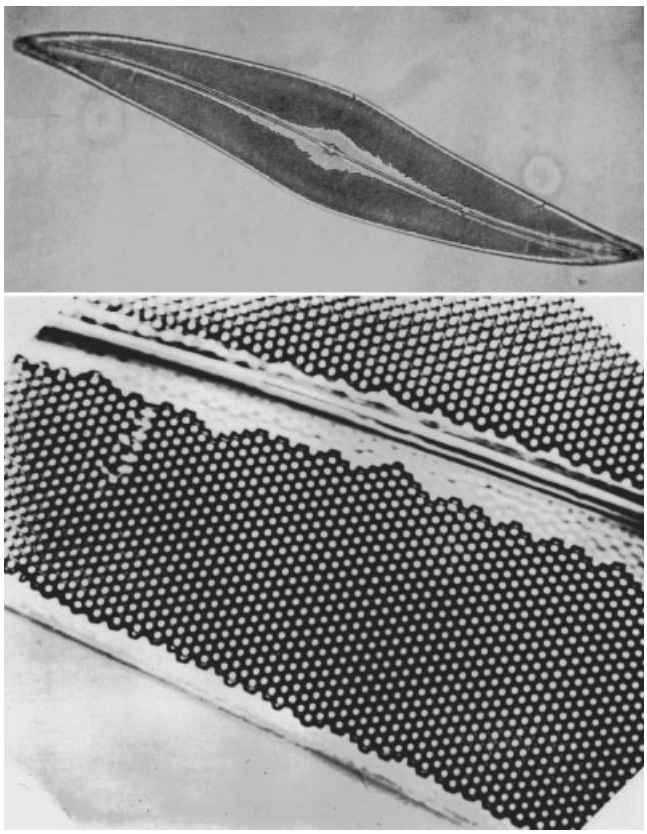

Figure 6.1
Resolution of the pores in a diatom shell with an apochromatic objective. Joseph Gall described these historic photographs of the diatom *Pleurosigma* prepared over 100 years ago using one of Abbé's lenses (Cover: *Molecular Biology of the Cell*, vol. 4, no. 10, 1993). "The photographs are taken from a Zeiss catalog published in 1888 in which Abbé's apochromatic objectives were advertised. Both figures show the silica shell of the diatom *Pleurosigma angulatum*. Because of the regular patterns of minute holes in their shells, diatoms have long been favorite objects for testing the resolution of microscope objectives. The top figure shows an entire shell at 500X, a magnification beyond which many 19th-century objectives would show little additional detail. The bottom figure, reproduced here and in the original catalog at a remarkable 4900X, was made with an apochromatic oil immersion objective of 2.0 mm focal length and a numerical aperture of 1.3. The center-to-center spacing of the holes in the shell is 0.65 μm, and the diameter of the holes themselves is about 0.40 μm. Almost certainly, this objective resolved down to its theoretical limit of 0.26 μm in green light."

that can capture light over a wide angle should give better resolution than an objective that collects light over a narrower angle. In the light microscope, the angular aperture is described in terms of the *numerical aperture* (NA), as:

$$\mathrm{NA} = n \sin\theta,$$

where θ is the half angle of the cone of specimen light accepted by the objective and n is the refractive index of the medium between the lens and the specimen. For dry lenses used in air, $n = 1$; for oil immersion objectives, $n = 1.515$.

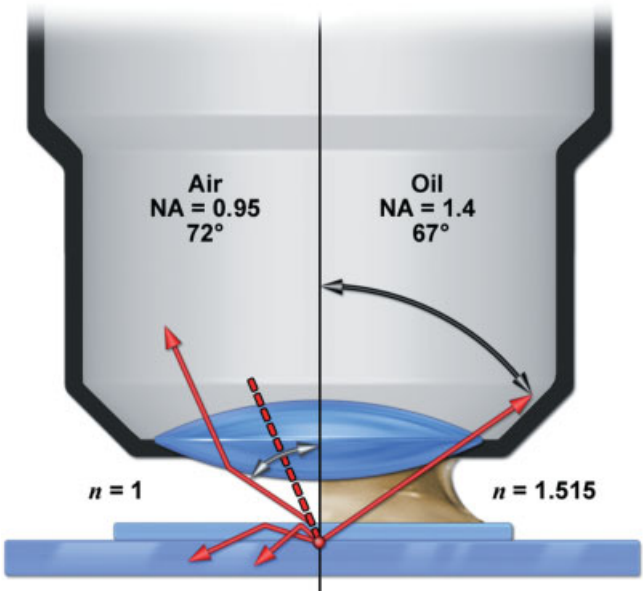

Figure 6.2
Effect of immersion oil on increasing the angular extent over which diffracted rays can be accepted by an objective. For dry objectives, NA is limited, because rays subtending angles greater than about 39° (angle formed at dotted line with the normal) are lost by total internal reflection and never enter the lens (downward deflected red arrows). This compares with an acceptance angle of 67° in the case of an oil immersion lens and accounts for the ability of an oil lens to collect much larger angles of diffracted light. Note, however, that the estimated maximum NA of 0.95 for the dry lens is actually calculated from the acceptance angle of 72° (double-headed arrow). The larger acceptance angle is due to the refraction of light at the air : coverslip interface. Snell's law, the critical angle for total internal reflection, and the refractive indices of the glass, oil, and air are all that are required to calculate these relationships. The newest TIRF objectives designed for use with special immersion oil have NA values of up to 1.49.

The diffraction angles capable of being accepted by dry and oil immersion objectives are compared in Figure 6.2. By increasing the refractive index of the medium between the lens and coverslip, the angle of diffracted rays collected by the objective is increased. Because immersion oil has the same refractive index as the glass coverslip (1.515), refraction of specimen rays at the coverslip–air interface is eliminated, the effective half angle is increased, and resolution is improved. Special total internal reflection fluorescence microscopy (TIRF) objectives are available with NA values of up to 1.49 using immersion oil, and even up to 1.65 using specialized immersion media and quartz coverslips. The reader can refer to Pluta (1988) for more details.

SPATIAL RESOLUTION

For point objects that are self-luminous (fluorescence microscopy, and darkfield microscopy), or for nonluminous points that are examined by brightfield microscopy in transmitted light where the condenser NA is greater than or equal to the objective NA, the *resolving power* of the microscope is defined as:

$$d = 0.61\,\lambda/\mathrm{NA},$$

where d is the minimum resolved distance in μm, λ is the wavelength in μm, and NA is the numerical aperture of the objective.

In the case of brightfield microscopy, where the condenser NA < objective NA (the condenser aperture is closed down and/or an oil immersion condenser is used in the absence of oil), the resolution is given as:

$$D = \frac{1.22\lambda}{\text{condenser NA} + \text{objective NA}}.$$

These equations describe the *Rayleigh criterion* for the resolution of two closely spaced diffraction spots in the image plane. By this criterion, *two adjacent object points are defined as being resolved when the central diffraction spot (Airy disc) of one point coincides with the first diffraction minimum of the other point in the image plane* (Fig. 6.3). The condition of being resolved assumes that the image is projected on the retina or detector with adequate magnification. Recording the real intermediate image on film or viewing the image in the microscope with a typical 10× eyepiece is usually adequate, but detectors for electronic imaging require special consideration (discussed in Chapter

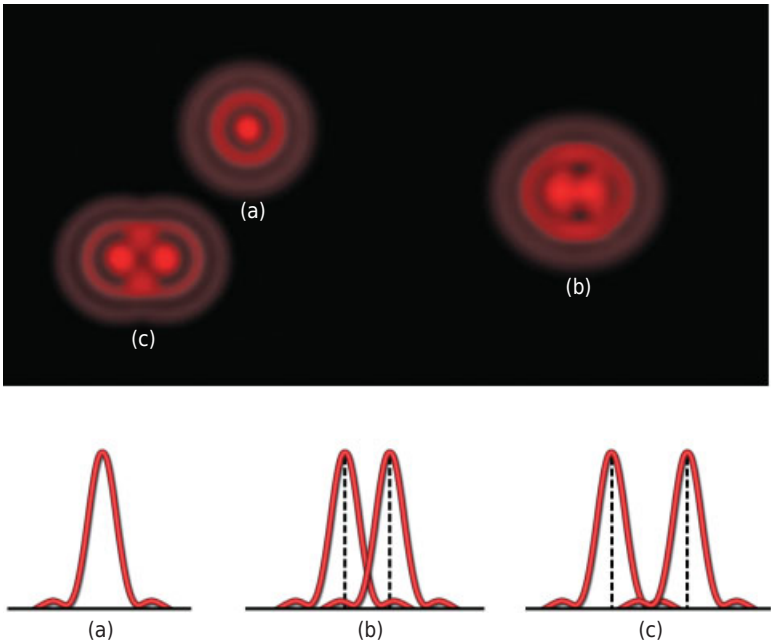

Figure 6.3

Rayleigh criterion for spatial resolution. (a) Profile of a single diffraction pattern: The bright Airy disk and 1st and 2nd order diffraction rings are visible. (b) Profile of two disks separated at the Rayleigh limit such that the maximum of a disk overlaps the first minimum of the other disk: The points are now just barely resolved. (c) Profile of two disks at a separation distance such that the maximum of each disk overlaps the second minimum of the other disk: The points are clearly resolved.

17). The Rayleigh resolution limit pertains to two luminous points in a dark field or to objects illuminated by incoherent light. For a condenser and objective with NA = 1.3 and using monochromatic light at 546 nm under conditions of oil immersion, the limit of spatial resolution is $d = 0.61\lambda/\text{NA} = 0.26\ \mu\text{m}$ and corresponds to the radius of the particle being examined. The NAs are engraved on the lens cap of the condenser and the barrel of the objective.

An image of an extended object consists of a pattern of overlapping diffraction spots, the location of every point x, y in the object corresponding to the center of a diffraction spot x, y in the image. Consider a specimen consisting of a crowded field of submicroscopic particles (point objects). For a given objective magnification, if the angular aperture of a microscope is increased, as occurs when opening the condenser diaphragm or when changing the objective for one with the same magnification but a higher NA, the diffraction spots in the image grow smaller and the image is better resolved (Fig. 6.4). Thus, larger aperture angles allow diffracted rays to be included in

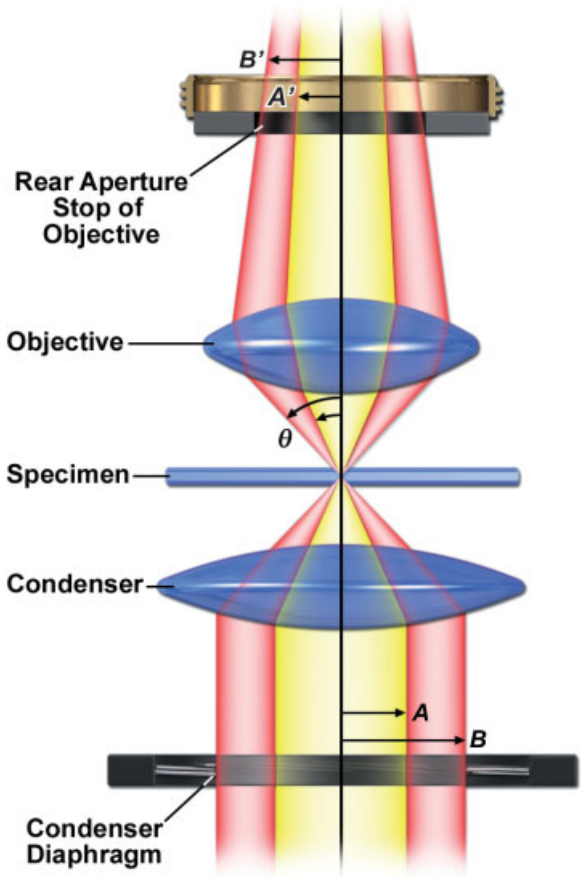

Figure 6.4

Role of the condenser diaphragm in determining the effective numerical aperture. Closing the front aperture diaphragm of the condenser from position *B* to *A* limits the angle θ of the illumination cone reaching the objective, and thus the effective numerical aperture. Notice that the rear aperture of the objective (*A*′) is no longer filled at the reduced setting.

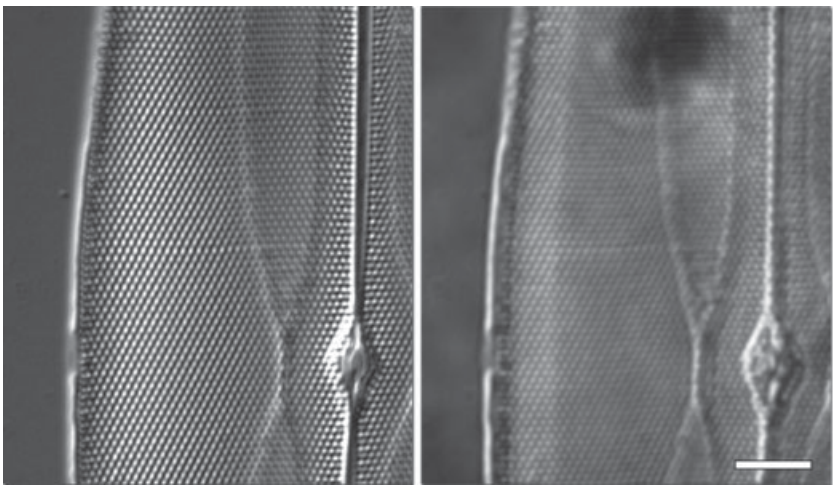

(a) (b)

Figure 6.5

Effect of numerical aperture on spatial resolution. The diatom *Pleurosigma* photographed with a 100×, 1.4 NA oil immersion lens using DIC optics. (a) Condenser aperture open, showing the near hexagonal pattern of pores. (b) The same viewfield with the condenser diaphragm closed. The 1st order diffracted rays from the pores are barely captured by the objective with a narrow cone of illumination. Spatial resolution is reduced, and many of the pores are poorly resolved. Bar = 10 μm.

the objective, permitting resolution of specimen detail that otherwise might not be resolved (Fig. 6.5).

The optical limit of spatial resolution is important for interpreting microscope images. Irregularities in the shapes of particles greater than the limiting size (0.52-μm diameter in the example cited previously) just begin to be resolved, but particles smaller than this limit appear as circular diffraction disks, and, regardless of their true sizes and shapes, always have the same apparent diameter of 0.52 μm (the apparent variability in the sizes of subresolution particles is due to variations in their intensities, not to variability in the size of their diffraction spots).

Thus, whereas minute organelles and filaments, such as microtubules, can be *detected* in the light microscope, their apparent diameter (for the lens given previously) is always 0.52 μm, and their true diameters are *not resolved*. It should therefore be apparent that two minute objects whose center-to-center distance is less than 0.26 μm cannot be resolved, but that two objects with physical radii smaller than this size can easily be resolved from each other if they are farther apart than 0.26 μm.

It must be remembered that *adjusting the condenser aperture directly affects spatial resolution in the microscope*. Since a large aperture angle is required for maximum resolution, the front aperture of the condenser must be fully illuminated. Stopping down the condenser diaphragm limits the number of higher order diffracted rays that can be included in the objective and reduces resolution. In an extreme case, the condenser aperture may be nearly closed in a mistaken effort to reduce light intensity. Then the half angle of the light cone entering the lens is greatly restricted, and resolution in the image is reduced significantly. The proper way to reduce light intensity

is to turn down the voltage supply of the lamp or insert neutral density filters to attenuate the illumination.

DEPTH OF FIELD AND DEPTH OF FOCUS

Just as diffraction and the wave nature of light determine that the image of a point object is a diffraction disk of finite diameter, so do the same laws determine that the disk has a measurable thickness along the *z*-axis. *Depth of field* (*Z*) in the object plane refers to the thickness of the optical section along the *z*-axis within which objects in the specimen are in focus; *depth of focus* is the thickness of the image plane itself. Our present comments are directed to the depth of field. For diffraction-limited optics, the wave-optical value of *Z* is given as:

$$Z = n\lambda/\mathrm{NA}^2,$$

where n is the refractive index of the medium between the lens and the object, λ is the wavelength of light in air, and NA is the numerical aperture of the objective. Thus, the larger the aperture angle (the higher the NA), the shallower will be the depth of field. The concept of depth of field is vivid in the minds of all of those who use cameras. Short-focal-length (fast) lenses with small focal ratios (<*f*/4) have a shallow depth of field, whereas the depth of field of long-focal-length (slow) lenses (>*f*/16) is relatively deep. At one extreme is the pinhole camera, which has an infinitely small NA and an infinite depth of field—all objects, both near and far, are simultaneously in focus in such a camera.

The depth of field along the *z*-axis is determined by several contributing factors, including principles of geometrical and physical optics, lens aberrations, the degree of physiological accommodation by the eye, and overall magnification. These variables and quantitative solutions for each are described in detail by Berek (1927), and are reviewed by Inoué (2006) and Pluta (1988). Calculated values of the wave optical depth of field for a variety of objectives are given in Table 4.1.

The depth of field for a particular objective can be measured quickly and unambiguously using the microscope. A planar periodic specimen, such as a diffraction grating, is mounted obliquely on a specimen slide by propping up one end of the grating using the edge of a coverslip of known thickness. When the grating is examined in the microscope, it will be seen that only a narrow zone of grating will be in focus at any particular setting of the specimen focus dial. The depth of field *Z* is then calculated from the width *w* of the focused zone (obtained photographically) and the angle of tilt α of the grating through the relationship:

$$Z = nw\tan\alpha,$$

where n is the refractive index of the medium surrounding the grating.

OPTIMIZING THE MICROSCOPE IMAGE: A COMPROMISE BETWEEN SPATIAL RESOLUTION AND CONTRAST

Putting these principles into practice, let us examine two specimens using transmitted light illumination and brightfield microscope optics: a totally opaque object such as a

copper mesh electron microscope grid and a stained histological specimen. These objects are called *amplitude objects*, because light-obscuring regions in the object appear as low intensity, high contrast regions when compared with the bright background in the object image. In comparison, transparent colorless objects, such as living cells, are nearly invisible, because the amplitude differences in the image are generally too small to reach the critical level of contrast required for visual detection. We discuss methods for visualizing this important class of transparent objects in Chapter 7.

With the microscope adjusted for Koehler illumination using white light, begin by opening the condenser front aperture to match the diameter of the rear aperture of the objective to obtain maximum aperture angle and therefore maximal spatial resolution. This operation is performed using an eyepiece telescope or Bertrand lens while inspecting the rear focal plane of the objective. Since this plane is conjugate with the condenser aperture, the edges of the condenser diaphragm appear when the diaphragm is sufficiently stopped down. With the telescope lens focused on its edges, open the diaphragm until its margins include the full aperture of the objective to obtain the maximum possible aperture angle. Expecting maximum resolution in normal viewing mode, we are surprised to see that the image of the opaque grid bars is gray and not black, and that the overall contrast is reduced. Similarly, fine details in the histological specimen, such as collagen bundles, cell organelles, and the edges of membranes and nuclei, have low contrast and are difficult to distinguish. The overall impression is that the image looks milky and washed out—in short, unacceptable. The poor definition at this setting of the condenser diaphragm is due to polychromatic illumination, scattered light, and reduction in the degree of coherence of the contributing waves. However, considerable improvements in the quality of the image can be made by using a bandpass filter to restrict illumination to a limited range of wavelengths and by partially closing the condenser diaphragm.

Monochromatic light assures that chromatic aberration is eliminated and that unit diffraction spots in the image are all of uniform size. With white light, diffraction spot size varies by nearly a factor of 2, due to the presence of different color wavelengths, with the result that diffraction features in the image are somewhat blurred. Monochromatic illumination sharpens the image and increases contrast, particularly for objects with inherently low contrast. For color objects such as histological specimens that are to be examined visually or recorded with a grayscale camera or black-and-white film, contrast can be improved dramatically by selecting filters with complementary colors: a green filter for pink eosin dye or a yellow filter for blue hematoxylin stain. A green filter, for example, removes all of the pink eosin signal, reducing the amplitude of eosin-stained structures and making them look dark against a bright background in a grayscale image.

To our surprise, closing down the condenser diaphragm also has a pronounced effect: It increases the contrast and greatly improves the visibility of the scene (Fig. 6.6). The grid bars now look black and certain features are more readily apparent. There are several reasons why this happens: (1) Part of the improvement comes from *reducing the amount of stray light* that becomes reflected and scattered at the periphery of the lens. (2) Reducing the aperture *increases the coherence of light*; by selecting a smaller portion of the light source used for illumination, the phase relationships among diffracted rays are more defined, and interference in the image plane results in higher amplitude differences, thus increasing contrast. (3) With reduced angular aperture, the

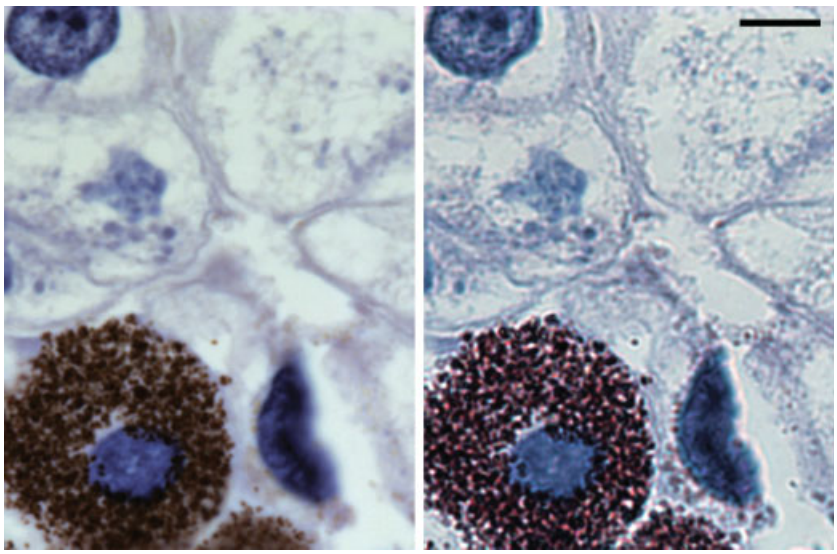

(a) (b)

Figure 6.6

Effect of the condenser aperture on image contrast and resolution. (a) With unrestricted aperture, resolution is maximal, but contrast suffers from stray light. (b) With the condenser aperture stopped down, light fills ~70% of the diameter of the rear aperture of the objective. Contrast is improved, but resolution is reduced. Brightfield light micrograph of a hematoxylin-stained thin section of *Amphiuma* liver containing hepatocytes and pigment cells. Bar = 10 μm.

unit diffraction spots comprising the image become larger, causing lines and edges to become thicker and cover a greater number of photoreceptor cells on the retina, thus making the demarcations appear darker and easier to see. Thus, the benefits of improved contrast and visibility might lead us to select a slightly stopped-down condenser aperture, even though spatial resolution has been compromised slightly in the process. If the condenser aperture is closed down too far, however, the image loses significant spatial resolution and the dark diffraction edges around objects become objectionable.

Thus, the principles of image formation must be understood if the microscope is to be used properly. A wide aperture allows maximal spatial resolution, but decreases contrast, while a smaller, constricted aperture improves visibility and contrast, but decreases spatial resolution. For all specimens, the ideal aperture location provides a balance between resolution and contrast. A useful guideline for beginners is to stop down the condenser aperture to about 70% of the maximum aperture diameter, but this is not a rigid rule. If we view specimens such as a diffraction grating, a diatom, or a section of striated muscle, stopping down the diaphragm to improve contrast might suddenly obliterate periodic specimen details, because the angular aperture is too small to allow diffracted light to be collected and focused in the image plane. In such a situation, the aperture should be reopened to whatever position gives adequate resolution of specimen detail and acceptable overall image visibility and contrast.

Exercise: Resolution of Striae in Diatoms

In this exercise, we will use a diatom test plate to examine the effect of NA and wavelength on resolution in the light microscope. Diatoms are unicellular algae that produce shells of silica containing arrays of closely spaced pores. They have been used to determine the spatial resolution of objectives in microscopes for well over a century.

Diatoms belong to the class Chrysophyta of yellow-green and golden brown algae. Their transparent quartz cell walls (valves or frustules) are usually composed of two overlapping halves (valves) that contain semi-crystalline and amorphous silica, which gives them a hard, brittle texture. The two overlapping valves are ornamented with tiny dots or perforations (pores) that are organized into rows (striae), both of which are commonly used to calibrate the magnification of microscopes. The ridge and pore spacings are constant for a given species. Figure 6.7

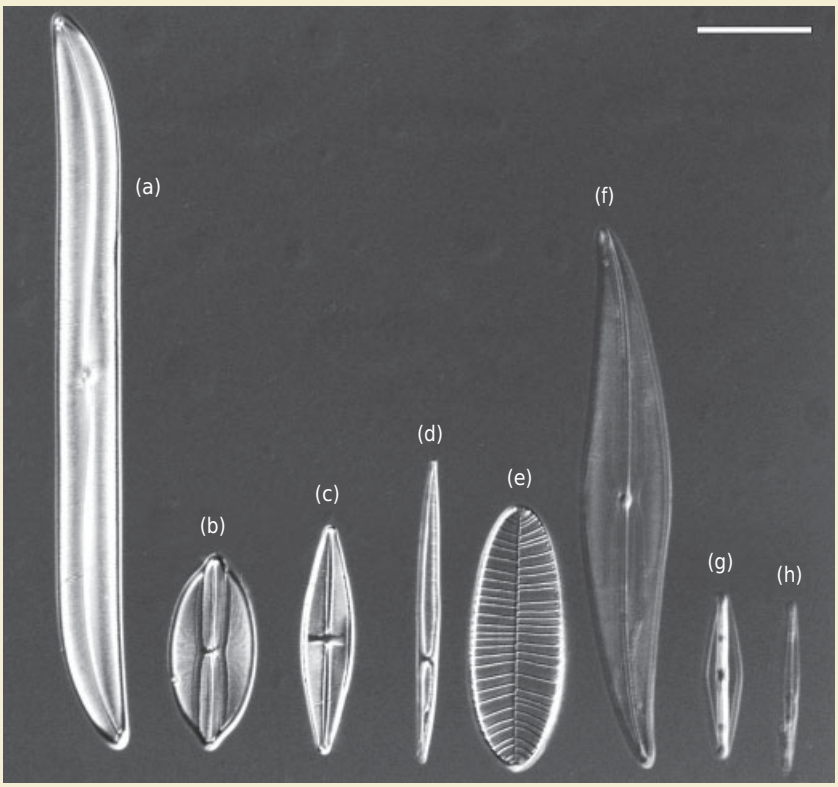

Figure 6.7

Diatom test plate and key (Genus, species, length (μm), period (μm/stria): (a) *Gyrosigma balticum*, 280, 0.67; (b) *Navicula lyra*, 160, 1.25; (c) *Stauroneis phenocenteron*, 150, 0.71; (d) *Nitzschia sigma*, 200, 0.43; (e) *Surirella gemma*, 100, 0.50; (f) *Pleurosigma angulatum*, 150, 0.53; (g) *Frustulia rhomboides*, 50, 0.29; (h) *Amphipleura pellucida*, 80–140, 0.27. Bar = 50 μm.

shows a diatom test plate obtained from Carolina Biological Supply Company, Burlington, North Carolina.

The accompanying table indicates the cell size and interstria spacing for the eight species of diatoms on the plate. While performing this exercise, compare the image of *Pleurosigma* produced with a modern lens with that produced by one of the first apochromatic lenses designed by Abbé (Fig. 6.1). If a test plate is not available, use a grain of dispersed diatomaceous earth (from a chemical supply house), or, failing that, some household scrubbing cleaner, which contains diatom shells as an abrasive.

1. Review the steps for adjusting the microscope for Koehler illumination. Identify and locate the positions of the four aperture planes and the four field planes, and prepare a list of each set in order, beginning with the lamp.
2. Adjust the condenser for brightfield mode. Image the diatom test plate using green light (546-nm bandpass filter) and the 40X objective. Focusing is difficult due to the extremely small size and transparent nature of the specimen. First locate the diatoms under low power (10×). Carefully move the *x* and *y* coordinates of the stage until the specimen comes into the field of view. Then swing in the 40× lens and refocus on the diatoms. Compare the image of the diatoms with Figure 6.7 and note the indicated spacings. Using brightfield optics and green light, open the condenser aperture to the proper location using the telescope lens, and note the species with the smallest spacing that it is possible to resolve with your microscope. Indicate the species and note the distance between the striae from the figure.
3. Calculate the theoretical resolution of the microscope under these conditions. The NA is indicated on the barrel of the lens. Show your work. The apparent and calculated resolution limits should roughly agree.
4. Now examine the diatom *Pleurosigma* with a dry 100× objective and close down the field-stop diaphragm to illuminate just this one diatom and no other. Make an accurate sketch of the hexagonal arrangement of the pores. Close down the condenser diaphragm to its minimum size. Now examine its diffraction pattern in the diffraction plane of the microscope using the telescope lens. Make an accurate sketch of the diffraction pattern.
5. How does the diffraction pattern relate to the spacing pattern of the diatom pores in the image plane?
6. Examine the diatoms in red and blue light and with the condenser aperture open or maximally closed. Which pair of conditions gives the lowest and the best resolution of the striae?
7. Examine the diatom *Pleurosigma* or *Diatoma* with a 100× oil immersion lens. Can the striae and pores be resolved? Examine the diffraction plane under these conditions. Make sketches of both views. Now oil the condenser as well as the objective and repeat your observations. Make sketches. Do you notice a difference in resolution?

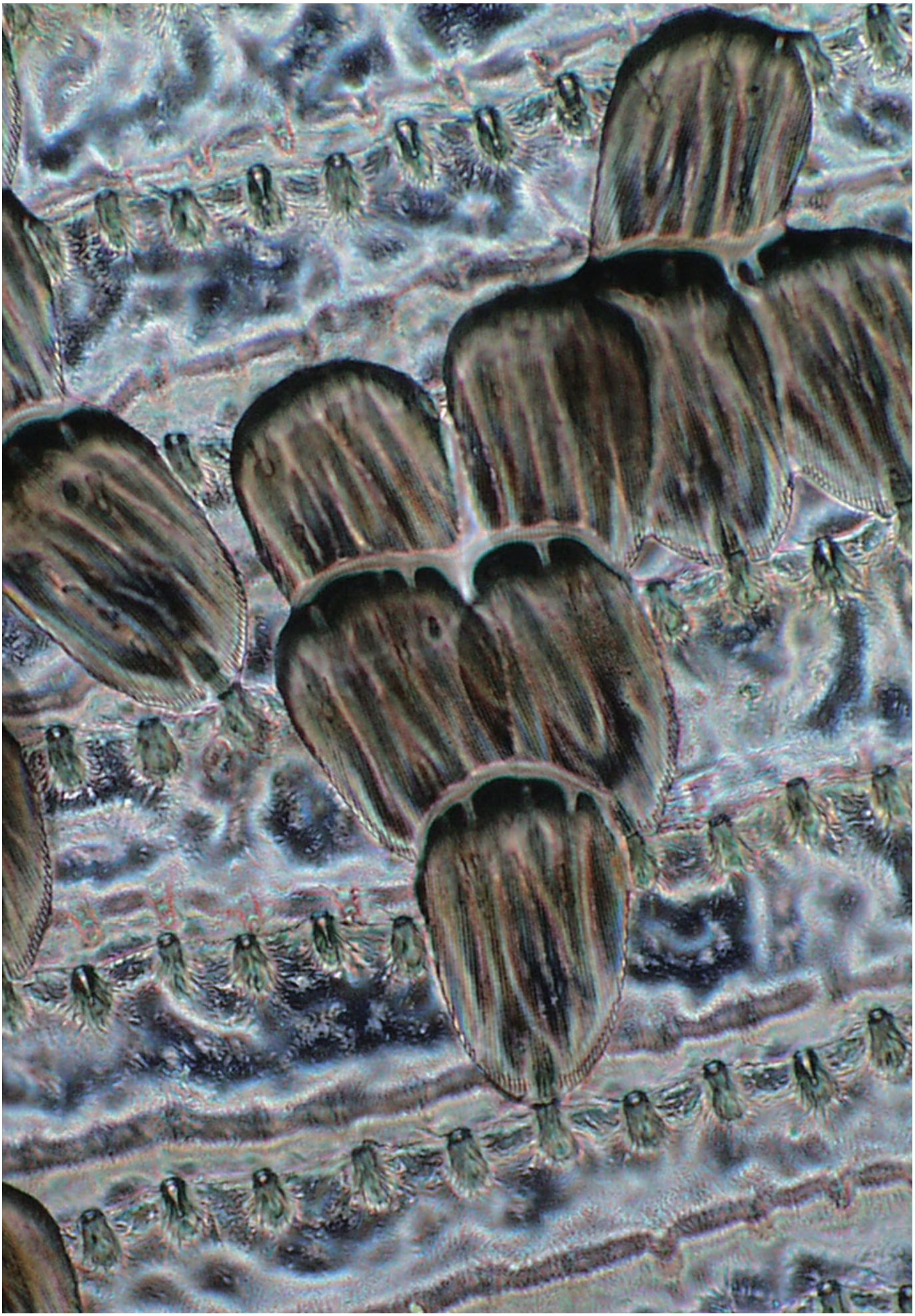

CHAPTER 7

PHASE CONTRAST MICROSCOPY AND DARKFIELD MICROSCOPY

OVERVIEW

Unstained objects, such as living cells, present a unique problem for the light microscopist because their images have very little contrast and are essentially invisible in ordinary brightfield microscopy. As we have seen in previous chapters, this is even true for transparent periodic specimens, such as diffraction gratings and diatoms. Although transparent objects induce phase shifts to beams of light due to scattering and diffraction, they remain nearly invisible because the eye cannot detect differences in phase. In this chapter, we examine two optical methods for viewing such objects: phase contrast microscopy, which transforms differences in the relative phase of object waves to amplitude differences in the image, and darkfield microscopy, where image formation is based solely on diffracted wave components. Phase contrast microscopy produces high contrast images of transparent specimens, such as cells and microorganisms, tissue slices, lithographic patterns, and particles such as organelles. Living cells in tissue culture can also be examined directly, without fixation and staining (Fig. 7.1).

PHASE CONTRAST MICROSCOPY

In the case of stained, histological preparations or specimens with naturally occurring pigments, specific wavelengths are absorbed by dyes or pigments, allowing objects to appear in color when illuminated with white light. With monochromatic illumination using a color filter complementary to the color of the specimen—for example, a blue object examined through a yellow filter—object rays are significantly reduced in

Phase contrast image of scales on a moth wing.

Fundamentals of Light Microscopy and Electronic Imaging, Second Edition.
Douglas B. Murphy and Michael W. Davidson.

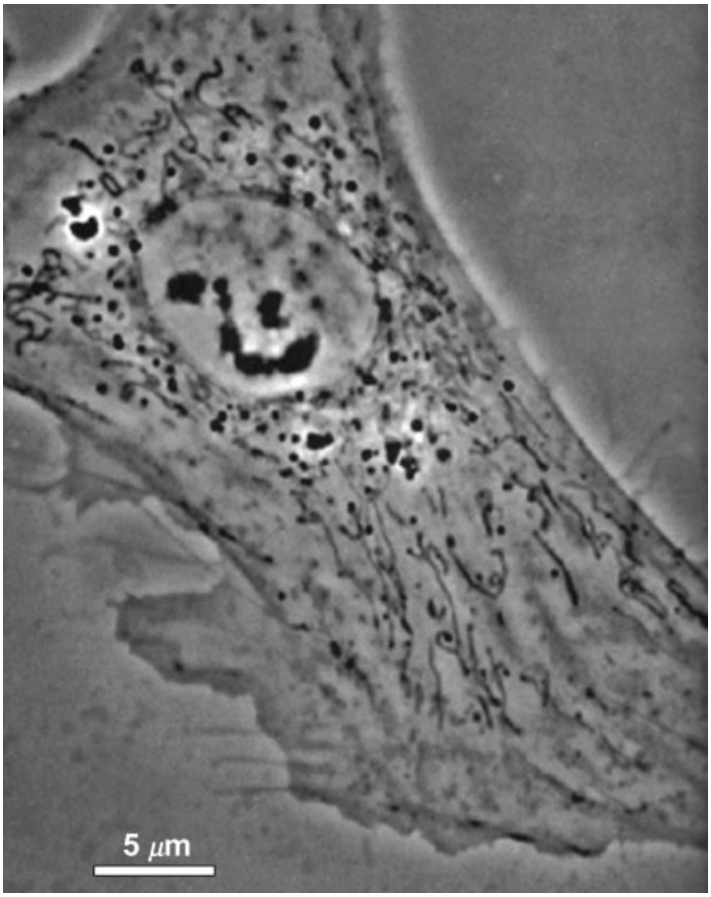

Figure 7.1

Phase contrast image of a living tissue culture cell. The cell nucleus, organelles, and membrane edges are clearly resolved in the normal rat kidney (NRK) cell. Phase-dense objects include mitochondria, lysosomes, nucleoli, and domains of nuclear chromatin. Phase-light objects represent lipid droplets and small vesicles. Bar = 5 μm.

amplitude, resulting in a high-contrast image. Such objects are called *amplitude objects* because they directly produce amplitude differences in the image that are detected by the eye as differences in intensity (Fig. 7.2). Although most transparent biological specimens do not absorb light, they do diffract light and cause a phase shift in the rays of light passing through them; thus, they are called *phase objects* (Fig. 7.2). The retardation imparted to a planar wavefront is shown in Figure 7.3. Phase contrast microscopes transform differences in the phase of object-diffracted waves to amplitude differences in the image, making objects appear as if they had been optically stained. Because the method is dependent on diffraction and scattering, phase contrast optics also differentially enhance the visibility of the light-scattering edges of extended objects and particles. The performance of modern phase contrast microscopes is remarkable. Under favorable conditions with present-day electronic enhancement and image processing, objects containing just a few protein molecules can be detected.

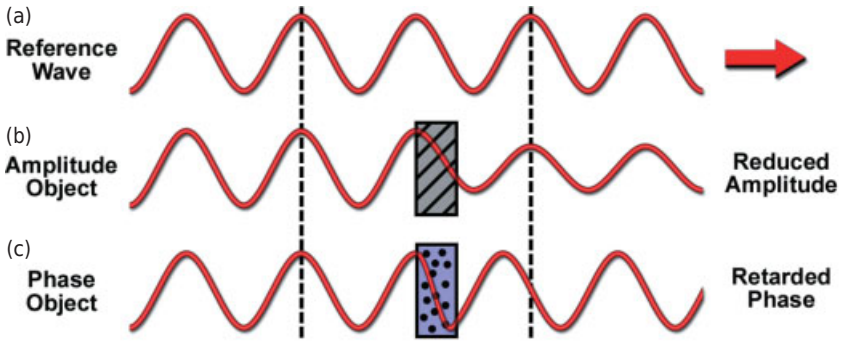

Figure 7.2

Effects of amplitude and phase objects on the waveform of light. (a) Reference ray with characteristic amplitude, wavelength, and phase. (b) A pure amplitude object absorbs energy and reduces the amplitude, but does not alter the phase, of an emergent ray. (c) A pure phase object alters velocity and shifts the phase, but not the amplitude, of an emergent ray.

In the 1930s, Frits Zernike, a Dutch physicist at the University of Groningen, created an optical design that could *transform differences in phase to differences in amplitude*. The development of phase contrast optics is a brilliant example of how basic research in theoretical optics led to a practical solution for viewing unstained transparent objects in the light microscope. The Zeiss optical works in Jena introduced phase contrast objectives and accessories in 1942, which transformed research in biology and medicine. For his invention and theory of image formation, Zernike won the Nobel Prize in physics in 1953 (Fig. 7.4). Excellent descriptions of the technique are found in Bennett et al. (2011), FranÇon (1961), Slayter (1970), Slayter and Slayter (1992), Strong (1958), and Pluta (1989).

In this chapter, we first examine the process of image formation using the terminology and diagrams that are commonly employed to explain phase contrast optics. Then we examine the relative contributions of diffraction and differences in optical path length in generating the phase contrast image.

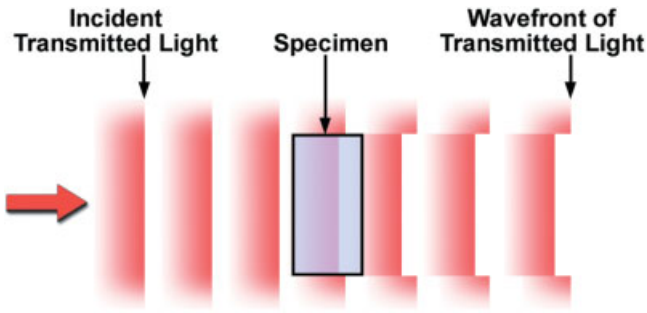

Figure 7.3

Disturbance by a phase object to an incident planar wavefront.

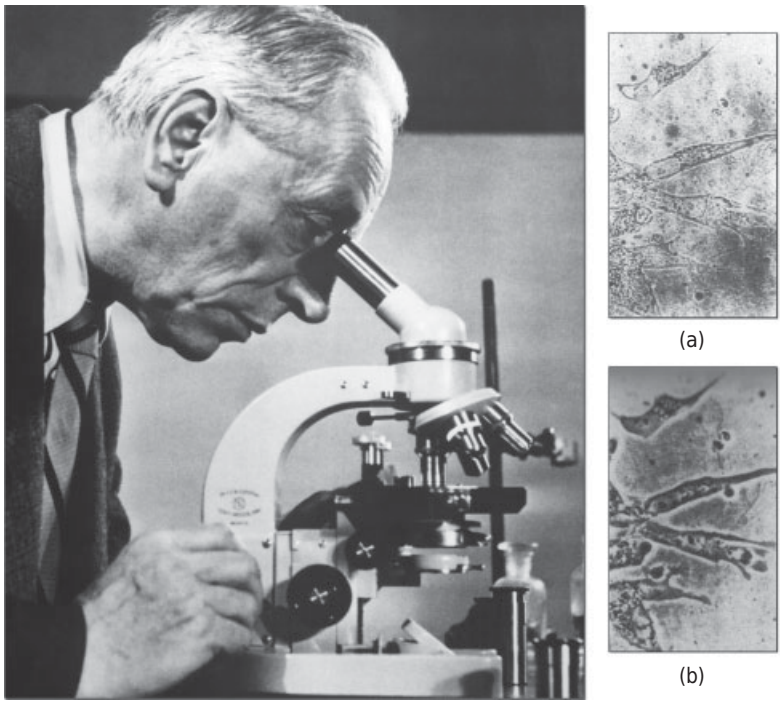

Figure 7.4

"How I Discovered Phase Contrast." Modified excerpts from Dr. Zernike's Nobel Prize address delivered in 1953 in Stockholm, Sweden, and published in the March 11, 1955 issue of *Science* (Zernike, 1955). Left: Dr. Zernike in his laboratory, November 1953. Right: Living tissue culture cells as seen with brightfield (a) and phase contrast (b). Phase contrast was not discovered while I was working with a microscope, but originated in my interest in diffraction gratings. About 1930 our laboratory obtained a large concave grating ruled by Robert Wood at Johns Hopkins University in Baltimore. Periodic errors in the grating lines made by ruling machines at that time caused the grating to exhibit a strongly striped surface, but when the grating was examined with a telescope at some 6 m distance and was exactly focused on the surface of the grating the stripes disappeared! By a succession of experiments and calculations I soon succeeded in explaining this. In a simpler case, a telescope was used to examine the phases of lines in a diffraction pattern of a vertical line-source of light after placing a 2 mm wide slit close behind the objective of the telescope. The diffraction maxima were observed but their phases could not be distinguished. However, the phases could be observed by throwing the diffraction image on a *coherent background* that served as a reference surface. Now I happened to know of a simple method Lord Rayleigh described in 1900 for making what I called *phase strips*—glass plates with a straight groove 1 mm wide and etched with acid to a uniform depth of half a wavelength. When a phase plate was placed in the spectrum of the faulty grating and examined with the telescope, the strips on the grating surface now stood out clearly. For a physicist interested in optics it was not a great step to change over from this subject to the microscope. Remember that in Ernst Abbé's remarkable theory of the microscope image the transparent object under the microscope is compared with a grating. Abbé examined gratings made of alternating opaque and transparent strips (amplitude gratings). Gratings made of transparent alternating thick and thin strips (phase gratings) produce diffraction spots that show a phase difference of 90°. For a phase object, my phase strip in the focal plane of the microscope objective brought the direct image of the light source into phase with the diffracted images, making the whole comparable to the images caused by an amplitude object. Therefore the image in the eyepiece appears as that of an absorbing object—that is, with black and white contrast, just as if the object has been stained. On looking back on these events I am impressed by the great limitations of the human mind. How quick we are to learn—that is, to imitate what others have done or thought before—and how slow to understand—that is, to see the deeper connections. Slowest of all, however, are we in inventing new connections or even in applying old ideas in a new field. In my case, the really new point was the diffraction pattern of lines of the grating artifacts, the fact that they differed in phase from the principal line, and that visualization of phases required projection of the diffraction image on a coherent background. The full name of the new method of microscopy might be something like "phase-strip method for observing phase objects in good contrast." I shortened this to "phase contrast."

THE BEHAVIOR OF WAVES FROM PHASE OBJECTS IN BRIGHTFIELD MICROSCOPY

Wave Terminology and the Importance of Coherence

Upon transit through a phase object, an incident wavefront of an illuminating beam becomes divided into two components: (1) an undeviated (0th order) wave or *surround wave* (S wave) that passes through the specimen but does not interact with it, and (2) a deviated or *diffracted wave* (D wave) that becomes scattered in many directions. Typically, only a minority of incident waves are diffracted by cellular objects. Both S and D waves are collected by the objective and focused in the image plane at the site corresponding to the image of the particle, where they undergo interference and generate a resultant *particle wave* (P wave). The relationship among waves is thus described as P = S + D. Detection of the object image depends on the intensities, and hence on the amplitudes of the P and S waves. *Only when the amplitudes of the P and S waves are significantly different in the image plane can we see the object in the microscope*.

Please note: In this chapter, the sine waves shown in the figures do not represent individual photons, rather the amplitudes and phases of wavefronts or wave bundles at the image plane, each bundle representing the combined contribution of many photons. Also, before we consider the interference mechanism, please note our earlier discussion of the partial coherence of light waves in the myriad small beams illuminating the specimen (Chapter 5). This condition is of great practical importance for phase contrast microscopy, because image formation through constructive and destructive interference requires coherent illumination, such that: (1) a definite phase relationship exists between the S and D waves, and (2) the phase relationship is preserved along the optical pathway between the object and the image.

Depiction of Wave Interactions with Sine Wave and Vector Diagrams

We begin by showing the relationship between S, D, and P waves as it normally occurs in the light microscope; the mechanism of phase contrast enhancement is shown in a separate section. First examine Figure 7.5a, which shows the S, D, and P waves as sine waves of a given wavelength in the image plane in normal brightfield imaging. The S and P waves, whose relative intensities determine the visual contrast, are shown as red and green lines; the D wave is shown in blue, and is not directly observed in the image. Thus, the amplitude of each wave represents the sum of the E vectors of the component photons. The D wave is lower in amplitude than the S wave, because there are fewer D-wave photons than there are S-wave photons at the image point. Notice that the D wave is retarded in phase by $\lambda/4$ relative to the S wave due to its interaction with the object particle. The basic $\lambda/4$ phase shift in the diffracted wave is a direct consequence of the physical process of scattering and diffraction (Zernike, appendix K in Strong, 1958). Phase shifts greater than $\lambda/4$ are observed for the beams traversing transparent objects that change the optical path length of the beam due to their thickness and/or refractive index. The P wave resulting from interference between the D and S waves is retarded relative to the S wave by only a small amount ($\sim\lambda/20$) and has an amplitude similar to that of the S wave. *Since the S and P waves have close to the same amplitude*

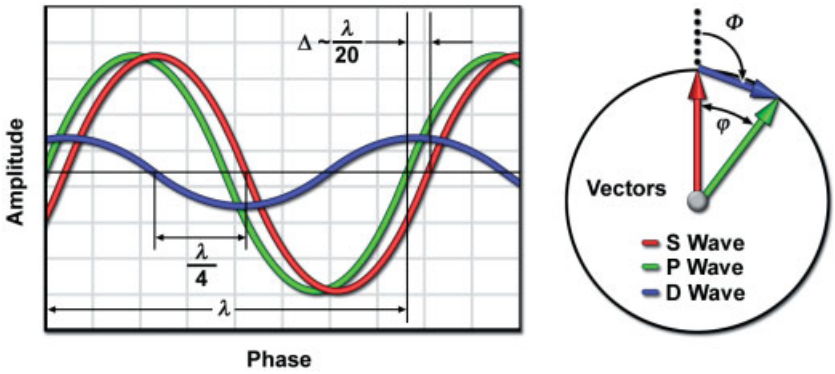

Figure 7.5

Phase relations between *S* (red), *D* (blue), and *P* (green) waves in brightfield microscopy. S and D waves, generated at the object, recombine through interference to generate the resultant particle image wave (*P*) in the image plane of the microscope ($P = S + D$). (a) Wave components shown as sine waves. (b) Vector diagram of *S*, *P*, and *D* waves. For explanations, see text.

in simple light microscopy, there is no contrast in the image and the object remains invisible.

The same phenomenon can also be described as a vector plot with polar coordinates (phasors), where the length of a vector radius represents the amplitude of a wave, and the angle of rotation of a vector relative to a fixed reference (angular phase shift ϕ) represents the amount of phase displacement, there being 2π radians in one wave (Fig. 7.5b). Phase retardations are shown as clockwise rotations. In this plot, the reconstructed P wave is shown as the vector sum of the S and D waves. This form of presentation is convenient because one can see more clearly how different degrees of phase shift in the D-wave affect the phase of the resultant P-wave and vice versa.

As stated above, the D-wave is usually shifted in phase by about $\lambda/4$ (90°) due largely to the effects of scattering (see below). A complete description of this form of wave analysis is given by Hecht (2001), Pluta (1989), and Slayter (1970), but for our purposes, a brief definition will be sufficient to explain the diagram. The position of D relative to S in Figure 7.5 is shown as Φ, where $\Phi = \pm 90° + \phi/2$ and ϕ is the relative phase shift (related to the optical path difference) between the S and P vectors. For very small phase shifts ϕ, Φ is ±90°. As shown in the figure, a D wave of low amplitude and small phase shift results in a P wave having an amplitude that is nearly equal to that of the S wave. With similar amplitudes for S and P, there is no contrast and the object remains invisible.

The Role of Differences in Optical Path Lengths

We encountered the concept of optical path length previously when we discussed the action of a lens in preserving the constancy of optical path length between object and image for coherent waves emerging from an object and passing through different regions of the lens (Fig. 5.6). For phase contrast microscopy, we are concerned with

the role of the object in altering the optical path length (relative phase shift ϕ) of waves passing through a phase object.

Since the velocity of light in any medium is $v = c/n$, where c is the speed of light in a vacuum, rays of light passing through a phase object with thickness t and refractive index n greater than the surrounding medium travel more slowly through the object and emerge from it retarded in phase relative to the background rays. The difference in the location of an emergent wavefront between object and background is called the *phase shift* δ (same as ϕ above), where δ in radians is:

$$\delta = 2\pi\Delta/\lambda,$$

and Δ is the *optical path difference*, which was defined in Chapter 5 as:

$$\Delta = (n_2 - n_1)t.$$

The Optical Design of the Phase Contrast Microscope

The key element of the optical design is to (1) isolate the surround and diffracted rays emerging from the specimen so that they occupy different locations in the diffraction plane at the rear aperture of the objective, and (2) advance the phase and reduce the amplitude of the surround light, in order to maximize differences in amplitude between the object and background in the image plane. As we will see, the mechanism for generating relative phase retardation is a two-step process: D waves are retarded in phase by $\sim\lambda/4$ at the object, while S waves are advanced in phase by a phase plate positioned in or near the diffraction plane in the rear aperture of the objective. Two special pieces of equipment are required: a condenser annulus and an objective bearing a phase plate for phase contrast optics.

The *condenser annulus*, an opaque black plate with a transparent annulus, is positioned in the front aperture of the condenser so that the specimen is illuminated by beams of light emanating from a ring (Fig. 7.6). (In some texts, the illuminating beam emergent from the condenser is described as a hollow cone of light with a dark center—a concept that is useful but not strictly true.) The condenser annulus replaces the variable diaphragm in the front aperture of the condenser. Under conditions of Koehler illumination, S waves that do not interact with the specimen are focused as a bright ring in the rear focal plane of the objective (the diffraction plane). Remember that under these conditions, the objective's rear focal plane is conjugate to the condenser's front aperture plane, so nondiffracted (0th order) waves form a bright image of the condenser annulus at the rear aperture of the objective. Light that is diffracted by the specimen (D waves) traverses the diffraction plane at various locations across the entire rear aperture, the amount and location depending on the number, size, and refractive index differential of light-scattering objects in the specimen. Since the direct (0th order light) and diffracted light become spatially separated in the diffraction plane, one can selectively manipulate the phase of either the S- or D-wave components.

To differentially alter the phase and amplitude of the direct (undeviated) light, a *phase plate* is mounted in or near the rear focal plane of the objective (Figs. 7.6 and 7.7). In some phase contrast objectives, the phase plate is a plate of glass with an etched ring of reduced thickness to selectively advance the phase of the S wave by $\lambda/4$. The same ring is coated with a partially absorbing metal film to reduce the amplitude of the

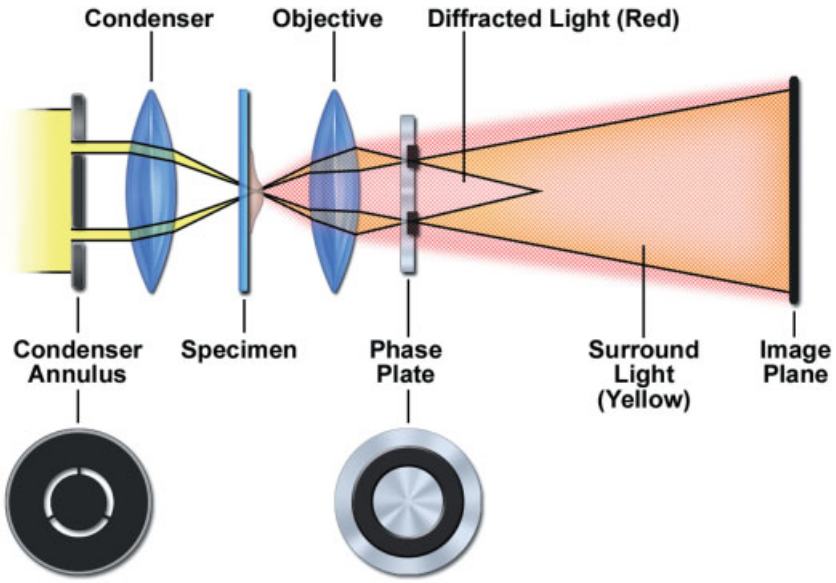

Figure 7.6

Path of nondiffracted and diffracted beams in a phase contrast microscope. An annular aperture in the front focal plane of the condenser generates a hollow cone of light that illuminates the specimen and continues (approximately) as an inverted cone that is intercepted by a phase plate at the rear aperture of the objective. The image of the annulus is in sharp focus in this plane because it is conjugate to the front aperture plane of the condenser. Diffracted specimen rays fill the shaded region of the illumination path.

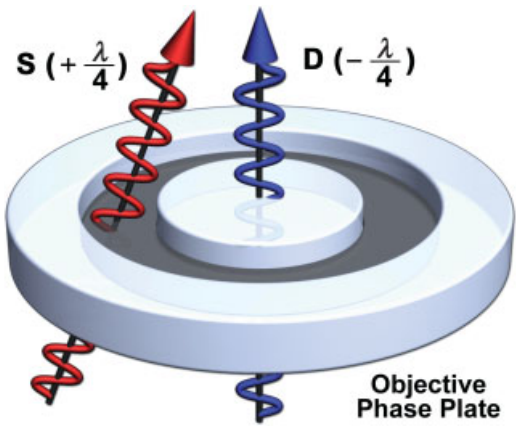

Figure 7.7

The action of a phase plate at the rear surface of the objective. Surround or background rays (*S*) are advanced in phase relative to the *D* wave by $\lambda/4$ at the phase plate. Relative phase advancement is created by etching a ring in the plate that reduces the physical path taken by the *S* waves through the high refractive index plate. Since diffracted object rays (*D*) are retarded by $\lambda/4$ at the specimen, the optical path difference between *D* and *S* waves upon emergence from the phase plate is $\lambda/2$, allowing destructive interference in the image plane. The recessed ring in the phase plate is made semitransparent so that the amplitude of the *S* wave is reduced by 70–75% to optimize contrast in the image plane.

light by 70–75%. In other lenses, the same effect is accomplished by acid etching a lens surface that is in or near the rear focal plane of the objective. Regardless of the method, it is important to remember that phase contrast objectives are always modified in this way and thus are different from other microscope objectives.

The optical scheme for producing positive and negative phase contrast images is given in Figure 7.8. As discussed in the preceding section, the D wave emergent from the object plane is retarded by $\lambda/4$ relative to the phase of the S wave. In positive phase contrast optics (left side of the diagram), the S wave is advanced in phase by $\lambda/4$ at the phase plate, giving a net phase shift of $\lambda/2$, which now allows destructive interference with D waves in the image plane. Generally, the manipulation of relative phase advancement, while essential to phase contrast optics, does not generate a high-contrast image, because the amplitude of the S wave is too high to allow sufficient contrast.

For this reason, the ring in the phase plate is darkened with a semitransparent metallic coating to reduce the amplitude of the S wave by about 70%. Since P = S + D, interference in the image plane generates a P wave with an amplitude that is now considerably less than that of S. Thus, the difference in phase induced by the specimen is transformed into a difference in amplitude (intensity). Since the eye interprets differences in intensity as contrast ($C = \Delta I/I_b$), we now see the object in the microscope (see Chapter 2 for discussion of formula). *Positive phase contrast* systems like the one just described *differentially advance the phase of the S wave relative to that of the D wave*. Cellular objects having a higher refractive index than the surrounding medium are dark in appearance, whereas objects having a lower refractive index than the surrounding medium appear bright.

It is also possible to produce optics giving *negative phase contrast*, where the S wave is retarded relative to the D wave, causing high-refractive-index objects to appear bright against a gray background. In this case, the phase plate contains an elevated ring that retards the phase of the 0th order S wave relative to the phase of the D wave. The effect of this action in generating negative phase contrast is shown on the right-hand side of Figure 7.8.

Alignment

To form a phase contrast image, the rings of the annulus and phase plate must have matching diameters and be perfectly aligned. A multiple-position condenser with a rotating turret may contain two or three annuli intended for use with different phase contrast objectives. Small annuli are used for low power dry objectives, whereas large annuli are employed with high power, oil immersion lenses. The nomenclature used by different microscope companies varies, but the proper selection can always be made by matching the designation on the edge of the turret with the corresponding designation on the barrel of the objective. Whenever a lens is changed and a new annulus brought into position, it is important to inspect the objective rear aperture to make sure the annulus and the phase plate match and that they are aligned. Since the objective is usually fixed into position by the nosepiece, alignment is performed by moving the condenser annulus with a set of special positioning screws on the condenser. The annulus adjustment screws, not to be confused with the condenser centration screws, are either permanently mounted on the condenser turret or come with separate driver tools that must be inserted into the condenser for this purpose. After bringing the rings into sharp focus with the telescope focus, move the bright image of the annulus to

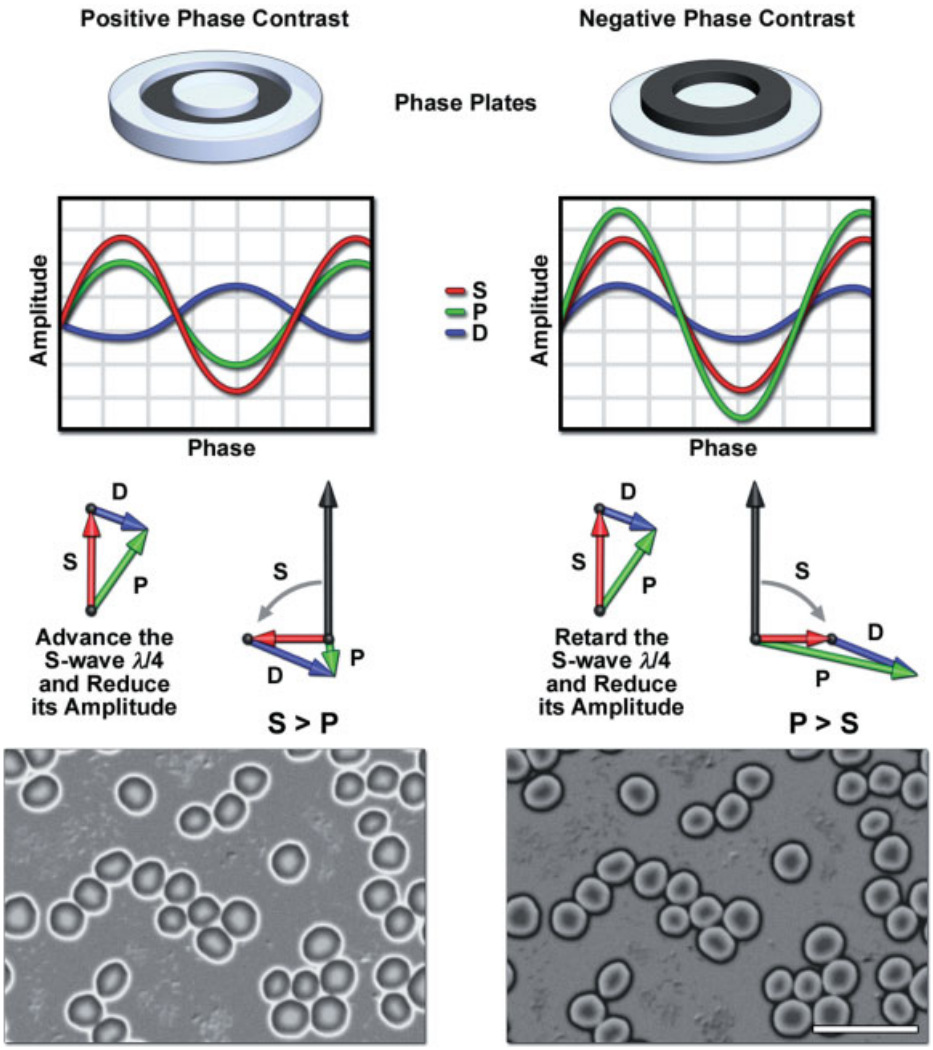

Figure 7.8

Comparison of positive and negative phase contrast systems. Shown in pairs, from the top down: phase plates for advancing (positive contrast) or retarding (negative contrast) the surround wave; sine wave diagrams showing destructive interference (positive phase contrast) and constructive interference (negative phase contrast) for a high refractive index object. Notice that the phase plate advances or retards the S wave relative to the *D* wave. The amplitude of the resultant *P* wave is lower or higher that the *S* wave, causing the object to look relatively darker or brighter than the background. Vector diagrams show advancement of the *S* wave by $\lambda/4$, which is shown as a 90° counterclockwise rotation in positive phase contrast, and retardation of the *S* wave by $\lambda/4$, which is shown as a 90° clockwise rotation in negative phase contrast. Phase plates also reduce the amplitude of the *S* wave by a significant amount. Addition of the *S* and *D* wave vectors gives *P* waves, whose amplitudes vary relative to the S waves. Images of erythrocytes in positive and negative phase contrast optics. Bar = 20 μm.

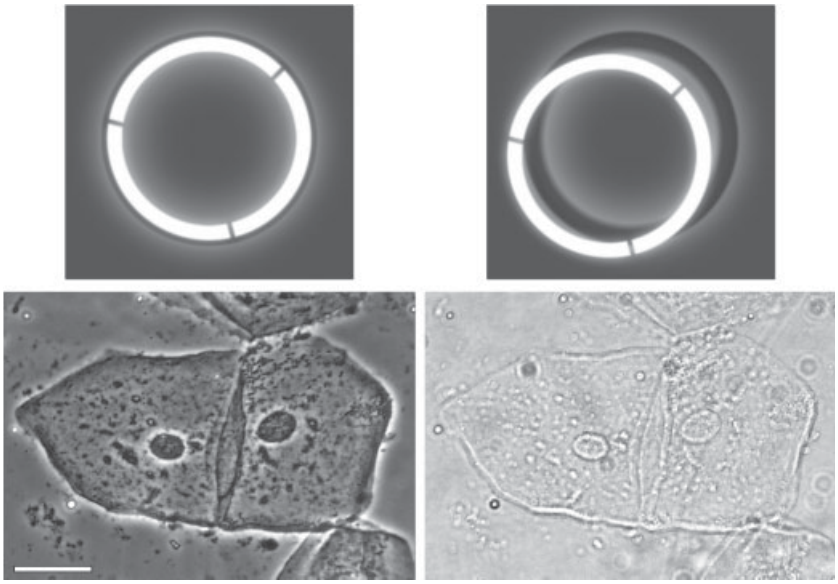

Figure 7.9

Alignment of condenser and objective annuli. An eyepiece telescope or Bertrand lens is used to examine the rear aperture of the objective. (a) The dark ring of the phase plate must be perfectly centered with the bright ring of light from the condenser annulus. The adjustment is made using two condenser plate-centering screws. These screws are distinct from the condenser centration screws, which are used to center the condenser lens with respect to the optical axis of the microscope. (b) Notice the low contrast shaded image resulting from a misaligned annulus. Bar = 20 μm.

exactly coincide with the dark ring on the phase plate (Fig. 7.9). Improper alignment gives a bright, low contrast image, because the bright background rays are not properly attenuated or advanced in phase as required by phase contrast theory.

Interpreting the Phase Contrast Image

Phase contrast images are easiest to interpret when the cells are thin and spread out on the substrate. When such specimens are examined in positive contrast mode, the conventional mode of viewing, objects with a higher refractive index than the surrounding medium appear dark. Most notably, phase contrast optics differentially enhance the contrast of the edges of extended objects, such as cell margins. Generally, positive phase contrast optics produce high contrast images that we interpret as density maps. As an approximation, this interpretation is usually correct, because the amplitude and intensity in an object image are related to refractive index and optical path length. Thus, a series of objects of increasing density (such as cytoplasm, nucleus, and nucleolus) are typically seen as progressively darker objects. However, the size and orientation of asymmetric objects also affect intensity and contrast. Further, there are optical artifacts we need to recognize that are present in every phase contrast image.

Interpreting phase contrast images requires care. In positive phase contrast optics, cell organelles having a lower refractive index than the surrounding cytoplasm generally appear bright against a gray background. Examples include pinocytotic vesicles, lipid droplets, and vacuoles in plant cells and protozoa. For objects that introduce relatively large phase retardations (phase shift Φ of the diffracted wave $\sim\lambda/2$), interference becomes constructive, making the objects appear brighter than the background.

To avoid confusion regarding bright and dark contrast in phase contrast images, it is useful to reconsider the term *optical path difference*, which is the product of refractive index and object thickness, and is related to the relative phase shift between object and background waves.

It is common to hear microscopists refer to high and low refractive index objects in a phase contrast image, but this is technically incorrect unless they know that the objects being compared have the same thickness. Thus, a small object with a high refractive index and a large object with lower refractive index can show the same optical path difference and yet appear to the eye as having the same intensity (Fig. 7.10). In particular, conditions that cause shrinking or swelling of cells or organelles can result in major differences in contrast. Likewise, replacement of the external medium with one having a different refractive index can result in changes in image contrast.

Finally, phase contrast images show characteristic patterns of contrast—halos and shade-off—in which the observed intensity does not correspond directly to the optical path difference of the object. These are sometimes referred to as phase artifacts or distortions, but should be recognized as a natural result of the optical system. *Phase halos* always surround phase objects and may be dark or light depending on whether the optical path through an object is greater or less than that of the medium (e.g., see Figs. 7.1 and 7.8.).

For objects that appear dark, the phase halo is light, and vice versa. Halos occur because the ring in the phase plate in the objective rear aperture also receives some

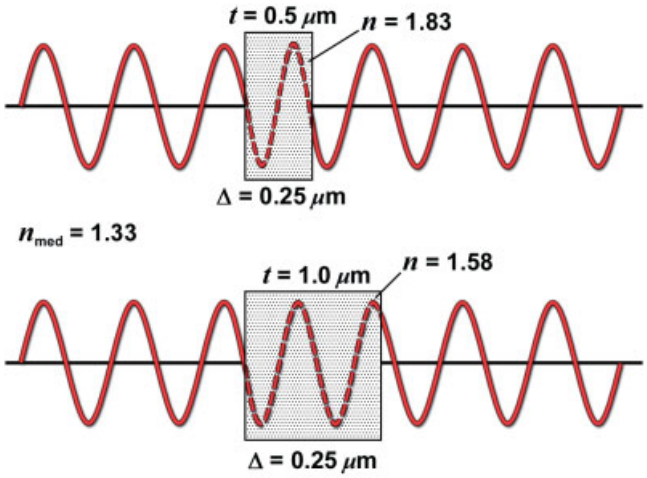

Figure 7.10

Effects of refractive index and specimen thickness on the optical path length. The phase contrast image reveals differences in optical path length as differences in light intensity, thus providing contrast. Since optical path length difference Δ is defined as the product of thickness t and refractive index n such that $\Delta = (n_1 - n_2)t$, two objects that vary both in size and refractive index can have the same optical path length and the same intensity in the phase contrast microscope.

diffracted light from the specimen—a problem accentuated by the fact that the width of the annulus generated by the 0th order surround waves is smaller than the actual width of the annulus of the phase plate. Due to requirements of optical design, the difference in width is usually about 25%. Since diffracted rays corresponding to low spatial frequencies pass through the annulus on the plate, they remain 90° out of phase relative to the 0th order light. The absence of destructive interference by these low spatial frequency diffracted waves causes a localized contrast reversal—that is, a halo—around the object. Halos are especially prominent around large, low spatial frequency objects, such as nuclei and cells. Another contributing factor is the redistribution of light energy that occurs during interference in the image plane. As in the case of the diffraction grating and interference filter, interference results in a redistribution of light energy, from regions where it is destructive to regions where it is constructive. High contrast halos can be objectionable for objects generating large optical path differences such as erythrocytes, yeast cells, and bacteria. In many cases, it is possible to reduce the amount of phase shift and diffraction and therefore the amount of halo, by increasing the refractive index of the medium using supplements such as glycerol, mannitol, dextran, or serum albumin. As will be seen in the next exercise, changing the refractive index of the medium can even reverse image contrast, turning phase-dark objects into the phase-bright ones.

Shade-off is another optical effect that is particularly apparent in images of extended phase objects. In a phase contrast mechanism based solely on optical path differences (one that does not consider the effects of diffraction), you might expect that the image of a large phase object of constant optical path length across its diameter would appear uniformly dark or light, but this is not the case. As shown schematically in Figure 7.11,

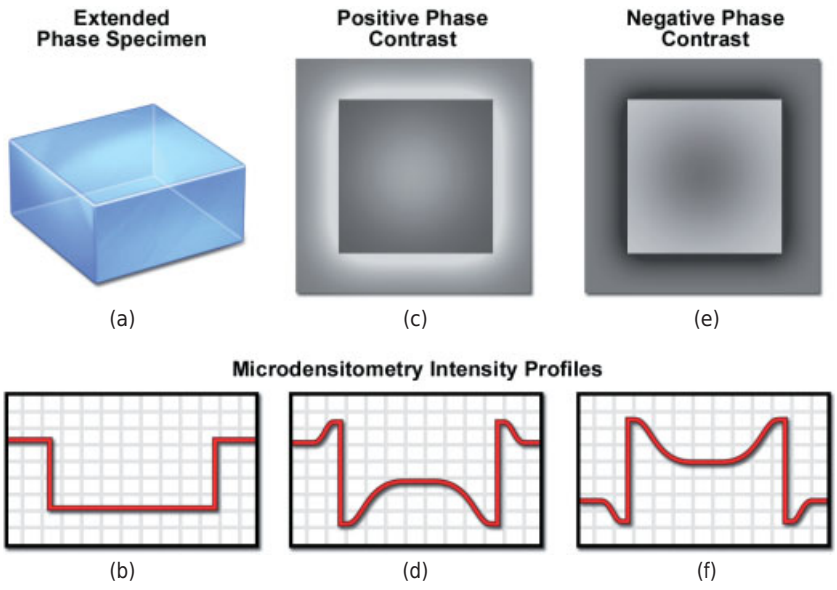

Figure 7.11

The effects of halo and shade-off in the phase contrast image. (a) Phase object. (b) Intensity profile of object shown in panel a. (c) Phase halo and shade-off in positive phase contrast. (d) Intensity profile of panel c. (e) Phase halo and shade-off in negative phase contrast. (f) Intensity profile of panel e.

the intensity profile of a phase-dark object gradually increases towards the center of the object. If the object is large enough, the light intensity in the central regions approaches that of the surrounding background. Shade-off is frequently observed on large, extended objects, such as extended or flattened cells (Fig. 7.1), flattened nuclei, and planar slabs of materials, for example, mica or glass. The phenomenon is also known as the *zone-of-action effect*, because central uniform zones and refractile edge zones of an object diffract light differently. In central regions of an object, the amount of diffraction and the angle of scattering are greatly reduced. Object rays, although retarded in phase, deviate only slightly from the 0th order component, and fall within the annulus of the phase plate. As a result, the amplitude and intensity of the central region are essentially the same as the background. The presence of shade-off in extended objects and high image contrast at edges reminds us that the phase contrast mechanism is principally one of diffraction and scattering.

Exercise: Determination of the Intracellular Concentration of Hemoglobin in Erythrocytes by Phase Immersion Refractometry

In this exercise, you will practice the proper alignment of phase contrast optics, examine blood cells in positive and negative contrast, and using a series of solutions of varying refractive index, calculate the concentration of hemoglobin in your erythrocytes.

The phase shift of light, δ, which occurs when light passes through a cell with refractive index n_o in a medium with refractive index n_m, is given by $\delta = (n_o - n_m)\, t/\lambda$, where t is the thickness of the object and λ is the wavelength. The phase contrast microscope converts the phase shift into an observable change in amplitude. When $n_o > n_m$ (the case for most cellular structures), objects appear dark against a gray background (positive contrast). When $n_m > n_o$, objects look bright against a gray background (negative contrast). When $n_o = n_m$, no relative retardation occurs and the object is invisible. If blood cells are placed in a series of albumin solutions of increasing concentration (made isotonic by adjusting the concentration of NaCl to prevent shrinking and swelling due to osmotic effects), positive and negative cells can be counted under the phase contrast microscope and a curve constructed, and the isotonic point can be determined from the point, at which 50% dark and bright cells are observed. This is a sensitive null method that can be used to obtain the concentration of solids in cells. In this case, we will calculate the intracellular molarity of hemoglobin in erythrocytes. *Note:* For erythrocytes, the intracellular concentration of hemoglobin is so high that cells look bright against a gray background when examined in normal isotonic saline. In the following exercise on erythrocytes, positive cells appear bright, and negative cells look dark.

1. Swab the tip of your finger with 70% ethanol and prick it with a sterile disposable lancet. Place a small drop of *fresh* blood (5 μL) on a microscope slide. Immediately place one drop (~60 μL) of albumin test solution on the droplet of blood, cover with a coverslip, and count the number

of positive and negative cells—100 cells total—for each sample. *Count only single cells that are seen face on. Do not count cell aggregates*. If necessary, you can check for "invisible" cells by turning away the condenser annulus, but perfect refractive index matching occurs only rarely, because the biconcave shape of the cells results in optical path differences through a single cell. Midpoint cells will appear both black and white simultaneously. It is recommended that you prepare and score one slide at a time. To recognize typical positive and negative cells, you should test the extreme albumin concentrations first. You should place your slides in a moist chamber (a sealed container with a moist paper towel) so that they do not dry out while you are busy counting other slides. Calculate the number of negative cells for each solution. Show your work.

2. Plot the % negative cells versus mg/mL albumin on a piece of graph paper, and determine the concentration of albumin giving 50% positive and negative cells.
3. Given that hemoglobin has about the same specific refractive index increment as albumin and comprises 97% of the cell solids, having determined the concentration of albumin that is isotonic to the cells, calculate the molar concentration of hemoglobin in the erythrocytes. The molecular weight of native hemoglobin tetramer is 64,000 Da. Treat the concentration (mg/mL) of bovine serum albumin (molecular weight, 67,000 Da) as if it were hemoglobin, and use the molecular weight (of either) to calculate the molarity of hemoglobin in erythrocytes. How many times more concentrated is hemoglobin in an erythrocyte than tubulin (2 μM) or aldolase (20 nM) in a fibroblast?
4. To what do you attribute the range of phase densities observed in the same erythrocyte sample? What are the estimated extremes of molarity of hemoglobin in your cells? How would you test if this is an artifact or represents real variation?

DARKFIELD MICROSCOPY

In most forms of transmitted light microscopy, both the diffracted rays (rays that interact with the specimen) and nondiffracted rays (rays that pass undeviated through the specimen) are collected by the objective and contribute to image formation. For unstained transparent specimens, we have seen that the component of nondiffracted background light is very large, resulting in bright, low-contrast images in which details are poorly visible. Another solution for viewing such objects is *darkfield microscopy*, in which the nondiffracted rays are removed altogether so that the image is composed solely of diffracted wave components. This technique is very sensitive because images based on small amounts of diffracted light from minute phase objects are seen clearly against a black or very dark background. Darkfield microscopy is most commonly used for minute light-diffracting specimens, such as diatoms, bacteria and bacterial flagella, isolated organelles and polymers, such as cilia, flagella, microtubules, and actin filaments, and silver grains and gold particles in histochemically labeled cells and tissues.

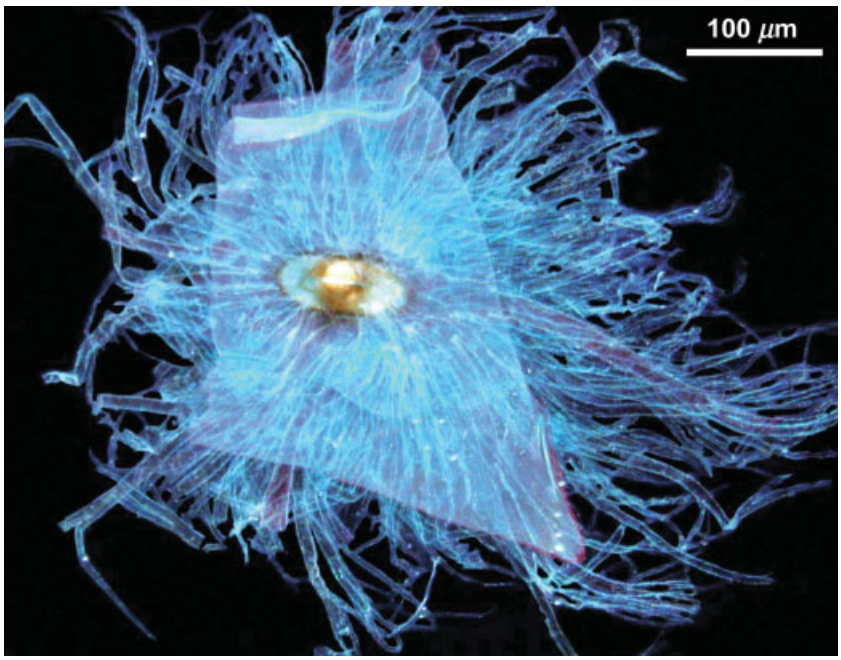

Figure 7.12
Darkfield image of the spiracle (breathing pore) and tracheae of a silkworm larva. Bar = 100 μm.

An example of a darkfield image of the spiracle and tracheae from a silkworm larva is shown in Figure 7.12. The number of scattering objects in the specimen is an important factor, because the scattering of light from too many objects may brighten the background and obscure fine details.

Theory and Optics

Darkfield conditions are obtained by illuminating the specimen at an oblique angle such that direct, nondiffracted rays are not collected by the objective. The effect of darkfield optics can be obtained quickly with brightfield optics by rotating the condenser turret so that rays illuminate the specimen obliquely. Only diffracted light from the specimen is captured by the objective, and the direct waves pass uncollected off to one side of the lens. The disadvantage of this technique is that unidirectional illumination of highly refractile objects can introduce large amounts of flare. Much better images are obtained with a special darkfield condenser annulus, which is mounted in the condenser turret. Special oil immersion darkfield condensers must be used for oil immersion objectives. Darkfield microscopy resembles phase contrast microscopy in that the specimen is illuminated by rays originating at a transparent annulus in the condenser. However, in darkfield optics, only diffracted rays are collected by the objective and contribute to the image; non-diffracted rays are pitched too steeply and do not enter the lens (Fig. 7.13). Since nondiffracted background light is absent from the image, light-diffracting objects look bright against a dark field.

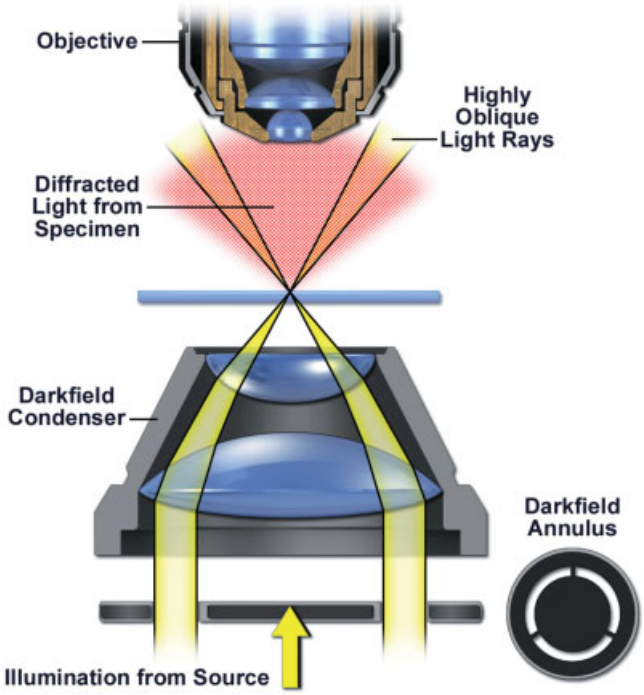

Figure 7.13

Optical scheme for darkfield microscopy. The geometry allows only diffracted light to be collected by the objective. Direct, nondiffracted rays (yellow) are inclined at a steep angle and miss the objective entirely.

There are several ways to create a darkfield image:

- Use the darkfield condenser stop, frequently labeled D on the condenser aperture turret, in combination with a medium power lens with numerical aperture (NA) < 0.8. If the NA of the objective is lower than the NA of the illuminating beam generated by the condenser and darkfield annulus, nondiffracted waves are excluded from the objective. If the objective contains an adjustable diaphragm, this can be stopped down slightly to help block any scattered direct rays that enter the lens.
- An effective and economical approach is to use a phase contrast annulus that is intentionally oversized so that nondiffracted illuminating rays do not enter the objective—that is, a high NA condenser annulus with a low NA objective.
- For high magnification work requiring oil immersion objectives, one can employ special oil immersion darkfield condensers with parabolic or cardioid reflective surfaces (Fig. 7.14). These condensers reflect beams onto the specimen at a steeply pitched angle, giving a condenser NA of 1.2–1.4. A *paraboloid condenser* receives a planar wavefront and reflects it off a polished paraboloidal surface at the periphery of the condenser to a point in the specimen plane. The front aperture of the condenser contains an opaque glass with transparent annulus similar to that used in phase contrast microscopy. A *cardioid condenser* receives a collimated beam

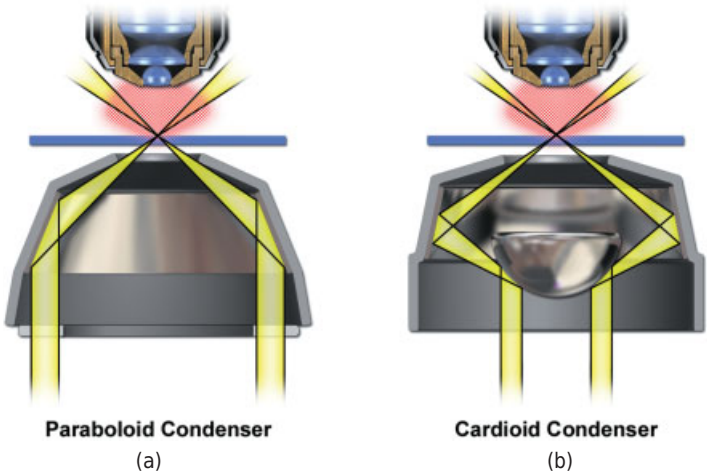

Figure 7.14

Two oil immersion darkfield condensers. (a) A paraboloid condenser receives a planar wavefront that is reflected off a polished paraboloidal surface to a spot in the specimen plane. The front aperture of the condenser contains an opaque glass with transparent annulus similar to that used in phase contrast microscopy. (b) A cardioid condenser receives a hollow cylinder of light, which is reflected by two spherical surfaces to generate a steeply pitched cone of light for specimen illumination: A central convex mirror reflects rays to a peripheral circumferential mirror with the figure of a cardioid, which reflects a steeply pitched cone of light onto the object.

that is reflected at two surfaces to generate a steeply pitched beam for specimen illumination: a central convex spherical mirror reflects rays to a peripheral concave cardioidal mirror that defines the shape of the beam. Illumination by this condenser is aplanatic and thus free of both spherical aberration and coma. Since both condensers work by reflection, there is no chromatic aberration. The oil immersion objectives used with these condensers should contain a built-in iris diaphragm so that the numerical aperture can be reduced to 0.9–1.0 to exclude any direct rays.

Image Interpretation

The appearance of a darkfield image is similar to one of self-luminous or fluorescent objects on a dark background, but with the difference that edges of extended, highly refractile objects diffract the greatest amount of light and dominate the image, sometimes obscuring the visibility of fainter smaller objects. In addition, details in darkfield images are broader and less distinct compared to other imaging modes such as phase contrast, because removal of one entire order of light information from the diffraction plane makes edge definition less distinct in the image. Further, if the NA of the objective selected is too restricted, many diffracted waves are also eliminated, resulting in a loss of definition of fine details in the specimen.

In summary, darkfield optics are advantageous because they allow detection of weak diffracted light signals, and may be the method of choice for viewing fine structural details. Specimens as small as lysosomes, bacterial flagella, diatom striae, and

microtubules are all easily seen in well-adjusted darkfield optics, even though these structures have dimensions that are ~20 times less than the resolution limit of the light microscope. Darkfield optics are also inexpensive, simple to employ, and do not require a lot of special equipment, such as DIC prisms, strain-free lenses, or phase contrast objectives.

Exercise: Darkfield Microscopy

1. Adjust the microscope for darkfield mode using a low NA objective (10 or 20×) and a high-NA phase contrast or darkfield annulus. These annuli produce steeply pitched cones of light that are not accepted by low NA, 10 or 20× objectives. Only the scattered light is accepted, which is what you want.
2. With the microscope adjusted for Koehler illumination, focus on a few isolated buccal epithelial cells (obtained from a scraping of the underside of the tongue) and compare with the image obtained by phase contrast microscopy. Notice that object edges are enhanced by both of these modes of microscopy. In darkfield, each speck of dirt is imaged as a beautiful Airy disk surrounded by higher order diffraction rings. This is an excellent chance to see the Airy disc, the diffraction pattern of a point source of light.
3. Using an oil immersion darkfield condenser (NA 1.4) and a 60 or 100× oil immersion objective, focus on the cilia and flagella of unicellular protozoa and algae. Cultures of protozoa can be obtained commercially, but a drop of pond water will do as well. *Note:* If the objective contains an aperture diaphragm, try stopping it down to improve contrast and visibility, as minute structures are difficult to detect.

The following specimens are suggested for darkfield examination:

- Buccal epithelial cells
- Culture of protozoa
- Axons and glial cells in sections of rat brain labeled with antibodies adsorbed on gold colloid particles
- Blood cells in a 10-μL drop of phosphate-buffered saline
- Taxol-stabilized microtubules in 15-mM imidazole, 1-mM Mg-GTP, 5-μM taxol. The microtubule stock is ~5–10 mg/mL. Dilute to 0.1 mg/mL for observation. Difficult specimen!
- Flagella of *Escherichia coli* bacteria. Difficult specimen!

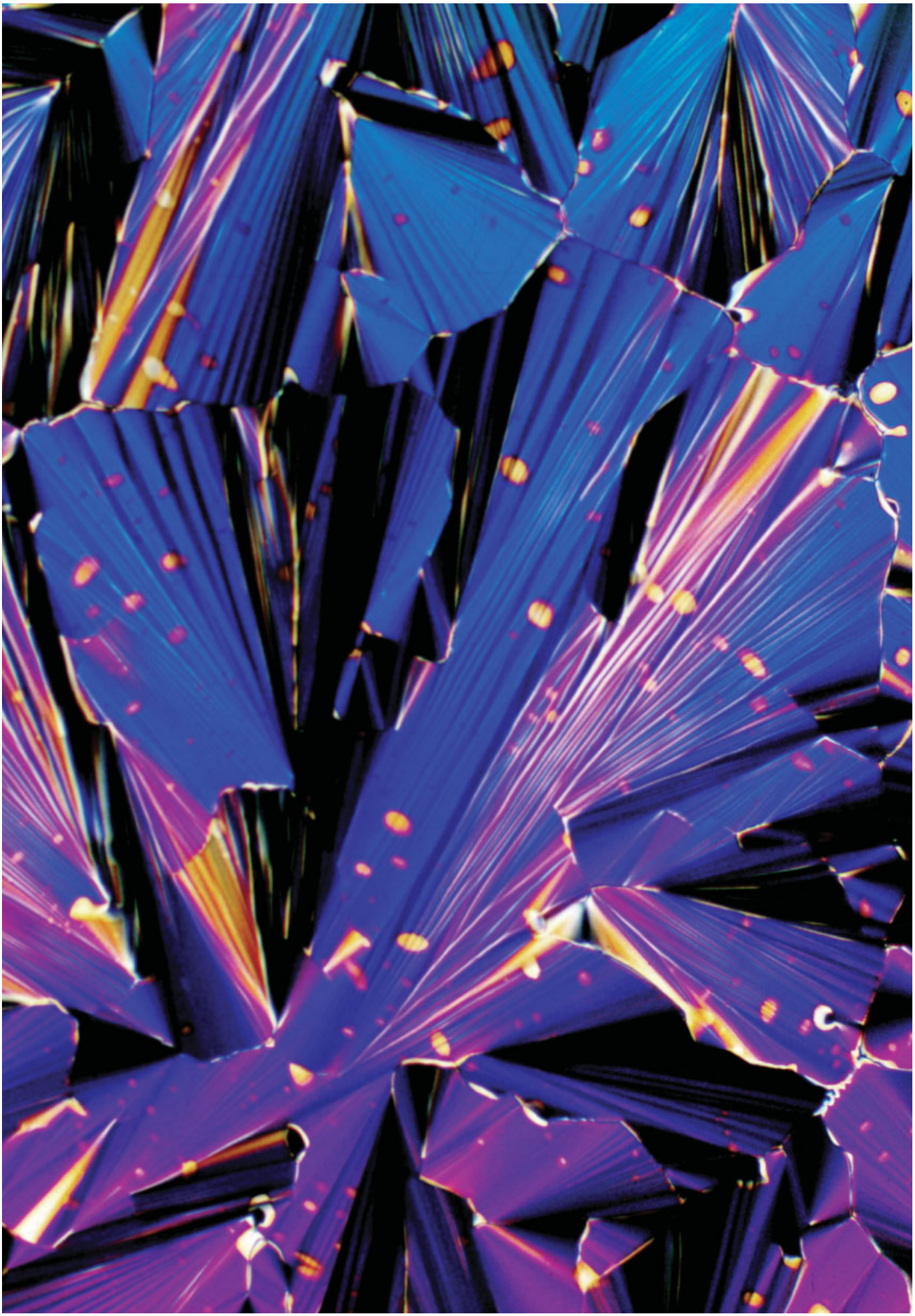

CHAPTER

8

PROPERTIES OF POLARIZED LIGHT

OVERVIEW

In this chapter, we turn our attention to polarization microscopy and a unique class of molecularly ordered objects that become visible upon illumination with polarized light. Figure 8.1 demonstrates the unique ability of a polarizing microscope to reveal molecular order in human hair, minerals, muscle tissue, and starch grains. Polarized light is also used in interference microscopy, including differential interference contrast (DIC) microscopy. Although we can observe high-contrast images of ordered objects using a polarizing microscope, it is remarkable that the eye has no ability in the usual sense to distinguish polarized light from random light. For this, we require special filters called polarizers. The relationships between the physics of polarized light and images of molecularly ordered specimens are remarkable in their economy and precision and are well worth mastering. Since the topic of polarized light is technically demanding, we use this chapter to describe its generation, properties, and interaction with different objects and optical devices. Our goal is to understand the working principles of the polarizing microscope, which is described in Chapter 9. Our reward will be in appreciating how the polarizing microscope reveals patterns of molecular order that otherwise can only be studied using more expensive, technically difficult methods, such as electron microscopy or x-ray diffraction, that operate at the resolution limit of molecules and atoms.

THE GENERATION OF POLARIZED LIGHT

The bulk light from most illuminators used in light microscopy is nonpolarized, the E vectors of different rays vibrating at all possible angles with respect to the axis of

Polarized light image of liquid crystalline DNA.

Fundamentals of Light Microscopy and Electronic Imaging, Second Edition.
Douglas B. Murphy and Michael W. Davidson.

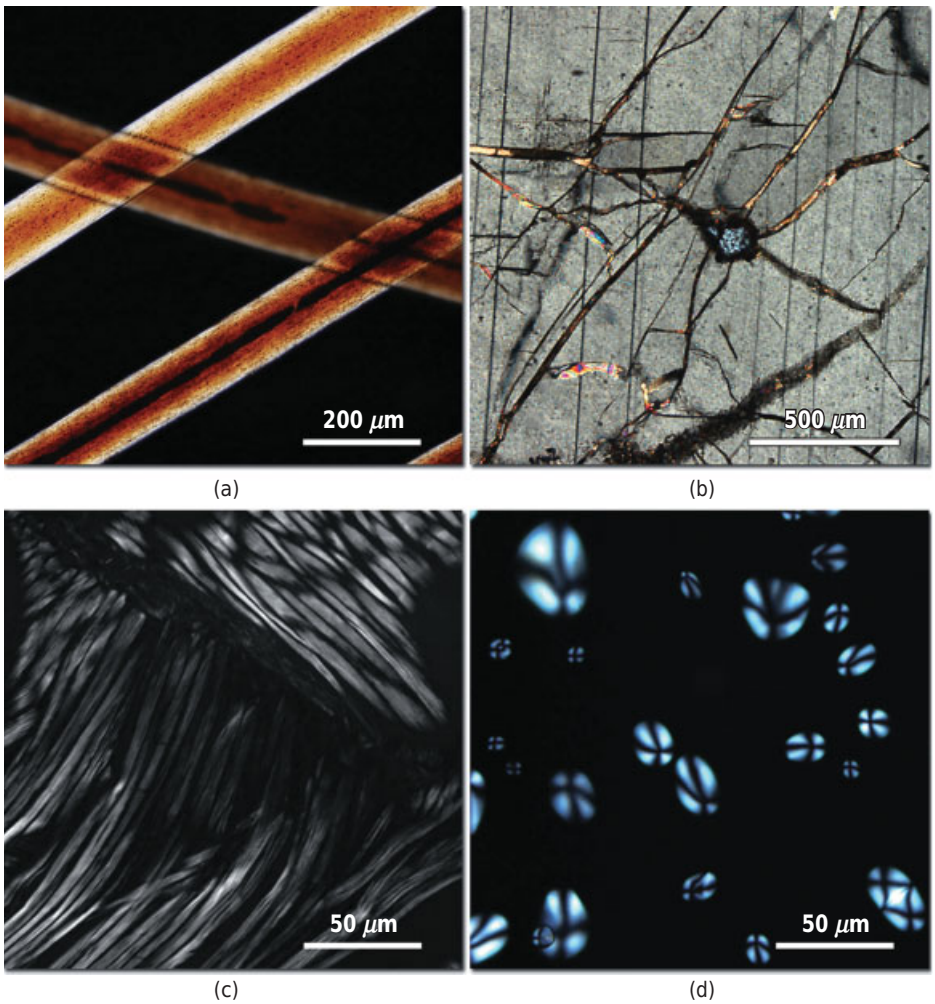

Figure 8.1

Materials imaged with polarized light. (a) Human hair. (b) Polished (30-μm) section of the mineral camptonite. (c) Rabbit smooth muscle. (d) Potato starch. The high contrast indicates a high degree of molecular order in these structures.

propagation (Fig. 8.2a). In a ray or beam of *linearly polarized light*, the E vectors of all waves vibrate in the same plane; the E vectors of beams of polarized light covering an extended area are *plane parallel*. Since the plane of vibration of the E vector can occur at any angle, to describe the orientation of the plane in a beam cross section, we describe the angle of tilt relative to a fixed reference plane designated 0° (Fig. 8.2b). A device that produces polarized light is called a *polarizer*; when used to determine the plane of vibration, the same filter is called an *analyzer*.

The most efficient polarizers are made of transparent crystals, such as calcite, but polarized light can also be generated simply and economically using a partially light-absorbing sheet of linear polarizing material similar to the type originally introduced by the Polaroid Corporation. Linear polarizers have a unique transmission axis (usually

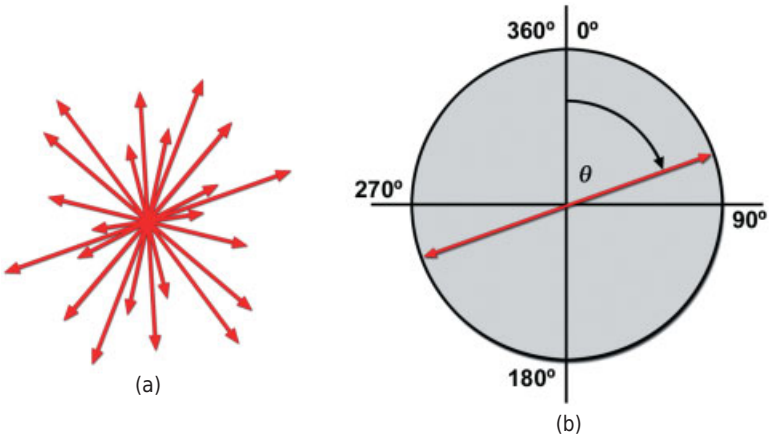

Figure 8.2

Random versus linearly polarized light. The drawings show two beams of light, each containing several photons, as they would appear in cross section, looking down the axis of the beam. Refer to Figure 2.2 for orientation. (a) Random light: The E vectors of the waves are randomly oriented and vibrate in all possible planes with different amplitudes. (b) Linearly polarized light: The E vectors of all waves comprising the beam vibrate in a single plane (red double-headed arrow). The angle of the plane of vibration of the E vector relative to the vertical reference line is designated θ. The angle of tilt is called the azimuthal angle.

marked on the plate) that defines the plane of vibration of the transmitted rays. Polarizers also play an important role as an analytic tool for determining the orientation of polarized light whose plane of vibration is not known. Two linear polarizers—a polarizer and an analyzer—are incorporated in the optics of a polarizing microscope.

Demonstration: Producing Polarized Light with a Polaroid Filter

A *Polaroid sheet*, or *polar*, is a polarizing device that can be used to demonstrate linearly polarized light. The sheet has a transmission axis, such that incident waves whose E vectors vibrate in a plane parallel to the axis pass through the filter, while other rays are absorbed and blocked (Fig. 8.3). Because of its unique action, the Polaroid sheet can be used to produce linearly polarized light or to determine the plane of vibration of a polarized beam whose orientation is not known. Used in these ways, the sheet is then called, respectively, a polarizer or an analyzer. To become familiar with polarized light, perform the following operations using a pair of Polaroid sheets:

- Place two polars on top of each other on a light box and rotate one of the polars through 360°. At two azimuths separated by 180°, light transmission reaches a maximum, while at two azimuths, separated from the first two by 90° transmission is substantially blocked, and the field looks black. In the

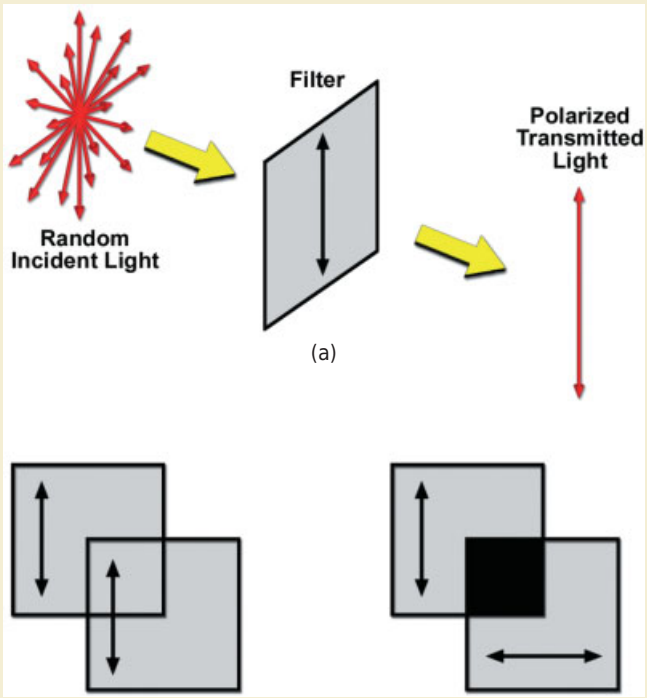

Figure 8.3

A Polaroid sheet generates linearly polarized light. (a) Only rays whose E vectors vibrate in a plane parallel with the transmission axis of the sheet are transmitted as a linearly polarized beam; other rays are partially transmitted or blocked. (b) A second overlapping polar transmits light of the first polar if its transmission axis is parallel to that of the first polar. (c) Transmission is completely blocked if the transmission axes of the two polars are crossed.

first case light is transmitted because the transmission axes of the two polars are parallel, and all of the light transmitted by the first filter passes through the second. The removal of light at the unique crossed position is called *extinction*. Here, polarized light from the first filter vibrates in a plane that is perpendicular to the transmission axis of the second filter and is substantially blocked by the second filter.

- Examine a beam of light reflected off a flat nonconducting surface (glass or plastic) with a polar while rotating it through 360°. The reflected beam is minimized at two azimuths, indicating that it is partially linearly polarized. Used this way, the Polaroid sheet is called an analyzer. If the transmission axis of the polar is known beforehand, you should be able to observe that the plane of vibration of the reflected rays is parallel to the plane of the reflecting surface. If the transmission axis of a polar is not known, inspection of a reflected beam can be used to determine the approximate orientation of its transmission axis.

- Using two crossed polars positioned on a light box, examine a piece of glass such as a microscope slide and a sheet of cellophane, while rotating them between the polars. The glass does not interact with polarized light and remains essentially invisible. Such materials are said to be *optically isotropic*. However, rotation of the cellophane sheet through 360° reveals four azimuths separated by 90°, at which the entire sheet looks very bright. The unique ability of cellophane to interact with polarized light is due to the presence of aligned parallel arrays of cellulose molecules and birefringence, which is described later in the chapter. Materials of this type are said to be *optically anisotropic*. All objects suitable for polarization microscopy exhibit some degree of molecular orientation and optical anisotropy.

POLARIZATION BY REFLECTION AND SCATTERING

Polarized light is also produced by a variety of physical processes that deflect light, including refraction, reflection, and scattering. Light reflected from the surfaces of dielectric materials and metal surfaces is partially linearly polarized, with the E vectors of the reflected waves vibrating parallel to the reflecting surface and the extent of polarization increasing with decreasing angles of incidence. For light incident on a transparent material, such as water or glass, there is a unique angle known as *Brewster's angle*, at which the reflected waves are completely plane-polarized (Fig. 8.4a). For the simple case of a beam of incident light traveling through air ($n = 1$), the critical angle is given as:

$$\tan\theta = n.$$

For water ($n = 1.33$) and glass ($n = 1.515$), the critical angles are 53° and 57°, respectively. As an interesting note on reflection polarization, manufacturers of Polaroid sunglasses mount sheets of polarizing material in the frames with the transmission axis of the Polaroids oriented perpendicularly in the field of view. Bright reflections off horizontal surfaces, such as the roofs of cars or water on a lake, are very efficiently blocked (Fig. 8.4b), while the random light is partially blocked, since only vertically polarized rays can reach the eye.

Linearly polarized light is also produced by light scattering. A common example is the polarization of light in the northern sky caused by the scattering of sunlight by air molecules. The extent of polarization (~50%) is readily appreciated on a clear day by rotating a polarizer held close to the eye. In accordance with principles of scattering, polarization is maximal at an angle 90° from the sun. For additional information on polarization by refraction, reflection, and scattering, see the interesting discussions by Minnaert (1954) and Hecht (2001).

VECTORIAL ANALYSIS OF POLARIZED LIGHT USING A DICHROIC FILTER

The Polaroid sheet described above commonly consists of a film of parallel arrays of linear polyvinyl alcohol molecules with embedded polyiodide microcrystals (H-ink)

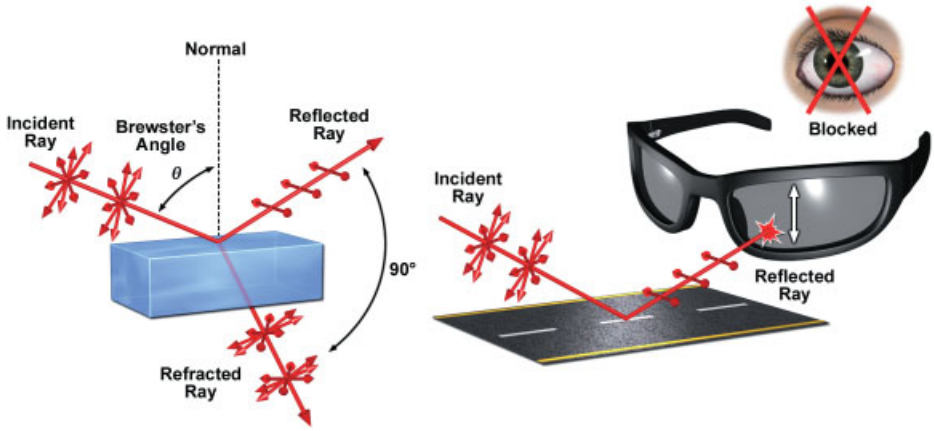

Figure 8.4

Reflection polarization and Brewster's critical angle. (a) The drawing shows an incident ray of random light (E vectors at random orientations) being reflected off a horizontal surface (glass or other dielectric material) as a linearly polarized beam to the eye. At a certain critical angle (Brewster's angle θ), the degree of polarization of the reflected ray is 100%, and the E vectors of reflected rays vibrate in a plane that is perpendicular to the plane of incidence (the plane defined by the incident, reflected and refracted rays). The refracted ray, oriented at a 90° angle with respect to the reflected ray, is only partially polarized. (Note: Brewster's angle is defined by the condition that exists when the reflected wave is at 90° to the refracted wave; the phenomenon occurs because in the second medium the electric vector of the component in the plane of incidence is pointing in the direction of propagation of the reflected wave and consequently has no resultant wave in that direction.) (b) A Polaroid sheet can be used to demonstrate the polarized nature of the reflected ray. If the transmission axis of the Polaroid is oriented at 90° with respect to the vibrational plane of the reflected ray, transmission is blocked. This principle is used to advantage in the design of Polaroid sunglasses to reduce or eliminate reflective glare.

aligned in the same direction as the organic matrix. The transmission axis of the filter is perpendicular to the orientation of the crystals and linear polymers in the filter. Thus, rays whose E vectors vibrate parallel to the crystal axis are absorbed. Waves with oblique orientations are partially absorbed, depending on the azimuths of their vibrational planes. Filters like the Polaroid sheet that differentially transmit rays vibrating in one plane while absorbing those in other planes are said to exhibit *dichroism*; hence the common name, *dichroic filter*. As we will see in later sections, the Polaroid sheet is a special kind of beamsplitter designed to transmit rays vibrating at a certain azimuthal angle as linearly polarized light. For H-series filters that are commonly employed in microscopy, only about 25% of incident random light is transmitted, but the degree of polarization of the transmitted rays is >99%.

If two polarizers are oriented so that their transmission axes are perpendicular to each other, they are said to be crossed, and all of the light transmitted by the polarizer (now linearly polarized) is extinguished by the analyzer (Fig. 8.3). The extent to which incident random light is extinguished by two crossed polars is called the *extinction factor*, and is defined as the ratio of the intensity of transmitted light observed for two polars when positioned in parallel and in crossed orientations ($I_{\parallel}/I_{\times}$). Extinction factors

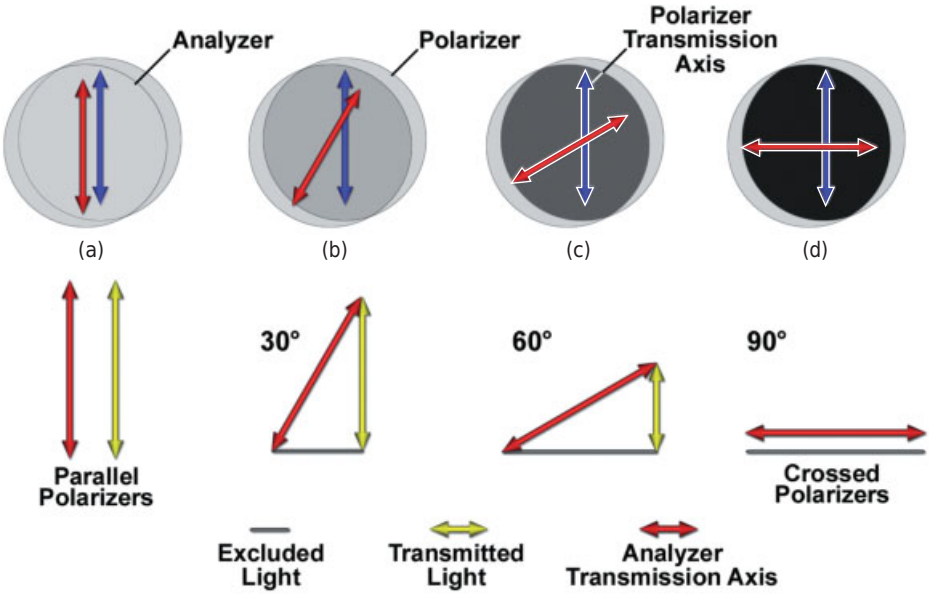

Figure 8.5

Transmission through a polarizer of linearly polarized rays vibrating in different planes. The upper row shows how the percent transmission of light through two overlapping linear polarizers depends on the relative orientation of their transmission axes (red and blue arrows). When the transmission axes are crossed at 90°, the transmission is close to 0 (d). The bottom row of figures shows how the amplitudes of rays (red and yellow vectors) vibrating at azimuthal angles different from the transmission axis of the polarizer can be resolved into their horizontal and vertical components by vector analysis. The amplitude of the transmitted ray (yellow) is equal to the vertical vector component.

of 10^3–10^5 or greater are required for polarization microscopy and can be obtained using two crossed dichroic filters.

The role of the analyzer in controlling the transmission of polarized light can be understood from vector diagrams showing the angular orientation (azimuthal angle) and magnitude of the E vectors of rays drawn from the perspective of viewing a ray end-on, down its axis of propagation. Figure 8.5 shows a vertically oriented analyzer, four incident waves of linearly polarized light that are equal in amplitude but vibrating in different planes, and the amplitudes of those waves after transmission through the analyzer. If each incident wave is resolved into its horizontal and vertical components, it can be seen that the entire vertical component of each ray passes through the analyzer. Further, the amplitude of the vertical component and that of the transmitted ray rapidly decrease as the plane of vibration of the incident ray approaches an azimuth perpendicular to the transmission axis of the analyzer.

The amount of light transmitted through two polars crossed at various angles can be calculated using *Malus' law*, which states that:

$$I = I_o \cos^2 \theta,$$

where I is the intensity of light passed by an analyzer, I_o is the intensity of an incident beam of linearly polarized light, and θ is the angle between the azimuth of polarization

of the incident light and the transmission axis of the analyzer. Thus, for two polars crossed at a 90° angle, $\cos^2\theta = 0$, and $I = 0$, so polarized light produced by the first filter (the polarizer) is completely excluded by the second filter (the analyzer). For polars partially crossed at 10° and 45°, the light transmitted by the analyzer is reduced by 97 and 50%, respectively.

DOUBLE REFRACTION IN CRYSTALS

Many transparent crystals and minerals, such as quartz, calcite, rutile, tourmaline, and others, are optically anisotropic and exhibit a property known as *double refraction*. When letters on a printed page are viewed through a calcite crystal, remarkably, each letter appears double (Fig. 8.6). Calcite is therefore said to be *doubly refracting*, or *birefringent*. Birefringent materials split an incident ray into two components that traverse different paths through the crystal and emerge as two separate rays. This occurs because atoms in crystals are ordered in a precise geometric arrangement, causing direction-dependent differences in the refractive index. In contrast, a sheet of glass, such as a microscope slide, which is an amorphous mixture of silicates, is usually optically isotropic and does not exhibit double refraction.

When a ray of light is incident on a birefringent crystal, it usually becomes split into two rays that follow separate paths. One ray, the *ordinary ray* or *O ray*, observes the laws of normal refraction, while the other ray, the *extraordinary ray* or *E ray*, travels along a different path. Thus, for every ray entering the crystal, there is a pair of O and E rays that emerges, each of which is linearly polarized. *The electric field vectors of these two rays vibrate in mutually perpendicular planes*. A sketch depicting this phenomenon is shown in Figure 8.7a. These features are easily observed by placing a crystal of calcite on a printed page and looking down on the crystal while rotating a dichroic filter held in front of the eye (see Demonstration); the double letters become alternately visible and invisible as the filter is rotated through an angle of 90°. There are two unique angles of incidence on the crystal for which the behavior is different. (1) The calcite crystal and others of its class contain a single unique axis known as the

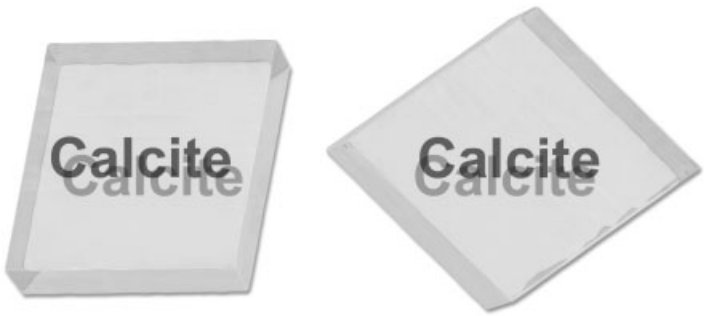

Figure 8.6

Double refraction in a calcite crystal. The word calcite viewed through a plane surface of the crystal appears double, the two images corresponding to the ordinary and extraordinary rays. As the crystal is rotated, the E-ray image (lighter gray) rotates around the O-ray image (darker gray). The O-ray image obeys the normal laws of refraction and does not rotate.

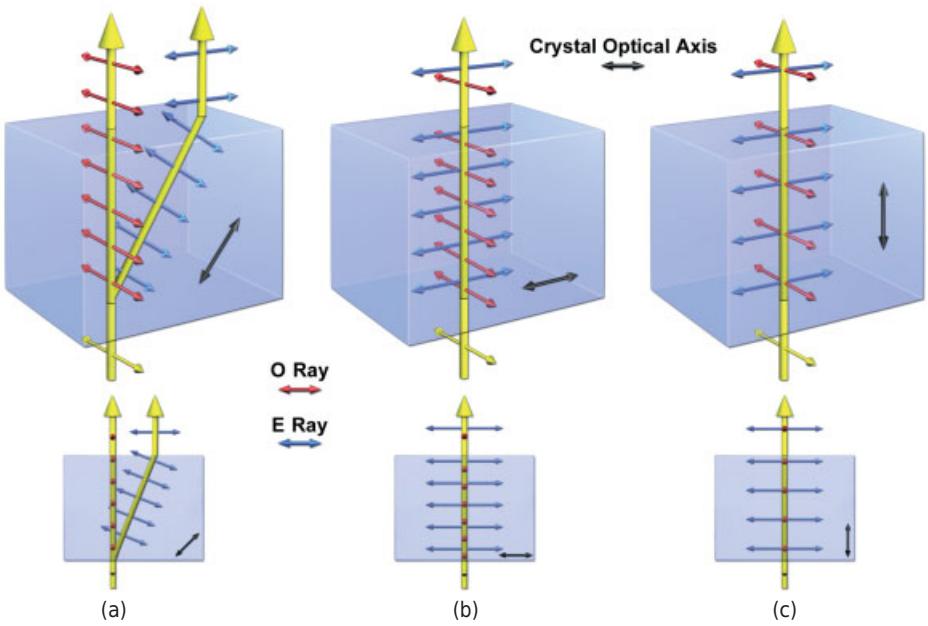

Figure 8.7

Splitting of an incident ray into O- and E-ray components by a birefringent crystal. The rectangular slabs shown in panels a, b, and c have been cut from parent crystals in such a way that the optical axes are oriented differently (indicated by a black double arrow), and are presented in 2D (lower) and 3D (upper) views. Incident light is linearly polarized. Red and blue double-headed arrows indicate the planes of vibration of linearly polarized O and E rays, respectively. (a) A ray incident on a crystal at an angle oblique to the optical axis of the crystal is split into O and E rays that traverse different physical paths through the crystal. The emergent O and E rays are linearly polarized, vibrate in mutually perpendicular planes, and exhibit an optical path difference. (b) An incident ray whose propagation axis is perpendicular to the optical axis is split into O and E rays, but the two rays follow the same trajectory through the crystal and do not diverge. Emergent rays can exhibit an optical path difference. This is the usual case for birefringent biological specimens. (c) An incident ray whose propagation axis is parallel to the optical axis is not split and behaves as an ordinary ray. The optical path lengths of the emergent rays are the same.

optical axis. Incident beams that are perpendicular to the optical axis are split into O and E rays, but the trajectories of these rays are coincident (Fig. 8.7b). At this unique angle of incidence, the O and E rays emerge at the same location on the crystal surface, but have different optical path lengths and are therefore shifted in phase. *This geometry pertains to most biological specimens that are examined in a polarizing microscope*. (2) Incident rays that follow trajectories parallel to this axis behave as ordinary rays and are not split into O and E rays (Fig. 8.7c). Under these conditions of illumination, calcite behaves as if it were optically isotopic, like glass. (It is difficult to demonstrate the optical axis of calcite because it runs obliquely across the diameter of the crystal, and it is necessary to look down crystal edges. One solution is to examine a specially prepared slab cut perpendicularly to the optical axis of the crystal.) These principles are displayed clearly in Hecht (2001), Pluta (1988), and Wood (1964).

Demonstration: Double Refraction by a Calcite Crystal

- Place a crystal on a page of printed text and rotate the crystal while looking down on it from above. One ray does not move as the crystal is rotated (the O ray), whereas the other ray (the E ray) rotates around the fixed ray according to the angle of rotation of the crystal (Fig. 8.6). The O ray does not move because it obeys the laws of normal refraction and passes through the crystal on a straight, undeviated trajectory. The E ray, in contrast, travels along a tilted or oblique path, and its point of emergence at the surface of the crystal changes depending on the orientation of atoms in the crystal and therefore on the orientation of the crystal itself. Because the angle of divergence is so great, wedges of calcite crystal can be cut and glued together in such a way that one of the two components is reflected and removed while the other is transmitted, making calcite an ideal linear polarizer.
- Examine the crystal resting on a black spot on a blank page through a dichroic polarizing filter held close to the eye while rotating the crystal through 360°. First, one ray, then the other ray alternately comes into view and becomes extinguished, and the black spot appears to jump back and forth as the filter is rotated through increments of 90°. The double images correspond to the O ray and E ray, each of which is linearly polarized and vibrates in a plane perpendicular to the other. For most birefringent crystals, the two rays are close together and must be magnified to be observed, but in calcite, the rays are so widely separated that no magnification is necessary. As we will see, this is due to large differences in the refractive index along different paths through the crystal. Notice too that polarized light cannot be distinguished from ordinary random light and that an analyzer is required to distinguish the different planes of polarization.

Materials such as calcite, quartz, and most molecularly ordered biological structures that contain a single optical axis are called *uniaxial*. Another class of *biaxial* crystals with two optical axes also exists, but is rarely encountered in biological systems. Biological examples of ordered macromolecular assemblies that can be seen in the polarizing microscope include such objects as lipid bilayers, bundles of microtubule and actin filaments, plant cell walls, crystalline granules of starch, lignin, and other materials, chromosomes from certain organisms, DNA kinetoplasts in trypanosomes, chloroplasts, and many other structures.

We have used the terms *double refraction* and *birefringence* to refer to the ability of molecularly ordered objects to split an incident ray of light into two components, the O and E rays, but the two terms refer to different aspects of the same process. Double refraction refers to the visible phenomenon: the splitting of a single incident ray into two resultant rays as exemplified by a crystal of calcite. Birefringence refers to the cause of the splitting: the existence of direction-dependent variation in the refractive index in a molecularly ordered material. Birefringence B also refers to a measurable quantity, the difference in the refractive index $(n_e - n_o)$ experienced by the O and E rays during transit through an ordered object such that:

$$B = (n_e - n_o).$$

Depending on the values of n_e and n_o, the *sign of birefringence* may be positive or negative, and specimens are therefore said to be either *positively* or *negatively* birefringent. Note also that birefringence is not a fixed value, but varies, depending on the orientation of the birefringent object relative to the illuminating beam of polarized light. We return to this important point in later sections.

Birefringence is related to another term, the *optical path difference*, Δ (or in the field of polarized light, the *relative retardation*, Γ), and both are defined as the relative phase shift expressed in nanometers between the O and E waves emergent from a birefringent object. As described in Chapters 5 and 7, the optical path length δ is given as $\delta = nt$, where n is the refractive index of a homogeneous medium between points A and B, and t is the object thickness. Notice that the optical path length is a distance given in units of parameter t and that this term is equal to the geometric distance only when $n = 1$. The optical path difference Δ for two objects spanning the same distance is:

$$\Delta = (n_1 - n_2)t.$$

Relative retardation and birefringence are related by the analogous expression:

$$\Gamma = (n_e - n_o)t,$$

where t is the thickness, the physical distance traversed through the specimen. Accordingly, small and large objects may give the same retardation depending on the magnitude of their birefringence and physical size. Retardation can also be expressed as the mutual *phase shift* δ between the two wavelengths, and is given (in radians) by:

$$\delta = 2\pi\Delta/\lambda.$$

Double refraction or birefringence is a property both of polarizers used in a polarizing microscope and of microscope specimens that are active in polarized light. Its presence in a specimen allows us to measure the pattern and extent of molecular alignments, refractive index differences, and specimen thickness.

KINDS OF BIREFRINGENCE

Birefringence can be an inherent physical property of specimens, such as the calcite crystal, or can be generated through cell biosynthetic activities (cellulose fibrils and starch granules in plant cells), or can arise from outside physical forces (cytoplasmic flow and cell movements) acting on components of an otherwise disorganized system. Various kinds of birefringence have been defined:

- *Intrinsic birefringence* is based on the asymmetry of polarizability of chemical bonds within naturally occurring materials, such as crystals. Examples: crystals of calcite and quartz.
- *Form birefringence* or *structural birefringence* is associated with extensive ordered arrangements of macromolecular assemblies having dimensions and spacings comparable with the wavelength of light. Form birefringence is sensitive to the refractive index of the surrounding medium. Examples: parallel arrangements

of actin and myosin filaments in muscle myofibrils (Fig. 8.1c), microtubule bundles in mitotic spindle fibers of dividing cells.

- *Flow birefringence* refers to the induced alignment of asymmetric, plate- or rod-shaped molecules in the presence of fluid flow or agitation. Examples: stirred solutions of detergents (shampoo), DNA, or flagella.
- *Strain birefringence* describes the forced alignment of molecules in a transparent solid deformed by an externally applied mechanical force. Example: stretched films of polyvinyl alcohol.
- *Stress birefringence* is descriptive when electronic deformation occurs in response to an external mechanical force without there being significant gross deformation. Example: a stressed lens caused by compression during mounting in a retaining ring or lens barrel.

PROPAGATION OF O AND E WAVEFRONTS IN A BIREFRINGENT CRYSTAL

In Chapter 5, we employed the concept of Huygens' wavelets to describe the location of a secondary wavefront generated by spherical wavelets and originating from a point source of light in a homogeneous medium. In a transparent birefringent material, the ordinary or O ray behaves in the same way, generating a spherical wavefront. However, the extraordinary or E wave behaves differently. As described by Huygens in 1690, the expanding wavefront of the E ray at a time t can be described as the surface of an ellipsoid (Fig. 8.8). An *ellipsoid* is the figure generated by rotating an ellipse about its

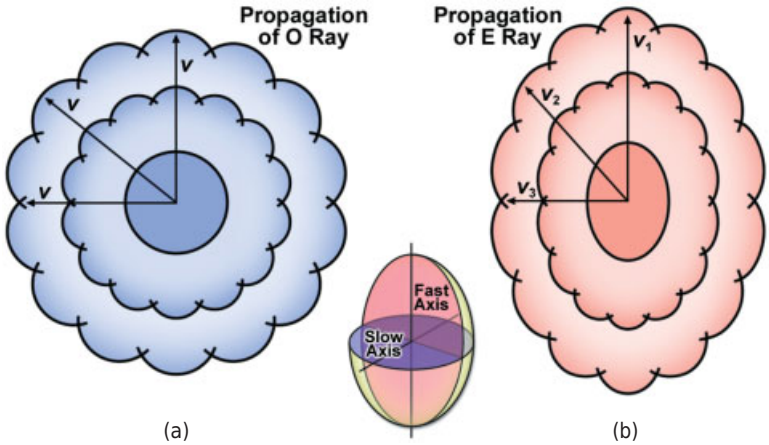

Figure 8.8

O and E rays emanating from a point in a birefringent material define spherical and ellipsoidal wavefronts. (a) The wavefront defined by O rays is spherical because the refractive index is uniform in all directions and waves propagate at a velocity given by the expression $v = c/n$. Circles are used to draw Huygens' wavelets to depict the spherical wavefront. (b) The wavefront defined by the E rays is ellipsoidal because the refractive index n varies in different directions depending on the three-dimensional distribution (shown as v_1, v_2, and v_3), resulting in a surface wavefront with the shape of an ellipsoid. Huygens' wavelets are drawn using ellipses instead of circles to depict the advancing wavefront.

major or minor axis. The ellipsoidal form indicates the presence of different velocities for the E ray along different trajectories in the crystal, where the upper- and lower-limit velocities define the long and short axes of the wavefront ellipsoid. The long axis corresponds to the direction along which the wavefront reaches its greatest possible velocity through the crystal, and is termed the *fast axis*, while the short axis corresponds to direction giving the smallest velocity and is called the *slow axis*. The velocities of waves traveling in all other directions have intermediate values.

Since the velocity of light in a medium is described $v = c/n$, where c is the speed of light in a vacuum and n is the refractive index, we may infer that n is not constant in a birefringent crystal, but varies, depending on the path taken by a ray through the crystal. Several additional points about the propagation of wavefronts in a crystal are worth noting:

- For uniaxial crystals, the O and E wavefronts coincide at either the slow or the fast axis of the ellipsoid, and the difference in surface wavefronts along the propagation axis is termed the optical path difference or relative retardation.
- If the O and E wavefronts coincide at the major axis of the ellipsoid, $n_e > n_o$ in directions other than along the optical axis, and the specimen is said to be positively birefringent (Fig. 8.9). This is the case for crystals, such as quartz, and most ordered biological materials. For materials such as calcite, whose O and E wavefronts meet at the minor axis of the ellipsoid, $n_o > n_e$ in directions other than along the optical axis. Such material are said to exhibit negative birefringence.
- For the unique case that the incident illuminating beam is parallel or perpendicular to the optical axis of the crystal, the paths of O and E rays follow the same trajectory and exit the crystal at the same location. If the incident ray is parallel to the optical axis, the E ray behaves as an O ray; if the incident ray is perpendicular to the optical axis, the O and E ray components experience different optical path lengths.

Double refraction is based on Maxwell's laws of electromagnetism. An explanation requires vector calculus and is beyond the scope of this text, but we can make a brief

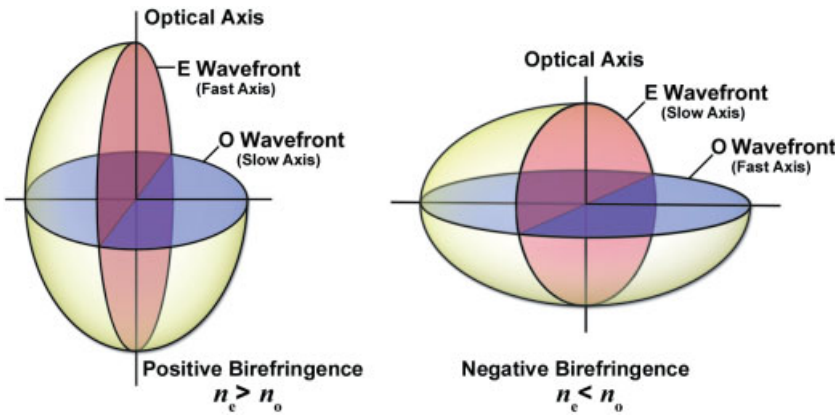

Figure 8.9
The relation of O and E wavefronts in specimens showing positive and negative birefringence.

qualitative explanation of the principles involved. Since light contains both electric and magnetic components, the velocity of light in a medium depends in part on the electrical conductivity of the material and the interaction of light with electric fields in that medium, a property called the *dielectric constant*, ε. For most dielectric substances and biological materials, magnetic permeability is close to 1 and can be discounted; however, for materials with reduced magnetic permeability (metallic films), this would not be the case. The dielectric constant ε is related to the refractive index n by the simple relationship:

$$\varepsilon = n^2.$$

Therefore, in crystals having a particular lattice structure of atoms and molecules, the value of n is different in different directions, depending on the orientations of chemical bonds and electron clouds around atoms and molecules. The short axis (slow axis) of the wavefront ellipsoid corresponds to the axis defining the highest refractive index value; the long axis (fast axis) corresponds to the axis having the lowest refractive index value. The ellipsoid describing the orientation and relative magnitude of the refractive index in a crystal is called the *refractive index ellipsoid* or simply *index ellipsoid*.

BIREFRINGENCE IN BIOLOGICAL SPECIMENS

We have seen that the velocity of light during transit through a specimen is retarded by perturbations and interactions with electrons in the transmitting medium. The susceptibility of an electronic configuration to distortion is termed its *polarizability*. The more polarizable the electronic structure of a molecule, the more extensively light can interact with it and, thus, the more slowly light is transmitted. In the extreme case, the interaction may be so strong that the specimen absorbs quanta of light.

Most chemical groups are asymmetric with respect to polarizability. For example, the electrons of carbon–carbon bonds in molecules with long carbon chains are most easily displaced along the direction of the bond (Fig. 8.10). A structure containing

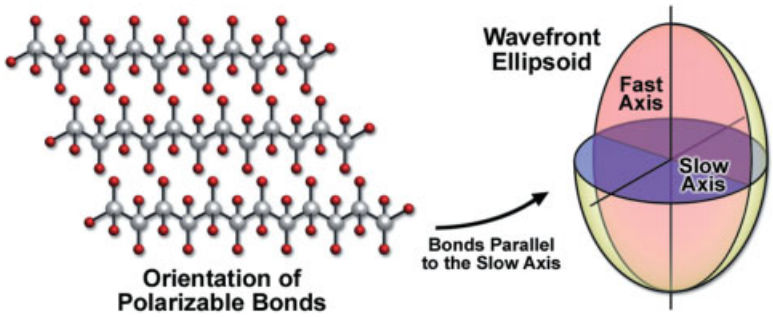

Figure 8.10

The axis of polarizability corresponds to the slow axis of the *wavefront ellipse*. In biological materials composed of linear arrays of macromolecules, the axis of strongest polarizability is usually determined by the direction of carbon–carbon bond alignments. Because polarizability and refractive index are highest in the direction parallel to the axis of bond alignment, this direction corresponds to the slow axis of the wavefront ellipsoid for this material.

parallel chains of carbon–carbon bonds like the cellulose polymers in cellophane is most polarizable in a direction parallel to the carbon chains. Since $\varepsilon = n^2$, the velocity of light is lowest and the refractive index is highest in this direction. Therefore, when long carbon chain molecules are regularly oriented in biological structures as they are, for example, in cellulose fibers comprising a plant cell wall, the polarizability of the structure as a whole varies with its orientation in the illuminating beam of polarized light. As shown in Chapter 9, the orientation of wavefront and index ellipsoids and the sign of birefringence of the specimen can be determined with the help of a compensator such as a full waveplate.

GENERATION OF ELLIPTICALLY POLARIZED LIGHT BY BIREFRINGENT SPECIMENS

Birefringent objects split rays of incident light into separate O- and E-ray components whose E vectors vibrate in mutually perpendicular planes. The O and E rays compromising each ray or wave bundle also become mutually shifted in phase owing to differences in refractive index experienced by each wave during transit through the specimen. With the calcite crystal, we observed that the O and E rays follow different trajectories and emerge at widely separated locations on the surface of the crystal, making it relatively easy to examine each linearly polarized component separately with the aid of a Polaroid sheet. Let us now consider the circumstance where the optical axis of the specimen is perpendicular to the incident beam, which is the usual case for retardation plates and most biological specimens that are mounted on a microscope slide and examined in the object plane of the microscope. Because the incident ray is perpendicular to the optical axis of the specimen, the O and E rays follow the same trajectory as the incident ray, with one ray lagging behind the other and exhibiting a phase difference according to the amount of birefringence. Since the O and E waves vibrate in mutually perpendicular planes, they cannot interfere to produce a resultant wave with an altered amplitude. This point becomes important in polarization microscopy, because interference is required to generate a contrast image. As a convenience for describing the behavior of the superimposed wave pair, we may add the two waves together to form a single resultant ray. The mutually perpendicular orientation of the two E vectors and phase difference between the two rays result in a three-dimensional waveform called *elliptically polarized light*.

As seen in Figure 8.11, the E vector of the recombined wave does not vibrate in a plane over the course of its trajectory, but progressively rotates about its propagation axis. When viewed perpendicular to its propagation axis, the E vector appears to follow the course of an elliptical spiral, and when viewed end-on, the E vector sweeps out the shape of an ellipse. The resultant elliptical wave is reconstructed using simple vector addition in three-dimensional space. For O and E waves of equal amplitude, the amount of ellipticity depends on the amount of phase shift (Fig. 8.12). For phase shifts of exactly $\lambda/4$ and $3/4\lambda$, the shape of the resultant wave can be described as a circular spiral; for phase shifts of λ or $\lambda/2$, linearly polarized light results; for all other phase differences (the vast majority), the shape is that of an elliptical spiral of varying degree of ellipticity. The component of elliptically polarized light that is able to pass through an analyzer varies depending on the amount of phase shift and is also shown in Figure 8.12. The description of circular or elliptical waveforms is simply a convenient device

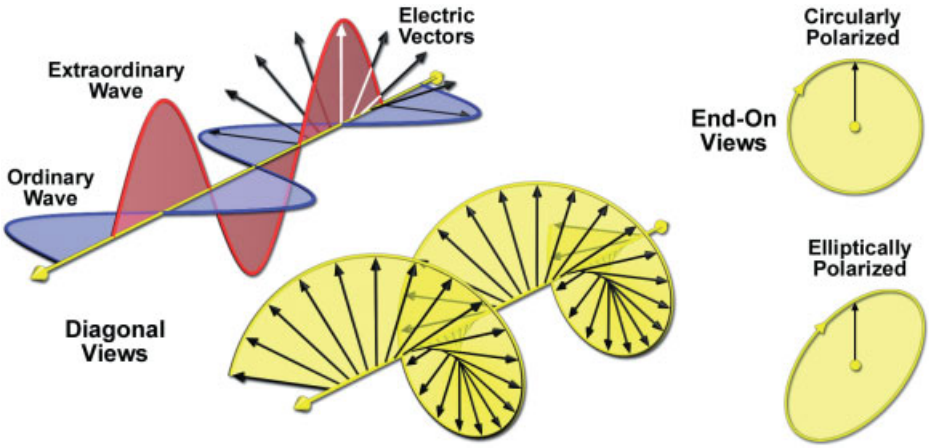

Figure 8.11

The waveforms of elliptically and circularly polarized light. O and E rays (red and blue waves) following the same propagation axis but vibrating in mutually perpendicular planes cannot interfere, but can be combined by vector addition and depicted as a single wave with an E-vector spiraling around the propagation axis (yellow wave). Depending on the relative phase difference between the two rays, the resultant wave may be linear or take on the form of a spiraling ellipse or circle. With a phase displacement of $\lambda/4$, the waveform is a circle.

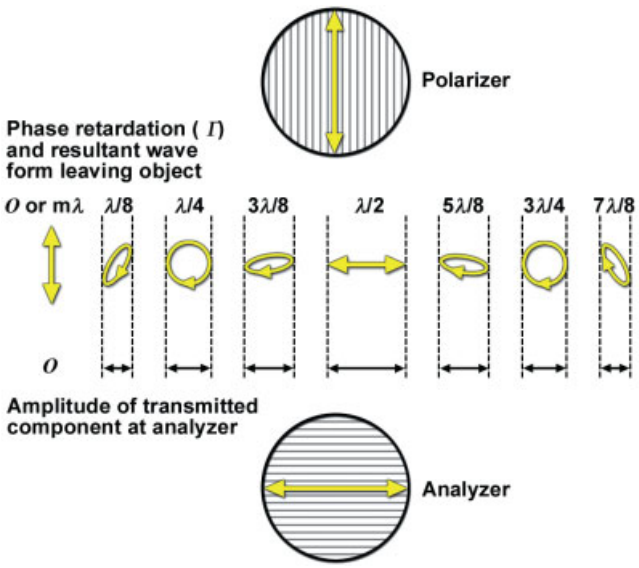

Figure 8.12

Effect of relative phase shift between O and E rays on the waveform of polarized light. Waves resulting from the combination of superimposed O and E rays have elliptical, spherical, or planar waveforms, depending on the amount of relative phase shift between the two rays. The orientations of transmission axes of the polarizer and analyzer are indicated. The amplitudes of the components of vibration passing the analyzer are also shown.

for visualizing how O- and E-ray pairs interact with analyzers and optical elements called retardation plates.

Interference between two intersecting waves of light occurs only when their E vectors vibrate in the same plane at their point of intersection. Only when interference causes a change in the amplitude in the resultant wave can an object be perceived due to differences in intensity and contrast. The observed intensity from the O and E waves vibrating in mutually perpendicular planes emergent from a birefringent object is simply the sum of their individual intensities; no variations in intensity are observed because interference cannot occur and the object remains invisible. A sheet of cellophane held against a single polarizer on a light box is an example of this behavior. Cellophane is a birefringent sheet made up of parallel bundles of cellulose. The optical axis is parallel to the axis of the bundles and contained in the plane of the sheet. When examined in polarized light without an analyzer, elliptically polarized light emerges from the cellophane, but since there is no interference or change in amplitude, the sheet remains invisible against the polarizer. However, if the cellophane is examined between two crossed polars, components of elliptical waves that are parallel to the analyzer are transmitted and emerge as linearly polarized light. Background rays from the polarizer are blocked by the analyzer, so the cellophane stands out as a bright object against a dark background. The sheet appears brightest when its optical axis is oriented at 45° with respect to the transmission axes of the two crossed polars.

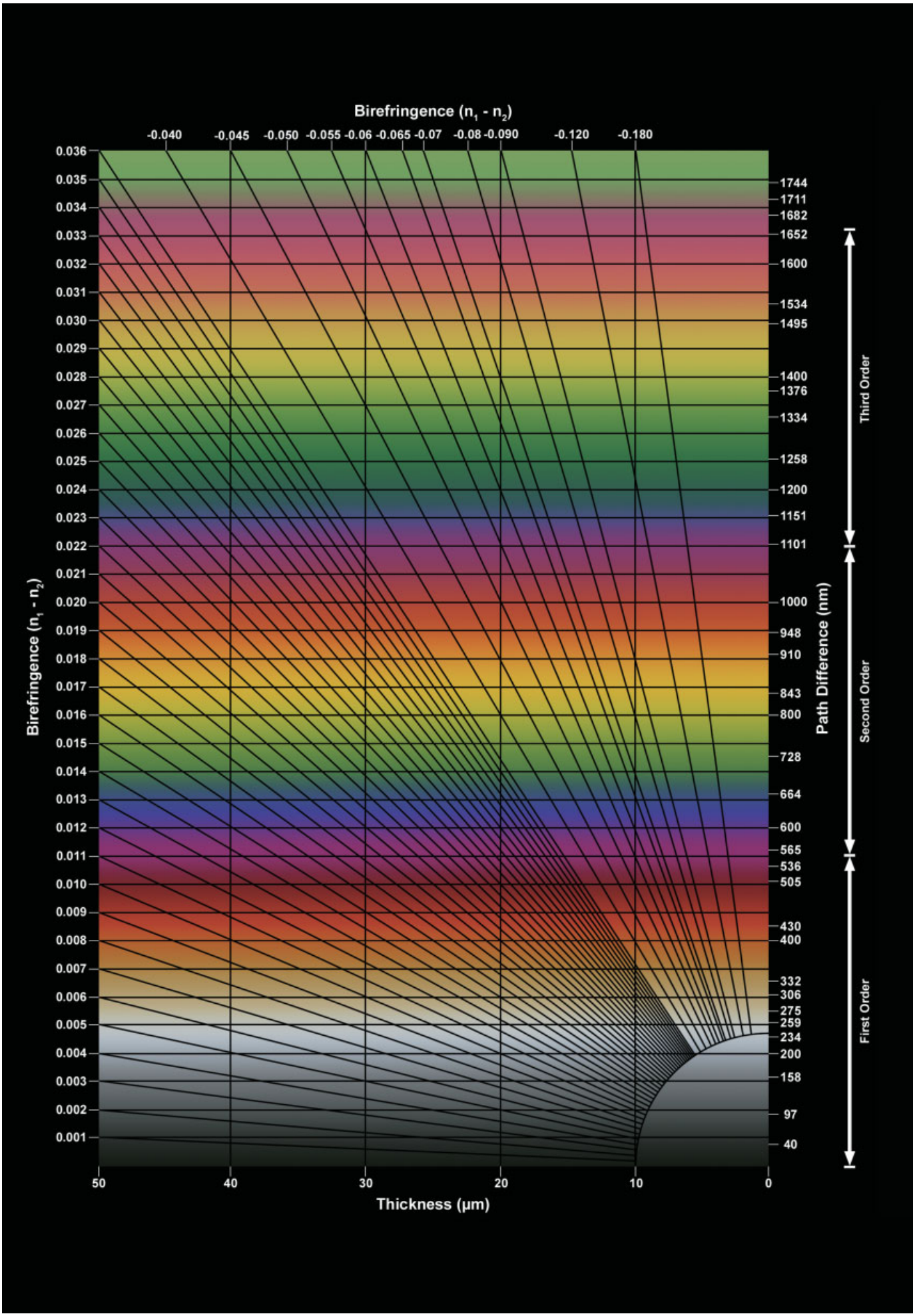

CHAPTER
9

POLARIZATION MICROSCOPY

OVERVIEW

Image formation in the polarizing microscope is based on the unique ability of polarized light to interact with polarizable bonds of ordered molecules in a direction-sensitive manner. Perturbations to waves of polarized light from aligned molecules in an object result in phase retardations between sampling beams, which in turn allow interference-dependent changes in amplitude in the image plane. Thus, image formation is based not only on principles of diffraction and interference, but also on the existence of ordered molecular arrangements. The degree of order encountered in objects ranges from near-perfect crystals to loosely ordered associations of asymmetric molecules or molecular assemblies. In the polarizing microscope, such structures generally appear bright against a dark background (Fig. 9.1). Polarization microscopy has been used to study the form and dynamics of many ordered cellular structures, including:

- Mitotic spindle fibers in dividing cells
- Actin filament bundles in a variety of cell types
- Actin and myosin filaments in the myofibrils of striated muscle cells
- Condensed DNA in certain sperm nuclei
- Kinetoplast DNA in the mitochondria of trypanosomes
- Helical strands of cellulose fibers in plant cell walls

Michel-Lévy polarization color chart. Details are given in Figure 9.9.

Fundamentals of Light Microscopy and Electronic Imaging, Second Edition.
Douglas B. Murphy and Michael W. Davidson.

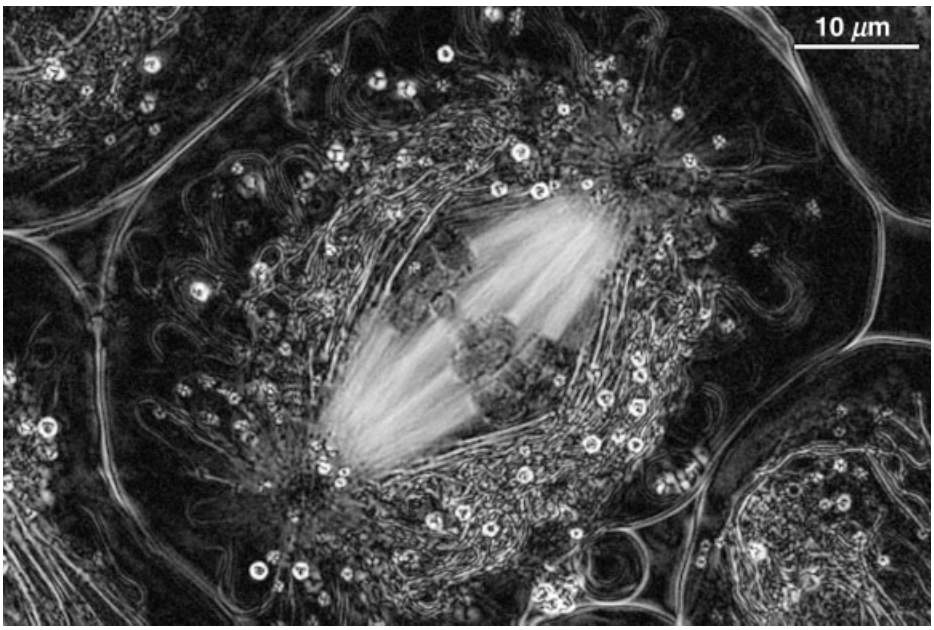

Figure 9.1
Polarized light image of meiosis in primary spermatocytes from the crane fly, *Nephrotoma suturalis.* (Image courtesy of Rudolf Oldenbourg, Marine Biological Laboratory, Woods Hole, MA.)

- Condensates of starch and lignin in plant cells
- Virus crystalloids and crystals of organic compounds in the cytoplasm of plant cells
- Lipid bilayers of the cell plasma membrane and mitochondria

In many cases, polarization microscopy is the only available method for studying the structure, formation, and dynamics of labile macromolecular assemblies or examining the effects of chemicals, drugs, or environmental conditions on cellular structures *in vivo*. For additional examples from the application of polarized light in studies of mitosis, see Inoué and Oldenbourg (1998) and Oldenbourg (1996, 1999).

The polarizing microscope is also a remarkable analytical instrument, capable of providing quantitative measurements of differences in optical path length (retardation), which in turn can be used to calculate refractive index differences and the thicknesses of ordered specimens. Geologists use these parameters together with a reference chart to determine the identities of unknown crystalline minerals.

These capabilities distinguish polarization microscopy from other forms of light microscopy and account for its popularity in biology, chemistry, geology, and materials science. Polarized light is also used for the many forms of interference microscopy, including differential interference microscopy. In this chapter, we discuss the function and alignment of polarizing optics and the action and method of deployment of several compensators.

OPTICS OF THE POLARIZING MICROSCOPE

A polarizing microscope is a compound light microscope fitted with a polarizer, an analyzer, and if quantitative measurements of birefringence are to be made, a compensator (see Fig. 9.2). A *compensator* (also called a *retarder*) is a birefringent plate that is used to measure optical path differences and improve visibility. The polarizer is placed between the light source and the specimen, commonly near the front aperture of the condenser; the analyzer is placed between the specimen and the eye, usually

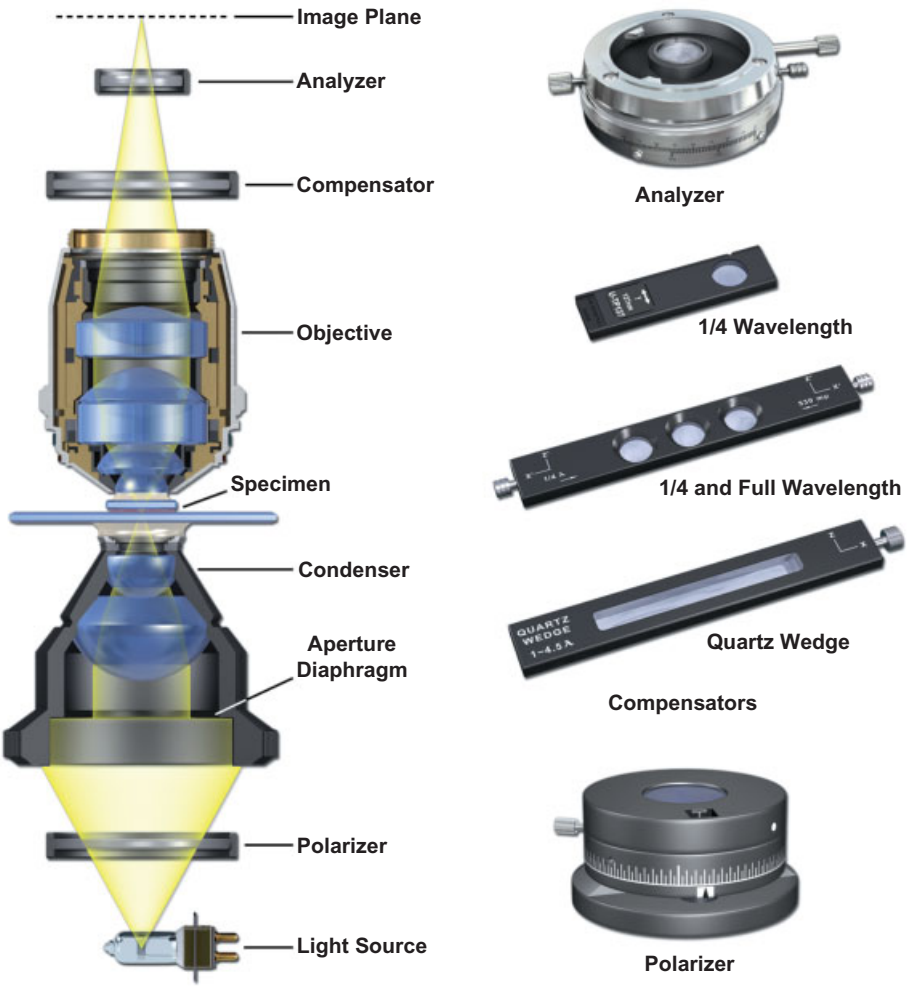

Figure 9.2

Optical components of a polarized light microscope. When examining the microscope, notice the presence of a polarizer and analyzer (right), a rotating stage (not illustrated), and a slot for accommodating a compensator (right). Fixed-orientation polarizers and analyzers are often mounted in sliders (similar to the 1/4 wavelength slider on the right) that can be easily inserted or removed from the light path. Polarization microscopy requires an intense light source.

some distance behind the rear aperture of the objective. The polarizer is mounted with its transmission axis fixed in a horizontal (east–west or right–left) orientation as seen facing the microscope and looking down the optical axis of the microscope; the analyzer is then rotated at 90° to the polarizer in a north–south or up–down orientation to obtain extinction. It is desirable that the polarizer or analyzer be rotatable. The rotatable holder is often marked out in degrees to facilitate adjustment to extinction. Having one of the polarizers in a rotatable holder assures proper orientation of the crossed polars along east-west and north-south axes and allows precise control for obtaining extinction. The use of a compensator also requires that the polarizers be adjusted precisely, because it is inserted into the optical path at a fixed orientation. It is also highly desirable that the specimen stage be rotatable, with its center of rotation adjusted to coincide with the optical axis of the microscope so that the fixed polarized light beam can illuminate a specimen at various angles simply by rotating the stage. Finally, there is an insertion slot for a compensator, which is located near and in front of the analyzer. For applications where birefringence is small and object contrast is very low, it is important to use strain-free, polarization-grade condenser and objectives. Strain birefringence exists in most lenses as a result of manufacture and mounting in a lens barrel. When severe, birefringence from a lens can obscure faint signals in images of weakly birefringent objects. For this reason, manufacturers carefully select only low strain objectives for use in polarization microscopy.

ADJUSTING THE POLARIZING MICROSCOPE

- Focus a specimen and adjust for Koehler illumination with both polarizing filters and the compensator removed from the optical path.
- Insert the fixed polarizer (depending on the microscope, either polarizer or analyzer might be fixed—i.e., glued into position in the holder so that it cannot rotate). If the polarizer is fixed, its transmission axis should be oriented horizontally east-west as seen looking in the microscope. If the polarizer is rotatable, check that the filter is positioned correctly by looking for the mark indicating the orientation of the transmission axis or checking the degrees of rotation on the holder.
- Insert the rotatable analyzer (or polarizer), and rotate it until the two polars are crossed and maximum extinction is obtained. Do this by examining a blank region on a specimen slide and making fine adjustments to the analyzer until the image is maximally dark. The transmission axis of the analyzer should now be oriented vertically or north–south. The critical adjustment for extinction can only be made while looking in the microscope. Extinction indicates that the polars are crossed, but does not guarantee that their azimuths are perfectly oriented east-west and north-south.
- Insert a telescope eyepiece or Bertrand lens and focus on the rear aperture of the objective. A dark *polarization cross* is observed at extinction (Fig. 9.3a), with brighter regions of intensity between the horizontal and vertical arms of the cross. Commonly, the horizontal and vertical components of the cross are broader in the center of the field and narrower at the periphery. This shape is caused by the depolarizing effects of spherical lens surfaces in the condenser and the objectives, and is normal for most microscope systems. The cross should be centered in the

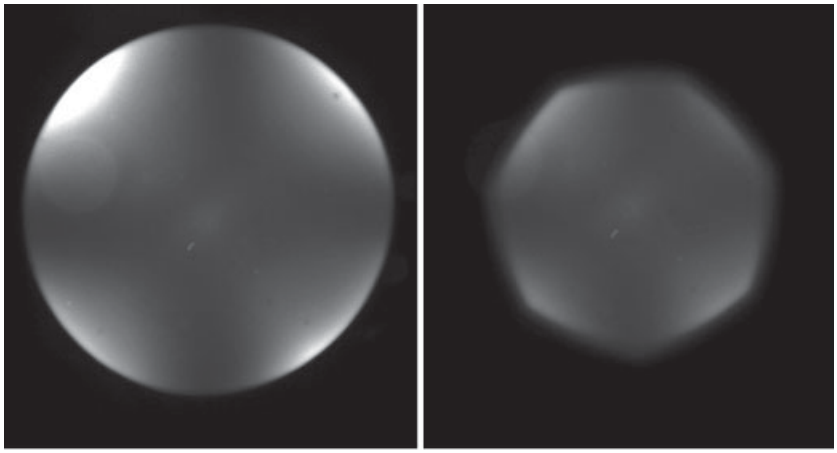

(a) (b)

Figure 9.3
View of the polarization cross in the rear aperture of the objective. Views before (a) and after (b) proper adjustment of the condenser aperture diaphragm.

field of view and should be perfectly upright. If not, the polarizer and analyzer may need to be rotated a bit to achieve proper orientation. Perfect alignment with respect to an azimuth at 0° is essential if quantitative measurements of azimuthal angles or birefringence are to be made with a compensator. Reference to the polarization cross is also useful in case a polar becomes misaligned in its holder, requiring the operator to readjust the polar's orientation.

- Using the telescope eyepiece or Bertrand lens, partially close the condenser aperture diaphragm so that bright outer regions of depolarized light visible at the edge of the aperture field are completely or mostly blocked (Fig. 9.3b). Although stopping down the condenser aperture reduces spatial resolution, it greatly improves the extinction factor of the microscope optics. Switching back to normal viewing mode, the field of view at extinction should now be very dark. Normally, it should only be necessary to rotate the specimen slide to examine the object at different azimuthal angles, leaving the positions of the polarizer and analyzer fixed and unchanged. Because it is often necessary to rotate specimens during examination, it is convenient to use a specially designed rotating stage that is marked in degrees at its periphery. Rotating stages must be adjusted so that their center of rotation is superimposed on the optical axis of the microscope.

APPEARANCE OF BIREFRINGENT OBJECTS IN POLARIZED LIGHT

Birefringent specimens exhibit characteristic patterns and orientations of light and dark contrast features that vary depending on overall shape (elongate vs. spherical) and the molecular orientation. In the absence of a compensator, spherical objects with radially

symmetric molecular structure exhibit a dark upright polarization cross superimposed on a disk composed of four bright quadrants. Thus, there are eight alternating bright and dark contrast regions distributed around the field of view. If a compensator, such as a λ/4 (quarter-wave) plate, is inserted into the beam so that its slow axis is oriented at 45° with respect to the transmission axes of the polarizer and analyzer, a pattern of four quadrants is observed, with one pair of opposite quadrants showing bright contrast and the other pair dark contrast. Instructions for performing this operation are given at the end of the chapter.

Linear objects such as elongate striated muscle cells with coaxial alignments of linear filaments have a different appearance. In the absence of a compensator, rotation of the specimen stage through 360° reveals eight angular azimuths at which the muscle cells alternately appear bright (45°, 135°, 225°, and 315°) or dark (0°, 90°, 180°, 270°); with a compensator present, there are four azimuths at 45°, 135°, 225°, and 315°, at which the object alternately appears light or dark with respect to the background.

PRINCIPLES OF ACTION OF RETARDATION PLATES AND THREE POPULAR COMPENSATORS

With the addition of a retardation plate or compensator, the polarizing microscope becomes an analytical instrument that can be used to determine the *relative retardation* Γ between the O and E waves introduced by a birefringent specimen. Since $\Gamma = t(n_o - n_e)$, either the birefringence or the thickness of a specimen can be determined if the other parameter is known (see Chapter 8). An excellent description of the action of compensators is given by Pluta (1993).

Transparent plates of birefringent materials, such as quartz, mica, or plastic that introduce a fixed amount of retardation between the O- and E-ray pairs are called *retardation plates* or *retarders*. Retarders are prepared at a certain thickness and with the optical axis contained in the plane of the plate. Since incident rays of linearly polarized light are perpendicular to the optical axis of the plate, the O- and E-ray components follow the same trajectory through the plate, but become retarded in phase relative to one another; waves emerge as linearly, circularly, or elliptically polarized beams, depending on the amount of relative phase retardation. Refer to Figure 8.12 to review how changes in the amount of phase retardation affect the waveform and plane of vibration of resultant waves emergent from the plate. The orientation of the optical axis of the plate relative to the plane of vibration of the incident polarized light beam is important. The most common retarders introduce phase retardations of 1λ, λ/2, and λ/4 (2π, π, or π/2 radians) for light of a specific wavelength and are called, respectively, full-wave, half-wave, and quarter-wave plates. As shown in Figure 9.4, a ray of the designated wavelength passing through a full-wave or λ plate remains linearly polarized and retains its original plane of vibration. In this figure, as previously discussed, and in other figures, wavelength spacings of the O and E rays are shown by the interval between sets of mutually perpendicular red and blue vectors. Note that the λ/2 plate rotates the plane of linearly polarized light by 90°, while the λ/4 plate converts linearly polarized light into light that is circularly polarized and vice versa. Retarders producing less than λ/4 phase retardation produce elliptically polarized light.

When a retarder is used as a nulling device to determine the relative retardation Γ in a specimen, it is known as a *compensator*. Commonly, the compensation plate is mounted in a device that permits rotation or tilting of the plate by a variable number

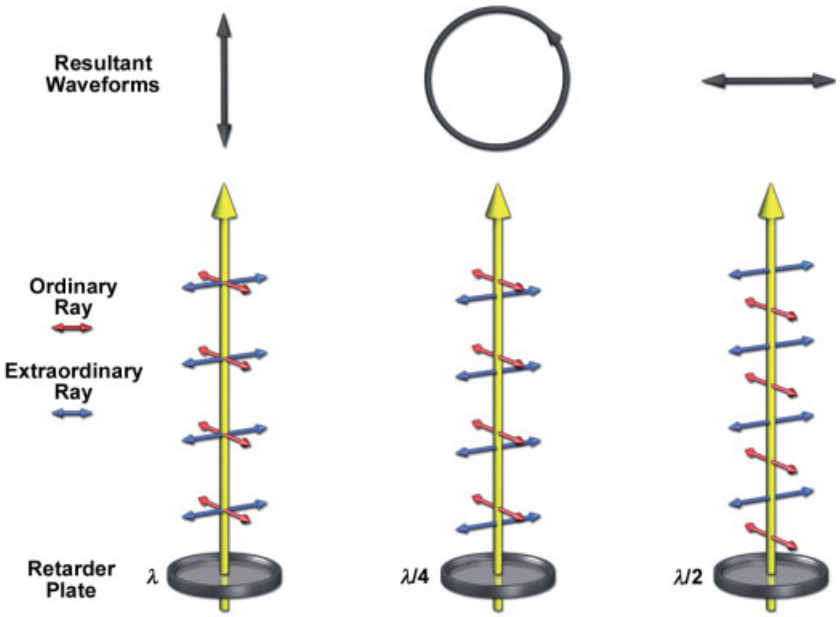

Figure 9.4

The action of three retarder plates. Retarders are special birefringent plates that introduce a fixed amount of relative retardation between ordinary (O) and extraordinary (E) rays, whose wavelength spacings are shown here as red and blue arrows, respectively. The incident rays are linearly polarized. Since the optical axis of the retarder is in the specimen plane and perpendicular to the incident ray, the O and E rays follow trajectories that are superimposable, but the waves are retarded in phase relative to one another. The resultant waveforms as they appear looking down the optical axis are presented at the top of the figure.

of degrees. Another method, known as de Sénarmont compensation, uses a fixed λ/4-plate compensator and requires the operator to rotate the analyzer. This action allows the compensator to be used as a nulling device to undo the phase shift imparted by the specimen through the introduction of an equal but opposite phase shift. The number of degrees of rotation on the compensator required to null the birefringence of an object and bring it to extinction is used to calculate Γ. If other variables are known, the retardation value Γ can be used to determine if birefringence is positive or negative, measure the amount of birefringence—the difference in refractive index ($n_e - n_o$) as experienced by the O and E rays—or determine the specimen thickness. It is even possible to deduce the geometry and patterns of molecular organization within an object (e.g., tangential vs. radial orientation of polarizable bonds of molecules in a spherical body). It is the compensator that makes the polarizing microscope a quantitative instrument.

Compensators are also used for qualitative purposes to control background illumination and improve the visibility of birefringent objects. In a properly adjusted polarizing microscope, the image background looks very dark, approaching black. Inoué has shown that the visible contrast improves if 5–10 nm retardation is introduced with a compensator, which increases the intensity of the background by a small amount (Inoué and Spring, 1997). The compensator can also be used to increase or decrease the amount of phase displacement between the O and E rays to improve the visibility of details in

the object image. Thus, birefringent objects are sometimes seen with greater contrast using a compensator than they are using the polarizer and analyzer alone.

λ-Plate Compensator

Retardations of a fraction of a wave to up to several waves can be estimated quickly and economically using a λ-plate retarder as a compensator (Fig. 9.5). The λ plate is also known as a full wave plate, a first-order red plate, red-I plate (read "red-one plate"), or a color tint plate. The plate is composed of a matrix of highly aligned linear organic polymers or of a sheet of mica, and thus is birefringent. The axis of polarizable bonds in the material defining the slow axis (higher refractive index) of the index ellipsoid is usually marked on the plate holder. When placed between two crossed Polaroid sheets at a 45° angle and back-illuminated with white light, the plate exhibits a bright 1st order red interference color, hence its designation as a 1st order red plate. Full-wave plates introduce vivid interference colors (polarization colors) to the image of a birefringent object and are useful for making rapid qualitative assessments of relative retardation, as well as for determining the orientation of index ellipsoids. In geology and materials science, full-wave plates are commonly used to identify birefringent crystalline minerals and determine specimen thickness. For retardations of ~λ/3 or less, phase retardations can be measured with an accuracy of ±2 nm.

When placed in front of the analyzer so that its slow axis is oriented 45° with respect to the crossed polarizers, a red-I plate introduces a relative retardation between the O and E rays of one wavelength centered at green wavelengths of 551 nm (Pluta, 1988). Green wavelengths therefore emerge from the retardation plate linearly polarized in the same orientation as the polarizer and are blocked at the analyzer. O and E waves of all other wavelengths experience relative phase retardations of less that 1λ; they emerge from the plate as elliptically polarized waves and are only partially blocked by the analyzer. The color of white light minus green is bright magenta red, thus accounting for the color of the red-I plate. (To review the principles governing the formation of interference colors, see Chapter 2.) You can confirm that the green wavelength has been removed by examining the red interference color with a handheld spectroscope. All of the spectral colors are seen except for a black band covering the wavelengths in the green portion of the spectrum. If now a birefringent object, such as a sheet of cellophane, is inserted together with the red-I plate between two crossed polarizers and rotated, the color shifts to blue and yellow. This is because the relative retardation for the combination of red plate plus object is now greater or less than 551 nm, causing the wavelength of linearly polarized light to be shifted and resulting in a different interference color. By comparing object colors with the background color of the plate and referring to a Michel-Lévy color chart, it is possible to determine the relative retardation introduced by the object (Fig. 9.9).

For birefringent biological materials, such as small spherical inclusion bodies, full-wave plates can be used to determine patterns of molecular arrangement (see exercise on plant cell inclusion bodies). The shifted blue and yellow colors are called, respectively, addition and subtraction colors, and immediately tell about the orientation and magnitude of the fast and slow axes of the specimen's index ellipsoid. Thus, the λ plate is a useful semi-quantitative device for estimating minute retardations and the orientations of index ellipsoids. As a survey device used to examine complex specimens, it may be even more convenient to use than other more precise compensators.

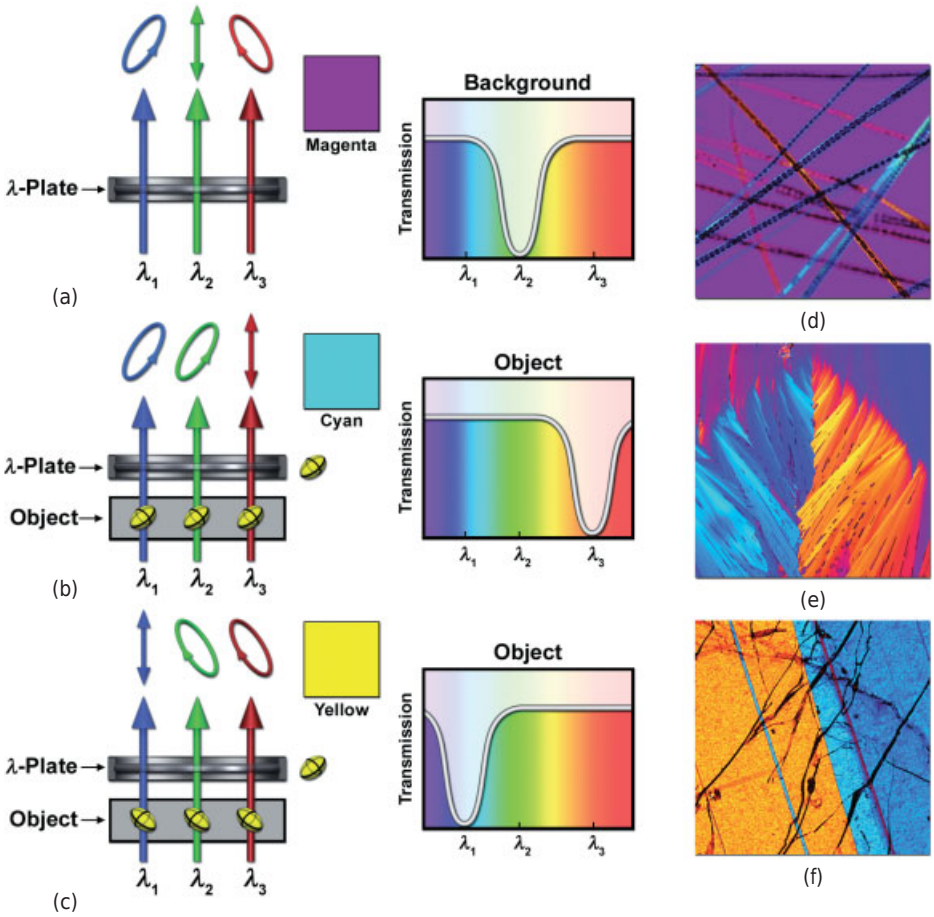

Figure 9.5

Action of a 1st order full-wave plate in white light. (a) A red-λ plate introduces a relative retardation for green light (λ_2), resulting in linearly polarized waves that are eliminated at the analyzer. Shorter (λ_1) and longer (λ_3) wavelengths produce elliptically polarized waves that are partially passed by the analyzer. The resulting spectrum shows extinction of green wavelengths, resulting in the perception of a magenta-red interference color (box; background color of the field of view). (b) The same plate with an object inserted whose wavefront ellipsoid has its slow axis parallel to that of the red plate. The relative retardation between O and E rays is increased so that now the wavelength giving linearly polarized light is shifted to a longer wavelength (λ_3), such as yellow, and the object exhibits a blue-cyan interference color (box), called an addition color. (c) The same plate with an object whose wavefront ellipsoid has its slow axis crossed with that of the red plate. In this case, the relative retardation between O and E rays is decreased, the wavelength giving linearly polarized light is shifted to a shorter wavelength (λ_1), such as blue, and the object exhibits a yellow interference color (box), called a subtraction color. Examples: (d) rabbit hair showing magenta background and yellow/cyan fibers. (e) Vitamin crystallites showing divergence of crystal growth along a central axis. (f) Anorthosite rock thin section.

Demonstration: Making a λ-Plate from a Piece of Cellophane

Crumple up a thin piece of cellophane and place it between two crossed polars on a light box. It is immediately obvious that cellophane is strongly birefringent. In regions where the sheet is a single thickness, the color of the birefringence is white, but in regions where the sheet is folded over on itself and overlapping, a surprising display of interference colors is observed. The colors indicate regions where the phase retardation between O and E rays subtends a whole wavelength of visible light, resulting in the removal of a particular wavelength and the generation of a bright interference color. In these colorful regions, cellophane is acting as a full-wave plate. The different colors represent areas where the amount of relative retardation varies between the O and E waves. The optical path corresponding to any of these colors can be determined using a color reference chart (Fig. 9.9). If we now insert an unknown birefringent object in the path, the color will change, and using the chart and the cellophane wave plate as a retarder, we can examine the color change and make a fairly accurate estimate of the path length of the unknown specimen. Used this way, the cellophane wave plate acts like a compensator. The following demonstration shows how to make a cellophane wave plate retarder, understand its action, and use it as a compensator:

- Place a sheet of clear unmarked cellophane between two crossed polars on a light box and rotate the cellophane through 360°. Use a thin thickness of the type used for wrapping CD cases, boxes of microscope slides, pastry cartons, and so forth. Cellophane dialysis membranes are also very good. Do not use the plastic wrap made for food products, or thick, stiff sheets. There are four azimuthal angles (located at 45° with respect to the crossed polars) at which the cellophane appears bright against the dark background. Mark the locations of these axes by drawing a right-angled X on the sheet with a marking pen. Cellulose is clearly birefringent, and the pattern of its action in polarized light is consistent with cellophane containing arrays of long-chain cellulose molecules arranged in parallel across the diameter of the sheet. Notice that the birefringence of a thin sheet of cellophane is colorless.
- Cut the sheet into a square or rectangle with a scissors or utility knife so that the arms of the X are perpendicular to the edges of the rectangle. At one corner of the sheet place another mark—this time, a straight line 2-cm long parallel to and 1 cm in from the edge of the sheet. Fold the corner of the sheet at a 45° angle, folding over the black line, and reexamine the folded cellophane between the crossed polars. The area of overlap now appears dark like the background and remains dark as the sheet is rotated. If not completely dark, slide the folded corner slightly while holding it between the crossed polars. Extinction occurs because the phase displacement of O and E rays induced by the first layer is exactly reversed and undone by the action of the second folded layer, whose orientation, relative to the main sheet, has been changed by 90°. This is confirmed by looking at the folded black line, which makes a 90° angle. This is the action of compensation, and the folded corner is acting as a compensator to nullify its own birefringence.

- Now fold the sheet in half so that opposite edges remain parallel to each other. Placed between crossed polars at a 45° angle, a bright interference color is seen, which in most cases will be yellow-gold. If the polars are parallel, the interference color will be blue. The folded sheet now has the properties of a full-wave plate and is capable of generating interference colors. If the sheet is rotated by incremental amounts between crossed polars while the analyzer is rotated back and forth, one will see the various colors of the first order interference spectrum. Since the retardation introduced by a single thickness of cellophane is ~230 nm, folding the sheet in this way doubles the retardation to 460 nm. The sheet looks yellow because 460 nm blue wavelengths are linearly polarized and are removed at the analyzer. Examination of the yellow color with a spectroscope reveals a prominent dark band in the blue region of the spectrum. Remember that for a full-wave plate, rays of a particular wavelength (here 460 nm) retarded by exactly 1λ emerge from the plate linearly polarized and vibrating in the same plane as the original incident rays. This component is removed completely at the analyzer. The O- and E-ray pairs of other wavelengths, being retarded by more or less than 1 wavelength, emerge from the plate as elliptically polarized light and are partially passed by the analyzer. Inspection of a Michel-Lévy color chart indicates that the yellow color corresponds to removal of wavelengths near 460 nm, and one-half this amount (230 nm) is the amount of retardation for a single thickness of cellophane. The reason that the color of birefringence of a single sheet of cellophane looks bright and colorless is also apparent: the relative phase retardation is too small to allow removal of a visible wavelength by the analyzer.
- The orientation of the index ellipsoid of the cellophane λ plate—a yellow-I plate—must still be determined. For this, we require a birefringent reference object whose index ellipsoid is known. We will use a strip of cellophane tape, such as transparent packing tape, since this is manufactured with the strands of cellulose (and direction of the slow axis of the wavefront ellipsoid) parallel to the length of the tape. Remove two 1-cm length pieces of tape and draw a wavefront ellipse on each piece. The slow (short) axis of the ellipse is parallel to the long axis of the strip of tape; the fast (long) axis is parallel to the cut edge of the tape. Place the two pieces of tape at 90° to each other on the folded piece of cellophane, with each piece of tape being parallel to the edge of the cellophane sheet. Place the folded sheet between the crossed polars and orient the sheet at a 45° angle. The regions covered with tape show two new interference colors—pale yellow and sky blue—superimposed on a yellow background. The polarization color chart shows that the blue color corresponds to the removal of a wavelength of 690 nm (460 + 230 nm). This can only occur if the retardation caused by the folded cellophane sheet is further retarded by additional retardation from the tape. The slow axes of the tape and cellophane must be parallel to each other for this to happen and the blue color is called an addition color. Conversely, the pale yellow interference color corresponds to removal of a much shorter wavelength (460 – 230 = 230 nm). The slow axis of the tape must be perpendicular to the slow axis of the folded cellophane sheet. This causes the

net retardation to be reduced, thus producing a pale yellow interference color, which is called a subtraction color. The ellipse drawn for the tape that appears blue can now be marked, retaining the same orientation, on the original cellulose sheet. We now have a calibrated cellulose yellow-I retarder that can be used to determine the amount of retardation and the orientation of the slow and fast axes of other birefringent materials.

- Further practice with the yellow-I plate will reinforce the concept of the compensator as a device for increasing or diminishing the relative phase retardation between the O and E rays and measuring the relative retardation Γ of unknown birefringent objects.

de Sénarmont Compensator

Compensation by the method of de Sénarmont requires a fixed quarter-wave plate (λ/4-plate) and a rotatable analyzer. Since λ/4 plates are designed for use at a specific wavelength, microscope illumination must be monochromatic, typically at the 546-nm green line of a mercury lamp, although λ/4 plates intended for use with other wavelengths, such as the 589-nm yellow line of the mercury lamp, are also available. Sénarmont compensation is commonly used to measure the amount of retardation in biological specimens, like cell organelles, plant cell walls and muscle fibers that induce retardations between λ/20 and 1λ. As explained, this compensator is also used to improve the visibility of birefringent specimens, because birefringent objects can be made to produce bright and dark contrast patterns against a medium gray background (Fig. 9.1).

The retarder (the λ/4 plate) is mounted in a *fixed* orientation between two crossed polars, usually between the rear aperture of the objective and the analyzer (Fig. 9.6). The analyzer is *rotatable* and is marked in degrees around its circumference so that the angle of rotation can be precisely determined. The λ/4 plate is made of a birefringent material, such as quartz, and is prepared so that the optical axis of the plate is parallel to the plane of the plate. When inserted into the optical pathway, the slow axis of the wavefront ellipsoid of the plate is oriented parallel to the transmission axis of the analyzer (the orientation is north-south when the analyzer is in the crossed position). The plate is fixed and does not rotate. As described in Chapter 8, a plane-polarized beam incident on the birefringent plate is split into separate O- and E-ray components. With the plane of vibration of incident polarized waves parallel to the slow axis of the λ/4 plate, O and E waves from background regions in the specimen emerge linearly polarized, are blocked by the analyzer, and cause the field to look maximally dark. As the analyzer is rotated, the field brightens until it becomes maximally bright at an analyzer setting 90° away from that giving extinction. At 45° of rotation, the field looks medium gray. Colors are not observed with incident white light because the amount of retardation introduced is considerably less than the one wavelength retardation required to generate an interference color. Thus, biological specimens, such as living cells, are frequently examined with the green line of a mercury arc lamp with a λ/4 plate designated for this wavelength. The use of monochromatic green light increases image contrast, allows more precise measurements of retardation, and helps protect living cells.

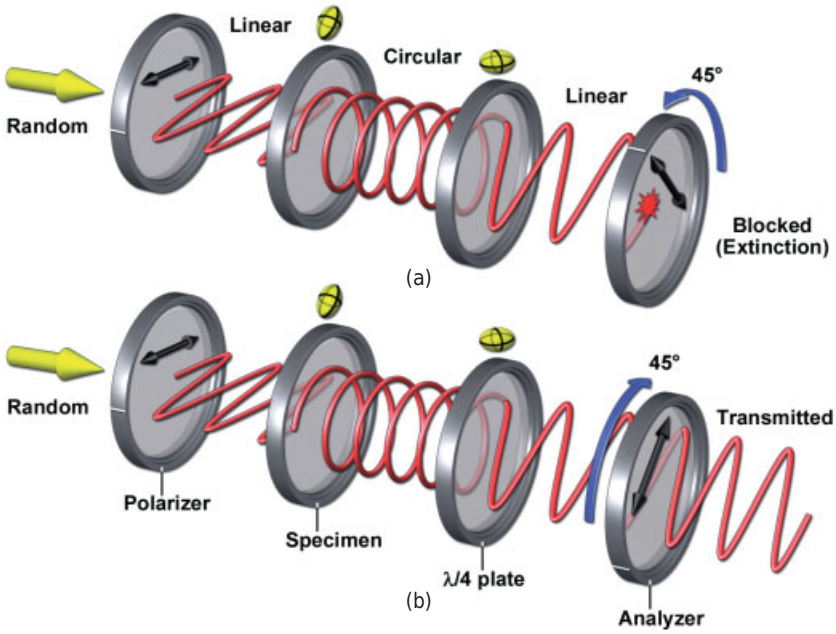

Figure 9.6

Compensation by the method of de Sénarmont. The equipment includes a fixed polarizer and λ/4-plate and a rotatable analyzer. The fixed λ/4-plate is inserted in the microscope so that the slow axis of its wavefront ellipsoid is oriented parallel to the transmission axis of the analyzer when the polarizer and analyzer are crossed. A λ/4 compensator produces circularly polarized light from incident linearly polarized waves and vice versa. To measure the amount of retardation from a specimen, the slow axis of the specimen is oriented at 45° with respect to the crossed polars. For convenience in the drawing, a specimen giving a relative retardation of λ/4 (the same as the λ/4-plate) is shown; hence, emergent waves are circularly polarized. The λ/4-plate converts these waves into linearly polarized light whose plane of vibration is now tipped 45° relative to the plane of the initial wave produced by the polarizer. When examined with the analyzer in crossed position, the object appears medium gray. Rotating the analyzer from its 0 position counterclockwise 45° blocks light transmission and gives extinction (a), while a clockwise 45° rotation gives maximum transmission (b). Since the relative retardation Γ by this method $= 2\theta$, we calculate that the retardation by the object is $2 \times 45° = 90°$, or λ/4. In a more typical case, a birefringent cellular object giving λ/20 retardation would require a rotation of the analyzer of 9° to give extinction.

If a birefringent specimen is positioned diagonally between two crossed polars, the combined action of the specimen plus the λ/4 plate generates linearly polarized waves whose E vectors are tilted at some azimuth θ depending on the amount of retardation at the specimen. This action occurs because the λ/4 plate produces linearly polarized light from incident, elliptically polarized waves. A rotation of the analyzer through 180° is equivalent to a relative retardation by the specimen of one wavelength. With every 90° of rotation of the analyzer, a birefringent object, such as a fiber, looks alternately dark or bright. Since retardations of most cells and organelles are usually less than 1λ, and because the compensation method is so sensitive, Sénarmont compensation is commonly used to analyze cellular specimens. Compensation with a λ/4 plate allows for measurement of relative retardations of up to 1λ with an accuracy of ±0.15 nm.

To measure Γ, the λ/4 plate is inserted into the optical path between two crossed polars as described. An elongated birefringent object (e.g., a muscle fiber containing aligned myofibrils) is first oriented at a 45° angle with respect to the transmission axes of the crossed polars with the rotating stage of the microscope. At this orientation, the fiber generates elliptically polarized light, which is converted into linearly polarized light by the λ/4 plate. These waves are partially transmitted by the compensator, causing the fiber to look bright against a maximally dark background. The analyzer is then rotated from its crossed position through an angle θ until the fiber's intensity appears maximally dark (extinction) against a gray background. Notice that as the analyzer is rotated to obtain extinction of the specimen, the background is brightening. Since the angle of rotation of the analyzer θ at extinction is equal to one-half of the full phase shift between the O and E rays, the relative retardation Γ is given as:

$$\Gamma_{\text{obj}} = 2\theta.$$

Γ can be used to calculate the values of the refractive index ellipsoid or the thickness of the object if one of these two parameters is known, since $\Gamma = t\ (n_o - n_e)$.

Brace–Koehler Compensator

For measuring very small phase retardations that occur in fine ultrastructural features, such as mitotic spindles, cleavage furrows, and stress fibers in living cells, a Brace–Koehler compensator can be employed (Fig. 9.7). This rotating compensator usually contains a thin birefringent plate made of mica, whose optical axis is contained within the plane of the plate. The compensator is used with monochromatic illumination—generally the 546-nm green line of the mercury arc lamp—and is capable of measuring retardations up to the limit of the compensator (a fixed value, but ranging from λ/10

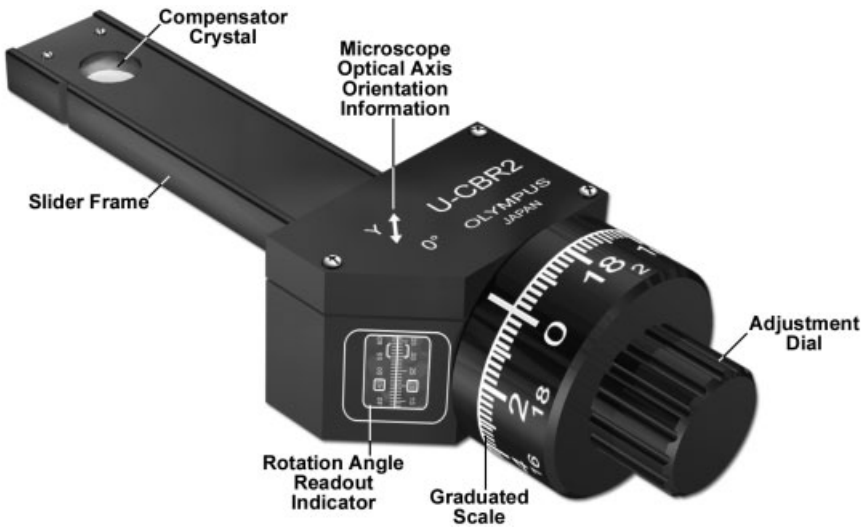

Figure 9.7
Brace–Koehler compensator.

to λ/30 depending on the particular compensator) with an accuracy of ±0.3 nm. These features make the Brace–Koehler compensator a highly sensitive measuring device.

In this method of compensation, the analyzer and polarizer remain fixed in position, because the compensator itself is rotatable. The slow axis of the plate (marked γ on the compensator mounting) is oriented parallel to the north–south transmission axis of the analyzer and corresponds to the 0° position on the compensator dial. A linear birefringent specimen, such as a bundle of actin filaments or microtubules, is first oriented at a 45° angle with respect to the transmission axis of the analyzer by rotating the stage of the microscope to give maximum brightness. Because the maximum optical path difference of the compensator is small (~λ/20), the background appears dark and remains relatively dark through different angles of rotation of the compensator. The compensator is then rotated counterclockwise from its 0° position until light from the specimen is extinguished, matching the dark background. The angle of rotation from the zero position on the compensator is used to calculate the relative retardation between the O and E rays using the equation:

$$\Gamma_{\text{obj}} = \Gamma_{\text{comp}} \sin 2\theta,$$

where θ is the angle of rotation of the compensator and Γ_{comp} is the maximum optical path difference of the compensator (~λ/20). The precise value of Γ_{comp} must be determined by calibration and is a constant in the equation. Depending on the particular compensator, retardations of ~λ/2000 can be measured under optimal conditions.

Exercise: Determination of Molecular Organization in Biological Structures Using a Full Wave Plate Compensator

First prepare the microscope for polarization microscopy. The analyzer and polarizer might already be installed in the microscope, in which case it is only necessary to bring them into position as described in the text. If not, strips of dichroic polarizing film can be used in the vicinity of the specimen slide, although this is not standard practice for a research grade instrument. The polarizer is mounted between the specimen slide and the condenser lens with its transmission axis oriented east–west. The analyzer is placed between the specimen slide and the objective with its transmission axis oriented north–south. The analyzer is rotated slightly until the background is maximally dark (extinction). If a red-I plate is used, it is inserted between the crossed polars with its slow and fast axes oriented at a 45° angle with respect to the transmission axes of the polars. (See Appendices B and C for sources and instruments on how to prepare red-I plates for this exercise.) The blackened edge of the red-I plate marks the direction of the slow axis of the wavefront ellipsoid.

For orientation, examine several birefringent materials between crossed polars without a red plate, including grains of corn starch, plant cell crystalloids, insect leg and flight muscle, and prepared slides of striated muscle, buttercup root, and pine wood. Notice that linear birefringent structures, such as myofibrils in striated muscle and plant cell walls, are brightest when their long axes are oriented at 45° with respect to the transmission axes of the crossed polars.

Spherical particles like starch grains are bright and exhibit a dark upright extinction cross through their centers. Reexamine the specimens after inserting the red plate. If the waveplate is a red-I plate, the background has a bright magenta-red (first order red) interference color. (*Note*: Other interference colors are possible if the thickness of the plate is not carefully controlled; in this case, the interference colors of objects will vary somewhat from the colors described in the exercise.) Muscle fibers, collagen bundles and elongate plant crystals look purple (an addition color) if their long axes are parallel to the slow axis of the wavefront ellipsoid of the red-I plate, and golden yellow (a subtraction color) if their long axes are perpendicular to the slow axis of the plate. Looking at the Michel-Lévy chart of polarization colors, it can be seen that the relative retardation between the purple and gold colors is about 100 nm. Further explanation of the interference colors is given below and in the text.

We will now use the red-I plate to determine the molecular orientation in two types of plant cell inclusion bodies. Amylose-containing starch storage granules and lignin-containing wood pits are birefringent spherical objects in plant cells consisting of parallel bundles of long-chain molecules and polymers. The two likely patterns for molecular order in these structures might be compared, respectively, with the needles projecting radially from a pincushion (radial pattern) or to surface fibers in the layers of an onion (tangential pattern). The axis of carbon–carbon bonds in these models differs by 90° and is easily observed in a polarizing microscope equipped with a λ-plate even though the inclusion bodies are extremely minute. The microscope is set up with the slow and fast axes of the wavefront ellipse of the λ-plate oriented at 45° with respect to the transmission axes of the crossed polars. The specimen background exhibits a bright magenta-red color, whereas the granular inclusion bodies appear as spheroids with opposite pairs of yellow-orange and purple-blue quadrants. It is remarkable that the yellow and blue color patterns are reversed for the two types of bodies, indicating differences in the pattern of molecular alignment! Each pair of yellow quadrants and blue quadrants depends on the orientation of the slow and fast axes of the wavefront ellipsoid of the λ-plate. The blue quadrants (the addition color) indicate the azimuth along which the slow axes of the specimen and plate are parallel to one another; the yellow quadrants (the subtraction color) indicate the azimuth along which the slow axes of the plate and object are perpendicular. By constructing a diagram where molecular alignment in each quadrant is shown as a series of parallel lines, you can deduce whether the molecules project radially like a pincushion or are ordered tangentially like the layers of an onion.

Roots of herbaceous plants contain an epidermis, a cortex, a pericycle (proliferative tissue), and a vascular cylinder or stele that runs along the axis of the root (Fig. 9.8). Inside the vascular cylinder identify the xylem—long, longitudinally oriented elements for conducting water and dissolved nutrients and minerals principally upwards to the leaves and branches. The phloem transports macromolecules and metabolites (principally downwards towards the roots). These are surrounded by a sheath of pericycle and endodermis cells. Outside the pericycle is an extensive layer of cortex containing starch storage granules. Notice the specific stains for the xylem and phloem cells. The walls of plant cells contain

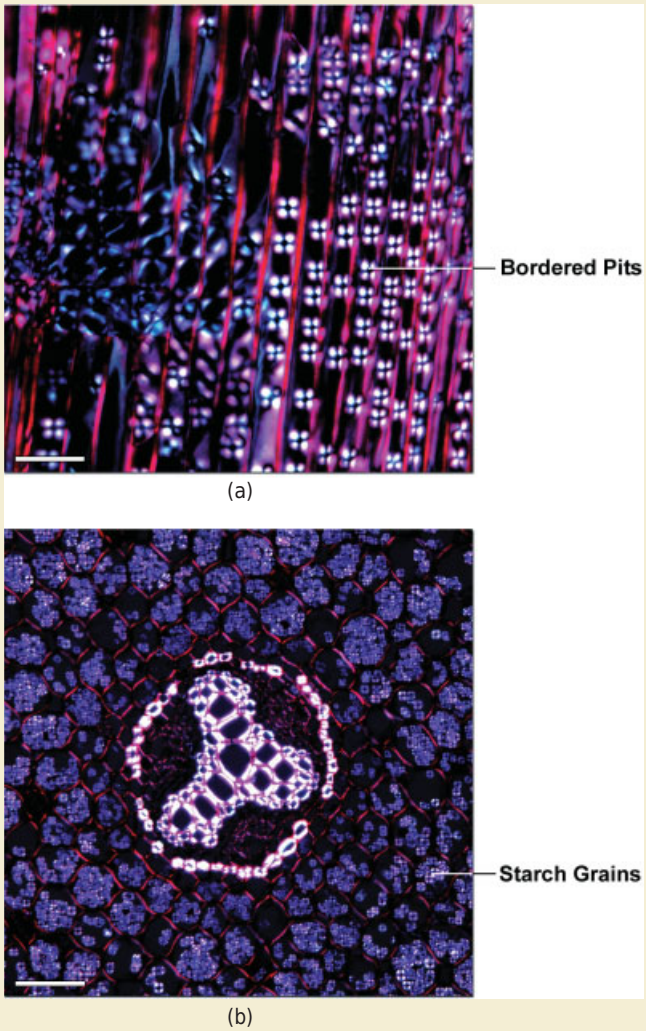

Figure 9.8

Polarized light images of histological sections of plant tissues with birefringent objects. (a) Radial section of pine wood containing cellulose walls and bordered pits. (b) Cross-section of a buttercup root, a herbaceous plant. The cortical cells are filled with starch gains. Bar = 50 μm (a) and 100 μm (b). (Specimen slides are from Carolina Biological Supply Company, Inc.)

ordered filaments of cellulose and lignin and thus are highly birefringent in a polarizing microscope

The section of pinewood contains mostly xylem (the water transport tissue), plus some vascular rays and pitch canals where pitch accumulates (Fig. 9.8). The xylem cells are called tracheids, and each is interconnected with neighboring tracheids by valve-like structures called bordered pits that regulate hydrostatic pressure in the xylem during fluid transport. The pits are made mostly of cell wall

materials, mainly lignin, a very dense phenolic polymer that gives wood its strength. Pinewood is about one-third lignin, the rest cellulose.

Examine the test slides of two plant tissues at 20–40×: a radial section of pinewood (*Pinus strobus*) containing bordered pits, and a transverse section of a buttercup root (*Ranunculus*) containing starch grains.

1. First examine each tissue by brightfield microscopy, carefully adjusting the microscope for Koehler illumination and positioning the condenser diaphragm. Identify bright spherical bodies in the cortical cells of the root and in the tracheid elements in pine wood.
2. Now examine the sections between two crossed polars by polarization microscopy. Insert the polarizer with its transmission axis east–west and the analyzer with its transmission axis north–south. Rotate the analyzer until the field of view is maximally dark (extinction). Now insert the focusing telescope eyepiece to examine the polarization cross in the rear

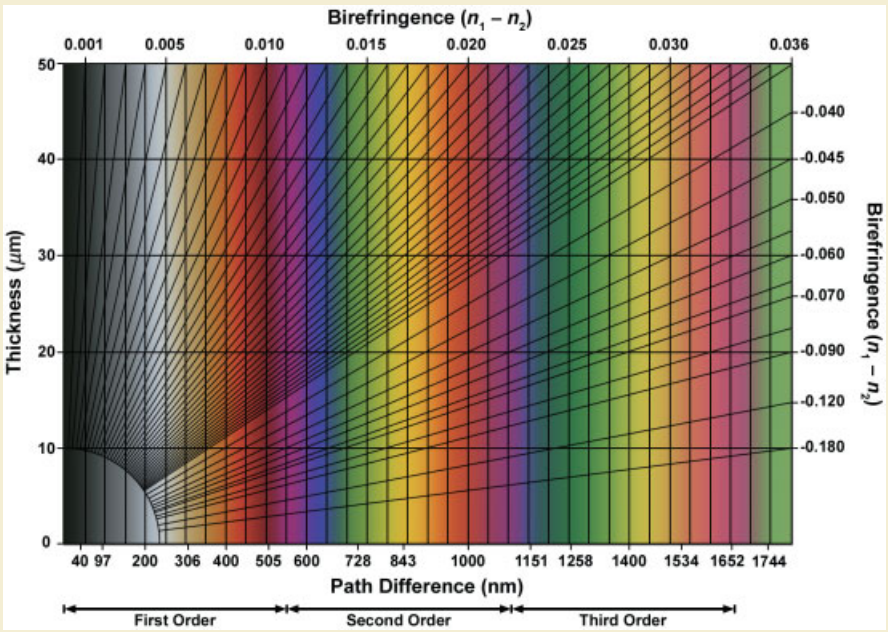

Figure 9.9

Michel-Lévy chart showing three orders of the interference color spectrum. The chart is used to determine the phase difference between O and E rays and birefringence (diagonal lines) of specimens examined in a polarizing microscope equipped with a λ-plate compensator. Removal of the wavelengths shown on the right-hand edge of the chart by the analyzer of a polarizing microscope yields the indicated interference colors. The Michel-Lévy chart can also be used to calculate the refractive index or thickness of a birefringent specimen if one of the two parameters is independently known. In geology, the chart is used to determine the identity, refractive index, or section thickness of birefringent crystals and minerals.

aperture of the objective and close down the condenser diaphragm to isolate the dark central portion of the cross, masking out the bright quadrants of light at the periphery; then replace the eyepiece to return to visual mode. What structures stand out? Make a sketch of the polarization cross in a bordered pit and explain the pattern of light and dark contrasts in the polarization image.

3. Place a red-I plate on top of the specimen slide with its slow axis at a 45° orientation to the polarizer and analyzer. Make sketches of a starch grain and a bordered pit indicating the colors seen in each of the polarization quadrants using a red-I plate.
4. Make drawings that show your interpretation of the molecular organization in starch grains and bordered pits as revealed by polarized light with the help of the Michel-Lévy color chart (Fig. 9.9). Starch and lignin are crystals of long carbon chain macromolecules. Assume that both structures exhibit positive birefringence.
5. Make sketches showing your interpretation for the orientation of cellulose in the xylem tracheids in pinewood. What evidence supports your conclusion?

CHAPTER
10

DIFFERENTIAL INTERFERENCE CONTRAST MICROSCOPY AND MODULATION CONTRAST MICROSCOPY

OVERVIEW

In Chapter 7, we examined phase contrast microscopy, an imaging system that converts optical path differences in a specimen to contrast differences in the object image. In this chapter, we examine two optical systems for viewing gradients in optical path lengths: differential interference (DIC) microscopy and modulation contrast microscopy (MCM). The images produced by these systems have a distinctive, relief-like, shadow-cast appearance—a property that makes the image appear deceptively three-dimensional and real (Fig. 10.1). The techniques were introduced within the past few decades and have gained in popularity to the point that they are now widely used for applications demanding high resolution and contrast and for routine inspections of cultured cells. Although the ability to detect minute details is similar to that of a phase contrast image, there are no phase halos, and there is the added benefit of being able to perform optical sectioning. However, there is no similarity in how the images are made. The DIC microscope uses dual-beam interference optics based on polarized light and two crystalline beamsplitters called Wollaston prisms. The generation of contrast in MCM is based on oblique illumination and the placement of light-obscuring stops part way across the aperture planes.

THE DIC OPTICAL SYSTEM

The DIC microscope employs a mode of dual-beam interference optics that transforms local *gradients in optical path length* in an object into regions of contrast in the object

DIC image of a crab megalops.

Fundamentals of Light Microscopy and Electronic Imaging, Second Edition.
Douglas B. Murphy and Michael W. Davidson.

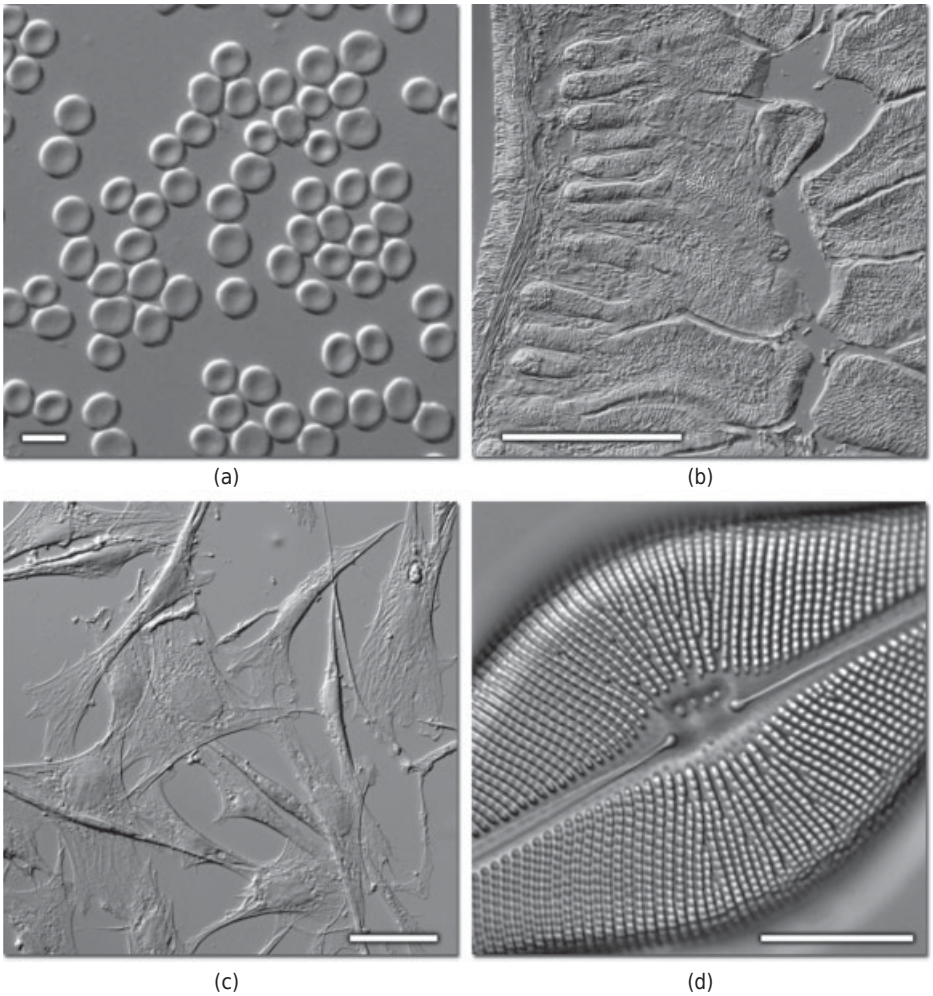

Figure 10.1

Biological structures imaged with DIC optics. The gradients of shading in the images indicate regions of rapidly changing optical path length in the cells and tissues. (a) Human red blood cells. (b) Mouse intestine thin section. (c) Indian Muntjac fibroblast cells. (d) *Cymbella* diatom frustule. Scale bars are 10, 100, 20, and 5 μm, respectively (a–d).

image. As will be recalled from Chapter 5 on diffraction, optical path length is the product of the refractive index n and thickness t between two points on an optical path, and is directly related to the transit time and the number of cycles of vibration exhibited by a photon traveling between the two points.

In DIC microscopy, the specimen is sampled by pairs of closely spaced rays (coherent wave bundles) that are generated by a beamsplitter. If the members of a ray pair traverse a phase object in a region where there is a gradient in the refractive index or thickness, or both, there will be an optical path difference between the two rays upon emergence from the object, and that optical path difference is translated into a change in amplitude in the image. Since an optical path difference corresponds to a relative

phase difference between the two rays, the presence of phase gradients is acknowledged in a DIC specimen. But because optical path length is the product of refractive index and thickness, we cannot tell from the image alone whether a phase gradient in the object is due to differences in refractive index or thickness, or both. Strictly speaking, amplitude differences in the image should be referred to as representing optical path differences, not refractive index differences or differences in physical thickness, unless other information about the object is known. Refer back to Figure 7.10 to distinguish among these points.

In the DIC microscope, two optically distinct planar wavefronts traversing a phase object become deformed and vary in their optical path length in the region of the object; DIC between the two wavefronts produces high contrast patterns of the phase gradient (e.g., between the edge of the object and the surrounding medium). The method uses polarized light and special beam-splitting prisms called Wollaston prisms to generate and recombine the two wavefronts. Although both DIC and phase contrast optics depend on relative phase differences between sampling beams, there are fundamental differences. In phase contrast, the amplitude corresponds directly to the optical path difference between a specimen ray and a general reference ray; in DIC microscopy, amplitudes correspond to the derivative of the optical path difference profile and not to the optical path difference directly. Thus, if we could make a curve showing optical path length versus distance across the diameter of a specimen and determine the first derivative of that curve, we would obtain the amplitude profile of the specimen as seen by DIC microscopy; hence the name, *differential interference contrast microscopy* (Fig. 10.2). The method was described in 1952 and 1955 by Georges Nomarski, a Polish-French optics theoretician, and was later developed as an optical system in the mid-1960s by Carl Zeiss, Inc. of Oberkochen, Germany. Excellent descriptions of the method are provided by Allen et al. (1969), Galbraith and David (1976), Lang (1968, 1969, 1970, 1971a,b), and Padawer (1968).

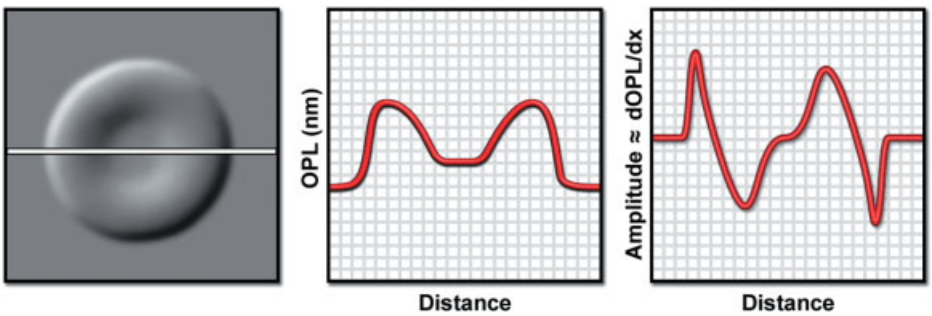

Figure 10.2

Gradients in optical path length yield differences in amplitude. (a) DIC image of a mammalian erythrocyte. (b) Plot of optical path length (OPL) across the diameter of the cell (indicated by the white line in panel a). (c) Derivative of the optical path length curve shown in panel b added to a constant, giving the amplitude profile perceived using DIC optics along the shear axis shown in panel a. Positive and negative slopes in panel a correspond to regions of higher and lower amplitude. Regions of the object exhibiting no change in slope (e.g., center of the cell) have the same amplitude as the background.

DIC Equipment and Optics

Differential interference contrast optics are commercially available for most research microscopes. The arrangement of four essential optical components is shown in Figure 10.3. (Instructions for aligning optics and evaluating imaging performance are given later in the chapter.) In order of their location on the optical pathway from the illuminator to the image plane, these include:

- A *polarizer* in front of the condenser to produce plane polarized light. The plane of vibration of the E vector of the waves is oriented horizontally on an east–west or right–left line when looking into the microscope just as in polarization micros-

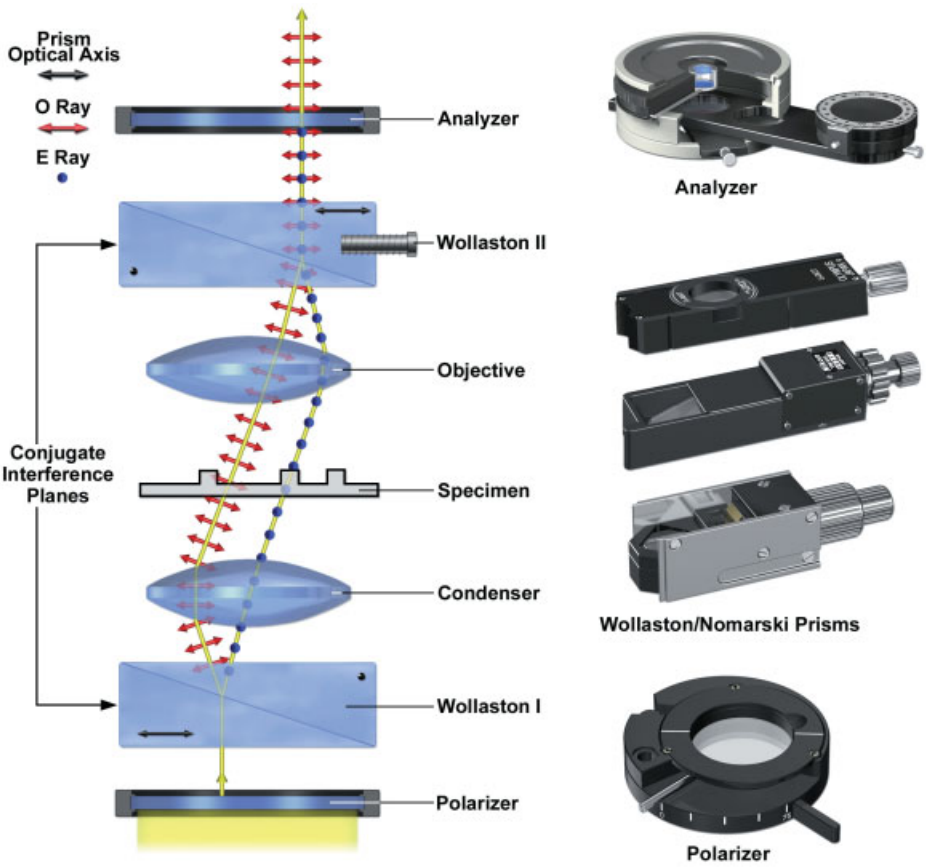

Figure 10.3

Optical components of a DIC microscope. Two polarizers (polarizer and analyzer) and two modified Wollaston prisms (DIC or Nomarski prisms) are required. The condenser DIC prism (Wollaston I) acts as a beamsplitter, producing two closely spaced parallel beams that traverse the object and are recombined by the objective DIC prism (Wollaston II). The red double arrows and blue dots (wave projecting out of the paper) indicate the mutually perpendicular vibrations of the two components of the split ray (defined in Fig. 8.7). On the right are shown examples of a polarizer, analyzer, and several Wollaston/Nomarski prisms. In some cases, the polarizers are mounted in sliders that can be inserted into or retracted from the light path.

copy. (The properties of polarized light and its application in polarization microscopy are discussed in Chapters 8 and 9.)

- A *condenser DIC prism* mounted close to the front aperture of the condenser acts as a beamsplitter. The design and action of this prism, technically known as a Wollaston prism, are described in this chapter. Every incident ray (wave bundle) of polarized light entering the prism is split into two rays—the O and E rays—that function as the dual beams of the interference system.
- An *objective DIC prism* mounted close to the rear aperture of the objective to recombine the two beams in the objective rear aperture. The action of this prism is essential for interference and image formation.
- An *analyzer* to "analyze" rays of plane and elliptically polarized light coming from the objective DIC prism and transmit plane polarized light that is able to interfere and generate a contrast image in the image plane. The analyzer has its vibrational plane oriented vertically in a north–south or top–bottom orientation when facing and looking in the microscope.

Alternative configurations based on the incorporation of a compensator provide greater control for adjusting image contrast. Since the system uses polarized light, special strain-free "pol lenses" are highly desirable, because ordinary objectives contain stress signatures in the glass that are birefringent and decrease contrast. Since the physical distance of separation of the wave pairs is as small as 0.18 μm for certain high-power oil immersion objectives (somewhat less than the diffraction-limited resolution of the lens itself), the specifications for lens performance are critical and must be met.

The DIC Prism

The DIC prism, known technically as a *Wollaston prism*, is a beamsplitter made of two wedge-shaped slabs of quartz (Fig. 10.4). Because quartz is birefringent, incident rays of linearly polarized light are split or sheared into two separate O- and E-ray components. The shear axis (direction of shear) and the separation distance between the resultant O and E rays are the same for all O- and E-ray pairs across the face of the prism. The E vectors of the resultant O and E rays vibrate in mutually perpendicular planes as they do for other birefringent materials.

In a standard Wollaston prism, the optical axes of two cemented wedges of calcite or quartz are oriented parallel to the outer surfaces of the prism and perpendicular to each other. If such a prism is placed between two crossed polarizers and examined face on, a pattern of parallel interference fringes is observed due to interference between obliquely pitched wavefronts of the O- and E-ray components. The interference fringes appear to lie inside the prism at a location termed the *interference plane*. This makes it difficult to use a conventional Wollaston prism for certain objectives, where the interference plane of the prism must lie within the rear focal plane (the diffraction plane) of the lens. This is especially problematic when the diffraction plane lies within the glass itself. Therefore, *modified Wollaston prisms* are generally used for the objectives, since the interference plane is displaced from the center of the prism to a distance several millimeters away from the prism itself (refer to the next demonstration). Such a prism does not have to be physically located in the aperture plane of the objective

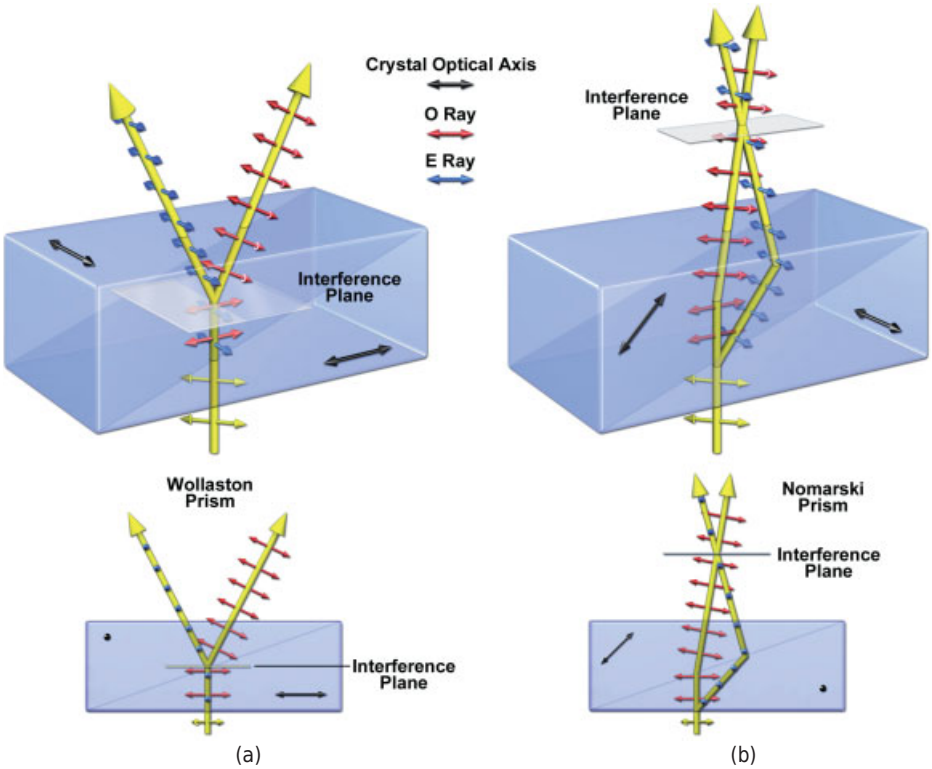

Figure 10.4

Design and action of Wollaston and Nomarski prisms. Conventional Wollaston (a) and modified Wollaston (or Nomarski) prisms (b) are used in DIC microscopy to generate and recombine pairs of O and E rays. The mutually perpendicular optical axes of the two quartz wedges comprising a Wollaston and Nomarski prism are indicated (↔,⊙) in the 2D drawings. The prisms are also drawn in 3D. The oblique orientation of the optical axis of one of the wedges in a Nomarski prism displaces the interference fringes to a site outside the prism. Interference and visualization of the interference fringes require the action of the analyzer.

and is much easier to employ. Interference fringes in the field of view are also avoided, and uniform contrast is achieved.

Nomarski cemented a conventional wedge with its optical axis parallel to the surface of the prism with another specially cut wedge whose optical axis was oriented obliquely with respect to the outside surface of the prism. For the condenser lens, there are fewer spatial constraints, and a conventional Wollaston prism can sometimes be used. In many cases, the condenser prism is a modified Wollaston prism as well, although its interference plane is usually closer to the prism. Thus, the two Wollaston prisms of the DIC microscope are cut differently and are not interchangeable. The condenser prism acts as a beamsplitter, while the objective prism recombines the beams and regulates the amount of retardation between O and E wavefronts. *Note the requirement for Koehler illumination to correctly position the interference planes of the DIC prisms in the conjugate aperture planes of the condenser and objectives.* The central or 0th-order interference fringe seen in the interference pattern just described is used to determine the proper orientation of the prisms during microscope alignment and is discussed later in this chapter.

Demonstration: The Action of a Wollaston Prism in Polarized Light

- Place a DIC prism between two crossed polarizers on a light box (white light) and rotate the prism until a dark interference fringe is observed. The intense dark band seen in the middle of the prism is the central 0th order fringe that results from destructive interference between the O and E wavefronts that have equal path lengths in the middle of the prism. Prisms intended for low magnification, low NA optics reveal several parallel interference fringes. Prisms intended for high magnification, high NA work reveal a single dark interference fringe.
- Observe that the higher order fringes appear in the colors of the interference spectrum if white light is used. Higher order fringes appear dark gray instead of black when illuminated with monochromatic light.
- Also notice that the interference fringes appear to float in space some millimeters above or below the prism. This is because modified Wollaston (Nomarski) prisms have their interference planes located outside the prism itself.
- Rotate the prism between the crossed polarizers again and notice that there are unique positions giving extinction. At these orientations, the phase retardation introduced between O and E rays by one slab of the prism is exactly reversed by phase displacements in the other slab, so that light emerges plane parallel and vibrating in the same plane as the incident polarized light. The resultant rays are blocked by the analyzer, giving extinction.
- In the microscope, examine the action of a DIC prism between crossed polarizers (the other prism has been removed) in the aperture plane using a telescope eyepiece or Bertrand lens. A brightfield is seen with a dark fringe running across it. When both prisms are in position and the rear aperture is observed, the field looks dark (extinction) because light emerging from each position from the condenser prism is now exactly compensated for by the objective prism. All beams emerging from the objective prism are again linearly polarized in the direction of the original polarizer, and thus are blocked by the analyzer (extinction).

Formation of the DIC Image

Both ray tracing and wave optics are useful for explaining image formation in the DIC microscope. By tracing the trajectories of rays from polarizer to image plane, we observe the actions of optical components and understand the DIC microscope as a double-beam interference device. By examining the form and behavior of wavefronts, we also come to appreciate that optimal image definition and contrast are affected by the amount of phase displacement (bias retardation) between the two wavefronts introduced by the operator. (Note, however, that properly adjusted DIC equipment can only insure good visibility of details that are within the resolution limit of the optics of the brightfield microscope.) Although complex, these details help one understand where

essential actions occur along the microscope's optical path, allow one to align and troubleshoot the optics, and help you use the microscope effectively. Before proceeding, one should keep in mind that the potential spatial resolution is limited, but not guaranteed, by the NA of the objective and condenser lenses.

Ray tracing of the optical pathway shows that an incident ray of linearly polarized light is split by the condenser prism into a pair of O and E rays that are separated by a small distance (Figs. 10.3–10.5). The E vectors of the two rays vibrate in mutually perpendicular planes. Between the condenser and objective, the trajectories of the ray pair remain parallel to one another and are separated by 0.2–2 μm—the *shear distance*—which is as small as or smaller than the spatial resolution of the microscope objective being employed. In fact, as the shear distance is reduced, resolution improves, although at some expense to contrast, until the shear distance is about one-half the objective's maximum resolution. Thus, every point in the specimen is sampled by pairs of beams that provide dual-beam interference in the image plane. Notice that there is no universal reference wave generated by an annulus and manipulated by a phase plate as in phase

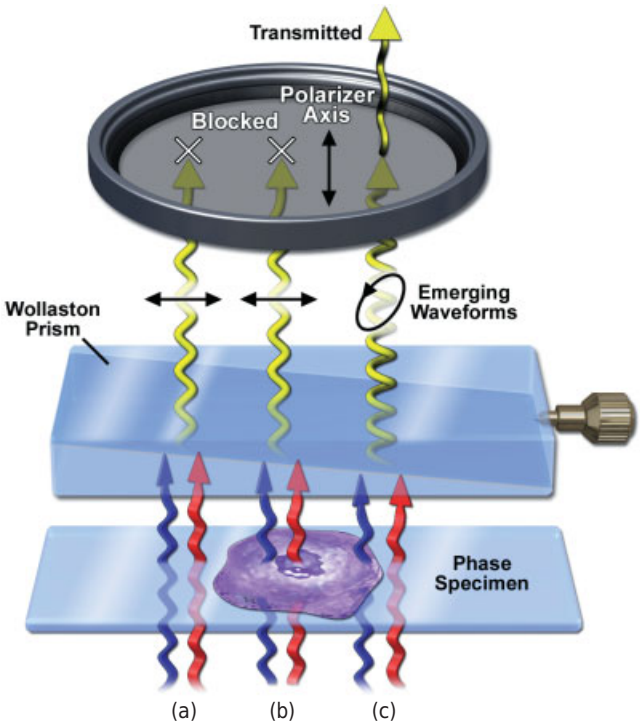

Figure 10.5

Progression of rays through the DIC microscope. An incident beam of linearly polarized light is split by the condenser DIC prism into O- and E-ray components that are focused by the condenser lens onto the specimen. The two rays follow separate parallel trajectories between the condenser and objectives. (a and b) In the absence of an optical path difference, the O and E rays are combined by the objective prism, giving linearly polarized light that vibrates in the same plane as the polarizer and is completely blocked by the analyzer. (c) If an optical path difference (phase shift) exists, the prism recombines the beams, giving elliptically polarized light that is partially transmitted by the analyzer.

microscopy, where the distance separating the object and background rays can be on the order of millimeters in the objective rear aperture.

In the absence of a specimen, the coherent O and E rays of each ray pair subtend the same optical path length between the object and the image; the objective prism recombines the two waves, generating waves of linearly polarized light whose electric field vectors vibrate in the same plane as the transmission axis of the polarizer; the resultant rays are therefore blocked by the analyzer, and the image background looks black, a condition called *extinction* (Fig. 10.5a,b). Thus, the beam-splitting activity of the condenser prism is exactly matched and undone by the beam-recombining action of the objective prism. Note that the axes of beam splitting and beam recombination of both DIC prisms are parallel to each other and fixed at a 45° angle with respect to the transmission axes of the crossed polarizer and analyzer. This axis is called the *shear axis* because it defines the axis of lateral displacement of the O and E wavefronts at the specimen and at all locations between the specimen and the image.

If, however, the O- and E-ray pair encounters a phase gradient in an object, the two beams will have different optical paths and become differentially shifted in phase. We treat the situation the same as we do in standard light microscopy: waves emanating from the same object particle in the specimen meet at their conjugate location in the image plane, with the difference that the waves must first pass through the objective DIC prism and analyzer. These waves emerge from the prism as *elliptically polarized light* (Fig. 10.5c). The E vector of the resultant ray is not planar, but sweeps out an elliptical pathway in three-dimensional space. These rays partially pass through the analyzer, resulting in a linearly polarized component with finite amplitude. This information plus our knowledge of diffraction and interference tell us that image formation will occur, but still do not provide a complete explanation for the unique shadow-cast appearance of the DIC image. For this we need to examine the formation and behavior of wavefronts.

Interference between O and E Wavefronts and the Application of Bias Retardation

As just described, incident rays of linearly polarized light are split by the condenser DIC prism into O- and E-ray pairs, traverse the specimen, and are recombined by the objective DIC prism, generating linearly and elliptically polarized waves that are differentially transmitted by the analyzer according to the azimuths of their vibrational planes. Since transmitted rays are linearly polarized and are plane parallel, they interfere in the image plane and generate an amplitude image of the object. Another useful way of viewing the situation is to decompose the transmitted rays into their corresponding O- and E-wave components so that we can appreciate the importance of phase displacements between the waves and the role of the objective DIC prism as a contrasting device. Knowledge of the action of the objective DIC prism is important, because the operator must adjust the position of this prism to regulate the amount of optical shadowing and image contrast.

The rays exiting the prism are observed to define two distinct planar wavefronts that meet in the image plane (see Fig. 10.6a). Each front shows localized regions of phase retardation—differential phase retardations—caused by phase objects in the specimen plane. Figure 10.6 (top) shows the reconstructed profiles of the O and E wavefronts in the image plane taken along an axis parallel to the direction of shear with

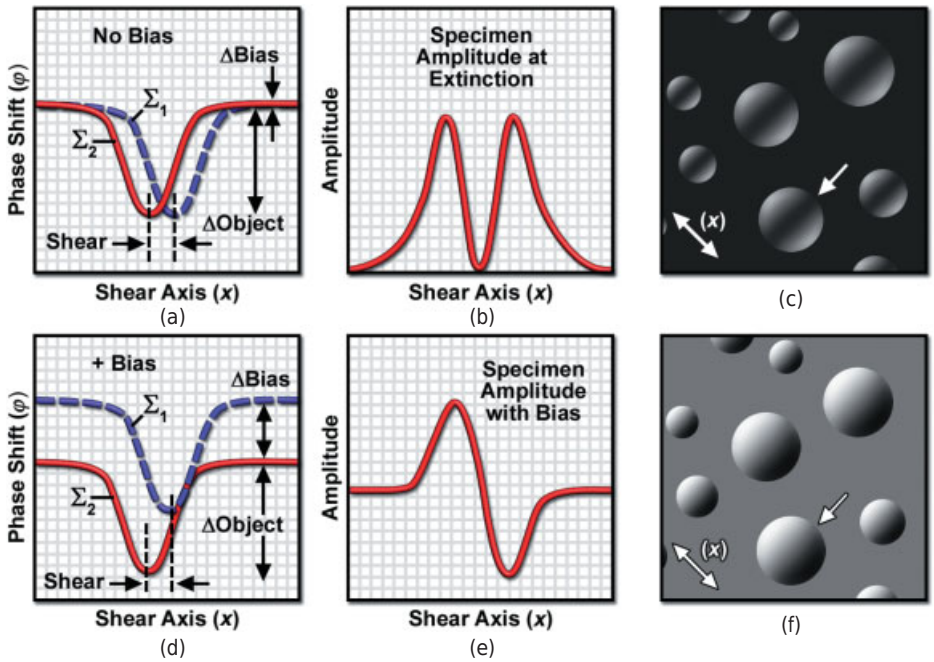

Figure 10.6

Interference between O and E wavefronts in the image plane. The two views of oil droplets show the DIC prism adjusted for extinction (top) and with the addition of bias retardation (bottom). The pairs of graphs for each condition show the positions of wavefronts (a, d), and the corresponding amplitudes (b, e) for profiles taken through an object in the direction of prism-induced shear, which gives the greatest contrast (c, f). The *x*-axis represents the distance *x* across the object. The graphs indicating the phase shift ϕ show the O and E wavefronts (labeled Σ_1, and Σ_2) in the image plane after passage through the object DIC prism and analyzer. The dips in the wavefronts represent phase retardations resulting from transit through a phase object. The amplitude graphs show the wave resulting from interference between the two original wavefronts. *Objective prism adjusted to extinction:* Notice that under conditions of extinction, the two wavefronts in the top panel are sheared laterally by a distance along the *x*-axis, but do not exhibit a phase difference in the regions corresponding to background. These regions have zero amplitude and appear black in the corresponding intensity plot. *Addition of bias retardation after movement of the objective DIC prism:* The two wavefronts remain sheared by the same amount, but are now relatively shifted in phase. The corresponding amplitude plot shows a bright edge on the left-hand side and a dark edge on the right-hand side. Moving the DIC prism changes the displacement between the two wavefronts along the *y*-axis and alters the contrast.

the instrument adjusted to extinction. Each wavefront shows a dip or trough whose width represents the magnified object diameter and whose depth represents the amount of phase retardation, ϕ, in nanometers. After combination and interference, the resultant image may be represented as an amplitude plot, from which we deduce that the image of the spherical object shows a dark central interference fringe flanked on either side by regions of brightness. With the background appearing dark, the overall effect is that of a darkfield image.

In practice, a prism setting giving total extinction of the background rays is not used. Rather, the 0th order interference fringe is displaced to one side of the optical

axis of the microscope using the objective prism adjustment screw, an action that introduces a phase displacement between the O- and E-ray wavefronts (Fig. 10.6, bottom). This manipulation is called *introduction of bias retardation*. Since background ray pairs are now differentially retarded and out of phase, they emerge from the objective prism as elliptically polarized waves and partially pass through the analyzer, causing the background to look medium gray. Adding bias retardation now causes the object image to exhibit dark shadows and bright highlights against a medium gray background in regions where there are phase gradients. The amplitude at the edges of objects relative to that of the background depends on whether the O- or E-ray wavefront was phase retarded or phase advanced at the specimen, and is determined by the direction of offset of the interference fringe.

On some microscopes bias retardation is introduced by advancing or retracting the objective DIC prism in the light path by turning a positioning screw on the prism holder; on other microscope designs containing in addition a $\lambda/4$ plate, the objective DIC prism is fixed, and the bias adjustment is made by rotating the polarizer (de Sénarmont method). The amount of displacement between the O and E wavefronts caused by the objective DIC prism is small, usually $<\lambda/10$. Introducing bias retardation makes objects much easier to see, because phase gradients in the specimen are now represented by bright and dark patterns on a gray background. The resultant image exhibits a shadowcast, three-dimensional, or relief-like appearance that is the distinguishing feature of DIC images and makes objects look like elevations or sunken depressions depending on the orientation of phase gradients. It is important to remember that the relief-like appearance of the specimen corresponds to phase gradients, not differences in elevation in the specimen, though it may do so if real topological features also correspond to sites of phase gradients.

Alignment of DIC Components

It is important to inspect the appearance of extinction patterns (polarization crosses) and interference fringes in the rear aperture of the objective to confirm that optical components are in proper alignment and to check for damage, such as stressed lens elements, scratches, lint, bubbles, and dirty lens surfaces. Adjustments of DIC optical components are critical to imaging performance, so it is important to recognize misalignments and faults and correct them if necessary.

The appearance of the image at different steps of alignment is shown in Figure 10.7, and the operation is performed as follows:

1. Cross the polarizer and analyzer. The polarizer (near the light source) is oriented in an east–west direction as you face the microscope. A mark on the mounting ring of the polarizer indicates its transmission axis. Before adjusting the analyzer, remove all optical components, including the condenser, the objective, and DIC prisms. When the analyzer is crossed at 90° with respect to the polarizer, the field looks maximally dark (extinction) when observed through the eyepieces (Fig. 10.8a). If the field of view is not dark, move the analyzer in its mounting until the transmission axis is oriented in a north–south direction.
2. If the analyzer is fixed and the polarizer is rotatable, this adjustment is made in the reverse order. When the objective and condenser are inserted (but without

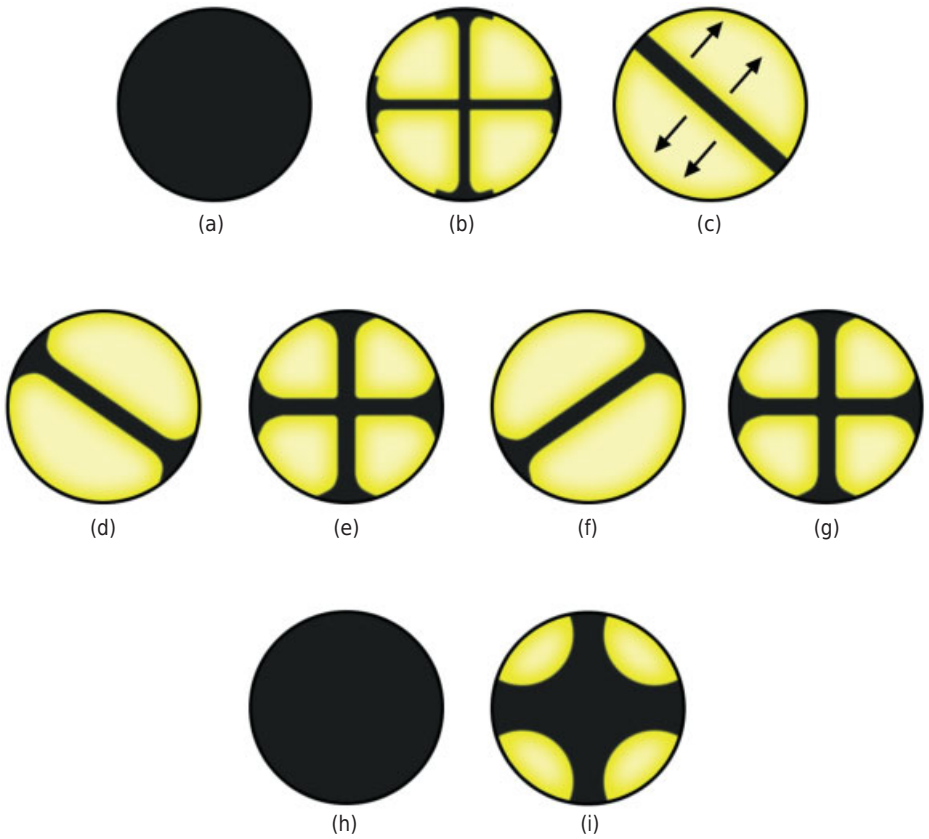

Figure 10.7

Alignment of DIC optical components. The following description is based on alignment of DIC prisms on a Zeiss microscope. The alignment procedure is different on other microscope designs, but the appearance of the expected interference fringes is the same. (a and b) Both DIC prisms removed, crossed polarizers: Image view (a) reveals a maximally dark field (extinction), while telescope view (b) shows the characteristic extinction cross. (c) Objective DIC prism only; crossed polarizers; telescope view: A prominent interference fringe is seen running diagonally from northwest to southeast across the field. Adjustment of the prism position with the bias adjustment screw shifts the fringe pattern laterally. For extinction, the fringe is positioned in the center of the field. (d–g) Condenser DIC prism only; crossed polarizers; telescope view: A prominent interference fringe runs diagonally from northwest to southeast across the field. The patterns seen at successive 90° rotations of the prism are shown, but only the first fringe pattern (d) is correct. Thus, the objective and condenser prism interference fringes must be parallel and overlapping. (h and i) Both DIC prisms in place; crossed polarizers; image and telescope views: In image view, the field looks uniformly dark. In telescope view, a dark, diffuse extinction cross is observed. Slight adjustments of the condenser and DIC prisms might be necessary to obtain perfect alignment. The condenser prism is then locked into position. The condenser aperture is stopped down to mask bright peripheral illumination at the objective rear aperture.

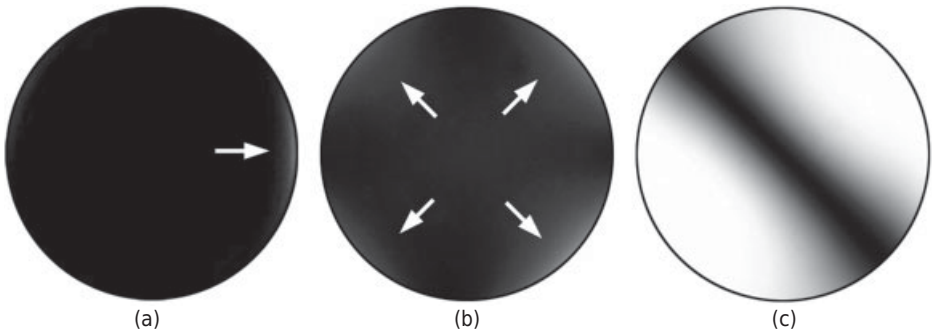

Figure 10.8

Observing the image and objective rear aperture in DIC microscopy with a Bertrand lens. (a) Polarizer and analyzer crossed with both DIC prisms removed from the optical train as viewed through the eyepieces. Note the slight misalignment of the polarizers or optical system indicated by the brighter region (white arrow). (b) Objective rear aperture with crossed polarizers viewed with a Bertrand lens. The white arrows show bright regions of the extinction cross. (c) Interference fringe extending from northwest to southeast viewed at the objective rear aperture when the objective DIC prism is inserted into the optical train.

the DIC prisms) and the microscope focused on a blank slide and adjusted for Koehler illumination, the field looks dark in visual mode, and a dark extinction cross can be seen in the rear aperture of the objective with an eyepiece telescope or Bertrand lens (Fig. 10.8b). If the polarizer and analyzer are mounted properly, the extinction cross will have straight horizontal and vertical components. There should not be any bright birefringent streaks, which are indicators of strained lenses and inferior performance in DIC.

3. Examine the objective rear aperture with the objective DIC prism in position and the condenser prism removed. A single dark interference fringe extends across the diameter of the rear aperture from the northwest to southeast quadrants at a 45° angle. The fringe should be well defined and run through the middle of the aperture (Fig. 10.8c). The objective prism is fixed in some microscope designs, but in others, it can be adjusted using a prism positioning screw. The image field as seen through the eyepieces looks bright and featureless.
4. Now inspect the front aperture of the condenser again using a telescope, this time with the condenser DIC prism in position and the objective prism removed. A single interference fringe running northwest to southeast at a 45° angle should be observed. To see the fringe clearly on some high NA condensers, it may be necessary to remove the front 1.4 NA cap lens of the condenser. If the fringe is not well defined or is oriented incorrectly, the condenser prism may need to be rotated to optimize the alignment. Usually, this adjustment is made by the manufacturer and remains fixed (or can be locked down with a set screw) so that it does not need to be altered. If it is not properly displayed, contact the manufacturer and get instructions on how to reset the alignment. The image field as seen through the eyepieces again looks bright and featureless.
5. Mount and focus a specimen (such as buccal epithelial cells; Fig. 10.9) on a slide and set Koehler illumination with both DIC prisms and polarizers in

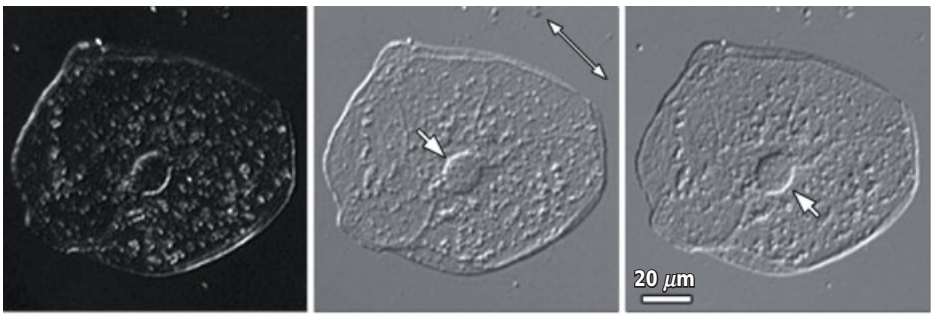

Figure 10.9

Positive and negative bias retardation in DIC microscopy. (a) When the DIC optical system is set at extinction, the field appears dark gray on a black background with bright highlights in regions having large refractive index and thickness gradients. (b) Shifting the DIC prism in one direction (positive bias) lightens specimen features at one edge (white arrow pointing to the nucleus) while darkening the same features on the opposite edge. (c) Shifting the DIC prism in the opposite direction (negative bias) reverses the intensity of features (white arrow). The shear axis is indicated by the double-headed white arrow.

position with the optics set at extinction. The image field looks very dark gray at extinction (Fig. 10.9a), while a sharply defined interference fringe or band is seen running in a northeast–southwest direction across the diameter of each refractile particle in the object (Fig. 10.6, top). The orientation of the interference fringe is shifted by 90° compared with the fringe orientation seen in aperture views of the individual condenser and objective DIC prisms already described, and is the correct orientation for the fringe in the image at extinction. While viewing the image, note that advancing the objective DIC prism (or rotating the analyzer a few degrees to either side of the extinction position) moves the interference fringe bisecting particles or organelles along an axis oriented in a northwest to southeast direction (the shear axis), causing one side of the organelle to look dark and the opposite side to look bright (Fig. 10.9b). For a given microscope, only one of these elements is adjusted (prism or polarizer or analyzer) to introduce bias retardation. Adjusting the bias retardation brightens the background, improves image appearance and contrast, and is an essential final step in the adjustment of DIC optics. In addition to the presence of discrete light and dark intensities at opposite edges of each organelle along the shear axis, a broad and indistinct field fringe is sometimes observed, a gradient of light across the entire field of view. With well-designed optics, the field fringe is so broad that the entire image background appears a uniform medium gray. More commonly, some evidence of the fringe remains, so that after introducing bias retardation (by adjusting the DIC prism or rotating the analyzer), the field exhibits a shallow gradient of light intensity from one edge to the other.

6. When the rear aperture of the objective is examined with an eyepiece telescope with the DIC prism set at extinction, the central region should look dark gray and uniform, but possibly with some brightening at four quadrants at the periphery, giving the appearance of a very broad extinction cross similar to the one

observed in the rear aperture of a polarizing microscope. The brightening represents an artifact due to partial depolarization of light at lens elements of the condenser and objective. Image contrast can be greatly improved if these regions are masked out by partly closing down the condenser aperture, leaving 75% of the aperture diameter clear. If the optics are in perfect adjustment at extinction, the cross stands upright and is seen to be composed of two broad interference fringes, each bent in the shape of a right angle and meeting in the center of the aperture. On most microscopes, the fringe pattern can be adjusted to make the central region of the aperture darker and more uniform. This is done by loosening and rotating the condenser DIC prism a small amount, or by slightly rotating the polarizer or analyzer. Now secure the components, leaving only one for adjusting bias retardation. As a final adjustment and check, move the condenser focus very slightly out of the Koehler position to determine if extinction at the rear aperture can be improved still further. However, too great a movement will bring the conjugate interference planes of the prisms too far apart and degrade optical performance.

Image Interpretation

The DIC image has a relief-like quality, exhibiting a shadow-cast effect as if the specimen were a three-dimensional surface illuminated by a low-angle light source. It must be remembered that the shadows and highlights in the shadow-cast image indicate the sign and slope of phase gradients (gradients in optical path length) in the specimen and do not necessarily indicate high or low spots. The direction of optical shear is obvious and is defined by an axis connecting regions having the highest and lowest intensity. Finally, the direction of the apparent shadow casting is reversed for structures with refractive indices that are lower and higher than the surrounding medium. Thus, dense nuclei, mitochondria, and lysosomes might have the appearance of raised elevations, while less dense pinocytotic vesicles and lipid droplets have reversed shadow orientations and look like sunken depressions. The degree of contrast and extent of three-dimensionality depend on the amount of bias retardation between wavefronts imparted by the objective prism. The axis of optical shear cannot be changed by changing a setting on the microscope. However, the orientation of bright and dark edges can be reversed 180° by moving the DIC prism to place the optical axis of the microscope on the other side of the null position of the prism. This has the effect of reversing the relative phase retardation of the O and E wavefronts. Therefore, the only way of changing the shear axis relative to the specimen is to rotate the specimen itself. For certain symmetric specimens, such as diatoms, specimen rotation can be used to highlight different features (Fig. 10.10). A precision-rotating specimen stage is very useful in deducing the direction of phase gradients in complex structures.

Finally, note that the intensity of shadows and highlights is greatest along the direction of the shear axis. If we examine the contrast at the edges of a spherical particle along diameters taken at different azimuths, we observe that the contrast between the particle and the background gradually decreases and reaches zero at 90° along a line defining the axis of the interference fringe. At this position, the irregularities in profiles of the O and E wavefronts are exactly aligned, so subtraction of the two wavefronts cancels out any retardation and gives a positive value that exactly matches that of the background.

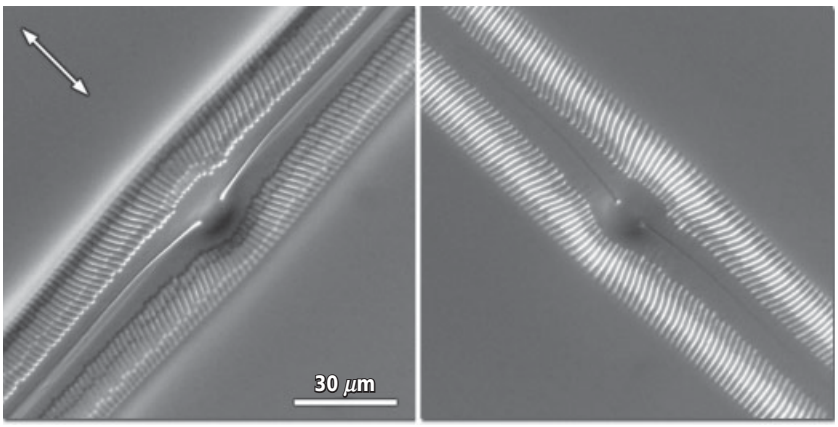

Figure 10.10

Effect of specimen orientation in DIC microscopy. Since the shear axis is fixed in DIC optics, the specimen itself must be rotated to highlight different features. Notice the differential emphasis of pores and striae in the shell of a diatom, *Gyrosigma balticum*, using DIC optics when the specimen is rotated. The white double-headed arrow indicates the shear axis.

The best amount of bias retardation is that giving optimum contrast to the object image and is unique for each object. Since the field of view usually includes many phase objects of different size and refractive index, the best overall bias setting is a compromise. The following guidelines are useful in performing this adjustment:

- The amount of bias retardation required to maximally darken one slope or edge of an object also gives the maximum possible contrast between the object and the background. Thus, for any given object, there is an optimal amount of bias retardation that requires a particular prism setting.
- If a bias retardation is chosen that is greater than the minimum amount required, the contrast will be reduced.
- Thick light-scattering objects may require a higher bias compensation setting in order to obtain extinction of one edge (gradient slope) of the object.
- When the condenser aperture exceeds about 75% of the objective aperture, resolution improves, but light scattering in the optical system increases significantly and contrast becomes reduced.

The Use of Compensators in DIC Microscopy

Although the DIC microscope is largely a qualitative instrument, a compensator can be used to manipulate the amount of bias retardation between O- and E-wave pairs more precisely and give more control to adjusting the contrast of specimen details in the image. The action of compensators as contrasting and measuring devices is described in Chapter 9. The compensator is placed in a specially designated slot between the crossed polarizers and introduces a known amount of retardation.

A full-wave plate or λ plate, such as the red-I plate with a retardation ~551 nm, can be used to color the image by introducing a spectrum of interference colors. The colors at the edges of objects and their immediate background can be compared using a Michel-Lévy color chart to estimate the magnitude of the optical path difference.

The de Sénarmont compensator contains a fixed $\lambda/4$ wave plate and a rotating analyzer, and is frequently used with DIC optics to introduce a known amount of bias retardation to a specimen. This might be needed in certain semi-quantitative applications or simply as a monitor of DIC optical alignment. Allen (1985) and Inoué (1989) used the technique to introduce a precise amount of retardation to optimize the contrast of microtubules imaged by video-enhanced DIC microscopy. When using this technique, the $\lambda/4$ wave plate and analyzer (adjusted for extinction) are inserted into the optical path and the objective DIC prism is adjusted to give extinction. The analyzer is then rotated to give the desired amount of bias retardation and background intensity (for details on de Sénarmont compensation, refer to Chapter 9). The degrees of rotation can be noted for future reference.

Comparison of DIC and Phase Contrast Optics

Figure 10.11 shows DIC and phase contrast images of buccal epithelial (cheek) cells on a glass microslide. Both images show a conspicuous nucleus and granules in the

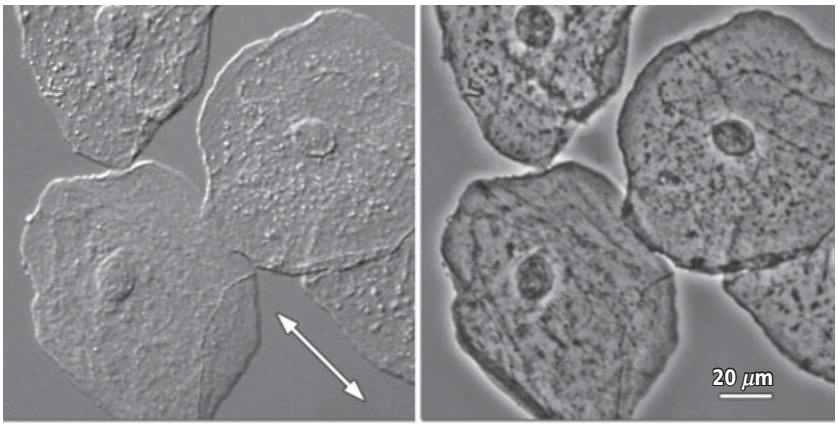

(a) (b)

Figure 10.11

Comparison of DIC and phase contrast images of buccal epithelial cells. (a) *DIC*: The direction of the shear axis is shown by the white double-headed arrow in the micrograph. The cells appear as if illuminated by a grazing incident light source located in the upper left corner. Bright edges at the upper margins of the cell, the nucleus, and some of the small granular inclusions indicate these objects are phase-dense (have a higher refractive index) compared with their surround. (b) *Phase contrast*: Positive phase contrast renders phase-dense objects as dark contrast features relative to the background. The cells themselves are surrounded by a bright phase halo, an artifact of the phase contrast optical system. The information content (spatial resolution, detection sensitivity) of the two optical systems is similar.

cytoplasm, but intensity differences in the phase contrast image show that the nucleoplasm is denser than the cytoplasm; notice too that the cytoplasm is denser than the surrounding medium. Small phase-dark mitochondria and granules are conspicuous. Phase halos around the cells indicate significant differences in optical path length compared with the surrounding medium, which is water.

In the DIC image, notice the orientation of bright and dark edges of the cell, nucleus, and granules perpendicular to the shear axis. Cytoplasmic granules are clearly defined, and there is no phase halo. The shadow-cast, three-dimensional appearance is the result of dual-beam interference.

MODULATION CONTRAST MICROSCOPY

Optical methods based on oblique or off-axis illumination provide an alternative to DIC optics for viewing phase gradients in an object. The principal systems are single sideband edge enhancement (SSEE) microscopy described by Ellis (1978) and MCM described by Hoffman and Gross (1975) (see also Hoffman, 1977). For examining tissue culture plates, Carl Zeiss introduced Varel optics, which uses a related optical system. Like DIC optics, MCM systems produce images that have a three-dimensional or shadow-cast quality, making objects appear as though they were illuminated by a low angle light source (Fig. 10.12).

In both MCM and DIC, brightly illuminated and shadowed edges correspond to *optical path gradients* (phase gradients) of opposite slope in the specimen, but unlike

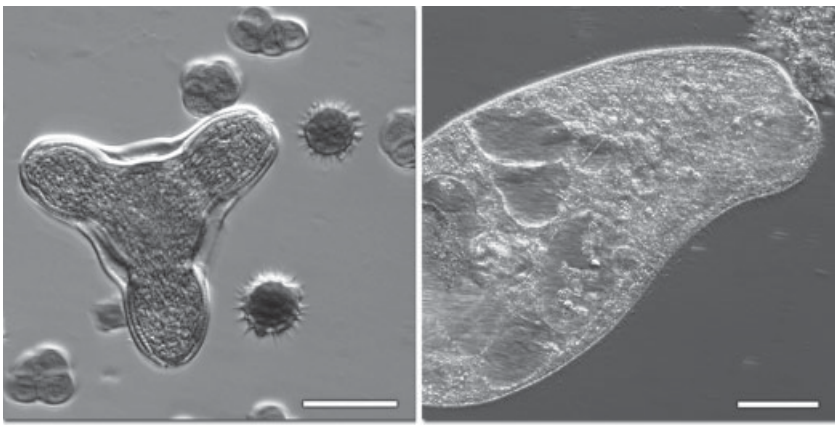

(a) (b)

Figure 10.12

Mixed pollen (a) and a living paramecium (b), imaged in modulation contrast microscopy. As in DIC microscopy, variations in intensity of the image correspond to gradients in optical path length in the specimen. The contrast image is generated by blocking one sideband of the diffracted light. There is no dependence on polarized light and no dual-beam interference mechanism as in DIC microscopy. Bars = 10 μm.

DIC, the MCM system does not require crystalline DIC prisms. Although resolution and detection sensitivity of the Hoffman MCM system are somewhat reduced compared with DIC, MCM produces superior images at lower magnifications, allows optical sectioning of rounded cell specimens, and offers certain advantages over DIC optics, including the ability to examine cells on birefringent plastic substrates, such as cell culture dishes. Hoffman modulation contrast optics are available from Modulation Optics, Glen Cove, New York.

Contrast Methods Using Oblique Illumination

Those who test optical surfaces will already be familiar with the essentials of the Schlieren system, which is related to the well-known knife edge test first employed by Leon Foucault in 1859 for measuring the radius of curvature of lens surfaces. Toepler later used the method to examine variations in the refractive index of a transparent medium in a sample cell, where inhomogeneities in the medium appear as high contrast streaks (Schlieren in German) (Fig. 10.13). The cell is illuminated with a narrow slit, and the light is refocused with a lens to reform an image of the slit. The sample cell is examined by placing the eye just beyond the slit image, while an opaque straight edge is inserted into the focused beam, with the edge aligned with the slit, so as to nearly completely mask the slit and reduce transmission to the eye. Brightness and contrast are modulated by the degree to which the knife edge blocks light from the slit. In forms of Schlieren microcopy, the optical design is similar. The specimen is illuminated by a slit in an opaque aperture mask placed in the front aperture of the condenser, and an adjustable knife edge located in the rear aperture of the objective is used to adjust brightness and contrast. The Schlieren image is formed in the following way: the object field appears evenly illuminated, but phase gradients in the object deflect rays through principles of diffraction, refraction, and reflection to regions outside the area of the

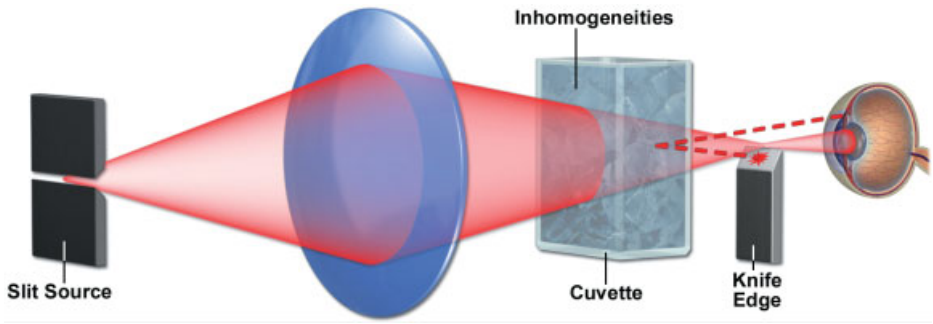

Figure 10.13
Optical plan for Schlieren optics with off-axis illumination. A knife edge placed close to the eye blocks one sideband of diffracted rays (dotted lines), creating a shadow-cast contrast image of phase gradients in the sample cell.

focused image of the slit, which represents the 0th order or direct light component. The eye sees the object as a relief-like pattern of shadows and highlights. Intensity differences perceived by the eye are due to interference in the image plane between the 0th order component and a single sideband of the diffracted light component.

Light microscopes using oblique illumination and MCM optics operate by similar principles. *Oblique illumination* can be obtained in a standard transmitted light microscope by selectively illuminating one side of the front lens of the condenser using an opaque mask with an off-axis slit in the front aperture position. Alternatively, one can simply rotate the condenser turret until light passing through the condenser iris diaphragm hits one edge of the condenser lens. This condition is analogous to using an illuminating slit as already discussed. The image of the offset condenser aperture is now offset in the conjugate rear aperture of the objective. Many of the rays diffracted by an object that would be brought to a position peripheral to the offset aperture are blocked by the edge of the lens and become excluded from image formation. In this case, the function of the knife edge at the aperture plane is provided by the edge of the lens itself. While the delivery of light is not well controlled, resolution is good because diffracted waves are included on one side of the 0th order spot in the rear focal plane of the objective.

The arrangement of components in a modulation contrast microscope resembles the design of the Schlieren optical system described above. The slit and knife edge of the Schlieren system occupy conjugate focal planes, and placement of the eye just behind the knife edge allows these planes to function as the condenser and objective aperture planes in a microscope. The object and retina define two conjugate field planes of the system. These features are modified in *Hoffman modulation contrast optics* as shown in Figure 10.14. An off-axis slit of some width is mounted in the front aperture of the condenser, while the knife edge at the rear aperture of the objective is represented by a modulator plate. The modulator is divided into three asymmetric regions: (1) a nearly opaque section of a circle at the extreme edge of the plate, (2) an adjacent, semidarkened rectangle giving 15% transmission, and (3) a large transparent zone that allows 100% transmission. When properly aligned, the image of the condenser slit exactly fills the semitransparent rectangle and produces even, attenuated illumination in the image plane. Sliding the modulator to the right or left exposes a greater or lesser area of the slit and brightens or darkens the background in the image. This right–left shear axis is the same axis that defines the bright and dark contrast regions in the image, but details along a north–south diameter through the object have minimal contrast. To examine contrast features of the specimen at different azimuths, it is necessary to rotate the specimen on the microscope stage.

Gordon Ellis demonstrated that the mechanism of contrast generation in this and other Schlieren-related systems is based on the selective removal of diffracted light on one side of the 0th order spot in the diffraction plane. This demonstration was made on a Schlieren microscope of his own design: the *SSEE microscope*. As in the Hoffman MCM microscope, there are complementary masks (half-aperture masks) in the front aperture of the condenser and in the rear aperture of the objective. Ellis showed (1978) that a transparent object (a water-immersed diffraction grating replica), which is invisible without the masks in a brightfield image, becomes visible at focus when the *diffracted light of one sideband is blocked* by the objective aperture mask. In the demonstration, there was no modification of the direct light, so it is possible to conclude that formation of a visible image is strictly a consequence of the change in interference between the diffracted sidebands and the direct light.

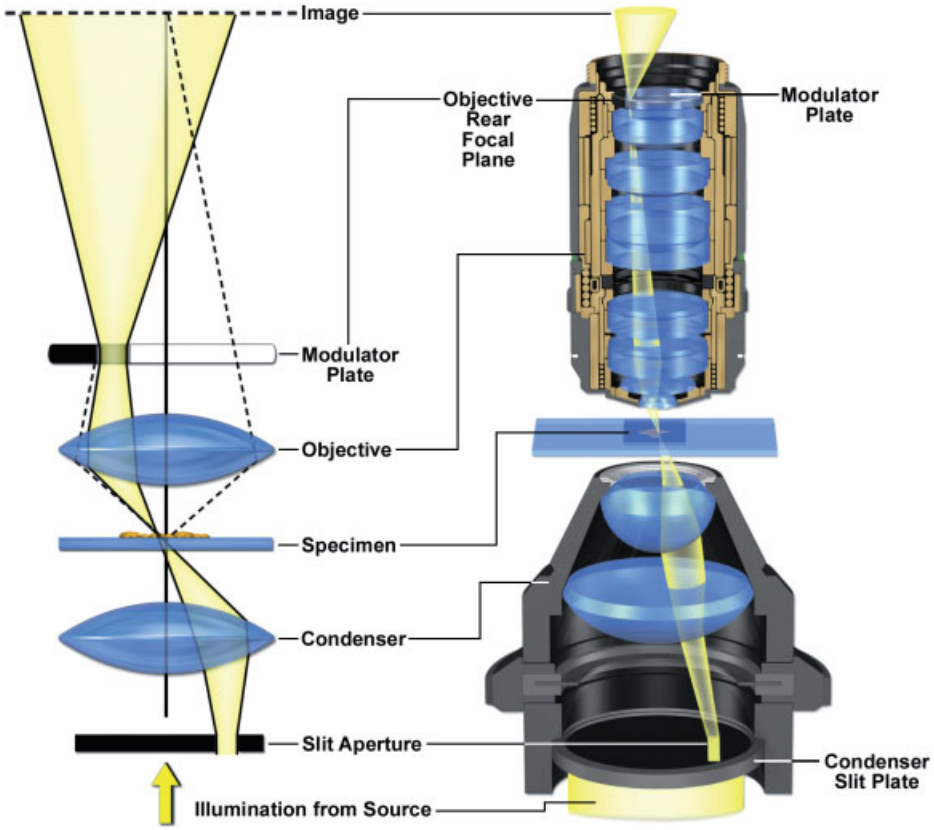

Figure 10.14

Equipment for modulation contrast microscopy. Oblique illumination is provided by an off-axis slit in the condenser aperture. A modulator plate with matching complementary slit in the objective rear aperture differentially blocks one sideband of diffracted light. Movement of the plate modulates the transmission of 0th order light, allowing for regulation of image contrast.

Alignment of the Modulation Contrast Microscope

The microscope is first adjusted for Koehler illumination. The condenser slit aperture is mounted in a vertical north–south orientation in the front aperture of the condenser (Fig. 10.15). Slit alignment is performed while viewing the objective aperture plane with an eyepiece telescope or Bertrand lens. The modulator is inserted in a slot near the rear aperture of the objective and likewise aligned, giving attention that the image of the condenser slit exactly fills the semi-darkened rectangle on the plate. A positioning screw on the modulator allows you to slide the plate along an axis perpendicular to the long axis of the condenser slit image. Other versions of MCM include two polarizing elements, one of which is rotated, to vary image brightness. Brightness can also be controlled by moving the modulator plate, but as movement of the plate affects the contrast of phase gradients, this method of control may not be desirable. Since both polarizing elements are located on the same side of the specimen, loss of contrast from birefringent plastic substrates, such as culture dishes, is not a problem.

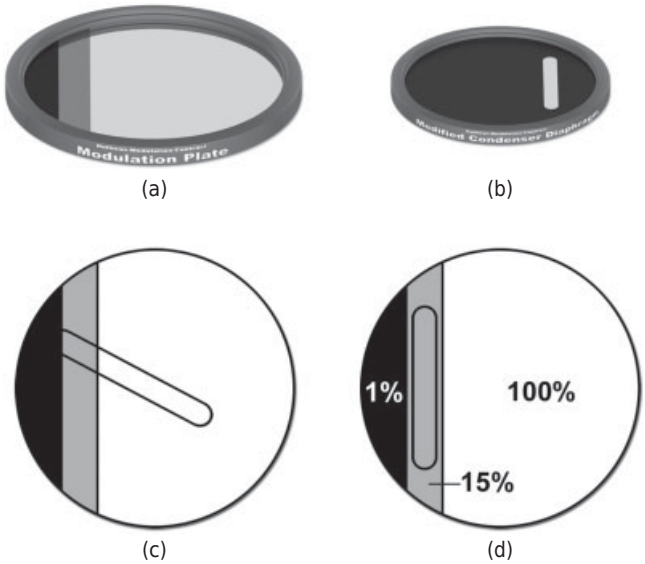

Figure 10.15

Alignment of optical components for modulation contrast microscopy. (a–b) 3D representation of HMC optical elements. The alignment of the condenser slit aperture and modulator plate is examined using an eyepiece telescope or Bertrand lens. (c) Unaligned system. (d) The condenser slit must be perfectly aligned with the rectangular gray area of the modulator plate to properly isolate and control the 0th order beam. The regions of varying light transmission (1, 15, and 100%) in the modulator plate are indicated in panel d. Note the requirement for Koehler illumination for the confocal positioning of the two conjugate aperture planes.

Exercise: DIC Microscopy

- *Review of procedures for aligning optical components for DIC microscopy.* In a sketch, indicate the proper sequence and orientation of the polarizer and analyzer, as well as the condenser and objective DIC prisms. Indicate the pattern and orientation of interference fringes seen with a Bertrand lens when the microscope is set at extinction and when the condenser or objective DIC prism has been removed.
- *Examination of diatom shells by DIC microscopy.* Examine the diatom test plate at 100× with DIC optics and determine if the striae and pores in *Frustulia* and *Amphipleura* can be resolved. Alternatively, examine the myofibrils of striated muscle in the thorax flight muscles of a fruit fly, *Drosophila*. Anesthetize one or two flies, remove the head and abdomen, and place the thorax in a 30–50 μL drop of water between a microscope slide and coverslip and squash the thorax to disperse the muscle. Blot off excess water, dry, and seal the edges of the coverslip with nail polish to prevent evaporation. Allow to dry thoroughly (!), and clean the glass surfaces before examination. To

obtain the highest resolution and contrast for these demanding specimens, oil both the objective and the condenser. Adjust the microscope for Koehler illumination and use the Bertrand lens to check that the condenser diaphragm masks some of the peripheral light, but does not significantly block the aperture. Does the spacing you observe approach the theoretical Abbé limit for resolution in the light microscope?

Since DIC microscopy uses polarized light, it can be used in combination with a compensator, such as a full-wave plate, to examine interference colors in phase objects. The high NA optics available for DIC mean that the specimen can be examined at very high resolution and with optical sectioning. Insert a red-I plate somewhere in the light path between the two crossed polarizers to observe the effect of optical staining. Be sure you have the correct orientation (axes of the refractive index ellipsoid of the plate at 45° to the axes of the polarizers). Note the colors of the background and of the edge of the shell and uniform portions of the shell itself using a 40× objective. Notice that each edge of the specimen is composed of a double band of interference colors. On the opposite side of the diatom, the same double-color band is observed, only in reversed order. The exact color observed depends on the optical path difference intrinsic to the specimen and the bias retardation introduced by the DIC prism. Although the interference colors indicate optical path differences in the specimen, the DIC microscope is primarily a qualitative instrument.

- *Examination of buccal epithelial cells.* Buccal epithelial cells are excellent specimens for practicing optical contrasting with the DIC prism and for examining the effect of the condenser diaphragm on image contrast and optical sectioning. The cells contain a centrally placed nucleus and have a modified stiffened plasma membrane that preserves the angular edges of their original polygonal shape in the epithelium, as well as patterns of multiple parallel ridges and grooves that exhibit an interridge spacing of ~0.4 μm. Gently scrape the underside of your tongue with the edge of a no. 1.5 coverslip to collect 10–20 μL of clear saliva and surface cells of the stratified squamous epithelium, and then mount the coverslip on a microscope slide.
  1. Examine the preparation by phase contrast and DIC optics using a 40 or 100× oil immersion objective, and compare the quality of the images. Focus through the specimen during observation and notice the clarity of optical sectioning using DIC optics.
  2. Carefully examine and test the alignment of polarizers and DIC prisms, as viewed at the rear focal plane of the objective with a telescope eyepiece or Bertrand lens.
- *Examination of living tissue culture cells.* Obtain a coverslip of tissue culture cells (COS7 cells, U2OS cells, or other flat epithelial cells are ideal). Cultures are prepared 1–2 days beforehand using plastic tissue culture dishes containing no. 1.5 coverslips presterilized by dipping in ethanol and holding briefly over a flame. Cell organelles that are identifiable in DIC include the nucleus, nucleolus, heterochromatin, lysosomes and peroxisomes, secretion granules, lipid droplets, mitochondria, rough endoplasmic reticulum, Golgi

apparatus, centrosome and centrioles, and stress fibers consisting of bundles of actin filaments. Membrane specializations, including the leading edge, membrane ruffles, filopodia, and microvilli should also be visible. DIC optics provide high sensitivity of detection and the ability to optically section through the specimen.

1. Carefully remove a coverslip with a pair of fine forceps, making sure not to damage the surface layer of cells. Next, clean off and wipe dry (carefully!) the back side of the coverslip with a water-moistened lab tissue, again being careful not to break the coverslip. The cleaned surface should be immaculate and dry.
2. Mount the coverslip with Vaseline spacers as shown in Figure 10.16. Clean off the back surface of the coverslip with a moistened lab tissue. Place the dry coverslip on a clean surface, cell-side up, and wipe away cells and medium within 1 mm or two opposite edges of the coverslip. Act quickly so the cells do not dry out. Smear a small bead over the surface to make a small, even ridge of Vaseline on the two dried edges of the coverslip (the side facing the cells). Mount the coverslip on a slide as shown, with the edges containing Vaseline parallel to the long axis of the slide, and gently tap the coverslip to ensure good attachment to the glass slide. Place a drop of HEPES-buffered Minimal Essential Medium (HMEM) against one open edge of the coverslip to nearly fill the chamber. Do not overfill, or the coverslip will float loose from the slide and be difficult to focus. Use the edge of a filter paper to wick away excess

Figure 10.16
A quick mount for the examination of cells grown on coverslips. A thin layer of petroleum jelly is spread evenly across a glass microscope slide or the palm of the hand, and a coverslip is drawn across the substrate sufficient to accumulate a small ridge of jelly on the side of the coverslip facing the cells. The coverslip is mounted on a microscope slide as shown, is gently tapped down to assure solid contact, and the chamber is filled with culture medium.

medium beforehand if necessary. It is better to leave a little airspace than to overfill the chamber. To prevent evaporation, you can seal off the two exposed edges with small drops of immersion oil.

Examine the preparation immediately with a 40× dry objective, but plan to make most of your observations using a 40, 60, or 100× oil immersion lens. Illuminate the cells with monochromatic green light. It is advisable to use UV- and IR-blocking filters. Make a labeled sketch of a well-spread cell showing all the recognizable organelles and structures. Include a scale bar with your drawings.

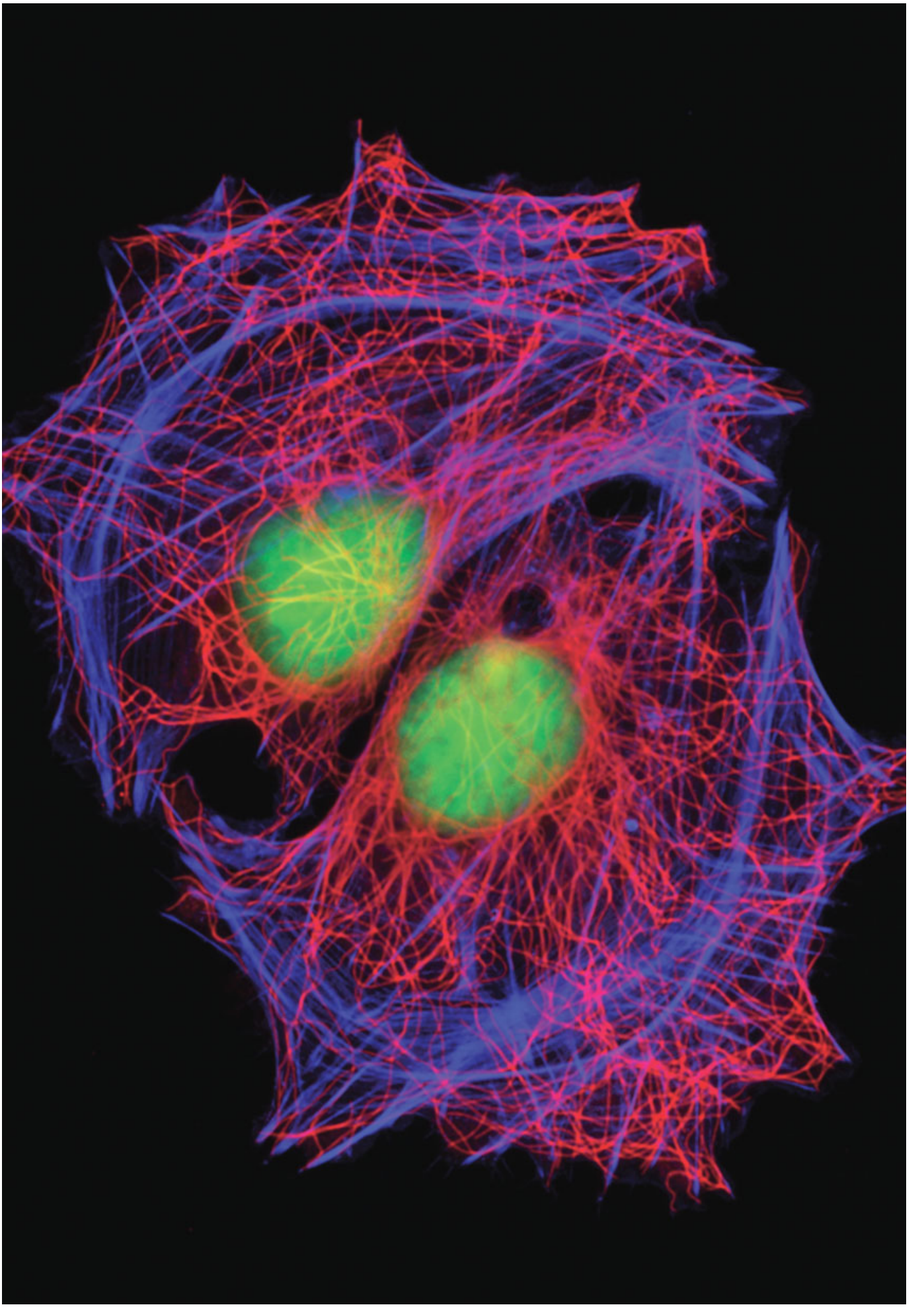

CHAPTER
11

FLUORESCENCE MICROSCOPY

OVERVIEW

With light microscope optics adjusted for fluorescence microscopy, it is possible to examine the distribution of a single molecular species in a specimen, and under specialized conditions, even detect individual fluorescent molecules. In contrast to other forms of light microscopy based on specimen-dependent properties of light absorption, optical path differences, phase gradients, and birefringence, fluorescence microscopy allows visualization of specific molecules that fluoresce in the presence of excitatory light. Thus, the amount, intracellular location, and movement of macromolecules, small metabolites, and ions can be studied using this technique. Figure 11.1 shows one such example: the distribution of several internal components in tissue culture cells. Typically, nonfluorescent molecules are tagged with a fluorescent dye or fluorochrome in order to make them visible. Examples of these are DAPI and the Hoechst dyes used to directly label nuclear DNA, or rhodamine-labeled phalloidin used to indirectly label cytoplasmic actin filaments. Alternatively, fluorochrome-labeled antibodies can be used to label fixed, permeabilized cells in a method known as *immunofluorescence microscopy*, one of the techniques used in Figure 11.1. These methods are commonly used to visualize the distribution of certain proteins in a cell or to make visible specific organelles, vacuoles, filaments, and biochemically distinct membrane regions. A variety of new tagging methods is also employed, including inserting short DNA sequences of known epitope into the coding sequences of proteins (epitope tagging), constructing protein chimeras with green or red fluorescent proteins (GFP, RFP), and several other methods.

Immunofluorescence image of rat epithelial cells showing microtubules, actin, and DNA.

Fundamentals of Light Microscopy and Electronic Imaging, Second Edition.
Douglas B. Murphy and Michael W. Davidson.

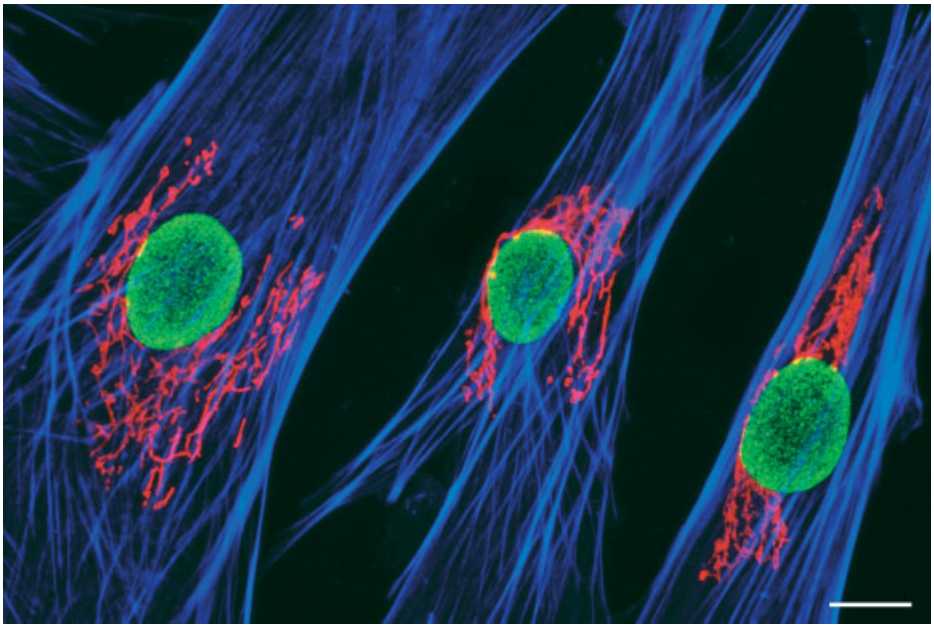

Figure 11.1

Demonstration of specific molecular labeling and imaging by fluorescence microscopy. Cultured fibroblast cells from Tahr ovary were fixed, detergent extracted, and labeled with primary antibodies to Giantin (a Golgi resident protein) and the nuclear pore coat protein (NPCP; nuclear pores surrounding the nucleus). Secondary antibodies conjugated to high-performance red and green fluorophores were used to highlight the Golgi and nuclear pores, while a blue fluorescent fluorophore conjugated to phalloidin was used to mark the filamentous network. Fluorescence microscopy is commonly used to determine the amount, distribution, and dynamics of specific macromolecules in cells. Bar = 10 μm.

Fluorescence microscopy has gained in popularity ever since Coons et al. (1941) developed methods to conjugate proteins to fluorochromes, and improvements in optics, thin-film technology, and optoelectronics increased the specificity and sensitivity of detection of emitted fluorescent light. Among the most important advances were the application of interference filters and dichromatic mirrors and their incorporation in a versatile epi-illuminator (Ploem, 1967), the introduction of special high numerical aperture (NA)-corrected objectives, and the emergence of highly sensitive detectors. Advances continue today in all of these areas. Because of its great specificity and relative ease of use, fluorescence microscopy is the most frequently employed mode of light microscopy used today in biomedical research.

Fluorescence microscopes contain special filters and employ a unique method of illumination to produce images of fluorescent light emitted from excited molecules in a specimen. The filters are designed to isolate and manipulate two distinct sets of excitation and fluorescence emission wavelengths. A band of shorter excitation wavelengths from the illuminator and filters is directed to the specimen, while a band of longer fluorescence wavelengths emitted from the specimen forms an image of the specimen in the image plane. To perform fluorescence microscopy effectively, the microscopist must be able to select the proper fluorophore, filters, and illuminator for a given application and evaluate the quality of fluorescence signals. In this chapter, we discuss the physical

basis of fluorescence, the properties of fluorescent dyes, the action of filters comprising a fluorescence filter set, the optical design of epi-illuminators, and the positioning of this equipment in the optical pathway. We also examine important variables that affect image quality and discuss methods for examining fluorescence in living cells.

APPLICATIONS OF FLUORESCENCE MICROSCOPY

Fluorescence microscopy is used extensively to study the intracellular distribution, dynamics, and molecular mechanisms of a large variety of macromolecules and metabolites. While it is impractical to discuss specialized labeling techniques and methods of fluorescence quantitation and analysis, it is important to note some of the principal applications for which fluorescence microscopy is applied. These include:

- *Determination of the intracellular distribution of macromolecules in formed structures, such as membranes, cytoskeletal filaments, and chromatin.* Fluorochrome-conjugated metabolites, ligands, and proteins can be used to label membrane channels and ion channels. Target molecules can also be labeled with fluorescent antibodies (immunofluorescence microscopy) or with biotin or epitope tags, or conjugated to fluorescent proteins, such as green fluorescent protein (GFP) and other genetically encoded agents. Multicolor labeling is possible (Fig. 11.1), whereby several different molecular species are labeled and viewed simultaneously using dyes that fluoresce at different wavelengths.
- *Study of intracellular dynamics of macromolecules in supramolecular structures and organelles (fluorescence recovery after photobleaching, or FRAP).* FRAP techniques give the half-time for subunit turnover in a structure, binding constants, and diffusion coefficients. Related technologies, such as photoactivation, photoswitching, and photoconversion, can also be used to study cellular dynamics.
- *Study of protein nearest neighbors, interaction states, and reaction mechanisms by fluorescence energy transfer or FRET and by fluorescence correlation microscopy.* In FRET, two different fluorophores are employed, and the excitation of the shorter-wavelength fluorophore results in the fluorescence of the longer-wavelength fluorophore if the two moieties come within a short molecular distance of one another.
- *Study of dynamics of single tagged molecules or molecular assemblies in vivo using an extremely sensitive technique called total internal reflection fluorescence (TIRF) microscopy.* TIRF is used to probe molecular events that occur very close to the membrane in living cells. The technique has a very short penetration distance (less than 200 nm) and is thus better suited to monitor fluorescence emitted by molecules within this distance from the glass coverslip.
- *Determination of intracellular ion concentrations, as well as changes in the concentrations, for several ionic species, including H^+, Na^+, K^+, Cl^-, Ca^{2+}, and many other metals.* Ratiometric dyes or specialized biosensor fluorescent protein combinations are used, whose peak fluorescence emission wavelength changes depending on whether the dye is in the free or bound state. The ratio of fluorescence amplitudes gives the ion concentration.
- *Organelle marking experiments using dyes that label specific organelles and cytoskeletal proteins.* Specialized fluorophores, such as MitoTracker and LysoTracker,

can be used to label specific organelles in living cells. Fusions of GFP to targeting peptides and proteins can also be used to monitor specific regions in cells for dynamic interactions using time-lapse microscopy. Fixed cells can be specifically labeled using immunofluorescence techniques.

- *Determination of the rates and extents of enzyme reactions using conjugates of fluorochromes whose fluorescence changes due to enzymatic activity.* An example is the use of nucleotide coenzymes (NADH and NADPH) where the reduced forms are fluorescent and the oxidized forms are nonfluorescent. Other synthetic reagents are capable of releasing a fluorescent dye during enzyme-catalyzed reactions.
- *Study of cell viability and the effects of factors that influence the rate of apoptosis in cells using a combination of dyes that are permeant and impermeant to the plasma membrane.* A synthetic fluorophore known as JC-1 can be used to analyze mitochondria membrane potential to monitor cell viability. Numerous other synthetic fluorophores can pass through the membrane of dead cells, but not those that are living.
- *Examination of cell functions, such as endocytosis, exocytosis, signal transduction, and the generation of transmembrane potentials, using fluorescent dyes.* Although a number of synthetic fluorophores, including quantum dots, have been developed for monitoring endocytosis and exocytosis, these assays are increasingly being fine-tuned with the application of genetically engineered fluorescent protein biosensors.

PHYSICAL BASIS OF FLUORESCENCE

Fluorescence is the emission of photons by atoms or molecules whose electrons are transiently stimulated to a higher excitation state by radiant energy from an outside source. It is a beautiful manifestation of the interaction of light with matter and forms the basis for fluorescence microscopy, so we will take a moment to examine the physical basis of the phenomenon.

When a fluorescent molecule absorbs a photon of the appropriate wavelength, an electron is excited to a higher energy state and almost immediately collapses back to its initial ground state. In the process of energy collapse, the molecule can release the absorbed energy as a fluorescent photon. Since some energy is lost in the process, the emitted fluorescent photon typically exhibits a lower frequency of vibration and a longer wavelength than the excitatory photon that was absorbed. The situation is depicted graphically in what is known as a *Jablonski diagram* (Fig. 11.2), which shows a series of increasing energy states as a stack of horizontal lines. Each energy level is in turn composed of a number of subenergy levels, which do not concern us here. There are two categories of excited states, characterized by different spin states of the excited electron—the singlet excited state and the triplet excited state. Most commonly, an excited electron occupies an excitation level within the singlet excited state (straight upward pointing arrows), and when it collapses to the ground state, energy can be given up as fluorescence emission (straight downward pointing arrows). Alternatively, energy can be given up as heat (internal conversion), in which case no photon is emitted (wavy downward pointing arrows). When excited above the ground state, there is a probability that an electron can also enter the triplet excited state through a process called inter-

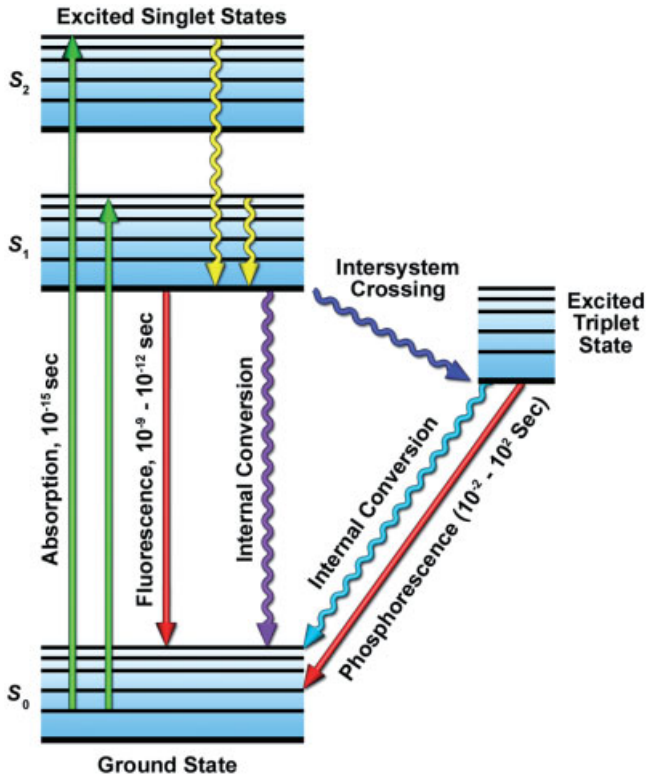

Figure 11.2

Jablonski diagram showing energy levels occupied by an excited electron within a fluorescent molecule (chlorophyll a). Chlorophyll a is unique in absorbing blue and red wavelengths of the visual spectrum. Once excited, energy is released through any of the following three pathways: Chlorophyll can give off a photon (fluorescence emission, straight downward pointing red arrow); it can release vibrational energy as heat without photon emission (internal conversion, wavy downward pointing purple arrow); or its electron can enter an excited triplet state (intersystem crossing, diagonal wavy blue arrow), which can make the molecule chemically reactive. Electrons in the triplet excited state can return to the ground state through internal conversion (diagonal wavy cyan arrow) or by emission of phosphorescence (red arrow). Refer to the text for details.

system crossing (diagonal wavy blue arrow). The triplet state is important, because molecules with electrons in this state are chemically reactive, which can lead to photobleaching and the production of damaging free radicals (discussed later in this chapter). During fluorescence, the absorption and re-emission events occur nearly simultaneously, the interval being only 10^{-9}–10^{-12} seconds; therefore, fluorescence stops the moment there is no more exciting incident light. The emission process is called *phosphorescence* if the period between excitation and emission is not instantaneous and lasts fractions of a second to minutes. These processes should not be confused with *bioluminescence*, such as that exhibited by firefly luciferase, in which electrons are excited by chemically driven processes rather than by absorbing external radiation.

Molecules that are capable of fluorescing are called *fluorescent molecules*, *fluorescent dyes*, or *fluorochromes*. If a fluorochrome is conjugated to a large macromolecule

(through a chemical reaction or by simple adsorption), the tagged macromolecule is said to contain a *fluorophore*, the chemical moiety capable of producing fluorescence. Fluorochromes exhibit distinct excitation and emission spectra that depend on their atomic structure and electron resonance properties. Fluorescent dyes usually contain several unconjugated double bonds and are usually heterocycles containing nitrogen, sulfur, and/or oxygen. The absorption and emission spectra for fluorescein-conjugated immunoglobulin (IgG) are shown in Figure 11.3. Molecules absorb light and re-emit photons over a spectrum of wavelengths (*the excitation spectrum*) and exhibit one or more characteristic excitation maxima. Absorption and excitation spectra are distinct but usually overlap, sometimes to the extent that they are nearly indistinguishable. However, for fluorescein and many other dyes, the absorption and excitation spectra are clearly distinct. The widths and locations of the spectral curves are important, particularly when selecting two or more fluorophores for labeling different molecules within the same specimen.

Re-emission of fluorescent light from excited dye molecules likewise occurs over a broad spectrum of longer wavelengths (*the emission spectrum*) even when excitation is performed with a monochromatic source, such as a laser. This is because electrons occupy excited states for various lengths of time during which they give up varying amounts of vibrational energy, some of it as heat, resulting in the re-emission of lower energy, longer-wavelength photons over a spectrum of wavelengths. Because some energy is lost during the process, the wavelength of a fluorescent photon is usually

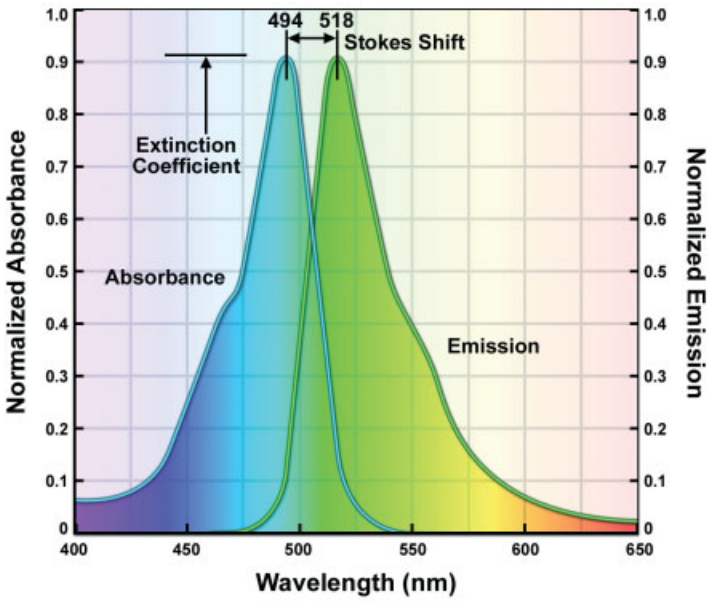

Figure 11.3

Normalized absorption and fluorescence emission spectra of fluorescein conjugated to IgG. Both spectra span a wide range of wavelengths. Fluorescein has an absorption/excitation peak at 494 nm and looks yellow-green to the eye, but actually fluoresces at wavelengths ranging from blue to red with a peak at 518 nm. The difference in nanometers between the excitation and emission maxima is called the Stokes shift. The molar extinction coefficient is measured at the peak of the absorbance spectrum as indicated in the figure.

longer than the wavelength of the photon exciting the molecule. It should be noted that the energy of a photon is given as $E = hc/\lambda$, where h is Planck's constant, c is the speed of light, and λ is the wavelength. Since the photon energy is reduced during absorption and re-emission, the wavelength increases. The reader is encouraged to review the relationships between the energy, frequency, and wavelength of photons described in Chapter 2.

Finally, the shapes of the spectral curves and peak wavelength of absorption and emission spectra vary, depending on factors contributing to the chemical environment of the system, including pH, ionic strength, solvent polarity, O_2 concentration, presence of quenching molecules, and others. This fact explains why the fluorescence of a dye, such as fluorescein, varies depending on whether it is free in solution or conjugated to a protein or other macromolecule.

PROPERTIES OF FLUORESCENT DYES

The excitation and emission spectra of fluorescent molecules are commonly observed to overlap. The difference in wavelength or energy between the excitation and emitted fluorescent photons is called the *Stokes shift*. In practice, the Stokes shift is the difference between the excitation and emission maxima (Fig. 11.3). Depending on the particular fluorescent molecule, the shift can range from just a few to several hundreds of nanometers. The Stokes shift for fluorescein is ~25 nm, while that for porphyrins is over 200 nm. Dyes exhibiting a large Stokes shift are advantageous in fluorescence microscopy, because the bands of excitation and fluorescence wavelengths are easier to isolate using interference filters. Another important criterion for dye selection is the *molar extinction coefficient*, which describes the potential of a fluorochrome to absorb photon quanta, and is given in units of absorbance (optical density) at a reference wavelength (usually the absorption maximum) under specified conditions. The *quantum efficiency (QE) of fluorescence emission* is the fraction of absorbed photon quanta that is re-emitted by the fluorochrome as fluorescent photons. QE varies greatly between different fluorochromes and for a single fluorochrome under different conditions. For soluble fluorescein dye at alkaline pH, the quantum efficiency can be as high as 0.9—an extremely high value—–but for protein-bound fluorescein at neutral pH, the quantum efficiency is typically 0.3–0.6.

Other important characteristics of dyes are their resistance to photobleaching, solubility in aqueous media, and chemical stability. Quenching and photobleaching reduce the amount of fluorescence and are of great practical significance to the microscopist. *Quenching* reduces the quantum yield of a fluorochrome without changing its fluorescence emission spectrum and is caused by interactions with other molecules, including other fluorochromes. Conjugation of fluorescein to a protein usually causes a significant reduction in the quantum yield because of charge-transfer interactions with nearby aromatic amino acids. Proteins like IgG or albumin that are conjugated with five or more fluorescein molecules, for example, fluoresce less than when bound to two to three molecules, because energy is transferred to nonfluorescent fluorescein dimers. *Photobleaching* refers to the permanent loss of fluorescence by a dye due to photon-induced chemical damage and covalent modification. As previously discussed, photobleaching occurs when a dye molecule, excited to one of its electronic singlet states, transits to a triplet excited state (Fig. 11.2). Molecules in this state are able to undergo complex reactions with other molecules. Reactions with molecular oxygen permanently

destroy the fluorochrome and produce singlet oxygen species (free radicals) that can chemically modify other molecules in the cell. Once the fluorochrome is destroyed, it usually does not recover. The rate of photobleaching can be diminished by reducing excitation energy or lowering the oxygen concentration. Methods for reducing oxygen concentration as a way to protect live cells are described at the end of the chapter.

Demonstration: Fluorescence of Chlorophyll and Fluorescein

The phenomena and principles of fluorescence can be demonstrated using a filtered alcoholic extract of spinach leaves and an aqueous solution of fluorescein. The procedures for preparing these samples are given in Appendix B.

Although an extract of spinach contains a mixture of chlorophylls a and b, plus carotene and xanthophyll, most of the fluorescence phenomena are due to chlorophyll a. The fluorescence spectra of chlorophyll a, the major chlorophyll component, are shown in Figure 11.4. The figure shows that the absorption/excitation spectrum is broad and distinctly bimodal, with absorption peaks widely separated in the blue and red portions of the visible spectrum. Fluorescence emission at red wavelengths with an emission peak at 670 nm is the same regardless of whether blue or red wavelengths are used to excite the molecule. Notice too the very large Stokes shift from 420 to 670 nm—a difference of some 250 nm. Normally, the chlorophyll and other pigments in intact chloroplasts act as energy

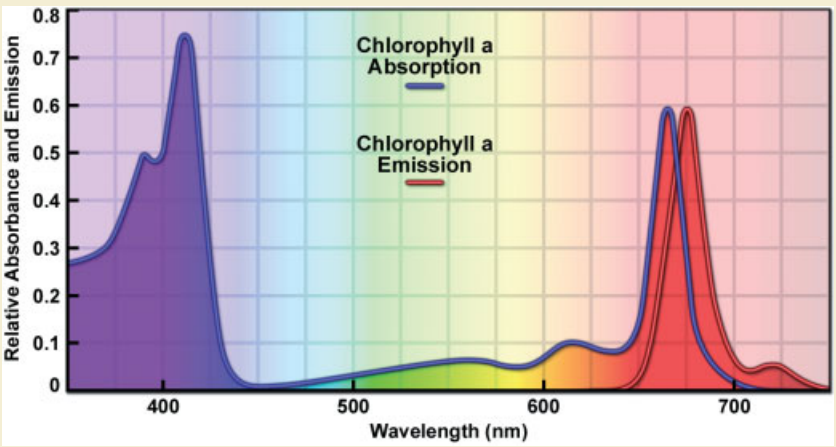

Figure 11.4

Absorption and emission spectra of chlorophyll a. The spectrum for absorption–excitation (blue curve) is unusual in showing two prominent peaks at ~420 and ~660 nm and a pronounced trough corresponding to green wavelengths of the visible spectrum. The emission curve is shown as a red curve. It might seem unusual that the major chlorophyll species of plants does not absorb in the green, where the peak of solar radiation occurs. This job is performed by other pigments (chlorophyll b, xanthophyll, and carotene), which transfer captured energy of incident radiation to chlorophylls a and b, thus providing an efficient design for light absorption across parts of the UV and much of the visual spectrum.

transducers and do not fluoresce; rather, the electrons excited by absorbed photons are transferred to nearby enzyme assemblies (photosystems I and II) for the fixation of carbon dioxide into carbohydrate. However, when chlorophyll is extracted into a soluble form in alcohol, no electron transfer is possible, and absorbed photons are re-emitted as deep red fluorescence.

If the flask of chlorophyll is placed over a bright white light source, a deep emerald green color is seen. Green wavelengths are observed because red and blue wavelengths are selectively absorbed. (Refer to subtraction colors in Chapter 2.) Red fluorescence is emitted by the solution, but its presence is masked by the bright green color of the nonabsorbed illuminating wavelengths. If the flask is now illuminated with deep blue wavelengths <450 nm or with long-wave ultraviolet (UV) (invisible) wavelengths from a black light in a darkened room, the red fluorescence can be easily observed. Chlorophyll demonstrates features important to fluorescence microscopy: the requirement to selectively isolate bands of wavelengths corresponding to the excitation and emission maxima, and the benefits of using molecules that exhibit both a large Stokes shift and high quantum efficiency.

We can examine a 10 μM solution of fluorescein using the same illuminators. Fluorescein appears bright yellow in white light (blue wavelengths are efficiently absorbed, leaving red and green wavelengths, which the eye perceives as yellow). Brilliant yellow-green fluorescence is observed under excitation illumination with the black light. The effect of environmental conditions can be demonstrated with fluorescein by adding a few drops of concentrated (10 N) sodium hydroxide, which causes a twofold increase in quantum efficiency and therefore a dramatic increase in fluorescence. If an opaque mask with a slit 5 cm long by 2–5 mm wide is placed up against the flask on the side facing the observer, and the slit of bright fluorescence examined in a darkened room while holding a holographic (sinusoidal) diffraction grating immediately in front of the eye, the full fluorescence emission spectrum of fluorescein can be examined. It begins with the longest of the blue-green wavelengths, reaches a peak in the green and yellow green, and then tapers off in the orange and red. It is clear that fluorescein re-emits light over a broad spectrum of wavelengths and that the yellow-green fluorescence color is not due to a single spectral line or narrow band of yellow-green wavelengths.

Tables 11.1 and 11.2 and Figure 11.5 catalog important properties of many valuable fluorescent dyes and fluorescent proteins commonly used in fluorescence microscopy. New classes of synthetic fluorochromes, such as the *Alexa Fluor* dyes (Life Technologies, Carlsbad, CA), *ATTO* dyes (ATTO-TEC GmbH, Siegen, Germany) and *cyanine* dyes (Amersham-Pharmacia, Piscataway, NJ), are especially notable, because they have very large quantum efficiencies and offer high resistance to photobleaching. *GFP,* isolated from the jellyfish *Aequorea victoria,* and its mutated allelic forms, blue, cyan, and yellow fluorescent protein (BFP, CFP, and YFP), are used to produce fluorescent chimeric proteins that can be expressed in living cells, tissues, and whole organisms (Table 11.2). Orange, red, and far red fluorescent proteins that are useful in fluorescence microscopy have been derived from chromoproteins and

TABLE 11.1 Properties of Commonly Used Fluorescent Dyes[a]

Fluorochrome	Color Band[b]	Excitation (nm)	Emission (nm)	Filter Set[c]
Acridine orange	Cyan	502	525	FITC
Allophycocyanin	Red	621/650	661	Cy5
AMCA	UV	350	445	DAPI
Alexa Fluor 405	UV	401	421	DAPI
Alexa Fluor 488	Cyan	495	519	FITC
Alexa Fluor 568	Yellow	578	603	TxRed
Alexa Fluor 647	Red	650	665	Cy5
ATTO 488	Cyan	501	523	FITC
ATTO 550	Green	554	576	TRITC
ATTO 594	Yellow	601	627	TxRed
ATTO 740	Far-Red	740	764	Cy7
BODIPY FL	Cyan	503	512	FITC
BODIPY TMR	Green	542	574	TRITC
Cascade blue	UV	400	425	DAPI
Carboxy-SNARF-1 (low pH)	Green	548	587	TRITC
Cy2	Cyan	489	506	FITC
Cy3	Green	548	562	TRITC
Cy5	Red	650	670	Cy5
Cy7	Far-Red	710	805	Cy7
DAPI (bound to DNA)	UV	350	470	DAPI
$DiIC_{18}$ (bound to lipid)	Green	549	565	TRITC
$DiOC_6$	Cyan	484	501	FITC
Fluorescein (FITC)	Cyan	494	518	FITC
Fluo-3 (with calcium)	Cyan	485	503	FITC
FM 1-43 (bound to Lipid)	Cyan	473	578	Special
Fura-2 (with calcium)	UV	335	505	Special
Hoechst 33258, 33342	UV	352	461	DAPI
Indo-1 (with calcium)	UV	350	405/482	Special
Lissamine-rhodamine B	Yellow	575	595	TxRed
Lucifer yellow	Blue	425	528	Special
LysoTracker green	Cyan	504	511	FITC
LysoTracker red	Yellow	577	590	TxRed
MitoTracker red	Yellow	581	644	TxRed
Oregon green 488	Cyan	496	524	FITC
Oregon green 514	Green	511	530	FITC
Phycoerythrin-R	Green	565	578	TRITC
Propidium iodide	Green	520	610	TRITC
SYTOX green	Cyan	504	523	FITC
SYTOX orange	Green	547	570	TRITC
Tetramethylrhodamine	Green	540	578	TRITC

TABLE 11.1 (*Continued*)

Fluorochrome	Color Band[b]	Excitation (nm)	Emission (nm)	Filter Set[c]
Texas red	Yellow	592	610	TxRed
TOTO-1	Green	514	533	FITC
TO-PRO-3	Red	642	661	Cy5
Ultralite T680	Red	656	678	Cy5
YOYO-1	Cyan	491	509	FITC

[a] Most values are from *Handbook of Fluorescent Probes and Research Chemicals* (2010). In most cases, the solvent used was methanol. Absorption maxima are typically close to the peak excitation wavelength.
[b] Excitation band.
[c] Recommended filter set.

TABLE 11.2 Physical Properties of Useful Fluorescent Proteins

Protein[a]	Color[b]	Excitation (nm)	Emission (nm)	Brightness[c]	Photostability[d]	Filter Set[e]
EBFP2	Blue	383	448	18	++	DAPI
mCerulean	Cyan	433	475	17	++	CFP
mTurquoise	Cyan	433	474	25	+++	CFP
mTFP1	Teal	462	492	54	+++	CFP
mEGFP	Green	488	507	34	++++	FITC/GFP
mEmerald	Green	487	509	39	++++	FITC/GFP
mVenus	Yellow	515	528	53	++	FITC/YFP
mCitrine	Yellow	516	529	59	++	FITC/YFP
mKO2	Orange	551	565	40	+++	TRITC
tdTomato	Orange	554	581	95	+++	TRITC
TagRFP	Orange	555	584	48	++	TRITC
mApple	Orange	568	592	37	+++	TRITC
mCherry	Red	587	610	17	+++	TxRed
mKate2	Far-Red	588	633	25	++	TxRed
mPlum	Far-Red	590	649	3.2	+++	TxRed
mNeptune	Far-Red	600	650	13	++++	Cy5

[a] Common literature abbreviation.
[b] Spectral class.
[c] Product of the molar extinction coefficient and the quantum yield $(\text{mM} \times \text{cm})^{-3}$.
[d] Relative to mEGFP (++++).
[e] Recommended filter set.

fluorescent proteins isolated from reef corals and sea anemones. The topic of fluorescent dyes and their applications is extensive and complex. Readers wishing to explore the subject in greater depth can begin by reading the chapters by Tsien (Tsien et al., 2006) and other authors in Pawley (2006) and by consulting the *Molecular Probes Handbook, A Guide to Fluorescent Probes and Labeling Technologies* (Johnson and Spence, 2010), which is available in electronic format on the internet (http://www.invitrogen.com) or on hard copy through Molecular Probes, Inc. (Eugene, OR; a division of Life Technologies). The spectra and properties of many fluorescent labels, including cyanine dyes,

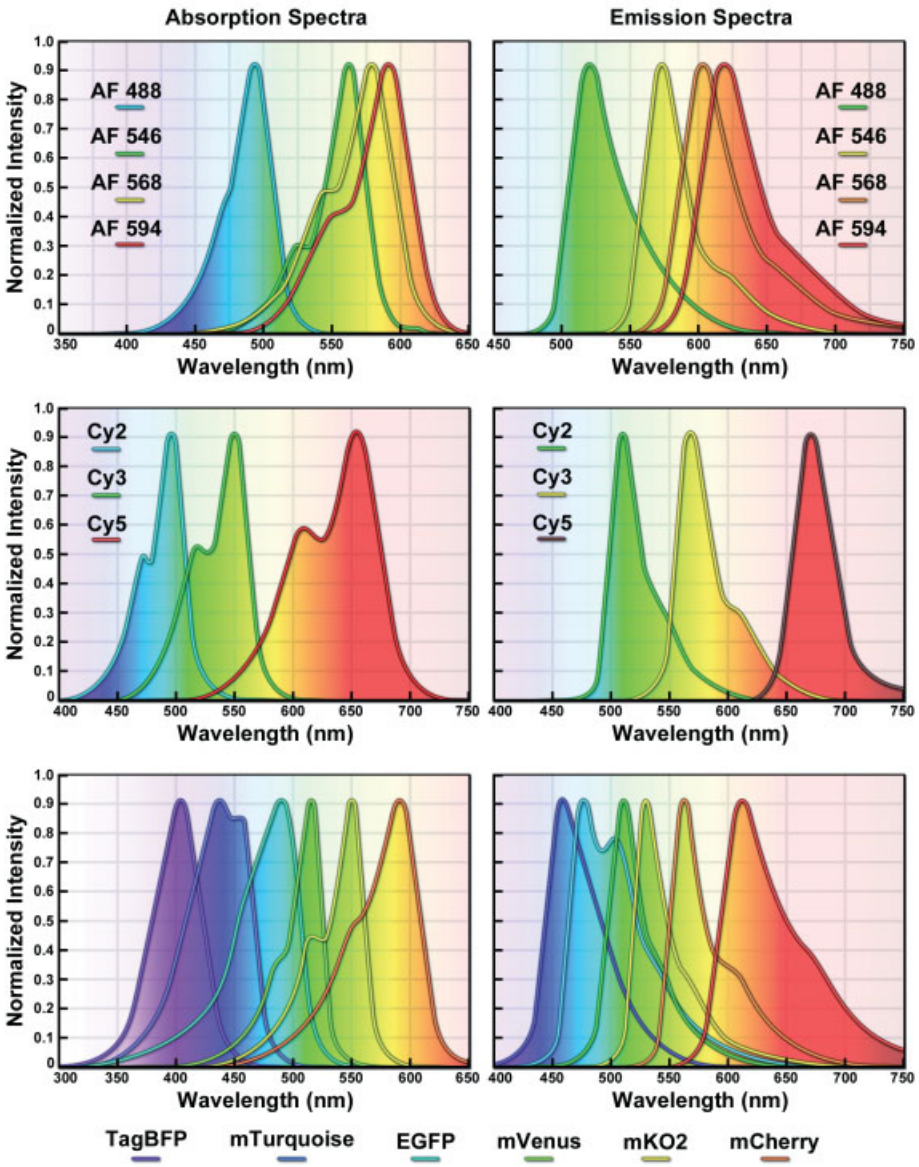

Figure 11.5

Absorption and emission spectra of synthetic dyes and proteins for fluorescence microscopy. The Alexa series of dyes introduced by Molecular Probes, Inc. (Eugene, OR), and the cyanine dyes by Amersham International, Inc. (available from Jackson ImmunoResearch Laboratories, Inc, West Grove, PA), are exceptionally photostable, have high quantum efficiency, and are soluble in aqueous media. The EGFP and mCherry proteins, provided as DNA vectors by Addgene (Cambridge, MA) and Clontech, Inc. (Palo Alto, CA), respectively, are used to construct fluorescent protein chimeras that can be observed in cells after transfection with the engineered vectors (see Table 11.2). This technique avoids the problem of purifying, tagging, and introducing labeled proteins into cells or having to produce specific antibodies. Fluorescent protein chimeras are also suitable for studies of protein dynamics in living cells. For examples and visualization methods, see Sullivan and Kay (1999).

are available at the website (http://www.jacksonimmuno.com) of Jackson ImmunoResearch Laboratories, Inc., and of GFP and other fluorescent proteins at the website of Clontech Laboratories, Inc. (http://www.clontech.com). Another excellent reference for spectral information is the website of Omega Optical (http://www.omegafilters.com). Websites covering all phases of fluorescence microscopy, including fluorophores and fluorescent proteins, and advanced microscopy techniques, can be found at Molecular Expressions (http://micro.magnet.fsu.edu), Nikon MicroscopyU (http://www.microscopyu.com), the Zeiss Microscopy Campus (http://zeiss.magnet.fsu.edu), the Hamamatsu Learning Center (http://learn.hamamatsu.com), and the Olympus Microscopy Resource Center (http://olympusmicro.com).

It is common practice to label cells with multiple fluorescent dyes to examine different molecules, organelles, or cells in the same preparation using different fluorescence filter sets. As an example, Figure 11.6 shows the excitation and emission spectra of three dyes (DAPI, fluorescein, and rhodamine) that are suitable for specimens illuminated with different spectral regions of a mercury arc lamp. Many factors influence the decision regarding dye selection, including spectral region, Stokes shift, quantum efficiency, solubility, and photostability of the dye; spectral profile of the illuminator; and availability of suitable filter sets. In the example shown here, DAPI and rhodamine are each excited by bright spectral lines of the mercury lamp at 366 and 546 nm, respectively; the excitation of fluorescein is not as favorable, but this is compensated by the fact that fluorescein (or Cy2 or Alexa 488) has a high quantum efficiency.

AUTOFLUORESCENCE OF ENDOGENOUS MOLECULES

All cells contain endogenous metabolites that autofluoresce and contribute background fluorescence to the image. In some cases, these signals are strong enough that they are mistaken for the signals of fluorescently tagged molecules. Some common sources of autofluorescence are the B vitamins, flavins, flavin proteins, and flavin nucleotides (FAD and FMN), reduced pyridine nucleotides (NADH and NADPH), fatty acids, porphyrins, uncoupled cytochromes, lipofuchsin pigments, serotonin, and catecholamines (see Demonstration and Table 11.3). Background fluorescence emission is greatest when live cells are examined with blue and UV excitation wavelengths. The strength of endogenous autofluorescence depends on the particular metabolite and excitation wavelength being employed and also on the cell type. Macrophages, neurons, and sperm cells exhibit particularly strong autofluorescence. Fixation of cells with aldehydes in preparation for labeling with fluorescently tagged marker molecules may also induce unwanted fluorescence, particularly in cell nuclei and organelles. For immunofluorescence studies, aldehyde-induced fluorescence can be diminished by treating fixed samples for 10 minutes with 20 mM sodium borohydride or ammonium chloride. Fortunately, autofluorescent signals are usually low in amplitude. Interference from autofluorescence can sometimes be avoided by simply selecting a longer wavelength fluorochrome.

Autofluorescence adds to the background signal in a cell and may overlap the signal of a fluorophore used in a labeling experiment, causing misinterpretation of the distribution pattern of the fluorophore. After acquiring fluorescence images of labeled specimens, it is therefore important to prepare similar exposures from unlabeled specimens. If necessary, a camera exposure time can be selected that minimizes the autofluorescent contribution, but still allows adequate imaging of the labeled experimental material.

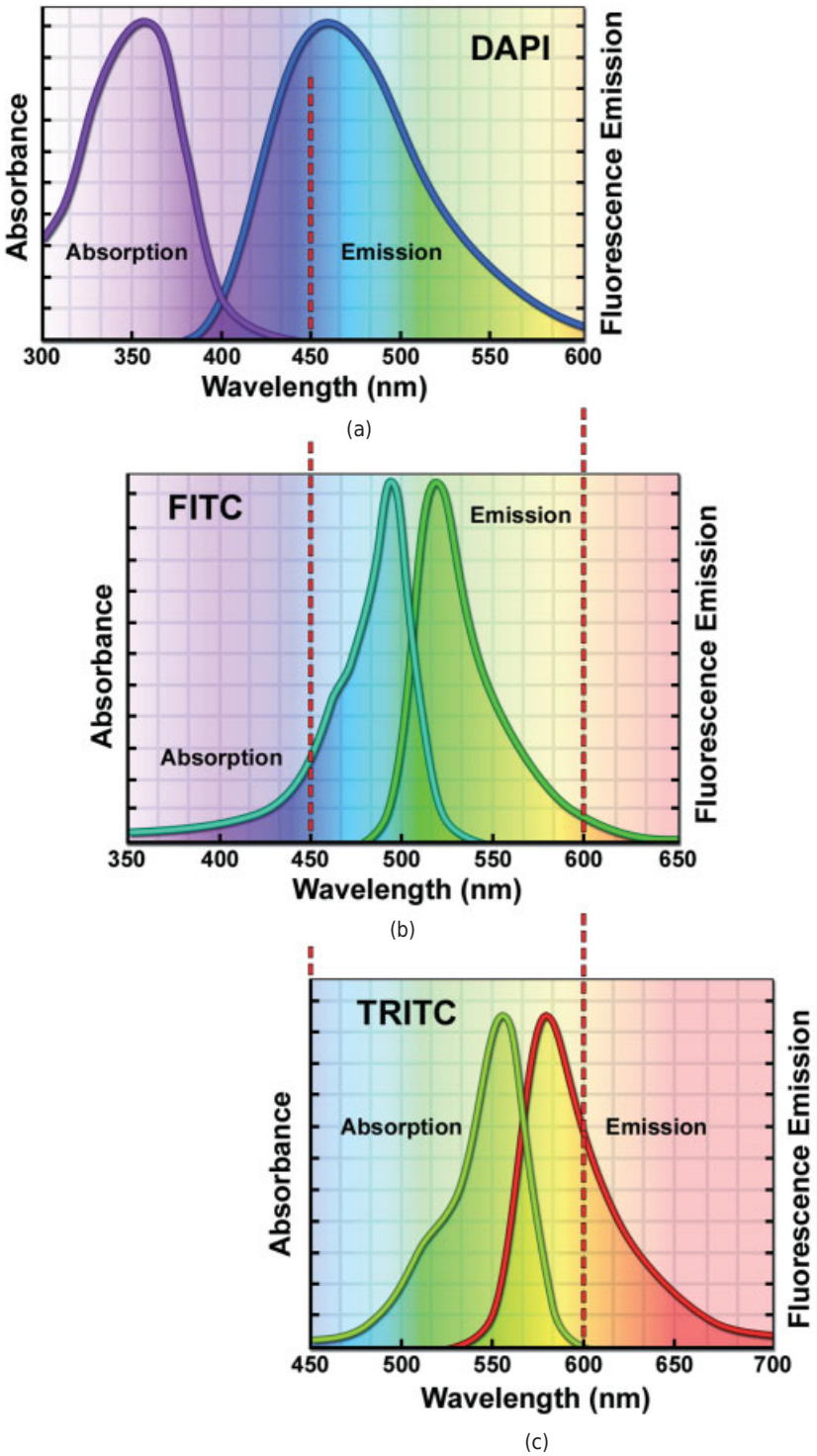

Figure 11.6

Use of multiple fluorescent dyes for examining cells with mercury illumination. The absorption and emission spectra of (a) DAPI, (b) fluorescein, and (c) rhodamine are shown. The absorption spectra of DAPI and rhodamine overlap strong spectral lines of the mercury arc lamp at 366 and 546 nm, respectively. Although the emission spectra of these three dyes partially overlap, it is possible to examine each dye separately using fluorescence filter sets that are specific for each dye. Dashed vertical lines indicate registration of wavelengths between plots.

Demonstration: Fluorescence of Biological Materials under UV Light

Fluorescent compounds and metabolites are abundant in living cells and tissues. To become familiar with these signals and recognize them when they occur, examine the fluorescence of naturally occurring compounds in foodstuffs and tissue extracts illuminated with a handheld black light in a darkened room. A list of common foodstuffs and their fluorescence properties is given in Table 11.3. Instructions for preparing certain extracts are given in Appendix B.

TABLE 11.3 Fluorescence of Naturally Occurring Substances

Specimen	Substance	Color
Powdered milk	Oxidized riboflavin (lumiflavin)	Blue
Margarine	Fatty acids	Blue
Yeast extract	Oxidized vitamin B_2 (lumiflavin)	Blue
Brain extract	Catecholamines, serotonin	Blue
Yeast on agar plate	Vitamin B_2 (riboflavin)	Green
Liver extract	Vitamin B_2 other B vitamins	Yellow
Carrot extract	β-carotene	Yellow
Butter, milk	Free riboflavin	Yellow
Spinach extract	Chlorophyll a, b	Red
Shells of brown eggs	Porphyrins	Red

FLUORESCENT DYES AND PROTEINS IN FLUORESCENCE MICROSCOPY

The history of synthetic fluorescent probes dates back over a century to the late 1800s when many of the cornerstone dyes for modern histology were developed. Among these were pararosaniline, methyl violet, and malachite green. Although these dyes were highly colored and capable of absorbing selected bands of visible light, most were only weakly fluorescent and would not be useful for the fluorescence microscopes that would be developed several decades later. However, several synthetic dye classes synthesized during this period, based on the xanthene and acridine heterocyclic ring systems, proved to be highly fluorescent and provided a foundation for the development of modern synthetic fluorescent probes. Most notable among these early fluorescent dyes were the substituted xanthenes, fluorescein, and rhodamine B.

Fluorophores were introduced to fluorescence microscopy in the early twentieth century as vital stains for bacteria, protozoa, and trypanosomes, but did not see widespread use until the 1920s when fluorescence microscopy was first used to study dye binding in fixed tissues and living cells. In the early 1940s, Albert Coons developed a technique for labeling antibodies with fluorescent dyes, thus giving birth to the field of immunofluorescence (Coons et al., 1941). Over the past 75 years, advances in immunology and molecular biology have produced a wide spectrum of secondary antibodies

and provided insight into the molecular design of fluorescent probes targeted at specific regions within macromolecular complexes.

Fluorescent probe technology and cell biology were dramatically altered by the discovery of GFP from jellyfish and the development of mutant spectral variants, which have opened the door to noninvasive fluorescence multicolor investigations of subcellular protein localization, intermolecular interactions, and trafficking using living cell cultures. More recently, the development of nanometer-sized fluorescent semiconductor *quantum dots* has provided a new avenue for research in fluorescence microscopy. All of these fluorescent probes are discussed below, and examples showing their use in organelle labeling are shown in Figure 11.7.

Alexa Fluor Dyes

Advances in modern fluorophore technology are exemplified by the Alexa Fluor dyes introduced by Molecular Probes (*Alexa Fluor* is a registered trademark of Molecular Probes). These fluorescent probes exhibit higher quantum yields for more intense fluorescence emission than spectrally similar probes, and have improved features, including enhanced photostability, absorption spectra matched to common laser lines, pH insensitivity, and a high degree of water solubility. In fact, the resistance to photobleaching of Alexa Fluor dyes is so substantial that even when subjected to irradiation by high-intensity laser sources, fluorescence intensity remains stable for relatively long periods of time in the absence of antifade reagents. This feature enables the water-soluble Alexa Fluor probes to be readily utilized for both live-cell and tissue section investigations, as well as in traditional fixed preparations.

Alexa Fluor dyes are available in a broad range of fluorescence excitation and emission wavelength maxima, ranging from the UV and deep blue to the near-infrared (IR) regions. Alphanumeric names of the individual dyes are associated with the specific excitation laser or arc-discharge lamp spectral lines for which the probes are intended. For example, Alexa Fluor 488 is designed for excitation by the blue 488-nm line of the argon or krypton-argon ion lasers, while Alexa Fluor 568 is matched to the 568-nm spectral line of the krypton-argon laser. Several of the Alexa Fluor dyes are specifically designed for excitation by either the blue diode laser (405 nm), the orange/yellow helium-neon laser (594 nm), or the red helium-neon laser (633 nm). Other Alexa Fluor dyes are intended for excitation with traditional mercury arc-discharge lamps in the visible (Alexa Fluor 546) or UV (Alexa Fluor 350, also useful with high-power argon-ion lasers), and solid-state red diode lasers (Alexa Fluor 680). Because of the large number of available excitation and emission wavelengths in the Alexa Fluor series, multiple labeling experiments can often be conducted exclusively with these dyes.

Cyanine Dyes

The family of cyanine dyes, Cy2, Cy3, Cy5, Cy7, and their derivatives, feature fluorescence excitation and emission profiles that are similar to many of the traditional dyes, such as fluorescein and tetramethylrhodamine, but with enhanced water solubility, photostability, and higher quantum yields. Most of the cyanine dyes are more environmentally stable than their traditional counterparts, rendering their fluorescence emission intensity less sensitive to pH and organic mounting media. In a manner similar to the Alexa Fluors, the excitation wavelengths of the cyanines are tuned specifically for use

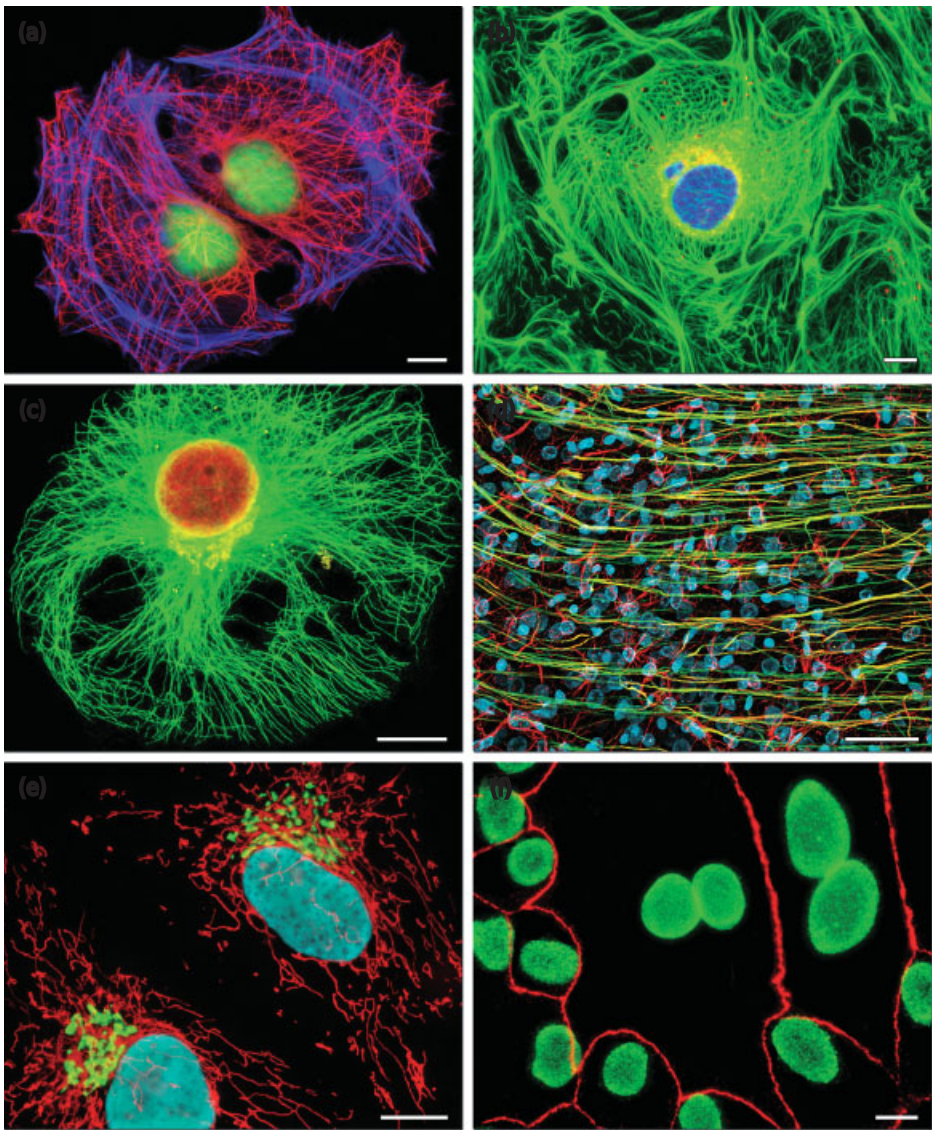

Figure 11.7

Imaging of synthetic fluorophores and fluorescent proteins in fluorescence microscopy. (a) Rat thoracic aorta cells stained with Alexa Fluor 350 (actin), Alexa Fluor 568 (tubulin), and SYTOX Green (DNA). (b) Kangaroo rat cells (PtK2) stained with Cy2 (keratin), Mito-Tracker Red (mitochondria), and DAPI (nucleus). (c) HeLa cell stained with QDot 525 (tubulin), QDot 585 (Golgi), and QDot 655 (histones). (d) Thirty-micrometer rat brain section stained with Alexa Fluor 488 (vimentin), Alexa Fluor 568 (GFAP), and DRAQ5 (nucleus). (e) HeLa cells expressing mTurquoise-H2B (nucleus), mEGFP-Gal-T (Golgi), and mCherry-pyruvate dehydrogenase (mitochondria). (f) Madin–Darby canine kidney cells stained with Alexa Fluor 488 (nuclear pores) and Alexa Fluor 568 (ZO-3). Bars = 10 μm (a)–(c), (e), and (f); and 50 μm (d).

with common laser and arc-discharge sources, and the fluorescence emission can be detected with traditional filter combinations.

Fluorescent Environmental Probes

A wide variety of fluorescent probes have been developed to monitor such effects as localized concentrations of alkali and alkaline earth metals, heavy metals (employed biochemically as enzyme cofactors), inorganic ions, thiols and sulfides, nitrite, as well as pH, solvent polarity, and membrane potential. Originally, the experiments in this arena were focused on changes in the wavelength and/or intensity of absorption and emission spectra exhibited by fluorophores upon binding calcium ions in order to measure intracellular flux densities. These probes bind to the target ion with a high degree of specificity to produce the measured response and are often referred to as *spectrally sensitive indicators*. Ionic concentration changes are determined by optical ratio signal analysis to monitor the association equilibrium constant between the ion and its host. The concentration values derived from this technique are largely independent of instrumental variations and probe concentration fluctuations due to photobleaching, loading parameters, and cell retention.

Organelle Probes

Fluorophores targeted at specific intracellular organelles, such as the mitochondria, lysosomes, Golgi apparatus, and endoplasmic reticulum, are useful for monitoring a variety of biological processes in living cells using fluorescence microscopy. Organelle probes consist of a fluorochrome nucleus attached to a target-specific functional group that assists in localizing the fluorophore through covalent, electrostatic, hydrophobic, or similar types of bonds. Many of the fluorescent probes designed for selecting organelles are able to permeate or sequester within the cell membrane and therefore are useful in living cells, while others must be applied using immunocytochemistry techniques. In living cells, organelle probes are useful for investigating transport, respiration, mitosis, apoptosis, protein degradation, acidic compartments, and membrane phenomena. Cell impermeant fluorophore applications include nuclear functions, cytoskeletal structure, organelle detection, and probes for membrane integrity. In many cases, living cells that have been labeled with permeant probes can subsequently be fixed and counterstained with additional fluorophores in multicolor labeling experiments.

Quantum Dots

Quantum dots are inorganic semiconductor nanocrystals composed of a cadmium selenide (CdSe) core surrounded by a zinc sulphide (ZnS) shell that exhibit fluorescent properties due to a phenomenon known as *confined exciton emission*. A passivation layer and hydrophilic coating must be applied to quantum dots for biological applications in fluorescence microscopy, and they must also be conjugated to streptavidin or antibodies for targeting. The fluorescence emission profile of quantum dots is remarkably symmetrical and generally exhibits a large quantum yield, while their broad absorption profile enables them to be excited over a large wavelength range (tens to hundreds of nm). The size of the CdSe core dictates the emission spectral profile, with

smaller cores (~2 nm) emitting in the blue regions and larger cores (5–7 nm) emitting in the yellow and red wavelengths. In general, the photostability for quantum dots dramatically exceeds that of all other known fluorophores. Because they do not penetrate the cell plasma membrane, targeting remains a problem with quantum dots in live-cell imaging applications, but conjugates to secondary antibodies are widely used in preparing samples using immunofluorescence techniques.

Fluorescent Proteins

The discovery and development of naturally occurring fluorescent proteins and their mutated derivatives have led to a virtual revolution in the investigation of a wide spectrum of intracellular processes in living organisms. These biological probes have provided scientists with the ability to visualize, monitor, and track individual molecules with high spatial and temporal resolution in both steady-state and kinetic experiments. Fluorescent proteins have become so useful that three of the pioneering investigators, Roger Tsien (University of California, San Diego), Martin Chalfie (Columbia University), and Osamu Shimomura (Marine Biological Laboratory) were awarded the 2008 Nobel Prize in chemistry for the discovery, demonstration of expression, and development of color analogs for these remarkable genetically encoded fluorescent probes.

A variety of marine organisms have been the source of more than 200 fluorescent proteins and their analogs, which arm the microscopist with a balanced color palette of noninvasive biological probes for single, dual, and multispectral fluorescence analysis. Among the advantages of fluorescent proteins over the traditional organic and new semiconductor probes described previously is their response to a wider variety of biological events and signals. Coupled with the ability to specifically target fluorescent probes in subcellular compartments, the extremely low or absent photodynamic toxicity and the widespread compatibility with tissues and intact organisms, these biological macromolecules offer an exciting new frontier in live-cell imaging.

The green fluorescent protein (GFP) was the first isolated from the North Atlantic jellyfish, *Aequorea victoria*, and exhibits a high degree of fluorescence without the aid of additional substrates or coenzymes. In native GFP, the fluorescent nucleus is a tripeptide derivative of serine, tyrosine, and glycine that autocatalytically forms and only requires molecular oxygen for activation, but no additional cofactors or enzymes. The GFP gene can be expressed in many other organisms besides the jellyfish, including mammals, to yield fully functional analogs that display no adverse biological effects. In fact, fluorescent proteins can be genetically fused to virtually any protein in living cells using DNA cloning technology to target virtually any organelle or cellular structure. Lack of a need for cell-specific activation cofactors renders the fluorescent proteins much more useful as generalized probes than other biological macromolecules, such as the phycobiliproteins, which require insertion of accessory pigments in order to produce fluorescence.

A broad range of fluorescent protein genetic variants have been developed that feature fluorescence emission spectral profiles spanning almost the entire visible light spectrum. These variants have often been given names of common minerals, celestial bodies, or fruits bearing colors similar to the emission spectral colors, such as emerald, turquoise, Venus, Neptune, cherry, and plum (Table 11.2). Mutagenesis efforts in the original jellyfish GFP resulted in new fluorescent probes that range in color from blue to yellow and are some of the most widely used *in vivo* reporter molecules in biological research. Longer wavelength fluorescent proteins, emitting in the orange and red spectral

regions, have been developed from the marine anemones and reef corals. Still other species have been mined to produce similar proteins having cyan, green, yellow, orange, red, and far-red fluorescence emission. Research efforts are ongoing to improve the brightness and stability of fluorescent proteins, thus improving their overall usefulness.

ARRANGEMENT OF FILTERS AND THE EPI-ILLUMINATOR IN THE FLUORESCENCE MICROSCOPE

The fluorescence microscope is modified in several important ways in order to obtain images that are bright and well defined:

- A bright light source, such as a mercury, xenon, or metal halide arc lamp, is required because only a narrow band of wavelengths, and consequently a small portion of the illuminator output, is used to excite fluorophores in the specimen.
- For efficient high contrast imaging, both the illuminator and objective are positioned on the same side of the microscope slide as the specimen. In this arrangement, the lamp and light delivery assembly are called an *epi-illuminator*, and the objective functions both as the condenser delivering excitatory light to the specimen and as the objective imaging lens, collecting fluorescent light and forming an image of the fluorescent object in the image plane.
- *Fluorescence filter sets* containing three essential filters (excitation filter, dichromatic mirror, and barrier [or emission] filter) are positioned in the optical path between the epi-illuminator and the objective. This arrangement is shown in Figure 11.8.
- High NA, oil immersion objectives made of low-fluorescence glass are used to maximize light collection and provide the greatest possible resolution and contrast.

Epi-illumination is made possible by the employment of a dichromatic mirror, which is mounted together with exciter and barrier filters as a fluorescence filter set in a filter cube (or optical block) that is positioned along the optical axis. The first component, the *excitation filter* (or exciter), selectively transmits a band of short wavelengths (relative to the fluorescence wavelengths) for exciting a specific fluorophore in the specimen. The second component, the *dichromatic mirror*, reflects the short wavelength excitation light toward the objective and specimen, while transmitting returning long-wave fluorescent light toward the detector. The dichromatic mirror also directs any excitation wavelengths reflected by the specimen back toward the exciter filter and illuminator. The third component is the *emission* or *barrier filter*, which transmits the band of fluorescence wavelengths while blocking any residual short excitation wavelengths. The fluorescent wavelengths then form an image on the eye or camera.

Lamps for Fluorescence Excitation

The excitation source can be a band of wavelengths isolated from a metal halide, mercury, or xenon arc illuminator with an interference filter, or it can be monochromatic light from a laser or light-emitting diode (LED), but illuminators must produce photons

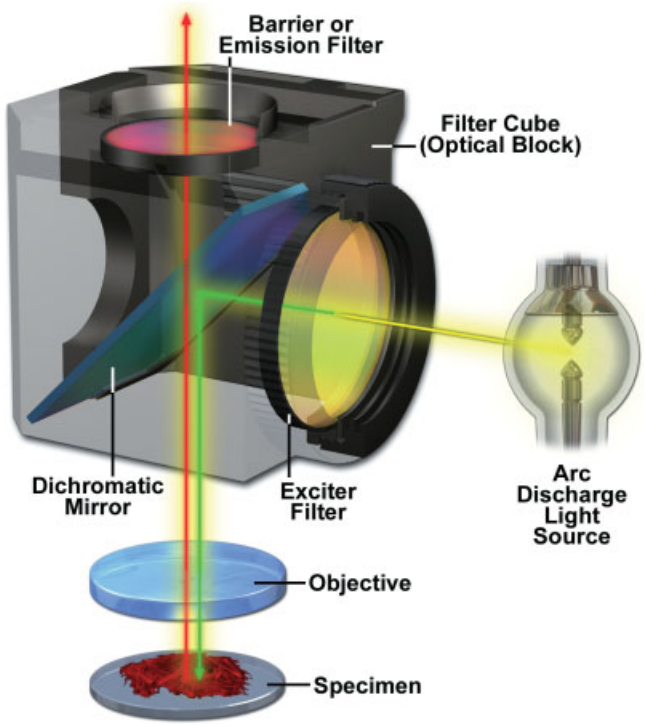

Figure 11.8

Arrangement of filters in a fluorescence filter cube. The diagram shows the orientation of filters in a filter cube in an epi-illuminator for an upright microscope. The excitation beam (yellow line) passes through the exciter and is reflected by the dichromatic mirror and directed toward the specimen (green line). The return beam of emitted fluorescence wavelengths (red line) passes through the dichromatic mirror and the emission filter to the eye or camera. Excitation wavelengths backreflected or scattered at the specimen are again reflected by the dichromatic mirror back toward the light source. Excitation wavelengths that manage to pass through the dichromatic mirror are blocked by the barrier (emission) filter.

of the proper wavelength and at a sufficiently high intensity to be efficient. To obtain a particular wavelength of the desired intensity, it may be necessary to use a certain illuminator—for example, a mercury arc excites DAPI much more effectively than a xenon arc, whereas a metal halide illuminator is far more efficient at exciting GFP and fluorescein than a mercury lamp. Therefore, it is important that the microscopist match the illuminator to the fluorescent dye in question.

For fluorescence microscopy, 100-W mercury, 75-W xenon, and 150-W metal halide arc lamps are commonly used. All three lamps produce bright, continuous emission over the visible spectrum (400–700 nm), but mercury and metal halide are distinct in containing sharply defined emission lines at 366 (UV), 405, 436, 546, and 578 nm. It is important to reexamine the spectra and characteristics of arc lamps, which are presented in Chapter 3. At 546 nm, mercury and xenon lamps are 10–100× brighter than a 100-W quartz halogen lamp, which is typically used for brightfield microscopy, but is too weak to excite most fluorophores adequately. The bright emission lines of the mercury and metal halide arc lamps are useful for exciting certain fluorophores, such as DAPI and Hoechst dye 33258, Lucifer yellow, rhodamine, Cy3, and Texas red,

but at other spectral regions, xenon is brighter and may be more useful (fluorescein, Alexa 488, Flo3, allophycocyanine, and Cy5). Refer to Table 11.1 and Figure 11.5 on fluorescent dyes and the spectra of xenon and mercury light sources in Chapter 3 to confirm this for yourself and to find other well-matched dye-illuminator partners.

The Epi-Illuminator

The epi-illuminator consists of the lamp and its collector lens plus a connector tube fitted with a field stop diaphragm, a relay lens, and slots for additional filters (Fig. 11.9). It is attached to the lamp at one end and is mounted at its other end to the microscope in the vicinity of the fluorescence filter cube. The lamp housing should contain a focusable collector lens to fill the rear aperture of the objective as required for Koehler illumination. On most research microscopes, the epi-illuminator is a built-in component of the microscope body. Apart from proper adjustment and focus of the lamp, little other manipulation of the illumination pathway is required. Check that the field stop diaphragm is centered and is opened to provide optimal framing of the specimen. Epi-illumination is much more efficient than transmitted mode (or diascopic) illumination because there is much less background in the fluorescence image.

One of the most important adjustments in fluorescence microscopy is the alignment of the illuminator. Since the amplitude of fluorescence signals depends directly on the amount of excitation, uneven illumination of the object by a misaligned lamp will result in bright and dark regions in the fluorescence image. This is especially detrimental for quantitative work. Lamp alignment is discussed in Chapter 3 and demands attention to two points: (1) centration of the image of the arc and its reflection on the optical axis, and (2) spreading of the illumination beam with the lamp collector lens to fill the rear aperture of the objective evenly and homogeneously.

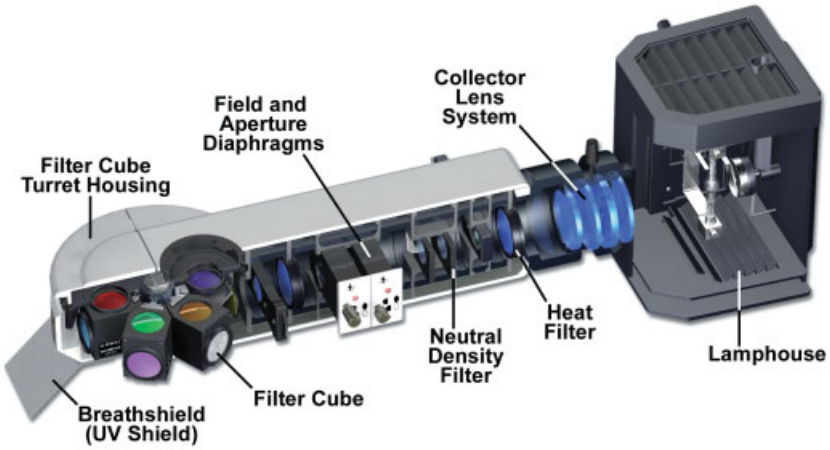

Figure 11.9

Internal anatomy of a fluorescence microscope epi-illuminator. The unit attaches to an upright microscope and contains a mercury arc-discharge lamphouse and a collector lens system to collimate light and direct it into the microscope optical train. Included are a heat filter to remove IR wavelengths, neutral density filters, aperture and field diaphragms, and a filter cube turret enabling a choice of up to six filter combinations.

Filters

Filters used to isolate bands of wavelengths in fluorescence microscopy include colored glass filters, thin-film interference filters, or a combination of filter types. The filters also include longpass or shortpass edge filters and narrow or broad bandpass filters. The design and action of filters are discussed in Chapter 3; the optical performance of representative filters used for fluorescence microscopy is shown in Figures 11.10 and 11.11. It is essential to understand the properties and value of these indispensable components of the fluorescence microscope. You will need to know how to "read" the absorption and emission spectra of a dye and the transmission profiles of the filters. This knowledge is required to select the best among several possible filter sets for examining the fluorescence of a certain fluorophore. You will also need to interpret and explain differences among fluorescence microscope images obtained using different filter sets. In addition, you may need to create new filter sets using components of filter sets already in hand. This will greatly extend the capacity of a limited collection of filters. As you install and remount filters, remember that interference filters are usually mounted in a specific orientation with respect to the illuminator and the specimen in order to obtain optimal performance (see Chapter 3). The transmission profiles of filter sets for fluorescence microscopy can be examined at the websites of Chroma, Inc., (http://www.chroma.com), Semrock, Inc., (http://www.semrock.com), and Omega Optical, Inc. (http://www.omegafilters.com), among others (see spectral viewers in Microscopy Web Resources section).

The Dichromatic Mirror

The dichromatic mirror or beamsplitter is a special longpass filter coated with multiple layers of dielectric materials similar to those contained in thin-film interference filters, but specially designed for reflection and transmission at certain boundary wavelengths. The mirror, which is the key component in a fluorescence microscope epi-illumination system, is mounted at a 45° angle with respect to the optical axis within a filter cube and faces the light source. At this angle, the dichromatic mirror reflects short excitation wavelengths at a 90° angle along the optical axis to the specimen, but transmits long fluorescence wavelengths that are collected by the objective and directed to the image plane. The transition from near total reflection to maximal transmission can be remarkably sharp, occurring over 20–30 nm, allowing the mirrors to act as precise discriminators of excitation and fluorescence wavelengths (Fig. 11.10). (For a description of the design and performance of interference filters, see Chapter 3.) The specifications for a dichromatic mirror assume a 45° angle between the axis of the incident beam and the plane surface of the mirror. Dichromatic mirrors should be handled with extreme care, because the exposed dielectric layers can be scratched and damaged during handling and cleaning. The cleaning procedure is the same as that used for cleaning other optical surfaces (Chapter 4).

Transmission profiles for dichromatic mirrors usually show multiple broad peaks and troughs that correspond to bands of wavelengths that experience high transmittance/low reflectance (at peaks) and low transmittance/high reflectance (at troughs) (Fig. 11.11). Filter sets are designed so that the band of excitation wavelengths (high-percent transmission) from the exciter precisely matches a trough in the dichromatic (low-percent transmission) so that these wavelengths are reflected to the specimen. Longer fluorescent wavelengths emitted by the specimen must also match the peak to the right

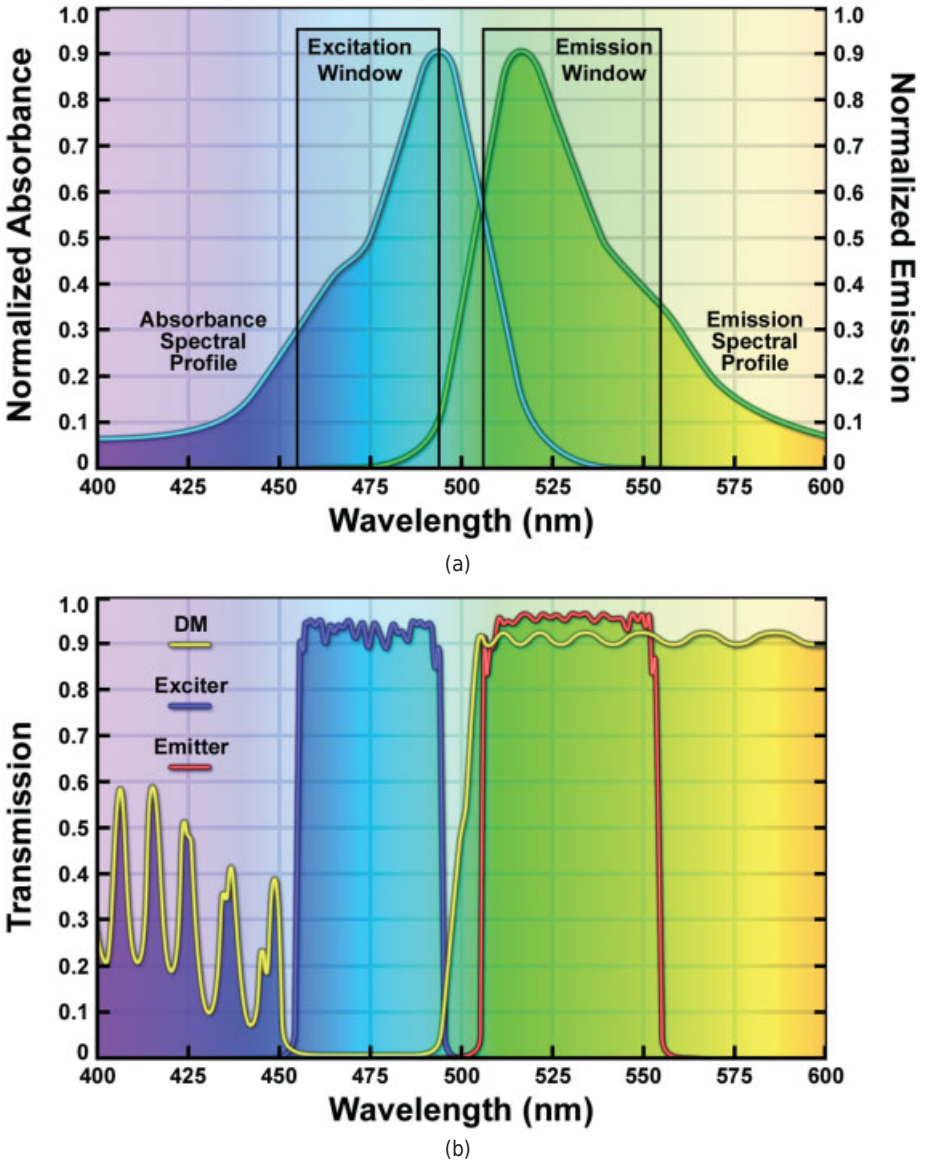

Figure 11.10

Transmission profiles of filters in a fluorescein filter set. The figure shows (a) the excitation and emission spectra of fluorescein and (b) the transmission profiles of three filters belonging to a high performance filter set (BrightLine® Single-Band FITC, Semrock, Inc., Rochester, NY). Bandpass excitation and emission filters (blue and red profiles shown in panel b) transmit bands of light that occupy the peak regions of the respective absorbance and emission spectra shown in the upper panel. To maintain a distinct separation of these components, the transmission profiles (gray boxes in panel a) are not exactly centered on the excitation and emission maxima of the dye. The dichromatic mirror (yellow line) reflects light (100% reflection corresponds to 0% transmission on the curve) or partially transmits light (90%), depending on the incident wavelength. The pronounced trough in the transmission profile, representing a peak of reflectance, is used to reflect the band of excitation wavelengths from the exciter filter onto the specimen. Boundaries between transmitted and reflected bands of wavelengths are designed to be as steep as possible to assure complete separation of the reflected and transmitted wavelengths. The pattern of rapidly rising and falling spikes (termed ringing), typical of dichromatic mirrors, indicates major improvements in thin-film technology over the last several years.

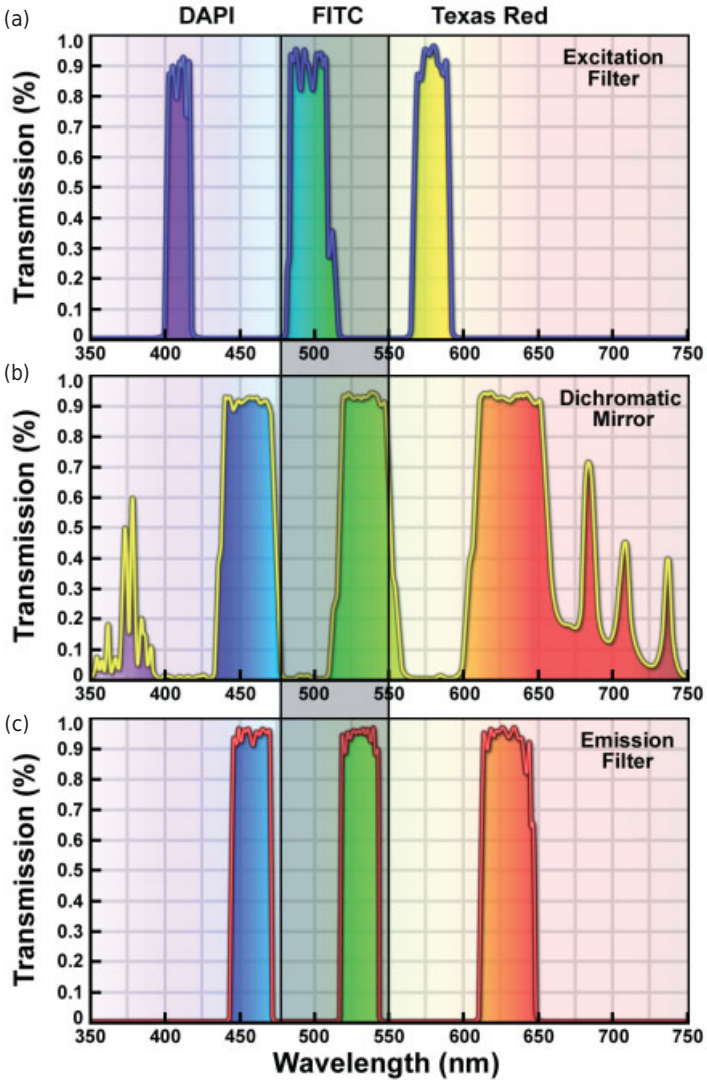

Figure 11.11

Transmission profiles of a triple-band filter set for DAPI, FITC, and Texas red (BrightLine® Triple-Band, Semrock, Inc., Rochester, NY). Each of the three filters contains multiple bandwidths that transmit or reflect three distinct bands of wavelengths simultaneously. The eye or camera sees a multicolor image based on the three dyes. Profiles of the exciter filter (a, top panel), dichromatic mirror (b, middle panel), and emission filter (c, bottom panel) are shown. The broad vertical gray band across the drawing distinguishes the spectral regions of the filters for FITC from those for DAPI and Texas red.

of the trough so that they are transmitted to the barrier filter and the detector. It is important that the transmission, reflectance, and emission characteristics of the exciter and dichromatic be closely matched, and that they be appropriate for the absorption and emission maxima of the dye; otherwise, excitation wavelengths can pass through the dichromatic and fog the image, or fluorescent wavelengths can be reflected at the

dichromatic mirror, reducing image brightness. Even when filters and fluorophores are appropriately matched, performance is usually compromised somewhat if the transmission profiles of the exciter and dichromatic mirror overlap. When this happens, some excitation light passes through the dichromatic mirror, reflects off the walls of the filter cube, and can be partially transmitted by the emission filter because the angle of incidence with that filter is oblique. Transmission of unwanted wavelengths through a filter set is called *bleedthrough*, and the amount of bleedthrough for typical filter sets is generally about 10%. Microscope manufacturers continue to improve fluorescence optical designs to give higher contrast images.

It is important to recognize that in addition to reflecting the excitation band of wavelengths, a dichromatic mirror usually reflects bands of wavelengths shorter than the excitation band. Therefore, you cannot always depend on the dichromatic filter to block transmission of unwanted short wavelengths, which to a greater or lesser extent always leak through the exciter filter. It is usually wise to insert an additional UV-blocking filter into the beam when examining live cells by fluorescence microscopy.

Dichromatic versus Dichroic Mirrors

Mirrors or beamsplitters that reflect or transmit selected bands of wavelengths are often referred to as *dichromatic* or *dichroic*, but the latter term can be confusing because it also refers to a property related to *pleochroism*, which describes the differential ability of a substance to absorb light based on the polarization azimuth of the incident light. Use of the term dichroic is widespread in the fluorescence filter literature, but here we will refer to fluorescence microscopy beamsplitters as dichromatic mirrors.

Advances in thin-film coating technology allow for the creation of multiple transmission peaks and alternating reflection troughs in a single interference filter or dichromatic mirror. When matched appropriately, two filters and a dichromatic mirror can be combined to create a *multiple fluorescence filter set* that allows simultaneous excitation and fluorescence transmission of multiple fluorophores (Fig. 11.11). Multiple-wavelength filters and dichromatic mirrors are now commonly employed in research-grade microscopes and confocal fluorescence microscope systems (see Chapter 13). Double, triple, and even quadruple fluorescence filter sets are available for fluorescence microscopy, although these sets are expensive and suffer somewhat from bleedthrough—that is, the transmission of fluorescence from one dye through bandwidths intended for other dyes. The clearest multifluorophore images are obtained by taking separate grayscale pictures with filter sets optimized for each dye and then combining the images into a single composite color image.

OBJECTIVES AND SPATIAL RESOLUTION IN FLUORESCENCE MICROSCOPY

Proper selection of an objective is important, especially for imaging dim fluorescent specimens. High-NA, oil immersion plan-fluorite lenses and plan-apochromatic objec-

tives are ideal, because at NA = 1.3 or 1.4, their light-gathering ability is especially high. These lenses feature excellent color correction, so different fluorescent wavelengths are brought to the same focus in the focal plane. They are also transparent to UV light—a requirement for examining UV-excitable dyes, such as DAPI, Hoechst, and AMCA. In addition, they contain low-fluorescence glass—a feature that minimizes background fluorescence and gives high contrast. Since image brightness (photon flux per unit area and time) is proportional to NA^4/M^2, where NA is the numerical aperture and M is the magnification, a 60×1.4 NA plan apochromatic objective is among the brightest objectives and is very well suited for fluorescence imaging.

The spatial resolution d for two noncoherent fluorescent point objects is the same as in brightfield microscopy with incoherent light, and is given as $d = 0.61\lambda/\text{NA}$, where λ is the mean wavelength of fluorescent light transmitted by the barrier filter. Resolution, brightness, and other features defining the optical performance of objectives are described in Chapter 4.

CAUSES OF HIGH FLUORESCENCE BACKGROUND

For research microscopes with properly selected fluorescence filter sets, the amount of background fluorescence in the image of a specimen containing a single fluorophore is usually 15–30% of maximum specimen brightness—not 0% as might be expected. An example of background signal in cells expressing a fluorescent protein is shown in Figure 11.12. Because background fluorescence is always present, it is important to take steps to keep the background signal as low as possible.

- Less than ideal performance of filter sets, where transmission and reflectance by interference filters and the dichromatic mirror are not 100% and where the transition boundaries between transmission and reflection are not sharply defined, is a major contributor to background signal. These problems are compounded when poorly performing filters are used together in a single filter set.
- Specimen preparation must include complete neutralization of unreacted aldehyde groups and blocking of remaining reactive sites to minimize nonspecific binding of the fluorescent probe. It is also necessary to completely remove unbound fluorophore by thorough rinsing. However, even if these precautions are followed, background fluorescence from unbound antibody can be high for a mounted coverslip containing labeled cultured cells. This is because the labeling reaction is an equilibrium between bound and free states of the antibody. Even with an equilibrium dissociation constant of 1 nM and a modest concentration of 10^6 antigen binding sites per cell, a significant fraction of antibody would be expected to dissociate and be free in the mounting medium.
- Use of lipid-based transfection reagents to introduce DNA vectors into living cells often increases autofluorescence and background signal when the cells are observed in fluorescence microscopy. In addition, fluorescent protein expression levels vary widely in transient transfection so that poorly expressing cells that are not bright enough to image increase the background when they are adjacent to cells that express well. After culturing the cells for a few days posttransfection, autofluorescence usually drops to acceptable levels.

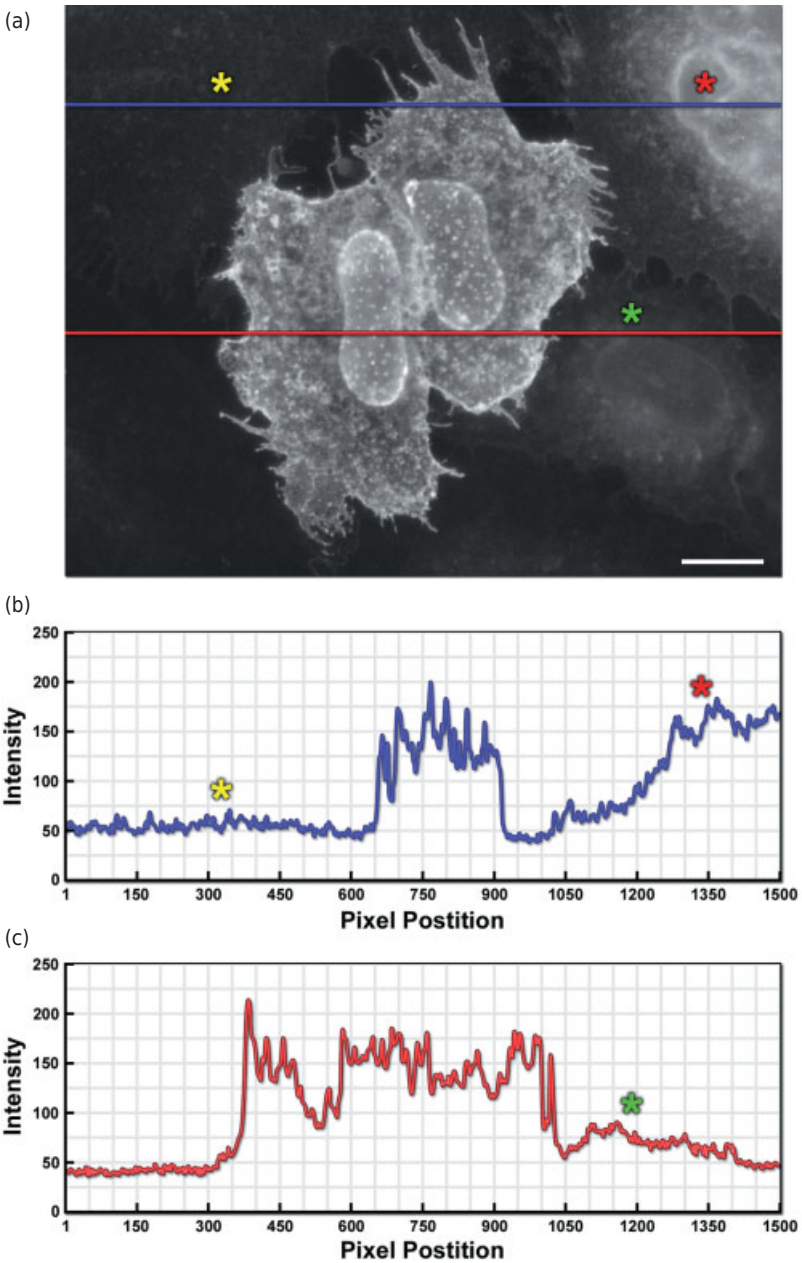

Figure 11.12

Comparison of specimen and background fluorescence in a typical fluorescence image. (a) Live HeLa cells were transiently transfected with mEmerald (a GFP derivative) fused to annexin A4, a protein involved in trafficking of vesicles and membrane organization. Upon induction of calcium by addition of ionomycin to the culture medium, the annexin fusion translocates to the plasma and nuclear membranes as illustrated in panel a. Three adjacent cells in the upper left (yellow asterisk) and right (red asterisk), as well as the lower right-hand side of the image (green asterisk), express the fusion at much lower levels and thus generate a high level of background. The horizontal blue and red lines represent rows of pixels whose numeric values are shown in panels b and c. (b) Intensity profile of the pixel values under the blue line in panel a, with regions corresponding to the asterisks marked. Note that the background is not black at any point, but shows a minimum intensity that is ~25% of that at the center of the bright cells. (c) Intensity profile of the pixel values under the red line in panel a with the region corresponding to the asterisk marked. This is typical of most transient transfections, as well as cells stained with synthetic dyes or labeled using immunofluorescence techniques. The causes of background fluorescence are discussed in the text. Bar = 20 μm.

- Reflections and scattering in the optical pathway cause rays to enter a filter at an oblique angle, reducing the filter's transmission/reflection efficiency. One site of concern is the rear wall of the filter cube, where excitatory rays that are partially transmitted by the dichromatic mirror are reflected and are transmitted by the emission filter because they are not incident at an angle perpendicular to the plane of the emission filter. In recent Zeiss designs where the back wall of the filter cube is removed, reflections at this location are removed, and image contrast is improved by 15–20%. Other filter cube manufacturers incorporate light-absorbing coatings on the interior of optical blocks to reduce or eliminate scattered light.
- Dust, fingerprints, and scratches on filters and lens elements scatter significant amounts of light, resulting in an increase in background signal and reduced contrast. Cleaning filters and optical surfaces significantly reduces this problem. Interference filters also deteriorate gradually over time due to handling and the presence of water vapor and chemicals in the air. Blemishes in old interference filters in the form of microscopic scaling, pinholes, and scratches can also scatter significant amounts of light.
- Fluorescence from other sources, including the glass in certain objectives, immersion oil, plastic tissue culture dishes, and autofluorescence from the specimen itself contribute to the background. Most microscope manufacturers make objectives of low fluorescence glass and provide low fluorescence immersion oil for fluorescence microscopy. The new low-fluorescence immersion oils available from microscope manufacturers and independent sources, such as Cargill, Inc. (Cedar Grove, NJ), increase contrast significantly and must be employed.

THE PROBLEM OF BLEEDTHROUGH WITH MULTIPLY STAINED SPECIMENS

Another problem in imaging double-stained specimens is bleedthrough, the crossover of fluorescence signal from one fluorophore through the filter set of the other fluorophore. A common example is double labeling with fluorescein and rhodamine using separate filter sets to capture different images of each of the two fluorophores. Bleedthrough can be reduced, but is never completely eliminated, because:

- The excitation spectra of two or more fluorophores are broad and overlap to a significant extent (Figs. 11.5 and 11.6). Thus, the excitation of fluorescein at 490 nm also causes rhodamine to fluoresce. The solution is to choose fluorophores with well-separated excitation spectra so that the excitation peak for one fluorophore is many wavelengths shorter than the excitation peak for the second fluorophore.
- The fluorescence spectra of the fluorophores may overlap, allowing fluorescence from the shorter-wavelength fluorophore to contribute to the image of the longer-wavelength dye. To minimize the problem, a narrow bandpass filter is used as an emission filter to collect only the peak fluorescence of the lower-wavelength fluorophore; a longpass barrier filter is usually used for the longer wavelength fluorophore.
- The fluorescence emission of one fluorophore (fluorescein) may stimulate a second longer-wavelength dye (rhodamine) to fluoresce. Selecting well-separated dyes

and assuring that labeling and fluorescence of the dyes are balanced help reduce this problem.

- If the amount of labeling and the intensity of fluorescence of the two fluorophores are not equally balanced, the brighter signal can overwhelm and penetrate the filter set for the second signal and cause a significant contribution to the image of the second dimmer signal. The intensity of fluorescence from dyes such as fluorescein and rhodamine should be similar and is adjusted according to the amount of dye in the specimen and the type of illumination used. Microscopists using epi-illumination with a mercury or metal halide arc lamp frequently forget that rhodamine is excited 10× more effectively than fluorescein owing to the bright 546-nm emission line in the mercury arc spectrum.

Even when these factors are controlled, the amount of signal crossover and bleedthrough generally remains about 10–15%. In experiments involving double labeling, you should always examine single-stained specimens using the filter set for the other fluorophore to assure that the amount of bleedthrough is minimal. In many cases, the main cause of bleedthrough is unequal staining by the two dyes. Remember that it is nearly always desirable to return to the lab bench to prepare a proper specimen, rather than to use unequal exposures and image processing on a poorly prepared specimen just to save time.

QUENCHING, BLINKING, AND PHOTOBLEACHING

The consequences of quenching, photobleaching, and molecular blinking occur in practically all forms of fluorescence microscopy, and result in an effective reduction in the levels of emission. The phenomena are distinct in that quenching and blinking are often reversible, whereas photobleaching is not. Quenching arises from a variety of competing processes that induce nonradiative relaxation (without photon emission) of excited state electrons to the ground state. Because these nonradiative transition pathways compete with the fluorescence relaxation, they usually dramatically lower or completely eliminate emission. A wide variety of simple elements and compounds behave as quenching agents, including oxygen, halogens, amines, some biological polymers, and many organic molecules.

Blinking is a phenomenon that occurs during continuous excitation of a fluorescent molecule where emission transitions between "on" and "off" states somewhat like twinkling stars in the night sky. This was predicted in 1913 by Niels Bohr in a quantum mechanical explanation of intensity fluctuations on short timescales. However, experiments have determined that fluorophores can remain in the off state for intermittent periods ranging from seconds to minutes. The mechanism underlying fluorescence blinking is not well understood, but it is thought to occur by a transition from the singlet excited state to a dark triplet state that occurs on a timescale much longer than fluorescence emission. In most cases, during routine imaging in fluorescence microscopy, blinking goes unnoticed, but it can become a problem (or solution) when examining specimens using superresolution techniques as discussed in Chapter 15. Blinking can be regulated to some extent by the addition of oxidizing and/or reducing agents into the imaging medium.

In contrast to quenching and blinking, photobleaching (also termed *fading*) occurs when a fluorophore permanently loses the ability to fluoresce due to photon-induced

chemical damage and covalent modification. Upon transition from an excited singlet state to the excited triplet state, fluorophores may interact with another molecule to produce irreversible covalent modifications leading to the destruction of fluorescence. The triplet state is relatively long-lived with respect to the singlet state, thus allowing excited molecules a much longer timeframe to undergo chemical reactions with components in the environment. The average number of excitation and emission cycles that occur for a particular fluorophore before photobleaching is dependent upon the molecular structure and the local environment. Some fluorophores bleach quickly after emitting only a few photons (Fig. 11.13), while others that are more robust can undergo thousands or even millions of cycles before bleaching.

An important class of photobleaching events is called *photodynamic,* meaning they involve the interaction of the fluorophore with a combination of light and oxygen. Reactions between fluorophores and molecular oxygen permanently destroy fluorescence and yield a free radical singlet oxygen species that can chemically modify other molecules in living cells. This serves as the basis for an advanced imaging technique

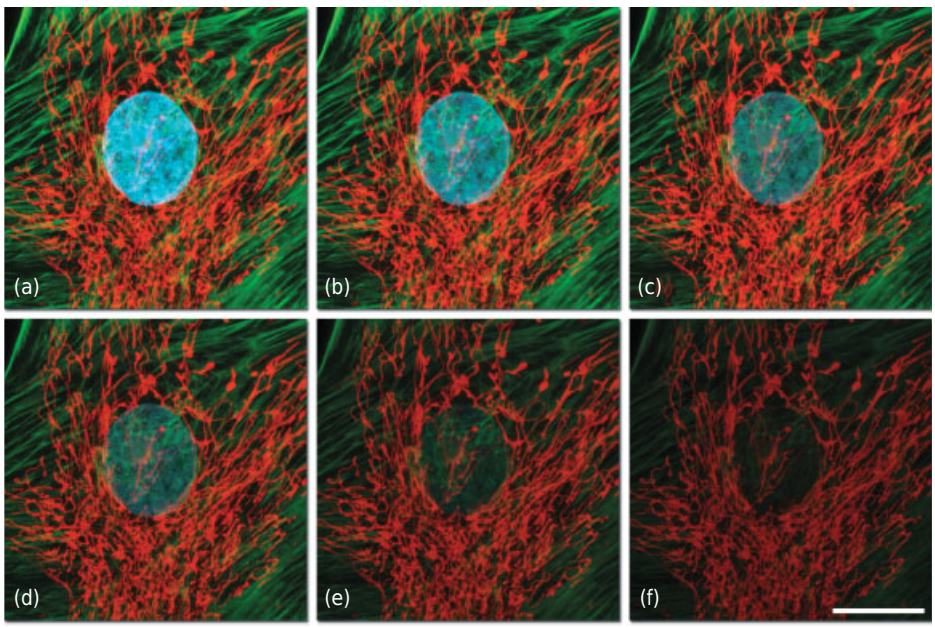

Figure 11.13

Photobleaching (fading) observed in a series of digital images captured at different time points for a multiply-stained culture of Indian Muntjac deerskin fibroblast cells. The nuclei were stained with DAPI (blue fluorescence), while the mitochondria and actin cytoskeleton were stained with MitoTracker Red (red fluorescence) and an Alexa Fluor phalloidin derivative (Alexa Fluor 488; green fluorescence), respectively. Time points were taken in 2-minute intervals using a fluorescence filter combination with bandwidths tuned to excite the three fluorophores simultaneously while also recording the combined emission signals. Note that all three fluorophores have a relatively high intensity in panel a, but the DAPI (blue) intensity starts to drop rapidly at 2 minutes and is almost completely gone at 8 minutes. The mitochondrial and actin stains are more resistant to photobleaching, but the intensity of both drops over the course of the timed sequence (10 minutes). (a) $t = 0$. (b) $t = 2$ m. (c) $t = 4$ m. (d) $t = 6$ m. (e) $t = 8$ m. (f) $t = 10$ m. Bar = 20 μm.

called *chromophore-assisted laser inactivation* (*CALI)*. The amount of photobleaching due to photodynamic events is a function of the molecular oxygen concentration and the proximal distance between the fluorophore, oxygen molecules, and other cellular components. Photobleaching can be reduced by limiting the exposure time of fluorophores to illumination or by lowering the excitation energy. However, these techniques also reduce the measurable fluorescence signal. Perhaps the best protection against photobleaching is to limit exposure of the fluorophore to intense illumination (using neutral density filters) coupled with the judicious use of commercially available antifade reagents (discussed below) that can be added to the mounting solution or cell culture medium.

Under certain circumstances, the photobleaching effect can also be utilized to obtain specific information that would not otherwise be available. For example, in FRAP experiments (see Chapter 12), fluorophores within a target region are intentionally bleached with excessive levels of irradiation. As new fluorophore molecules diffuse into the bleached region of the specimen (recovery), the fluorescence emission intensity is monitored to determine the lateral diffusion rates of the target fluorophore. In this manner, the translational mobility of fluorescently labeled molecules can be ascertained within a very small region of a single cell.

EXAMINING FLUORESCENT MOLECULES IN LIVING CELLS

Fluorescence microscopy is potentially damaging to living cells, since light sources are intense and rich in damaging UV and IR wavelengths, and because fluorescence filter sets are not totally efficient in removing these unwanted wavelengths. The chief concern is phototoxicity to the cell through absorption of photons by introduced and endogenous fluorophores and the generation of reactive oxygen species, including singlet oxygen ($^1O_2$), superoxide ($O_2^{\bullet -}$), hydroxyl radical ($OH^\bullet$), various peroxides (ROOR'), hydroperoxides (ROOH), and others. They react with oxidizable metabolites and components in the cell, such as the pyridine nucleotides in nucleic acids, several amino acids, glutathione, lipids, and ascorbate. Among the immediate effects is damage to membrane lipids and proteins, including ion pumps, channels, and gates, which leads to loss of ion balance, loss of transmembrane potential, and rapid cell death. We discussed the consequences of phototoxicity on cell shape and cell behavioral responses in Chapter 3, and will cover live-cell imaging in detail in Chapter 16. Briefly, cells cease movement; intracellular organelle trafficking ceases; cells round up and form vacuoles and eventually lyse. Excitable cells, such as neurons and free-living amoebae, are among the most sensitive to light exposure in the microscope. Just 3 seconds of continuous exposure to the blue excitation wavelengths from a mercury lamp filtered by a standard fluorescein filter set is sufficient to cause *Acanthamoeba* and *Dictyostelium* amoebae to stop moving and round up. The requirement to minimize the exposure of living cells to light can place extreme demands on photography, because short exposures reduce the signal-to-noise ratio and result in grainy images. Control of the exposed dose is especially difficult during the acquisition of time-lapse sequences. The following approaches reduce the effects of phototoxicity:

- Additional UV and IR cutoff filters should be inserted near the illuminator, since the majority of the spectral output of metal halide, mercury, and xenon lamps

occurs in the UV and IR regions of the spectrum, and because most fluorescence filter sets are not completely effective in removing these unwanted wavelengths.

- Minimize exposure to light to allow time for dissipation and degradation of free radicals. Phenol red-free basal salt solution is recommended to reduce photon absorption.
- Addition of millimolar concentrations of anti-free radical reagents to live cells and *in vivo* preparations of purified cell organelles and filaments minimizes free radical damage, because the reagents readily react with free radicals and help spare endogenous molecules. Sodium ascorbate, reduced glutathione, or Trolox (a water-soluble form of vitamin E) at 10 mM concentrations are effective, particularly for *in vivo* systems.
- To retard the rate of free radical formation, the concentration of dissolved oxygen can be reduced to ~4% of the saturating value for buffer in room air by adding oxygen-depleting enzymes to the medium. Low oxygen concentration is usually not damaging to tissue culture cells—in fact, cells exist at similarly low values of oxygen tension in body tissues. One effective commercial product is Oxyrase (Oxyrase, Inc., Mansfield, OH), a preparation of respiratory particles from *Escherichia coli* membranes. Alternatively, an oxygen-scavenging system can be constructed based on a combination of catalase, glucose oxidase, and D-glucose. Cells in well chambers open to the air can be covered with a layer of embryo-grade mineral oil, such as that available from Sigma Chemical Company (St. Louis, MO), to prevent resaturation of the medium with oxygen.

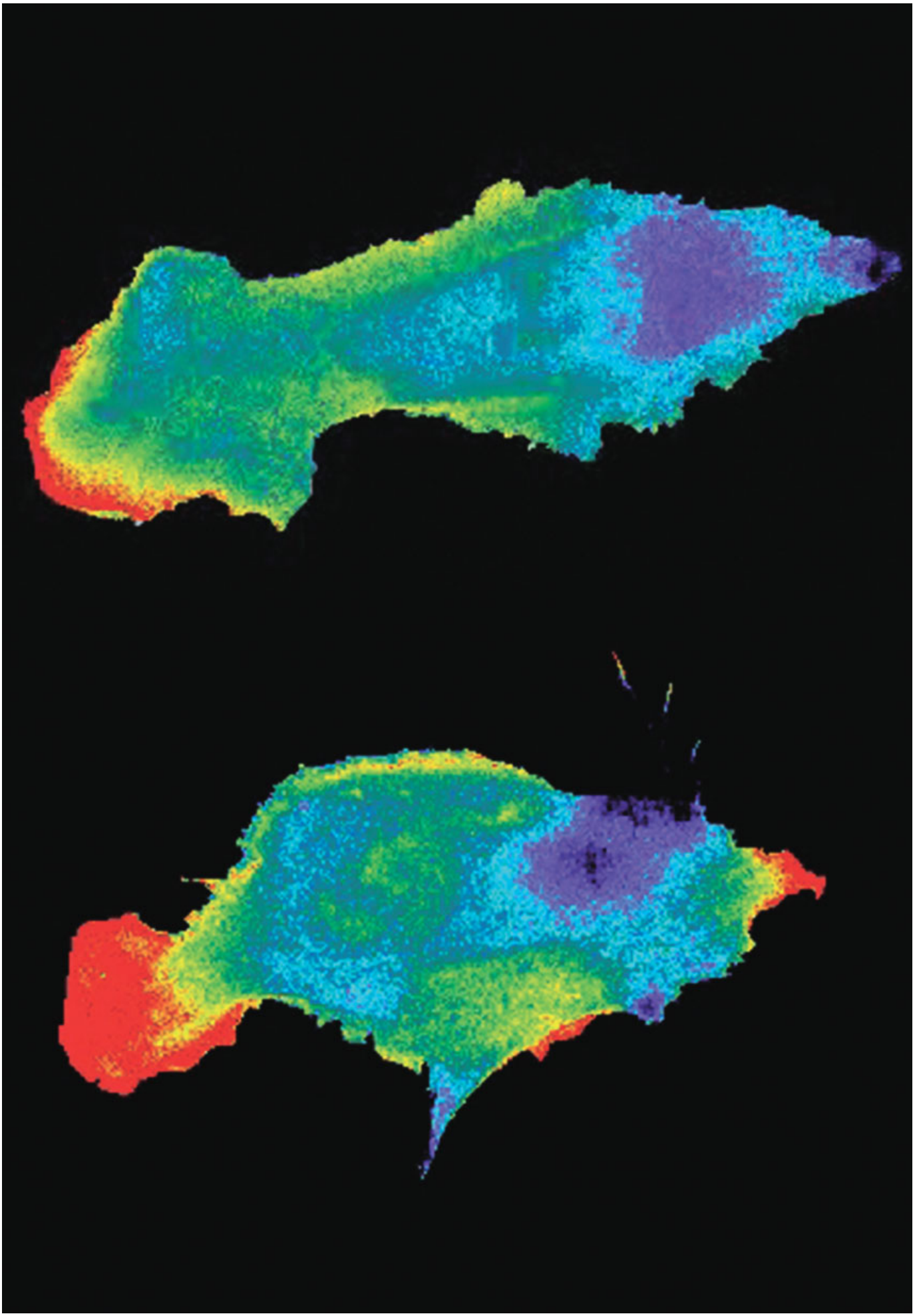

CHAPTER
12

FLUORESCENCE IMAGING OF DYNAMIC MOLECULAR PROCESSES

OVERVIEW

A remarkable feature of fluorescence microscopy is that the signals making up an image are molecule-specific. This means that fluorescence images are molecular distribution maps with information about the location and abundance of unique molecular species. With the addition of time-lapse methods, one can track time-dependent changes of bulk populations of molecules, and with sensitive detectors, even the complex behaviors of individual molecules. In this chapter, we show how fluorescence microscopy can be used to define the mechanisms underlying dynamic molecular events by careful choice of illumination and fluorescent probes. FRET and FRAP are two commonly used methods that allow one to study molecular mechanisms underlying cell functions. *Förster (fluorescence) resonance energy transfer,* or *FRET,* is used to examine molecular interactions in polymers and complexes and can also be used to report the activities of certain enzymes and the concentrations of signaling molecules and cofactors; *fluorescence recovery after photobleaching,* or *FRAP,* is used to determine the rate of molecule exchange into formed structures, such as filaments and organelles, and can even be used to measure rates of diffusion and determine the diffusion coefficients of proteins. Finally, we describe a unique method of fluorescence illumination called *total internal reflection fluorescence* or *TIRF,* that allows one to image structures with exceptionally high contrast and which has become a valuable tool for imaging and tracking single fluorescent molecules. It is methods such as these that have made fluorescence microscopy such an important analytical tool.

Pseudocolor image of FRET intensities showing rac activation in Dictyostelium cells. Courtesy of Klaus Hahn, University of North Carolina School of Medicine.

Fundamentals of Light Microscopy and Electronic Imaging, Second Edition.
Douglas B. Murphy and Michael W. Davidson.

MODES OF DYNAMIC FLUORESCENCE IMAGING

The following methods are used to measure the dynamics of molecules in live cells. Three of these—FRET, FRAP, and TIRF—are discussed in more detail below.

4D/5D *Time lapse microscopy in x, y, and z spatial dimensions in time (4D imaging) and in multiple color channels (5D imaging).*

These methods are used to measure the bulk dynamics of molecules in formed cellular structures, such as filaments and membranes. Multidimensional imaging reveals changes in the steady-state distribution of molecules over time and enables monitoring of dynamic interactions.

BRET *Bioluminescence resonance energy transfer.*

Optical-based resonance energy transfer approaches are founded on the nonradiative transfer of excitation energy between the electromagnetic dipoles of an energy donor and acceptor. In the case of FRET, both the donor and acceptor are fluorescent molecules, whereas for bioluminescence resonance energy transfer (BRET), the donor is bioluminescent and the acceptor is fluorescent. A prerequisite for these processes is that the emission spectrum of the donor and the excitation spectrum of the acceptor must overlap and that the donor and acceptor be in close proximity. BRET is a naturally occurring phenomenon in certain marine coelenterates, such as *R. reniformis*; the emitted luminescence from the degradation of coelenterazine by luciferase is transferred to green fluorescent protein (GFP), which then emits fluorescence at its characteristic wavelength.

CALI *Chromophore assisted laser inactivation.*

CALI is a light-mediated technique used to determine the functions of proteins in living cells by selectively inactivating them by local production of free radicals. A protein species of interest binds to a nonblocking antibody conjugated to a dye such as malachite green. The absorption of light from a focused laser generates short-lived free radicals that damage and inactivate adjacent proteins in the illuminated area. A variety of dyes and fluorescent proteins can be used.

FCS *Fluorescence correlation spectroscopy.*

FCS measures the rate of movement of individual fluorescent molecules into and out of a focused laser beam. The residence time of molecules in the beam varies, depending on their mass and diffusional properties and indicates whether they are free or bound to other macromolecules or small ligands. This method can be used to calculate diffusion coefficients and molecular concentrations *in situ* and can even be used to calculate the association and dissociation rate constants for binding reactions.

FISH *Fluorescence in situ hybridization.*

Short sequences of DNA complementary to the DNA sequence of interest are produced, labeled with fluorescent tags, and hybridized with DNA (chromatin, chromosomes) in fixed, permeabilized cells. Fluorescent signals from FISH can also be used to localize specific mRNAs in cells and tissues.

FLAP *Fluorescence localization after photobleaching.*

This method is used to track the dynamics of fluorescently labeled molecules in cells. The molecular species of interest is labeled with two fluorophores: one is photobleached in a small defined spot in the cell; the other serves as a reference label. The bulk movement of the labeled molecules is followed by subtracting the bleached signal from the unbleached reference signal.

FLIM *Fluorescence lifetime imaging microscopy.*

Lifetime imaging measures the state of molecular associations in cells. A fluorescent molecule is stimulated by a short burst of light and fluorescence is monitored by very high speed recording equipment. Fluorescence lifetime changes depending on whether molecules are free in solution, bound to other (nonfluorescent) macromolecules, or partnering with another molecule to produce FRET.

FLIP *Fluorescence loss in photobleaching.*

In FLIP, one measures the rate of molecule exchange within and between formed structures in the cell. A small defined region on a fluorescent structure is bleached, followed by measuring the rate of fluorescence reduction in neighboring regions of the structure as fluorescent molecules outside the bleach zone equilibrate with bleached molecules in the targeted spot.

FRAP *Fluorescence recovery after photobleaching.*

FRAP gives the half-time for molecule exchange in formed structures and can be used to measure the diffusion coefficient (D) of molecules. In FRAP, you photobleach a region on a cell structure (similar to FLIP), then monitor the rate of fluorescence recovery and analyze the recovery in terms of diffusion and the binding-dissociation of soluble and stationary molecules.

FRET *Förster (fluorescence) resonance energy transfer.*

FRET is sensitive to the distance between fluorophores and hence can be used to examine the proximity between fluorophores in cells and *in vivo*. Two proteins tagged with different fluorophores (acceptor and donor fluorophores) can be tested for Förster resonance energy transfer (a measure of molecular proximity) by exciting the shorter wavelength fluorochrome and monitoring the fluorescence emission of the longer wavelength fluorochrome. By placing two fluorochromes on a single molecule, one can study changes in molecular conformation within a molecule (intramolecular FRET). The latter method is also used to study changes in ion concentration, pH, and the activities of second messengers, kinases, and other interactions.

TIRF *Total internal reflection fluorescence microscopy.*

TIRF microscopy is used for sensitive imaging of fluorescent molecules located at the plane of reflection of an excitation beam of light. Typically, a laser beam is reflected from the surface of the specimen-coverslip interface. Fluorescent molecules located within 100 nm of the reflection plane are excited by an evanescent wave field present at the reflection interface.

FÖRSTER RESONANCE ENERGY TRANSFER

Förster resonance energy transfer—also known as *fluorescence resonance energy transfer*, or *FRET*—is the transfer of energy from an excited-state fluorophore to another fluorophore in the complete absence of photon emission and reabsorption. The mechanism of radiationless energy transfer was first described by Theodor Förster in 1946 when he was a professor of physical chemistry at the State University of Poznan. Because FRET requires very close physical proximity between the two fluorophores, microscopists have used the method as a mechanism to study questions of molecular proximity and interaction, such as the identification of interacting proteins in multimolecular complexes, filament systems, transcription centers, and other assemblies. For a review of FRET applications in light microscopy, see Jares-Erijman and Jovin (2003). FRET probes called *biosensors* are also used to examine changes in enzyme activities and report on the concentrations of intracellular metabolites.

The Molecular Mechanism of FRET

FRET involves the radiationless transfer of energy between closely spaced *donor and acceptor fluorophores*. When the donor and acceptor are brought into close proximity (1–10 nm), excitation of the donor results in fluorescence, not of itself, but from the acceptor. The mechanism of FRET is related to the behavior of excited fluorescent molecules as electric dipoles (or antennas), where electron resonances in an excited molecule establish a state of electronic polarity and an associated dipole moment (the product of the charge on either pole of a dipole and the distance separating them) (Fig. 12.1). If a second suitable fluorophore comes in very close proximity to the first, interaction can occur if the resonance frequency of the donor's electric field can induce electrons in the acceptor to oscillate and undergo transitions. Energy transfer of this kind is *radiationless and occurs in the absence of emission and absorption of an intermediate photon*. Under conditions of FRET, the donor fluorophore does not fluoresce and is said to be *quenched*, while the acceptor fluoresces. This form of *stimulated emission* returns the energy level of the two molecules back to the ground state. The reader is referred to Clegg (1996) and Lakowicz (2006) for comprehensive discussions of the physics of the phenomenon.

The main requirements for FRET are fluorophore proximity, spectral overlap, dipole alignment, and favorable environmental conditions:

- Energy transfer only occurs when donor and acceptor fluorophores are within 1–6 nm (up to 10 nm) of each other. This proximity relationship is very strong. The efficiency of energy transfer varies as the inverse 6th power of the intermolecular distance, and for this reason, probing molecular proximity by FRET exhibits a spatial resolution (1–6 nm) that is very high, up to a hundred times greater than that obtained by conventional fluorescence microscopy (limit of 200 nm). The distance at which there is a 50% probability of FRET transfer versus donor fluorescence is called the *Förster distance*, R_0. For CFP and YFP fluorescent proteins R_0 is about 4–5 nm.
- Energy transfer requires that the emission spectrum of the donor fluorophore overlap the excitation spectrum of the acceptor fluorophore (Fig. 12.2). The amount of overlap, also called the spectral overlap integral, determines both FRET

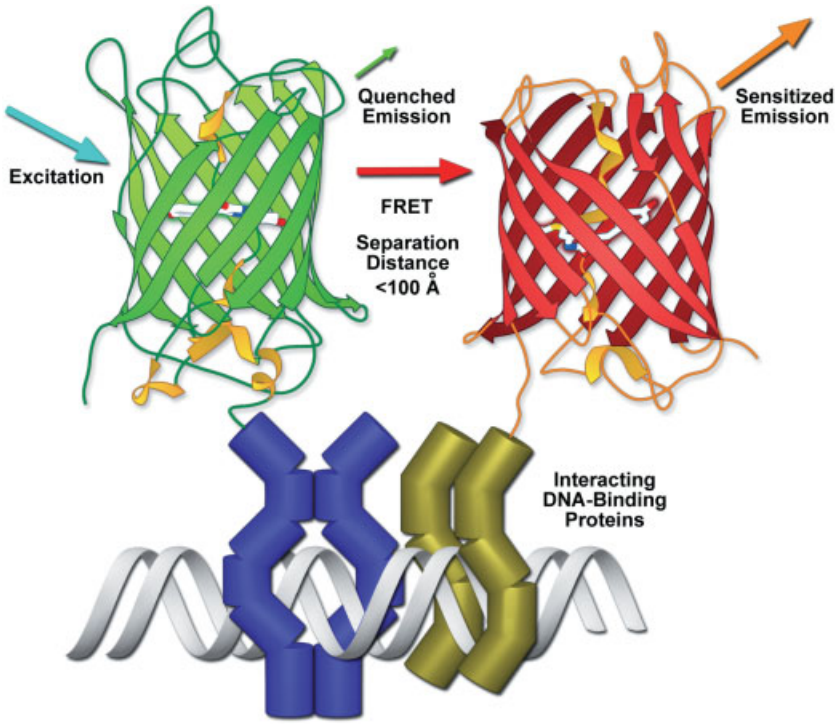

Figure 12.1

A pair of interacting nuclear proteins attached to green and red fluorescent protein reporters are used for FRET. For intermolecular FRET, two interacting DNA-binding proteins of interest are joined to GFP and RFP reporters. When the proteins are bound to DNA, their interaction brings the reporters into close proximity, and they can then undergo FRET. Intramolecular FRET involves a conformational change to a host protein that has two fluorescent proteins directly attached (usually to the C- and N-termini). Changes to the conformation of either bring the two fluorescent proteins closer together (FRET) or spread them farther apart (no FRET).

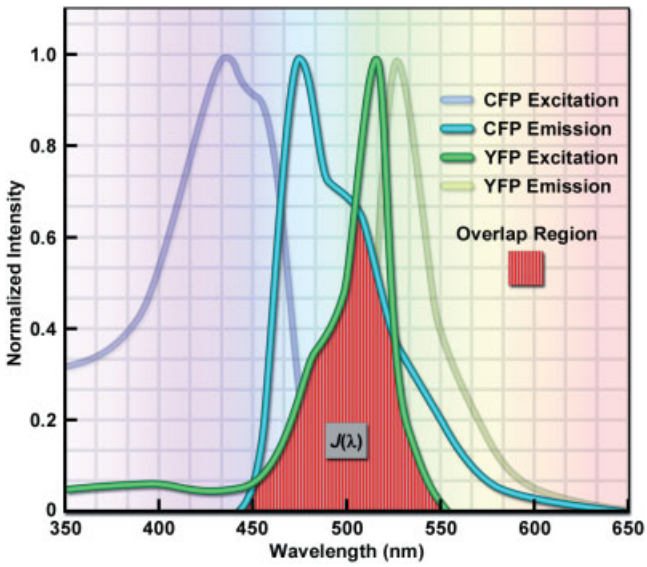

Figure 12.2

Spectral overlap integral ($J(\lambda)$) for the cyan and yellow fluorescent proteins, CFP and YFP, is highlighted as a hatched red region in the spectral profiles. The amount of overlap is related to the FRET efficiency and the Förster distance, R_0.

efficiency and *Förster distance*, R_o, with more overlap giving stronger FRET. The overlap integral for CFP and YFP is shown in Figure 12.2.

- The efficiency of Förster energy transfer depends on dipole orientation and is greatest when both dipoles are in line and parallel and least when they are perpendicular to one another. This means that some experimentation is required when designing FRET probes so that conditions for both distance and dipole orientation are satisfied.
- Finally, FRET is sensitive to environmental conditions that affect dipole interactions, including solvent type, degree of hydration, ionic strength, pH, and temperature, among other factors.

FRET Probes

The fluorophores used for FRET can be fluorescent atoms, small dye molecules, or macromolecules, such as fluorescent proteins. Fluorescent dyes can be more accurate proximity reporters because of their small size, but their use usually requires that the investigator purify proteins, conjugate the dyes, and microinject the conjugated molecules into cells. Various combinations of dyes can be used as donor and acceptor, such as fluorescein (or Cy2)-Cy3, Cy3-Cy5, and Cy3-Cy5.5.

Fluorescent proteins have become very popular as FRET reporters (FP-FRET) because of the relative ease of producing DNA constructs of chimeric proteins and transfecting cells using standard molecular biology techniques. The favored FPs at the present time are CFP variants "Cerulean," "mTurquoise," or "mTFP1" (teal fluorescent protein) for the donor, and the YFP variants "Venus" or "Citrine" for the acceptor. These proteins have improved maturation kinetics, high quantum yield, and photostability, making them suitable for live cell imaging and FRET analysis. New and better versions are continually being developed. Because FRET signals depend so strongly on the spacing and orientation between fluorophores, and because of the size of FPs, it can be valuable to know the three-dimensional structures of the host proteins when designing FP chimeras so that the fluorophores are brought as closely together as possible and have mutual orientations suitable for dipole–dipole energy transfer.

Paradigms for FRET

There are two paradigms for arranging donor and acceptor fluorophores:

- *Intermolecular FRET:* Donor–acceptor fluorophores are located on two separate molecules that interact with each other, and FRET indicates the proximity of the two reporters, and indirectly, the proximity of the two test molecules.
- *Intramolecular FRET:* Donor-acceptor fluorophores are placed on different regions of a single polypeptide that undergoes conformational changes upon binding to a substrate, causing the fluorophores involved in FRET to come together or move apart. Such molecules are called *biosensors*. Tsien and collaborators have created biosensors, such as *yellow chameleon*, *camgaroo* (based on calcium-sensitive peptides like calmodulin for reporting changes in calcium concentration), and *Raichu ras* (based on ras protein for reporting changes in cell signaling),

among other sensors for measuring FRET, as described in Tsien (2009). FRET biosensors have also been created for measuring changes in pH, Cl^-, redox potential, Ca^{2+}, Zn^{2+}, cAMP, cGMP, as well as kinase and protease activity.

Evaluating FRET from Fluorescence Images

From the fluorescence intensities in image frames acquired in the presence and absence of FRET (*image-FRET*), one can calculate the *FRET efficiency, E*, and the *intermolecular distance, R*. *E* is calculated from the ratio of fluorescence intensities of the donor with acceptor (I_{da}) and without the acceptor (I_d):

$$E = 1 - (I_{da}/I_d).$$

FRET efficiency can also be obtained from fluorescence intensity measurements of the acceptor in the presence and absence of donor (see below). FRET efficiency is related to the *intermolecular distance R* between the donor and acceptor fluorophores. Since *E* and *R* are related:

$$E = R_0^6/(R_0^6 + R^6),$$

it is possible to calculate *R*:

$$R = R_0(1/E - 1)^{1/6}.$$

In this equation, R_0 is a unique value called the *Förster distance*, the distance at which energy transfer is 50% efficient, meaning that there is a 50–50 probability that an excited donor will exhibit FRET versus fluoresce on its own. Notice that dipole–dipole coupling and FRET efficiency are related to the inverse 6th power of the donor–acceptor distance. This degree of sensitivity makes FRET very useful as a "spectroscopic ruler" for measuring intermolecular distances in the range of 1–10 nm. The magnitude of the Förster distance R_0 depends on the extent of overlap between the donor emission and acceptor excitation spectra, the quantum yield of the donor, the absorption coefficient of the acceptor, and the relative orientation of the two fluorophores, and is further defined:

$$R_o = [8.8 \times 10^{23} \kappa^2 n^{-4} Q_d J]^{1/6} \text{ (in Angstrom units)},$$

where:

- κ^2 (kappa squared) is a dipole orientation factor and is assumed to be equal to 2/3 assuming the movements are free and isotropic, but ranges from 0 to 4 depending on the orientation of dipoles that may have fixed positions.
- Q_d is the fluorescence quantum yield of the donor in the absence of acceptor.
- *n* is the refractive index of the medium at the site of fluorescence and is generally assumed to be 1.4 for a protein. The value *n* in this expression generally ranges from 1.33 (water) to 1.6.
- *J* is the spectral overlap integral, the degree of overlap between the donor emission spectrum and the acceptor absorption spectrum.

Most of these values are readily available from the literature.

Methods for Detecting FRET

With specialized equipment, one can make precise FRET measurements by measuring the decrease in donor fluorescence lifetime, the depolarization of donor fluorescence, and by using flow cytometry, as well as other methods. In particular, *FLIM* provides very accurate measurements of E and R because the process is measured directly and is unaffected by spectral bleedthrough as described by Chen et al. (2003). However, we focus here on three methods based on *image FRET* using widefield and confocal fluorescence microscopes to provide a practical, working example of the steps involved.

SENSITIZED ACCEPTOR EMISSION FRET

In this method, fluorescence emission of excited acceptor fluorophores increases, while donor fluorescence decreases. A standard way of measuring FRET involves imaging FRET samples and control samples with three fluorescence filter cubes, either on a widefield or confocal microscope: (1) a cube for donor excitation/emission, (2) a cube for acceptor excitation/emission, and (3) a FRET cube containing a donor exciter filter and donor dichromatic mirror and an acceptor emission filter. The spectral profiles of a CFP/YFP FRET pair in a typical three-cube set are shown in Figure 12.3. So-called three-cube FRET requires fluorescence measurements from donor-only and acceptor-only samples, as well as the experimental FRET sample using all three filter cubes. The operator must calculate correction factors for donor bleedthrough (donor fluorescence that contributes to signal in the FRET image) and crosstalk (donor excitation that directly excites acceptor fluorescence). Representative methods for performing and analyzing "three-cube FRET" are described by Elangovan et al. (2003), Erickson et al. (2001), and Gordon et al. (1998).

Practical Example of Three-Cube FRET

As a practical example of how results are analyzed in a sensitized-emission FRET experiment, we will focus on the three-cube FRET approach described by Erickson et al. (2001). Their 3-cube solution is based on FRET using CFP as the donor and YFP as the acceptor, and was devised to control for variability in recombinant fluorescent protein expression, the inability to selectively excite CFP due to spectral overlap, and also control for small aberrations in optical components. Three fluorescence filter cubes are installed on a widefield or confocal fluorescence microscope as normally used for fluorescence imaging. The *FRET ratio (FR)*, indicating the fractional increase in acceptor-YFP emission due to FRET is obtained from the fluorescence intensity measurements of acceptor-YFP signal in the presence of donor (F_{AD}) and by itself (F_A). Because the FRET ratio is based on YFP emission, YFP should be attached to the limiting molecular species in the molecular association under study. The ratio, (F_{AD}/F_A), is calculated as:

$$\mathrm{FR} = F_{AD}/F_A = [S_{FRET}(\mathrm{DA}) - R_{D1} \cdot S_{CFP}(\mathrm{DA})]/R_{A1} \cdot [S_{YFP}(\mathrm{DA}) - R_{D2} \cdot S_{CFP}(\mathrm{DA})].$$

Terms with the form "S_{CUBE}(SPECIMEN)" in this expression denote an *intensity measurement,* where S is the signal, *CUBE* means the filter cube for CFP, YFP, or FRET, and *SPECIMEN* indicates whether the cell contains donor (D-CFP), acceptor (A-YFP), or both (DA). In addition to cell images, the expression also contains correction constants (R), which are defined below. The numerator in the above expression represents

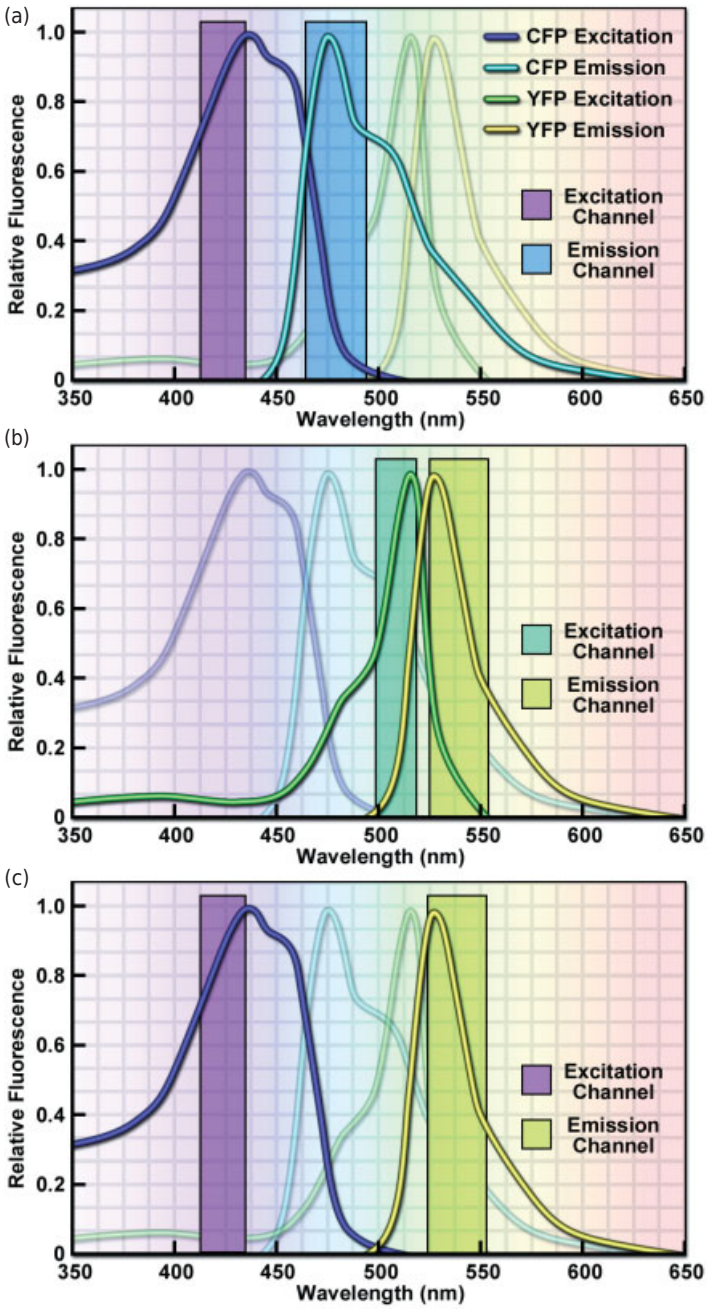

Figure 12.3

Filter cubes used for three-cube FRET involving a CFP-donor and YFP-acceptor. (a) Cube for donor excitation and emission gives a specific donor fluorescence signal, but excitation of donor also excites acceptor to some extent. In some cases, the donor emission overlaps the spectral region used for detecting acceptor emission. (b) Cube for acceptor-YFP excitation and emission. Acceptor excitation and acceptor emission are usually both fairly clean and specific. (c) FRET cube has bandpass filters for donor excitation and acceptor emission. Notice that the FRET signal contains unwanted signal from direct excitation of acceptor and bleedthrough of donor fluorescence.

an intensity component due to FRET plus a component due to the direct excitation of YFP; the denominator is the intensity from the direct excitation of YFP; the ratio gives FRET.

Images are prepared of cells containing both CFP and YFP together (DA) and are corrected by subtracting the background:

$S_{FRET}(DA)$ FRET intensity of DA
$S_{CFP}(DA)$ CFP intensity of DA
$S_{YFP}(DA)$ YFP intensity of DA

Both numerator and denominator contain correction factors for bleedthrough and crosstalk. To calculate the FRET ratio, three correction factors must first be determined from measurements of cells expressing separately only CFP- or YFP-tagged molecules. The correction factors, calculated from background-subtracted images, are:

$R_{D1} = S_{FRET}(D)/S_{CFP}(D)$ is the ratio of donor intensities in FRET and CFP filter sets. This factor allows calculation of non-FRET donor fluorescence occurring at the overlapping YFP emission wavelength and is subtracted from $S_{FRET}(DA)$ to obtain the YFP signal resulting from FRET.

$R_{D2} = S_{YFP}(D)/S_{CFP}(D)$ is the ratio of donor intensities in YFP and CFP filter sets. Multiplying $S_{CFP}(DA)$ by this value corrects for bleedthrough of directly excited CFP collected in the emission signal for YFP.

$R_{A1} = S_{FRET}(A)/S_{YFP}(A)$ is the ratio of acceptor intensities in FRET and YFP filter sets. Multiplying the measurement $[S_{YFP}(DA) - R_{D2} \cdot S_{CFP}(DA)]$ gives the YFP emission signal due to direct excitation.

Once the constants are determined, one simply acquires the FRET, CFP, and YFP images of a cell, subtracts the background, extracts the cell intensities from the images, and does the math to obtain the FRET ratio. With the FRET ratio in hand, one can then readily calculate the *FRET efficiency* (*E*) and *intermolecular distance* (*R*) from the relationships described above. The FRET ratio rises with increasing FRET efficiency, becoming ~12 when the FRET efficiency approaches 100%. A complete explanation together with a thorough description of important controls is given in Erickson et al. (2001).

Additional Considerations

- The concentrations of donor and acceptor need to be controlled so that the efficiency of FRET transfer is optimal. Ideally, there is molar excess of acceptor over donor (but not a 10-fold or greater molar excess).
- Photobleaching should be minimal to maximize the number of functional molecules generating the FRET signal.
- Spectra for donor emission and acceptor excitation must overlap substantially.
- The best FRET pairs have a donor with a large fluorescence quantum yield and an acceptor with a large absorption extinction coefficient.
- Minimize direct excitation of acceptor during excitation of donor.

- Donor's absorption and emission spectra should overlap minimally to avoid donor–donor transfer, the case where emission of the donor molecules stimulates other donors to fluoresce, thus increasing a nonspecific background signal.
- Ideally, one would like to compare signals from a cell in the presence and absence of FRET. Therefore, it is a great advantage if the conditions allowing FRET can be controlled experimentally, such as through chemical, electrical, or mechanical stimuli.
- The dichromatic mirror *from the donor filter set* must be used to avoid excitation of the acceptor molecule. For a CFP/YFP FRET system, optics would include a 440/20 exciter, 455 dichromatic long-pass mirror, and 480/40 emission filters.
- Labeled donor and acceptor molecules must retain their biological functions.

Adjustments Required to Obtain an Accurate FRET Measurement

- Direct excitation of the acceptor at the donor excitation wavelength. This is unwanted but is usually unavoidable, since the excitation spectra overlap and have long tails.
- Emission of the excited donor at the acceptor emission wavelengths.
- Effects of varying concentrations of donor and acceptor molecules.
- Poor filter performance and therefore poor spectral discrimination when performing FRET.
- Factors complicating measurements are: cell movement during image acquisition, cell autofluorescence, and noise inherent to electronic imaging systems. To minimize the problems of movement, donor, acceptor, and FRET images can be acquired *simultaneously* (for instance, a DualView from Photometrics splits image pairs on the CCD surface) or very close together in time (Sutter, Till, or Ludl filter wheels for moving exciter filters). Noises introduced by the mercury lamp, microscope reflections, camera read, and processing noises must also be carefully considered.

ACCEPTOR-PHOTOBLEACHING FRET WITH DEQUENCHING OF DONOR FLUORESCENCE

In this method, acceptor fluorophores are bleached to make them nonfunctional; the donor fluorophore, now dequenched, is able to emit fluorescence (Fig. 12.4). The strategy here is to photobleach the acceptor so that it no longer fluoresces; donor excitation causes donors to fluorescence because energy cannot be released through stimulated emission of the acceptor. Under these conditions, the increase in donor fluorescence, called the *dequenching of donor fluorescence*, indicates close physical proximity of the reporter fluorophores and therefore the host proteins. The technique can be applied to both fixed and live cells and has the advantage that it is not sensitive to spectral bleedthrough. This method provides a built-in (and valuable) internal control, since the *same cell is examined before and after acceptor photobleaching*. To demonstrate the presence of FRET, it is not essential to perform a control where the FRET signal is turned on and off experimentally with drugs or environmental changes, and the cell-to-cell variability caused by different transfection efficiency of donor and acceptor constructs is not an issue. It is important to determine that the illumination used to bleach acceptor fluorescence does not also destroy some of the donor fluorescence.

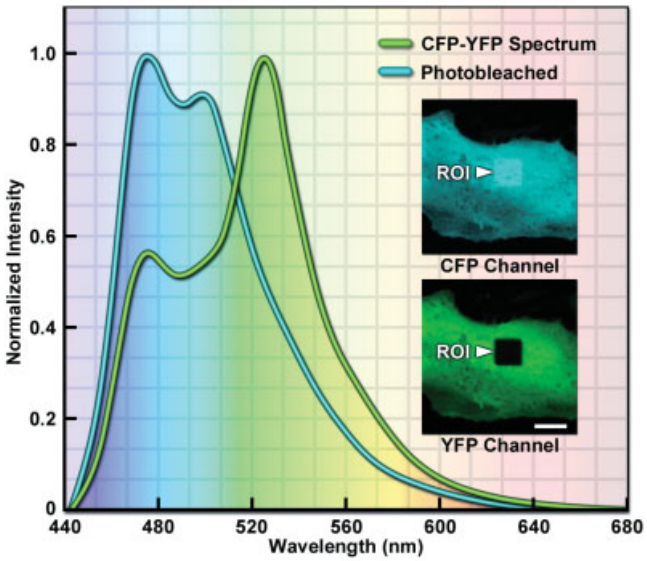

Figure 12.4

Spectral imaging FRET with acceptor photobleaching. Spectral curves for a FRET reference molecule containing CFP and YFP tethered together with a linker containing 10 amino acids and excited with a 405-nm laser before (green curve) and after (cyan curve) photobleaching with a 514-nm laser. A region of interest (ROI) was chosen for recording the spectra. Note the lack of signal in the YFP channel in the ROI as the result of photobleaching, coupled to a corresponding increase in the amount of cyan fluorescence in the CFP channel due to donor dequenching. Bar = 10 μm.

SPECTRAL IMAGING FRET

When performing acceptor-photobleaching FRET on a confocal microscope equipped with a spectral imager, fluorescence emission can be acquired in a single channel to measure the entire emission spectrum of the FRET pair upon excitation of the donor (Fig. 12.4). Many confocal microscopes (Chapter 13) are equipped with spectral detectors that enable recording the spectral profiles of fluorophores over a wide wavelength range. The underlying concept is that the combined emission spectrum allows the overlapping fluorophore spectra to be separated using both the peak emission wavelength data as well as the distinct shapes of the spectral curves. Thus, by gathering the entire spectrum, quantitative analysis can be conducted on the amount of donor and acceptor fluorescence when FRET is occurring. Spectral imaging FRET is often accompanied by acceptor photobleaching so that comparisons can be made between the FRET and no-FRET spectral profiles. The spectral profiles of a CFP-YFP FRET pair are shown in Figure 12.4 before and after photobleaching the YFP acceptor. CFP was excited with a 405-nm laser and the emission spectrum was recorded between 450 and 650 nm.

APPLICATIONS

Investigators have examined a wide variety of molecular interactions using FRET. These include: conformational changes in proteins and nucleic acids, the assembly of

protein subunits into higher order polymeric structures, assays involving nucleic acid hybridization, including PCR assays and detection of single nucleotide polymorphisms, the special case of receptor–ligand interactions including antigen-antibody binding and immunoassays, the distribution and transport of lipids as well as membrane fusion, plus a wide range of other functions, such as the monitoring of metabolites like cAMP, membrane potentials, and enzyme activities.

Cameleons: FRET Biosensors for Calcium Ions

Cameleons are fluorescent calcium ion indicators, recombinant chimeric proteins, based on the calcium-binding protein calmodulin (CaM), the calmodulin-binding domain of myosin light chain kinase (M13) and two fluorescent proteins, CFP and YFP (Fig. 12.5). In the presence of calcium, CaM binds ions, changes conformation, and wraps around the M13 domain, causing the CFP and YFP fluorophores to come close enough together to exhibit FRET. Mutations in the CaM domain allow the sensor to detect calcium at concentrations ranging from 10^{-2} to 10^{-8} M, a one million-fold range. By incorporating targeting sequences for specific localization in the cell, it is also possible to obtain cameleon expression in cytosol, nuclei, or endoplasmic reticulum of transfected cells. Miyawaki et al. (1997), who designed this sensor, named it "cameleon," both for its CaM activity and its ability to change its fluorescence emission color. In a low calcium environment, cameleon is extended, the CFP and YFP moieties remain relatively far apart, and excitation with deep blue light causes the molecule to fluoresce cyan. But in the presence of calcium, conformation changes bring the CFP and YFP domains close together, fluorescence resonance energy transfer occurs, and cameleon now fluoresces yellow-green. Cameleon sensors are an excellent example of *intramolecular FRET*.

FLUORESCENCE RECOVERY AFTER PHOTOBLEACHING

FRAP, also known as *fluorescence photobleaching and recovery (FPR)*, is commonly used to examine molecules that exist in equilibrium between a bound state in some cellular structure and a free (unbound) state in the cytoplasm. The technology has been significantly advanced and has become very popular with the emergence of GFP and its color variants as an imaging tool, discussed in detail by Edidin (1994) and Lippincott-Schwartz et al. (2001). Fluorescently tagged molecules at equilibrium in a structure are photobleached with brief exposure to an intense beam of light, and the scene is monitored to determine the half-time of recovery (Fig. 12.6a). Fluorescence recovery can be analyzed by measuring fluorescence intensities or fluorescence lifetimes. We will focus on the analysis of fluorescence intensities obtained by measurement of images from time-lapse sequences. By applying certain assumptions and controls, it is possible to relate the half-time of fluorescence recovery to the half-time for molecule exchange in the structure. In addition, FRAP is useful in biochemical and biophysical studies of purified proteins for calculating the *apparent diffusion coefficient*, a hydrodynamic parameter that contains information regarding the mass and shape of a molecule. Under ideal circumstances, probing equilibria by FRAP alters the fluorescence equilibrium

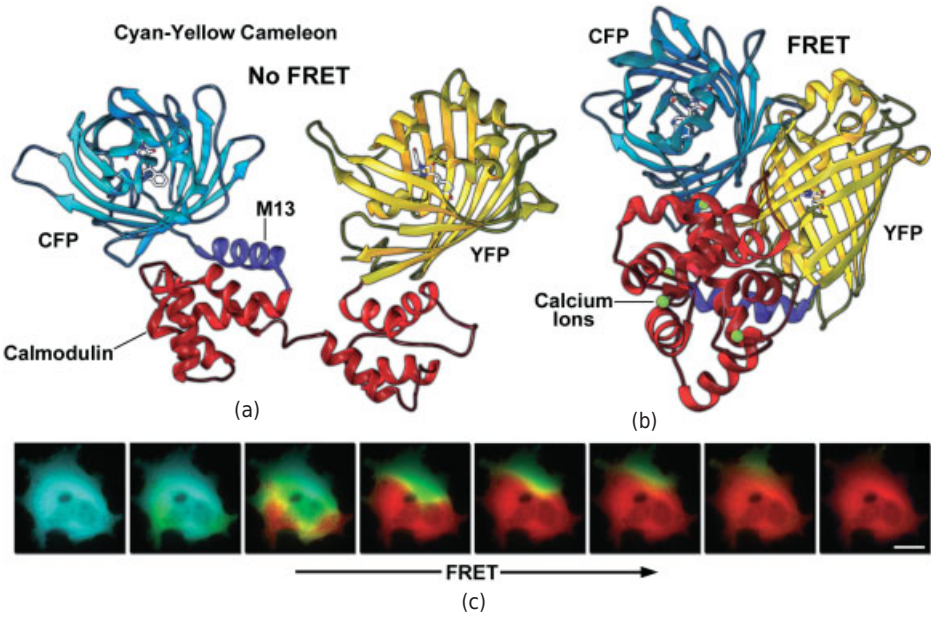

Figure 12.5

Calcium sensing by a cyan-yellow (CFP-YFP) cameleon. (a) Molecular arrangement of CFP, calmodulin, M13 peptide, and YFP in the chimeric biosensor called cameleon. In environments containing calcium ion (b), calmodulin binds ions, changes conformation, and wraps around the M13 peptide, creating a conformation suitable for FRET and allowing a shift in fluorescence emission from cyan to yellow-green. (c) A series of images covering a time window of 2 seconds showing a calcium wave in HeLa cells expressing cameleon (pseudocolored in a cyan to red range) after addition of ionomycin to the culture medium. Bar = 20 μm.

without perturbing biochemical processes or disrupting the cell in any way. Finally, FRAP measurements in cells reveal the *percent mobile fraction*, the fraction of a molecular species that is free in the cell and therefore able to participate in the dynamic equilibrium under study.

A related technique called *FLIP* is performed by continually photobleaching a small portion of a fluorescent structure while simultaneously documenting the fluorescence intensity of the whole structure by time-lapse imaging (Fig. 12.6b). During FLIP, bleaching a patch on a fluorescent structure causes the entire structure to bleach if the parts are physically connected. Therefore, the rate at which adjacent fluorescent areas diminish in fluorescence intensity tells one about the mobility of molecules comprising a structure and indicates whether neighboring fluorescent domains are physically contiguous, since the rate of fluorescence decrease in nonbleached areas is very slow if the bleached and nonbleached areas are not physically connected. Another variation similar to FLIP is termed *iFRAP* (inverse FRAP), where a small region of interest in a cells is selected and the inverse region is photobleached before examining recovery kinetics (Fig. 12.6c).

Recently, new fluorescent proteins have been developed that can be activated to initiate fluorescence emission from a quiescent state or can be optically converted from one fluorescence emission bandwidth to another. These probes offer an excellent alternative to the very high laser powers necessary to conduct FRAP experiments in living

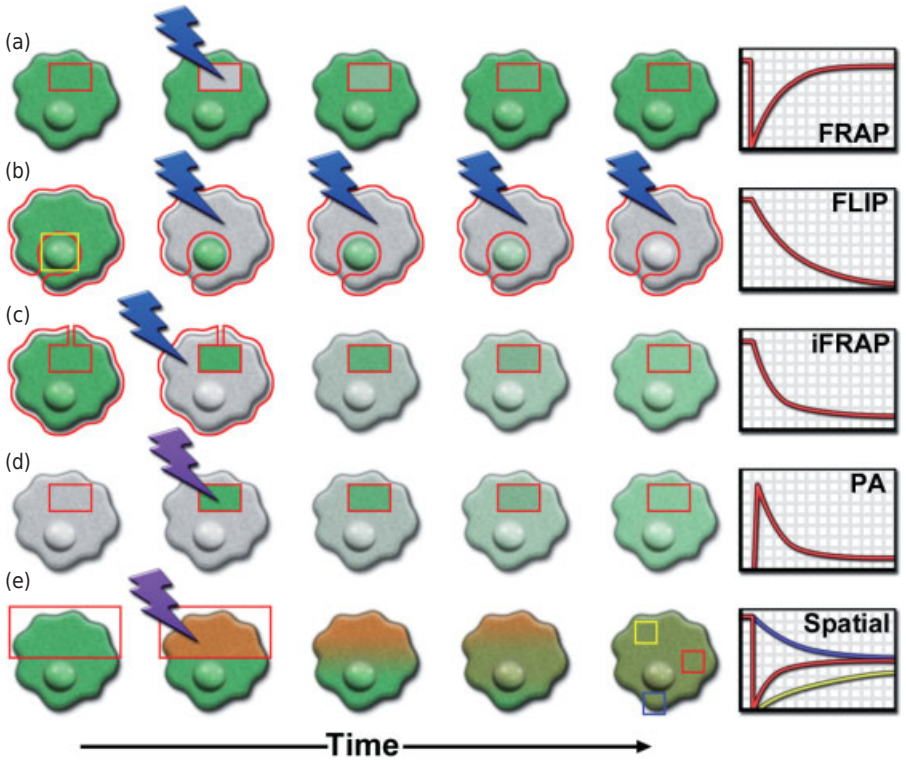

Figure 12.6

Techniques used in FRAP and related dynamic imaging modalities. The blue and purple lightning bolts represent high intensity laser excitation at 488 and 405 nm, respectively. Graphs on the right indicate typical recovery kinetics. (a) FRAP; (b) FLIP; (c) iFRAP; (d) photoactivation; (e) photoconversion.

cells. Termed *optical highlighters*, these fluorescent proteins can be either *photoactivated* (turned fluorescent from a dark state; Fig. 12.6d), *photoconverted* (converted from one fluorescence emission color to another; Fig. 12.6e), or *photoswitched* (turned "on" or "off" using different laser wavelengths). Similar to traditional FRAP experiments, the ability to selectively highlight distinct molecular pools within the cell is a powerful tool in the study of cellular dynamics. Optical highlighters have the added benefit that only a limited population of photoactivated molecules exhibits noticeable fluorescence (or a change in emission color), so their half-life and diffusion behavior can be followed independently of other proteins that are newly synthesized.

A Molecular Model for Analyzing FRAP Measurements

FRAP is applied to cells to study the chemical equilibrium of binding and dissociation of molecules in organized structures, such as filament biopolymers (intermediate filaments, actin filaments, microtubules), proteins and lipids composing cell membranes and organelle surfaces, nucleic acid-protein complexes, supramolecular assemblies, such as focal adhesions, as well as other structures. These and many other subcellular

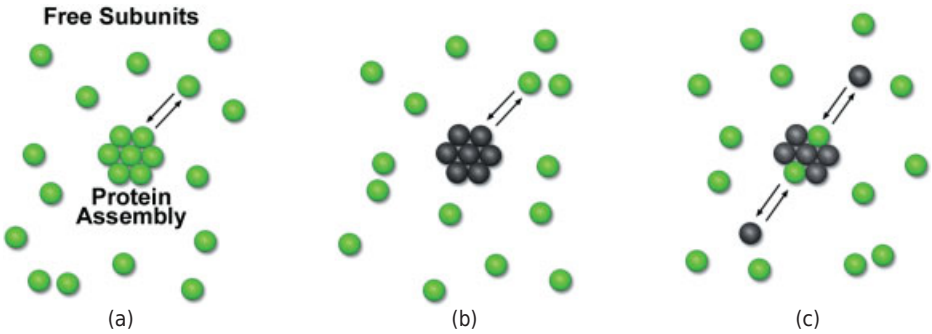

Figure 12.7

Equilibrium binding of subunits in a supramolecular structure as revealed by FRAP. (a) Molecules before photobleaching are fluorescent. (b) After photobleaching, the structure is bleached and fluorescence is reduced. (c) After partial recovery bleached molecules dissociate from the structure and are replaced by soluble nonbleached subunits.

structures consist of molecular assemblies whose subunits are noncovalently bound to one another and exist in a dynamic equilibrium with free unbound molecules in the cytoplasm (Fig. 12.7a). FRAP analysis provides the half-time for fluorescence recovery and hence the rapidity of molecule exchange, as well as the percentage of molecules participating in recovery.

First, we will focus on the use of FRAP to study the dynamics of molecular assembly in cells. In applying FRAP to a structure containing a fluorescent protein, we are probing the equilibrium between free and bound states of the molecule, a process governed by rates of association and dissociation of molecules composing a structure. After photobleaching leaves a dark mark on a structure, fluorescence recovery may take several seconds or even several minutes to occur (Fig. 12.7b). Ideally, a small photobleach mark is made in order to maximize the size of fluorescence recovery signal. An initial rapid part of the recovery lasting just a few seconds is due to the diffusion of unbleached free molecules into the bleached zone; a second slower phase of recovery involves recovery of bleached subunits in the fluorescent structures themselves. In this second phase, bleached molecules in the structure dissociate and are replaced by incoming fluorescent molecules that are part of the pool of unbound fluorescent molecules (Fig. 12.7c).

Generally, the rate of fluorescence recovery depends on the rate at which bleached molecules dissociate from the structure, the rate varying for different molecules and structures depending on the strength and stability of the bonds holding the molecules together. Therefore, the "characteristic half time for fluorescence recovery," the principle metric resulting from FRAP analysis, is mainly determined by the *rate of molecular dissociation* from structures. The *rate of association* of new fluorescent molecules is typically diffusion limited and very rapid, with a half-time of a few seconds, evidence that the association process itself is not rate limiting. Thus, the initial phase of fluorescence recovery is a mixture of two overlapping phases: (1) a rapid recovery phase involving diffusion of free fluorescent molecules, where bleached soluble molecules are replaced with fluorescent molecules from outside the bleach zone; and (2) a slower overlapping phase based on *recovery of the bleached structure* that depends on the replacement of bleached molecules with new fluorescent ones. A panel of fluorescence images from a typical FRAP experiment is shown in Figure 12.8.

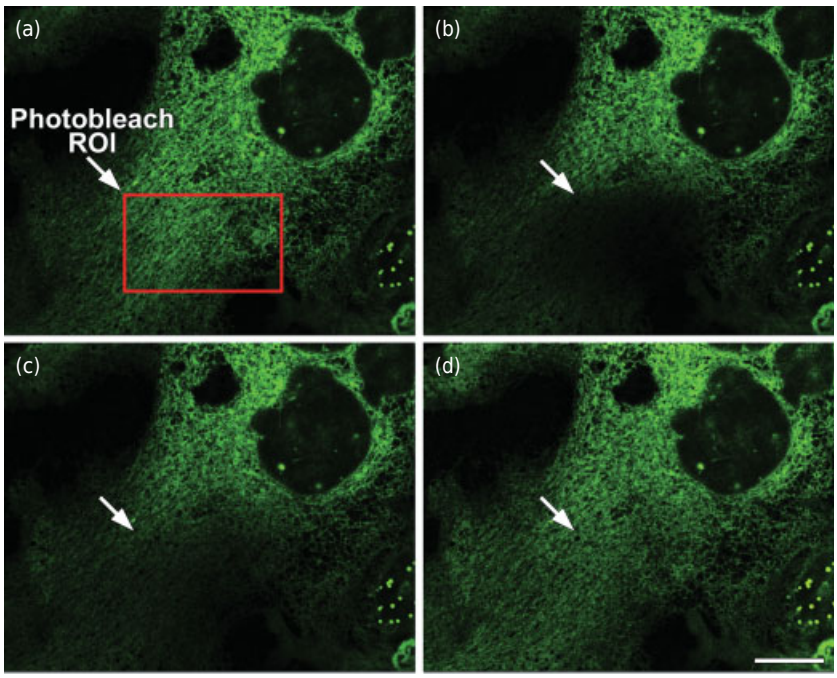

Figure 12.8

FRAP experiment of GFP fused to an endoplasmic reticulum targeting signal in a living cell. Image frames show (a) prebleach and the selected ROI (red rectangle); (b) 2 seconds postbleach; (c) 5 seconds postbleach; and (d) 50 seconds postbleach. Bar = 10 μm.

In performing FRAP, time-lapse imaging is used to record the specimen before and after photobleaching. The photobleach mark is typically limited to a small patch, such as a diffraction-limited focused spot or slit of light, and the region-of-interest used to measure intensity is limited to this area. Typically, the target is illuminated for a few milliseconds to reduce fluorescence intensity to 30–50% of the prebleach level. Small marks made within short time intervals minimize perturbation to the cell and help preserve the total amount of cell fluorescence. Time-lapse recordings are made as early as possible after the bleach event to capture early stages of fluorescence recovery. A representative sequence of recovery photos for cell endoplasmic reticulum is shown in Figure 12.8, and a general curve of a FRAP experiment is shown in Figure 12.9. Notice the rapid drop in fluorescence at the photobleach event followed by the slower recovery to a stable plateau. Usually, the level of recovered fluorescence (F_∞) is less than the original level before photobleaching (F_i). This can occur if photobleaching removes a significant amount of the total fluorescence signal in the system, or if there is a fraction of molecules in the structure that recovers at a much slower rate or does not recover at all, or for yet other reasons—a so-called *nonmobile fraction* of the fluorescence. The *mobile fraction*, the fraction of molecules that does show recovery, is calculated from the curve as: (F_∞/F_i), whereas the balance is the nonmobile fraction, $(F_i - F_\infty)/F_i$. Another useful statistic for describing fluorescence recovery is the *percent recovery*, the percent of the initial fluorescence that is recovered, where:

$$\% \text{ Recovery} = (F_\infty - F_0)/(F_i - F_0),$$

and F_0 is the fluorescence intensity immediately after bleaching.

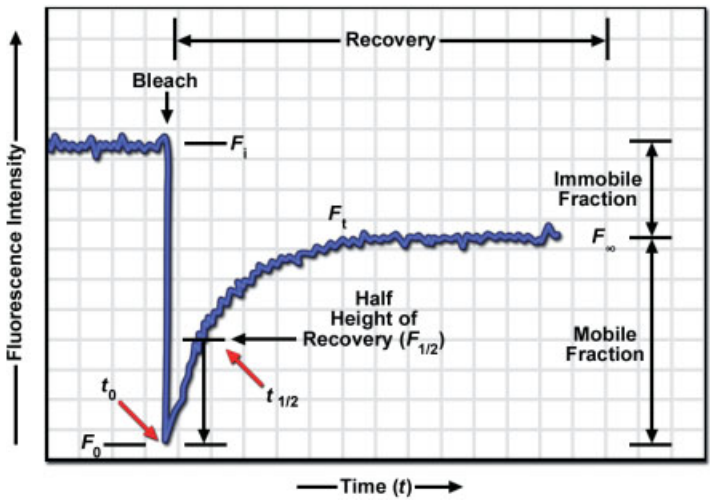

Figure 12.9

FRAP kinetics. Fluorescence intensity of a structure prebleach (F_i), immediately after photobleach (F_0), at time = t during recovery (F_t), at the half-time for recovery ($F_{1/2}$) and at fluorescence equilibrium (F_∞) is shown. The percent recovery is calculated as % Recovery = $(F_\infty - F_0)/(F_i - F_0)$, and the percent mobile fraction and percent immobile fraction are indicated.

One principal goal of FRAP is the determination of the *characteristic half-time for recovery*, $t_{1/2}$, from time lapse sequences of the fluorescence recovery. The theory used to analyze many photobleach-recovery events is called *perturbation–relaxation* and is based on kinetic theory for physical–chemical processes. In our example, a structure in a cell is perturbed from equilibrium very quickly by laser photobleaching, and fluorescence recovery is monitored to observe the relaxation to equilibrium. For simple first-order reactions, a basic approach is to fit FRAP recovery data to the exponential equation:

$$F_t = F_\infty - (F_\infty - F_i)\, e^{-kt},$$

where F_t, F_i, and F_∞ are the fluorescence at time t during recovery, the initial fluorescence, and the final fluorescence, respectively, and k is a constant. A convenient way to analyze recovery is to plot the natural logarithm of the fluorescence increment $(F_f - F_t)$ at each recovery time point versus time:

$$\ln(F_\infty - F_t) = -kt + b.$$

This function gives a straight-line plot, where the slope ($-k$) is related to the recovery half-time and the y-intercept (b) is related to the amount of fluorescence immediately after photobleach. Examination of a semi-log plot of the recovery data is a good way to confirm the presence of a first-order process (you should obtain a straight line).

Our brief overview of FRAP kinetics ends here. However, with additional knowledge of the equilibrium constant, the intracellular concentration of the molecule, and the order of the reaction, one can calculate the unique values of the association and

dissociation rate constants defining the chemical equilibrium. For examples and insights on the use of FRAP for determining diffusion coefficients and fluorescence recovery half-times in cells, see Axelrod et al. (1976), Wadsworth and Salmon (1986), Tardy et al. (1995), and Tsay and Jacobson (1991).

Measurement of Diffusion Coefficients Using FRAP

Fluorescence recovery methods can also be used to measure the *diffusion coefficients (D)* of fluorescently tagged macromolecules, such as a protein labeled with a small fluorescent dye like fluorescein (Axelrod et al., 1976). A drop of labeled molecule forms a thin film when sandwiched between a slide and coverslip. The laser beam is spread into a large spot (diameter 40–50 μm), and FRAP is performed in the usual manner. The kinetics of fluorescence recovery of the photobleached zone can then be analyzed by various equations, such as the equation developed by Axelrod et al. (1976) to calculate D in a two-dimensional system:

$$\tau_D = \omega\gamma/4D,$$

where ω is the radius of the waist or focused laser beam, γ is a photobleaching correction factor, and τ_D is the time for fluorescence recovery. Other equations are available for calculating D for GFP-tagged fusion proteins in the cytoplasm or membranes of living cells as described by Ellenberg and Lippincott-Schwartz (1999).

FRAP Examples

- Mobility of cell adhesion molecule E-cadherin in plasma membrane.
- Lamin B receptor motility in nuclear envelope versus in endoplasmic reticulum.
- Microtubule dynamics in the chromosomal and astral fibers of the mitotic spindle.
- Vinculin mobility in focal adhesions.

FRAP Equipment

Imaging can be performed on a widefield or confocal fluorescence microscope. If widefield, a bright light source, such as a laser, is essential for producing a photobleach mark on the specimen within a few milliseconds. A short photobleach period minimizes the amount of molecular exchange that can occur before time-lapse monitoring begins, while a small spot helps maintain a large pool of fluorescent molecules within the sample. Both criteria are important. Since the laser beam is usually focused to a spot at the specimen, one must apply extreme caution, regarding both the cell and the objective. Since the upper limit for the power of a focused laser beam in an objective is ~100 mW, powers greater than this should be used with caution. Given that the decrease in beam intensity due to scattering by upstream optics is around 50%, laser beams around 200 mW can be useful. Because of potential photodamage to the cell, careful controls must be used when performing FRAP (see below).

A filter cube should be chosen that is suitable for both laser photobleaching (high percent transmission of the laser line) and monitoring fluorescence recovery (optimized dichroic and emission filters), and in the case of widefield microscopy, possibly with a mercury lamp. It is also necessary to arrange for controlling the duration of exposure to the laser beam (such as with an electronic shutter) and to design the illumination pathway so that one can switch back and forth between laser spot illumination and full frame imaging. These steps are readily configured on a confocal microscope, but widefield systems may require some modification of the illumination pathway.

The laser should be sufficiently powerful to induce 30–50% photobleaching in a short time period, about 50–100 ms, so that an appreciable photobleach signal is captured in the first recovery frame. Since molecules can diffuse across the diameter of a cell in about 2 seconds, it is important to keep the bleach time as short as possible and obtain the first recovery frame quickly if the full range of recovery is to be recorded. It is often necessary to use additional optics to shape the laser beam and bring the beam to the epi-illuminator and the specimen.

A similar arrangement can be made with a single point scanning confocal microscope, with the caveat that the confocal monitoring of recovery may cause photodamage to the live cell. The software is set up to raster scan the specimen over a point or small area to induce photobleaching. The recovery phase is typically monitored by a large area raster that images the entire cell. Intensity values are extracted from the image sequence and analyzed as above.

FRAP Controls

It is essential to perform controls for photodamage and cell viability to show that FRAP recovery reflects a real biological process and that the cell specimen is free of photodamage. In selecting the time and intensity of exposure for bleaching, the goal is to expose the target only long enough to photobleach molecules without damaging the biological functions of the molecules. Therefore, one needs to establish that the photobleach event does not cause chemical or physical damage other than extinguishing fluorophores (GFP or fluorescein, for example). Ideally, one would prepare purified, fluorescently tagged molecules and perform bioassays on photobleached preparations to show that their activity is the same as untreated samples. To test for cell viability, one can examine live photobleached cells to establish that sensitive processes are still intact, such as mitosis, cell locomotion, and organelle transport.

TIRF MICROSCOPY: EXCITATION BY AN EVANESCENT WAVE

Total internal reflection fluorescence (TIRF) microscopy uses a specialized method of illumination to excite fluorescence in molecules located within 100 nm of the surface of the coverslip to which specimens (cells, molecules, and other fluorescent objects) are attached (see Axelrod et al., 1984). Compared with widefield or confocal modes of fluorescence microscopy, TIRF images can have very high contrast and S/N ratio, because the thickness of the zone emitting fluorescence (100 nm) is much less than the corresponding optical slice represented in a confocal image (700 nm), and because there are no sources of fluorescence outside the illuminated zone that can blur the image. Photodamage is also reduced and cell viability is prolonged, because excitatory photons

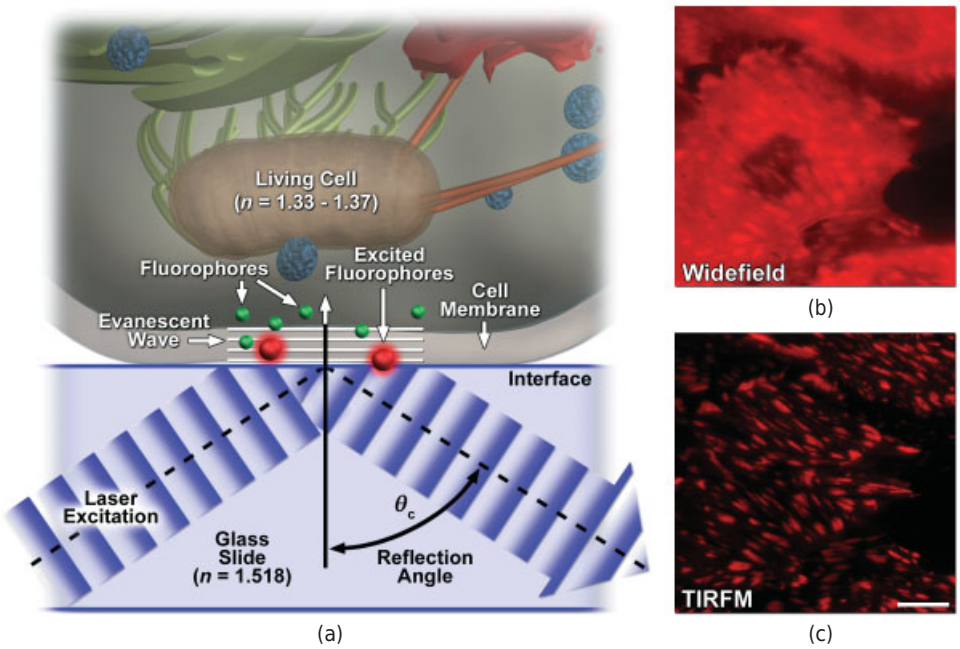

Figure 12.10

Principles of TIRF microscopy. (a) Cartoon of a cell on the surface of a coverslip labeled with fluorophores that are excited by the evanescent wave field from the reflected laser. (b) Widefield image of living cells expressing a red fluorescent protein fused to paxillin, a focal adhesion component. (c) Same field of view in TIRF illumination. Note the high contrast and S/N in the TIRF image compared with the widefield image. Bar = 10 μm.

do not pass through the specimen. One can use TIRF to examine membrane proteins, cell signaling events, receptor clustering in membranes, focal adhesions, cytoskeletal components, and other membrane-associated molecules (Fig. 12.10). Provided the detector has adequate sensitivity, one can even image individual fluorescent molecules using this illumination method as demonstrated by Funatsu et al. (1994) and Ishii and Yanagida (2000), including GFP (Pierce and Vale, 1999). As a special note, many optical devices from fiber optic cables to binocular prisms and diamond rings are based on the principle of TIR. In the case of optical fibers, light traveling along the fiber reflects off the walls of the fiber by TIR and experiences very little energy loss, even over long distances.

Total Internal Reflection

As explained previously in Figure 4.3, under certain conditions, a beam of light can be made to totally internally reflect at the interface between two transparent media. Notice from that figure and Figure 12.11 that TIR is possible when beams of light encounter a medium of lower refractive index. In the microscope and for practical discussion, let us consider the case of a glass coverslip as the *first medium* ($n_1 = 1.515$) *and a living cell attached to its surface as the second medium* ($n_2 = 1.34$–1.38). *At angles* of

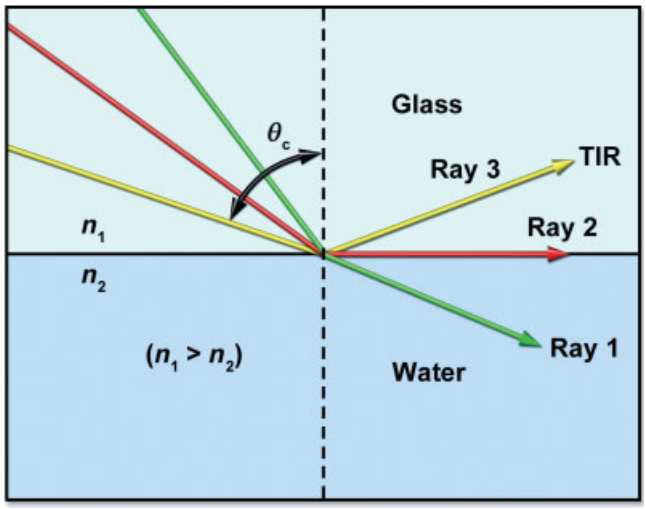

Figure 12.11

Conditions required for total internal reflection. Beams directed towards an interface between two media where $n_1 > n_2$ behave differently depending on the angle of incidence at the interface. At angles less than θ_c, rays are refracted and enter the second medium (ray 1). At the so-called critical angle θ_c, a ray is deflected at a 90° angle to the normal and travels along the interface (ray 2). At angles greater than θ_c, rays experience total internal reflection (ray 3).

incidence greater than the critical angle θ_c, beams are totally internally reflected back into the first medium. The critical angle of illumination required for TIR is obtained from Snell's law:

$$n_1 \sin\theta_1 = n_2 \sin\theta_2,$$

which relates the angle of refraction for rays of light traveling from one medium into another medium with a different refractive index, n. The angles θ are the angles subtended by the incident and transmitted rays relative to the normal at the interface. The conditions for TIR are unique: the refractive index in the first medium must be greater than in the second ($n_1 > n_2$) and the angle of the transmitted ray must be >90°. (Notice that if the transmitted ray is exactly 90°, the ray travels along the interface, and if at >90°, the "transmitted ray" is then reflected back into the first medium.) If the two refractive indices are known, then by setting the angle θ_2 in the second medium to 90°, the critical angle θ_c can be calculated as:

$$\theta_c = \sin^{-1}(n_2/n_1).$$

For the case of a cell ($n = 1.35$) attached to a glass coverslip (1.518), θ_c is 62°, and angles greater than this are required to obtain TIR.

The Evanescent Wave

Under conditions of TIR, incident wavelengths do not refract and carry energy into the second medium but instead are totally reflected away from it. It seems counterintuitive

that TIR illumination could excite fluorophores in the second medium at all. However, the physics of wave reflection under conditions of TIR from a dielectric material like glass requires that there be a "transmitted" wave component, represented as a standing, evanescent wave at the interface, even though all wave energy is reflected. The electric field of this standing wave penetrates into the second medium a short distance and is called an *evanescent wave* because it tends to vanish or to fade away into emptiness, meaning its intensity decreases exponentially with increasing distance from the interface (Fig. 12.10a). As a result, fluorophores located within about 100 nm from the surface can become excited in this field, draw energy from the reflection surface, and emit photons into the second medium, which otherwise does not occur. This specialized mode of illumination is very useful for producing fluorescence images of molecules and objects at the interface with exceptional clarity and resolution.

The *intensity I of the evanescent wave* at a depth z from the interface is given as:

$$I_z = I_0 e^{-(z/d)},$$

where I_0 and I_z are the light intensities at the coverslip surface at a perpendicular distance z, and d is the penetration depth. *Penetration depth d* depends on the refractive indices of the two interfacing media, the critical angle of incident illumination, and the wavelength, and is given by:

$$d = \frac{\lambda(\sin^2\theta - \sin^2\theta_c)^{-1/2}}{4\pi},$$

where λ is the wavelength of incident light in a vacuum and n is the index of the glass coverslip. Notice that the penetration depth decreases with increasing θ and increasing λ. When doing two-color TIRF with different laser lines at the same angle of incidence, the penetration depth of the evanescent wave at the two wavelengths may be slightly different and require some adjustment by the operator. The variation in illumination angle required to give the same penetration depth for wavelengths at 405 and 630 nm can be on the order of several degrees. Some commercial motorized TIRF modules automatically change the illumination angle at different wavelengths to give the same penetration depth. Relative intensity versus distance from the coverslip surface is shown in Table 12.1.

Microscope Configurations Used to Obtain TIRF

There are several methods for directing an illuminating beam at the critical angle to a coverslip as required for TIRF imaging. Beams of light can be delivered through the

TABLE 12.1 Depth of Penetration versus Intensity of the Evanescent Wave

Distance (nm)	Relative Intensity
1	0.99
10	0.92
100	0.43
1000	0.0002

objective itself, or positioned by mounting a prism on the coverslip surface, or even brought in through the condenser. Low power lasers of 10–100 mW are frequently used as light sources for TIRF illumination, as laser beams are bright, monochromatic, and polarized, all of which can be convenient features for manipulating the beam. If multiple lasers are employed for imaging different fluorescent dyes, the particular laser line and brightness can be controlled by an AOTF and the illumination delivered through a fiber optic to a TIRF module coupled to the epi-illumination port of the microscope. A commercial TIRF module contains a moveable lens to focus the laser at the rear focal plane of the objective and a positioning device with x,y controls for moving the focused beam (~0.5-mm diameter) within the rear aperture of the objective (~3–4-mm diameter). Positioning is needed to shift back and forth from TIRF illumination (edge of lens aperture) to widefield illumination (center of lens aperture) or for adjusting the TIRF angle to accommodate different wavelengths or to standardize the depth of penetration of the evanescent field. In a manual unit, these adjustments are performed by hand, but motorized TIRF modules perform these functions quickly and can be much more efficient and convenient. With a 100× lens, the area of TIRF illumination is variable, but is typically 50–200 μm in diameter.

Through-the-lens-TIRF is commonly used because it takes advantage of the epi-illumination light path of the microscope. In this case, the laser beam is focused on one edge of the rear aperture of an immersion type objective with a numerical aperture (NA) large enough to give TIR. The reflected beam is immediately collected and delivered out of the opposite side of the rear aperture of the same lens. Since the aperture of a 1.4 NA oil objective can just barely do the job, companies have responded by providing so-called TIRF objectives with very large NAs.

An alternative method that can be used to advantage on inverted microscopes is "prism-TIRF." In this method, a small glass prism (triangle, trapezoid) with polished optical surfaces is placed in contact with the coverslip with immersion oil, and a laser beam is directed at the prism to give TIR at the coverslip surface (Fig. 12.12).

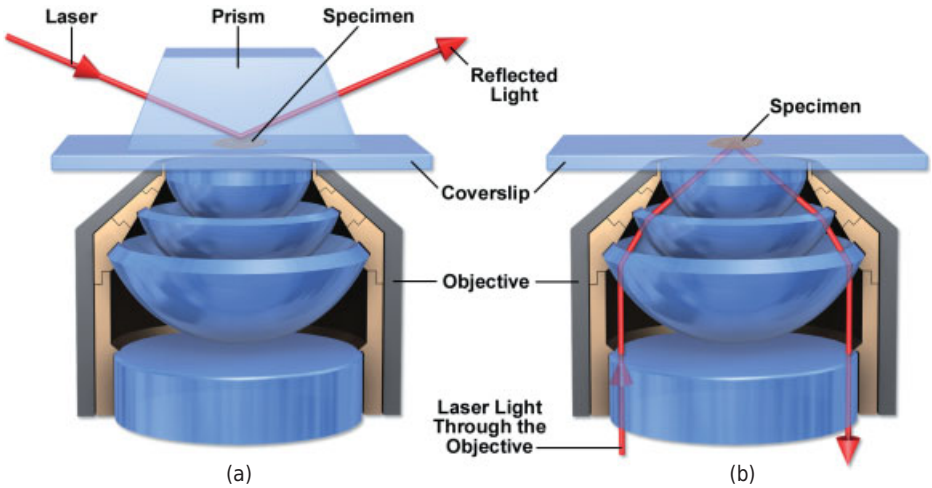

Figure 12.12
Modes of TIRF illumination. (a) Prism TIRF, and (b) through-the-lens TIRF.

Alternatively, a laser beam can be brought to the TIR interface along the transillumination light path of an inverted microscope using a high NA oil-immersion condenser. Using either method, the incident and reflected beams are external to the microscope and not part of the epi-illumination pathway used to image fluorescence. Prism-TIRF is often favored by researchers because of flexibility: this mode is suitable for both inverted and upright microscopes, one is not constrained to using high NA TIRF objectives—a variety of immersion and dipping lenses can be used, including long working-distance lenses for physiology experiments; there is greater freedom in manipulating the angle of incidence of the laser beam to obtain TIR; and the contrast is often improved, because the incident and return laser beams do not scatter light in the objective.

TIRF Objectives

TIRF illumination is commonly obtained by focusing a laser beam at one side of the rear aperture of a high NA objective. The reflected beam enters the other side of the lens and exits back out the rear aperture (Fig. 12.13). This method of illumination is called "through-the-lens-TIRF." As described above, the beam must be delivered to the

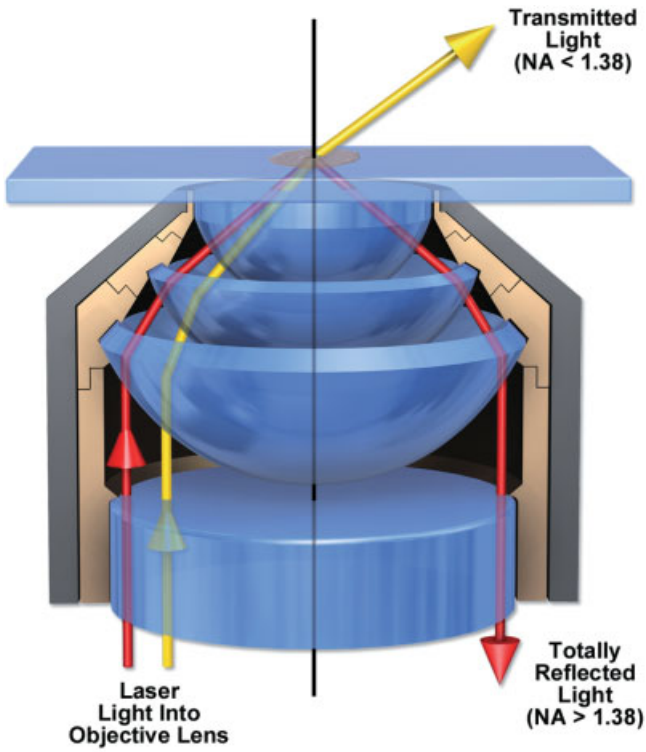

Figure 12.13

Adjustment of the critical angle for TIRF illumination. The laser beam is focused at the objective's rear aperture and then moved to one edge of the aperture. TIRF illumination is obtained when the angle of incidence at the specimen is greater than the critical angle. For a glass coverslip and living tissue culture cell, this angle is ~62°.

cell: coverslip interface at an angle of approximately 62° to the normal to the interface so that it totally internally reflects back into the objective and does not refract and penetrate the cellular space. This requires a large NA.

In Chapter 4, we described a 60×/1.49 NA oil objective for through-the-lens TIRF with a half angle of the acceptance light cone of 79.6°. Assuming a critical angle 61.2° for cells attached to a glass coverslip, such a lens provides ample room to obtain TIR and normalize the penetration depth using different wavelength beams. These manipulations are difficult to make using a standard 1.4 NA oil immersion lens. Another 100×/1.65 NA TIRF lens from Olympus uses special immersion oil and coverslips (both with $n = 1.78$) and has a corresponding critical angle of 49.3°, making it easier to adjust for TIRF. The high NA also produces images that are about 20–30% brighter than other 100× TIRF lenses. However, the advantages of this lens are partly offset by the cost of special coverslips and the need for high index oil that readily crystallizes. All of the microscope companies now make objectives with NA ≥ 1.45 that provide high-quality TIRF images.

The TIRF Illuminator

Using a motorized or hand-operated TIRF illuminator, one can position a laser's fiber optic cable at the epi-illumination port to adjust the focus and position of the laser to give widefield fluorescence or TIRF illumination. One end of the illuminator housing attaches to the epi-illumination port on the microscope and the other receives the fiber optic cable, while two threaded screws or motorized actuators push on the tip of the fiber to adjust its position in the light path (Fig. 12.14). The module also has a moveable projection lens to focus the laser beam into a spot at the rear aperture of the objective. The controls for positioning the fiber optic tip are then used to move the laser

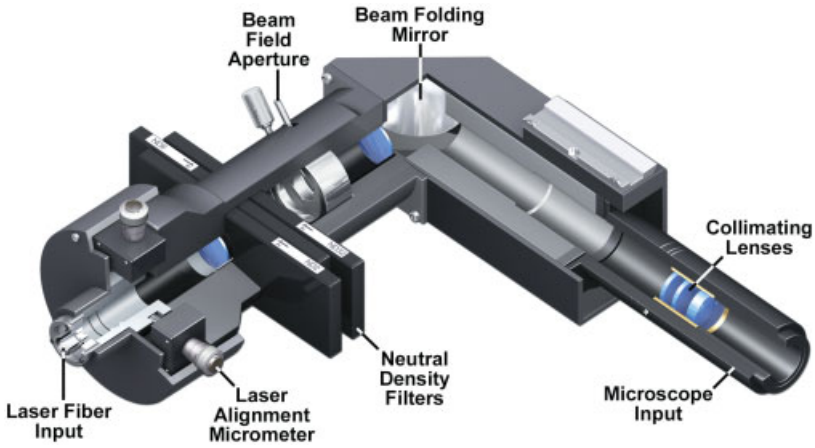

Figure 12.14

TIRF Illuminator for an inverted microscope. A laser optical fiber input can be adjusted with alignment micrometers, and the illumination passed through neutral density filters and a field aperture before being directed into the microscope optical train.

spot from the center of the aperture (widefield illumination) to the edge of the aperture (TIR). If multiple lasers are used, adjustments can be applied to optimize TIR for different laser wavelengths, or to adjust the depth of penetration of the evanescent zone on the specimen side of the coverslip.

Filters for TIRF

In widefield fluorescence microscopy, a matched filter set containing an excitation, emission, and dichromatic mirror filters is housed as a unit in an optical block (or cube; Chapter 11). TIRF microscopy requires the same type of filters, but usually of higher precision with much tighter specifications to eliminate unique artifacts induced through the use of lasers (Fig. 12.15 and Table 12.2). TIRF instruments benefit from a *laser cleanup filter* that removes unwanted spectral lines and noise from the laser that might interfere with imaging. This precision filter, which has a bandwidth between 5 and 20 nm and requires tight tolerances (low wedge, no pinholes or autofluorescence), can be placed at a slight incline (3–5°) in a filter wheel or mounted externally in the laser optical train. An *excitation filter* is placed in the optical block to supplement the laser cleanup filter. TIRF excitation filters differ from those designed for widefield microscopy by having much steeper edges and low ripple to ensure low noise and high transmission at specific laser lines.

Perhaps the most important optical component in the TIRF configuration is the dichromatic mirror, which is positioned at 45° to the illuminator and optical train, and can have significant impact on the system efficiency and image quality. In standard widefield fluorescence microscopes, the dichromatic mirror has less demanding

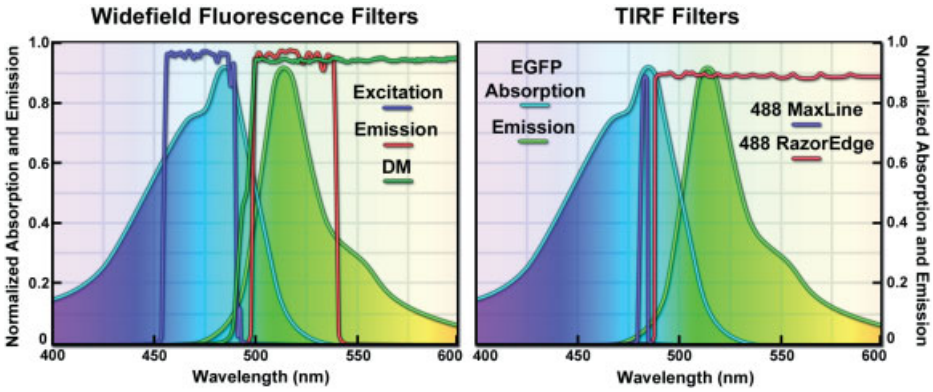

Figure 12.15

Comparison of standard widefield fluorescence and specialized TIRF filter accessories. (a) High transmission single-band filter set optimized for EGFP and similar fluorophores. The bandpass regions are ~40- to 45-nm wide to maximize signal throughput. (b) Optimized laser clean-up filter (Semrock MaxLine 488) and longpass edge filter (Semrock RazorEdge 488) can be used for TIRF applications to transmit the laser light effectively while providing a steep edge on the emission filter.

TABLE 12.2 Recommended TIRF Filter Parameters

Filter	Placement	Comments
Laser cleanup	Laser port or optical block	Limits laser damage, noise, and unwanted spectral lines
Excitation	Optical block	Steep edges, high transmission, low ripple, low damage threshold
Dichromatic mirror	Optical block	2- to 3-mm thickness, high flatness, steep edges, high transmission, low autofluorescence, low wedge and ripple, low damage, matched to laser lines
Notch filter	Optical block or filter wheel	Optional, sharp bandpass, high blocking, low autofluorescence
Emission filter	Optical block or filter wheel	Bandpass or longpass, steep edges, high transmission, low blocking, low wedge, autofluorescence, and ripple

specifications than those used for laser applications. Thus, the reflected and transmitted wavelength distortion should be 20 and four times better for laser mirrors, respectively, and the scratch/dig specification must also be higher. All laser dichromatic mirrors should have antireflection coatings applied to those surfaces lacking an interference coating to reduce secondary laser reflections and scatter, as well as to increase transmission efficiency. Widefield fluorescence dichromatic mirrors are 1-mm thick, but specialized mirrors designed for TIRF can be 2 or 3 mm in thickness and are usually fabricated using fused silica. In some cases, installing these thicker mirrors may require modifications to the optical block to avoid introducing stress when mounting the mirror. The 45° surface to which the mirror is applied should be polished to a similar flatness, and the mirror clip or mounting spring must not exert uneven pressure. Some manufacturers offer custom optical blocks specifically designed for the thick mirrors in TIRF applications. For multicolor imaging scenarios, dichromatic mirrors having two or more passbands (termed *polychromatic mirrors*) can be used to reflect multiple wavelengths in order to visualize several fluorophores without having to change the dichromatic mirror.

The primary function of the emission filter in fluorescence microscopy is to block unwanted excitation wavelengths from reaching the detector, while the secondary function is to transmit the desired emission band from the fluorophore being imaged. In a practical sense for TIRF applications, the emission filter must block any incident laser light transmitted through the excitation filter and dichromatic mirror with a high degree of extinction. Emission filters feature either bandpass or longpass spectral profiles and typically have high blocking levels for out-of-band wavelengths. Because they reside in the imaging pathway, the fabrication specifications of these filters are more stringent than excitation filters with regards to distortion, wedge, and scratches, or pinholes, and they may require antireflection coatings depending on the application. For TIRF, the minimum requirements for emission filters are blocking at the laser wavelengths to a minimum of 6 optical density (OD) units (often up to 8 OD), and they should contain antireflection coatings. These filters are often mounted in the optical block at an angle ranging up to 5° from incidence to reduce internal reflections.

In summary, the primary consideration in a TIRF microscope configuration is that the optical filters should work together as a set. Overall, the filters should achieve high blocking efficiency as well as high transmission levels at specific wavelength bands without compromising the diffraction-limited image quality. This simplified set of requirements influences not only the design of individual filters, but the combination of filters that must all perform separate functions. Therefore, the design characteristics of exciter, emission, and dichromatic filters should be complimentary in order to obtain the highest fidelity imaging. As an example, edge steepness of the excitation and emission filters is coupled and significantly affects the efficient utilization of the limited bandwidth. In this regard, the wavelength separation of excitation and emission filters should be as small as possible (typically less than 2% of the longest laser wavelength). On the other hand, the blocking ability of these filters should ensure that excitation light does not leak into the emission channel. Image registration (especially in multicolor experiments) is affected by the combined performance of the dichromatic mirror and emission filter. The thicker (up to 3 mm) flat glass substrates used for TIRF dichromatic mirrors should minimize any wedge angles and glass curvature arising from coating stress forces.

ADVANCED AND EMERGING DYNAMIC FLUORESENCE TECHNIQUES

Researchers have developed a wide spectrum of useful techniques designed to aid in contrast enhancement, provide better observation, and assist in the collection of fluorescence digital images of a wide variety of specimens. Many of these advanced techniques are especially important in imaging biological specimens and have led to widespread use of the optical fluorescence microscope as an indispensable tool in cell biology. Discussed briefly above, several of the more important techniques are described in a bit more detail here.

Fluorescence Lifetime Imaging Microscopy

Fluorescence lifetime imaging microscopy is a sophisticated technique that enables simultaneous recording of both the fluorescence lifetime and the spatial location of fluorophores throughout every location in the image. The methodology provides a mechanism to investigate environmental parameters, such as pH, ion concentration, solvent polarity, and oxygen tension in single living cells, presenting the data in a spatial and temporal array. FLIM measurements of the nanosecond excited state lifetime are independent of localized fluorophore concentration, photobleaching artifacts, and path length (specimen thickness), but are sensitive to excited state reactions, such as resonance energy transfer.

Fluorescence Correlation Spectroscopy

Used primarily with laser scanning confocal or multiphoton microscopy (Chapters 13 and 14), FCS is a technique designed to determine molecular dynamics in volumes containing only one or a few molecules, yielding information about chemical reaction

rates, diffusion coefficients, molecular weights, flow rates, and aggregation. In FCS, a small volume (approximately one femtoliter) is irradiated with a focused laser beam to record spontaneous fluorescence intensity fluctuations arising from the number or quantum yield of the molecules occupying the volume as a function of time. Relatively small fluorophores diffuse rapidly through the illuminated volume to generate short, random bursts of intensity. In contrast, larger complexes (fluorophores bound to macromolecules) move more slowly and produce a longer, more sustained time-dependent fluorescence intensity pattern.

Harmonic Generation Microscopy

Harmonic generation occurs when an optical excitation event involving two or more photons at a particular frequency results in cooperative emission at multiple harmonics (primarily, the second and third) without absorption of the photons (see Chapter 14). Generation of the harmonic frequencies is essentially a nonlinear scattering process yielding an emitted photon wavelength that is twice the frequency or half the wavelength (for second harmonic generation) of the incident illumination. In optical microscopy, transparent specimens that lack symmetry are ideal candidates for imaging with harmonic generation techniques. Unlike the situation with typical probes and traditional fluorescence microscopy illumination techniques, changing the excitation illumination wavelength produces a corresponding change in the emission wavelength. In addition, the emitted light is coherent and retains phase information about the specimen.

Coherent Anti-Stokes Raman Scattering Microscopy

The major benefit of *coherent anti-Stokes Raman scattering microscopy* (CARS) is that it enables investigations of biomolecules without the addition of synthetic fluorescent labels or endogenous coupling to fluorescent proteins. Instead, the technique is based on the vibrational properties of the target molecule and does not require the species to be electronically excited by ultraviolet or visible light. In practice, fast (picosecond or lower) laser pulses in the near-infrared region from two sources are focused onto the specimen with a microscope objective and raster scanned in the lateral and axial planes. The pulses are separated in frequency by a selected molecular vibrational mode and generate a new beam, which has a wavelength shorter than the incident beams, at the objective focal point. The secondary beam produces a concentration profile of the target species and enables the construction of a three-dimensional image of the specimen.

Fluorescence Speckle Microscopy

The inherent dynamics and spatial distribution of fluorescently labeled structures can be difficult to analyze when these entities are densely packed and overlapping within specific regions of living cells. *Fluorescent speckle microscopy* (FSM) is a technique compatible with almost all imaging modalities that takes advantage of a very low concentration of fluorescently labeled subunits to reduce out-of-focus fluorescence and

improve visibility of labeled structures and their dynamics in thick regions. FSM is accomplished by labeling only a fraction of the entire structure of interest. In that sense, it is similar to performing FCS over an entire field of view, albeit with more emphasis on spatial patterns than on quantitative temporal analysis. Speckle microscopy (as it is often called) has been especially useful in defining the mobility and polymerization of cytoskeletal elements, such as actin and microtubules, in highly motile cells.

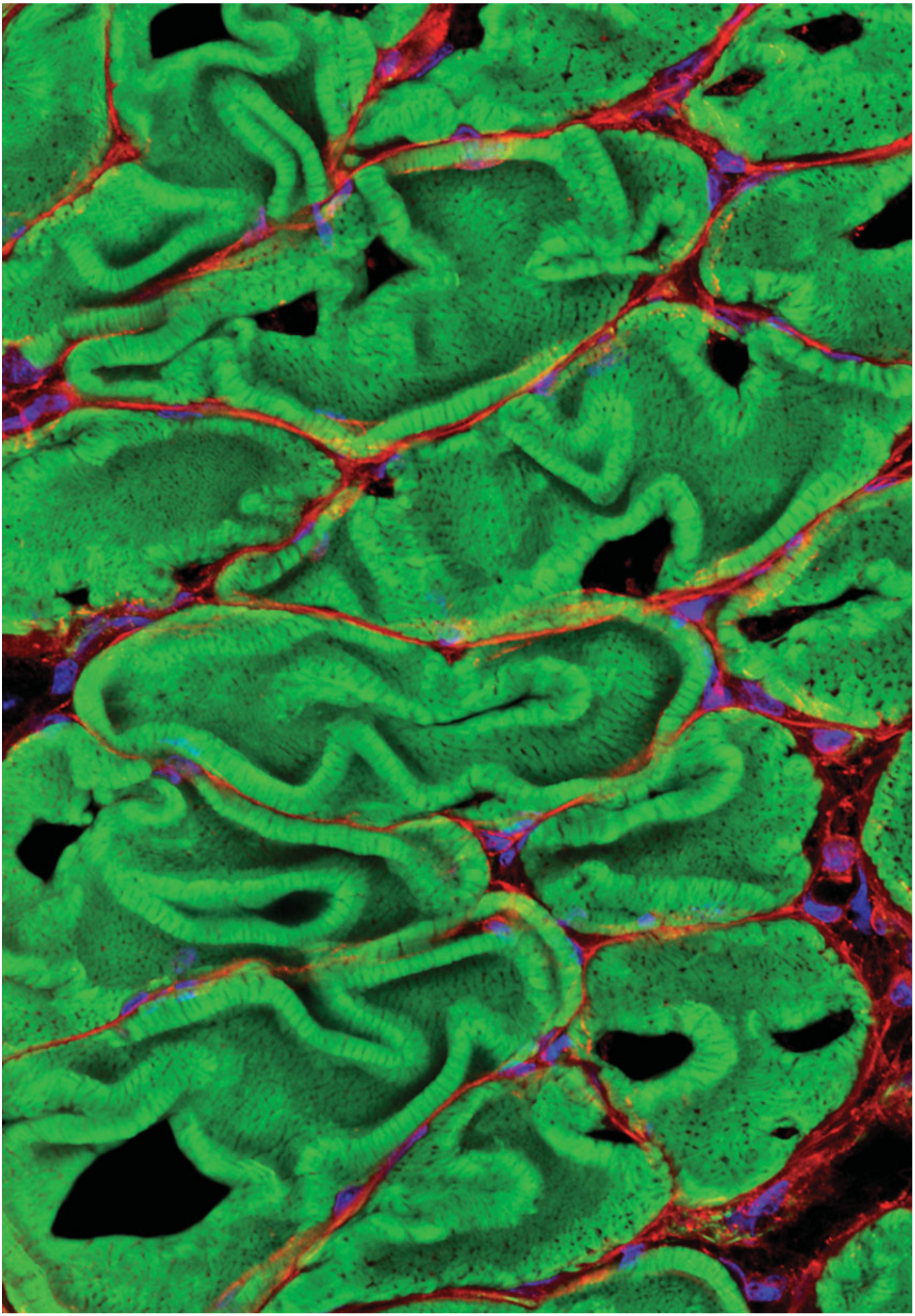

CHAPTER
13

CONFOCAL LASER SCANNING MICROSCOPY

OVERVIEW

Thick fluorescent specimens, such as rounded cells and tissue sections, can pose problems for conventional widefield optical systems because bright fluorescent signals from objects lying outside the focal plane increase the background and yield low-contrast images. Confocal microscopy and deconvolution imaging solve the problem by rejecting signals from nearby sources above and below the focal plane. In confocal microscopes, this is accomplished optically by illuminating the specimen with a focused scanning laser beam (point scanning) and by placing a pinhole aperture in the image plane in front of an electronic photon detector. Both fluorescent specimens and reflective surfaces can be examined using the technique (Fig. 13.1). Confocal images can also be produced using a spinning Nipkow disk that gives tandem scanning with literally thousands of scanning beams, and optical sections can be obtained by an optical computational method called structured illumination. In deconvolution microscopy, a standard widefield fluorescence microscope is used, and the image of an optical section is obtained computationally with a computer that removes out-of-focus light from the image. Deconvolution microscopy is briefly covered in the last section of this chapter. The high contrast images provided by confocal and deconvolution methods can provide clear answers to commonly asked questions about fluorescent microscope specimens: Is a fluorescent signal distributed on a membrane surface or contained throughout the cytoplasm as a soluble factor? Within the limits of resolution of the light microscope, are different fluorescence signals colocalized in the same structure? What is the three-dimensional structure of the specimen?

Confocal image of rat diaphragm showing muscle fibers (green), endomysium connective tissue (red), and cell nuclei (blue).

Fundamentals of Light Microscopy and Electronic Imaging, Second Edition.
Douglas B. Murphy and Michael W. Davidson.

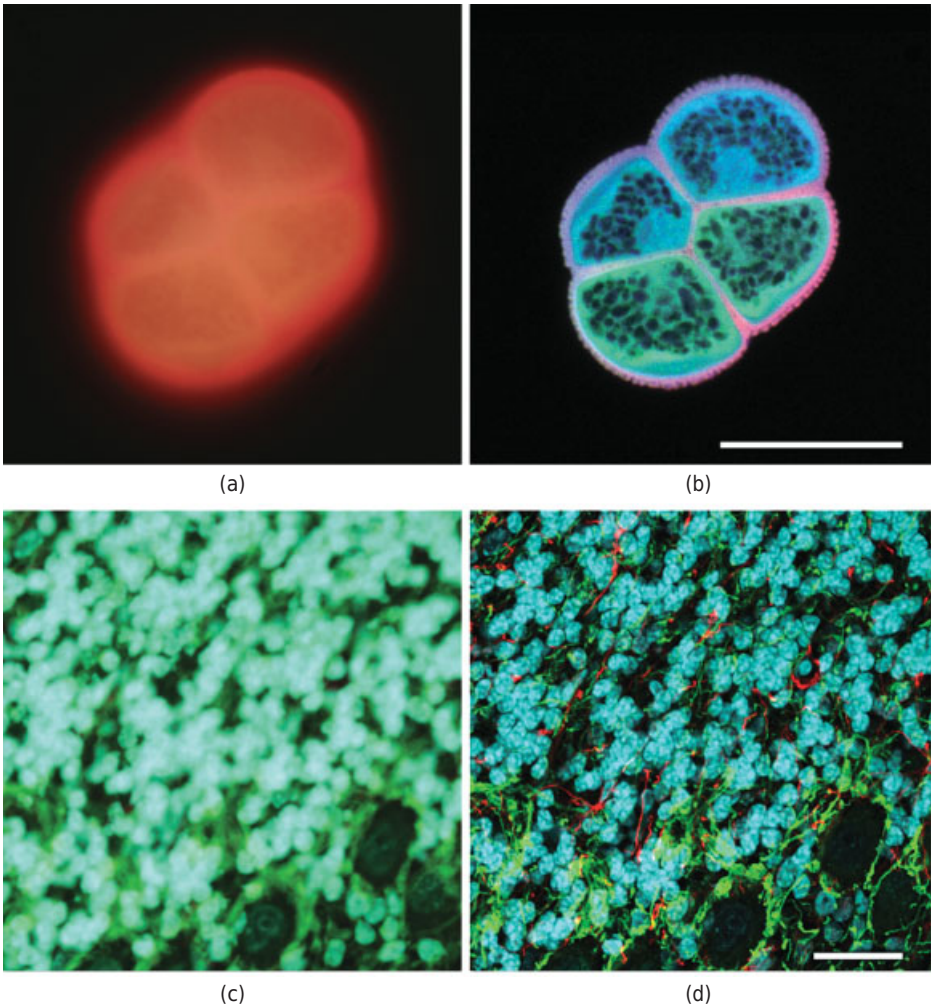

Figure 13.1

Widefield fluorescence (a,c) and confocal optical sections (b,d) of autofluorescence in a pollen grain (top row) and a thick (30 μm) section of rat brain triple-labeled with Alexa Fluor 568 (glial fibrillary acidic protein; GFAP), Alexa Fluor 488 (neurofilaments), and DAPI (nuclei; bottom row). Although the widefield images highlight the overall shape of the pollen grain and the outline of the nuclei in the brain section, the images are blurred by emission originating away from the focal plane. In contrast, the confocal optical sections reveal many fine structural details. Bars = 50 μm.

By using a stepper motor that changes the microscope focus in small steps along the *z*-axis, confocal and deconvolution microscopes make it possible to acquire a stack of images, or *z*-series, at different focal planes and generate a three-dimensional view of the specimen using computer software. Microscopists commonly acquire *z*-section stacks of live cells in multiple color channels, with stacks acquired at regular time intervals, so an entire color movie can be constructed showing dynamic events in a cell

in three dimensions—a truly valuable and exciting experience! Such sequences are called five-dimensional, because intensity information for every point in *x*, *y*, and *z* dimensions in a specimen is available at various times (as in a time-lapse sequence) and in color. Confocal and deconvolution microscopy already provide this capability.

The principle of confocal imaging was developed and patented in 1957 by Marvin Minsky, who is well known for work on neural network computing and artificial intelligence, while he was a postdoctoral fellow at Harvard University. In subsequent years, Brakenhoff, Sheppard, Wilson, and many others contributed to the design of a practical working instrument. Amos and White demonstrated the value of confocal imaging for fluorescent biological specimens around the time the first commercial instruments appeared in 1987. Since then, interest in confocal microscopy and improvements in the capacity of confocal imaging have increased at a rapid pace. For a historical perspective and annotated bibliography of this technology, refer to articles by Inoué (2006) and Webb (2006). In this chapter, we discuss the optics and essential electronic features of the confocal microscope, review briefly the parameters that are important in acquiring and evaluating an electronic image, and then consider how these parameters are affected by the operating controls of the confocal microscope.

THE OPTICAL PRINCIPLE OF CONFOCAL IMAGING

The confocal microscope is an integrated system consisting of a fluorescence microscope, multiple laser light sources, a confocal scan head with optical and electronic equipment, a computer and monitor for display, and software for acquiring, processing and analyzing images. The scan head contains the following devices:

- Inputs from one or more external laser light sources
- Fluorescence filter sets
- A galvanometer-based raster scanning mechanism
- One or more variable pinhole apertures for generating the confocal image
- Photomultiplier tube (PMT) detectors for different fluorescent wavelengths

The general configuration of a confocal microscope is shown in Figure 13.2 and the arrangement of components in the scan head in Figure 13.3. An analog-to-digital converter changes voltage fluctuations of the PMTs into digital signals for image display on the computer monitor.

The optical principle of confocal microscopy is shown in Figure 13.4 and is described as follows:

- *Epi-illumination* is used, where the light source and detector are both on the same side of the specimen plane and separated from it by the objective, which functions in dual duty as both a condenser and objective. The components of fluorescence filter sets (exciter filter, dichroic filter, and emission filter) perform the same functions as they do in widefield fluorescence microscopy.
- A laser beam is expanded to fill the rear aperture of the objective and forms an intense diffraction-limited spot that is scanned from side to side and from top to

Figure 13.2

Basic components of a confocal laser scanning microscope (CLSM). The laser provides a beam of light that is scanned across the specimen by the scan head under the control of a computer. The scan head also directs fluorescence signals from the specimen to its pinhole and photomultiplier tube (PMT). The computer holds the image in a buffer until it is processed and displayed on a computer monitor. On many instruments, a second monitor (not shown here) displays software menus for image acquisition and processing. It is important to realize that a confocal image is never generated in the microscope. Instead, the image is built up electronically, point by point and over time, from fluorescent signals received by the PMT and accumulated in the image memory board of the computer.

bottom over the specimen in a pattern called a *raster*. This procedure is called *point scanning*.

- The heart of confocal optics is the *pinhole aperture*, which receives fluorescent photons from the illuminated focused spot in the raster, but largely excludes fluorescence signals from objects above and below the focal plane, which, being out of focus, arrive at the pinhole as diffuse extended disks. Because the size of the disk of an out-of-focus object is spread out over such a large area, only a fraction of light from out-of-focus objects passes through the pinhole. The pinhole also eliminates much of the stray light in the optical system. Examine Figure 13.4 carefully to see how the pinhole blocks out-of-focal-plane signals. The combination of point scanning and the use of a pinhole as a spatial filter at the conjugate image plane are essential for producing the confocal image.
- Fluorescent wavelengths emanating from an excited point in the specimen at any time t are collected by the same objective and focused as a small diffraction spot that just fills the diameter of a variable pinhole aperture placed in front of a photomultiplier (*PMT detector*) in a plane that corresponds to the image plane in a widefield fluorescence microscope. The pinhole is optically confocal with, and conjugate to, the specimen plane. Thus, the PMT does not see an image, but produces a voltage that corresponds to the intensity of incident fluorescent photons; the computer in turn digitizes the signal and displays it on the monitor.

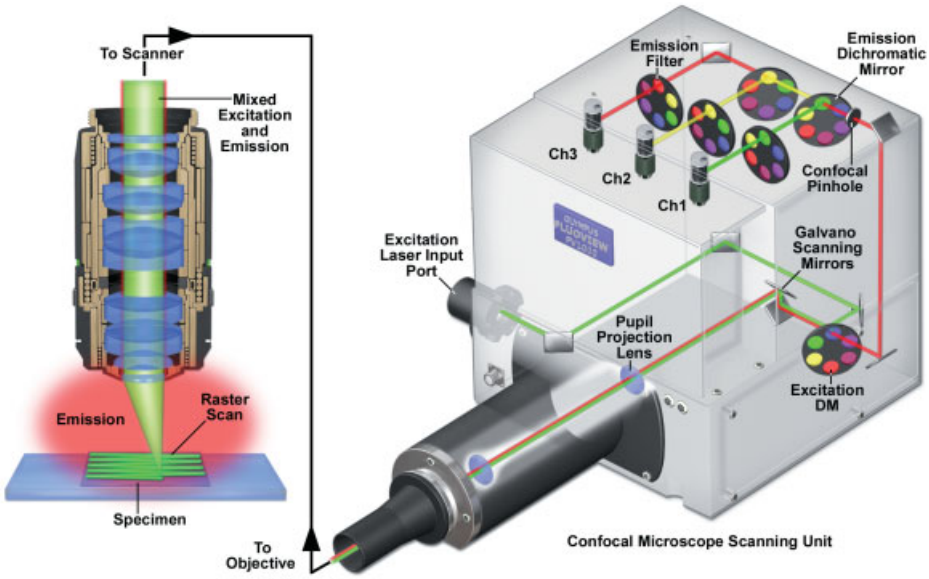

Figure 13.3

Optical pathway in a confocal microscope point-scanning unit. A laser beam is reflected by the excitation dichromatic mirror (DM) onto the galvanometer scanning mirrors of the scan-control mechanism, which sweep the beam in a raster pattern back and forth across the specimen to excite fluorophores. The objective simultaneously collects fluorescent emission, which is passed back to the scanning unit and descanned by the same galvanometer mirrors, transmitted through the confocal pinhole, reflected from the appropriate emission dichromatic mirror, and passed through an emission filter to the detection PMT. The excitation light is colored green and the emission light is colored red (mixed together in the objective). For clarity and instruction, only one excitation beam is shown, whereas three emission wavelengths are diagrammed in the upper right-hand section in the detection channels. In practice, only one excitation line is usually employed for each fluorophore. The drawing also shows the dichromatic mirror and filter arrangement used for collecting up to three fluorescence emission signals on separate detectors.

- To generate an image of an extended specimen, the laser beam is scanned across the object by a raster pattern that is typically based on two high-speed vibrating mirrors driven by galvanometer motors (Fig. 13.5). The two mirrors oscillate in mutually perpendicular directions. Fluorescent photons emitted from an excited point in the specimen are collected by the objective. Because the speed of the galvanometer mirrors is inconsequential relative to the speed of light, fluorescent light follows the same light path on its return and is brought to the same position on the optical axis as the original exciting laser beam. This process is called *descanning*. The fluorescent light then passes through a dichromatic mirror and becomes focused at the confocal pinhole. Because descanning is instantaneous, the image in the pinhole always remains steady and does not move back and forth like the beam in the plane of the specimen; however, the focused spot varies in intensity over time as the spot excites different locations in the specimen.
- Fluctuations in light intensity are converted into a continuously changing voltage (an analog signal) by the PMT detector. The analog signal is digitized at regular

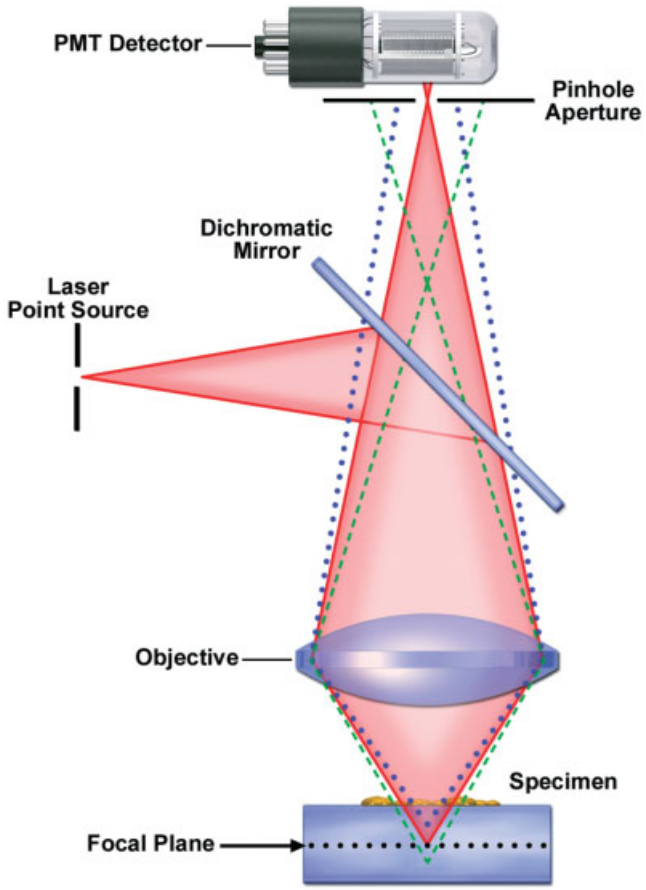

Figure 13.4

The confocal principle in epi-fluorescence laser scanning microscopy. Excitation wavelengths from a laser point source are confocal with a scanning point in the specimen. Fluorescent wavelengths emitted from a point in the specimen are focused as a confocal point at the detector pinhole (red waves). Fluorescent light emitted at points above (blue dots) and below (green dashes) the plane of focus of the objective is not confocal with the pinhole and forms extended disks in the plane of the pinhole. Since only a small fraction of light from out-of-focus locations is delivered to the PMT detector, out-of-focus information is largely excluded from the detector and final image. The dichromatic mirror and emission filter (the latter is not shown) perform the same functions as in a widefield epi-fluorescence microscope.

time intervals by an analog-to-digital converter to generate pixels (digital picture elements) that are stored in an image frame buffer board and are displayed on a computer monitor. Thus, a confocal image of an object is reconstructed from photon signals that are built up over time and displayed on the computer monitor; the confocal image never exists as a real image that can be seen by the eye in the microscope.

- A microscope system of this design is called a *confocal laser scanning microscope* (*CLSM*).

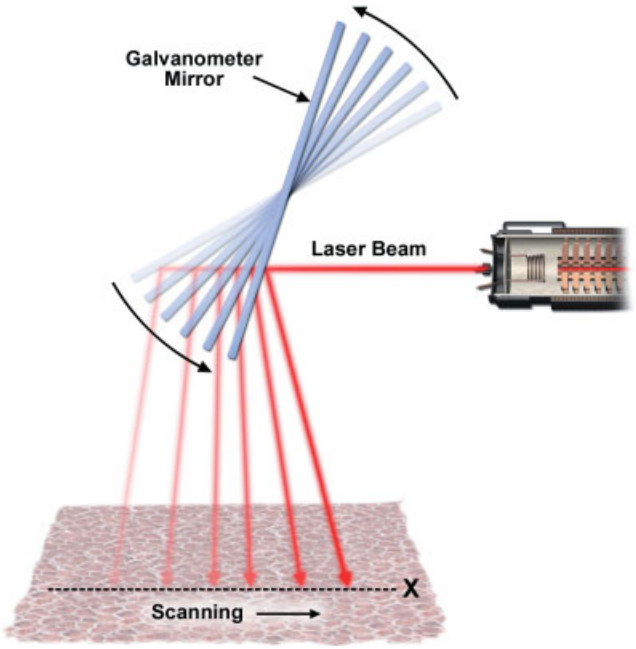

Figure 13.5

The scan-control mechanism in a CLSM. The sketch shows the delivery of the excitatory laser beam to the specimen by one of two galvanometer-driven mirrors that vibrate in mutually perpendicular axes within the confocal scan head. One mirror controls scanning along the *x*-axis, the other along the *y*-axis; both motions are coordinated to generate a pattern of a raster on the specimen. The speed and angular extent of deflection of the mirrors can be controlled to regulate the scanning rate and the extent of the scan.

Demonstration: Isolation of Focal Plane Signals with a Confocal Pinhole

Warning

Care should be taken not to accidentally reflect the light beam into the eye during the exercise!

To become familiar with confocal optics, construct the confocal reflection optical system shown in Figure 13.6 using common optical components mounted on an I-beam optical bench, a small diode or HeNe laser (1–5 mW), and a coin as a specimen. The specimen support plate must be rigid enough so that you can slide a coin or other reflective specimen on its surface without moving the plate. Position the objective so that reflections from the coin are refocused at the pinhole aperture (a pinhole pierced in a white card) mounted in the confocal image plane. A white card allows you to see if the laser beam is diffuse or focused at the pinhole. The detector behind the pinhole can be a white screen for visual inspection, or for demonstration before a large group, a video camera connected to a TV monitor. Fluctuations in light intensity reaching the camera are seen as a brightening or darkening on the monitor. Note that a large portion of light from the laser passes

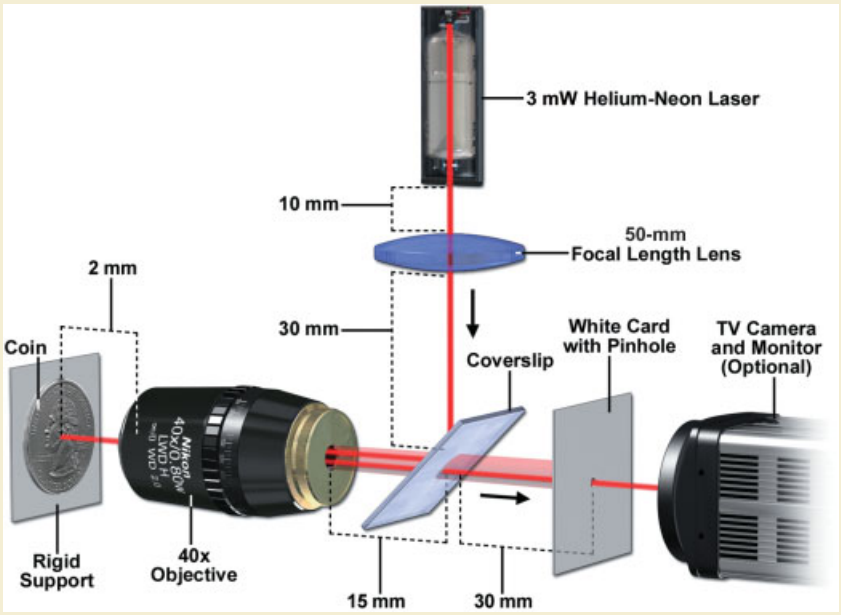

Figure 13.6
Optical bench for demonstrating confocal reflection optics.

through the coverslip instead of being reflected toward the objective, and that a large portion of light is reflected back to the laser instead of being transmitted to the pinhole. With a 1- to 3-mW laser, sufficient light will reach the pinhole.

- Use a reflective specimen, such as a coin with a high relief surface (or some other reflective irregular surface), that can be held up against a rigid but adjustable support. Move the support and coin back and forth along the I-beam until the laser beam appears as a tightly focused spot on the surface of the coin. As the coin is moved on a rigid surface in the specimen plane, adjust the position of the objective (and/or pinhole support) so that reflections from the highest points on the coin are focused as a bright spot at the pinhole and give a bright signal on the camera monitor screen.
- Reflected light from out-of-focal-plane features (recessed background regions on the coin) forms an expanded 5- to 10-mm disk at the pinhole rather than a focused point. The decreased transmission of photons through the pinhole is seen as a darkening on the TV monitor. The rejection of out-of-focal-plane signals is easy to observe.
- If the coin is moved around on its support plate as it is scanned by the fixed laser beam, the pinhole screen and monitor show bright and dark signals that look like flickering, but an actual image is not observed. This reinforces the idea that the confocal signal is a continuously changing voltage, not an image. In the scan head of an actual confocal system, the voltage signal is digitized at regular intervals into pixel values that are stored in a computer in an image frame buffer board and displayed on a computer monitor.

ADVANTAGES OF CLSM OVER WIDEFIELD FLUORESCENCE SYSTEMS

The principal gain in imaging performance using CLSM is the ability to optically section through fluorescent objects up to 10- to 50-μm thick or to obtain high contrast images of surface topologies using confocal reflection optics. Contrast and definition are improved, sometimes considerably, due to the reduction in background signal and a greatly improved signal-to-noise (S/N) ratio. With a stack of images representing different focal planes spaced at regular intervals along the optical axis (the *z*-axis), the specimen can be displayed in a variety of ways:

- *Composite or projection view*, where the information contained in an image stack is projected into a single focused image. Consider a three-dimensional object, such as a fluorescent neuron with thin extended processes in a tissue section. In a single widefield fluorescence image, out-of-focus processes appear blurry and indistinct. A single confocal image shows the muscle tissue as a pattern of bright and dark blotches, but a composite view of all of the focal planes contained in a stack or *z*-series shows the muscle fibers clearly and uniformly labeled (Fig. 13.7).
- *Three-dimensional views* of an object can be obtained using a *z*-stack of confocal images and computer software. Most confocal software programs can display an object in 3D at different angular perspectives with rotation about the *x*-, *y*-, or *z*-axis, or a combination of axes. This mode of viewing is valuable for examining complex three-dimensional objects, such as columnar epithelial cells and details in thick tissue sections (Fig. 13.8).

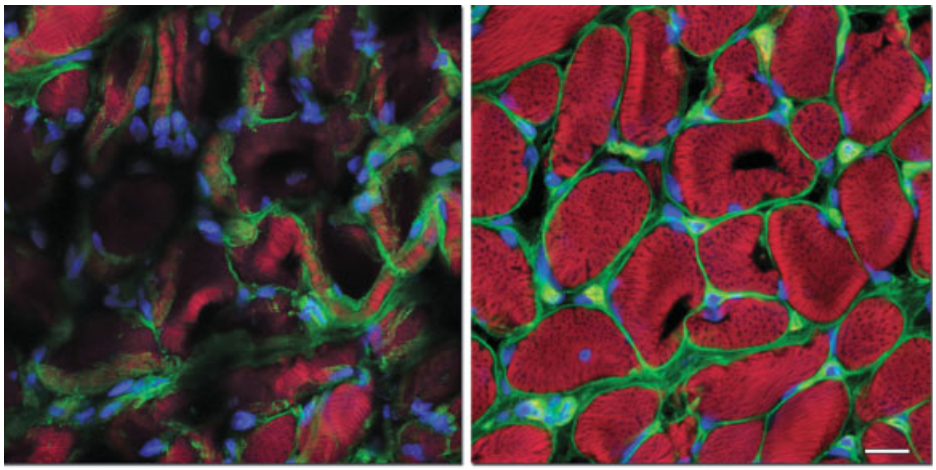

(a) (b)

Figure 13.7

Single optical section and a composite or projection view of muscle fibers in a 16-μm thick section of rat diaphragm tissue. Alexa Fluor 488 conjugated to wheat germ agglutinin (green) was used to highlight extracellular matrix structures and Alexa Fluor 568 conjugated to phalloidin labels actin in the myofibrils (red). Nuclei were counterstained with DAPI (blue). (a) Single optical section of the muscle fibers. (b) A composite of 20 optical sections form the projection view. Complete diaphragm muscle structure is revealed, as contrasted by the limited number of structural elements in the single optical section. Bar = 20 μm.

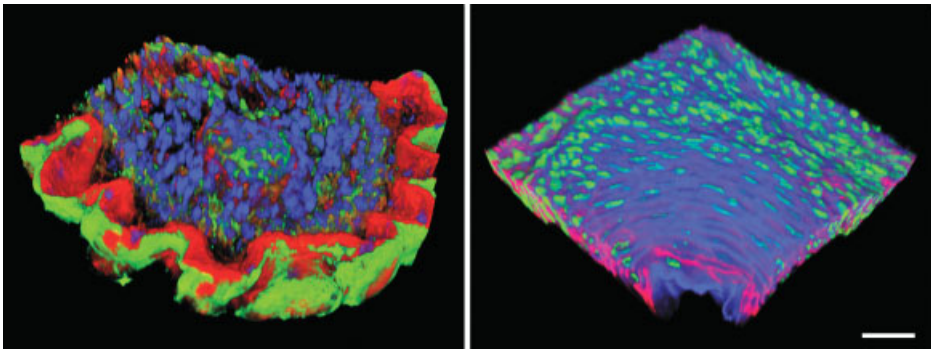

(a) (b)

Figure 13.8
Volume views of triple-stained rodent embryo tissue. (a) Mouse embryo (17 day) section (30 μm) stained with Alexa Fluor 488 conjugated to wheat germ agglutinin (labels glycoproteins), Alexa Fluor 568 conjugated to phalloidin (filamentous actin), and DAPI (nucleus). (b) Rat embryo (19 day) section (30 μm) immunofluorescently stained with Alexa Fluor 350 (glycoproteins), Alexa Fluor 568 (actin), and SYTOX Green (nuclei). Bar = 20 μm.

- Transverse *x–z* or *y–z cross-sectional views* can be generated by most confocal software programs. The object appears as if it had been cut transversely—that is, in a plane oriented parallel to the optical axis.
- *Five-dimensional views*, including information in *x*, *y*, and *z* dimensions, in a timed sequence, and in multiple colors. Such sequences can be displayed as a three-dimensional, multicolor movie in real time or time-lapse mode. Five-dimensional viewing will become more convenient as computer processing speed and storage capacity continue to improve.

The following additional advantages of CLSM should also be considered:

- Magnification can be adjusted electronically by varying the area scanned by the laser (zoom factor) without having to change the objective. Since the display area of the monitor remains unchanged, the image appears magnified or zoomed.
- Digitization by an *analog-to-digital converter* transforms the continuous voltage signal into discrete digital steps of light intensity, thus allowing you to obtain quantitative measurements of fluorescence intensity.
- There are few restrictions on the objective. However, for accurate color focus and proper spatial resolution of light intensities, high numerical aperture (NA) fluorite or apochromatic oil immersion objectives should be employed. Using the *zoom* feature on most confocal microscopes (see below), lower magnification 40 and 60× objectives that have high light transmission can be used to capture high-quality images instead of higher magnification 100× objectives that are compromised by lower light transmission efficiency.
- Epi-illumination and point scanning are ideal for *confocal reflection microscopy*, in which the laser beam scans the three-dimensional surface of a reflective object.

Fluorescence filter sets are not used for this mode of imaging; rather, the focused spot of the laser is reflected off the surface. Reflections from features lying in the focal plane pass through the confocal pinhole aperture, whereas light from reflections above and below the focal plane is largely excluded just as in confocal fluorescence microscopy.

CRITERIA DEFINING IMAGE QUALITY AND THE PERFORMANCE OF AN ELECTRONIC IMAGING SYSTEM

The quality of a confocal image or any image is determined by four principal factors:

1. Spatial resolution
2. Resolution of light intensity (dynamic range)
3. S/N ratio
4. Temporal resolution

Spatial resolution describes the smallest resolvable distance between two points in an image. Resolution between two points in the image plane and along the *z*-axis depends on the excitation and fluorescence emission wavelengths and the NA of the objective and settings in the confocal scan head. The NA of the objective is crucial, since this determines the size of the diffraction-limited scanning spot on the specimen and the size of the focused fluorescent spot at the pinhole. The role of the NA in determining spatial resolution has already been discussed (see Chapter 6). In widefield fluorescence optics, spatial resolution is determined by the wavelength of the emitted fluorescent light; in confocal mode, both the excitation and emission wavelengths are important, because the size of the scanning diffraction spot inducing fluorescence in the specimen depends directly on the excitation wavelength. (See Chapter 5 for the dependence of the size of the diffraction spot on the wavelength of light.) Thus, unlike widefield fluorescence optics, the smallest distance that can be resolved using confocal optics is proportional to $(1/\lambda_1 + 1/\lambda_2)$, and the parameters of wavelength and NA figure twice into the calculation for spatial resolution (Pawley, 2006; Shotton, 1993; Wilhelm et al., 2010).

In the confocal microscope, spatial resolution also depends on the size of the pinhole aperture at the detector, the zoom factor, and the scan rate, which are adjusted using software that controls the scan head. Decreasing the size of the pinhole reduces the thickness of the focal plane along the *z*-axis, thereby allowing higher resolution in optical sectioning, which is essential for high-quality projection images and high-resolution three-dimensional viewing. Reducing the size of the pinhole also improves contrast by excluding out-of-focal-plane sources of light. Under certain conditions, the lateral spatial resolution in the *x,y*-plane obtainable in a confocal fluorescence microscope can exceed that obtainable with widefield optics by a factor of ~1.4, a condition sometimes called *superresolution*. Normally, the detector pinhole is adjusted to accommodate the full diameter of the diffraction disk. However, if the pinhole is stopped down to about one-quarter of the diffraction spot diameter, the effective spot diameter is slimmed down so that the disk diameter at one-half maximum amplitude is reduced by a factor of ~1.4. Oldenbourg et al. (1993) have shown that contrast is also improved by stopping down the pinhole.

As referenced by R. Webb in Pawley (2006), the minimum resolvable distance d between two points in the horizontal x,y-plane of the confocal microscope can be approximated as:

$$d_{x,y} \approx 0.4\lambda/\mathrm{NA}.$$

Resolution along the z-axis is described:

$$d_z \approx 1.4\lambda n/\mathrm{NA}^2.$$

The effect of pinhole diameter on section thickness is described below. The effects of zoom factor and scan speed on resolution are also discussed later in the chapter. A constricted pinhole in confocal optics increases horizontal resolution in the x,y-plane by a factor of ~1.4 but decreases the axial resolution by the same factor. The effects of zoom factor and scan speed on resolution are discussed later in this chapter.

Dynamic range (DR) describes the *resolution of light intensity* in the image and is defined as the number of gray levels that are assigned to an image by the analog-to-digital converter. The DR of the PMT detector is defined as the ratio of the saturated signal to the detector readout noise, and is calculated in volts or electrons. The DR of a detector is therefore an inherent feature of the imaging system. To achieve the imaging potential of the detector, the operator should try to acquire images that fill its dynamic range, from black (no signal) to white (saturating signal). This is accomplished by adjusting the amplitude range of the photon signal using the electronic gain and offset controls of the PMT. The procedures for adjusting gain and offset are discussed in this chapter.

Signal-to-noise (S/N) ratio defines the degree of visibility or clarity of an image. It depends directly on the amplitudes of the object and its background, and on the electronic noise of the imaging system. For bright images, S/N is determined mainly by the intensities of the specimen and background; however, for dim images, the electronic noise of the imaging system becomes a determining factor. Image brightness at the pinhole is affected by many variables, including laser power, fluorophore density in the specimen, NA of the objective, confocal zoom factor, raster scan rate, the choice of fluorescence filter sets, and other factors. Reduced photon optical system throughput and/or noisy performance by the detector can result in images that lack contrast and appear grainy. Generally, there is little we can do to improve the imaging performance of a detector other than to provide more light. Typically 50–100 photons/s/pixel are detected from a moderate to bright specimen by CLSM, which corresponds to an S/N ratio of 25 for a sensitive confocal system. This value compares with maximum S/N ratios of 100 to several hundred for video and digital CCD camera systems. Thus, the image quality of a bright object in confocal is okay, but not good or excellent. The usual way to improve S/N is to increase the amount of light by reducing the scan rate or opening the pinhole. Alternatively, a number of individual frames can be averaged, which is called *frame averaging or Kalman averaging*, because S/N improves in proportion to the square root of the number of averaged frames. We return to the topic of improving S/N later. One of the compromises in obtaining optical slices by confocal imaging is a reduction in photons contributing to the image and therefore to image quality.

Temporal resolution depends on the raster scan rate and the processing rates of the detector, the analog-to-digital converter, and the computer. Frames are typically cap-

tured at a rate of 1–2 per second (fps) for a 512 × 512 pixel image, but rates of 100 fps or higher can be acquired for images of limited size.

In summary, optical performance in the confocal microscope is affected by several variables, all of which must be evaluated and controlled by the microscopist. It almost never happens that time, space, and intensity are all resolved optimally for a given combination of specimen and microscope. Generally, it is necessary to make compromises. For example, to optimize resolution of light intensity to obtain smooth looking images with high S/N ratio, one could decrease the spatial and/or temporal resolution of the image. Recognizing how to balance these parameters requires education and experience and is the key to successful confocal imaging.

CONFOCAL ADJUSTMENTS AND THEIR EFFECTS ON IMAGING

A number of mechanical adjustments made in the confocal software affect the brightness and resolution of the image. These include adjustments for:

- Detector pinhole aperture
- Laser scan rate and image size
- Zoom factor
- Laser selection and laser intensity
- Gain and offset of the PMT detector
- Objective selection

Pinhole Adjustment

The pinhole aperture mounted in the image plane of the microscope is the heart of confocal imaging. This simple optical device acts as a filter to remove the majority of fluorescent signals that have their origin outside of the focal plane. Many parameters are affected by the adjustment of the pinhole, including focal plane thickness, spatial resolution, image brightness, and susceptibility to photodamage. Since the pinhole is frequently adjusted to control these parameters, the confocal operator needs to become familiar with its effects. The pinhole is a typically square or hexagonally shaped aperture, created by two partially overlapping notched metal blades, which are motorized to vary the aperture diameter from ~0.1 to 1.0 mm. The pinhole is adjusted to accommodate the diameter of the Airy disk that is the sole object of the confocal image. The effect of the pinhole diameter on the thickness of the optical section is shown in Figure 13.9. As already described, a small pinhole gives the thinnest optical section. It also improves horizontal resolution and contrast in the image. However, reducing the size of the pinhole too much also decreases the number of photons reaching the detector. If we compare two images of comparable amplitude made at different pinhole settings, the image corresponding to the smaller pinhole diameter requires a longer exposure, and causes more photobleaching, for the same S/N ratio. A wide pinhole setting reduces confocality, but also increases photon flux and reduces photobleaching by requiring shorter exposures. If we compare images made at different pinhole settings but with the same exposure time, we see that the image acquired using a wider pinhole is brighter and contains less noise.

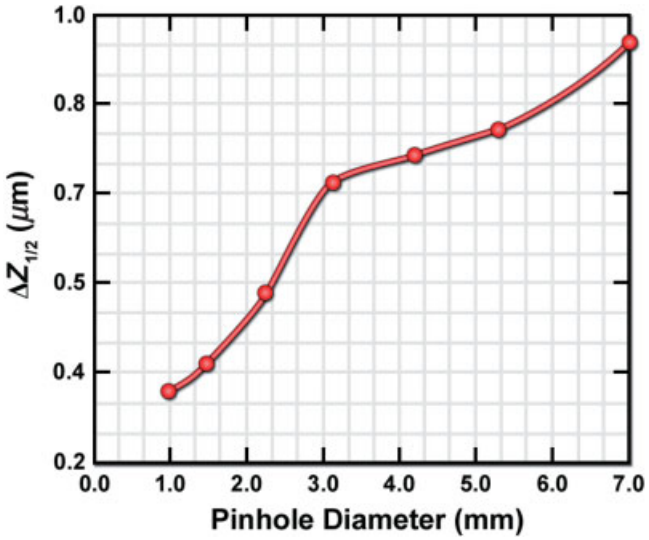

Figure 13.9

Confocal microscope pinhole diameter versus optical section thickness. The thickness of the optical section through the *z*-axis of the confocal image (*Z*) is plotted versus the diameter of the pinhole aperture in millimeters. Fluorescent beads (0.2 μm) were examined with a Nikon Plan Apo 60×, 1.4 NA oil immersion lens. Smaller pinhole sizes are used in today's instrument designs.

The optimum average pinhole setting corresponds to an aperture giving 50% of maximum intensity. At this position, ~75% of the light of the Airy disk still passes the pinhole, and resolution will be 20% better than obtained by a widefield fluorescence system. This corresponds to a pinhole diameter that is slightly smaller than the first dark ring in the Airy disk pattern.

Scan Rate, Image Size, and Dwell Time

Picture elements or *pixels* and volume elements or *voxels* are the basic spatial units that compose 2D and 3D digital images acquired by the confocal microscope. Unlike silicon area array detectors like CCD cameras, where pixels are actual physical units, pixel size in confocal microscopy is adjustable and is defined by settings made in the acquisition software (see the box for an explanation of how voxels are used to define a 3D confocal image). Here is how the pixel size is determined. The user first selects the number of pixels for resolving the image, typically in the range of 512×512 to 1024×1024, although arbitrary numbers can also be used. If the area to be covered on the specimen is 100×100 μm, the pixels in a 512-pixel image would each be 0.2 μm. Since a scanning laser spot moves over the image at a given rate, each pixel is also defined as a time interval equal to the time required for a full deflection on the *x*-axis divided by 512. The time interval is set in the software. This interval is also called the *laser dwell time*, the length of time the laser dwells on an area of the specimen that corresponds to one pixel in the image. If the scan rate is increased, the pixel clock changes, and the time interval corresponding to one pixel is reduced.

The Voxel Concept in Confocal Images

Every image produced by a confocal microscope and projected onto the surface of the PMT detector is an "optical section," a two-dimensional representation of a specimen that really exists in three-dimensional space. The image of a particular section is divided into a 2D array of pixels, represented graphically by *x* and *y* coordinates. In the confocal microscope, pixel size is determined by the lateral resolution and magnification of the objective, as well as electronic factors, such as zoom factor and the number of pixels assigned to the *x* and *y* dimensions in the image. A volume element or *voxel*, includes the *x*, *y* dimensions plus a *z* dimension, which is the step size between optical sections along the *z*-axis of the microscope (see Fig. 13.10). The operator can change the *z*-step size depending on the NA and magnification of the lens and pinhole size. These parameters govern the dimensions of the point spread function and determine how big the voxel should be (Chapter 6). Voxels are the basic spatial unit in 3D confocal imaging.

Voxels having equal dimensions along each axis are called *isotropic voxels*, whereas those having different dimensions in at least one of the planes are called *anisotropic voxels*. Each voxel in an image has a unique digital address within 3D space (*x*, *y*, and *z*) and is assigned a single intensity value. Voxel information can be retrieved to display a single optical section in the specimen, and multiple planes can be stacked to generate a 3D map or volume rendering of the entire specimen. Digital voxels can be manipulated during image processing in a manner similar to 2D pixels (see Chapters 17 and 18), such as histogram stretching or unsharp mask filtering.

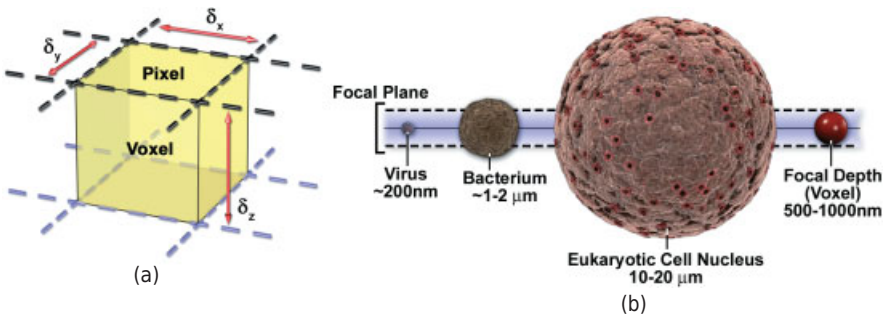

Figure 13.10

To illustrate the voxel concept, a sub-resolution fluorescent point object can be described in three dimensions with an *x*,*y*,*z* coordinate system, as illustrated in panel a. The typical focal depth of an optical microscope is shown relative to the dimensions of a virus, bacteria, and mammalian cell nucleus in panel b.

If the amplitude of deflection of the galvanometer mirrors is small and the scan rate is high, a smaller image area can be presented on the monitor at rates up to hundreds of frames per second. High-speed sampling (20–30 fps) gives the appearance of a live image on the monitor and is convenient for focusing the specimen. High speed is also useful for monitoring rapid kinetic events in the specimen. With rapid scanning, the dwell time can be reduced to about 0.1–1.0 μs/pixel. In contrast, a large amplitude deflection of the galvanometer mirrors coupled with a slow scan rate produces a large-size image at high resolution but at a rate of 1 fps or slower. For high resolution imaging of fixed, stained fluorescent specimens, the capture rate is typically 2–4 fps for an area covered by 512 $\times$ 512 pixels. The scan rate options indicated in the confocal software accommodate a range of scanning speeds and image sizes. It is useful to remember that the pixel size changes depending on the image size and zoom factor selected by the user and that the values of these parameters are readily available from the software. Of significance for successful imaging, one should also remember that the scan rate and dwell time directly affect the rate of photobleaching of the specimen (slower scan rates bleach more), the S/N ratio in the image (faster scanning reduces S/N), and in living specimens, the amount of photon-induced damage (faster rates decrease damage).

Zoom Factor

Electronic zoom is used for two reasons: (1) to reduce pixel size and maintain spatial resolution, and (2) to magnify the image for display and printing. Implementing the zoom command while maintaining the same number of pixels in the image causes the galvanometer scanners to cover a smaller area on the specimen and scan at a reduced rate. Since a smaller area of the specimen now fills the whole monitor, the image appears zoomed in or magnified (Fig. 13.11). Zooming also reduces the size of the pixels, a consequence of using the same pixel format (512 or 1024, etc.) to cover a smaller area on the specimen. However, if significant changes in magnification are required, it is always preferable to use a higher power objective rather than increase magnification electronically using the zoom, because the higher-magnification, higher-NA objective gives better image resolution and definition. In most cases, zoom control is used to make minor adjustments in the magnification and to adjust the pixel size to maintain resolution. However, specimens photobleach faster at higher zoom factors because the same amount of laser light is delivered to a smaller area at a slower speed when the zoom is increased. The effect of increasing the zoom on reducing the size of the image, decreasing pixel size, and improving resolution is shown in Figure 13.12.

To preserve the maximum resolution afforded by the objective, you should calculate and employ the required zoom factor. Using the resolution equation for confocal imaging, a 100×/1.35 NA objective receiving 520-nm blue-green light is calculated to have a spatial resolution of 0.20 μm. The required sampling interval is then calculated as 0.20 μm/2 = 0.1 μm. The factor of 2 means that there are two samples per spatial unit of 0.20 μm, and it is related to the requirements of the Nyquist sampling theorem for maintaining the spatial resolution provided by the optics. We discuss this topic in greater detail in Chapter 17. The sampling period of any given zoom setting is usually indicated in a statistics table that accompanies an image. If the sampling period is not indicated on the monitor or in an image statistics menu, the dimensions of the scanned field can be adjusted with the zoom command to obtain the same result. The correct size is determined as the desired sampling period times the number of pixels across

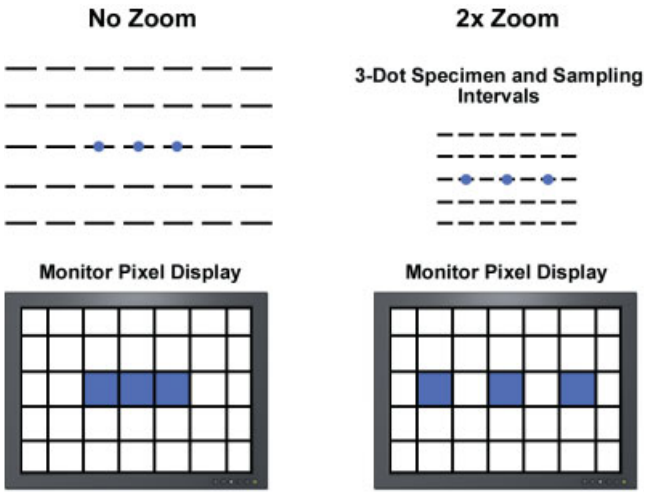

Figure 13.11

Effect of electronic zoom on electronic sampling and image resolution. Increasing the zoom factor reduces the area scanned on the specimen and slows the rate of scanning. The increased number of sampling intervals (pixels) along a comparable length in the specimen increases the spatial resolution and magnifies the display on the monitor. Zoom is employed when it is necessary to preserve the diffraction-limited optics of the objective and optical system.

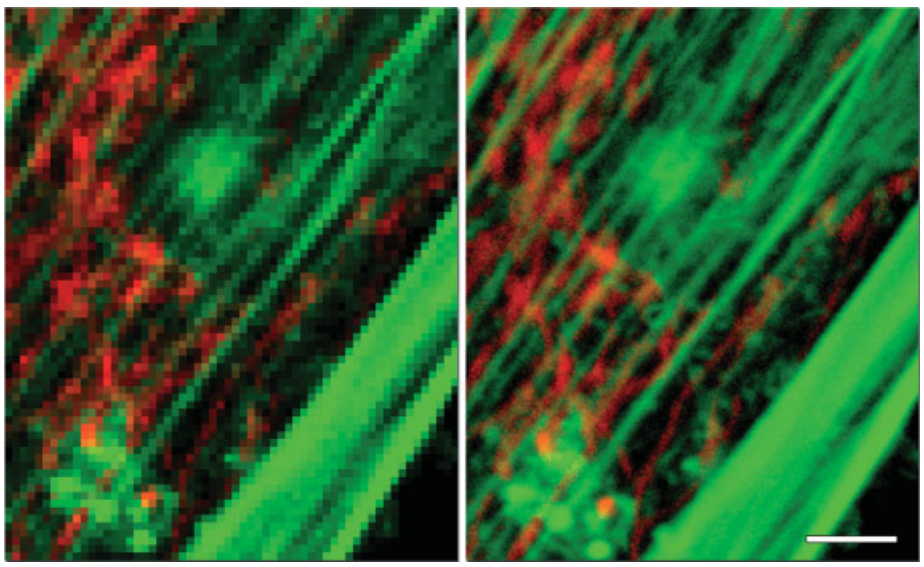

(a) (b)

Figure 13.12

Effect of zoom on confocal image resolution. Bovine pulmonary artery endothelial cells labeled with BODIPY FL-phalloidin (green, actin filaments) and MitoTracker red (red, mitochondria) were imaged on a point-scanning confocal microscope with a 20× objective in a pixel format of 1024 × 1024 with 1× zoom (a) and with 4.3× zoom (b). (BODIPY and MitoTracker dyes are available from Life Technologies.) When shown at equal magnification, the image acquired with 1× zoom appears undersampled and pixelated. Bar = 2 μm.

one edge of the image. For an image format of 512×512 pixels, we calculate $512 \times 0.1\ \mu m = 51\ \mu m$ as the required size of the scanned area.

Zoom settings above and below the optimum value are called *oversampling* and *undersampling*. Oversampled images (zoom too high) are a bit smoother and easier to work with in image processing, but the rate of photobleaching is greater. Undersampling (zoom too low) degrades the spatial resolution provided by the objective, but reduces the rate of bleaching. Undersampling is sometimes used in live-cell imaging to optimize viability. For low magnification applications using low NA objectives, the Nyquist sampling factor may need to be as high as 3–4 (instead of 2) to maintain the resolution provided by the objective.

Lasers for Fluorophore Excitation

Confocal microscopes employ several types of lasers to obtain the wavelengths required for fluorophore excitation and to guarantee sufficient fluorescence intensity at the confocal pinhole. A variety of lasers—diode lasers, diode-pumped solid state lasers, and noble gas ion gas lasers containing helium-neon and argon—provide excitation lines across the visible spectrum, the most common being lines at 405, 440, 458, 488, 515, 532, 561, 594, 633, and 647 nm (see Table 13.1).

The laser beam is expanded by a lens to fill the rear aperture of the objective uniformly to give the minimum-size focused spot on the specimen. Because the rear aperture of the objective must be evenly illuminated across its diameter, and since the light intensity profile across a laser beam is Gaussian and not flat, the beam is overexpanded somewhat so that the portion filling the lens is more uniform. The power of lasers fitted by manufacturers for confocal illumination (range, 5–50 mW) is chosen based on the factor of light loss from beam spreading and the intensity of light required to give close to saturating excitation of the appropriate fluorophores in the focused beam in the specimen.

Laser power is commonly adjusted with an *acousto-optic modulator (AOM)*. For systems with several laser wavelengths, either a selection of dichroic filters or an *acousto-optic tunable filter (AOTF)* is used to select a specific laser line for excitation. Normally lasers are operated at or below their mid-power range during acquisition to prolong the lifetime of the laser, and in cases where specimens are subject to photobleaching or biological damage, laser beam intensity is reduced to a point where fluorescence emission is still adequate for acquiring an image. Since a focused laser beam

TABLE 13.1 Solid-State and Gas Lasers for Confocal Microscopy

	Wavelength (nm)			
Laser Type	Violet	Blue	Green	Red
Argon-ion		458, 477, 488	515	
Helium-neon			543	594, 633
Diode	405	440, 473, 488	539, 559	638, 647
Diode-pumped solid state			532, 561	640

of just a few milliwatts can damage the eye, confocal microscopes contain an *interlock device*, an electromechanical shutter, which is automatically actuated to prevent the operator from seeing the laser when looking through the eyepieces during laser scanning or during visual inspection of the sample.

A recently introduced option for illumination in the confocal microscope is the *supercontinuum white light laser*. Leica Microsystems currently offers this option on its SP5-X confocal microscope system, and other confocal manufacturers will probably follow. Supercontinuum lasers offer high brightness and broad spectral coverage, making them valuable for microscopy. The advantage for confocal imaging is complete freedom in creating an excitation bandwidth of any size and wavelength region in the visible and near-infrared (IR) spectrum to optimally excite fluorophores. This degree of versatility is not currently available, even using a collection of fixed wavelength lasers. Supercontinuum lasers are based on an IR, mode-locked laser, whose narrowband IR output is converted to a broad spectral bandwidth that covers the visible and near IR spectrum (Fig. 13.13). Spectral broadening, a kind of laser rainbow effect, is achieved by passing the beam through a strongly nonlinear medium, such as a short segment of photonic crystal fiber with high spectral dispersion. Spatial coherence of selected bandwidths within the white light spectrum remains very high and is suitable for confocal imaging. Wavelength and intensity are controlled with an AOTF and *acousto-optic beamsplitter (AOBS)*, making it easy, fast, and convenient to select any excitation wavelength. The system is very useful for on-the-fly adjustments in FRET and other applications.

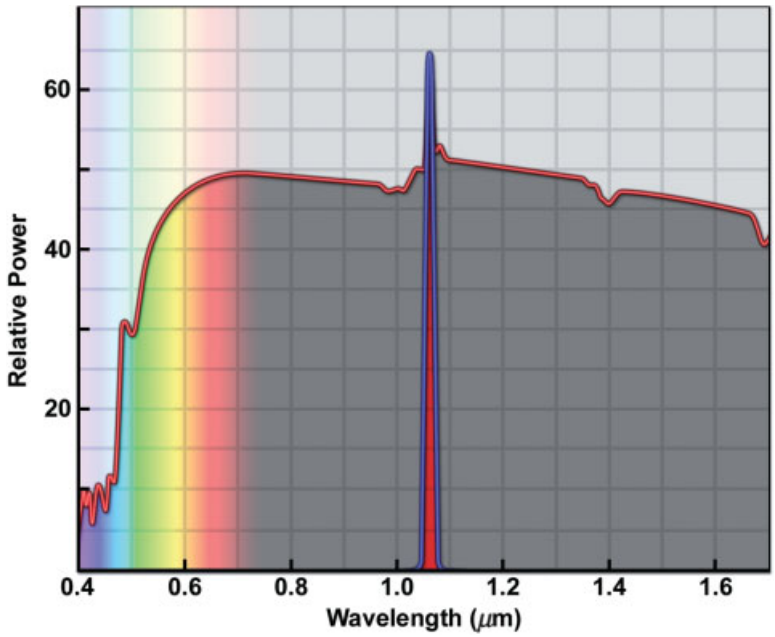

Figure 13.13

Spectrum of a supercontinuum white light laser. The emission line of a pulsed, mode-locked laser (narrow band under the blue curve) becomes broadened into a continuum of emission wavelengths (red curve) by a suitably matched photonic crystal fiber. The broadened spectrum looks like white light. Bands of wavelengths ranging from blue-violet to IR suitable for confocal imaging (white light) are both bright and coherent.

Gain and Offset Settings of the PMT Detector

The gain and offset controls of the PMT are used to adjust the light intensities in the image to match the full dynamic range of the detector (Fig. 13.14). These adjustments assure that the maximum number of gray levels is included in the output signal of the PMT. After digitization in the computer, the photon signal is displayed as shades of gray ranging from black (no signal) to white (saturating signal) on the computer monitor. PMTs with a dynamic range of 10 or 12 bits have 2^{10} (1024) or 2^{12} (4096) gray levels, respectively, which is also the number of gray levels in the respective image files in the computer. Setting the gain and offset of the PMT should not be confused with adjusting the contrast and brightness of the image during image processing. Processing can stretch existing pixel values to fill the black-to-white display range on the monitor, but can never create new gray levels. Thus, when a poorly captured image containing only 50 out of a possible 4000 gray levels is stretched from black to white during image processing, the resulting image looks grainy. Sometimes,

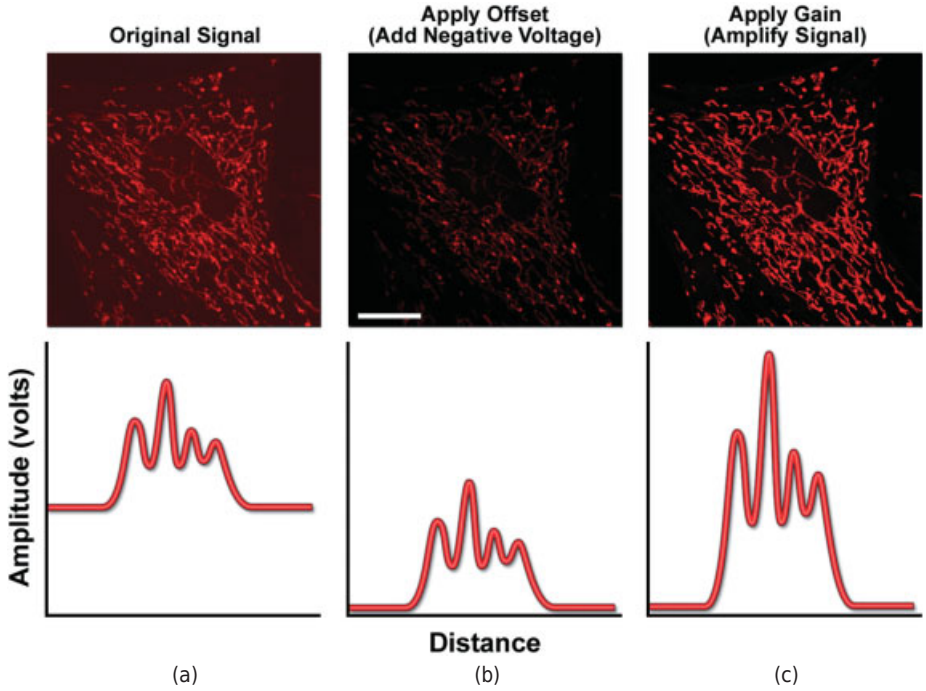

Figure 13.14

Adjustment of gain and offset. Gain and offset are electronic controls used to stretch the available photon signals from an object to fill the dynamic range of the detector in order to include the maximum number of gray levels, from white to black, in the captured image. In the example above, the specimen is a bovine pulmonary artery cell labeled with MitoTracker red (a) showing a high degree of background due to unbound fluorophore. (b) Offset adds a voltage (positive or negative) to the output signal so that the lowest signals just approach the threshold for detection on the PMT (black level). (c) Gain amplifies the signal by multiplying the output voltage from the PMT by a constant factor prior to its digitization at the analog-to-digital converter. Gain should be increased until the maximum signal values just approach saturation. Offset should be applied first before adjusting the gain. Bar = 20 μm.

it is not possible to fill all of the gray levels during an acquisition, but ordinarily this should be the goal. We will discuss the gray level ranges of images in Chapters 17 and 18.

Offset is an electronic adjustment that adds a positive or negative voltage to the signal so that a selected background signal corresponds to a PMT output of ~0 V (black). *Gain* is an electronic adjustment that amplifies the input signal by a voltage multiplication process that causes it to be assigned to a higher gray level value. Generally, offset should be set first, followed by adjustment of the gain. Increasing the gain beyond its optimal setting can make an image look somewhat grainy, but it is sometimes desirable to capture the maximum number of gray levels, even if the gain must be increased somewhat to do so. In practice, these adjustments are often made using a special color display function to depict pixel values on the monitor. In one commonly used function, the saturating pixels (typically the top 2%) are shown in red, black-level pixels (bottom 2%) are shown in blue, and all intermediate gray levels are shown in shades of gray. When properly adjusted, a few red and blue pixels will be seen in the image, indicating that the full dynamic range of the PMT is being utilized.

Objective Selection

The quality of the confocal image is critically dependent on the optical performance of the objective. The objective should be well corrected for chromatic and spherical aberrations discussed in Chapter 4, because different color wavelengths must be focused precisely both on the specimen and in the confocal pinhole. Off-axis aberrations of the objective, such as coma and astigmatism, must also be corrected to a high degree. First, the objective must form a well-defined diffraction spot on the specimen and at locations on and off the optical axis; second, emitted fluorescence wavelengths must be collected and focused to a spot in the pinhole. The NA of the objective is important, because it determines the spatial resolution in the horizontal and vertical dimensions, as well as the brightness of the image and the depth of focus in the specimen (Chapter 6). Image brightness (photon flux per area per unit time) is also determined by the NA and is of great practical importance for confocal microscopy. Since the amount of light reaching the PMT is usually small, we are frequently forced to operate the confocal system at high electronic gain, which tends to produce noisy images. Since image brightness is proportional to NA^4/Mag^2 (Chapters 4 and 6), system gain can be reduced and image quality improved by providing a brighter diffraction spot at the pinhole with a high NA objective. For these reasons, a well-corrected plan-fluorite or plan-apochromatic objective of 60–100× magnification is ideal for the examination of cellular details.

In addition to the confocal pinhole, the objective plays an equally important role in determining depth of field in the specimen, the thickness of the optical slice represented in a confocal image. Since depth of field is proportional to λ/NA^2 (Chapter 6), high-NA objectives reduce the size of the diffraction spot for laser excitation in the specimen and define a thinner focal plane. Reducing the size of the pinhole diaphragm also defines the thickness of the confocal optical section, but only to the limit set by the microscope optics. Therefore, it is the combination of high NA objectives and small pinhole apertures that generates the thinnest optical sections. The effects of the objective and principal mechanical adjustments on image brightness and spatial resolution are summarized in Table 13.2.

TABLE 13.2 Effect of Increasing Confocal Parameters on Image Intensity and Spatial Resolution

Parameter	Effect
↑ Pinhole diameter	↑ Intensity ↓ Spatial resolution
↑ Zoom	↑ Intensity ↑ Spatial resolution
↑ Scan rate	↓ Intensity ↑ Temporal resolution
↑ Objective NA	↑ Intensity ↑ Spatial resolution

PHOTOBLEACHING

Confocal specimens are subject to photobleaching from repetitive exposure to the intense beam of the laser. The rate and extent of bleaching are generally greater than for specimens examined with a widefield fluorescence microscope and can make it difficult to obtain suitable images of weakly fluorescent specimens. If an immunolabeled specimen appears dim and its image does not look acceptable due to improper staining, a new specimen should be prepared. Otherwise, photobleach-resistant dyes such as cyanine dyes or Alexa Fluor dyes can be used in combination with a good antifade reagent, such as Prolong Gold, SlowFade Gold, or Vectashield. To reduce the rate of photobleaching, the microscope operator can do one or more of the following:

- Reduce the beam intensity (AOTF control, neutral density filter, laser power) while increasing the gain.
- Scan at a faster rate while increasing the gain.
- Widen the pinhole (least attractive option, as this action reduces the confocal effect).
- Reduce the number of frames used for frame averaging.

For *z*-series intended for three-dimensional viewing, the operator can sometimes collect the stack of images from front to back so that more distant details, made dimmer by photobleaching from repetitive scanning, match the viewer's expectations that fluorescent signals from more distant locations will appear fainter in the three-dimensional view.

GENERAL PROCEDURE FOR ACQUIRING A CONFOCAL IMAGE

Acquiring a confocal image involves adjusting each of the instrument and specimen parameters just described and usually proceeds as follows:

1. *Prepare for acquisition.*
   - Focus the specimen in fluorescence widefield mode.
   - In the acquisition software, pick the appropriate laser line and filters (dichromatic mirror and emission filter) and PMTs.
   - Adjust the system for low intensity transmission (5% transmission on AOTF and 1–2% laser power).
   - Check that the offset settings of the PMTs are near 0 and gain settings are adjusted to mid-range.
   - Select the pixel format of the image (512×512 pixels is a good choice to begin) and dynamic range (8-bit or 12-bit).
   - Choose the scan mechanism: unidirectional versus bidirectional scanning, and sequential versus simultaneous scanning of multiple wavelengths. Avoid filtering until you have a good idea what is necessary to get acceptable images.
2. *Adjust the pinhole, zoom factor, scan speed, offset, and gain. Then fine-tune these parameters.*
   - Pick live (continuous) view confocal mode to evaluate and adjust the image. The goal in setting adjustable parameters is to obtain a clear image while keeping photobleaching of the specimen to a minimum.
   - Adjust the pinhole diameter to one Airy disk diameter. The setting of the pinhole varies depending on wavelength and objective and usually changes automatically.
   - Increase the zoom factor, if necessary, to match the pixel size to the required spatial resolution. Zoom can be used to maintain the spatial resolution provided by the objective. Remember that increasing the zoom decreases the diameter of the field of view and increases the rate of photobleaching.
   - Adjust the scan speed. For bright specimens, this is typically 2/3 of maximum rate, but adjust up or down depending on photobleaching rate and the total sample scan time.
   - Set the offset (dark or black level). If the image intensity is bright, it may be necessary to reduce intensity first using the AOTF or ND filters. Examine a dark background region in the image. Increase the amount of offset slowly and notice on progressive scans how the screen display becomes increasingly darker. When the image background approaches a black color, the offset is set properly.
   - Set the gain. Increasing the gain amplifies the light intensity through voltage multiplication. Increase the gain until bright highlights approach saturation. The use of a color display function (saturation = red; black level = blue) makes it easier to adjust offset and gain.
3. *Acquire the final image.* If the image is somewhat grainy, use frame averaging and average two to four frames. As described in a later chapter, the factor improvement in S/N is the square root of the number of averaged frames or the square root of the factor by which the exposure time has been increased.
4. *Adjust the step size for a z-series.* For *z*-series used in 3D displays, if it is desirable to preserve diffraction-limited resolution of the objective, the step size

along the *z*-axis is adjusted to give a sample period of two steps per diffraction disk radius. If the radius is 0.2 μm, the step size should be 0.1 μm.

5. *Review the following general points.*
   - Use the highest NA objective available (NA 1.3–1.4) to reduce focal plane thickness and increase image brightness. Dry objectives are convenient, but at equal magnification, an immersion objective can be many times brighter than a dry one. Brightness is inversely proportional to magnification (a 40× objective produces brighter images than a 100× objective).
   - Excitation of the specimen at high laser power maximizes fluorescence emission, but causes rapid bleaching and reduces image quality.
   - Low transmission is usually employed even if the resulting image is somewhat noisy in order to reduce the rate of photobleaching. Noise in dimmer images can be removed by frame averaging or frame accumulation.
   - Be mindful of the bit-depth and dynamic range when saving images. Subtle details in 8-bit images do not tolerate much adjustment during subsequent processing.

PERFORMANCE CHECK OF A CONFOCAL SYSTEM

The confocal microscope has many adjustable parameters that affect the final image, so that a feature like light intensity, for example, is affected by multiple adjustments. Since electromechanical devices can drift from their original settings and eventually become degraded through use, it is important to implement a monitoring protocol to spot check the performance of basic functions: (1) *z*-Stacks of large fluorescent beads (>5 μm diameter) are useful for examining some of the main functions in the confocal scan head: constancy of light intensity (laser power, PMT function); even pattern of superimposed colors (pinhole alignment); and absence of image jump and jagged edges (galvanometer scanners). (2) *z*-Stacks of small fluorescent beads (<0.2-μm diameter) can be used to obtain point-spread (PSF) functions of the objective. PSF analysis reveals performance faults in the objective itself, as well as defective beamsplitters, vibrations from faulty fans, uneven illumination of the rear focal plane and fidelity flaws of piezo motors. (3) It can also be important to check peripheral equipment associated with environmental controls, stage performance, shutter action, and other devices. Tests like these safeguard projects lasting weeks or months, where the consistency of performance is of critical importance. The reader is referred to detailed protocols and discussions by Murray et al. (2007), White et al. (1987), and Zucker and Price (2001) that address these issues.

FAST (REAL-TIME) IMAGING IN CONFOCAL MICROSCOPY

The growing application of fluorescent proteins in live-cell imaging now requires microscope imaging speeds on the millisecond timescale in order to unravel the intricate dynamics that occur in many biological processes. Unfortunately, as we saw above, CLSMs are limited in acquisition speed by the galvanometer mirrors, which are driven at the rate of several microseconds per pixel. This translates to a scan rate ranging from 500 ms to 2 seconds, depending upon the image dimensions. In order to acquire images

on faster timescales, microscopes must be reengineered to incorporate advanced scanning scenarios that enable the beam to be scanned across the specimen at higher speeds. A number of instruments have been introduced to increase the speed of confocal imaging, as will be discussed below.

Confocal Imaging with a Spinning Disk

Instead of illuminating the object by raster scanning using a single spot, it is possible to scan the specimen with thousands of points simultaneously using a spinning *Nipkow disk* (Fig. 13.15). A Nipkow disk contains thousands of minute pinholes arranged in multiple nested rows of outwardly spiraling tracks. The laser beam is expanded to illuminate an extended area on one side of the disk covering about 1000 pinholes and excite multiple point locations in the specimen. The pinhole spiral patterns are designed so that a complete image is created with each 30° rotation of the disk (~1700 point scans across the specimen; 12 images per one disk rotation).

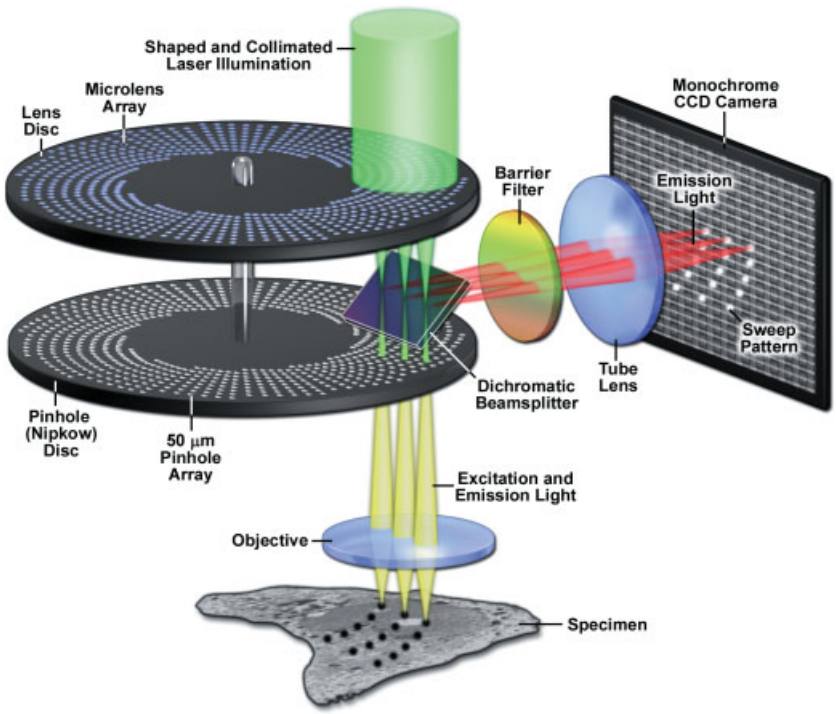

Figure 13.15

Tandem scanning confocal microscopy using a spinning Nipkow disk. The Yokogawa design features two disks each with >20,000 pinholes (50 μm in diameter) that rotate as a single unified piece around a central axis. The upper disk is fitted with microlenses about 250 μm in diameter that focus incident rays on a pinhole in the second disk. The pinholes of the disk are confocal with a specimen and the surface of an electronic imager, such as a CCD camera. A fixed dichromatic mirror positioned in between the rotating disks transmits excitatory wavelengths from the laser while reflecting fluorescent wavelengths to the camera.

The pattern of pinholes in the spirals assures that the specimen is completely scanned. There are substantial advantages inherent to this method of parallel scanning:

- The fluorescent light generates an extended *real confocal image* that can be seen by the eye or recorded on a camera. Spinning disk systems are also simpler and easier to use than single-point scanning systems.
- With a sensitive CCD camera as a detector, the *dynamic range in the image is extended* to thousands of gray levels, and light intensity can be quantitated with greater accuracy. For the same exposure time, the S/N ratio of a spinning disk image is increased and images look smoother and less noisy. Conversely, when acquired to the same S/N ratio as a single point scanned image, the total amount of exposure of the specimen is reduced, thus *reducing the rate of photobleaching* and prolonging cell viability.
- *Time resolution* is greatly improved. For complete scanning coverage, the fastest spinning disk systems provide up to 2000 full fps versus ~1 full fps for single-point scanning confocals. Note that acquisition speed in spinning disk microscopy is usually limited by the frame rate of the camera.
- Scanning at a rapid rate but at relatively low intensity results in efficient fluorescence emission. Among the benefits is improved detection of fine structural details represented by clusters of only a few fluorescent molecules.

The pinholes in the Nipkow disk perform the same function as the pinhole in a single-point scanning system in generating a confocal image of an optical section. Incorporation of a stepper motor for the *z*-axis and three-dimensional imaging software also permits volume viewing and single-plane composite or projected views. Early spinning disk imaging systems had the disadvantage of very low light transmission, but the double-disk design by Yokogawa Electronics, Inc., (Tokyo) remedies the problem by including microlenses that greatly boost light-gathering efficiency and transmission. This system has been thoroughly reviewed by Inoué and Inoué (2000) and by Wang et al. (2005). Spinning disk technology provides an attractive low-cost imaging solution and the method is now widely used for live-cell imaging, where it is necessary to image for long periods of time while minimizing photon damage. The ability to obtain confocal images at high frame rates has also made spinning disk technology attractive for documenting rapid kinetic processes, such as cell movement and calcium imaging.

The Yokogawa spinning disk uses a dual disk system to increase imaging sensitivity. Microlenses on the upper disk deliver about 70% of the incident laser light to the specimen. Although the return path for fluorescence emission does not include microlenses and delivers only ~1–2% of the fluorescent light to the detector, sensitive CCD cameras help compensate, particularly EMCCD cameras (discussed in Chapter 17), which are excellent for imaging faint signals. Another advantage is the ability to synchronize scan speed with acquisition frame rate to allow the capture of an integral number of complete scans in an image. This feature eliminates the appearance of scanning stripes in images made with short exposures (high rotation speeds) in the absence of synchronization. Some of the features of the Yokogawa CSU spinning disks are summarized in Table 13.3. By illuminating with a 10-mW laser, it has been possible to document calcium spikes in neurons and fast flow in physical systems at 2000 fps.

TABLE 13.3 Comparison of Spinning Disk and Single-Point Scanning Systems

Parameter	SD Fast System	SD Standard System	Point Scanning Confocal
Max spin rate	10,000	1,800	N/A
Frame rate	2,000	360	~1–2

Data are for the Yokogawa CSU-10 (standard) and -X1 (fast) systems.

Despite the simple design, there are nevertheless certain disadvantages to spinning disk imaging in general that one needs to consider. Because the 20,000 pinholes are spaced closely together on the disk, there is some crosstalk, because the fluorescent light emitted from one site enters several pinholes on the disk, not just one pinhole. This crosstalk adds to the background signal (background haze), reducing the S/N ratio of the object. If required, deconvolution algorithms can be applied to acquired image stacks to remove background signal. Another disadvantage of many of the available spinning disk systems is that the pinholes in the disk are fixed in physical size and not variable. Thus, imaging may be somewhat compromised in resolution and *z*-section thickness for certain objectives (i.e., those having a magnification less than 60×). However, imaging performance is remarkably good overall, and the microlens technology presently in place offers good transmission ranging from 405 to 650 nm.

Microscope companies offer different spinning disk mechanisms. Besides the Yokogawa double-disk system described here, there are also single disk designs with patterns of pinholes or linear slits. Some microscopes allow the user to choose among different disks with pinholes of different sizes in order to best match the NA of the objective.

Sweptfield Confocal Imaging

Prairie Technologies offers a *sweptfield* solution for rapid confocal imaging (Fig. 13.16) that can be used on Nikon and similar microscope frames. The scan head contains two identical aperture plates with sets of slits and rows of pinholes of various sizes that the user selects. The plates are fixed and do not move. Laser light is directed to the plate, and the pinhole pattern is then swept across the specimen with galvanometer and piezo-driven scanner mirrors. The return fluorescence beam is directed to the second aperture plate and scanning mirrors, which this time sweep the focused pinhole images across the face of a sensitive CCD detector. The second plate performs the function of a confocal pinhole and effectively removes photons with origins above and below the focal plane. In this case, scanning is done by scanning mirrors, rather than by the pinhole disk itself. The number of pinholes is limited to 32, but the scanning mechanism sweeps the entire specimen and builds up a full image on the camera.

Resonant Scanning Confocal Microscopy

The high-performance linear galvanometers used in CLSMs are a marvel of engineering, designed to accurately rotate the attached mirrors and position the beam with

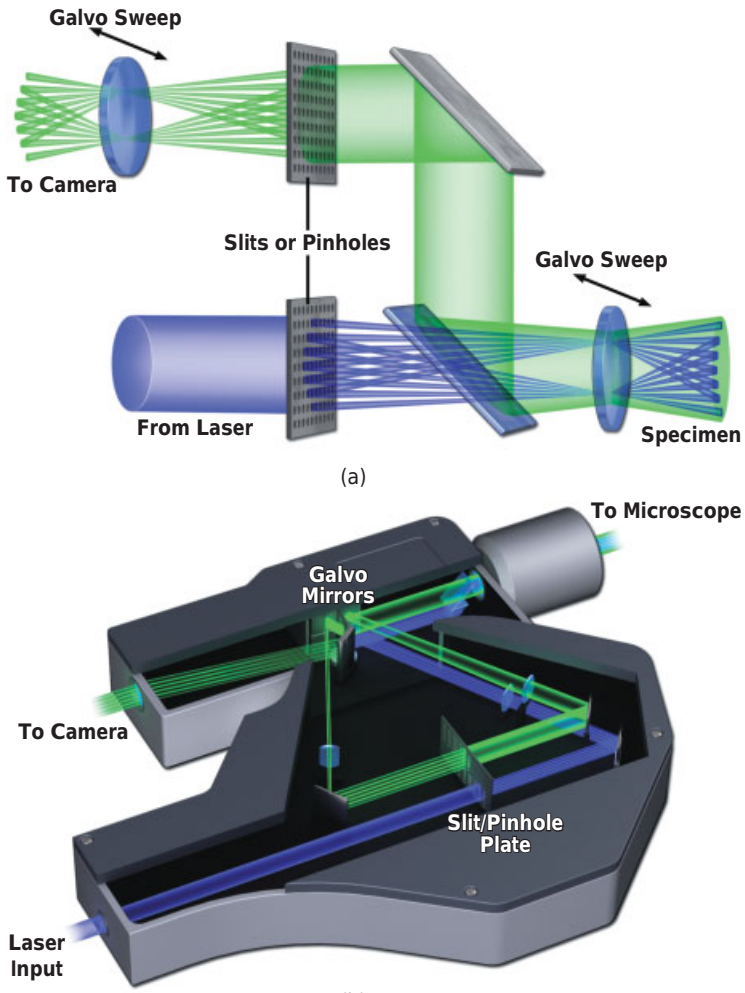

Figure 13.16

Principle of sweptfield confocal imaging. (a) Schematic drawing of sweptfield optical pathway. Two aperture plates are used. One illuminates the specimen with a slit or row of pinholes. A second identical plate acts as the confocal pinhole. In sweptfield imaging, the *x*,*y*-galvanometer mirrors sweep the spot pattern or slit over the specimen, while the two aperture plates remain fixed and stationary. (b) Cutaway diagram of sweptfield confocal scan head.

extreme precision over a lifetime exceeding several billion cycles. Unfortunately, linear galvanometers are limited in their scanning speed due to inertia, and, therefore, can only raster-scan a specimen at image acquisition rates of one to two images per second at standard frame sizes. In order to achieve faster scanning rates, the slower linear galvanometer used for horizontal line scanning can be replaced with a much faster resonant scanning galvanometer that vibrates at fixed frequency and is the rotational equivalent of a tuning fork. In resonant galvanometers (also known as *counter rotation scanners*), the energy stored in a torsion spring or rod assembly is used to oscillate the

mirror in a sinusoid manner. These devices cycle at a resonant frequency on the order of 4–8 kHz. When a resonant scanner operating at 7900 Hz is used to acquire 512 lines that are progressively scanned in a bidirectional orientation (odd lines are left-to-right and even lines are right-to-left), the result is an individual line period of approximately 125 ms and image capture rates on the order of 30 fps, equivalent to video rates.

The Achilles' heel of resonant galvanometers is their nonlinearity in velocity. Thus, a fluorescent specimen is scanned at the highest speeds in the central region, with the velocity progressively decreasing as the scan reaches the edges. As a result, when the image dataflow derived from a resonant scanner is acquired with a frame grabber clocked at a constant pixel rate (which assumes the beam is scanned linearly), the images appear stretched at the edges (Fig. 13.17). Furthermore, the uneven distribution of laser excitation intensity (greater at the edges) produces excessive photobleaching (and potentially phototoxicity) at the edges of the scanned region because of the increased exposure to the laser light. Image distortion induced by nonlinear resonant

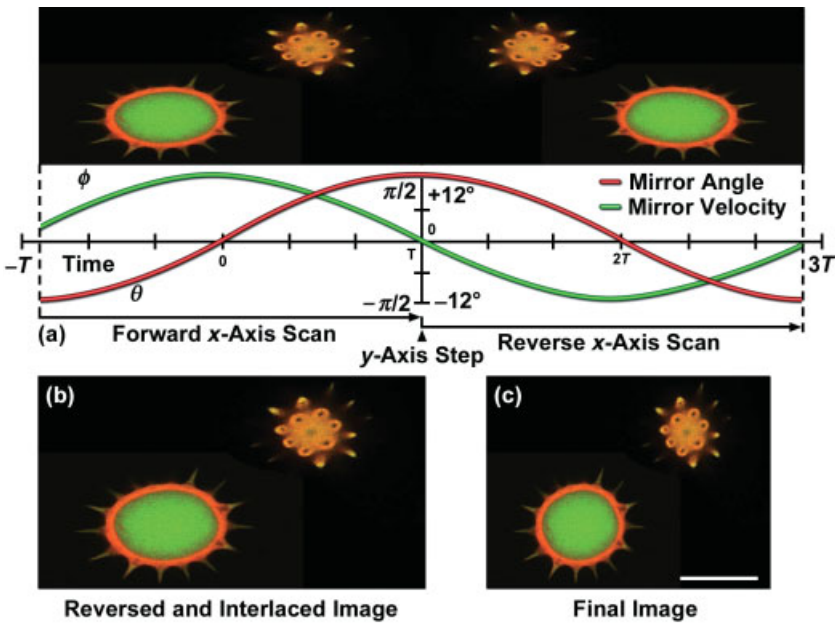

Figure 13.17

Resonant scanning confocal microscopy with a linear pixel clock. (a) During oscillation, the angular velocity of a resonant galvanometer varies in a cosinusoidal manner, reaching maximum velocity at a scanning angle of zero degrees (in the center of the scanning field), but lower velocity at the edges of the field, where the scan direction changes. When generating images using resonant scanners, these nonlinear variations present a significant problem in terms of pixel clocking. (b) Processing images involves inverting data points from the second half of the horizontal scan line, followed by interlacing the inverted data between the data lines for the first half of the image. Note the distorted oval shapes of the pollen grains. (c) The final step in the sequence is to apply a correction factor for each pixel or phase position relative to the center pixel. Each pixel is then relocated to the correct position in the final image. The pollen grains now reveal their true shapes. Bar = 20 μm.

galvanometer scanning is fortunately predictable and can be corrected using either software or hardware solutions. Regardless of the correction scheme involved to produce images, the most effective scanning strategy involves collecting data during both the forward and backward scans of the galvanometer mirror. Recording data during the forward scan is straightforward, but due to the fact that the backward scan reverses the direction in which pixels are recorded, the image data must be inverted using specialized read-write buffers or software, as described in Figure 13.17. The most common hardware solution for nonlinear scanning involves using an analog pixel clock and optical grating to measure the mirror position in real time in order to correct the final images.

Additional Options for Rapid Confocal Imaging

Acquisition speed on conventional single-point scanning confocal microscopes is limited mainly by the rate of deflection of the galvanometer mirrors and the serial pixel-by-pixel detection of the fluorescence signal at the PMT. Spinning disk and sweptfield systems increase speed by using rapid parallel scanning with multiple pinholes combined with image detection on a CCD camera, and resonant scanners replace slower galvanometer motors on fast-rated confocal systems. But there are other methods to increase acquisition speed:

- *Line-scanning confocal.* The Zeiss LSM 7 Live confocal uses a cylindrical lens to spread the laser beam into a line or slit, which is swept across the specimen, while the return fluorescence is detected by a silicon-based bar code reader (Fig. 13.18a). The combination of these methods gives a 20-fold increase in imaging rate with little expense to confocal image quality.
- *AOM.* AOM devices manipulate laser beams much faster than galvanometer motors and rotating filter wheels (Fig. 13.18b). The Leica SP5 uses a single AOTF

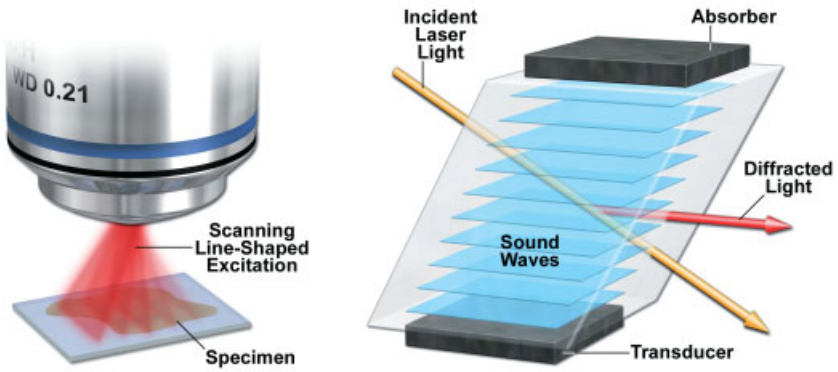

Figure 13.18
Additional methods for rapid confocal imaging. (a) Slit scanning is based on rapid movement of a line or slit across the specimen. (b) AOM-based devices rapidly select, attenuate, or deflect laser beams in the absence of any mechanical movement or filter wheel rotations.

in place of individual dichroic filters for rapid wavelength switching and high fluorescence transmission. Many systems use AOBS devices to select and attenuate the intensity of laser beams. The VT-Eye from VisiTech International is unique in using an *acousto-optic deflector (AOD)* for raster scanning in the *x* dimension in their single-point scanning confocal microscope.

SPECTRAL ANALYSIS: A VALUABLE ENHANCEMENT FOR CONFOCAL IMAGING

Detecting two different fluorophores in a specimen without cross-contamination of signals can sometimes be challenging, because there is usually some overlap between their excitation spectra and between their emission spectra, even when the two dyes are chosen to be largely separated and "distinct." Depending on the amount of overlap, the excitation of one dye simultaneously excites the other, and the filter profile designed to collect the emission wavelengths of one dye also captures some of the emission of the other. This capture of unwanted signal is called *crosstalk* or *bleedthrough*, and is commonly observed, even for widely separated pairs of dyes like DAPI-fluorescein or fluorescein-rhodamine (Fig. 13.19). Usually, fluorescence of the shorter wavelength dye bleeds into the signal of the longer wavelength dye, but sometimes, bleedthrough occurs the other way around. The use of interference filters with specific cut-on and cut-off boundaries helps increase the specificity of detection, but sometimes does not eliminate the problem. Bleedthrough interferes with colocalization analyses, FRET measurements, and is sometimes a factor in samples with bright autofluorescence. The

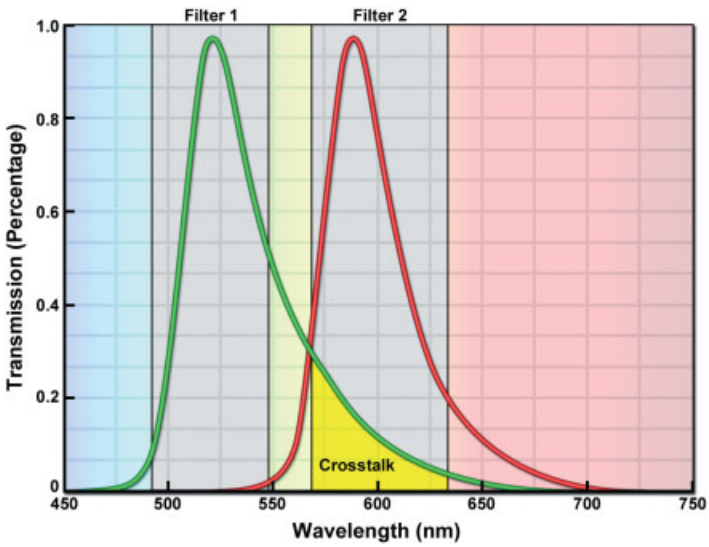

Figure 13.19

Emission spectra of two fluorescent dyes with spectral profiles similar to fluorescein and rhodamine. In this example, the region of overlap labeled "crosstalk" in the rhodamine channel (yellow) means the rhodamine signal is not dye-specific.

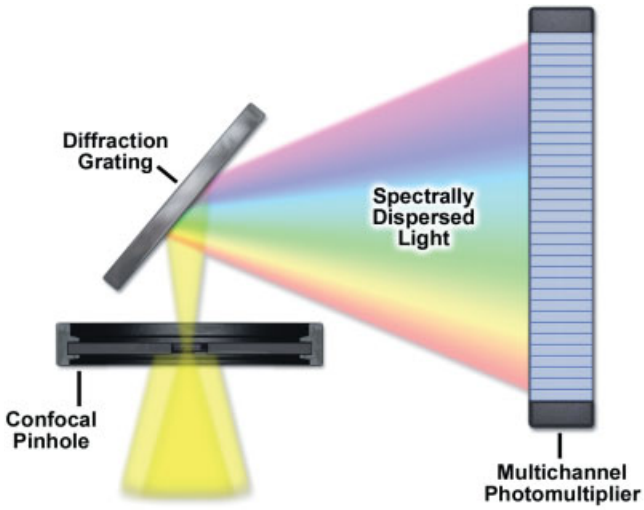

Figure 13.20
Spectral imaging equipment. A grating or prism disperses the fluorescence emission beam into spectral components; a multiple photomultiplier device records intensities in adjacent 10-nm wide bandwidths.

problem can usually be avoided by optimizing the choice of excitation lines, dichromatic mirrors, and emission filters. But if this strategy fails, it is usually possible to collect dye-specific signals using *spectral imaging*, a method based on equipment that acquires a stack of images at closely spaced wavelength intervals and employs software that can construct emission spectra of the dyes, calculate their relative contributions, and construct dye-specific images. Spectral imaging has its origins in the analysis of satellite images of different reflection signatures from the earth, where different types of terrain are associated with different spectral signatures.

For Nikon and Zeiss confocal microscopes, the optical device for spectral imaging consists of a diffraction grating for dispersing the return fluorescence emission beam and a multichannel photomultiplier capable of detecting up to 32 separate channels each 2–20 nm in width (Fig. 13.20). The fluorescence emission from each pixel equivalent in the specimen is dispersed and recorded on a variable number of adjacent channels on the PMT. The result is a *lambda-stack*, a series of images arranged by wavelength, with each image representing a 10-nm bandwidth of light. Thus, a spectral image stack can be considered as either a collection of images each corresponding to a different wavelength, or as a collection of different wavelengths for each pixel location.

The spectra of the individual fluorophores are then obtained from dye-specific objects on the same slide or from specimens on two separate reference slides, the operator selecting a feature in the image, and the software determining the corresponding fluorescence emission spectrum. Once the spectra have been recorded, it is then possible to image a slide and determine the proportion of dyes at each pixel location by employing an algorithm called *linear unmixing* or *linear decomposition* (Fig. 13.21). The software uses linear algebra to analyze the combined spectrum from multiple dyes at each pixel location and calculates the respective contributions of the two

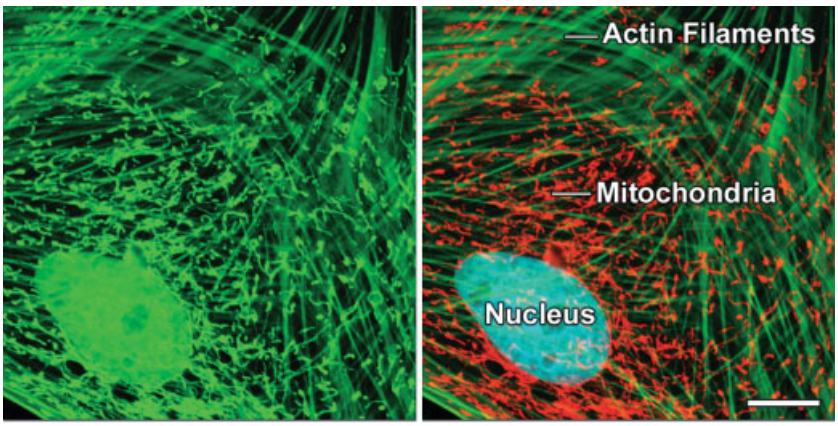

(a) (b)

Figure 13.21

Indian Muntjac fibroblast cell stained with a combination of SYTOX Green (nucleus), Alexa Fluor 488 conjugated to phalloidin (filamentous actin network), and Oregon Green 514 conjugated to goat anti-mouse primary antibodies (targeting mitochondria). (SYTOX and Oregon Green dyes are available from Life Technologies.) These dyes have emission maxima at 523, 518, and 528 nm, respectively, and each appears green to the eye when viewed in widefield fluorescence using a standard FITC cube (a); Using a spectral imaging detector, the entire spectrum of fluorophores in the specimen was first gathered, and then linearly unmixed (b) and assigned pseudocolors: nucleus, cyan; actin, green; mitochondria, red. Bar = 10 μm.

dyes and stores the results in image frame buffers. This operation is then repeated, pixel for pixel, until all of the pixels are analyzed. The result is separate dye-specific images without bleedthrough (Fig. 13.21). Of the different algorithms that can be used for spectral imaging, linear unmixing is the most specific and efficient for colocalized fluorophores.

Leica and Olympus perform spectral imaging using one or more PMTs masked by pairs of adjustable slits that generate a wavelength window that ranges from just a few nanometers to 100 nm or more in width. Simple adjustment of the slit optimizes the band of emission wavelengths. If the specificity is not good enough, emission spectra can be obtained by scanning a narrow-band slit over the spectrum to generate a lambda stack (Olympus) or by optimizing multiple PMT spectral windows and employing one of several spectral separation algorithms (Leica). All of these methods are effective, but may require setting priorities and making compromises regarding system flexibility, spectral accuracy, detection sensitivity, acquisition time, and degree of image correction.

OPTICAL SECTIONING BY STRUCTURED ILLUMINATION

Optical sectioning on widefield fluorescence microscopes can be difficult when fluorescent sources above and below the focal plane contribute significantly to the image, particularly in the case of thick, extended specimens. Effective solutions include confocal microscopes, which use a pinhole mask (optical filter) to reject signals outside of the

focal plane, and deconvolution (image processing) of an image stack, which reassigns background signals to their origins in other nearby focal planes. A third solution is illumination of the specimen, without lasers, with a grid pattern using devices that are inserted into the epi-illumination light path in a widefield fluorescence microscope at a focal plane conjugate with the specimen (Heintzmann, 2006; Neil et al., 1997). Such equipment is available from Quorum-Leica (Angstrom system), Carl Zeiss (ApoTome), and Qioptiq (OptiGrid). One should note that the application of structured illumination for optical sectioning is distinct from the structured illumination techniques used for obtaining subdiffraction resolution as described in Chapter 15. In the method described here, in-focus and out-of-focus information is acquired by a CCD camera and analyzed in a computer; signals lying outside the focal plane are eliminated by a phase sampling technique; in-focus information is retained in the optical section, resulting in a "confocal-like" image. A nice feature of imaging with a structured illumination device is that the light source, filters, and optics are the same as those used for standard fluorescence microscopy.

A pattern of closely spaced parallel lines is projected onto the specimen at the fluorescence excitation wavelength so that the image of the specimen shows a grid of bright and dark parallel lines running through it (Fig. 13.22a,b,c). At short distances away from the focal plane, the grid is strongly blurred, the grid projection pattern is not seen, and defocused specimen structures remain very dim or invisible. Thus, the grid generates a strong signal wherever specimen details are in focus and a weak signal when features are out of focus. In order to display an optical section, the grid is translated in a direction perpendicular to the grid axis in three steps (each step is 1/3 of the basic grid spacing), so that all the information in the dark stripes is covered, and the three resulting images are analyzed to compute the image for that focal plane. Thus, each site on the specimen and corresponding pixel location on the detector experiences a series of illumination intensities, corresponding to translation phases of the grid. The grid itself is translated using a tilting glass plate, or a length-variable piezoelectric crystal, so that acquisition of the required three images per focal plane takes less than a second. A demodulation algorithm analyzes changes in intensity at a given pixel location in the three images and creates an image of the focal plane, where pixel locations showing the greatest rates of change have the highest amplitudes. The microscope focus is shifted to the next *z*-location and the process repeated until an entire *z*-stack is obtained. Optical sectioning by structured illumination is most impressive for moderately bright specimens imaged at medium to low magnifications (Fig. 13.22). It is therefore useful for extended objects, such as tissue sections, Drosophila embryos, nematodes, zebrafish embryos, and similar specimens. Because the focal plane is frequently deep within the specimen and because multiple wavelengths are used, it is helpful to use apochromatic objectives with spherical aberration correction.

DECONVOLUTION MICROSCOPY

Deconvolution is an image processing technique that requires extensive computation using any one of a variety of algorithms designed to improve contrast by removing or reversing the blurring present in fluorescence images. Some algorithms reassign the blurring photons to other locations in the image volume, thereby restoring photometric accuracy to optical sections. Nearly any image acquired on a fluorescence microscope

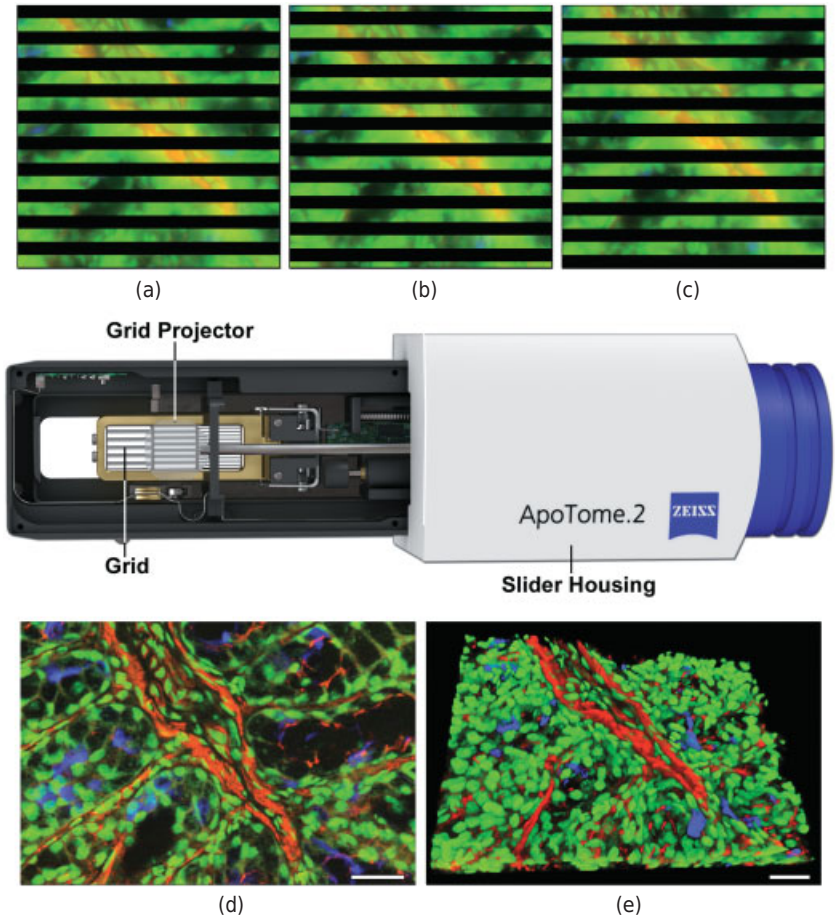

Figure 13.22

Optical sectioning by structured illumination with the Zeiss ApoTome. The ApoTome.2 features three grids to cover the magnification range between 10 and 100×. Grid lines are projected onto the specimen and translated in 1/3 steps of the period length with a glass plate. (a–c) Images of a 30-μm triple-labeled mouse colon section showing the three grid projections. (d) Optical section created from the images in panels a–c. (e) Volume rendering of the optical section image stack from the entire mouse colon section. Bars = 50 μm.

can be deconvolved, and several applications have been developed that can apply deconvolution techniques to transmitted light images, as well (including DIC and phase contrast). Among the most suitable subjects for improvement by deconvolution are three-dimensional image stacks consisting of a series of optical sections along the *z*-axis of the microscope. Deconvolution is often suggested as a good alternative to confocal microscopy, as confocal images also contain some image blur and can be improved by deconvolution techniques, often with outstanding results. In comparison, confocal microscopy and widefield deconvolution microscopy both work by removing image blur, but they do so by different mechanisms. As we learned earlier, confocal microscopy prevents out-of-focus blur from being detected by placing a pinhole aperture between

the objective and the detector. In contrast, widefield microscopy allows blurred light to reach the detector, but deconvolution techniques can then be applied to the resulting images either to subtract blurred light or to reassign it to a different optical section. Confocal microscopy is especially well suited for examining thick specimens, such as embryos or tissues, while deconvolution microscopy has proven to be a powerful tool for imaging specimens requiring extremely low light levels, such as living cells expressing fluorescent proteins. Practical aspects of deconvolution microscopy are discussed in Wallace et al. (2001), Biggs (2010), and McNally et al. (1999), as well as papers by early pioneers and developers of the method, David Agard and John Sedat (Agard et al., 1989).

Microscope Configuration for Deconvolution

Deconvolution has several rather strict microscope hardware and software requirements that must be met in order to get datasets that produce the optimum results. All of the major microscope manufacturers offer instruments and software capable of performing deconvolution, but several companies specialize in turnkey systems designed specifically for deconvolution analysis. Among them, Applied Precision of Issaquah, Washington, offers the most sophisticated instrumentation. The major requirements are a research-grade fluorescence microscope, deconvolution software, a stabilized illumination source, axial (z) stepper motor, and a high performance CCD camera system. Deconvolution algorithms require tightly spaced optical z sections ranging in thickness from ~250 to ~750 nm and captured with high precision, thus necessitating a highly accurate axial focus control motor that is stabilized against mechanical and thermal drift. The illumination system must also be free of spatial and temporal fluctuations, which can be accomplished using light scramblers coupled to lasers, LEDs, or arc-discharge lamps. The camera should be a cooled scientific CCD, with low read noise, selectable readout rates, 12-bit A/D conversion, high sensitivity at low light levels, and relatively even quantum efficiency across the visible spectrum.

The key to obtaining good results with deconvolution is to capture high precision image stacks that are matched in spatial resolution to the specifications of the objective. For example, high NA objectives should have a lateral Nyquist sampling range of 90–100 nm and an axial range of 250–300 nm. The exposure time must be carefully controlled to limit photobleaching and avoid saturation, but still long enough to obtain high S/N image stacks. Suitable imaging fields can be selected using phase contrast or DIC to avoid exposing the specimen to fluorescence illumination prior to image acquisition. Image stacks should extend beyond the main specimen features into a region that is dark or has uniform fluorescence (~4 μm above and below the signal from a 10-μm thick specimen). Finally, the deconvolution software should record image metadata that includes the microscope optical configuration, voxel dimensions, exposure time, filter data, and other critical variables of the experiment.

Determination of the Point-Spread Function

Depending upon the algorithm applied (see below), the success of deconvolution processing can depend heavily on the accuracy of the objective point-spread function model applied to the calculations. The most sophisticated software requires a measure-

ment of the PSF using subresolution fluorescence beads mounted in the same medium and emitting at a similar wavelength band as fluorophores in the specimen. The beads can be imaged on a separate slide or mixed with the specimen. A through-focus 3D image stack of beads acquired under the same conditions as those used for the specimen should be obtained for each emission wavelength. Subroutines for PSF calculation are usually available with commercial deconvolution algorithms or the microscope control software. Before gathering a PSF image stack, it is a good idea to get an empirical estimate of the objective quality by focusing through the fluorescent beads. As focus is adjusted up and down through a bead, look for equivalent diffraction rings above and below the focal plane of the bead. If the rings are asymmetrical, this is an indication of aberration or a mismatch in refractive index between the immersion oil and mounting medium. It should be noted that a truly accurate determination of the objective PSF is difficult to obtain because noise is always introduced into the measurement, and using a theoretical PSF does not compensate for subtle aberrations in the microscope optical train. It is therefore best to mix the fluorescent beads with the specimen for PSF measurements. Examples of a good PSF and two showing severe aberrations are shown in Figure 13.23.

Deconvolution Algorithms

Deconvolution algorithms for microscopy are based on mathematical formulae that describe the imaging process. In theory, the fundamental equation for image formation in the microscope is:

$$I(X, Y, Z) = S(X, Y, Z) \otimes \mathrm{PSF}(X, Y, Z),$$

where the three-dimensional image, $I(X,Y,Z)$, is treated as a mathematical convolution of the spatial light distribution of the specimen, $S(X,Y,Z)$, with that of the objective point-spread function, $\mathrm{PSF}(X,Y,Z)$. The convolution operation shifts the PFS so that it is centered at each point in the image and then sums the contributions of all the shifted PSFs. Because the contribution from the image, $I(X,Y,Z)$ is known, and the $\mathrm{PSF}(X,Y,Z)$ for the objective can be determined, the process of solving for $S(X,Y,Z)$ is usually conducted by first performing a Fourier transformation on both sides of the equation and then solving for S. A number of algorithms of varying sophistication have been developed to deconvolve image stacks:

Deblurring: Among the simplest in the deconvolution family of algorithms, deblurring methods attempt to remove blur and haze from images and were some of the first algorithms used for deconvolution due to their low computational and computer memory requirements. The *nearest neighbors* deblurring algorithm examines three adjacent optical sections and removes the blur contribution in the center section by subtraction of defocused features from the adjacent sections. The process is repeated throughout an entire 3D stack and sharpens image features, but results in >90% reduction in brightness due to the removed signal. The related *no-neighbors* approach operates on a single optical section and is basically equivalent to the unsharp mask tool in Photoshop. These algorithms are best used for screening data before committing to more complicated deconvolution methods.

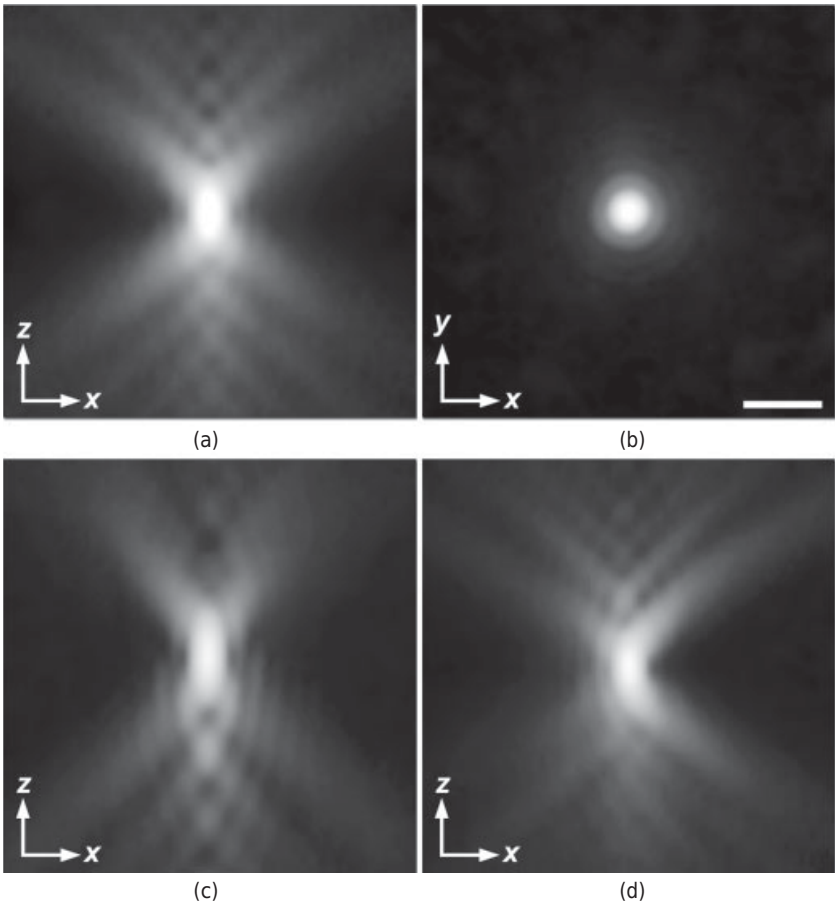

Figure 13.23

Point-spread function quality. (a) PSF of highly corrected and aligned objective showing symmetry through *x*–*z* axis. (b) Same PSF in the *x*–*y* plane. (c) PSF of objective with spherical aberration skews the symmetry. (d) PSF revealing coma aberration. Bar = 1 μm.

Linear filtering: These algorithms are designed to restore true image intensities to the raw data, and are comprised of methods called *inverse filtering*, *Wiener filters*, and *linear least squares*. Filtering algorithms examine information from all the focal planes in an image stack using the 3D optical transfer function (OTF), which is the Fourier transform of the PSF. Inverse filtering divides the Fourier transformed image data by the OTF, but is complicated by two serious factors: (1) the OTF contains components with a value of zero, and (2) high spatial frequencies in the image (at the limits of detection) are corrupted by noise because of their small magnitude. In contrast, the Wiener filter takes noise and negative pixel values into account and uses the full 3D OTF to produce deconvolved images. This technique, which is one of the most popular linear methods, is limited to restoration of frequency values residing within the band-

width of the OTF. The linear least squares method is based on linear algebra and restores images by reducing the effects of noise and high spatial frequency components, but is hampered by the tradeoff between image sharpness and noise amplification.

Iterative restoration: Iterative algorithms are the most sophisticated methods for deconvolution and require multiple calculation cycles to converge toward the best image solution. Examples of iterative algorithms are called *nonlinear least squares*, *maximum likelihood*, and *Richardson–Lucy*. In the best case, iterative algorithms can effectively remove noise and recover frequencies beyond the objective bandwidth limit. Their only downside is that these complex mathematical treatments require intensive computational processing with significant computer memory requirements. Iterative algorithms work by first making an estimate of the specimen image, followed by creating a blurred version using the measured PSF, and finally comparing it to the actual image data. The calculation is optimized to generate an improved estimate, and the entire process repeated until the data converges to the best solution. Iterative algorithms that impose constraints, such as nonnegative pixel values, are called *constrained iterative deconvolution*. In practice, the algorithm operates until a predetermined convergence criterion has been reached or when a defined number of iterations has been completed. The best image result balances the removal of blur with low noise amplification (see Fig. 13.24).

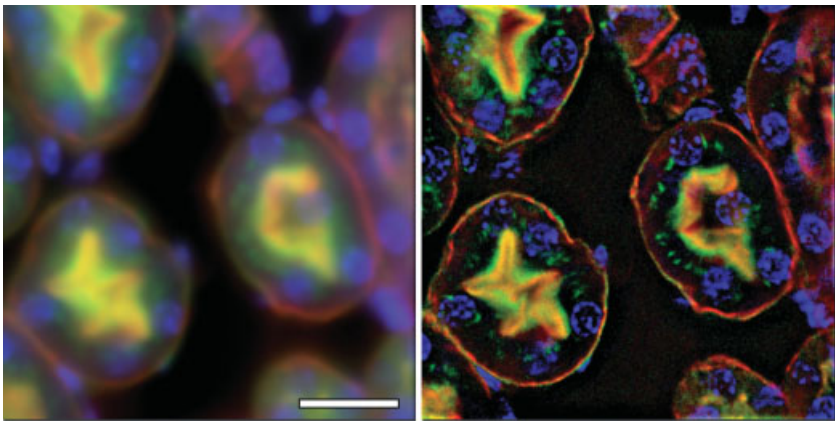

(a) (b)

Figure 13.24

Widefield and deconvolution images of a triple-stained mouse kidney thick (16 μm) section. (a) Widefield fluorescence image of kidney labeled with Alexa Fluor 488 conjugated to wheat germ agglutinin (glomeruli and convoluted tubules; pseudocolored green), Alexa Fluor 568 conjugated to actin (brush border; pseudocolored red), and DAPI (nuclei; blue). (b) Same viewfield after deconvolution using iterative restoration (20 iterations) with a calculated PSF and 3D frequency filter in SlideBook software (Intelligent Imaging Innovations, Denver, CO). Images were acquired with an Olympus 60× 1.42 NA plan-apochromatic objective in 100-nm steps to create a 20-image (2-μm) *z*-stack. Bar = 20 μm.

Blind deconvolution: The *blind* deconvolution method is so named because it relies on determining both a calculated PSF and the best image estimate from blurred image stacks. Blind deconvolution eliminates the need to accurately measure the objective PSF, making deconvolution much easier because the microscopist does not have to collect PSF data for each experiment. During the calculation, the image and PSF estimates are modified after each deconvolution iteration so that the final solution converges to the best fit for the original blurred image data. This method takes about twice the computational time as iterative techniques, but it avoids some of the pitfalls that arise when the PSF is not accurate (one of the largest sources of artifacts in the image restoration). Blind deconvolution works amazingly well, but it will not compensate for poor sample preparation, improper microscope configuration, or inferior quality objectives.

Evaluating Deconvolution Results

The results of deconvolution experiments should be carefully compared with key optical sections from the original image stack, as well as maximum intensity projections obtained from the analysis. Structural features that appear in the deconvolved image should be apparent (albeit, blurred) in the original images, and new textures featuring fine details should be examined to ensure they didn't arise as a result of noise amplification (Fig. 13.24). The brightness of deconvolved images, which is scaled to the features with the highest intensity, may appear to be much less than the average value in the original image stack, but this is usually due to reassignment of image intensities and an increase in dynamic range. In general, specific regions in deconvolved images should be carefully examined for artifacts, including the specimen borders (especially if they stretch to the image boundaries), brightness, background, and fine specimen detail.

Several artifacts may be encountered in deconvolution, including alternating bright and dark stripes in the *x*–*z* plane arising from fluctuations in the light source, and concentric rings (ringing) around bright features. Poor PSF quality resulting in asymmetric specimen details in the *x*–*z* plane and edge artifacts (i.e., increased sharpness) are common to many algorithms. In addition, filamentous structures (such as actin or tubulin) might be lost or become fragmented when using some of the algorithms described above.

Exercise: Effect of Confocal Variables on Image Quality

This exercise should be performed on a confocal microscope together with an experienced user.

- The following adjustments can all be used to brighten a confocal image. Examine the effects of each manipulation on image quality beyond the effect on brightness:
  1. Adjust AOTF, remove ND filter, or increase the laser power.
  2. Open pinhole diaphragm.

3. Increase the PMT gain.
4. Decrease the PMT offset.
5. Reduce the scan speed.
6. Increase the zoom factor.

- Examine the effect of pinhole diameter on the thickness of the optical section.
- Compare the effects of built-in confocal filter sets with bandpass versus longpass emission filters using a specimen labeled with multiple fluorophores. Note the effects on brightness/quality of the image and bleedthrough of nonspecific fluorophores.

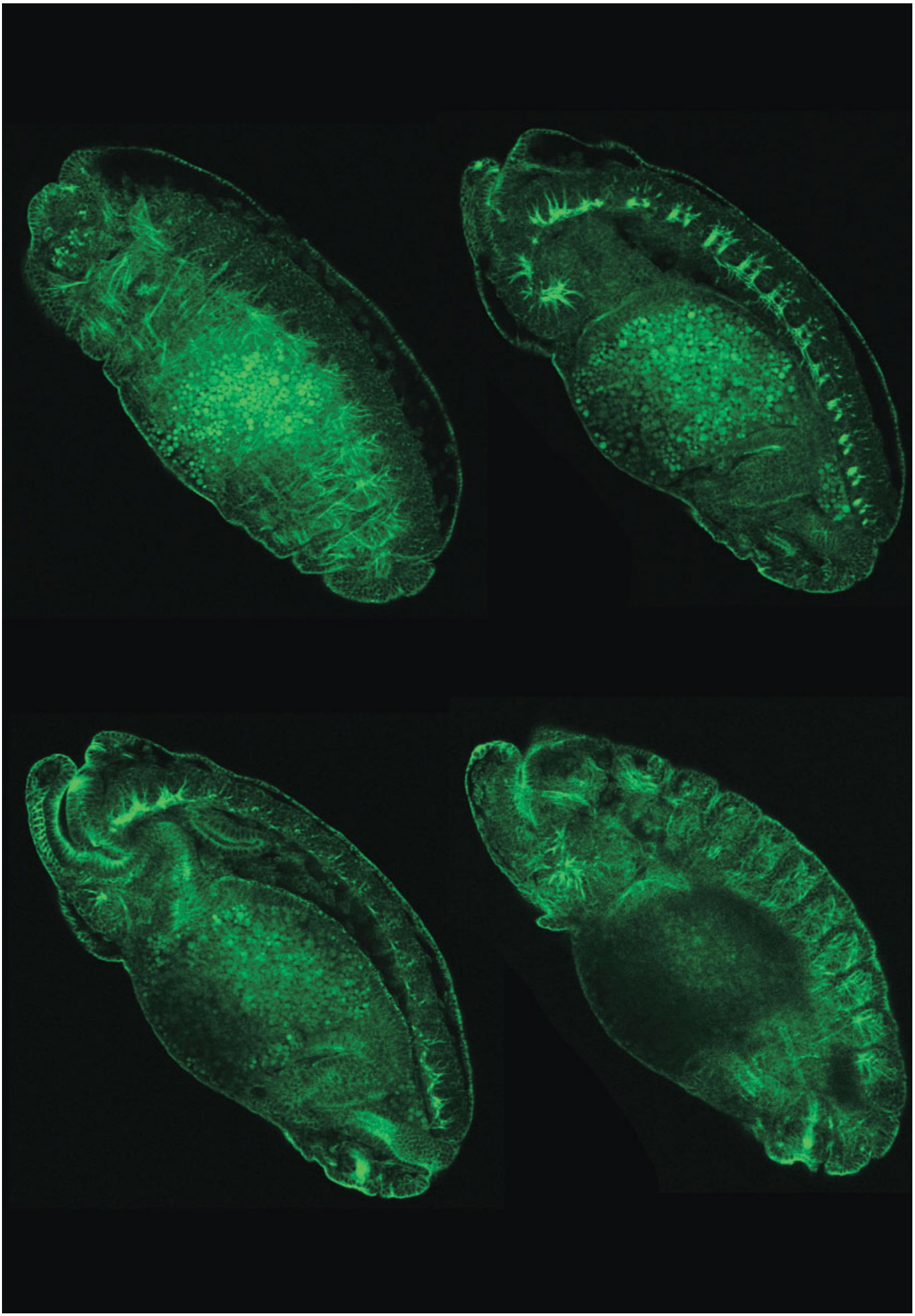

CHAPTER
14

TWO-PHOTON EXCITATION FLUORESCENCE MICROSCOPY

OVERVIEW

Fluorescence microscopy reveals the distribution of molecules in cells and tissues at great specificity and sensitivity. For widefield microscopy, the useful imaging depth in uncleared tissue sections is usually less than 10 μm, and for confocal imaging, no more than 50 μm. But there are specimens, such as neuronal tissues and developmental systems, where it is desirable to image fluorescent objects with the same specificity and sensitivity, but at depths of hundreds of micrometers. Fluorescence imaging in these cases must overcome a number of problems: structural components strongly scatter visible wavelengths, resulting in weak excitation of fluorophores, and images become distorted from lens aberrations, especially spherical aberration, in different refractive index environments. The result is faint, blurry images lacking in object detail. One solution is a form of laser-scanning microscopy with a *pulsed near-infrared (IR) laser* that excites fluorescence excitation by two-photon absorption and results in a highly *localized excitation of fluorescence*. Together these features reduce scatter, decrease fluorescence background, and produce bright, high contrast, fluorescence images even at great depths in thick specimens (Fig. 14.1). *Two-photon excitation fluorescence imaging*, along with a two-photon scattering method called *second harmonic generation (SHG) microscopy* (Franken et al., 1961; Freund et al., 1986), as well as the three-photon correlates of these methods and other methods are collectively referred to as *multiphoton microscopy* (see reviews by Mertz, 2004; Svoboda and Yasuda 2006; Zipfel et al. 2003). Two-photon microscopy was introduced as a new method for biological

Two-photon images of a Drosophila embryo. Courtesy of Byeong Cha, College of Medicine, University of South Florida.

Fundamentals of Light Microscopy and Electronic Imaging, Second Edition.
Douglas B. Murphy and Michael W. Davidson.

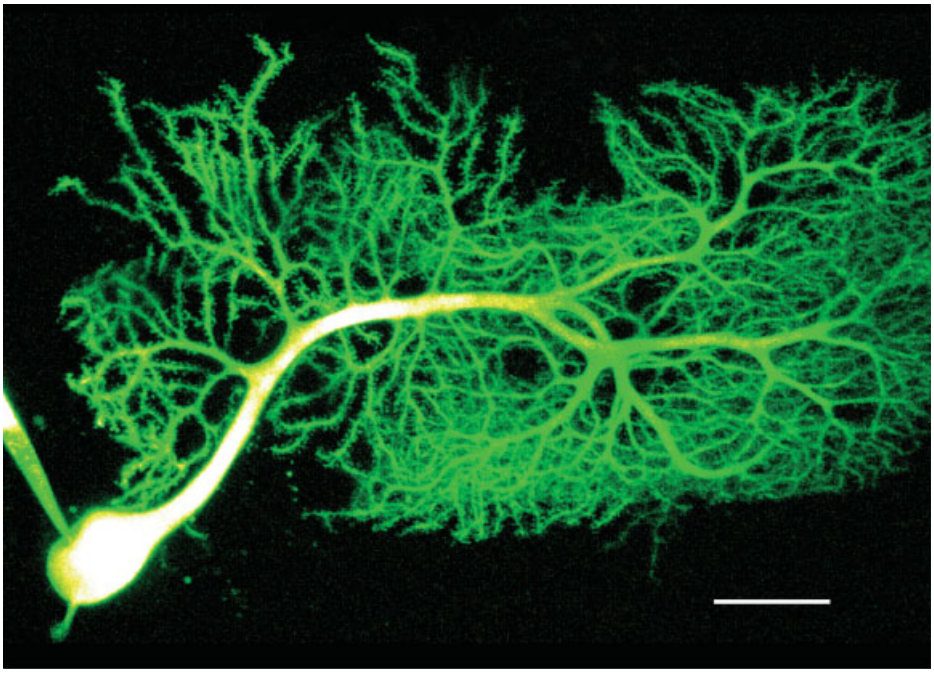

Figure 14.1

Dendritic spines of a neuron in a thick slice of brain tissue were imaged by two-photon fluorescence microscopy. These particular neurons, which were used for physiological recording, are 300 μm below the surface of the slice, which was imaged with a 25×/1.05NA water immersion lens. Bar = 5 μm. (From Denk and Svoboda, 1997, with permission, Cell Press.)

imaging in 1990 (Denk et al., 1990). Our goal is to describe the mechanism of two-photon excitation and SHG microscopy, define some of the unique terms required to understand the process, outline the special equipment that is needed, and provide some examples that highlight the advantages of this special form of fluorescence imaging.

THE PROBLEM OF PHOTON SCATTERING IN DEEP TISSUE IMAGING

The greatest impediment to fluorescence imaging deep in tissues is light scattering, which weakens the beam exciting the specimen and reduces the number of fluorescent photons reaching the detector. The scattering of light in tissues is largely due to the presence of objects like cell bodies and cell components that are larger than the wavelength of light (Mie scattering), a phenomenon that increases exponentially with increasing specimen thickness. In confocal microscopy using visible light, scattering is so severe that imaging is usually limited to specimens less than 10- to 50-μm thick.

Two-photon microscopy with near-IR illumination solves some of these problems. For one thing, certain tissues like neural tissue are relatively transparent to near IR wavelengths, so that only about half of the incident excitation photons are scattered for every 50–100 μm of tissue thickness. IR light is also absorbed less in tissues and

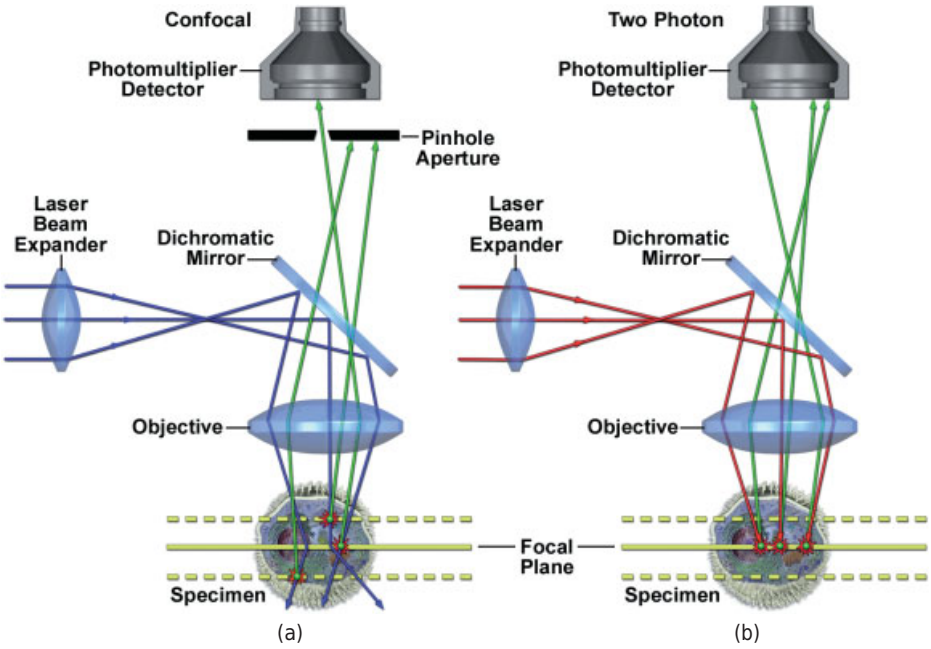

Figure 14.2

Light scattering limits fluorescence imaging. (a) In confocal imaging, scattering reduces excitation of the specimen and diverts confocal fluorescent rays (green arrows) from the pinhole, cutting signal strength. (b) In contrast, for two-photon imaging with near-IR rays, scattering of excitation rays is reduced, and fluorescence emission from the focal plane (green arrows) is efficiently collected on a wide area PMT. The improvement by two-photon imaging of deep tissue imaging is substantial.

produces less autofluorescence than does visible light, which further improves the efficiency of penetration and excitation. In addition, photon damage is avoided because of the pulsed nature of light delivery with a mode-locked laser, and because fluorescence excitation is highly localized (Fig. 14.2). As a result, it is possible to use two-photon microscopy to image structures in samples of brain tissue that are in excess of 1-mm thick (Fig. 14.3).

TWO-PHOTON EXCITATION IS A NONLINEAR PROCESS

In one-photon fluorescence excitation (standard fluorescence imaging), a molecule like fluorescein or GFP is excited by a wavelength within its excitation spectrum and then emits a longer wavelength photon. In this case, molecular excitations show a linear response to illumination intensity and are not excited by longer or shorter wavelengths outside their excitation spectra. However, in a two-photon process, two photons, usually of the same wavelength and each with half the energy required to excite a fluorescent molecule, are absorbed simultaneously and have the same effect as a single photon of half the wavelength and twice the frequency and energy. The result is emission of a

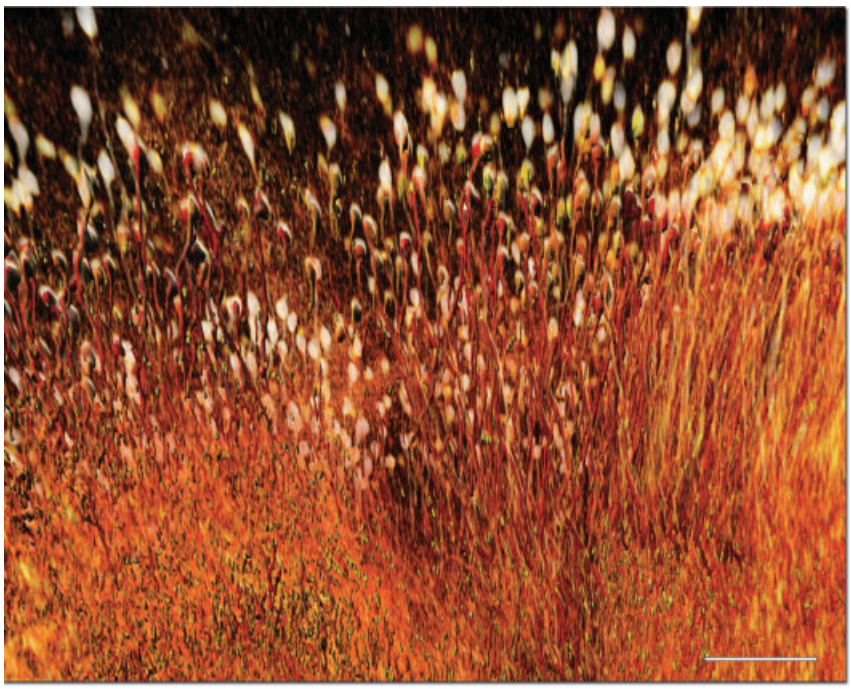

Figure 14.3

Two-photon imaging allows deep tissue imaging. Reconstructed tiled *z*-stack from a through-focus series of a 3.5-mm thick section of mouse brain hippocampus tissue expressing enhanced yellow fluorescent protein (EYFP). High-quality images are obtained at depths up to 500 μm, and useful information is still obtained at depths of up to 800 μm and beyond. Bar = 200 μm. (With permission, Olympus America Inc.)

single fluorescent photon (Fig. 14.4). It seems implausible that long wavelengths completely ineffective in one-photon stimulation are exactly what are needed for two-photon excitation. Because two-photon excitation depends on two simultaneously absorbed photons, *stimulation to the excited state is proportional to the square of the light intensity, and it is therefore a second-order, nonlinear process. Thus, to double absorption by the two-photon mechanism, one needs to quadruple the excitation intensity.*

To estimate the wavelength required to stimulate a fluorescent dye by the two-photon process, one just doubles the one-photon absorption maximum, but excitation spectra are blue-shifted compared with the expected values and are complex, sometimes bearing little resemblance to their one-photon correlates. Nevertheless, as an approximation we can say that dyes excited in the 400–500 nm range require ~800- to 1000-nm IR excitation for two-photon fluorescence. The two-photon excitation spectra of small fluorophores in particular are somewhat unpredictable and irregular; the spectra for larger molecules like fluorescent proteins are more regular (Figs. 14.5 and 14.6). Fluorescence emission resulting from two-photon excitation has exactly the same spectrum as emission resulting from one-photon excitation, so those accustomed to one-photon fluorescence microscopy must consider that emission photons from a two-photon process have a shorter wavelength and higher energy than the excitation photons used to produce them (Fig. 14.5).

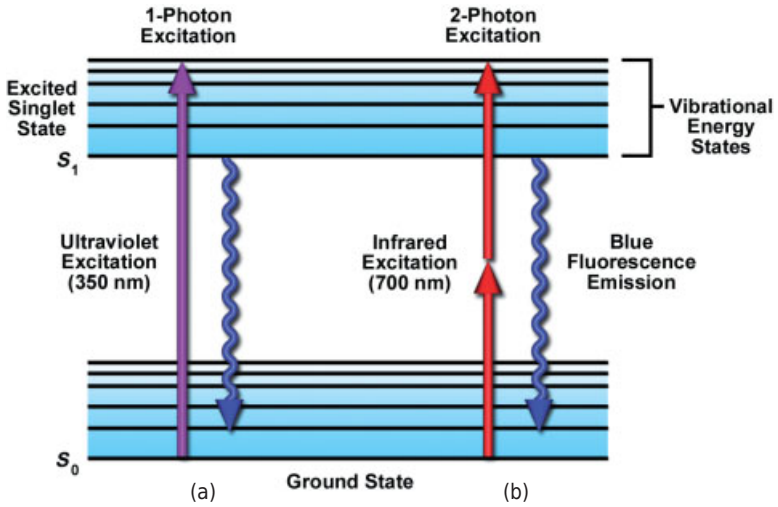

Figure 14.4

A J ablonski diagram showing one- and two-photon modes of fluorescence excitation. In one-photon excitation, fluorophores excited to the singlet excited state by absorption of a single photon of a specified energy (purple arrow) can return to the ground state through emission of a *lower energy* photon and vibrational energy (wavy blue arrow). In two-photon imaging with an IR laser, two photons, each with half the required energy, are absorbed simultaneously (red arrows), and the emitted fluorescent photon can have *higher energy* than the excitation photons (wavy blue arrow).

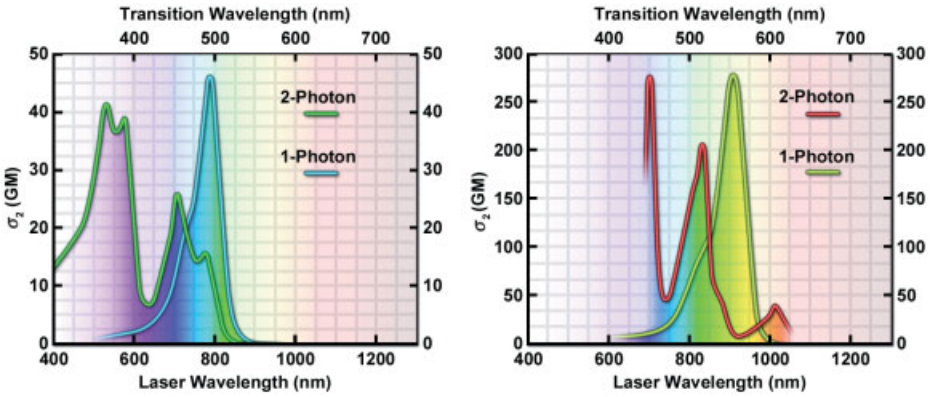

Figure 14.5

Relative two-photon excitation spectra for common probes used in fluorescence microscopy. (a) One- and two-photon excitation spectra of fluorescein. (b) One- and two-photon excitation spectra of rhodamine-b. Two-photon excitation spectra for dyes are frequently irregular profiles, but have wavelength maxima that are roughly twice those of their one-photon counterparts. Fluorescence emission spectra (not shown) are the same for both one- and two-photon mechanisms.

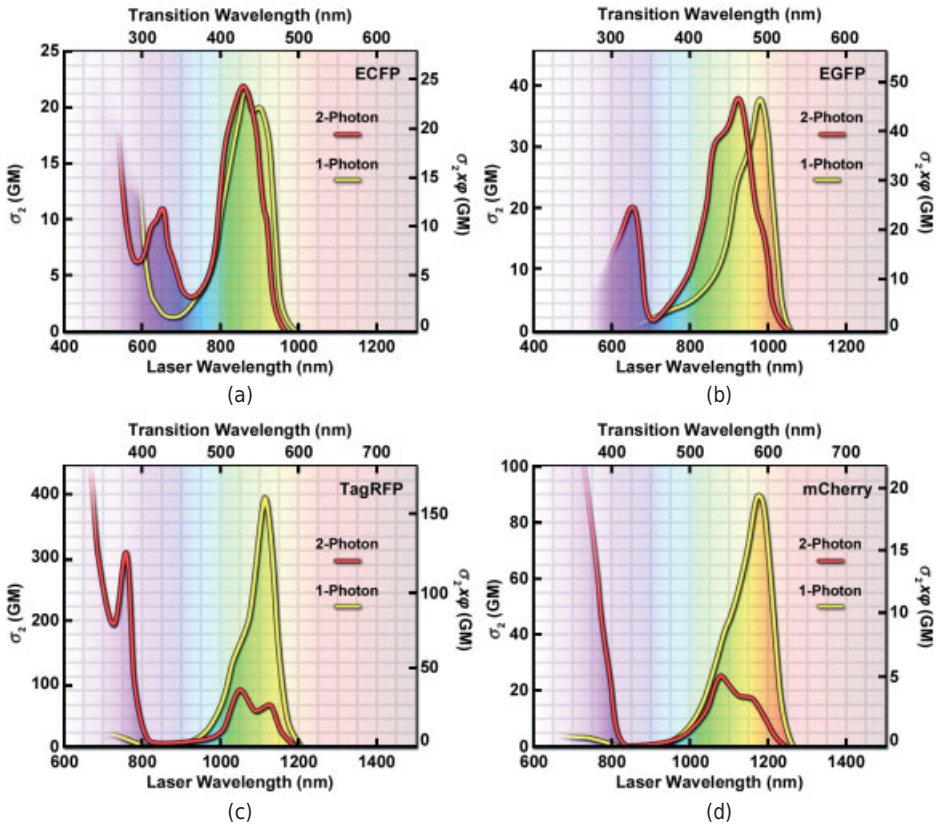

Figure 14.6

Relative one- and two-photon excitation spectra of fluorescent proteins. (a) Enhanced cyan fluorescent protein (ECFP). (b) Enhanced green fluorescent protein (EGFP). (c) TagRFP, a monomeric orange-red fluorescent protein designed to create fusions for localization studies. (d) mCherry fluorescent protein, one of the best performers in the orange-red spectral region. The two-photon excitation spectra of fluorescent proteins are more regular and generally exhibit maxima above 900 nm. In practice, GFP and mCherry proteins are excited at 900 and 1100 nm. Using one-photon excitation, these proteins are excited between ~450 and 590 nm.

Molecular Cross-Sections and Göppert-Mayer (GM) Units

Since two-photon excitation is rooted in principles of quantum mechanics, it is not convenient to describe two-photon absorption in terms of Beer's law and molar extinction coefficients; instead, absorption is related to the *probability of molecular excitation* in the electric field of light and is described by the term *molecular two-photon cross-section*, σ. The term σ includes the product of the areas of two excitation photons times the very short length of time within which a target molecule simultaneously absorbs two photons and enters an excited state ($\sim 10^{-18}$ s).

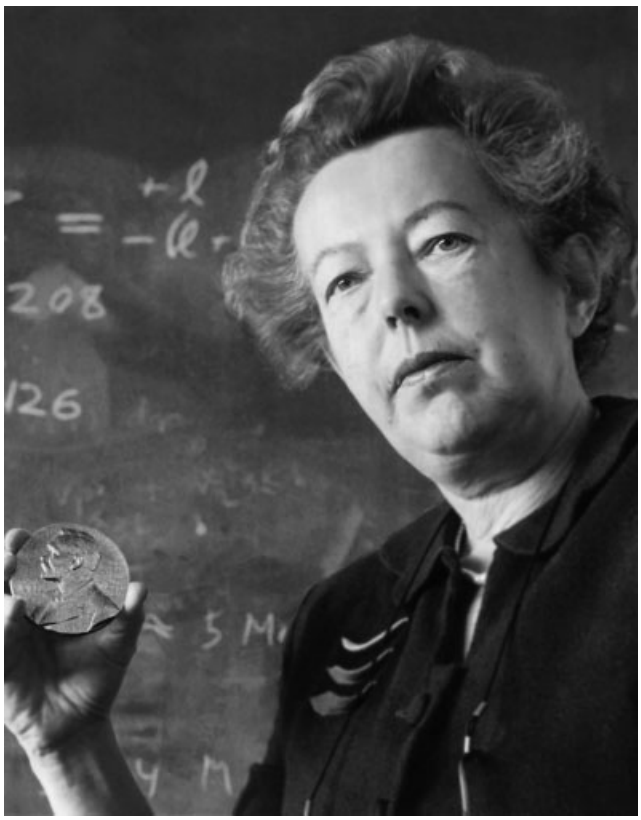

Figure 14.7
Maria Göppert-Mayer (1906–1972), a German-born American nuclear physicist, received the Nobel Prize in physics in 1963 for extensive contributions to the shell nuclear model of the atom. For her doctoral thesis in physics (1931 in Göttingen, Germany), Göppert-Mayer described the theory of two-photon absorption by atoms, although the phenomenon was not observed in the laboratory until some 30 years later after development of the laser. (With permission from Corbis Images.)

In practice, investigators refer to two-photon *action cross-sections*, the product of σ and fluorescence quantum efficiency, which are given for a particular wavelength in *GM units* (Fig. 14.7), where 1 GM = 10^{-50} $cm^4 \cdot s \cdot photon^{-1}$. Cross-section values vary greatly for different fluorescent molecules. In two-photon fluorescence excitation, most molecules have cross-sections in the range of 1–300 GM, but fluorescent molecules span a wide range of values, from 10^{-4} GM for NADH to 10^4 GM for certain quantum dots. Another related term, relative two-photon excitation spectrum, refers to the distribution of the relative amount of fluorescence emitted at different excitation wavelengths.

LOCALIZATION OF EXCITATION

The most important property of two-photon microscopy that makes it valuable for deep tissue imaging is a feature called *localization of excitation*, the confining of all fluorescence excitation to a tiny volume at the focal point. In fact, fluorescence excitation is restricted to the volume of the central diffraction spot of the point-spread function of the focused beam, a spot in the focal plane (Fig. 14.8). Due to the nonlinear effect of photon excitation (two-photon excitation diminishes with the 4th power of the distance from the focal plane) the light intensity is immediately too weak outside the focal plane, and there is no fluorescence. Because fluorescence is restricted to the focal plane, two-photon images have excellent contrast and definition, 3D images can be obtained from image stacks of through-focus series, and photodamage and photobleaching are greatly reduced. Resolution in two-photon imaging is discussed later in this chapter.

The effect of the nonlinear intensity-squared relationship, frequency doubling, and the localization of excitation is demonstrated in Figure 14.9. The figure shows areas of photobleaching (dark areas) where one-photon excitation with a confocal microscope was used to excite a small patch in the middle of a plastic slab embedded with a green-yellow fluorescent dye. A laser beam focused to a point in the middle of the slab was scanned back and forth in a raster to create a bleached region after which a conventional *z*-stack of images was prepared with a confocal microscope. The *x*,*z*-projection of an

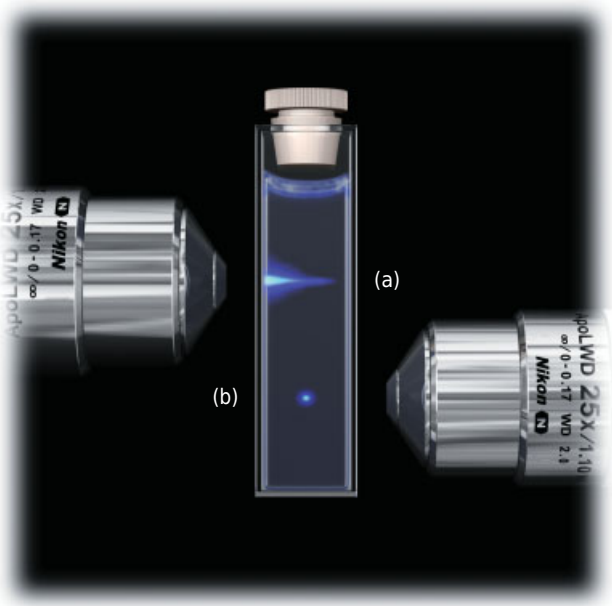

Figure 14.8

Localization of excitation by two-photon excitation. (a) One-photon excitation of fluorescein dye in a cuvette by a focused 488-nm beam of a laser shows an extended path of excitation above and below the focal plane. (b) Two-photon excitation of the same dye with a 960-nm near-IR beam shows just a single isolated point.

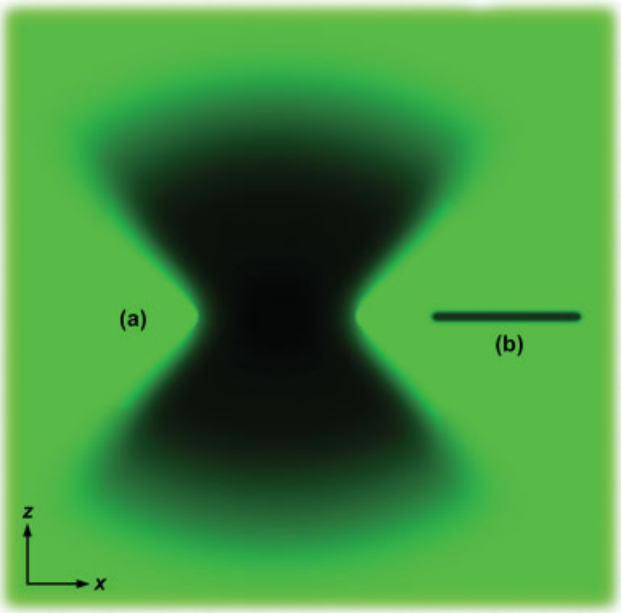

Figure 14.9

Localization of excitation by a microscope objective in a fluorescent substrate. A confocal microscope (a) and a two-photon microscope (b) were used to photobleach an area of interest at the same depth of focus of a rhodamine-containing plastic substrate. The plastic block was scanned with a confocal microscope to produce an image stack through the bleached area and the stack displayed as an *x*,*z* plane perpendicular to the surface of the block. Two-photon excitation bleached a sharply defined line in the focal plane (b), whereas confocal imaging bleached the figure of two cones meeting in the focal plane (a) and indicating the numerical aperture of the objective.

image stack through the region (a sideways *x*,*z*-view of the region) shows, for the one-photon case, the characteristic hourglass shape of the photobleached zone, where the focal plane resides at the waist of the hourglass figure. The bleached zone represents the cone of light between the lens and the focus, and the steepness of its shape and the rate of fall-off in fluorescence away from focus depend on the numerical aperture (NA) of the objective. Clearly, conventional one-photon confocal imaging stimulates (and bleaches) fluorescent molecules at all planes along the *z*-axis. However, in the case of two-photon imaging with an IR beam, fluorescence excitation is localized exclusively to the focal plane, and there is no fluorescence excitation at locations on the *z*-axis above and below the focal plane (Fig. 14.10).

To explain the localization effect, it is helpful to examine the intensity squared relationship further and compare the amount of fluorescence observed for one- and two-photon excitation in transverse sections of the light cone at different distances from the focal plane along the *z*-axis. The total fluorescence (Φ) in each plane is described as the product of the absorption rate (ϕ) and the area (A) of the excitation zone at a distance (z) from the focal plane: $\Phi = \phi A$. The relations of factors are summarized in Table 14.1, and a sketch showing the different distributions of excitation energy in one- and two-photon processes is shown in Figure 14.10.

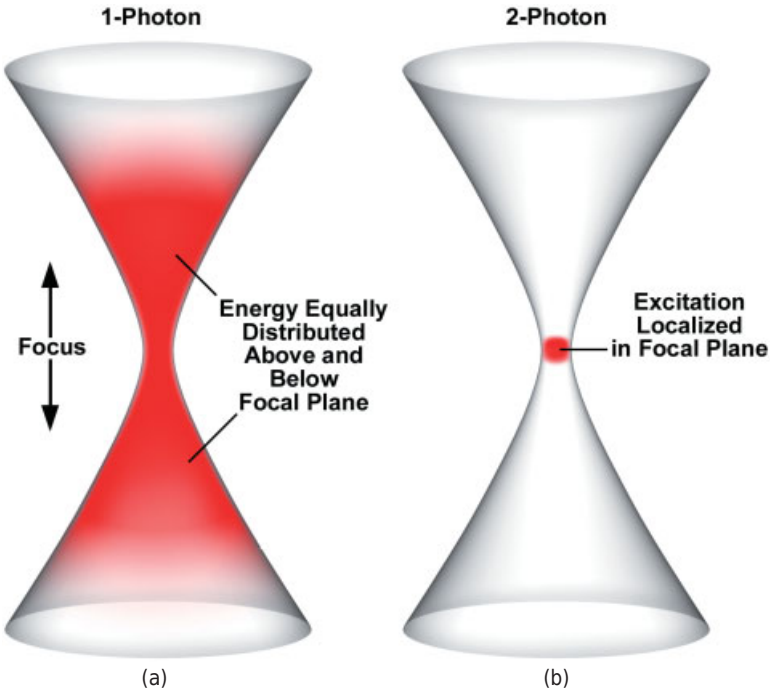

Figure 14.10

Localization of excitation deduced from basic principles. (a) Light path in a one-photon microscope showing fluorescence constricted at the focal plane but occupying all planes above and below the focus and showing the same total amount of fluorescence in each plane. (b) Light path in a two-photon microscope shows fluorescence excitation is localized (and limited) to the focal plane.

TABLE 14.1 Factors Governing Total Fluorescence Present at Different Distances from the Focal Plane by One-Photon and Two-Photon Mechanisms

Terms	1 Photon	2 Photon
Absorption rate ϕ	$\phi \sim I$	$\phi \sim I^2$
Intensity I	$I \sim 1/z^2$	$I \sim 1/z^2$
Rewriting ϕ	$\phi \sim I/z^2$	$\phi \sim I/z^4$
Area A of illuminated spot at each distance z from the focal plane[a]	$A \sim z^2$	$A \sim z^2$
Total amount of fluorescence Φ at each focal plane	$\Phi \sim \phi A \sim 1/z^2 \cdot z^2 = 1$ Φ is constant in each cross-sectional area at every distance z from the focal plane	$\Phi \sim \phi A \sim 1/z^4 \cdot z^2 = 1/z^2$ Φ decreases as the square of the z distance, which localizes fluorescence to the focal plane

[a] For a typical objective of NA = 1, the z distance along the z-axis from the focal plane equals the radius of the illuminated plane at that z distance; therefore, the illuminated cross-sectional area $A \sim z^2$.

A key difference between one-photon and two-photon excitation is that the absorption rate (ϕ) is directly proportional to intensity I in one-photon excitation, but is proportional to I^2 in two-photon excitation and is thus a nonlinear process. Since intensity (I) is proportional to $1/z^2$ in two-photon excitation, the absorption rate ϕ at a given location x,y, is proportional to $1/z^4$, and fluorescence decreases precipitously. Thus, in one-photon excitation, the amount of fluorescence Φ is constant at every cross sectional area of the light cone at distance z from the focal plane, which explains the substantial fluorescence intensities above and below the focal plane. In two-photon excitation, by contrast, Φ is proportional to $1/z^2$, which gives a strong localization of excitation effect.

What intensities are required for two-photon excitation? Since the probability of excitation by simultaneous two-photon absorption is extremely low and several orders of magnitude weaker than one-photon absorption, unique conditions are employed to obtain it. Expressing light intensity in terms of W/m^2, a power of some 10^{14} W/m^2 is required for two-photon excitation. We can compare this with much lower values of 10^7 W/m^2 for the intensity of light at the surface of the sun or 10^8 W/m^2 for a 1-mW continuous laser power in a confocal microscope. The tremendous intensities required for two-photon excitation are usually obtained with pulsed IR lasers, such as a mode-locked titanium-sapphire (Ti:sapphire or Ti:S) laser as described below. At the light intensities used to excite one-photon fluorescence, say in a confocal microscope, the probability of two-photon fluorescence is practically zero.

WHY TWO-PHOTON IMAGING WORKS

The unique ability of two-photon microscopy to image fluorescence in thick specimens is due to the combined effects of several phenomena:

- Excitation is provided by IR light, typically 800–900 nm, which is absorbed and scattered less strongly than visible wavelengths.
- IR photons are scattered in tissues, but the scattered light is too weak to excite fluorescence, so fluorescence only occurs in the central diffraction spot of the Airy disk at the focal plane. This remarkable fact means that fluorescence emission is localized to a 1 femtoliter (fL) volume in the focal plane and is not hidden by a fog of fluorescence in adjacent regions (localization of excitation). As in other point-scanning methods, the scattering of the fluorescence photons is usually not an issue, because the detector is a wide area photomultiplier tube.
- Light is delivered in interrupted bursts by a femtosecond (fs) pulsed laser. The interval between pulses, ~10 ns, is about 1–10 fluorescence lifetimes, a lifetime being the time it takes for excited molecules to return to the ground state through fluorescence emission. At this rate of stimulation, there is ample time for molecules to return to the ground state rather than accumulating in a potentially damaging triplet excited state, which can lead to photobleaching and free radical formation. When pulses are of such short duration as 100 fs, extremely high powers can be attained (1000 W peak pulse intensity) even though the average power output is only about 10 mW. Therefore, peak power can be up to a million times stronger than the power of a 1-mW continuous laser in a confocal

microscope. Short pulses of such high energy are sufficient for two-photon fluorescence excitation, but (amazingly) are relatively harmless to cells and tissues. The use of pulsed, high intensity light is of key importance for the success of this method.

RESOLUTION

The optical resolution in two-photon imaging might be predicted to be worse by a factor of 2 due to the ~2-fold longer wavelength of near-IR light. But since as mentioned above, excitation by a nonlinear, two-photon process is proportional to the square of the light intensity, the *intensity point spread function* is likewise squared ($IPSF^2$). Thus, the IR beam scanning the specimen might have a PSF or Airy disk radius of a certain size, but the effective PSF in exciting two-photon excitation will be considerably smaller, and the effective PSF will have a considerably reduced excitation volume compared with that for one-photon imaging at the same near-IR wavelength (Fig. 14.11). The squared relationship of the linear and nonlinear PSFs can be seen in the graph in the figure. The distance corresponding to 50% of maximum intensity in the one-photon case, when squared, now corresponds to just $(0.50)^2$ or 25% of maximum in the nonlinear two-photon case.

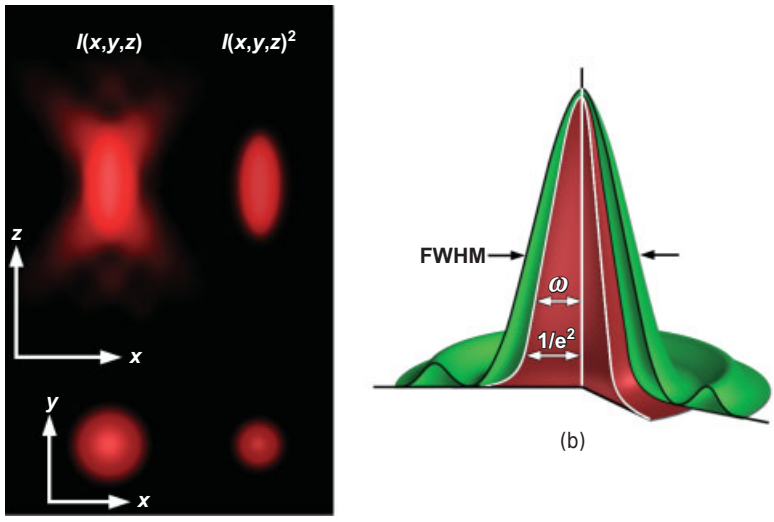

Figure 14.11

In two-photon imaging resolution is proportional to the square of the intensity point spread function ($IPSF^2$). The sketch shows the point spread function of a standard Gaussian beam from a focused laser and the radius (ω, omega) of the central diffraction spot in two-photon imaging is calculated here at $1/e$ of the height of the $IPSF^2$ distribution, where e is the base of the natural logarithm. (a) Cross-sectional and longitudinal profiles of the IPSF and (b) graph of the same showing profiles for the effective IPSFs in one-photon (green) and two-photon imaging (red).

For objective NAs >0.7, the lateral and axial resolutions can be calculated as:

$$\omega_{xy} = 0.325\lambda/\sqrt{2}\ \mathrm{NA}^{0.91}, \text{ and}$$
$$\omega_z = [0.532\lambda/\sqrt{2}]\cdot[1/(n-\sqrt{(n^2-\mathrm{NA}^2)}],$$

where ω values are $1/e$ times the value of the respective lateral and axial radii of the two-photon point spread function (IPSF[2]), and n is the refractive index. For a 1.0 NA water immersion objective at 800 nm and $n = 1.333$, the values of ω_{xy} and ω_z are 0.18 and 0.66 μm, respectively. The reader is referred to Zipfel et al. (2003) for additional useful discussions.

The excitation volume has been calculated to be a femtoliter (10^{-15} L) or less, but the volume may vary depending on laser power settings, degree of specimen saturation, and imaging conditions. It is important to remember that despite the advantages of the intensity squared relationship for resolution, for a given dye like fluorescein in a thin specimen, similar resolution will be obtained using a confocal microscope and shorter wavelengths. The unique advantage of two-photon imaging is therefore not so much in its resolution, but the localization of excitation and the ability to image deeply in specimens. In thick sections and tissues, two-photon imaging can produce much clearer, more highly resolved images than any other imaging mode.

EQUIPMENT

A two-photon microscope is typically equipped with a water-immersion, long working distance objective especially suited for deep tissue imaging; a pulsed IR laser; an optical modulator to regulate beam intensity, wavelength selection, and blanking; scan mirrors for scanning the laser beam in a raster on the specimen; photomultiplier tubes and bandpass filters for detecting particular bandwidths of fluorescence emission; and a computer for device control, image processing, and display (Fig. 14.12). The instrument might be set up as a dedicated two-photon imaging system, or, alternatively, incorporated into a general-purpose instrument equipped for widefield or confocal fluorescence imaging.

Ti:Sapphire Laser

The central feature of a two-photon microscope is the mode-locked Ti:sapphire laser for producing pulsed IR light. High-end, near-IR lasers produce 100 fs pulses at a repetition rate of 80 MHz at a peak power of 1–2 W. Such a laser produces a pulse every 10 ns, sufficient for the relaxation of fluorophores from singlet and triplet excited states back to the ground state. With each pulse occupying only 1/100,000 of a cycle time (pulse width ~100 femtoseconds), pulse energy is extremely high, sufficient for two-photon fluorescence excitation (Fig. 14.13). Thus, delivery of light from a pulsed laser is unusual, with peak pulse energy at about 1 W at 800 nm but a modest average intensity of 10 mW. When using such a beam on cells, it is possible to excite about 10% of the possible target molecules. Ti:sapphire lasers have a tuning range from ~680 to 1100 nm. Laser beam intensity is controlled with an electro-optic modulator (EOM) or an acousto-optic modulator (AOM) as in a confocal microscope.

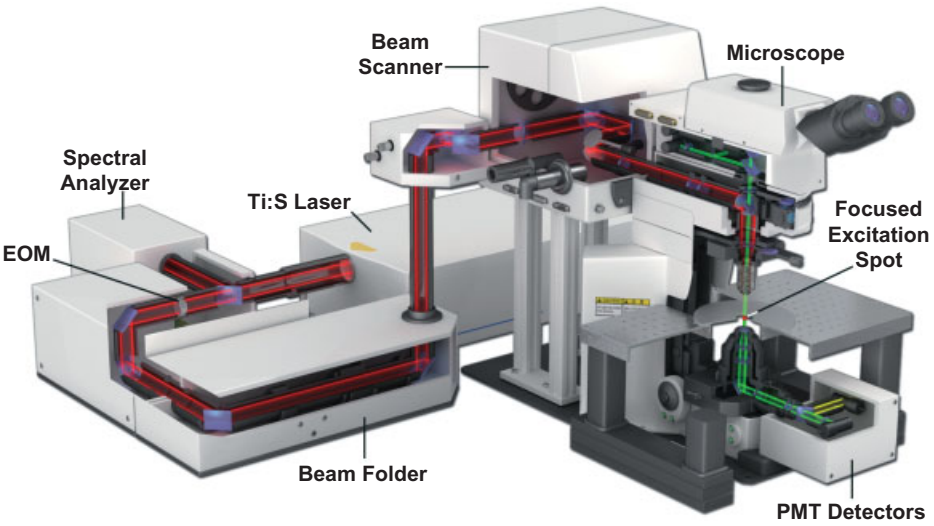

Figure 14.12

Equipment configuration for two-photon microscopy. A titanium:sapphire (Ti:S) laser producing a near-infrared beam is expanded to fill the rear aperture of the objective to form a focused point on the specimen, and the specimen is scanned in a raster pattern. Two-photon fluorescence emission is reflected by appropriate dichromatic mirrors and captured by "nondescanned" photomultiplier tube detectors. The spectral analyzer allows checking of the laser beam for proper spectral output. The electric optical modulator (EOM) controls intensity or blocks the beam.

In two-photon imaging, it is important to maintain the shape (duration) of the laser pulses and not allow them to broaden or become reduced in amplitude. The following points relate to measures that can be taken to control the pulsed laser output. On passage through the entire optical system (but primarily the objective) on the way to the specimen, the laser pulses become broadened and reduced in amplitude, resulting in weaker fluorescence signals and greatly increasing risk of tissue damage from overly long pulses. This pulse-broadening effect is called dispersion. If we examine the 100 fs pulse of 900-nm IR light in detail, we see it is actually a narrow spectrum of wavelengths with a bandwidth of ~9 nm. Lens-induced dispersion and broadening of a pulse occur because lower (redder) frequencies emerge from a lens slightly ahead of higher (bluer) frequencies, broadening the pulse, by one estimate to about 175 fs, nearly twice the length of the original pulse. This broadening phenomenon is called "chirp" (Fig. 14.14). The pulsed laser beam used for two-photon imaging can be maintained by applying a "negative chirp" of equal and opposite chromatic effect as that induced by the lens, with the result that the laser pulse length remains sharp and well defined. Prechirp optics based on a pair of prisms are sometimes contained in a separate unit, but in some instances may be contained within the Ti:sapphire laser housing.

Another form of beam modification is the use of a *passive pulse splitter*. By passing the beam through an array of prisms, it is possible to divide the pulse interval into 2, 4, 8, and so on subpulse intervals and thus produce a modified beam with progressively shorter pulse intervals, and, at the same time, smaller pulse amplitudes. By increasing power, the pulse amplitudes can be restored to their original size. Laser beams modified

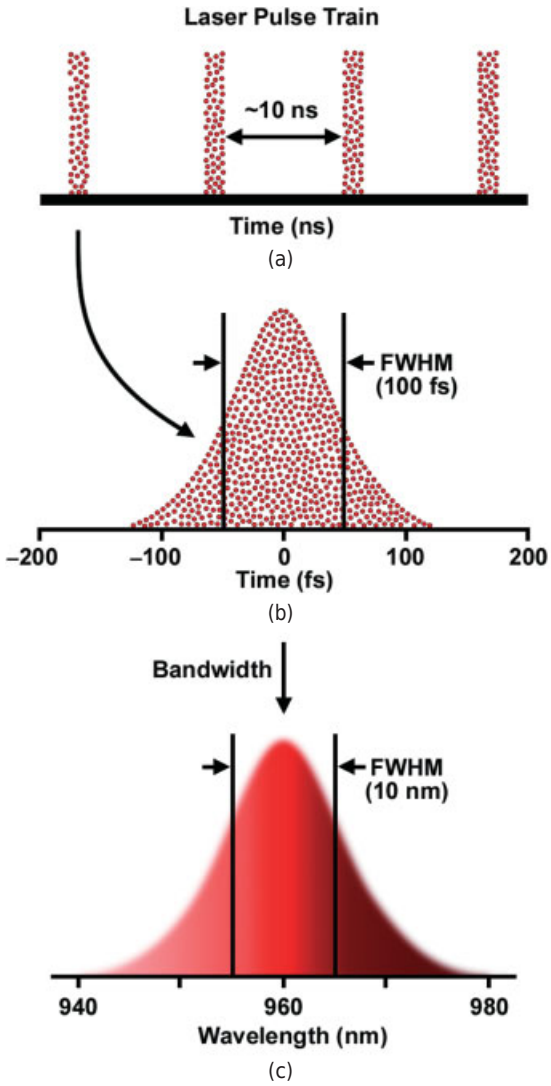

Figure 14.13

The pulsed near-IR beam of a mode-locked laser. The output of a titanium:sapphire laser is a series of pulses (a) with a pulse interval of ~10 ns and a duration (FWHM) of ~100 fs (b). Peak power is 1–2 W, but average power is about 10 mW. The spectral bandwidth is in the range of 10–20 nm (c), but the laser can be tuned from 680 to 1100 nm.

by pulse splitting reduce the rate of photobleaching and give more intense fluorescence excitation.

Scan Head

Galvanometer-driven mirrors scan the focused IR beam in a raster pattern over the specimen as they do in a confocal microscope. The dwell time of the laser spot on the specimen is adjustable, but a speed giving 100 laser pulses per pixel is useful.

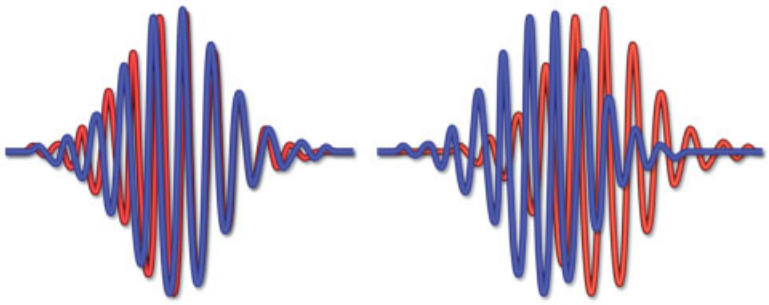

Figure 14.14

Laser chirp. Laser beams (a) become dispersed on passage through an objective because long wavelengths experience a slightly lower refractive index in the lens than do longer wavelengths, causing them to emerge sooner from the lens (b). This chromatic dispersion of the beam is called chirp. Two-photon microscopes contain prism-based devices to apply a negative chirp before the beam enters the lens, thus minimizing broadening of the pulse width and risk of photobleaching and damage.

Detectors

Since fluorescence signals from locations deep in a tissue are often weak and noisy, methods must be employed to improve signal detection. Several techniques not commonly encountered in widefield and confocal microscope designs may be encountered.

- Fluorescence photons emitted in directions away from the objective can be *collected by the condenser*, directed to a separate set of filters and PMTs, and combined with the fluorescence signal coming from the objective to increase signal strength and improve detection.
- *Nondescanned detectors*, large area PMTs suitable for collecting wide beams coming directly from the objective, are mounted near the objective and give improved detection because photons are not lost by scatter on multiple optical surfaces and scan mirrors. These detectors are sometimes called "proximity detectors" because of their location near the objective. Because the fluorescence beam in this instance does not pass back through the scan mirrors as happens in a confocal microscope, the design is also called nondescanned detection (NDD). On confocal/two-photon hybrid microscopes, the confocal PMTs are sometimes used, but limited signal capture from photon blockage at the pinhole aperture, as well as further losses from scatter on the scan mirrors, significantly reduce the signal.
- For the most sensitive detection, *GaAsP PMTs* are used, whose photocathodes are coated with gallium-arsenide-phosphide (GaAsP). GaAsP detectors have up to twice the quantum efficiency of typical PMTs (40%) and unlike many PMT designs are sensitive even out to deep red wavelengths (700 nm).

Objectives Used for Two-Photon Imaging

For the example of deep tissue fluorescence imaging in nervous tissue, where it is necessary to detect fine structures and still retain a widefield of view, a high-resolution objective of moderate magnification is very useful. The Olympus 25×, 1.05 NA water-immersion (WI) objective is ideal (Fig. 14.15a,b). This is a "dipping" type objective that can be placed in aqueous media near a tissue surface. The lens elements and optical coatings give very high transmission, and apochromatic correction spans the visible range from 400 to 1000 nm, making it suitable for IR excitation and fluorescence emission at visible and UV wavelengths.

This objective is also corrected to provide a full 27.5-mm view of the intermediate image plane formed in the front aperture of the eyepiece; the magnification of 25× gives a widefield-of-view suitable for nervous tissue, while the NA of 1.05 provides great light collection efficiency. Using the correction collar, one can correct the image for spherical aberration caused by the refractive index of the medium around the specimen, temperature, and the distance of the specimen from the coverslip; the correction collar, which controls movable internal lens elements (Fig. 14.15b), allows one to image through hundreds of micrometers of tissue and still see faint signals clearly. The working distance of 2.0 mm also allows access to the specimen when using micropipettes. Finally, the ceramic top element provides thermal insulation so that the lens does not behave as a heat sink and cool down the specimen.

A more advanced objective for deep-tissue imaging (Fig. 14.15c) employs a proprietary clearing reagent immersion medium called ScaleView-A2, designed to enable imaging up to an incredible 8 mm beneath the surface of tissue. The ScaleView reagent acts to clarify fixed biological tissue, rendering it gelatinous and clear to produce detailed, crisp images at remarkably deep penetration depths.

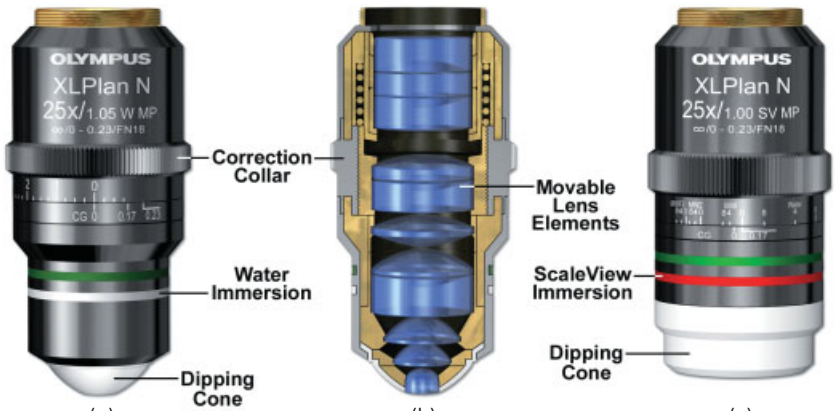

Figure 14.15

Olympus 25×/1.05 NA water immersion (a, b) and (c) 25× 1.00 NA ScaleView immersion (dipping) objectives for two-photon imaging. Note the correction collar for adjusting for spherical aberration and the ceramic tip to help maintain constant temperature of the specimen. The objective working distances are (a) 2 mm and (c) 8 mm.

Examples and Applications of Two-Photon Fluorescence Microscopy

The following examples highlight the benefits of two-photon excitation in reducing phototoxicity, increasing the depth of imaging in deep tissues, and inducing localized photochemistry.

- Two-photon excitation microscopy is generally less phototoxic than confocal microscopy, as demonstrated by recent time-lapse studies of deep brain imaging (Fig. 14.16), embryo development, and other systems.
- The nontoxic nature of two-photon excitation means it is possible to image live human skin at depths of up to 150 μm.
- Using two-photon excitation, it has been possible to avoid the phototoxic effects of UV irradiation and use UV fluorescent dyes. This feature is especially beneficial in imaging the naturally occurring reduced pyridine nucleotides (NAD(P)H) as indicators of cellular respiration, differentiation, and metabolic responses in a variety of cultured cells. Repetitive imaging of these cells cannot be performed using confocal microscopy, because of the limitations imposed by photobleaching and UV-induced photodamage.
- Because two-photon excitation microscopy utilizes mode-locked (pulsed) lasers, it can be used in combination with fluorescence lifetime imaging. Images based on nanosecond fluorescence decay times allow one to get an unambiguous value of fluorescence resonance energy transfer (FRET) efficiency between two

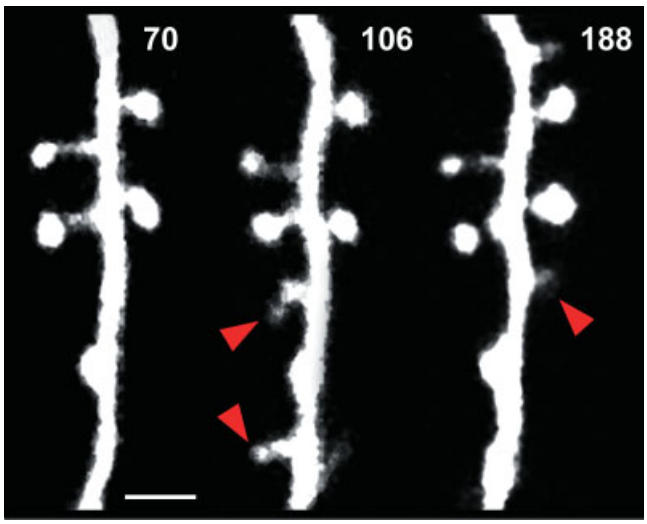

Figure 14.16

In vivo deep brain imaging, over a period of 4 months, of dendritic spines by two-photon microscopy. Dendritic spines expressing EGFP persisted and new spines appeared (red arrowheads) on mouse pyramidal cell neurons. Neurons in layer 5B were imaged in intact animals over a 4-month period (the white numbering in the upper right-hand corner of each panel indicates the postnatal day on which images were captured). Bar = 2 μm. (From Holtmaat and Svoboda, 2009, with permission, Nature Publishing Group).

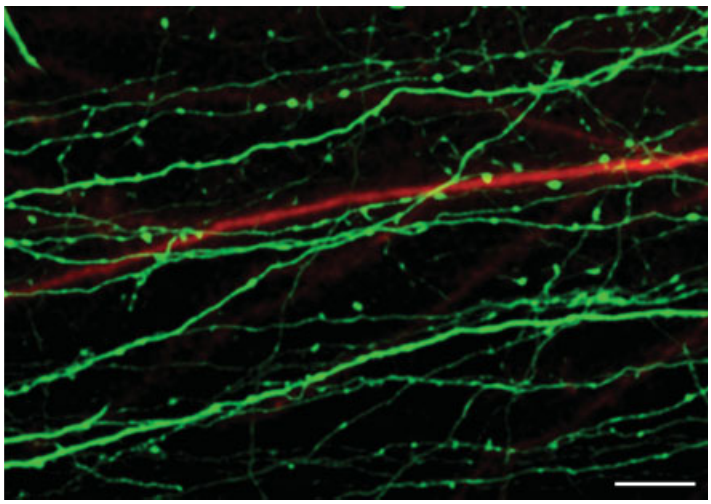

Figure 14.17
Live simultaneous imaging of green and red emitting fluorophores by two-photon microscopy in a 400-μm thick section of rat brain. Dendrites of rat hippocampal neurons were filled with Alexa Fluor 594 (red) with a patch pipette. Cortical neurons containing channelrhodopsin2-EGFP (green) course through the field. Bar = 5 μm. (Image courtesy of Dr. Bertalan Andrasfalvy, HHMI Janelia Farm Research Campus.)

molecules. Alternatively, two-photon excited lifetime imaging microscopy can be used to obtain the concentrations of metabolites like NAD(P)H in different subcellular compartments.

- Several researchers have employed genetically encoded calcium indicators or used techniques of bulk loading of calcium indicator dyes combined with two-photon excitation microscopy to map the microcircuitry of neurons in mouse brain slices.
- Another powerful application of two-photon excitation microscopy is the uncaging or photo release of certain caged compounds whose 3D distribution can then be followed by imaging in 3D over time. The method has been used to mark cells in certain embryos to follow cell movements in development.
- Two-photon excitation can be used to excite specific sites on neurons in cultured slices where neurons synthesize and incorporate channel-rhodopsin molecules into their plasma membranes. In the presence of blue light, channels transport ions leading to neuronal transmission. Using two-photon excitation to selectively excite certain locations, whole neurons, dendrites, or even single synapses can be stimulated within 1 ms to produce action potentials. Exciting work like this prepares the way for using light and membrane channel regulators to turn neurons on or off, even by stimulation at specific synapses (Fig. 14.17).

THREE-PHOTON EXCITATION

Three-photon excitation resembles the two-photon process except that three photons must interact simultaneously with the fluorophore to produce emission. The photon

density required for excitation is about 10-fold greater than the density needed for two-photon absorption, but three-photon excitation is possible on most two-photon instruments. As an example, an IR beam at 1050 nm can produce 3-photon excitation of a fluorophore absorbing UV light at 350 nm. The same illumination could also be used for simultaneous two-photon excitation of a green-absorbing fluorophore at 525 nm in the same sample. Additionally, three-photon excitation can be employed to extend the region of useful imaging into the deep ultraviolet (UV). For example, near IR light at 720-nm light can be used to excite a fluorophore that normally absorbs deep UV light of 240 nm. By extending the range of excitation in this way, three-photon excitation becomes a valuable imaging tool, since most microscope optics are opaque to UV wavelengths below approximately 300 nm. Higher order nonlinear effects, such as four-photon absorption, have been demonstrated, but it is unlikely that these phenomena will find any immediate application in biological research.

SECOND HARMONIC GENERATION MICROSCOPY

In addition to two-photon fluorescence imaging, there are also nonlinear methods for imaging light scattering, such as *second harmonic generation (SHG) microscopy* and *coherent anti-Stokes Raman scattering (CARS) microscopy*. SHG images produced by nonlinear scattering are distinct from images produced by ordinary light scattering (linear scattering) that are detected by darkfield microscopy as described in Chapter 7, because, optically, the scattered light signal is coherent (waves vibrating in same plane and in phase with each other), and because the intensity of the signal shows a nonlinear relationship to the intensity of the illuminating beam. As described below, *images are obtained through a two-photon effect by point-scanning the specimen with a pulsed IR laser* as in two-photon fluorescence excitation. Objects that exhibit SHG scattering are also distinct in exhibiting molecular order (aligned assemblies of asymmetric molecules collagen, myosin, microtubules, starch grains, and certain styryl dyes oriented in lipid bilayers; Campagnola et al., 2002). An image of collagen fibers in a section of tendon is shown in Figure 14.18. SHG images in some ways resemble images obtained by polarization microscopy, both in their appearance and requirement that specimens exhibit molecular order, and because the images are sensitive to specimen orientation. However, in polarization microscopy, signals are polarized but incoherent and imaging is based on birefringence and factors, such as polarizability of atomic bonds and refractive index differences along different axes in the specimen. In contrast, SHG images are dependent on the orientation of electric dipoles under conditions of intense illumination.

The SHG effect was first demonstrated by Franken et al. in 1961 and is now commonly used in physics, radio, and photonics. Freund and co-workers introduced SHG for biological imaging in 1986. For a familiar, practical example, the 532-nm light in a green laser pointer is made by a SHG process in which 1064-nm light from an IR laser diode, which itself is generated from another source, illuminates a crystal of potassium dihydrogen phosphate (KDP) to generate a frequency-doubled beam of coherent green light at 532 nm. Some of the key characteristics of SHG imaging and features that distinguish it from two-photon fluorescence excitation imaging are summarized as follows:

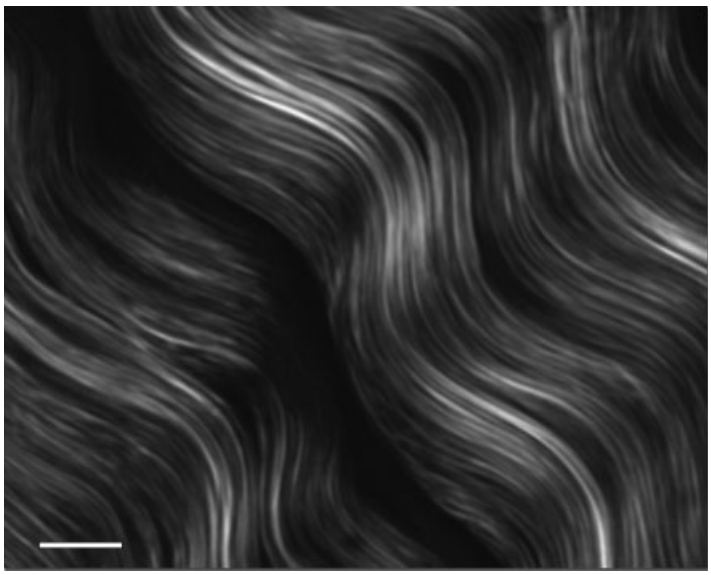

Figure 14.18
Forwards scattered SHG image of collagen bundles in a mature tendon. Bar = 10 μm. (From Williams et al., 2005, with permission, Cell Press.)

- SHG specimens behave as *electric dipoles* in an intense beam of light. Thousands of dipoles aligned in the microscope field scatter light coherently under conditions of intense laser illumination, and the intensity of the scattered light signal responds nonlinearly to the intensity of the illuminating beam. A pulsed IR laser beam focused on a suitable object generates frequency-doubled scattered photons. A process of *phase matching* among frequency-doubled scattered photons means that the forward-scattered photons vibrate in the same phase. Dipole emission is very sensitive to the orientation of the dipole axis, since emission goes as $\sin^2\theta$ where θ is the angle from the dipole axis. Because photons do not lose energy in the scattering process, they remain monochromatic, and since elastically scattered photons do not experience energy loss (there is no Stokes shift), scattered photons have exactly twice the frequency, twice the energy, and one-half the wavelength as the illuminating beam (also called the *fundamental wavelength*). Mathematically, the frequency-doubled beam is the same as the squared fundamental wavelength (the driving wavelength), and scattered photons are phase-matched with it.
- The nonlinear scattering that is imaged in SHG microscopy typically has a very strong *forward-directed* component and a substantially weaker *backward-directed* component. This pattern of scattering, called Mie scattering, is typical for scattering objects larger than the wavelength of light (collagen fibrils, muscle fibers, mitotic spindles, and cells), and is distinct from Rayleigh scattering involving atoms and small molecules where the scattering envelope is much more symmetric. The ratio of forward/backward signals is not fixed and is determined by the axial extent of the scattering object relative to the wavelength. Whereas *the*

forward component in SHG scattering is coherent, coherence in the backward scattered signal depends on specimen thickness and the amount of phase advance across the specimen. Because of coherence, the forward-scattered signal can be examined using a linear polarizer just as in polarized light microscopy.

- SHG specimens are unique. Examples of SHG specimens include anisotropic crystals or parallel arrays of polymeric structures such as collagen filaments, myosin filaments, microtubule bundles, starch grains, and special dyes and nanocrystals. All of these objects show a high degree of molecular order, are *noncentrosymmetric*, that is, have no molecular symmetry about a central point, and act as polarizable dipoles in the electric field of an intense beam of light. Such specimens are said to exhibit *dielectric hyperpolarizability*, with the dipole axis usually oriented parallel to the long axis of the molecule. SHG generation is also sensitive to the ionic strength of the surrounding medium, with low ionic strength media producing brighter signals. This fact can be useful when imaging isolated specimens *in vivo*.
- *Fluorescence excitation by a two-photon mechanism is different from SHG*, because in fluorescence, energy is always lost when molecules relax to the ground state (a Stokes shift is observed). Therefore, wavelengths of fluorescence emission are longer than the frequency-doubled excitation wavelength.
- Like two-photon fluorescence excitation, the intensity of scattered light in SHG microscopy increases with the square of the illumination intensity, and intensity decreases with the inverse of the fourth power of the distance from the focus, meaning frequency-doubled scattering is essentially restricted to the focal plane in a manner similar to two-photon fluorescence imaging. This relationship gives *precise optical sectioning without the requirement of a pinhole*, and is therefore suitable for creating image stacks for 3D reconstruction. The method works even for objects located up to 500-μm deep in a tissue.
- Because scattering in SHG is elastic, *target molecules do not absorb energy*. SHG imaging therefore *greatly reduces photodamage* to living specimens.

A two-photon fluorescence microscope can be modified for SHG imaging. A pulsed femtosecond IR laser is imaged as a point and scanned in a raster pattern across the specimen. Because the emergent scattered beam coming from the specimen is both coherent and dependent on specimen orientation, the microscope requires optics for rotating the planes of the illuminating and scattered SHG beams. A rotatable quarter-wave plate or half-wave plate placed before the scanner or objective is convenient for orienting the laser beam. An absorbing glass filter or dichromatic is used to remove the IR illumination wavelengths, and a rotatable analyzer before the detector is employed to optimize contrast. For efficient forward-directed scattering along the optical axis, the specimen is oriented so that the E-vector of the coherent laser beam is parallel to the orientation of the dipoles. For many types of filament arrays, such as collagen and microtubules, this means placing the filaments parallel to the surface of the microscope slide and perpendicular to the propagation axis of the imaging beam and then orienting the filaments with their long axes parallel to the plane of the E vector of the illuminating laser beam. SHG images of the forward scattered component show longitudinal profiles of filament bundles (Fig. 14.18).

At present, methods for SHG imaging in living cells are still in development, but useful clinical applications have emerged, such as the examination of abnormal

collagen arrangements in connective tissue diseases. New directions for SHG imaging include treatment of specimens with polarizable nanocrystals and *electrochromic styryl dyes* that fill intracellular spaces and incorporate asymmetrically into one face of lipid bilayers, thereby allowing clear SHG views of cells and delimiting cell membranes. There are also ongoing attempts to use dyes to reveal the action potentials in living neurons.

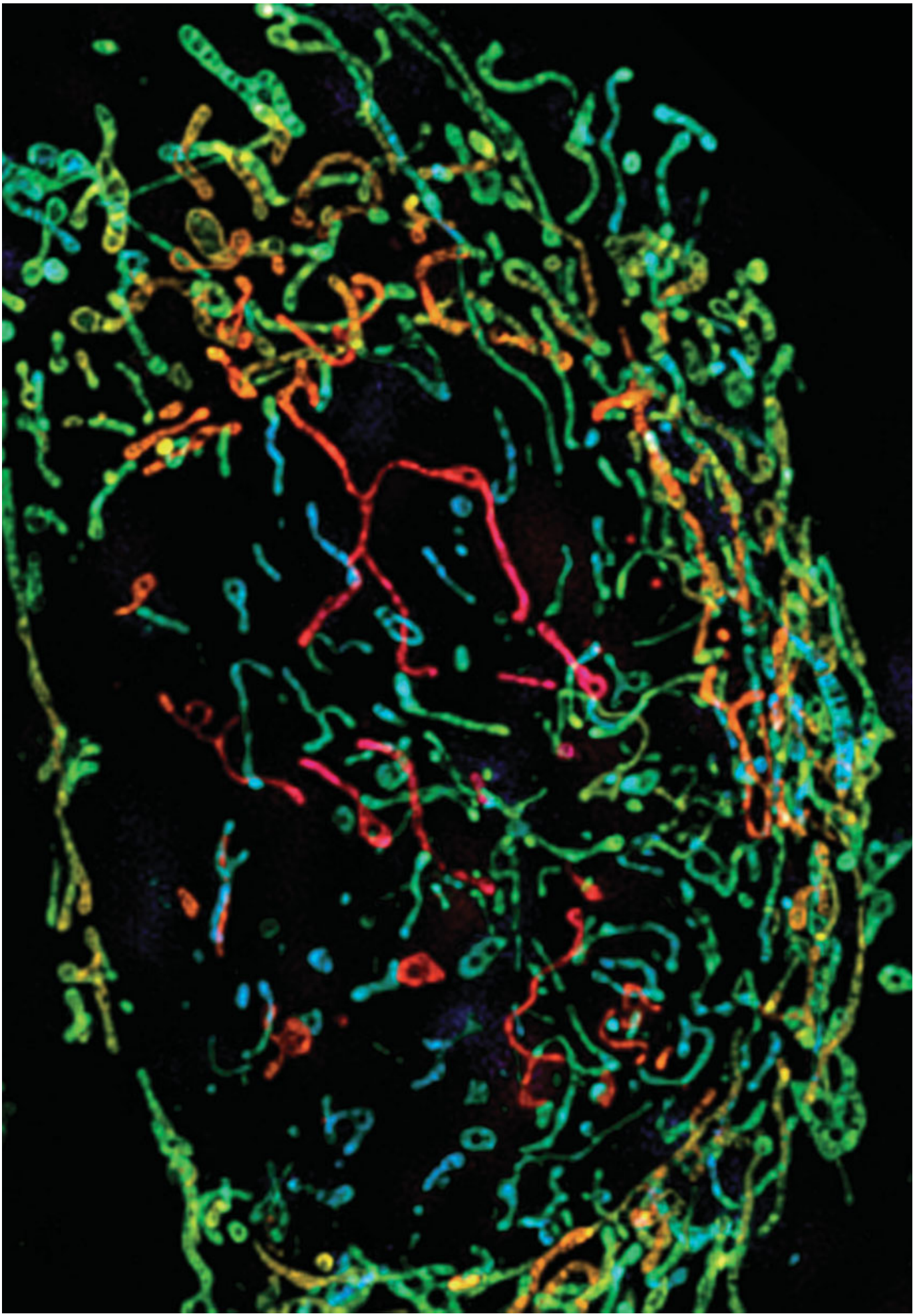

CHAPTER
15

SUPERRESOLUTION IMAGING

OVERVIEW

Abbé's equation for resolution in a light microscope, $d = \lambda/2\text{NA}$, has been useful for calculating spatial resolution since it was first proposed in 1882, as we learned in Chapter 6. Thus, microscope resolution entails the ability to distinguish between two closely spaced objects in the image plane, but is limited by diffraction of light as the wavefronts pass through the objective aperture. Regardless of the optical quality of the lenses, lateral resolution (in the x–y plane) is restricted at the highest numerical aperture (NA) to around 200–250 nm whereas axial resolution (in the z plane, along the microscope optical axis) is over twice as poor, somewhere in the range of 500–700 nm. The reason axial resolution is lower than that in the lateral dimensions is due to the asymmetrical nature of the almost spherical light wavefronts focused on the specimen. This limitation is often referred to as the *diffraction barrier* and is a serious impediment in our ability to distinguish many of the important subcellular features present in living and fixed cells.

In fluorescence microscopy using a high NA oil immersion objective (NA = 1.4 or greater), the excitation light is focused on the specimen in what is termed a *diffraction limited spot* that has dimensions of 200–300 nm^2, depending upon the illumination wavelength. All of the fluorophores within this diffraction volume are simultaneously excited and emit their fluorescence in concert to produce a blur of unresolved signal that obscures both the number of fluorescent molecules, as well as any details smaller than the illumination spot size. Therefore, two fluorophores spaced 200 nm or less apart

Structured illumination (SIM) image of mitochondria in a cultured cell. Courtesy of Lin Shao, HHMI Janelia Farm Research Campus.

Fundamentals of Light Microscopy and Electronic Imaging, Second Edition.
Douglas B. Murphy and Michael W. Davidson.

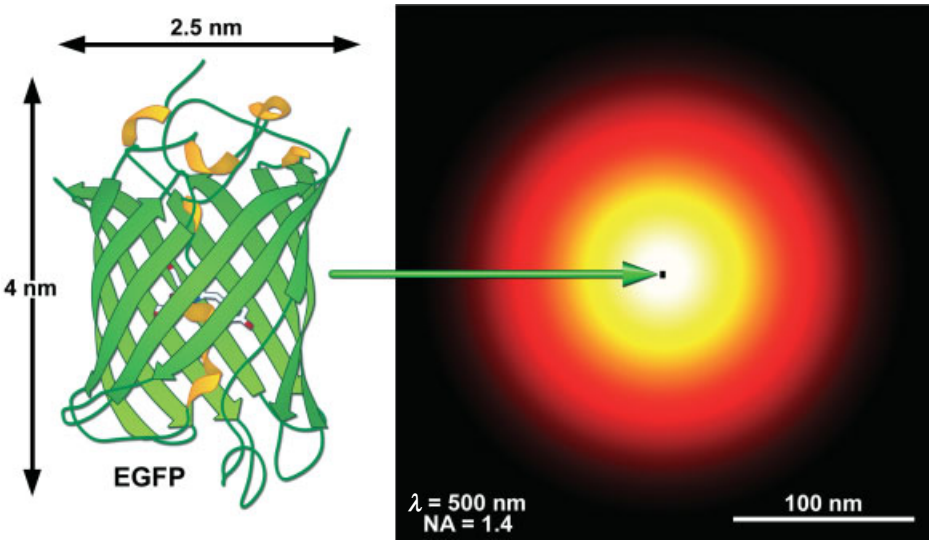

Figure 15.1

Enhanced green fluorescence protein (EGFP) and a comparison of its physical size to the size of its image in the fluorescence microscope.

will appear to be a single object. This is true regardless of whether only one or 100 or more molecules reside within the area excited by the illumination spot. As a result, many of the features present in very small cellular structures, such as mitochondria, the Golgi complex, lysosomes, peroxisomes, and the cytoskeleton appear as unresolved fluorescent blobs.

As research interests have become increasingly more molecular in scope, so too has the need for increased resolution using convenient optical instruments. Shown in Figure 15.1 is the 200-nm diameter, diffraction limited point-spread function (PSF) of a fluorescent EGFP molecule, an average size protein, produced by a widefield objective. In comparison, a single EGFP molecule, measuring 2.5×4 nm and the source of the photons making up the PSF, is represented by the small black speck at the center. The large PSF is what gives rise to blurring in widefield fluorescence images. It seems improbable that light in the visible spectrum could be used to resolve spatial details much smaller than a wavelength, but this in fact has become an active area of research and development. New superresolution imaging techniques are being developed at such a rapid pace that it does not seem unreasonable to expect true molecular resolution by light-based instruments in the near future.

In the early 1990s, a wide range of instruments and methods was introduced aimed at improving spatial resolution. Some of the main developments at that time were microscopes with opposed dual objectives sporting names like 4Pi and I^5M that achieved resolution in the range of 100 nm by dual-beam interference (Stefan Hell, Mats Gustafsson, David Agard, and John Sedat), standing wave microscopy (Fred Lanni, Lans Taylor, and collaborators), and near-field microscopy (Ash, Betzig, and others) that were capable of 1-nm resolution. These instruments improved resolution in significant ways, but were limited in performance and applicability, and, in some cases, were technically demanding. Later in the 1990s, Stefan Hell introduced STED microscopy

together with new concepts dealing with the use of certain fluorescent dyes in high resolution imaging. Together, these developments led to a revolution in superresolution fluorescence microscopy and the introduction of new methods that offered lateral and axial resolution in the tens of nanometers and even less. A common feature of many of these methods is that they use Stefan Hell's discovery that fluorophores can be photoswitched on and off, sequentially in time, so that the signals can be recorded consecutively in the microscope.

In this chapter, we introduce three methods for superresolution microscopy that are effective, user-friendly, and commercially available. These include: (1) *single-molecule localization*, including *PALM (photoactivated localization microscopy)* and *STORM (stochastic optical reconstruction microscopy)*; (2) *structured illumination microscopy (SIM)*, a combination of optical and image processing methods for extracting high frequency information from microscope images in so-called reciprocal space; and (3) *STED (stimulated emission depletion)* as well as *GSD (ground state depletion)* microscopy, where the Airy disk itself is engineered to smaller physical dimensions so that established methods of point scanning microscopy can produce higher resolution.

THE RESOLFT CONCEPT

Many of the superresolution methods described here are based on a principle first advanced by Stefan Hell and associates called *RESOLFT, reversible saturable (or switchable) optical fluorescence transitions* (Hofmann et al., 2005 and Bossi et al., 2006). This concept is based on switchable fluorescent probes that can be reversibly turned "on" (a fluorescent state) or "off" (a dark, nonfluorescent state). As shown in the Jablonski diagram in Figure 15.2a, these on–off states of a fluorophore can be the ground and excited singlet states (S_0 and S_1) as will be discussed below for STED

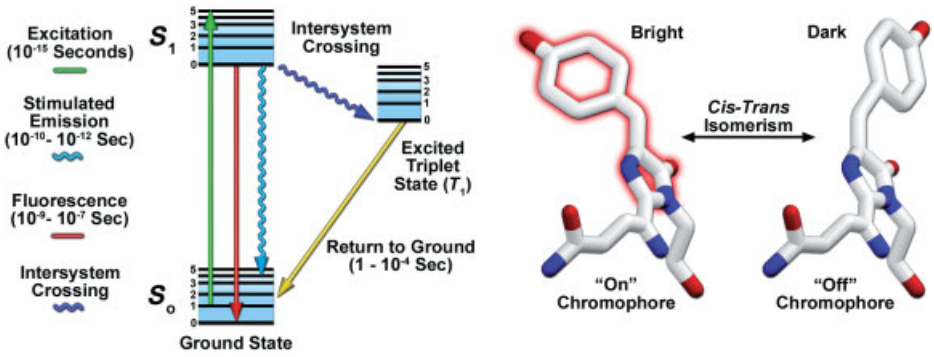

Figure 15.2

Key concepts of superresolution imaging using RESOLFT techniques. (a) Jablonski fluorescence diagram showing excitation and emission pathways, ground state depletion, such as through intersystem crossing into a metastable triplet state (GSD), and stimulated emission depletion (STED). (b) Photoswitchable fluorescent protein based on a mechanism of *cis/trans* isomerization.

microscopy, the excited singlet and dark triplet states utilized in ground state depletion (GSD) microscopy and ground state depletion-individual molecule return (GSDIM) microscopy, or the bright and dark states of a reversibly photoswitchable fluorophore (such as Cy5, kindling fluorescent protein, rsTagRFP, or Dronpa). In contrast, many of the popular optical highlighter fluorescent proteins, such as Eos, Kaede, Dendra2, and PA-GFP, which are capable of being permanently photoconverted from one emission bandwidth to another, are not suitable probes for RESOLFT, because the molecular transitions are not reversible. The RESOLFT concept also includes fluorescent molecules that can switch between *cis-trans* isomerization states (Fig. 15.2b), bound and unbound conformations, or other stable optical states.

It is useful to examine the basic principles and terms that are used to describe optical transitions in molecules. When a molecule photoswitches from one state to the other (e.g., dark to bright), the probability that the molecule will remain in the first (dark) state decreases exponentially with increasing excitation light intensity. The exponential response is a "nonlinear" behavior, and for many of the schemes described in this chapter, this nonlinearity is essential for the success of the imaging scenario. The term *saturation intensity* is used to define the light intensity at which the switching transition occurs (e.g., when 50% of the molecules have transitioned from dark to bright) and is inversely proportional to the ratio of lifetimes of the two states. In general, molecules used for superresolution microscopy have high fatigue levels (a measure of the ability to repeatedly photoswitch before being destroyed) and show characteristic saturation intensities and lifetimes that differ significantly for their on and off states.

SINGLE-MOLECULE LOCALIZATION MICROSCOPY

By single-molecule localization microscopy, one can localize molecules with an accuracy of several nanometers and resolve details down to 10 nm or less. Selvin and collaborators introduced *fluorescence imaging with one-nanometer accuracy* (*FIONA*) (Yildiz et al., 2003), and in 2006, closely related technologies were introduced—*PALM* by Betzig et al. (2006), *STORM* by Rust et al. (2006), and FPALM (*fluorescence photoactivated localization microscopy*) by Hess et al. (2006). The difference between these techniques is in the nature of the probes that were initially used. Today, the method is referred to as *PALM/STORM microscopy*. Although resolution down to 10 nm is theoretically possible with these methods, the actual observed resolution is typically 20–50 nm, still many times better than the Abbé diffraction limit of 200 nm that can be obtained using standard widefield microscopy. The concept of identifying and localizing individual molecules was first described by Werner Heisenberg in the 1930s and was formally buttressed with a solid mathematical foundation during the 1980s and 1990s by several groups. Basically, in a lateral specimen field containing single molecule emitters, the central portion of each diffraction-limited spot recorded on a digital camera image plane corresponds to the position of a molecule and can be localized with high nanometric precision by analyzing the distribution of its photons on the pixels of a CCD detector. A molecule-localization image is composed of the sum of tens of thousands of individual points and has been compared with the painting technique called *pointillism*. Because of the finite number of points, the method works best for point and line objects like vesicles and filaments, and less well for wide extended objects, except under conditions of high sampling density.

Special Requirements and Conditions for PALM/STORM Imaging

The idea behind PALM/STORM is as follows: if one could use the *x,y*-locations (centroids) of each Airy disk or PSF to construct an image based on the location coordinates of thousands of Airy disks, then it should be possible to improve spatial resolution 10- to 20-fold. In order to acquire Airy disk images of individual fluorescent molecules, two conditions are used: (1) an area array detector with small highly sensitive pixel photosites, commonly an EMCCD camera capable of imaging single fluorescent molecules; and (2) a high contrast mode of fluorescence imaging, such as TIRF illumination, where fluorescence emission is confined to a 100-nm zone adjacent to the coverslip and where signals are negligible from flanking out of focus regions along the *z*-axis. An alternative method is to examine thin sections of fluorescent, plastic-embedded specimens. It is important to minimize background fluorescence such as that arising from autofluorescence and to use fluorescent molecules that are bright and emit plenty of photons, that is, molecules that have a high quantum efficiency and high ratio of fluorescence between bright and dark states (called a high *contrast ratio*). Molecular localization works best when there is a high density of label (*molecular density*), so generally, the denser the labeling, the better the resolution of fine details. Illustrated in Figure 15.3 are the steps involved in localizing single molecules with high precision by fitting the PSF to a Gaussian function. In Figure 15.3a, the PSF of a widefield fluorescence microscope is superimposed on a wireframe representation of the pixel array from a digital camera in both 2D (upper left) and 3D diagrams. The pixelated PSF of a single fluorophore as imaged with an EMCCD is shown in the upper left of Figure 15.3b, and modeled by a three-dimensional Gaussian function, with the intensity for each pixel color-mapped in the central portion of Figure 15.3b. A contour map of the intensities is presented in Figure 15.3c. As a practical matter, the density of Airy disks must be sparse and nonoverlapping in the acquired images; otherwise, it becomes impossible to determine the distribution of photons in individual disks when they are strongly overlapping. The requirements for high probe density in the specimen and sparse density of fluorescent Airy disks in the image should not be confused.

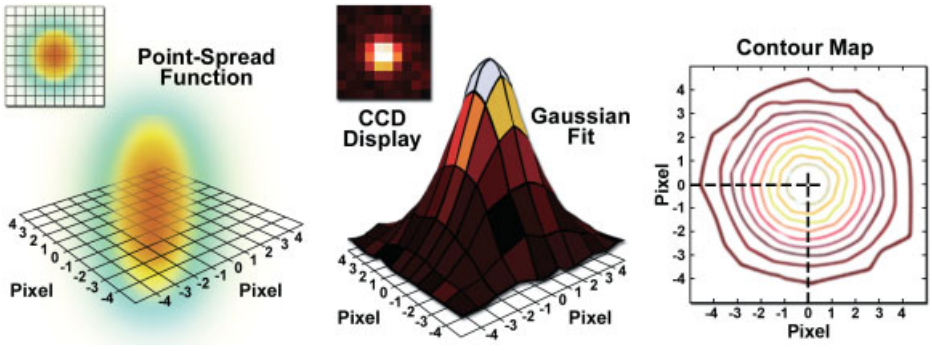

Figure 15.3

Method for localizing single molecules. (a) The point-spread function (PSF) of a single molecule is superimposed on a grid representing the pixel array of a digital camera. The PSF as imaged with an EMCCD is shown in two and three dimensions in panel b, while the centroid of the PSF is localized on a contour map in panel c.

Many methods of single-molecule localization microscopy rely on stochastic photoswitching, where most of the molecules remain dark and it is possible to record fluorescence as individual PSFs of separate molecules. However, new methods are appearing where photoswitchable probes are not required (see BaLM method below). As we will see, there are many ways to obtain the required blinking behavior. Upon excitation with an activation laser at low power, a small percentage of the molecules are stochastically switched on, imaged, localized, and then photobleached to remove them from the ensemble (Fig. 15.4). This is accomplished by taking a series of hundreds or thousands of replicate images from the same field of view and determining the centroid locations for thousands of Airy disks. Images of fluorescent emitters are captured using a low power readout laser (usually spanning from one to three camera frames) until most of the molecules photobleach or re-enter a dark state. Repeating this process for multiple cycles is the creative idea behind single-molecule localization microscopy and the

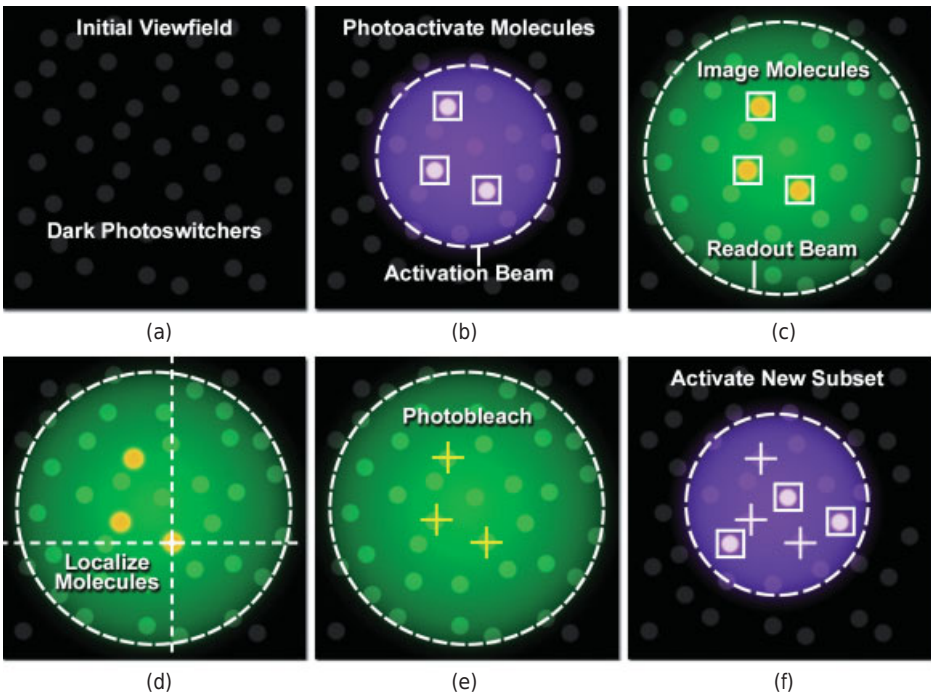

Figure 15.4

Cartoon drawing of PALM/STORM single-molecule localization microscopy. (a) A densely labeled network of structures that are labeled with photoswitchers residing in the dark or inactive state. (b) A sparse set of the fluorescent probes that do not overlap (boxed circles) is activated by near-UV light (purple activation beam). (c) The activated molecules are imaged (orange boxed circles) with a readout laser (green beam) and an EMCCD camera. (d) Enough photons are collected from each photoactivated molecule to localize the PSF with high precision. (e) The active molecules are photoswitched or photobleached to a dark state. (f) The process begins again and continues until all of the fluorescent probes are exhausted due to photobleaching or because the background fluorescence becomes too high. The final superresolution image is constructed by plotting the measured positions of the localized fluorescent probes.

reconstruction of a superresolution image. The basic steps involved in creating a PALM or STORM superresolution image are presented using a series of cartoon drawings in Figure 15.4. The target structure shows a densely labeled extended specimen decorated with a photoconvertable fluorophore. In Figure 15.4b, a sparse set of the fluorescent probes is activated to produce single-molecule images (represented by orange circles in Fig. 15.4c) that do not overlap. After capturing the images with an EMCCD, the PSFs of the individual molecules are localized with high precision based on the photon output (Fig. 15.4d) before the probes spontaneously photobleach or switch to a dark state (Fig. 15.4e). The positions of localized molecular centers are indicated with yellow crosses. The process is repeated (Fig. 15.4f) until all of the fluorescent molecules are exhausted due to photobleaching or because the background fluorescence becomes too high to distinguish single molecules. The final superresolution image is constructed by plotting the measured positions of the fluorescent probes.

Although the image of a single fluorescent emitter is an Airy disk-diffraction spot that covers several adjacent pixels on the detector, the exact position of the molecule can be determined to within just a few nanometers, provided enough photons are captured. The precision of the measurement of centroid location is proportional to the square root of the number of photons captured, the read noise of the camera, and the pixel size in the detector. Determining the center precisely requires statistical curve-fitting of the measured photon distribution to a Gaussian distribution. The localization errors for 1000 and 10,000 photon signals are approximately 10 nm and 1–2 nm, respectively.

The single-molecule localization technique is unique in requiring special photoswitchable fluorescent molecules that exist in equilibrium between bright and dark states. A specimen labeled with such molecules can then be imaged thousands of times to give the desired number of centroids.

Microscope Configuration for Single-Molecule Superresolution

Single-molecule superresolution microscopy techniques require minimization of background fluorescence in order to optimally detect faint emission from single molecules. Existing commercial TIRF microscope configurations can be utilized for PALM/STORM imaging with minor modifications, but new turnkey instruments designed specifically for superresolution imaging have been introduced (Fig. 15.5). Specific hardware components for superresolution imaging include a very powerful laser system, high NA objectives, a precision mechanical stage, vibration isolation, sensitive EMCCD or scientific CMOS detector, efficient fluorescence filters, and a fast data acquisition computer. TIRF is especially useful for single-molecule superresolution because the evanescent excitation wave penetrates only approximately 100–200 nm into the specimen (about the same width as the PSF), leading to rejection of the background fluorescence common in most applications. TIRF is also a widefield technique, so that many molecules can be imaged simultaneously in each frame, thus increasing the acquisition speed. Additionally, TIRF is an ideal method for imaging fluorescently labeled structures that lie close to the membrane, such as focal adhesions, endosomes, clathrin, and cytoskeletal components. Note that TIRF is not an absolute requirement for single-molecule imaging as certain specimens (such as bacteria) are sufficiently thin that autofluorescence does not impede the localization of single molecules illuminated in epifluorescence.

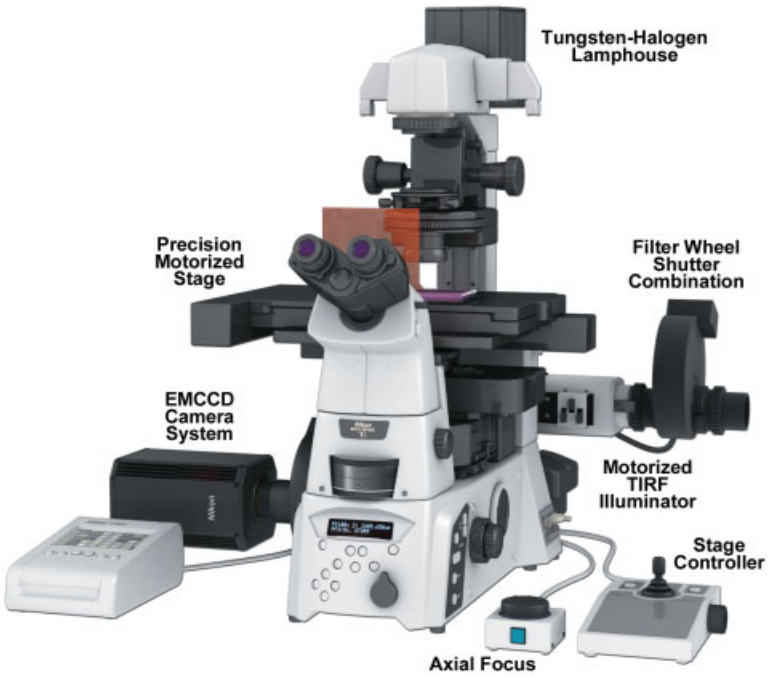

Figure 15.5

Single molecule localization microscope configuration. An inverted fluorescence microscope with TIRF illuminator features a precision stage, EMCCD camera, axial focus drift correction, motorized illuminator, and laser cleanup filters with a shutter mounted in an external filter wheel. The laser system is not shown in this illustration.

High NA objectives (>1.40) typically exhibit very good photon collection efficiency and are therefore the best choice for PALM and STORM imaging. Objective magnification should be selected to match the pixel size of the detector when coupled with a relay lens. The final configuration should produce images of single molecules that span at least two pixels, but not substantially more. For example, for a camera having 16-μm pixels, the effective pixel size at the specimen plane is approximately 270 nm and can be roughly determined by dividing the camera pixel size by the objective magnification. On the CCD, the image should span approximately 9 pixels (a central pixel with eight neighbors involved) so that the relative level of intensity in each of the adjacent pixels can be used to more accurately determine the molecular position.

Single-molecule superresolution configurations require interference filters and dichromatic mirrors of the highest quality to ensure the best signal-to-noise ratios and eliminate or reduce stray light and autofluorescence. Because lasers are used for photoactivation and readout, laser cleanup filters having a narrow bandwidth (in the range of 10 nm) are often useful. Dual or triple band polychromatic mirrors are employed to simultaneously reflect both activation and excitation wavelengths to avoid switching single-band mirrors during the experiment. Bandpass emission filters are usually the best choice (as opposed to longpass or shortpass filters). When selecting filters, the new hard-coat filters offer steeper cut-on and cut-off slopes, as well as higher transmission.

They are marketed under a variety of special brands and are produced by all of the major filter manufacturers.

PALM and STORM instruments should be equipped with lasers under AOTF control having output power ranging between 50 and 200 mW to provide sufficient energy for single-molecule photoswitching and imaging. Most of the fluorescent proteins and several of the synthetic dyes used in these superresolution techniques are efficiently activated at 405 nm, so a laser in this wavelength range is quite useful. Other laser wavelengths that match the typical fluorophores for single-molecule imaging have emission lines at 488, 561, 594, and 647 nm.

Microscope stability is a critical factor in all forms of single-molecule imaging, including PALM, STORM, and related techniques. Even nanometer-sized lateral drift can interfere with the precise localization of single emitters, and axial drift can completely wipe out signal if the specimen moves away from the focal plane. In general, a motorized microscope firmly mounted on an air-suspension vibration isolation platform on a solid concrete slab will provide reasonable positional stability over timescales of several minutes. Automatic focus drift correction hardware is useful to maintain the specimen within a few nanometers of the axial focal plane.

Modes of Single-Molecule Localization Microscopy

Many combinations of molecules and environmental conditions have been described that show photoswitchable properties and thus make them suitable for single-molecule localization microscopy. Two-color imaging using these approaches is also available.

PALM

The original PALM method introduced by Betzig et al. in 2006 relied on the use of photoswitchable GFP variants (Fig. 15.6). Some of the more successful variants are:

- Monomeric and tandem dimer Eos, mEos and tdEos (native green fluorescence, but once activated with 405-nm light, can be excited at 561 nm and emit orange-red fluorescence).
- Dronpa fluorescent protein (green when excited with 488-nm light, but it rapidly photoswitches to a dark form that can be made fluorescent again with 405-nm light).
- PA-GFP (photoactivatable GFP is dark until activated with 405-nm light, after which excitation with 488-nm light induces green fluorescence).
- PS-CFP2 (cyan fluorescence until activated to green fluorescence with 405-nm light).
- PA-mCherry1 (orange-red fluorescence with 561-nm illumination after being photoactivated with 405-nm light). Used as a second color for PALM with PA-GFP.

PALMIRA

PALMIRA is an acronym for PALM with Independently Running Acquisition. In this mode, the digital camera runs at high speed, without synchronization to the activation laser or the switching cycles of the fluorescent probes (Egner et al., 2007). The method works using photoswitchable fluorophores and increases acquisition speed up to 100-fold.

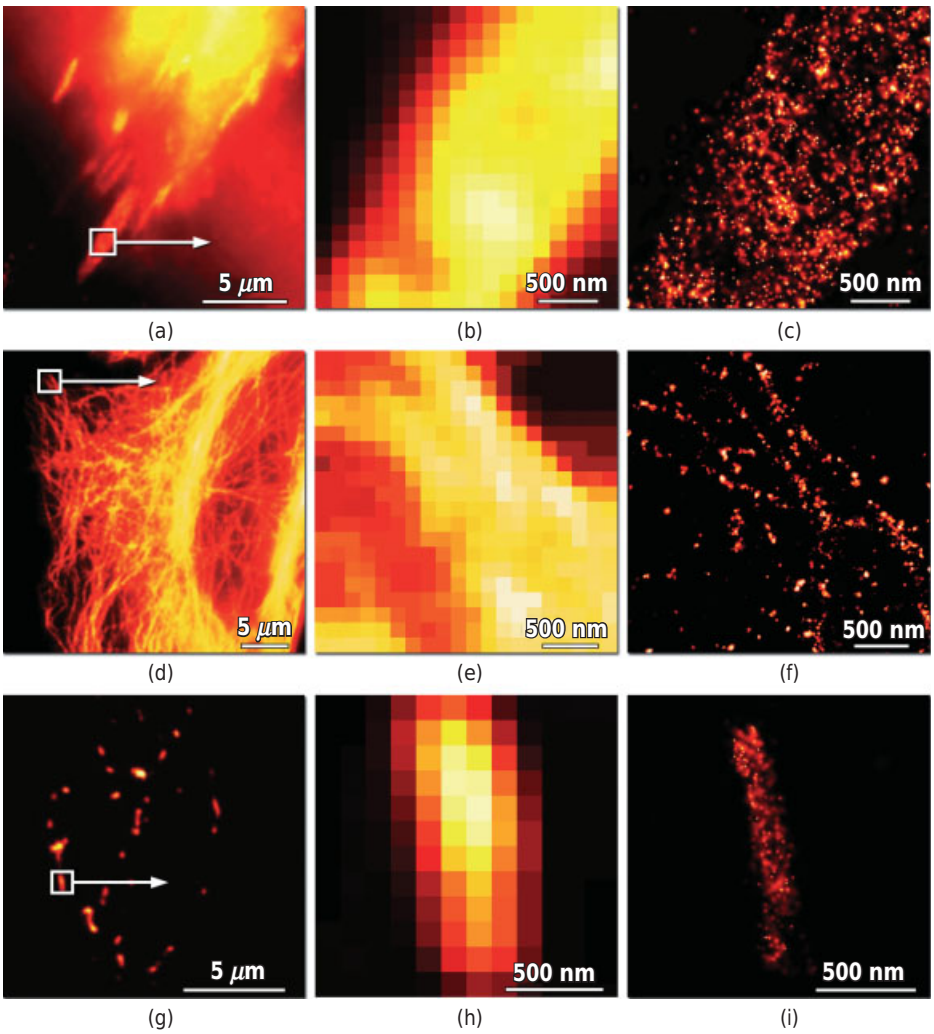

Figure 15.6

PALM images based on Eos fluorescent protein. (a–c) Dimeric Eos (dEos) fused to vinculin, localizing in focal adhesions in widefield TIRF imaging mode. The boxed region in panel a is also shown magnified in panel b and as a superresolution PALM image (c). Similar sets of images were captured for panels d–i. (d–f) Tandem dimer (td) Eos fused to human *alpha*-tubulin targeting microtubules (widefield and PALM). (g–i) dEos fused to a mitochondrial targeting signal (widefield and PALM). Note the detailed structure down to 30–50 nm in the PALM images. (Panels a–c and g–i courtesy of Eric Betzig, HHMI Janelia Farm Research Campus.)

STORM

This method, introduced by Rust, Bates, and Zhuang in 2006, uses the carbocyanine dye pair Cy3 and Cy5, or alternatively, Cy3 plus Alexa Fluor 647, as the photoswitching ensemble. (Cyanine dyes are available from Amersham Pharmacia Biotech; Alexa Fluor dyes from Life Technologies.) The Cy3-Cy5 dye pair is referred to as a *cyanine switch*: dark Cy5 is activated with green 532-nm light when in close proximity to Cy3,

which converts Cy5 to a fluorescent form that can be excited with red light at 633, 647, or 657 nm. Specimens are examined under reducing conditions and oxygen depletion. For imaging, the 532- and 647-nm lasers work simultaneously. Imaging of Cy5 for localization of single molecules drives the dye back to the dark state. The "fatigue rate" of the Cy3-Cy5 pair is excellent, allowing hundreds of switching events before permanent photobleaching occurs. Many other photoswitchable dye pairs have been discovered, including Alexa Fluors and ATTO dyes. The combination of Alexa Fluor 405 and 647 works very nicely in STORM (Fig. 15.7). Despite the utility of the cyanine switch, its physical basis is not well understood. STORM works best in the presence of reducing reagents (including thiols) and reduced concentrations of molecular oxygen.

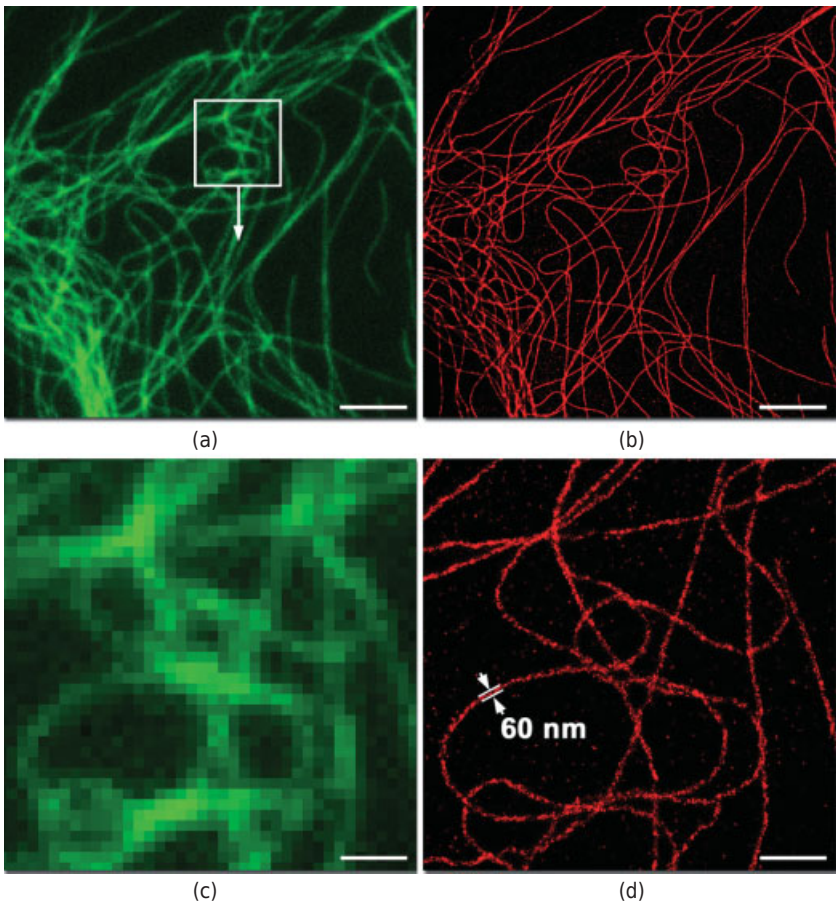

Figure 15.7

Superresolution imaging of microtubules with STORM. Microtubules in rat kangaroo kidney cells (PtK2 line) were labeled with antitubulin primary antibodies and secondary Fab antibody fragments conjugated to Alexa Fluor 405 and Alexa Fluor 647 (Life Technologies). STORM images were generated using a pulsed violet activation laser (405 nm) and a far-red imaging laser (657 nm). (a) Conventional widefield fluorescence image. (b) STORM image of viewfield in panel a. (c) Enlarged widefield image of boxed area in panel a. (d) STORM image of the area shown in panel c with a single microtubule diameter (60 nm) indicated by the white arrows. (a, b), bar = 5 μm. (c, d), bar = 1 μm.

DSTORM (DIRECT STORM)

Single fluorescent dyes (Cy5, Alexa Fluor 647, and several of the ATTO series fluorophores) can be driven into photoswitchable light and dark states with reducing reagents and under conditions of oxygen depletion, and can be selectively turned on or off with a single laser (Heilemann et al., 2008). The requirement of one dye and one laser greatly simplifies the imaging process compared with the original STORM procedure with cyanine switching. A number of techniques are closely related to dSTORM, including reversible photobleaching microscopy (RPM) and "blink" microscopy.

GSDIM (GROUND STATE DEPLETION WITH INDIVIDUAL MOLECULE RETURN) OR SIMPLY GSD

Fluorescent dyes are driven into a dark, metastable triplet excited state using a continuous wave laser in widefield mode (Fölling et al., 2008). For more on GSD principles using point-spread modification techniques rather than single-molecule localization, refer to the STED section at the end of the chapter. Images are recorded when single molecules stochastically become fluorescent and return to the ground state. Related methods called blink microscopy and reversible photobleaching microscopy (RPM) are two variants of the technique. Standard fluorescent dyes, such as fluorescein, Alexa Fluors, ATTO dyes, BODIPYs, DyLights, and carbocyanine dyes, are used in aqueous buffer supplemented with oxygen scavengers and aliphatic thiols. In GSDIM microscopy, resolution down to 50–70 nm is readily achieved; however, single-molecule localization methods require a low ratio of "time on" to "time off," and this has been difficult to achieve with existing dyes and buffer conditions. Similar methods for converting fluorescent probes in a dark state have also been described (Biteen et al., 2008; Lemmer et al., 2009). A GSD/GSDIM microscope for molecular localization with continuous wave laser illumination called SR-GSD is presently available from Leica Microsystems.

BALM (BLEACHING/BLINKING ASSISTED LOCALIZATION MICROSCOPY)

Rapid molecular localization microscopy can be performed using nearly all commonly used fluorescent probes without a requirement for photoswitchable properties (Burnette et al., 2011). The method depends on inherent photobleaching and blinking properties of most fluorophores, including synthetic dyes and fluorescent proteins. To detect single molecules, a sequence of images is obtained under illumination that is significantly higher than normal conditions of fluorescence excitation (~40–50% full laser power); blink-off events are detected by subtracting from each image of the series the subsequent one, and blink-on events are revealed by subtracting from each image of the series the previous one. Molecule localization is then performed in the usual way by fitting the single-molecule PSFs to a theoretical 2D Gaussian distribution and mapping the coordinates.

3D SINGLE-MOLECULE LOCALIZATION MICROSCOPY

Obtaining high resolution along the *z*-axis for 3D imaging using single-molecule localization techniques has proven to be more difficult, although several clever solutions have been used. One method (3D STORM) features a cylindrical lens to skew the PSF of single-molecule fluorescence in the lateral direction depending on its position along

the *z*-axis. Another method, Biplane (BP) FPALM, employs a dual-plane imaging configuration to project an image of the same molecule into two different focal planes. Yet another technique named double-helix PSF (DH-PSF) engineers the PSF of the microscope with a spatial light modulator (SLM) into two lobes, which are rotated with respect to the image depending on their axial position. Finally, interferometric PALM (iPALM) gathers light from single emitters using twin juxtaposed objectives, recombines the emission with a special prism, and uses interference of the photons based on their location in the focal plane to determine the axial location. While most of these methods provide a somewhat lower resolution along the *z*-axis, the resolution provided by iPALM along the *z*-axis is actually comparable or better than resolution in the lateral dimension.

Fluorescent Probes for PALM/STORM Imaging

Fluorescent probes suitable for imaging with PALM/STORM and related superresolution methods (Table 15.1) have high absorption coefficients and quantum efficiency (are very bright), and have high contrast levels (bright state signal/dark state signal), and emit a maximum number of photons per molecule before photobleaching or returning to a dark, nonfluorescent state. Fluorophores suitable for STORM must be photoswitchable, exhibit high switching reliability, have low fatigue rates, and have switching kinetics that can be readily controlled. The best probes are those whose inactivation can be balanced with the activation rate to ensure that only a small population of molecules is activated at any particular time. STORM superresolution probes must also be conjugated to an antibody to bind specifically and exhibit low background noise.

STRUCTURED ILLUMINATION MICROSCOPY

In widefield microscopy, spatial resolution is limited by the illumination wavelength and the numerical aperture of the objective (see Chapters 5 and 6). *SIM* extends resolution to twice the Abbé diffraction limit by illuminating the specimen with highly structured illumination, such as a pattern of parallel lines, which acts as a carrier of high frequency information (image details). Thus, details that are invisible because they lie beyond the diffraction limit of the objective become convolved with the image of a grid. Images of the superimposed pattern are recorded, and by working with spatial frequencies in reciprocal space, it is possible to extract the high frequency information and view the details in a reconstructed real image. This technique, sometimes called high resolution or superresolution (HR or SR) SIM, is performed using precision optics and special image processing algorithms and is commercially available on microscopes marketed by Applied Precision, Nikon, and Zeiss. (Note: High resolution SIM described here is distinct from another form of structured illumination employed in devices such as OptiGrid [Qioptiq], ApoTome [Zeiss], and Angstrom [Quorum/Leica]). These devices do not provide "superresolution," but rather are used for optical sectioning to obtain high contrast, confocal-like z-stacks of specimens using standard widefield fluorescence optics (see the section on optical sectioning using structured illumination in Chapter 13).

TABLE 15.1 Properties of Fluorescent Probes for Single Molecule Imaging

Probe Name[a]	Ex[b] (nm)	Em[c] (nm)	EC[d] ($\times 10^{-3}$)	QY[e]	N Photons[f]
Photoactivatable fluorescent proteins					
PA-GFP (N)[g]	400	515	20.7	0.13	70
PA-GFP (G)	504	517	17.4	0.79	300
PS-CFP2 (C)	400	468	43.0	0.20	NR
PS-CFP2 (G)	490	511	47.0	0.23	260
PA-mCherry1 (R)	564	595	18.0	0.46	1300
Photoconvertible fluorescent proteins					
tdEos (G)	506	516	34.0	0.66	NR
tdEos (R)	569	581	33.0	0.60	750
mEos2 (G)	506	519	56.0	0.74	NR
mEos2 (R)	573	584	46.0	0.66	500
PSmOrange (O)	548	565	113.3	0.51	NR
PSmOrange (FR)	635	662	32.7	0.28	350
Photoswitchable fluorescent proteins					
Dronpa	503	517	95.0	0.85	120
rsFastLime	496	518	39.1	0.77	200
Padron	503	522	43.0	0.64	NR
bsDronpa	460	504	45.0	0.50	NR
rsCherry	572	610	80.0	0.02	NR
rsCherryRev	572	608	84.0	0.005	NR
Synthetic fluorophores					
Alexa Fluor 488	495	519	71.0	0.92	1000
ATTO 488	501	523	90.0	0.80	1200
Cy3B	559	570	130.0	0.67	2000
Alexa Fluor 568	578	603	91.3	0.69	2000
Alexa Fluor 647	650	665	240.0	0.33	4000
Cy5	649	670	250.0	0.28	5000
Cy7	747	767	200.0	0.28	1000
DyLight 750	752	778	220.0	0.25	750
C-Rhodamine[h]	545	575	90.0	0.90	1100
C-Fluorescein	494	518	29.0	0.93	525

[a] The common name and/or acronym for each fluorophore.
[b] Peak excitation (Ex).
[c] Peak emission (Em) wavelengths.
[d] Molar extinction coefficient (EC).
[e] Quantum yield (QY).
[f] Number of photons emitted per molecule per switching cycle (N Photons) are indicated.
[g] Terminology: (N) native, (C) cyan, (G) green, (O) orange, (R) red, (FR) far-red.
[h] C-Rhodamine and C-Fluorescein refer to caged derivatives.
NR, not reported.

NA Limits the Spatial Resolution in an Image

For imaging devices involving a lens, rays of light entering at the periphery of the lens define its angular limit and numerical aperture. These beams determine the point-spread-function of the system and define the resolution of the image. Thus, lenses with higher NA have larger aperture angles and they generate smaller PSFs to provide finer image details. Specimen details smaller than the resolution limit are not visible because wider aperture angles and smaller PSFs are required to image them. This is the usual case for widefield imaging in either fluorescence or brightfield modes, and defines what is known as *diffraction-limited imaging*.

Viewing and Manipulating Images in Frequency Space

SIM involves manipulating intensity features of an image in *frequency space*, so we need to review some of the basic features of this term. We introduced the concept of spatial frequencies when discussing diffraction and its role in Abbé's theory for image formation in the light microscope (Chapters 5 and 6). In microscopes, spatial features measured in units of distance in the real intermediate image are reciprocally related to distributions of spatial frequencies in the rear focal plane, or diffraction plane, of the objective. The images in these two nonconjugate planes are referred to as being in *real space* and *frequency space*. The latter is also called "Fourier space, reciprocal space, or spatial frequency space." The diffraction plane is visible as a circular image with a central or 0th order diffraction spot surrounded by features of increasing spatial frequency at increasing distance from the center. Features located at the image periphery represent the highest spatial frequencies of the image. Frequency space is the reciprocal of real space: just as the wavelength (in centimeters) is reciprocally related to the frequency of light (1/cm), there is a reciprocal relationship between smallest resolvable distance ($d = 0.5\ \lambda/\mathrm{NA}$) and maximal spatial frequency ($f = 2\mathrm{NA}/\lambda$). In Chapters 5 and 6, we examined the relationship of diffraction spots associated with specific spatial frequencies in figures and exercises dealing with striations in skeletal muscle and the patterns of pores in diatom shells, where reinforcement of repeated patterns makes diffraction features particularly apparent.

In SIM, image transforms are obtained by a mathematical operation called Fourier transformation, which generates a pair of amplitude and phase images of the scene. The amplitude image, also called the reciprocal transform, corresponds precisely to the diffraction image that we would see in the rear focal plane of a microscope. With amplitude and phase images in hand, an *inverse transform* can again be made, which generates a real image. *In processing for SIM, the transform is examined to extract embedded harmonic frequencies that are otherwise invisible without the application of patterned illumination.* The real image that results from reversing the Fourier process using the amplitude and phase images is the inverse transform. SIM images are inverse transforms that have been created by SIM image processing in the frequency domain.

High Frequency Information Is Contained in Low Frequency Moiré Fringes

In SIM, high frequency information in the specimen generates new harmonic frequencies that become visible as coarse, low frequency structures in the image. An analogous situation in the generation of new frequencies is seen in *moiré fringes*, when two finely spaced overlapping patterns are viewed together (Fig. 15.8a). In the example shown, patterns of light and dark vertical lines (fringes) appear superimposed on the scene. Moiré patterns can have complex shapes—straight, wavy, circular, and so on—and have the important feature that they "magnify" high frequency information. In the example shown, the spacing between moiré fringes is 10 times larger than the spacing between the parallel line elements in the sample. Another example of the moiré magnifying effect can be seen when viewing two overlapping sections of a chain-link fence.

When the distance between the viewer and the fence is just right, deviations in the wire structure of one of the fences appear magnified, not by any optical means, but as large, easily visible distortions in the moiré fringes. In applying the fence analogy to structured illumination in the microscope, one of the patterns would represent unresolved specimen details and the other the pattern of structured illumination. The high frequency details become mixed with the patterned light (carrier wave), generating harmonic frequencies analogous to moiré fringes. Careful inspection of the line pattern reveals distortions and intensity fluctuations in the line pattern caused by the mixing of the two sets of spatial frequencies. These pattern changes can be imaged, and the information can be demodulated (extracted from the carrier wave) in frequency space by the application of special algorithms, revealing the hidden high frequency details.

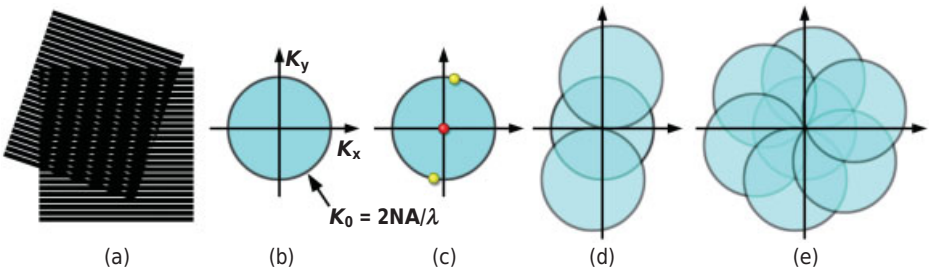

Figure 15.8

The principle of resolution enhancement by structured illumination. (a) Moiré fringes are generated by two overlapping patterns of parallel lines. (b) The observable region of reciprocal space produced by an objective (analogous to its diffraction image) is limited at its edge by the highest spatial frequencies that the lens can transmit ($2NA/\lambda$); the central spot represents the 0th order component of the image. (c) The 0th and ±1st order diffraction components of a pattern of parallel lines imaged by the objective (red and yellow spheres, respectively). If the pattern is at the limit of resolution, the 1st order spots fall at the very edge of the "observable field" shown in panel c. (d) By frequency mixing, the observable region is seen to contain, in addition to the normal image of spatial frequencies (center circle), two new offset frequency images, each centered on the edge of the original field. The offset images contain spatial frequencies that are not observed using conventional widefield optics. (e) From a set of images prepared from three phases at each of three orientations, a real image can be generated that has twice the spatial resolution. (From Gustafsson, 2000.)

Spatial Frequencies Are Extracted from SIM Images, Extending Resolution Twofold

For SIM, one projects a fine grating spacing on the specimen plane. Various methods have been used to do this, including: projecting the diffraction image of a sinusoidal phase grating (a diffraction grating) on the rear aperture of the objective (Gustafsson, 2000); using spatial light modulators (SLMs), which have the advantage of moving the pattern 1000 times faster, because no rotation of the specimen or any optical component is required (Kner et al., 2009); and by creating interference patterns in the focal plane using standing wave total internal reflection fluorescence microscopy (Chung et al., 2007). In Gustafsson's method, a grating is selected so that the ±1st order spots just enter the objective at opposite sides of the rear aperture. By definition, this gives the finest grating pattern that it is possible to resolve while viewing the real image of the specimen. The wavelength chosen is the excitation wavelength of the particular fluorescent dye or protein. For SIM, images of the image plane are acquired at the fluorescence emission wavelength and are taken at different angular rotations and phases as described below. For purposes of clarity in the description that follows, we focus on the method originally used for structured illumination imaging in two dimensions, even though the more involved 3D procedure is the one frequently implemented today.

Let us now consider a single SIM image containing both the structured illumination grid and specimen details, and examine its reciprocal transform (Fig. 15.9a). Additional high frequency information (arrows, Fig. 15.9b) is now visible, indicating that high frequency details have been carried into the image using structured illumination.

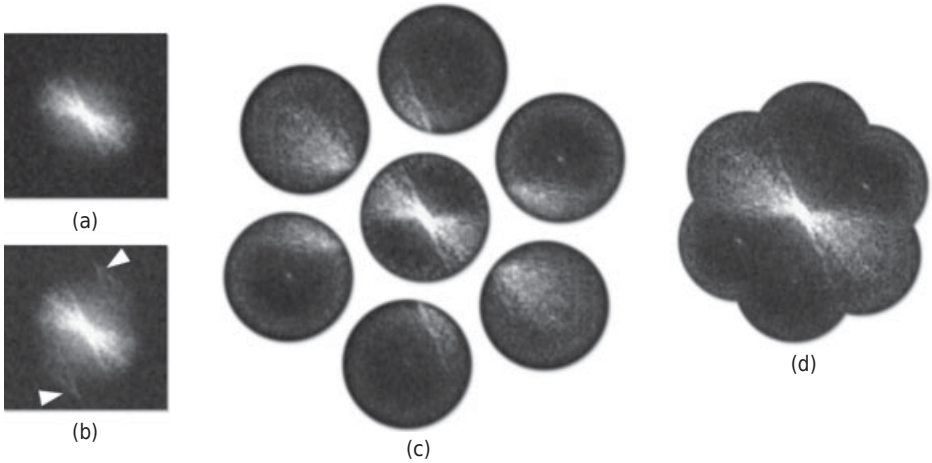

Figure 15.9

The procedure of reconstructing high frequency information in reciprocal space. Fourier transforms of a microscope image without (a) and with (b) structured illumination. Information is contained in the "observable region" in both cases, but in panel b, moiré effects have displaced high frequency information (arrowheads) and carried it into the observable region. (c) Seven components shown separately as calculated from nine images taken at three azimuthal rotations of the grid pattern. (d) Reconstruction of the image transform extends the visible region outwards by a factor of 2 compared with the original image shown in panel a, allowing a twofold enhancement in resolution. (From M. Gustafsson, 2000.)

Since the location of the grating spots is known, it is possible with special algorithms to reassign the distribution of these features to their proper location in reciprocal space. The displacement is defined by the location of the two diffraction spots corresponding to the grid. In fact, three images result, the central (normal) image and two other images separated by 180° and each located on either side of the central transform (Fig. 15.9c). If the highest possible resolution is used, the center of each calculated transform lies exactly at the outside edge of the original transform (Fig. 15.9d). This operation extends the range of spatial frequencies in reciprocal space by a factor of 2, thus doubling the spatial resolution in the real image (reciprocal transform). The process is shown graphically in Figure 15.9d and in terms of images in Figure 15.9c,d. Notice that new features in the offset circles shown in Figure 15.9d falling outside the central circle contain new information that is not visible by standard widefield fluorescence microscopy.

In practice, one SIM image in the two-dimensional mode requires three rotations of the grid pattern, with three translations of the grid at each rotational angle for a total of nine separate photographs in all. The nine raw images, which yield one SIM reconstruction, are referred to as a "SIM frame." *Each translation increment is equal to 1/3 of the grating period*. Translating the grating and obtaining images at three different phases is required to separate the three components summed up in each image (Fig. 15.9c). Because resolution is only improved in the direction perpendicular to the line pattern of the grid, the grating must also be rotated and the process repeated at two additional rotation angles, three rotations in all, to fill the Fourier space. Three or five or even more rotations can be used (Frohn et al., 2000), but at the expense of longer time and photobleaching of the specimen. Spatial frequencies are calculated and plotted in a new expanded spatial frequency image, and an inverse transform is performed to create a SIM image showing the new "superresolution details." This method improves conventional widefield resolution by a factor of two, giving resolutions of ~100 nm laterally (Gustafsson, 2000). Recently, 100-nm resolution in all three dimensions has been obtained using two apposed objectives that are focused on the specimen to generate interference (Shao et al., 2008). Even higher resolution can be obtained by nonlinear *saturated SIM (SSIM)*, which arises from saturation of the excited state and sharpening of the structured illumination pattern and allows higher spatial frequencies to be resolved (Gustafsson, 2005; Heintzmann and Jovin, 2002).

Important Guidelines and Conditions for SIM Microscope Optics

- SIM illumination is provided by lasers, whose light is scrambled and then polarized to provide uniform polarized light.
- The orientation of the grid lines on the specimen should be parallel to the polarization vector azimuth of the excitation illumination.
- Diffraction orders other than the ±1st orders should be blocked.
- In the Gustafsson method, a sinusoidal phase grating is used to create structured illumination of the specimen. Approximately 80% of the light is diffracted into the first order diffraction spots, producing a high-contrast pattern with a periodicity of approximately 200 nm.

- The modulation depth (visible as percent contrast) of the stripe pattern projected onto the specimen should lie between 70% and 90%, and the grating should be mounted on a translation device that can also be rotated. Some commercial instruments allow three or five grid rotations (120° or 72°) to optimize imaging speed or resolution, respectively.

Several grating sizes are required to match multiple laser line excitation sources, because the diffraction angle is wavelength dependent.

SIM for 3D, Multicolor Imaging of Living Cells in Time-Lapse Mode

As originally formulated, SIM improves lateral resolution to approximately 100 nm, but is only applicable to 2D samples or 3D samples illuminated in TIRF mode. However, advanced methods have been developed that allow 3D SIM imaging with a *z*-resolution of 300 nm (Shao et al., 2008). In this application, three beams generated by a diffraction grating form a three-dimensional interference pattern in the focal plane. For 3D imaging, there are five phase translations per grid rotation and three rotational angles, yielding a total of 15 images per focal plane. The 15 images are required to thoroughly sample the focal volume in *x*, *y*, and *z* dimensions. Image processing of the data maintains the 100-nm resolution in the lateral (*x*,*y*) plane, and gives 300-nm axial (*z*) resolution (almost twice as good as laser scanning confocal microscopy). With an efficient EMCCD camera to increase the sensitivity and speed and reduce specimen damage, it is possible to do 3D imaging of live cells at a rate of 75 ms/*z* plane (Shao et al., 2011) (Fig. 15.10). This rate can be improved using a scientific CMOS camera. Because additional exposures are required for 3D SIM, specimens should be moderately bright and contain a high density of fluorescent label. For this application, bright, stable fluorophores are used, such as EGFP, Emerald, and tdTomato (tandem dimer) fluorescent proteins as well as synthetic dyes, such as MitoTracker Green and Alexa Fluor 568 (Fig. 15.10) .

STIMULATED EMISSION DEPLETION (STED) MICROSCOPY: SUPERRESOLUTION BY PSF ENGINEERING

In *stimulated emission depletion* microscopy, the size of the PSF is reduced to provide superresolution imaging by a method similar to laser point-scanning. STED uses two superimposed, colinear excitation and STED laser beams of different wavelengths and requires the use of certain photoswitchable fluorescent dyes in the specimen in order to obtain PSF shape engineering. In standard widefield or confocal microscopes, the excitation beam is expanded to fill the rear aperture of the objective, and resolution is determined by the size of the focused diffraction spot, which is dependent on the wavelength and the NA of the objective. Confocal and two-photon fluorescence microscopy can both surpass Abbé's resolution limit by more than a factor of $\sqrt{2}$, although imaging by these methods is still limited by diffraction. In STED microscopy, the PSF is engineered to be considerably smaller, allowing resolutions down to 50–70 nm, and in some cases less. The shaping or engineering of the PSF is performed using two superimposed laser beams, and equally as important, fluorescent molecules that can be switched

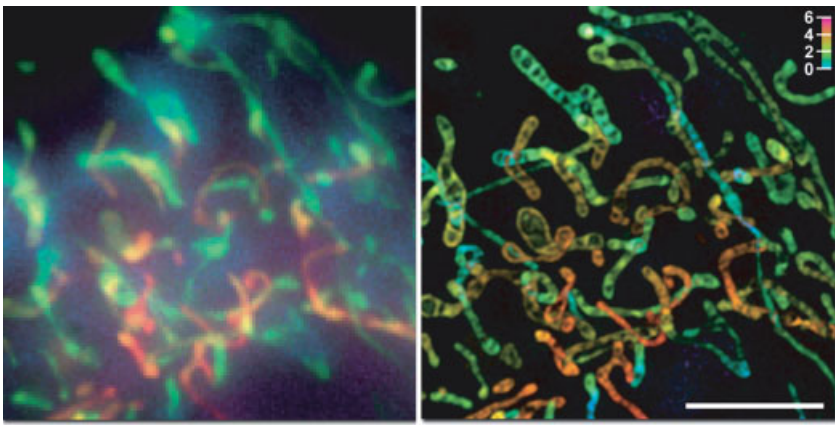

(a) (b)

Figure 15.10

3D SIM imaging. (a) Widefield fluorescence and (b) SIM images of a living HeLa cell stained with MitoTracker Green (Life Technologies). The SIM image is a maximum-intensity projection along 38 planes through the cell, while the widefield image is represented by a single exposure. The *z*-depth (μm) in the SIM image is coded with colors as shown in the scale bar (indicating the height in μm above the coverslip surface). Clearly SIM reveals details of mitochondrial matrix and cristae that are not visible in the conventional widefield image. Bar = 5 μm. For more details, see Shao et al. (2011). (Image courtesy Dr. Lin Shao, HHMI Janelia Farm Research Campus.)

between bright and dark states by a mechanism of stimulated emission depletion. Stephan Hell adapted PSF engineering strategies as one of several methods he called RESOLFT for high resolution microscopy (see Introduction to this chapter; RESOLFT was also discussed in the section on PALM/STORM microscopy). Hell introduced the STED concept in 1994 (Hell and Wichmann, 1994), and the first working microscope was described in 2000 (Dayba et al., 2003; Klar et al., 2000). STED microscopes are now commercially available as the TCS STED microscope from Leica Microsystems.

Shaping the Scanning Spot

The major principle behind PSF engineering is STED, the stimulated emission depletion of specific fluorescent dyes. STED is performed using synchronized laser pulses by irradiating dye molecules immediately after they have been stimulated into an excited state but before they have had a chance to re-emit photons using wavelengths near the longer wavelength end of their own emission spectrum. The excitation pulse is short (0.1 fs), but the STED pulse is up to 100 times longer. This illumination strategy forces the excited molecules back into the upper vibrational level of the ground state, and their immediate vibrational decay allows dissipation of the excitation energy and prevents further excitation. For these molecules, fluorescence is quenched and extinguished. Thus, in STED, a scanning laser spot excites molecules in the usual manner, but PSF shaping is accomplished by near-simultaneous quenching of a portion of the excited molecules so that they do not fluoresce.

STED Depends on Two Essential Factors: Nonlinear Emission Depletion and RESOLFT-Compatible Dyes

Stimulated emission depletion of fluorescence depends on two important factors. First, the process is *nonlinear*, meaning the relation of molecular relaxation to the intensity of the STED beam is exponential, not linear. It is the combination of the linear process of dye excitation coupled with the exponential, nonlinear response to emission depletion that allows the sculpting of such a minute intense spot. If the STED response was linear, crafting such a small scanning spot would not be possible.

Second, STED depends on the RESOLFT properties of certain fluorescent dyes, which makes them uniquely suitable for STED compared with other dyes. For this reason, the STED technique has focused on just a subset of fluorescent dyes and fluorescent proteins. We discuss fluorescent dyes used for STED at the end of the section.

Actual shaping of the PSF in STED is brought about by focusing two overlapping laser beams on the specimen with the objective: an excitation beam in the standard TEM_{00} mode giving a Gaussian spot, and a second emission beam in TEM_{01*} mode having the shape of a ring or donut (the depletion or STED beam). The need for photoswitchable dyes is immediately apparent. The effect of light within the circular donut is to force molecules into a dark state, which trims down the size of the Airy disk and reduces the area of fluorescence excitation. The first STED microscopes used Ti:sapphire mode-locked lasers for imaging with ATTO-647 and other deep red emitting dyes. In recent years, STED systems have been introduced that can also be configured with continuous wave lasers (CW STED) to reduce cost and increase compatibility with a variety of dyes, including synthetic dyes and fluorescent proteins. Fluorophores located in the middle of the donut hole region of the STED beam are allowed to fluoresce upon exposure to the excitation beam, whereas those fluorophores exposed to the STED beam in the region of the donut are transferred back to their nonfluorescent state (ground state) by means of stimulated emission (Fig. 15.11b). This action creates a physically smaller excitation diffraction spot for point scanning, and allows higher resolution during scanning. The wavelength and duration of the STED beam pulse are chosen to coincide with the emission maximum and amount of light required for saturation, respectively, for each fluorophore in the sample. These values are predetermined and are selected in the software. Deactivation of the fluorophores occurs throughout the focal volume *except at the center of focus*. At the high depletion laser powers used for STED (often exceeding 250 mW per square centimeter), the fluorophores are almost instantaneously driven to the ground state by stimulated emission. Substantially reducing the laser power (as discussed below) enables formation of a nonfluorescent state via a number of other mechanisms, including driving the fluorophores into a metastable triplet state, formation of charge-transfer states, or photoswitching. Because the physical dimensions of the zone for STED are so small, vibration must be eliminated to the greatest extent possible, and the excitation and STED laser beams are fine-aligned periodically by an automatic procedure to guarantee peak performance.

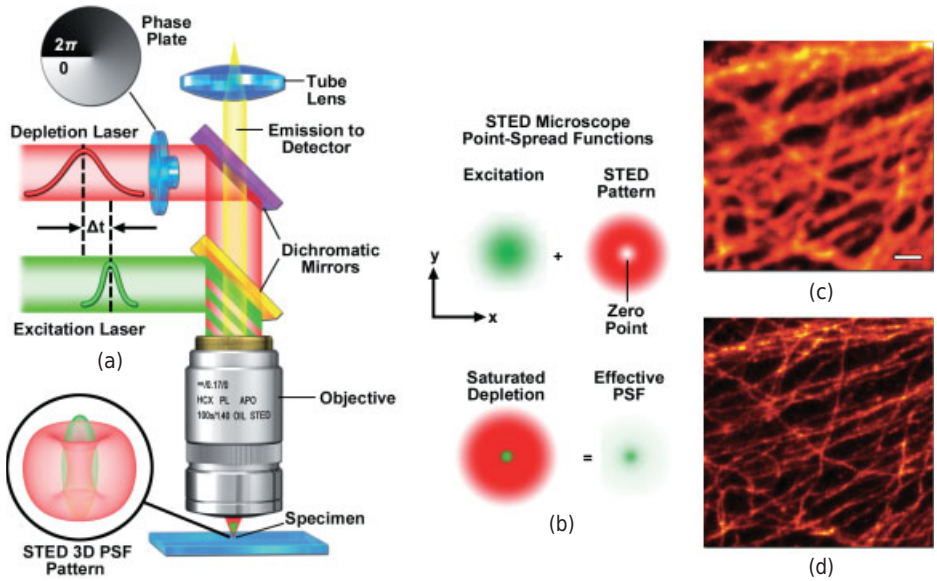

Figure 15.11

STED microscope configuration and point-spread functions (PSFs). (a) STED microscope optical train showing excitation and depletion lasers, helical phase plate, and 3D STED PSF. (b) STED PSF. (c) Widefield image of microtubules stained with Alexa Fluor 594. (d) Same viewfield as panel c imaged with STED laser system. (Panels c and d courtesy of Leica Microsystems, Inc., with permission.)

A typical arrangement of the STED optical path is shown in Figure 15.11a, which includes the phase plate, excitation and depletion lasers (red and green beams, respectively), dichromatic mirrors, tube lens, and objective. The STED beam at the specimen plane is also shown. Excitation and depletion are performed with synchronized laser pulses that are focused by the objective onto the specimen plane. Fluorescence emission is registered on a photomultiplier or avalanche photodiode detector (not shown). The focal spots produced by the STED and depletion lasers are simulated as green and red patterns, respectively, in Figure 15.11b. The green laser excitation spot is superimposed on the red donut-shaped STED depletion profile to reduce the size of the effective PSF. Comparison of widefield (Fig. 15.11c) and STED (Fig. 15.11d) images of microtubules stained with Alexa Fluor 594 demonstrates the increased spatial resolution afforded by PSF engineering methodology.

For imaging, the trimmed down laser excitation spot is raster scanned laterally across the specimen as in confocal microscopy. Among the benefits of STED microscopy are that the effective resolution increase is dictated by the experimental configuration, characteristics of the fluorescent probe, and the laser powers applied to the specimen. Furthermore, the image is recorded as the beam scans along the specimen and requires no additional processing. Image acquisition times equal those of a laser scanning confocal microscope. The effective resolution increase with STED is proportional to the power of the depletion laser, but can become problematic at extremely high laser powers that are likely to result in rapid photobleaching and destruction of the probe. Regardless, many fluorophores have been successfully used with STED (see Table 15.2), including fluorescent proteins, ATTO dyes, Alexa Fluor and DyLight dyes,

TABLE 15.2 Fluorescent Probes for STED Microscopy

Probe Name[a]	Ex[b] (nm)	Pulse Width[c] (ps)	STED[d] (nm)	Pulse Width[e] (ps)	Resolution[f] (nm)
Synthetic dyes					
ATTO 425	440	130	532	1,000	70–80
Alexa Fluor 488	488	CW	592	CW	<60
ATTO 532	488	100	615	200	60–70
ATTO 565	532	90	640	90	30–40
Alexa Fluor 594	570	90	700	90	60
ATTO 590	570	90	700	90	30–40
ATTO 633	635	100	750	200	30–40
Fluorescent proteins					
EGFP	490	100	575	200	70
EYFP	490	100	598	300	70
Citrine	490	100	598	300	50

[a]Synthetic fluorescent dyes and fluorescent proteins are listed with respect to their [b]excitation maxima, [c]optimum pulse width, [d]depletion beam wavelength, [e]pulse width of the depletion beam, and [f]resolution. CW, continuous wave laser.

as well as numerous other dyes. There are many studies showing the value of STED in providing the resolution required to answer difficult questions in cell biology. For example, Willig and coworkers (2006) resolved synaptic vesicles in presynaptic termini and reported receptor recycling in patches with other synapse proteins. In another example, Eggeling et al. (2009) reported that the distribution of certain lipids occurs in nanodomains in the plasma membranes of cells.

Advanced versions of STED have been implemented to address improvements in axial resolution for three-dimensional superresolution imaging of ensembles. By coupling two STED depletion lasers with an apposed-objective configuration, Stefan Hell and coworkers have succeeded in generating significantly improved resolution in both the lateral and axial dimensions. The technique has been termed iso-STED due to the fact that it yields a tunable, nearly isotropic (spherical) PSF with a resolution approaching 40 nm along the axes. Such a symmetrical focal spot should prove beneficial in obtaining high resolution optical sections from deep within biological cells and tissues. The complex instrumental configuration consists of dual STED lasers that are combined and sent to both objectives using a beamsplitter. Digital image processing can additionally be employed to reduce the effect of side lobes and other artifacts that compromise the PSF. A more compact and simpler STED instrument based on a supercontinuum laser source gives three-dimensional imaging using a single objective with respective lateral and axial resolutions of 45 and 100 nm.

Shaping the PSF by Ground-State-Depletion (GSD)—An Alternative to STED

An alternative to quenching the excited state by STED is depleting the ground state of the dye by shelving excited dye molecules in the triplet state or another long-lived "dark

state" (Bretschneider et al., 2007). The advantages for imaging are that 1000-fold lower illumination intensity is required for GSD compared with STED and that standard fluorescent molecules can be used. Similar to STED, the depletion laser in GSD microscopy has a doughnut-like geometry with a zero node in the center. Raster-scanning the specimen with superimposed lasers (excitation and depletion) generates images with subdiffraction resolution. As in STED, the key requirements are being able to saturate the depleted condition and having a nonlinear relationship between the illumination intensity and the amount of dark state of the dye.

The same RESOLFT principles described above for STED microscopy also hold for ground state depletion (GSD) microscopy. In GSD, the photoswitching mechanism involves transiently shelving the fluorophore in a metastable dark triplet state (T_1) (Hell and Kroug, 1995). Electronic transitions to metastable energy levels occur only with very low probability. Regardless, the triplet state can be populated by repetitively exciting the fluorophore to the first excited singlet state (S_1) to increase the probability of a nonradiative intersystem crossing from S_1 to T_1 (also shown in the basic Jablonski diagram in Fig. 11.2 in Chapter 11). Electrons remain in the metastable state for times ranging from microseconds to milliseconds. The depletion laser power necessary to drive fluorophores into the triplet state (usually several kilowatts per centimeter squared) is significantly less than that required for STED microscopy.

Among the greatest challenges for implementing GSD microscopy is choosing suitable fluorescent probes due to the potential involvement of fluorescent dark states in photobleaching. In addition, those fluorophores that can be effectively driven to the triplet state must be able to recover after removal of the depletion laser. Fluorescence recovery is essential, because GSD relies on scanning the specimen in a manner similar to confocal and STED microscopy. Thus, fluorophores trapped in the triplet state must be able to relax to the ground state before the depletion beam moves to the next spatial location. As a result, in GSD microscopy there must be a finely-tuned balance between the optical shelving time, the intersystem crossing rate, and photobleaching activity. The number of potential fluorophores and demonstrations of GSD imaging have been limited, but theoretically there are many fluorescent probes that might be successfully imaged using this technique.

Note that there is a potential for fluorophores to be shelved in other dark states (in addition to the metastable triplet state) using GSD microscopy, but the technique will still produce excellent high resolution images provided the fluorophores are eventually able to return to the ground state. The ability to exploit saturation of the triplet state with GSD using much lower depletion laser powers stems from the millisecond lifetime of the dark state. Furthermore, the low light levels employed by GSD microscopy and the single-molecule version, GSDIM, are compatible with the use of digital cameras. Optical shelving in the triplet state has been demonstrated in common synthetic probes, such as ATTO dyes, rhodamine, carbocyanines, Alexa Fluors, BODIPYs, and fluorescein. Among the imaging media found to be useful for GSD are polyvinyl alcohol, aqueous solvents, and several commercially available mounting media formulations.

Illustrated in Figure 15.12 are the effective PSFs (Fig. 15.12a), population densities of the electronic excited states (Fig. 15.12b), and typical images for widefield and GSD microscopy (Fig. 15.12c,d). As depletion laser power is increased in GSD mode from 1 to 100 mW (Fig. 15.12a), the effective PSF decreases to a full width at half maximum of 90, 33, and 12 nm, respectively. The population probability of the ground state (S_0,

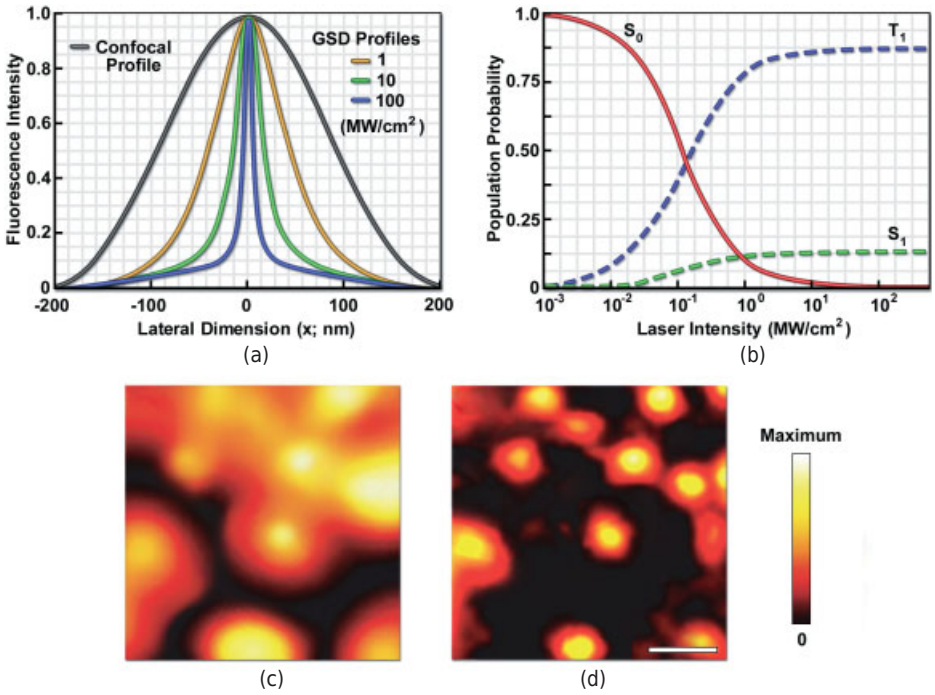

Figure 15.12

Features of Point-spread function (PSF) engineering using GSD. (a) PSFs for three power densities of the GSD beam. (b) Relative abundance of electronic states (ground, S_0; singlet excited, S_1; triplet, T_1) of a fluorescent dye at different GSD beam intensities. (c–f) Simulated fluorescence images of fluorescent beads (c, d) obtained by widefield fluorescence and GSD-mediated PSF engineering. Scale indicates intensity. Bar = 500 nm.

red curve) versus the first excited singlet state (S_1, green curve) and the forbidden triplet state (T_1, blue curve) as a function of laser excitation intensity for a traditional fluorophore (fluorescein) is also shown (Fig. 15.12b). Note the dramatic increase in triplet state population as the laser power is increased. Images of fluorescent beads in widefield fluorescence (Fig. 15.12c) and with GSD (Fig. 15.12d) demonstrate the dramatic improvement in resolution.

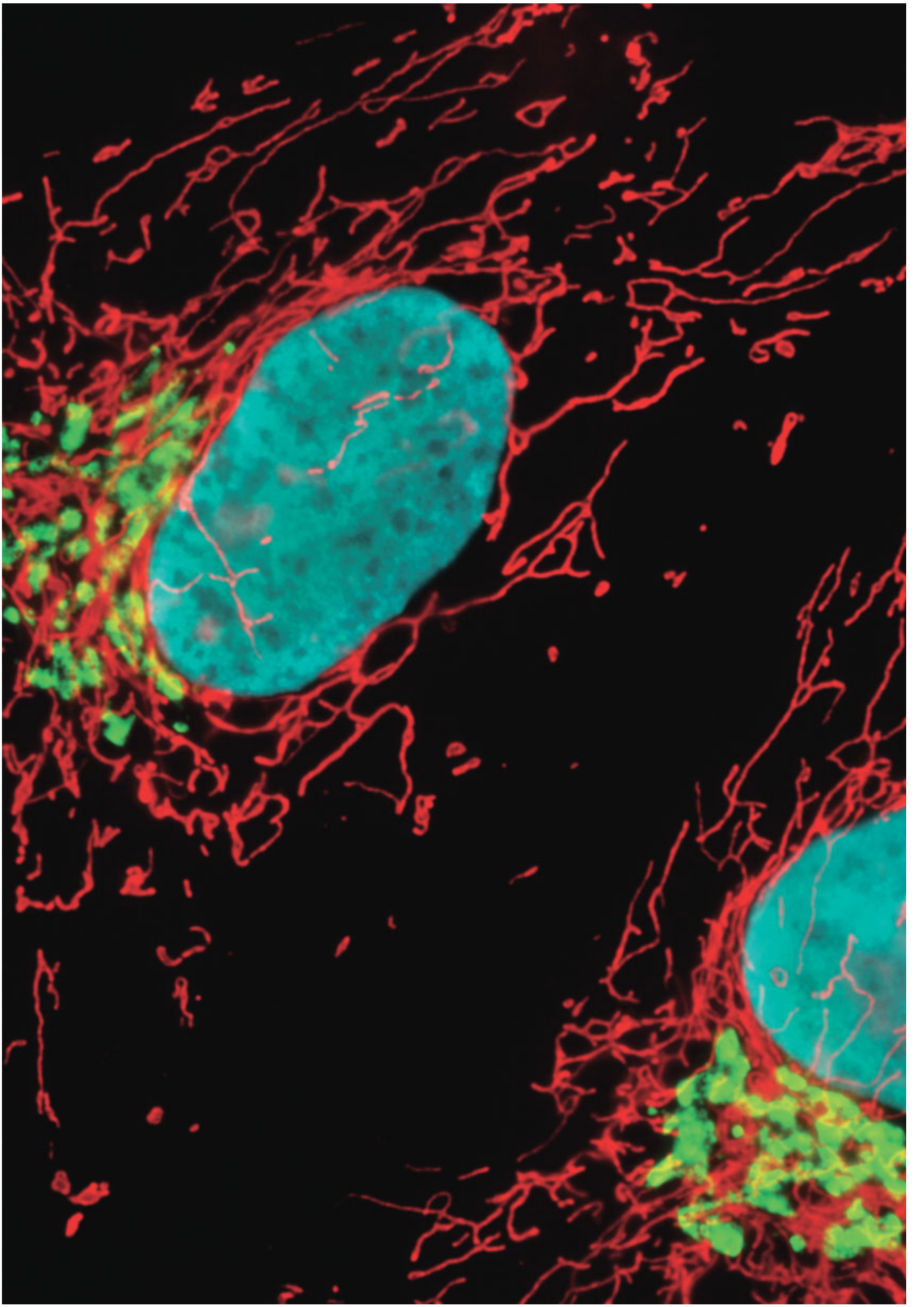

CHAPTER
16

IMAGING LIVING CELLS WITH THE MICROSCOPE

OVERVIEW

Imaging living cells on the microscope stage over time (called *live-cell imaging*) has become a major research focus in cell biology laboratories. Some of the principal concerns are maintaining cell viability on the microscope, minimizing phototoxicity from exposure to light, and reducing the rate of photobleaching of fluorescent dyes. New developments in instrumentation have helped in meeting these challenges, including turnkey microscope systems (Fig. 16.1), climate-controlled environmental incubation systems, high-performance digital cameras, advanced thin-film filter technology, and narrowband illumination sources. Substantial advances have also been made in the development of synthetic fluorophores and fluorescent proteins used to label cells for live-cell fluorescence imaging. In fact, the engineering of bright and photostable new fluorescent protein variants, which can be genetically coupled to virtually any targeting peptide or protein of interest, has been the hallmark breakthrough in enabling routine single and multicolor live-cell imaging. Together, these new technologies have allowed investigators to use live-cell imaging to monitor a variety of dynamic intracellular events with high spatial and temporal resolution over a wide range of time scales. Readers interested in advanced topics on live-cell imaging can refer to "Live Cell Imaging: A Laboratory Manual," by Goldman et al. (2010). In this chapter, we review four areas of concern for live-cell imaging: labeling strategies with fluorescent probes; control of illumination; control of environmental conditions; and optics, detectors, and hardware.

Living cells showing organelles (mitochondria, Golgi, and nucleus) labeled with fluorescent proteins.

Fundamentals of Light Microscopy and Electronic Imaging, Second Edition.
Douglas B. Murphy and Michael W. Davidson.

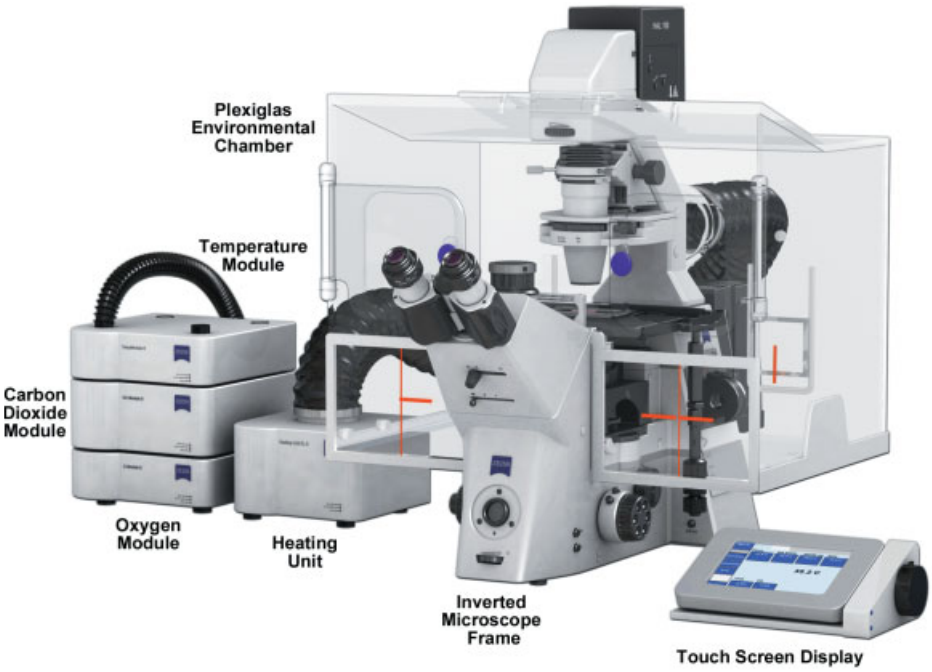

Figure 16.1

Live-cell imaging microscope configuration. The upper portion of an inverted microscope frame is enclosed in a Plexiglas environmental chamber to maintain temperature. Warm, humidified air mixed with 5% CO_2 is forced into the chamber. Several hinged and sliding doors provide access to the stage and specimen. The microscope control panel is easily accessible to the operator.

LABELING STRATEGIES FOR LIVE-CELL IMAGING

Fluorescent proteins have become the reagent of choice for labeling structures in most live-cell imaging applications in cell biology. Fusions of GFP and its color variants, which act as faithful reporters of protein expression and localization, can be easily generated using standard molecular biology cloning techniques (Fig. 16.2). Despite advances in fluorescent protein technologies that have produced high-performance reporters having minimal artifacts, it is still important to determine whether your particular fusion behaves correctly, does not induce toxicity, and is functional in living cells. Furthermore, because fluorescent proteins have much wider emission bands than most synthetic dyes, filter selection is critical, especially in multicolor imaging scenarios. Microscope manufacturers and aftermarket filter dealers (Chroma, Semrock, and Omega) offer fluorescence filter sets that are tailored for imaging fluorescent proteins alone or in combinations of green and red. FRET filter sets for cyan and yellow fluorescent proteins are also available. Imaging three or more fluorescent proteins is tricky due to the large spectral overlaps, but carefully selected narrow bandpass filters can often enable multiple imaging of three or more fluorescent proteins in the same cell.

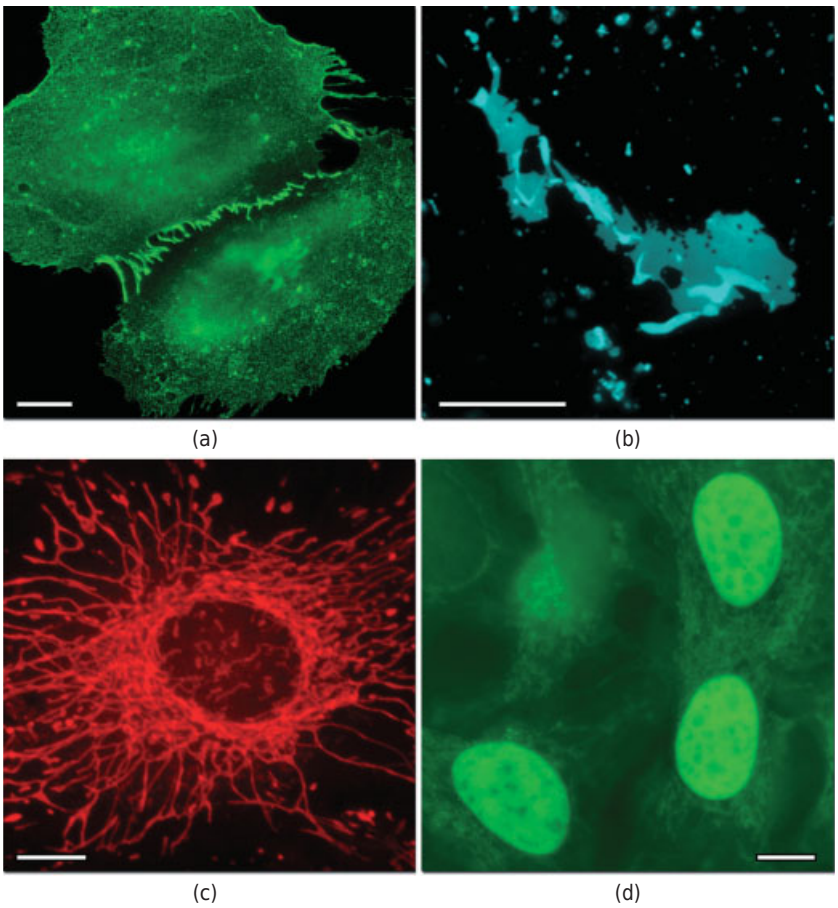

Figure 16.2

Tagging live cells with fluorescent proteins, synthetic fluorophores, and hybrid labeling systems. (a) mEmerald fluorescent protein, a high-performance derivative of EGFP, used to highlight tight junctions in epithelial cells. (b) mTurquoise (a cyan fluorescent protein) fused to connexin 26 marks gap junctions in HeLa cells. (c) MitoTracker Red, a synthetic fluorophore, is used to label mitochondria in living bovine pulmonary artery cells. (d) The FlAsH hybrid labeling system employs a combination of a genetically expressed target and a membrane-permeant fluorescein derivative to label nuclei in HeLa cells. Both mEmerald and mTurquoise are bright fluorescent proteins and can be imaged with very short exposure times to eliminate background artifacts usually arising from autofluorescence. In contrast, the MitoTracker and FlAsH dyes produce higher background levels. Bars = 10 μm.

Introducing Fluorescent Proteins into Living Cells

The most commonly used mechanism to introduce fluorescent protein fusion DNA into living cells is *transient transfection* using liposome-based reagents. Alternative methods include using virus vectors or electroporation for cell lines that are difficult to transfect. Many of the necessary transfection reagents, viral vectors, and electroporation chemicals are commercially available from companies such as Clontech or Life Technologies.

The expression level of fluorescent protein fusions is determined by the promoter included in the cloning vector. Some promoters are highly active and produce very high expression levels of the fusion product. For more controlled expression, the fluorescent protein fusion can be moved to a vector that has an inducible promoter controlled by chemicals, such as tetracycline. RNA interference (RNAi) technology has become very useful in live-cell imaging by allowing the behavior of fluorescent protein fusions to be studied while selectively depleting a competing or endogenous gene product by RNAi. Since introduction of small interfering RNA also involves transfection, a protocol can be developed where both the fusion and siRNA are introduced in the same step. Although fusions can also be introduced by microinjection, commercial transfection reagents (such as Lipofectamine 2000 from Invitrogen, Fugene from Promega, and Effectene from Qiagen) are preferred by most researchers due to their convenience and flexibility.

One of the most important facts to be appreciated about fluorescent protein transfections is that the fusions are expressed above the natural levels of the endogenous protein and therefore are, by definition, *overexpressed*. As a consequence, when the localization of a fluorescent protein fusion depends on other cellular products or the fusion is a component of a multiprotein complex, the observed localization may differ from the endogenous protein. In addition, the details regarding fusion construction (N- vs. C-terminus fusion of the fluorescent protein, as well as the amino acids comprising the linker sequence) can affect expression and localization, as described by Snapp (2009). It is therefore a good idea to generate a cell line that expresses the fusion at a low level by selecting mutants that stably express the fusion using an antibiotic selection marker (such as G-418) built into most vectors.

Labeling with Synthetic Fluorophores

Many synthetic fluorophores are useful in live-cell imaging, and manufacturers are continually developing new derivatives for this purpose. Some fluorophores have molecular characteristics that render them excellent reporters of cellular function, such as calcium indicators, apoptosis sensors, organelle probes, live-dead indicators, and nuclear labels. Synthetic probes for mitochondria (MitoTracker; Fig. 16.2c), lysosomes (LysoTracker), the plasma membrane ($DiOC_6$), Golgi complex (rhodamine-ceramide), and calcium (Fura and Indo) can be easily used to quickly and conveniently label living cells in imaging chambers (see Chapter 11). An excellent source of information on synthetic reagents for labeling can be found in Johnson and Spence (2010). It is important to keep in mind that while synthetic probes are an attractive tool to label live cells, they are usually more toxic than fluorescent proteins and may interfere with normal cellular function.

Hybrid Labeling Systems

The future of live-cell imaging depends on increasing the specificity and labeling efficiency of very bright fluorophores while simultaneously decreasing the size of the targeting agents used to deliver the fluorescent payload to the cells. A wide spectrum of hybrid systems designed to couple synthetic fluorophores with genetically encoded targets may one day be capable of achieving this goal. All of these systems utilize a

peptide or protein sequence that is expressed in living cells and is capable of recruiting a small synthetic molecule to bestow fluorescence. One of the most sophisticated reagents in this class utilizes a tetracysteine motif fused to a variety of genetic targets to recruit blue, green, or red fluorophores (called FlAsH, ReAsH, and CHoAsH, respectively) capable of binding to the cysteine residues to generate a probe similar in specificity to fluorescent proteins (Fig. 16.2d). Other hybrid reagents have proprietary names, such as CLIP-Tag, SNAP-Tag, and HaloTag, which rely on a recognition peptide that is fused to the protein of interest to enable a naturally occurring or engineered enzyme to ligate the synthetic probe to the recognition peptide. The major disadvantage of hybrid combinations is the inability to overcome the high background levels of unbound fluorophore that lower contrast, but continuing development may someday yield suitable probes for live-cell imaging.

CONTROL OF ILLUMINATION

When imaging fixed cells and tissues labeled with fluorescent dyes or proteins, we are primarily concerned with controlling the illumination level to reduce the rate of photobleaching. Likewise, photobleaching is a concern for live-cell imaging, but the detrimental effects of light on the health and biology of living cells must also be taken into consideration. As we will see in this chapter, there is a tradeoff between limiting the amount of light exposure to prevent toxicity while still being able to acquire images having adequate detector signal-to-noise (S/N) ratio.

Phototoxicity and Photodamage

Aside from cellular toxicity due to high concentrations of synthetic dyes and overexpression of fluorescent proteins, living cells are subject to light-induced damage, called *phototoxicity*, which occurs upon exposure to light from lasers and arc lamps. Light, especially at short wavelengths, reacts with a variety of molecules to create free radicals. The presence of molecular oxygen enhances this process. Additionally, some constituents of standard culture media, including the vitamin riboflavin and the amino acid tryptophan, may also contribute to adverse light-induced effects in cultured cells. Certain fluorescent molecules in their excited state can also react with molecular oxygen, and in the process destroy the fluorescence properties of the fluorophore and produce free radicals that go on to damage subcellular components and compromise the cell. Fluorescent proteins are generally not phototoxic to cells because their fluorophores are buried deep within a protective polypeptide envelope. However, many synthetic dyes, such as MitoTracker Red and nuclear stains (Hoechst, SYTO cyanine dyes, and DRAQ5), can be highly toxic to cells when they are illuminated for even relatively short periods of time (Fig. 16.3). When imaging cells, it is best to minimize exposure to light, use fluorophores with long excitation wavelengths, and to avoid exposing cells to short wavelength illumination, as described by Khodjakov and Rieder (2006).

Even in the absence of fluorophores, the sensitivity of mammalian cells to ultraviolet (UV) light exposure has been well established, and many cell lines are at least equally sensitive to blue light in the wavelengths used to excite cyan and green fluorescent proteins. Mammalian cells are very sensitive to UV, blue, and infrared (IR)

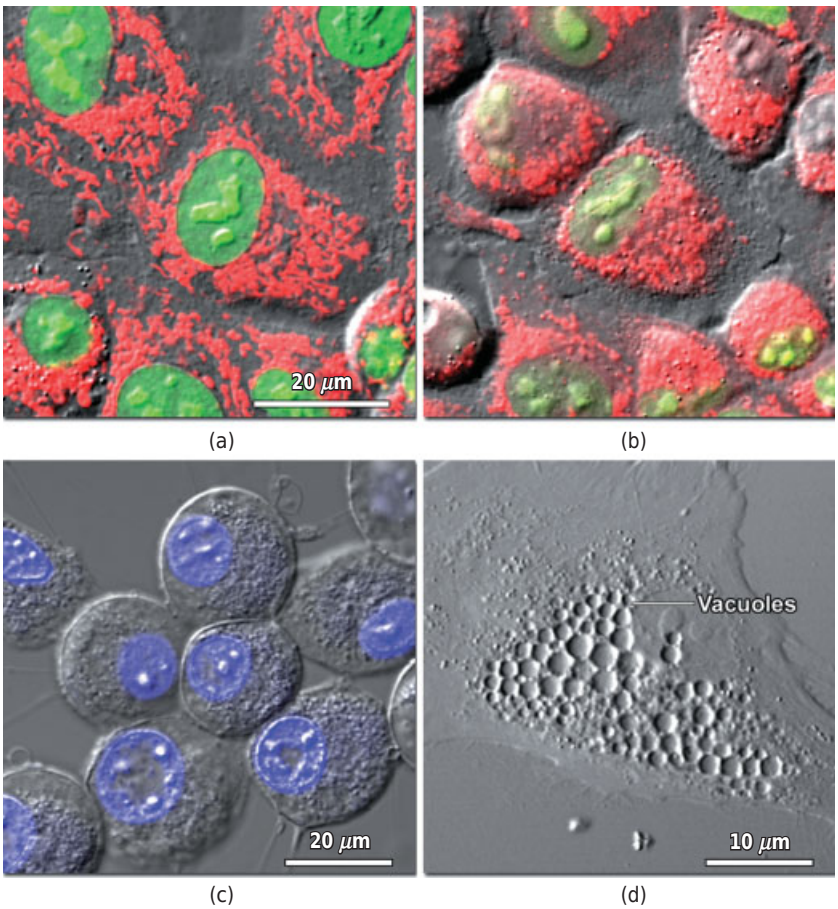

Figure 16.3

Phototoxicity during live-cell imaging. (a) Rabbit kidney (RK-13 line) cells expressing EYFP fused to a nuclear localization signal (green nucleus) were treated with the synthetic dye MitoTracker Red and imaged in fluorescence and DIC mode. (b) Same viewfield as panel a after time-lapse imaging for 2 hours at 15 second intervals. Note the fragmentation of mitochondria and rounding of the cells due to phototoxicity. (c) HeLa cells labeled with Hoechst 33342 imaged for 30 minutes at 10-second intervals with a 405-nm laser in a confocal microscope. Cells have detached from the coverslip and are rounding. (d) Vacuole formation in a fibroblast cell after imaging for 8 hours at 30-second intervals using tungsten halogen illumination and DIC optics.

light, and are least sensitive to green, yellow, and red light. To minimize photodamage and phototoxicity when setting up an imaging experiment, cells should first be observed at very low light levels to avoid damage even before the experiment has begun. Neutral density filters or very low laser power should be used to attenuate the illumination source while choosing a cell or region for imaging. Alternatively, candidate cells can be chosen using brightfield, phase contrast, Hoffman, or differential interference contrast (DIC) imaging modes with far less toxic tungsten-halogen illumination. In this case, photodamage can be further minimized by inserting a green or red interference filter into the illumination pathway.

Phototoxicity can be reduced by choosing efficient bandpass filters and using sensitive cameras and PMTs. When choosing filters for live-cell imaging experiments, bandwidths should be carefully selected so that even trace levels of IR and UV light are eliminated. Even though modern bandpass filter designs perform well in the central regions of the visible light spectrum, they often pass radiation at very low and very high wavelengths. It is therefore advisable to install filters near the illumination source to block damaging UV and IR wavelengths. Electronic shutters should also be used to limit exposure of the cells to damaging radiation during periods when images are not being captured. Judicious shuttering of the illumination source is one of the most important factors in successful live-cell imaging experiments. (Note: It is important to review the spectra of common illuminators shown in Chapter 3; about half of the total output of a mercury arc lamp is in UV, and the majority of tungsten-halogen lamp and xenon arc lamp output is in the IR.)

Improvements in detector sensitivity have made it feasible to further reduce illumination levels in live-cell imaging experiments. Increasingly sensitive photomultiplier tubes (PMTs) for confocal microscopy and advanced CCD cameras for widefield microscopy allow high-quality imaging at light levels that are exceedingly low. Many of these cameras employ back-thinned charge-coupled devices (CCDs), which are usually cooled and feature high quantum efficiency across the visible and near-IR spectral regions to further increase sensitivity. If the best cameras are not available, sensitivity can be increased by combining the signal from multiple pixels (a process known as binning; see below and Chapter 17) at the expense of spatial resolution. In confocal microscopy, maintaining low zoom ratios also reduces phototoxicity. Increasing the confocal zoom factor causes the total amount of laser light to be scanned over a smaller region of the specimen, thus exposing the cells to more intense illumination.

Choosing the exact level of light attenuation and the correct exposure time is always an empirical exercise. For a new cell line with unknown parameters, the best strategy is to attenuate the light as much as possible and apply very short exposure times so that subcellular structures are just barely visible in the acquired image. A good place to start is a neutral density filter with an optical density of 1.0 and an exposure time of 100 ms or less. For laser scanning confocal microscopes, start with a laser power of approximately 1% and increase the voltage (and gain, if necessary) of the PMT. Use pixel dwell times about 50% shorter than those that usually produce adequate signal levels. If the cells are able to tolerate this light level through a long-term time-lapse experiment, then the illumination intensity and exposure time can slowly be increased in subsequent experiments until a workable compromise is achieved between S/N and cell viability. Note that a nonlinear relationship often exists between the total amount of light exposure a cell can tolerate and the length of individual exposure times. In general, cells appear to be the healthiest when exposed to very brief pulses of light, since extended exposures (greater than one-half second) are often lethal over long periods of time. Examples of the effects of phototoxicity on cells are shown in Figure 16.3.

Monitoring Cell Viability and Variability

After the imaging chamber has been loaded with fresh cells, assembled, and mounted on the microscope stage, the next step is to visualize the cells to establish their overall

condition and morphology, and to identify candidates that are appropriate for imaging. In most experiments, especially when imaging cells that have recently been transiently transfected with fluorescent proteins, there will be a significant amount of morphological variability in the cell population. It is not uncommon to observe cells that were either not transfected or exhibit poor localization of the GFP fusion proteins. In addition, a percentage of the transfected cells overexpress the fluorescent protein, often to the point of creating a potentially toxic effect. Other cells may exhibit stress, such as detachment from the substrate, excessive vacuole formation (Fig. 16.3d), swollen mitochondria, cytoplasmic blebs (Fig. 16.4a), and multiple nuclei (Fig. 16.4b). Cells showing even a slight deviation from a normal and healthy appearance should not be considered for imaging and data collection. Furthermore, if more than 50% of the population is judged as unhealthy, the entire culture should be discarded and exchanged for one that is in better physiological condition.

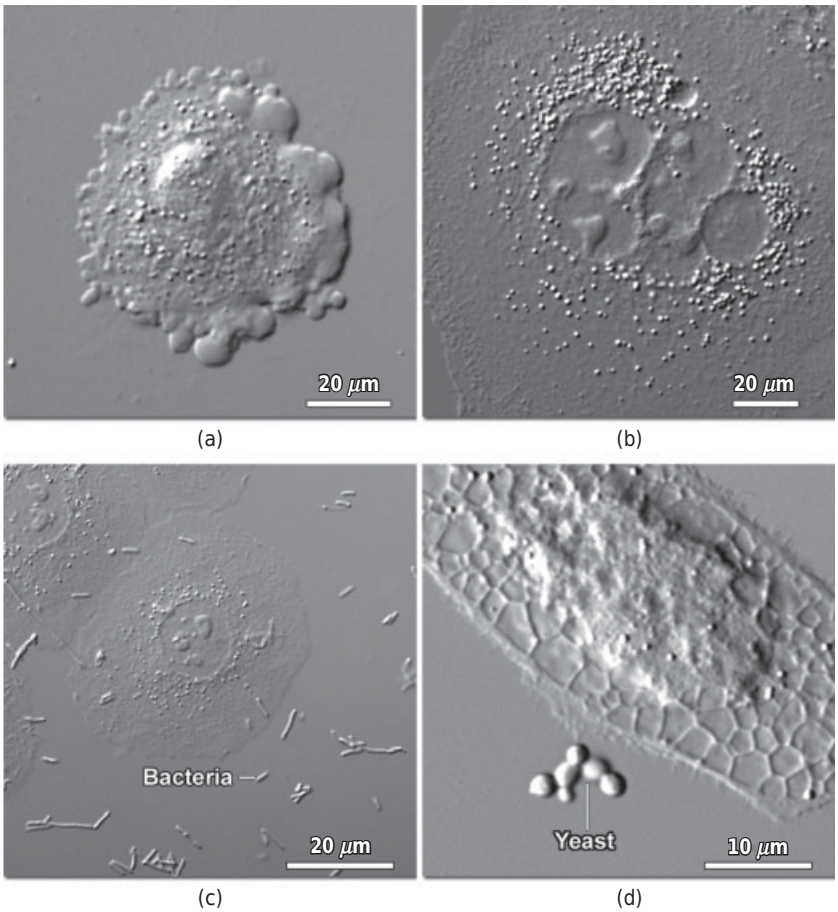

Figure 16.4
Common health problems and infections of cultured mammalian cells. (a) Membrane blebbing. (b) Multiple nuclei. (c) Bacterial contamination. (d) Yeast contamination and vacuole formation.

Aside from the problems associated with phototoxicity and maintaining cells on the microscope, one must be alert to the possibility of microbial contamination during the course of an experiment. The most common infections are due to bacteria (Fig. 16.4c), fungi, mycoplasma, yeasts (Fig. 16.4d), and, in rare circumstances, protozoa. Unless it becomes a frequent event, the nature of the infection or species involved is not as important as determining where the contamination originated. In general, rapidly growing microorganisms are less problematic due to the fact that they are usually readily detected and the culture can be quickly discarded. Overuse of antibiotics in the culture medium is a common problem that often results in a low-level contamination, which can remain undetected for long periods of time and may ultimately interfere with normal mammalian cellular function. A comprehensive discussion of basic techniques, cell viability, and microbial contamination in animal cell cultures is provided by Freshney (2010).

CONTROL OF ENVIRONMENTAL CONDITIONS

Keeping Cells Alive and Healthy on the Microscope Stage

Control of environmental factors is critical for successful live-cell imaging. While it may be easy to maintain cells in a tissue culture incubator, the task of growing cells on the microscope stage for long-term imaging experiments is far more demanding. Table 16.1 lists some of the environmental parameters that must be regulated within specific boundaries to guarantee health and normal function (Freshney, 2010).

- *Buffer.* Culture medium must be maintained at a specific pH using a combination of bicarbonate and CO_2 gas (5–7%), which equilibrate to produce the desired pH. Live-cell imaging usually requires special culture chambers to regulate the concentration of CO_2. In room air, the CO_2 concentration goes down and the medium becomes more alkaline, so buffers, such as HEPES, are sometimes added to control pH for short periods of time. HEPES is somewhat toxic and reduces growth rates, and bicarbonate is essential for optimum cell growth, so the addition of HEPES is only a temporary solution. The pH indicator dye, Phenol Red, is

TABLE 16.1 Environmental Variables for Mammalian Cell Cultures

Variable	Optimum Range	Comments
Humidity	97–100%	Closed chamber or humidified environmental chamber
pH	7.0–7.7	Use HEPES-buffered media or change medium regularly or use perfusion
Osmolarity	260–320 mOsm	Avoid evaporation, seal chamber or use humidified environmental chamber
Oxygen	Variable	Perfuse or change media regularly or use large chamber volume
Temperature	28–37°C	Control with chamber heaters, objective heaters, inline heaters, or environmental control boxes

usually omitted when observing live cell fluorescence in order to reduce background noise and prevent phototoxicity. For cells not tolerant of HEPES, Leibovitz L-15 medium, or "air-buffered medium," is designed to eliminate the need for CO_2 by buffering with sodium pyruvate and high concentrations of amino acids. The presence of sodium pyruvate allows cells to increase their endogenous production of CO_2 and bicarbonate ion, theoretically rendering them independent of the gas. Unfortunately, many cell lines do not adapt well to L-15 medium and each should be thoroughly examined for several passages before planning live-cell imaging experiments based on this formulation.

- *Osmotic pressure and ionic strength.* Mammalian cells grow well at osmolarities between 260 and 320 mOsm. In cases where cells are grown in Petri dishes or open-plate cultures, hypotonic medium can be substituted to compensate for evaporation. To minimize changes, a sealed system can be created by covering the medium with light mineral oil; alternatively, the chamber can be humidified during imaging. The microenvironment provided by the small volume in the live-cell imaging chambers described below is inherently less stable than a CO_2 incubator and requires considerably more attention to detail.
- *Oxygen concentration.* Cell lines vary widely in their oxygen requirement, although normal atmospheric oxygen tension levels are compatible with most cultures. Mammalian cells require oxygen for respiration *in vivo*, but can substitute glycolysis (an anaerobic process) when grown in culture vessels as primary lines or after immortalization. During fluorescence illumination, oxygen is often depleted as a way to reduce the photodamage and photobleaching from the presence of oxygen free radicals. Generally, this is not harmful, because in the body most epithelial and connective tissue cells exist at partial pressures of oxygen that are only 3–4% of the level found in arterial blood. Oxygen can be reduced by the application of a commercial oxygen depletion system, such as Oxyrase, or enzyme mixtures, such as glucose, glucose oxidase, and catalase, or the PCA/PCD oxygen scavenging system (Aitken et al., 2008). Oxygen-free radicals can also be depleted with scavengers such as ascorbate (ascorbic acid; vitamin C) or Trolox (a derivative of vitamin E), and can also be controlled by filtering the illumination to remove blue and UV wavelengths, reducing light intensity, and using sensitive camera systems that need shorter exposures (see below). The height of the culture medium above the cells affects the rate of oxygen diffusion to adherent cells growing on a glass or plastic surface and should be kept below 5 mm.
- *Temperature.* Temperature control is important for maintaining the consistency of physiological processes and for minimizing focus drift caused by the thermal expansion and contraction of the microscope and its optical system. Too often, attention is limited to the chamber itself. The microscope stage, frame, and objectives act as heat sinks and must also be considered. Heating problems are compounded when immersion objectives are used because the optical coupling medium—oil, glycerin, or water—has a much higher thermal conductivity than air. In static, unheated chambers, the area directly under the objective is often up to 3–5°C cooler than the remainder of the specimen chamber.

Objective heaters that employ circulating heated water or resistive heating elements are useful to partially offset temperature gradients between the specimen and the front lens

Figure 16.5
Objective heaters. (a) Economical setup having a metal foil blanket wrapped around the objective with a Velcro fastener. (b) Copper tubing water jacket requires external source of pumped heated water. Panels a and b are essentially the same from a thermodynamic point of view. (c) High-performance proportionally controlled closed loop heating unit attached to the objective nosecone through a band that contains the heating element. Note that all three designs require removal of the objective decorative barrel.

elements (see Fig. 16.5). However, even with an objective heater, there can still be a temperature gradient along the objective barrel or between the objective and the microscope itself. Adjustable heating blanket and circulating water jacket objective heaters (Fig. 16.5a,b) are both relatively inefficient, with much of the heat being radiated away to the region directly beneath the specimen instead of being transferred into the objective. The result is excessive external heat being convectively channeled upwards in the vicinity of the specimen to produce large temperature variations and excessive thermal cycling in the chamber control system. The best solution is a closed loop heater (Fig. 16.5c) designed specifically to heat the region of the objective housing the front lens element. Objective heaters of this type are available from Bioptechs, Inc. and several other manufacturers.

Most objectives are designed and sold for the purpose of fixed-cell microscopy (conducted at room temperature), so when selecting an objective to be employed in live-cell imaging, care should be taken to choose only those objectives with the ability to be efficiently heated. The following issues should also be considered:

- Cycling of the heating system can alter the coverslip position (so-called *coverslip flex*) and cause the specimen to drift out of focus.
- Repeated heating and cooling have been incorrectly reported to considerably shorten the lifespan of objectives. In fact, there is little reliable evidence that temperature cycles affect the strain characteristics in objectives, and most can withstand temperatures up to 50°C without damage.
- Heating the objective may dry out lubricants for the retraction stopper barrel prematurely, making the action sluggish.

A final consideration is tight control of temperature not only for the microscope, but also the entire laboratory. Even a seemingly minor change of 1°C from air conditioning

or heating ducts near the microscope can produce unwanted shifts in the microscope optical train, resulting in focus or alignment drift. For critical long-term observation, consider building a large thermostatically controlled box around the stage (see the discussion below) or even place the entire microscope in a room that is maintained at 37°C. A comprehensive discussion of objective heaters is provided by Focht (1998).

Live-Cell Imaging Chambers

Specimen chambers stabilize environmental conditions and allow cells to be examined for varying amounts of time. Simple experiments—20–30 minutes or less—can be conducted by attaching a coverslip containing adherent cells onto a microscope slide using spacers to keep the cells from being damaged (Fig. 16.6). The coverslip is secured to the slide with a sealant, which can be molten agarose, rubber cement, vacuum grease, or a preparation known as *VALAP* (a 1:1:1 mixture of Vaseline, lanolin, and paraffin), to eliminate evaporation of the culture medium. Thin gaskets cut from silicone rubber or broken pieces of coverslip can be used as spacers to keep the cells from coming in direct contact with the microscope slide. After sealing, cells will function normally for only a few minutes without fresh medium, but this is often sufficient for observations.

Specially designed chambers are useful for maintaining environmental conditions over extended periods of time. Such chambers include a glass window, usually the thickness of a coverslip, through which the cells can be readily viewed with objectives

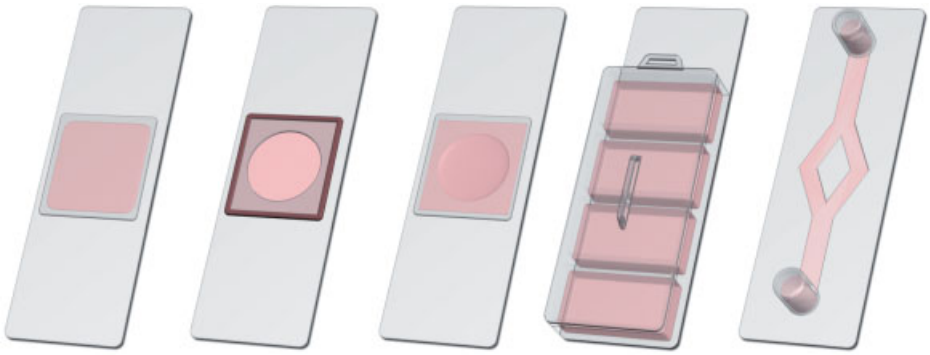

Figure 16.6

Simple live-cell imaging chambers made with microscope slides. (a) Coverslip attached to the microscope slide with rubber cement. (b) Coverslip with adhesive-backed silicone gasket to seal the chamber. (c) Coverslip attached to concave microscope slide for imaging thicker specimens, such as embryos of small intact organisms. (d) Multichamber slide (called "lab-on-a-slide") for holding several individual cultures. These slides are available from several manufacturers in a number of configurations, ranging from a single chamber to 12 separate chambers. (e) Flow chamber for simulating blood vessels for studies on endothelial cells. These slides have Luer-style adapters for perfusion couplers.

operating at high numerical aperture (NA). Temperature control is achieved using peripheral sources of IR radiation or heated air (such as a hair dryer or egg warmer), a metal heating plate coupled directly to the chamber, or with optically transparent thin coatings of electrically conductive metal oxides applied by evaporation onto the coverslip surface to provide a more efficient conductive heat transfer to the chamber.

There are generally two types of chambers: *open* chambers, similar to Petri dishes, which have free access to the atmosphere; and *closed* chambers that are sealed to protect cells from evaporation of the culture medium. Open chambers allow access for microinjection, addition of drugs, and changing of the culture medium. In contrast, closed chambers provide better insulation from the external environment, but make access to the cells more difficult. Most closed chamber designs include ports that allow the addition of fresh medium and drugs without interrupting image acquisition (Fig. 16.7). In these systems, perfusion is regulated by a peristaltic pump, motor-driven syringe, or through a gravity-controlled manifold. When new solutions are added to a closed imaging chamber, it is critical that they are equilibrated to the same temperature as the cells before addition. Many cell lines are sensitive to shear, so perfusion of adherent cells should be performed at very low flow rates. Several of the more advanced chambers allow one to control the flow rate.

The simplest commercial open chamber imaging systems are constructed by mounting a coverslip onto the bottom of an ordinary tissue culture vessel or Petri dish. Standard 35-mm and 60-mm sterile Petri dishes are available that have a small hole drilled in the dish with a 170-μm coverslip fused to the plastic to enable high-resolution imaging (these are commercially available from the MatTek Corporation and other manufacturers). Rectangular coverslips and microscope slides with a small single- or

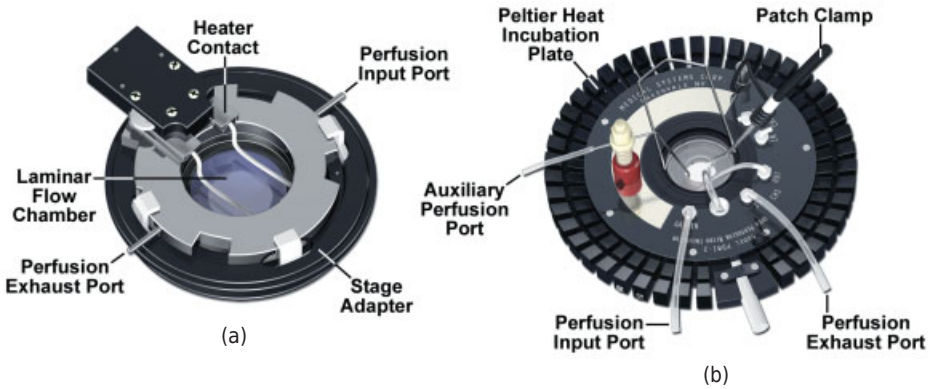

Figure 16.7

Advanced live-cell imaging chambers. (a) Closed perfusion chamber with a thin coating of indium-tin oxide film for temperature control. The glass plate is transparent and temperature control is provided by resistance heating. This system can operate at rapid media flow rates and temperatures up to 50°C. Both bicarbonate and organic buffers are compatible with the chamber, which is interfaced with a stand-alone controller unit. (b) Open-chamber system designed to be used with 35-mm Petri dishes having a coverslip fused to the base, multiple perfusion ports, and a Peltier heating device for controlling the temperature. The chamber is also equipped with a patch clamp for electrophysiology.

multiple-well plastic imaging chamber sealed to the glass are also commercially available (Fig. 16.6d). Both of these chamber designs are simple to use, but they are not tightly sealed, so the amount of culture medium that evaporates over the course of an experiment must be carefully monitored. In addition, simple imaging chambers do not include any heating system, and must be mounted on a microscope stage equipped with an auxiliary heating unit designed specifically to house the chamber. Without temperature control, the performance of simple open chambers is only marginally better than using the sealed coverslip method described above.

Robust environmental control is best provided by a Plexiglas enclosure that surrounds the microscope stage and nearby objectives, fluorescence filters, and transmitted light condenser of the microscope (Fig. 16.1). These chambers can be used with a variety of culture vessels and many of the open and closed systems described above. Temperature is maintained with an external heating unit (usually forced air) and the CO_2 concentration is controlled with a sensing unit coupled to a regulator that is fed by a cylinder of pure gas or a mixture of 5% CO_2 in air. These units can also be equipped with humidity control and advanced designs provide rubber glove access to avoid disturbing the environmental equilibrium when manipulating the cells during imaging. In order to maintain a high degree of temperature control, more sophisticated incubator chambers enclose virtually the entire microscope with the exception of the eyepieces, camera, and lamphouses. Unfortunately, environmental chambers can impede rapid access to the specimen and are cumbersome when repeated manipulation is necessary. In addition, the high humidity level inside the chamber can add to the expense of maintaining the instrument due to premature degradation of gear lubricants, metal surfaces, and lens or filter coatings. Microscope manufacturers offer custom incubators for their inverted microscopes, while aftermarket suppliers fill the gaps with simpler and more advanced models, as well as a host of useful accessories.

Laboratory Environment and Isolation of Vibration

When choosing a room for live-cell imaging experiments, the following key factors should be considered:

- Ensure that adequate ventilation is available to dissipate the ozone released by mercury and xenon arc-discharge lamps, as well as the fumes from organic solvents used to clean optical surfaces and disinfect the microscope stage.
- Allow sufficient space around the microscope system for proper ventilation, as well as cleaning of the floors, benches, tables, and experimental apparatus.
- The laboratory should be kept as clean as possible to reduce the levels of dust, smoke, and other damaging vapors that can diminish optical as well as electronic performance.
- In order to reduce culture contamination by microorganisms, the microscope stage and surrounding space should be kept free of unnecessary equipment to enable the area to be periodically wiped with 70% ethanol or commercial antiseptic towels.
- Culture media spills should be cleaned immediately and the surrounding area thoroughly disinfected.

Figure 16.8

Vibration isolation for live-cell imaging. (a) Economical Neoprene vibration damping pads can be obtained from scientific supply houses. (b) Sorbothane damping pads are available in a variety of shapes and sizes. The pads illustrated here are the size of tennis balls. (c) Commercial vibration isolation tables are expensive, but offer the best solution.

Among the mechanical vibration sources that can affect microscope performance are central heating and cooling units in the attic or on the roof of the building, refrigerators, low-temperature incubators, and traffic through nearby hallways. Vibrations from refrigerators and other sources that may not be immediately obvious can have an impact on microscope stability. Room and building low-frequency vibrations can be mitigated using vibration isolation tables that are gas-filled or relatively low-cost flexible synthetic polymer isolation pads (see Fig. 16.8). Vibration isolation pads are marketed in a variety of geometries and damping levels to suit almost all configurations. A combination of the vibration pads and a heavy sheet of half-inch aluminum or a predrilled isolation platform often will reduce vibrations. High-frequency vibrations can be reduced by loading the table top with additional mass, such as lead bricks. For more information about system integration to combat harsh laboratory conditions and vibration, the reader is referred to Inoué and Spring (1997).

When setting up a system for live-cell imaging, the following checklist can be used as a guide to potential environmental focus drift and vibration hazards:

- Vibration from equipment cooling fans, refrigerators, building heaters, and air conditioning blower units.

- Acoustic noise from noisy fan units, auxiliary equipment, and hallway traffic.
- Heat generated by microscope light sources, cameras, computers, auxiliary equipment, and power transformers.
- Poor ventilation, insufficient laboratory heating or cooling, and building vibration.
- Heat and vibration from motorized microscope components, including nosepieces, focus controls, shutters, filter changers, and automatic stages.

OPTICS, DETECTORS, AND HARDWARE

Focus Drift

Fluctuations in the axial (z) position of the focal plane during time-lapse imaging (*focus drift)*, can quickly destroy image sequences. A seemingly minor 1°C change in room temperature can shift the focus by approximately 500 nm, enough to completely change focus at high magnification. Other causes of drift are irregularity in glass coverslips, microscope instability, gear slippage, and other mechanical factors. One of the best remedies for focus drift is to employ a thermostatically controlled enclosure that fully envelops the microscope and associated components. Alternatively, a feedback device can be used to continuously monitor and correct focus. Defeating focus drift should be a principal consideration during configuration of a microscope for time-lapse imaging:

- For time-lapse sequences lasting several days, the entire imaging system, including the microscope, camera, shutters, filter wheels, illuminators, live-cell chamber assembly, and host computer should be brought to operating temperature for at least 24–48 hours prior to initiating sequence acquisitions.
- When assembling the imaging chamber, ensure that coverslips containing adherent cells are mounted securely in their housings and that the chamber itself does not move in lateral or axial directions.
- Oil immersion objectives can be the source of focus drift as the oil spreads across the chamber coverslip and the front lens element.
- An objective heater (Fig. 16.5) should be used for samples that require immersion objectives.
- Once the microscope is at the correct operating temperature, monitor the focus with a test sequence over a period of 12–24 hours using a fixed specimen.

Several hardware devices for correcting focus drift operate by measuring the distance between the objective front lens and the specimen by sensing light (near-IR laser or LED) or sound reflected from the coverslip surface. A special detector controls a feedback circuit to adjust the position of the objective in relation to the interface between the coverslip and the culture medium for oil immersion objectives or between the coverslip and air for dry objectives (Fig. 16.9). Instantaneous feedback of specimen position enables the distance between the coverslip and objective to be detected in millisecond intervals during observation, thus automatically correcting for focus drift

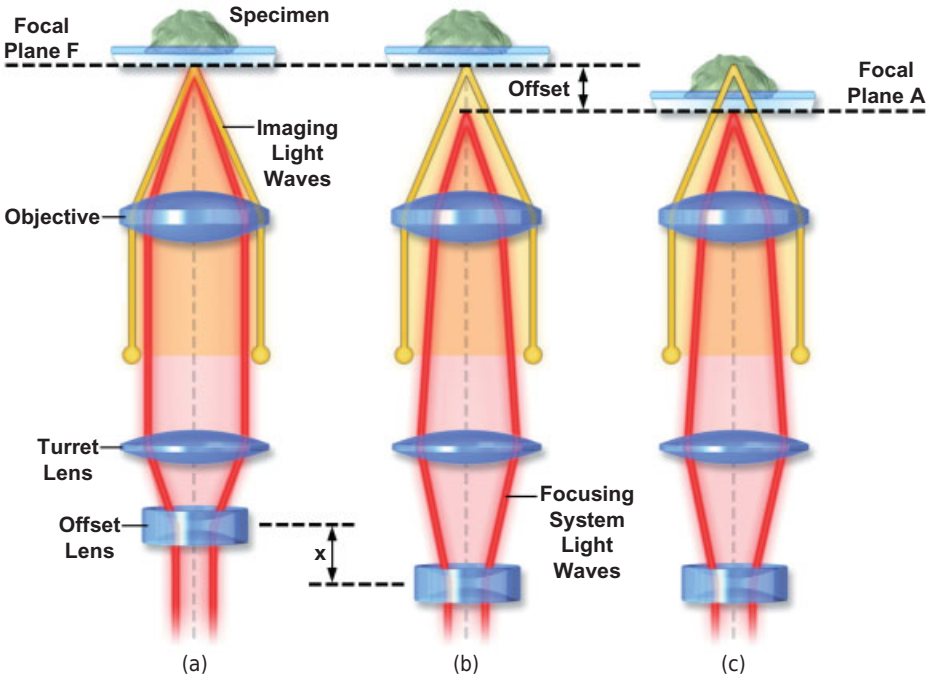

Figure 16.9

Microscope focus drift correction optical train operation. Yellow ray traces depict image-forming light waves, and red ray traces represent focus-detection light waves that monitor and correct drift. The drift correction rays are focused onto the air:glass interface of the coverslip by the turret and offset lenses, the configuration used for dry objectives. The offset system is designed to enable the operator to select a region of the specimen for imaging while maintaining a fixed distance between the objective front lens element and the coverslip using the drift-correction hardware and software. (a) The focal point of the objective (focal plane F) and that of the drift-correction optics (focal plane A) coincide at the interface region, a condition called *zero offset*. (b) The offset lens in the figure is adjusted by the operator to a distance *x*, which results in a shift in focal plane from F to A. (c) Drift-correction hardware shifts the objective position so the coverslip interface coincides with focal plane A bringing the selected region of the specimen into focus and thus establishing an offset value that is maintained whenever the coverslip shifts position due to thermal or mechanical drift.

in real time. Software accompanying the focus stabilization systems allows freely selectable focal planes through adjustment of an offset control (Fig. 16.9b). Due to the long wavelengths used, the detection system does not interfere with wavelengths used for observation and is invisible to the fluorescence detector.

Optimizing Signal-to-Noise with Binning, Gain, and Exposure Time

Compared with live-cell imaging, working with fixed cells offers greater flexibility in attempting to locate a suitable field of view and when defining electronic parameters

for image acquisition. As a result, it is easier to acquire images that utilize the full dynamic range of the camera system, thus producing the optimal S/N ratios. Unfortunately, there is limited flexibility with live cells due to the stringent requirements for maintaining cell viability. Frequently, the intensity of the specimen is only a few gray levels higher than that of the background. Therefore, the most important consideration becomes the dark current and read noise levels of the detector. Cheaper cameras often feature higher noise levels, leading to noise (graininess) in the background that can obscure signals from the specimen, an effect that becomes more serious as the readout speed is increased. In virtually all live-cell imaging applications, the detector choice is paramount in determining the success or failure of an experiment. Furthermore, understanding the balance between binning, gain, and exposure time is critical for producing the best images of living cells (Goldman et al., 2010).

The primary sources of noise in digital imaging arise from the specimen and illumination systems themselves, the so-called *Poisson* or *shot* noise (due to the stochastic nature of a photon flux) associated with features in the image and stray light. There are also significant noise sources from the detector (see Chapter 17). These include:

- *Detector noise* is specific for each type of detector and includes spurious electrons for PMTs, as well as dark current and read noise for CCDs.
- *Poisson (shot) noise* is a function of photon statistics with an uncertainty associated with signal detection. For a signal with N photons, the uncertainty is $N^{1/2}$, which also equals the S/N.
- *Illumination noise* occurs due to spatial and temporal fluctuations in illumination. Variations up to 10% are common if not corrected using stabilized power supplies.
- *Stray light* and spurious photons contained in the microscope optical train are of great concern in extremely low light level applications, such as single molecule imaging. Choosing a very sensitive EMCCD or PMT with high quantum efficiency can help offset noise.

The tradeoff between camera sensitivity and readout speed with regard to image quality is illustrated in Figure 16.10. When specimens are bright and exposure time is not limiting, the entire dynamic range of the camera is available, and image quality does not significantly suffer as a function of readout speed. However, with dim samples, a slower readout speed produces much higher image quality, but using this setting is often not possible when trying to capture very fast events in living cells.

BINNING

In order to overcome the low light levels associated with live-cell imaging, CCD cameras can be configured to deliver a significant increase in sensitivity by implementing a process known as *binning* (Chapter 17). In a binned image, the photoelectrons from a group of adjacent pixels on the image sensor are combined and assigned to a single pixel value during readout. In the case of 2×2 binning, there is a twofold loss in resolution, a fourfold increase in signal, and a twofold improvement in signal-to-noise. The improvement in signal-limited applications can be significant, although at the cost of spatial resolution.

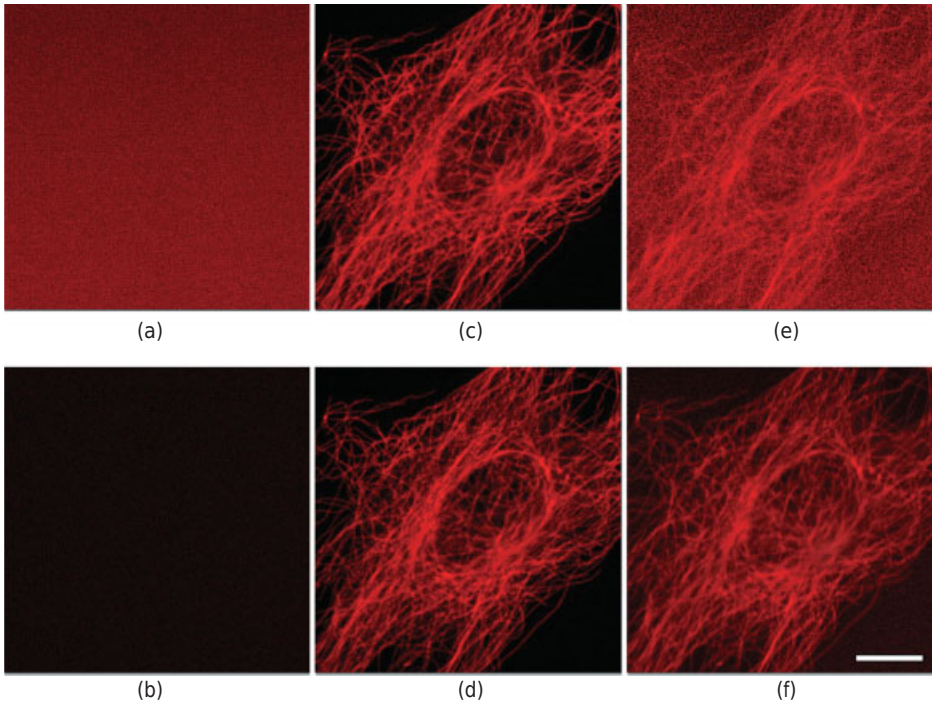

Figure 16.10

Effect of exposure time and camera readout rate on image quality in live-cell imaging. HeLa cells expressing a fusion of mCherry fluorescent protein (pseudocolored red) and human *alpha*-tubulin imaged in widefield fluorescence mode demonstrate three important points. The readout rates in panels a, c, and e and in panels b, d, and f were 10 MHz and 1.25 MHz, respectively. All images are displayed with the same range of gray level values. (1) Under conditions of shuttering (no light) and long exposure, background noise is dramatically lower at the slower readout speed (a, b). (2) Readout rate does not seriously affect image quality when exposure time can be adjusted to utilize the entire dynamic range (c, d). (3) Under low light level conditions where light intensity was 10-fold lower, slower readout speeds produced superior image quality (e, f). Bar = 10 μm.

Effects of Binning on Spatial Resolution and Image Dimensions

The effects of combining adjacent pixels on spatial resolution and the final dimensions of digital images captured using increasing levels of binning are illustrated in Figure 16.11. With no binning enabled (Fig. 16.11a), the signal is too low to be distinguishable at exposure times that produce negligible phototoxicity and photobleaching. Binning 2×2 and 4×4 progressively increases the signal level, but at the cost of spatial resolution (Fig. 16.11b,c). The brightest image is produced by binning 8×8 pixels (Fig. 16.11d), but it suffers significant loss in spatial resolution. Notice that the image dimensions are also decreased as binning is increased. While the unbinned (1×1) image in Figure 16.11 was originally 1360×1024 pixels, the pixel number in the binned images was decreased by a factor of 4, 16, and 64, respectively. The relative sizes of the images are shown at the bottom.

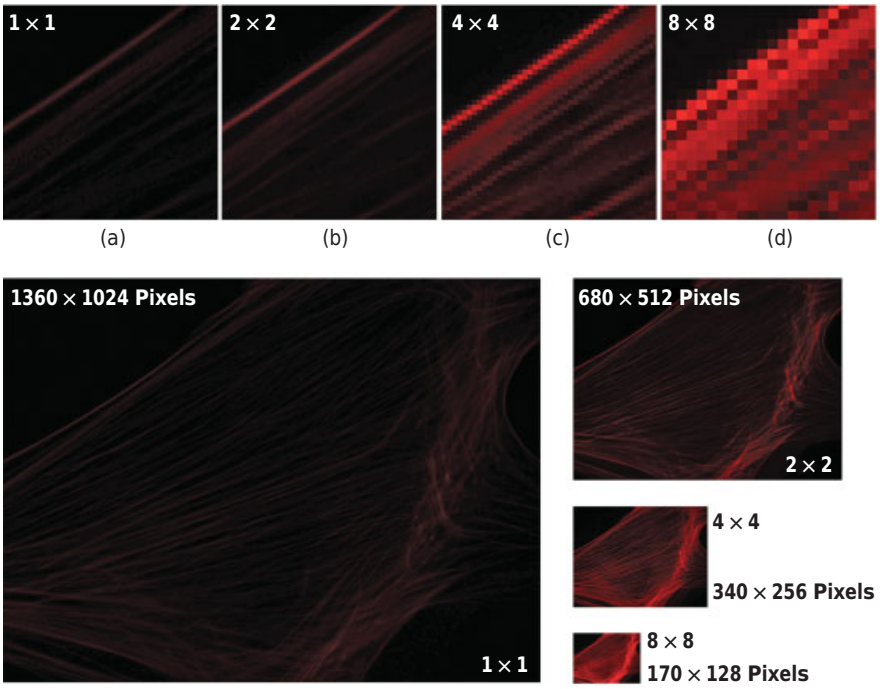

Figure 16.11

Effects of pixel binning on image brightness and dimensions. Indian Muntjac fibroblasts expressing a fusion of mCherry fluorescent protein and human *beta*-actin (pseudocolored red), which localizes in stress fibers comprising the filamentous cytoskeletal network.

The following key points summarize binning in live-cell imaging:

- Read noise occurs after the binning process, so even though several pixels are being combined, there is only one read event per binned pixel, eliminating the separate noise contribution from each pixel in an unbinned image.
- Binning sacrifices spatial resolution, but leads to a significant increase in the S/N ratio (i.e., image brightness).
- Binned images have smaller dimensions than unbinned (1 × 1) images (Fig. 16.11).
- Binning should be used in cases where low illumination levels and short camera exposure times are necessary to preserve cell health and reduce phototoxicity and photobleaching.
- As an alternative to binning, you can set the camera software to read only a subarray or selected region of interest on the full CCD, a useful mechanism to preserve spatial resolution while simultaneously reducing the amount of time cells are exposed to harmful illumination.

GAIN

The gain adjustment of a digital CCD camera system defines the number of accumulated photoelectrons that determine each gray level step distinguished by the readout

electronics, and is typically applied at the analog-to-digital (A/D) conversion step (see Chapter 17). An increase in electronic gain corresponds to a decrease in the number of photoelectrons that are assigned to each gray level, and allows a given signal level to be divided into a larger number of gray level steps. Although electronic gain adjustment provides a method to expand the limited signal amplitude often encountered in live-cell imaging to a larger number of gray levels, if it is used excessively, the small number of electrons that distinguish adjacent gray levels can lead to digitization errors. However, increasing gain does not increase the S/N, unlike the case for binning. Furthermore, high gain settings can result in more noise due to inaccurate digitization, which appears as graininess in the final image, and increasing gain decreases the useful dynamic range of the camera due to saturation before photodiodes reach full well capacity. In most cases, the lowest camera gain setting produces the best results in live-cell imaging experiments.

EXPOSURE TIME

Camera exposure (or *integration*) time is defined as the amount of time that photons are allowed to accumulate in pixel wells before the CCD chip is read. Longer exposure times enable pixels to gather more photoelectrons, generating larger signal levels (Chapter 17). In cooled scientific CCD cameras, the only increase in noise that accompanies longer exposure times is higher Poisson or shot noise, leading to an increase in S/N. Bear in mind that the higher S/N that accompanies longer exposure times also comes at the risk of greater phototoxicity to the cells and increased photobleaching of fluorescent probes. In addition, longer exposure times can produce artifacts, such as blurring and reduced spatial resolution, when imaging dynamic events in living cells due to movement of labeled structures during the exposure. Frame rates are also decreased if long exposure times are employed, thus limiting the number of images acquired per unit time. Therefore, the tradeoff between S/N increases, minimizing specimen damage, and gathering images fast enough to record specimen dynamics must be carefully balanced with exposure time.

The introduction of electron multiplying CCDs (EMCCDs) for amplifying weak signals above the CCD read noise floor has helped overcome the pitfalls and S/N issues associated with live-cell imaging. These advanced cameras feature an on-chip multiplication gain register to achieve single-photon detection sensitivity without compromising the quantum efficiency and resolution characteristics of the conventional CCD architecture (see Chapter 17). For critical live-cell investigations with low-intensity signals, such as those encountered in single-molecule imaging, total internal reflection, spinning disk and sweptfield confocal microscopy, flux determinations of calcium or other ions, and time-resolved three-dimensional microscopy, the EMCCD offers significant advantages over other sensors designed for low signal levels. Additionally, when employed with the higher signal levels of conventional fluorescence imaging techniques, the extreme sensitivity of the EMCCD system allows the application of lower fluorophore concentrations and/or lower power levels from the excitation source, thereby reducing both phototoxicity and photobleaching of fluorophores.

Microscope Optics for Live-Cell Imaging

Optimizing the S/N in live-cell imaging calls for careful attention to the microscope optical system to ensure that the maximum amount of information is transferred from the specimen to the detector. Stray light can be minimized, and visual detection in the

eyepieces improved by keeping the overhead lighting off or placing the microscope in a darkened room. Reducing the number of mirrors, beamsplitters, prisms, and other optical components also helps increase throughput of photons to the detector, and it is important to remember that any light sent to the eyepieces during image acquisition is done so at the expense of light sent to the camera (therefore, if possible direct 100% of the light to the camera port).

For live-cell imaging, detectors must provide both sensitivity and speed. The relatively high light intensities and long exposure times typical of fixed-cell imaging must be avoided when working with living cells. In most cases, live-cell microscopy represents a compromise between achieving the best possible image quality and preserving the health of the cells, and spatial and temporal resolutions set by the experiment should be designed to match the goals of the investigation. In principle, the ideal live-cell image acquisition system should be sensitive enough to acquire superior images from weakly fluorescent specimens while simultaneously being fast enough to record dynamic processes of interest. In addition, the system would have sufficient resolution to capture the finest specimen detail and a wide dynamic range capable of accurately measuring small differences in intensity. Unfortunately, optimizing any one of these criteria is only accomplished at the expense of the others. It is therefore currently impossible to design an all-purpose generalized live-cell imaging system that will be ideal for the entire range of possible investigations. Instead, the investigator must compromise by determining the most important parameters for optimization while still attempting to limit the sacrifice made by those variables that are of lesser interest.

The following microscope components deserve particular attention for live-cell imaging:

- *Objective NA.* Objectives with very high NA are required to maximize the amount of light that is collected from the specimen. NA defines how much light from a single point source can be gathered by the lens (Chapter 5). Since image brightness is proportional to M^2/NA^4, NA is an important consideration in selecting objectives for live-cell imaging. Thus, a small increase in NA can yield significant improvement in the signal.
- *Objective magnification.* Signal intensity decreases with M^2, so that among lenses with the same NA, the lower magnification objective is often beneficial when imaging dim samples. For example, if the S/N becomes a limiting factor in a specimen imaged with a 100× objective of NA 1.4, changing to a 60 or 40× objective of the same NA will produce a significant improvement in brightness.
- *Corrections for optical aberrations.* The highly corrected objectives (such as plan apochromats) suitable for imaging fixed cells contain more optical elements and have less light throughput than less corrected achromats and fluorites. As an example, a plan apochromatic 40× objective having a NA of 1.4 should be approximately six times brighter than a similarly corrected 100× objective, but is really only about four times as bright. It is often, but not always, a better choice to use fluorite objectives for live-cell imaging.
- *Immersion media.* Remember that refractive index changes with temperature, so the optimal combination of immersion medium and coverslip thickness will differ between room temperature and 37°C. Newer immersion objectives with correction collars can be used to combat temperature-induced refractive index fluctuations. Normally, the coverslip thickness that should be used with a given objective is

specified on the barrel. However, if conditions should require (blurry image for an object lying several micrometers from the coverslip), the refractive index of the immersion medium or the thickness of the coverslip can be changed to compensate for the effects of spherical aberration. Use extreme caution when choosing coverslips of different thickness or different immersion oils to avoid creating additional artifacts. Immersion oils of various refractive indices are commercially available (Cargille, Inc.).

- *Contrast-enhancing optical components.* These components include polarizers and prisms for DIC, or condenser annuli and phase rings for phase contrast and Hoffman modulation contrast. Because the overall throughput of light for bright-field imaging mode is much higher than with fluorescence, good S/N is usually attained. More important is filtering the tungsten-halogen illumination source to remove heat-producing IR wavelengths and avoid damage to the specimen. Wavelengths reaching the specimen can easily be controlled using a green or red interference filter, heat filter (absorbs IR), or hot mirror (reflects IR).
- *Fluorescence filters.* At low light levels, choosing the appropriate fluorescence filters is important for achieving optimal S/N in the image. However, narrow bandpass filters used to minimize bleedthrough may also reduce the number of photons contributing to the signal. Therefore, one should choose the high-throughput, large-bandpass filters that still minimize bleedthrough, often termed "hard-coated" filters. A wide variety of filter and dichromatic mirror combinations are available from the microscope manufacturers and aftermarket optical filter companies.

Effects of NA on Image Brightness

In Figure 16.12, the same viewfield was imaged using objectives having the same optical correction (plan fluorite) and NA (1.3), but with magnifications ranging from 40 to 100×. Although the number of pixels and detector conditions utilized in collecting the images for Figure 16.12 were identical, the mitochondria are brightest when imaged through the 40× objective (Fig. 16.12a). In contrast, the

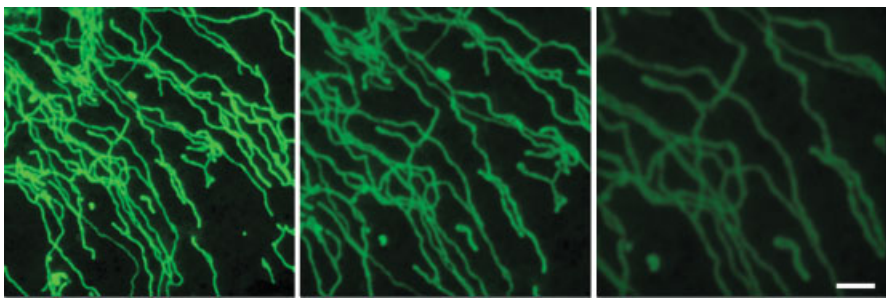

(a) (b) (c)

Figure 16.12

Effect of NA on image brightness. Confocal images of HeLa cells containing EGFP fused to a mitochondrial targeting peptide were created using immersion objectives with the same NA but different magnifications: (a) 40×/1.3 NA; (b) 60×/1.3 NA; (c) 100×/1.3 NA. Images are shown at the same dynamic range. Bar = 5 μm.

higher magnification 60 and 100× objectives (Fig. 16.12b,c, respectively) yield progressively darker images, with the 100× image being almost indiscernible. This objective can still be used to image the specimen, but the detector gain must be significantly increased, resulting in a deterioration of the S/N and a generally inferior image. Note that the resolving power of the objectives is comparable due to the identical NA values.

Apart from the effect of NA on image brightness, another important lesson to be learned from Figure 16.12 is the need to avoid excessive magnification. Simply increasing the digital enlargement (zoom) during image collection on a confocal microscope using the 40 or 60× objectives would produce images of equivalent size and the same resolution (see Chapter 13). The resolution of all three objectives is the same because their NAs are the same. This does not mean that the 60 or 100× objectives are not beneficial. High magnification objectives are necessary when imaging very small objects, such as peroxisomes or secretory granules, using a widefield microscope. Because the image size relative to detector size plays an important role in determining spatial sampling frequency, the optimal magnification is determined by the parameters of the digital camera system (CCD pixel size and the intermediate magnification factor). Thus, the best choice of objective usually depends on the optical configuration of the instrumentation in addition to the specific requirements of a particular experiment.

Time-Lapse Imaging

Dynamic imaging of biological activity first was introduced in 1909 by the French doctoral student Jean Comandon, who presented the earliest reported time-lapse cinema films of living syphilis-producing spirochaetes, 5 years before Charlie Chaplin made his first movie (Gastou and Comandon, 1909; Roux et al., 2004). Comandon's technique, which he called *microcinematography*, enabled the production of movies capturing events in the microscopic world that could be recorded using an enormous cinema camera bolted onto a fragile darkfield microscope. These films were useful in teaching physicians how to distinguish disease-causing spirochaetes from those that are harmless, and demonstrated how time-lapse observations can be employed to gain important biological information without recourse to image analysis, processing, or even empirical quantitative measurements. With the advanced digital camera systems available in the twenty-first century, the increasingly popular technique of time-lapse cinemicrography is being broadly applied to capturing events that occur in living cells over periods ranging from a few seconds to several weeks (or even months). The technique involves repeated imaging of a cell culture at defined time points, thereby providing information on myriad dynamic processes that often occur with a wide distribution of time scales. As we will see, when time-lapse investigations are coupled to labeling cells with synthetic fluorophores and genetically encoded fluorescent proteins, dynamic events and interactions at the subcellular and molecular levels can be investigated.

Time-lapse imaging can be performed in two spatial dimensions using widefield techniques and extended to three-dimensional imaging with confocal microscopy. In addition, modern confocal microscopes are equipped with line-scanning software for rapid and repeated imaging of single scan lines. Two-dimensional time-lapse imaging involves sequential capture of single focal planes (Fig. 16.13), whereas three-

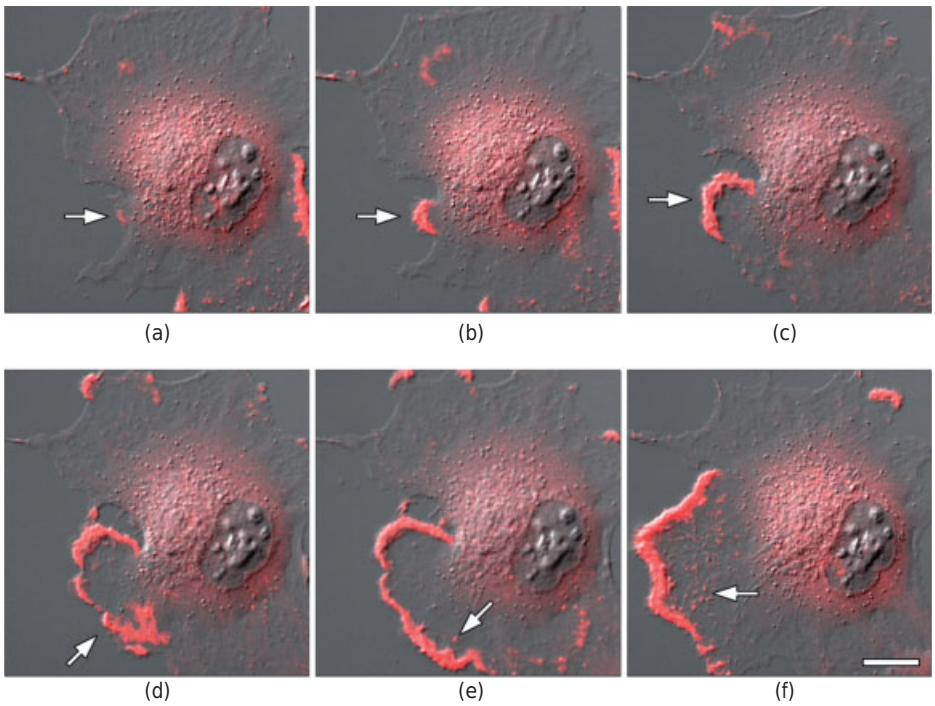

Figure 16.13

Selected images from a 24-hour time-lapse sequence of adherent rabbit kidney epithelial (RK-13 line) cells that were captured using a combination of fluorescence and DIC. The cells contain a chimeric vector composed of mCherry fluorescent protein and human *beta*-actin to reveal the distribution of actin in lamellipodia. (a) Elapsed time (ET) = 1 minute; the white arrow points to the initiation of a cytoplasmic ruffle near the large pool of actin in the central region of the cell. (b) ET = 5 minutes; arrow points to growing ruffle. (c) ET = 10 minutes; ruffle continues to grow. (d) ET = 15 minutes; the small ruffle begins to swell and extrude toward the upper left-hand side of the image, in a wave-like motion, concentrating the brightly labeled actin fusion protein into the leading edge as it grows. (e) ET = 20 minutes; as the lamellipodium spreads to cover a large area, small clusters of labeled actin form behind the leading edge to form structural elements that may be podosomes (white arrows in panels e and f) that play a role in cell adhesion to the glass substrate. (f) ET = 25 minutes. Bar = 20 μm.

dimensional imaging produces *z*-stacks from multiple focal planes. When a single focal point in the lateral plane (*x* and *y*) is combined with *z*-stack imaging as a function of time, the technique is referred to as 4D time-lapse imaging. Likewise, adding a fifth dimension (wavelength) yields 5D imaging, and adding either multiple wavelengths or multiple lateral regions to the 4D stack is referred to as 6D time-lapse imaging.

Time-lapse imaging techniques require auxiliary components, such as electronic shutters, filter wheels, motorized stages, and focus drift correction mechanisms, which can be coordinated and controlled by a host computer:

- *Electronic shutters* are necessary to block illumination of the specimen between camera exposures when imaging fluorescently labeled cells in order to minimize photodamage, phototoxicity, and photobleaching, thus dramatically extending the quality of images and cell viability over the long periods of time often used in

time-lapse experiments. Shutters can be triggered by the software on the host computer or through controller units for the shutter.

- *Filter wheels* are useful for simultaneous imaging of multiple fluorophores, as well as combined fluorescence and DIC imaging, which requires the ability to switch rapidly between different fluorescence filter sets and/or a polarizer. Temporal resolution in rapid time-lapse sequences is usually determined by the amount of time necessary to switch between filters. High performance wheels are able to switch between filters at times ranging from 10 to 50 ms.
- *Motorized filter turrets* are useful for multicolor fluorescence imaging either alone (fitted with filter cubes) or when used in combination with filter wheels (a dichromatic mirror is placed in the turret and excitation/emission filters in wheels). Because filter turrets often have much longer switching times than filter wheels, they are best used when the experiment requires lower temporal resolution.
- *Motorized stages* enable imaging of several different fields of view in a single experiment. Several coordinates in the imaging chamber can be programmed into the software and time-lapse image sequences gathered sequentially from each specimen that has been chosen. The number of fields that can be imaged depends on the time interval between image frames.
- *Focus drift correction* is absolutely necessary when conducting long-term time-lapse imaging in order to maintain focus of the specimen. All of the major microscope manufacturers offer optional focus drift hardware correction for the inverted microscopes, and several aftermarket products are also available.

In confocal microscopy, time-lapse image collection is limited by the speed of the scanning mirrors. The highest scanning rates are achieved by reducing the image pixel dimensions and employing the fastest raster speed available on the instrument, but this is usually still limited to, at best, 8–10 frames/s. Collecting image sequences over shorter time intervals requires single-line scanning, resonant scanners, sweptfield instruments, or spinning disk microscopes (see Chapter 13). Modern spinning disk and sweptfield microscopes can routinely capture image sequences at high rates, ranging from one to several hundred or even thousands of frames per second, and are usually only limited by the speed of the digital camera system or PMT.

Incubator Microscopes

Environmental variables that create stress in cell cultures and are difficult to control when cells are grown directly on the microscope stage can be partially offset by integrating the cell culture, microscope optics, incubator, and detector into a single motorized system for long- and short-term time-lapse imaging. With this idea in mind, several microscope companies have developed *incubator microscopes* that are specifically designed to image cultured cells under controlled environmental conditions (Fig. 16.14). By optimizing the imaging environment, fragile cell lines, such as stem cells and primary cultures, can be cultured and observed as if they were growing in a 5% CO_2 incubator with controlled relative humidity. Incubator microscopes are ideal for long-term time-lapse imaging and help to eliminate problems associated with thermal focus drift.

The commercial incubator microscopes such as those offered by Nikon and Olympus feature the ability to conduct multidimensional time-lapse imaging (x, y, z,

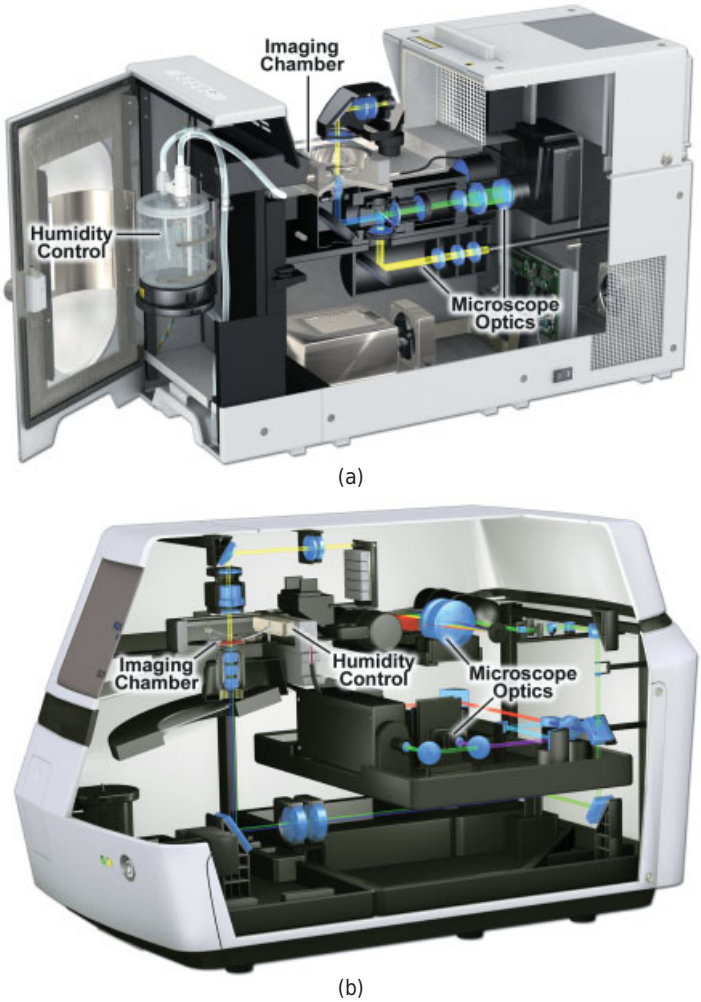

Figure 16.14

Cutaway drawings of commercial incubator microscopes. (a) Widefield fluorescence and phase contrast. (b) Laser scanning confocal and DIC.

and wavelength) as a function of time and position in the imaging chamber (Fig. 16.14). These microscopes are equipped with LED sources for brightfield, phase contrast, and DIC imaging, as well as metal-halide, LED, and laser illumination sources for fluorescence. The microscopes have motorized stages and objective turrets that are controlled by proprietary software, which is also used for image acquisition and processing or analysis. Typical problems associated with live-cell imaging on inverted microscopes, such as preparing a dark room at controlled temperature, eliminating air currents and vibration, and managing the location of peripheral devices (filter wheels, shutters, etc.) are eliminated with the incubator microscopes. Confocal incubator microscopes (Fig. 16.14b) feature multiple laser excitation sources, and water or oil immersion objectives, and have the ability to acquire crisp optical sections.

EVALUATING LIVE-CELL IMAGING RESULTS

The goal of live-cell imaging experiments is to uncover some facet related to the dynamic aspects of cell biology. As such, it is important to make sure that the environmental and imaging conditions do not perturb normal cellular function and therefore do not substantially alter the experimental result. In effect, if you are studying the dynamics of microtubule polymerization, for example, strive to make certain the culture conditions are such that you are not really observing what occurs as a result of light-induced apoptosis or necrosis. It is wise to establish a criterion for examining the health of the culture so the success of the experiment can be judged on the results with a high degree of certainty that the imaging process itself did not damage the cells and lead to a false conclusion. The experimental conditions (culture medium, pH, temperature, humidity, etc.) should not significantly change the growth rates, the mitotic and apoptotic indices, or any other normal cell function. Controls should be run simultaneously, with the absence of imaging, in a standard incubator using the same medium as the imaging experiments to assay for cell viability, division time, and other critical parameters. In some cases, the results of live-cell imaging experiments can also be compared with what is seen with fixed cells.

Because the cells are exposed to high doses of light and free radicals when using fluorophores, it should be assumed that some type of damage occurs during the experiment. The key here is to determine whether the level of damage is significant enough to affect the events under investigation. One excellent method is to leave the cells on the microscope after the experiment is completed and determine whether they initiate and complete mitosis. Apoptosis is often difficult to identify simply by examining live cells, but mitotic events can be readily observed. By extending time-lapse imaging over a number of hours after an experiment has been terminated, clues to the overall health of the culture can be gathered. Another good control is to compare cells that have been imaged with neighboring cells in the same culture that have not been exposed to light. If the imaging experiment does not harm the cells, the two populations should appear identical or nearly so in phase contrast and/or DIC, and localization of fluorescent proteins or synthetic fluorophores should be the same. Such comparisons will often reveal whether significant damage has occurred to the cells being studied.

Exercise: Fluorescence Microscopy of Living Tissue Culture Cells

The purpose of this exercise is (1) to learn how to prepare and examine live cells whose organelles are labeled with specific fluorescent dyes; (2) to examine the effects of fixatives on organelle morphology; (3) to become familiar with the action of narrow bandpass and longpass filter sets that are used to examine double-stained specimens; (4) to evaluate and select filter sets based on their transmission profiles; and (5) to learn how to balance the intensities of different fluorophores to minimize bleedthrough in inappropriate filter sets. Note: Read the entire text of the exercise before beginning the work. Work in pairs to make the exercise go smoothly.

In this exercise, we will stain tissue culture cells with organelle-specific fluorescent dyes to examine the morphology and abundance of organelle systems and

to compare the performance characteristics of different filter sets. Many, but not all, of these dyes can be used to stain cells in the living state. Large, well-spread cells, such as COS-7, U2OS, CHO, LLC-PK1 cells, or primary cultures of endothelial cells, if available, are appropriate for this exercise. Prepare representative sketches of the labeled cells. Keep a record of your observations, including the time course of the staining response, the stability of fluorescence, and other relevant information. For this exercise, pick one or more of the following marker dyes. Instructions for preparing dye solutions are given in Appendix B.

Dye Set	Structure	Target/Action	Filter
DiOC6	Mitochondria (dilute); ER	Potential uptake dye	FITC
BODIPY FL-ceramide	Golgi apparatus	Lipids	FITC
Ethidium bromide	Chromosomes, chromatin	DNA	TRITC
MitoTracker Red	Mitochondria	Potential uptake dye	TxRed
LysoTracker Red	Lysosomes	Potential uptake dye	TxRed
Rhodamine-phalloidin	Actin stress fibers	Actin filaments	TRITC

Procedure

Transfer a cell-containing coverslip from a culture dish to a 35-mm dish containing HMEM (MEM culture medium plus 10 mM HEPES pH 7.2 and without serum). Buffering with HEPES (10 mM, pH 7.2) is necessary when handling and examining cultured cells in room air. Serum and phenol red should be omitted because their fluorescence decreases contrast. Remove the culture medium; add 2 mL HMEM and tilt gently to wash the medium over the cells. Pull off the medium with a Pasteur pipette and replace it with 2 mL HMEM containing a specific fluorescence dye at the appropriate concentration. Disperse the dye by gently rocking the culture dish. Incubate for the indicated time, retrieve and save the dye solution for reuse at a later time, rinse the coverslip 3× with 1 mL HMEM to remove any excess unbound dye, wipe off the back of the coverslip with a damp Kimwipe to remove cells and medium, and prepare a Vaseline mount as described in Figure 10.16. Draw off extra medium from the edge of the coverslip chamber with a filter paper and examine the preparations immediately. For each dye employed, describe the degree of staining specificity for organelles and explain why a dye might not appear to stain specifically. Where appropriate, describe changes in organelle distribution that occur as the result of fixation. Also, describe the intracellular abundance and morphological pattern exhibited by each type of labeled organelle. Make sketches and include scale bars on your drawings.

Microscope set-up. Examine the cells with a 40–100× oil immersion lens using epi-illumination with a 100-W mercury arc lamp. The microscope should also be fitted with phase-contrast or DIC optics so that structural features in the cells can be examined in transmitted light without having to move the specimen or change the lens.

Precautions regarding fixatives. If formaldehyde or glutaraldehyde is used as a fixative, use ventilation during preparation to prevent fumes from contacting

the eyes or skin. Place all fixatives and dyes in a toxic waste container for proper disposal afterwards. Be sure to consult an experienced cell biologist for advice and supervision.

Specific details

DiOC$_6$/ER, mitochondria. $DiOC_6$ is a lipophilic dye that stains organelles according to the lipid composition of their membranes. Cells are stained with 2 mL of a 2.5 μg/mL solution of $DiOC_6$/HMEM for 1–2 minutes. Remove the dye and rinse the cells 2× with HMEM. Mount and examine. Can you distinguish the mitochondria from the ER? Does the nucleus also stain? Why? At dilute concentrations of dye (1/10 the indicated concentration), only the mitochondria are stained. Living cells can be treated for 30–60 minutes and examined the same as fixed cells. With longer labeling times or at higher concentrations of dye, the ER also becomes labeled and is seen as a beautiful lacy network at the periphery of the cell. Make sketches of the stained organelles.

BODIPY-ceramide/Golgi apparatus. Rinse a coverslip containing cells in HMEM; fix with 5 mL 0.5% glutaraldehyde in HMEM for 5 minutes. Remove the fixative and rinse cells with HMEM several times. Incubate for 30 minutes at 5°C in 5 μM C_6-BODIPY-ceramide/BSA complex in a refrigerator. Ceramide is a lipid that partitions to certain lipid environments in the cell, and BSA serves as a carrier for the lipid. Remove and save the ceramide, rinse the cells at 22°C with HMEM containing 3.4 mg/mL delipidated BSA several times over 1 hour, and then mount and examine the cells. (The BSA removes excess ceramide and improves the specificity of labeling.) If things go well, you're in for a treat! Make drawings of the Golgi apparatus from several cells. Are there any indications of staining of pre-Golgi or post-Golgi structures? As an alternative, label living cells and observe the pathway of dye uptake and partitioning from the plasma membrane to endosomes to the Golgi. Wash a coverslip 3× with HMEM. Place the coverslip in 5 μM ceramide/BSA for 15 minutes at 37°C, then replace the solution with complete culture medium and incubate for an additional 30 minutes (for endosomes) or 60 minutes (for Golgi) at 37°C.

Ethidium bromide/nucleus. After rinsing in HMEM, the cells are fixed in 4 mL 0.5% glutaraldehyde in HMEM for 15 minutes. Remove the fixative, dehydrate the cells in 100% ethanol for 1 minute, and rinse in HMEM. Add ethidium bromide to 5 μg/mL (alternatively, DAPI to 0.5 μg/mL) in HMEM, being careful not to contact the skin, and incubate the cells at 22°C for 60 minutes. Alternatively, stain living cells with Hoechst dye 33258 (or Hoechst 33342) at 0.5 μg/mL for 15 minutes at 22°C. Mount and examine. Remove the dye and rinse the cells. Look for reticular patterns caused by euchromatin and heterochromatin in the nuclei. Also, look for nucleoli, which are sites of RNA processing in the nucleus. What do mitotic chromosomes look like? Make sketches.

MitoTracker or LysoTracker/mitochondria, lysosomes. Simply add these potential uptake dyes to 250 nM in the culture medium and incubate the cells at 37°C for 5–10 minutes. Mount and examine. Carefully discard the stain-

ing solution. Are the dyes specific for mitochondria and lysosomes? How many mitochondria/lysosomes are there in a typical cell? What is the distribution of their lengths/diameters? Determine if you can see mitochondria round up and migrate toward the center of the cell, a stress response of the cell to nonideal environmental conditions and prolonged observation. Make sketches.

Rhodamine-phalloidin/actin stress fibers. After rinsing in HMEM, fix the cells in 4 mL 0.5% glutaraldehyde in HMEM for 15 minutes. Dilute the dye 1 : 40 in the culture medium containing 0.1% Triton X100 detergent and incubate the cells at 37°C for 30 minutes. Mount and examine after thorough rinsing in HMEM. Are the filaments you see individual actin filaments or filament bundles? How are stress fibers oriented with respect to the long axis of the cell, cell borders, and vertices that represent points of cell attachment? Estimate the amount of fluorescence associated with stress fibers versus unorganized filaments subjacent to the plasma membrane. Prepare careful drawings.

Examination of double stained specimens. If the microscope is equipped with two different filter sets for the same dye (e.g., for examination of fluorescein, a filter set with a narrow bandpass emission filter and another set with a longpass emission filter), it is useful to examine specimens double stained with fluorescein and rhodamine.

It is possible to directly examine the transmission profiles of the dichromatic mirror-emission filter combination of a given filter set right at the microscope. Just switch the microscope to transmitted white light, mount a diffraction grating on the stage, close the condenser diaphragm down to a minimum, and examine the colors of the 1st order diffraction spectra with the aid of a Bertrand lens. Examine all of the filter sets to determine the bands of wavelengths transmitted by the sets.

1. Is there any bleedthrough of fluorescence of one dye through the filter set intended for viewing the other dye?
2. Is the amount of rhodamine bleedthrough different for the two types of fluorescein filter sets? Why? In preparing to answer why bleedthrough occurs, it is useful to compare transmission profiles of the various filters of the filter sets and to compare them with the excitation and emission spectra of fluorescein and rhodamine (Fig. 11.6).
3. Is rhodamine fluorescence totally excluded from the fluorescein filter set with the narrow bandpass filter? Why? Since the longpass fluorescein filter set shows transmission of red wavelengths, it should be obvious that rhodamine fluorescence will also be transmitted by this filter set design, making it unsuitable for examination of double-stained specimens.
4. What is the purpose of equipping a microscope with a filter set containing a longpass emission filter?
5. Name two steps you could take to reduce the amount of rhodamine bleedthrough in a fluorescein filter set.

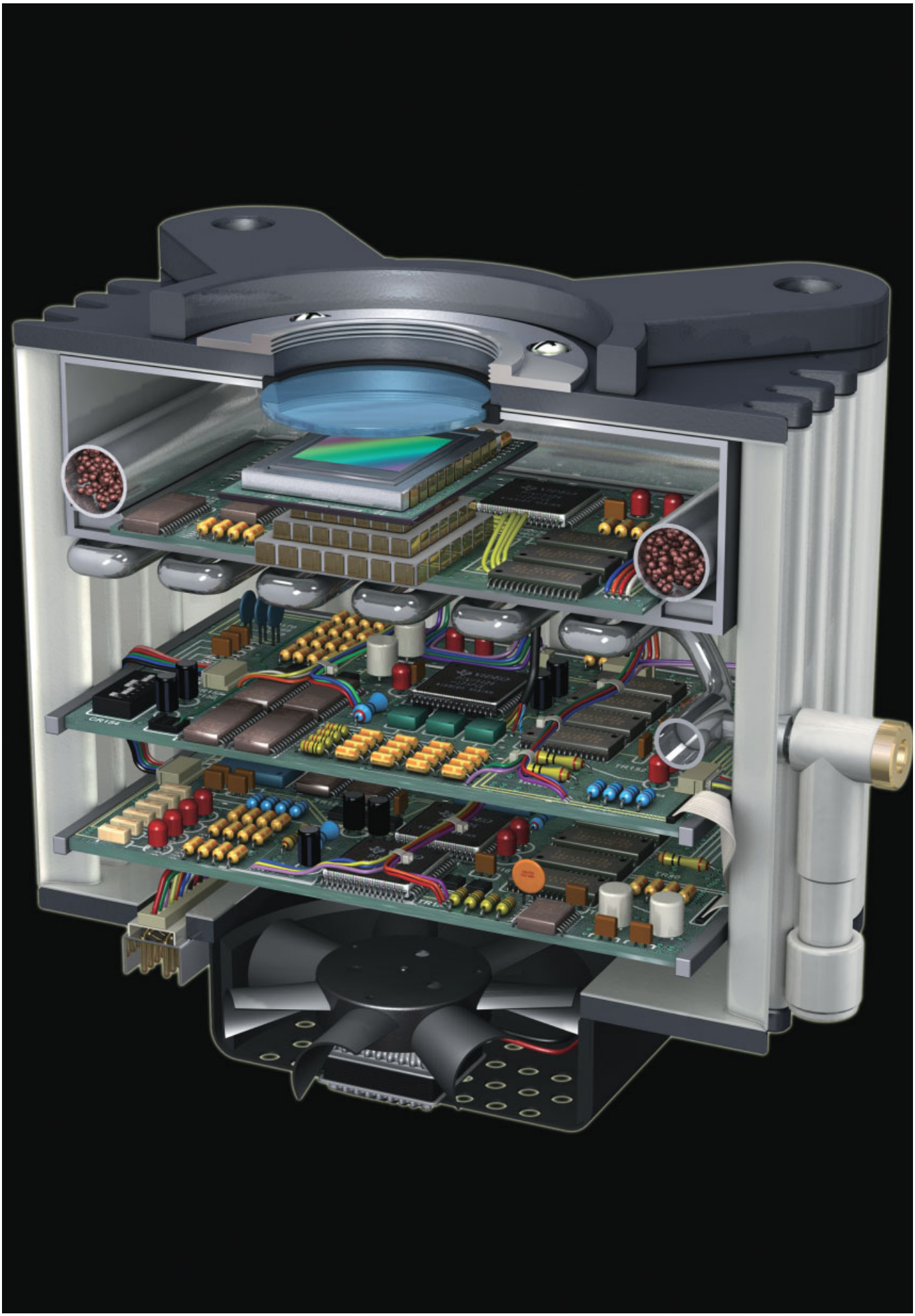

CHAPTER
17

FUNDAMENTALS OF DIGITAL IMAGING

OVERVIEW

Charge-coupled device (CCD) and complementary metal oxide semiconductor (CMOS) detectors are small, centimeter-size chips of silicon that are divided up into millions of tiny picture elements capable of storing photoelectrons during an exposure. The photon count in each pixel is then digitized and displayed on a computer monitor or other display device. The light-sensitivity, dynamic range, and spatial resolution of these detectors are extraordinary. The efficiency of light collection is so great that even weak fluorescent images in a microscope can be recorded in just a few milliseconds. Because they give a linear response over a large range of light intensities, CCD and CMOS cameras can function as imaging spectrophotometers, producing tens to hundreds of times better resolution of light intensity than video or film cameras. They also have a high spatial resolution comparable with film (Fig. 17.1), and can acquire "full frame" images at close to the standard video rate of ~30 fps. Because digital imaging is so fast, one can see and interact with the images on the computer monitor in real time.

The combination of microscope and digital camera, together with computer with imaging software, defines what is called a *digital imaging system* (Fig. 17.2), a mainstay of the laboratory that has greatly stimulated the use of light microscopy in research (Hiraoka et al., 1987). To use the equipment properly, some basic study is needed to master several software-dependent procedures for image acquisition, processing, analysis, and display. In this chapter, we examine the principals and design of the CCD camera, the cameras presently in use in most laboratories, and review the variables one

Cutaway drawing of the internal electronics and sensor element of a CCD camera.

Fundamentals of Light Microscopy and Electronic Imaging, Second Edition.
Douglas B. Murphy and Michael W. Davidson.

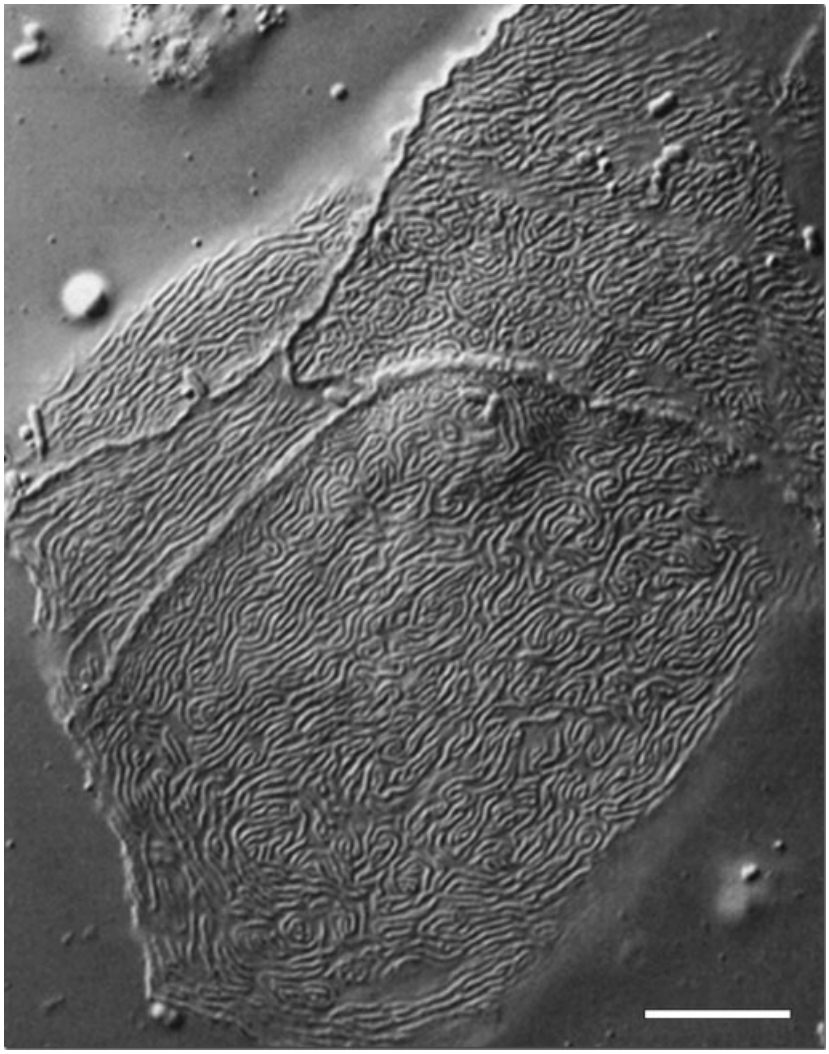

Figure 17.1

Spatial resolution of a CCD detector. This DIC image of the surface of a buccal epithelial cell was recorded on a 1.4 megapixel CCD camera having a pixel size of 6.8 μm. Since the unit diffraction spot radius projected on the CCD by a 100×, 1.3 NA objective is 26 μm, full optical resolution is retained. The spacing between ridges is approximately 0.4 μm. Bar = 5 μm.

must consider for obtaining high-quality images. Scientific CMOS devices are an emerging digital imaging technology, and we discuss them briefly later in the chapter.

THE CHARGE-COUPLED DEVICE (CCD IMAGER)

The CCD device, sometimes called a chip or imager, is located in a hermetically sealed chamber covered with a transparent glass or quartz window. The CCD is mounted on

Figure 17.2

Components of a digital CCD imaging system. (a) A CCD camera is mounted on a light microscope. A camera control unit connected to the camera communicates with a host computer. (b) Scientific cooled CCD cameras, color cameras, EMCCDs, and scientific CMOS cameras (discussed below).

a block that is backed by Peltier cooling elements designed to reduce the so-called thermal noise in the photoelectron signal. The CCD device contains electronics for controlling the readout of photoelectrons from the light-sensitive pixels, a low noise amplifier, and an analog-to-digital converter. A sketch showing the arrangement of these components is shown in Figure 17.3. Readers will find detailed descriptions of CCD operation and design in volumes by Holst (1998) and Buil (1991).

A CCD *chip* or *imager* is composed of a thin wafer of silicon, a semiconductor material capable of trapping and holding photon-induced electron/ electron hole pairs (Fig. 17.4). The silicon surface is covered with an orthogonal gridwork of narrow transparent strips that carry a voltage, thereby defining thousands or millions of square picture elements or *pixels* in the silicon matrix.

The pixels are *photodiodes*, photosites that act as potential wells and store charge carriers derived from incident photons (one electron/electron-hole pair per absorbed photon). The charge carriers are usually called photoelectrons. Photoelectrons can be accumulated and stored for long periods of time until they are read from the chip by the camera electronics. The peak *quantum efficiency (QE),* the percent of incident photons resulting in photoelectrons, is very high (40–90%), and varies depending on the incident wavelength and design of the chip. Pixels in CCDs used for microscope imaging range from 4 to 16 μm on a side and have a typical holding capacity, or full well capacity, of ~1000 electrons/μm^2 when the camera is used in the multi-pin phase (MPP) mode. This mode of operation is used to reduce the spillover of saturated pixels into neighboring pixels, a phenomenon called *blooming*. Therefore, a 6.8 μm pixel in a MPP-operated CCD holds ~45,000 electrons.

The face of a CCD in a *full frame CCD camera* contains thousands of pixels that make up the *parallel register*, the imaging surface that accumulates and stores photoelectrons (Fig. 17.5). (Note: Several CCD designs are described below. Although today most laboratories use interline CCD cameras, the first and simplest design was the full

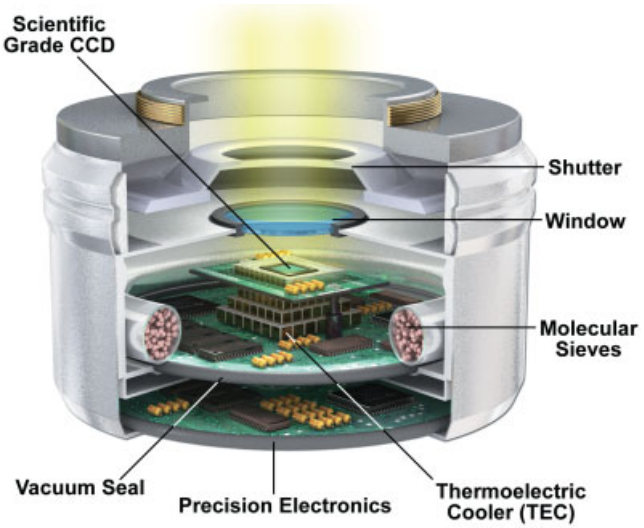

Figure 17.3

CCD camera architecture. The CCD detector is mounted in a hermetically sealed chamber charged with dry nitrogen gas or containing a vacuum. A transparent faceplate or window at the front of the chamber is located just in front of the CCD, which is mounted on a thermoelectrically cooled block to reduce thermal noise in the image signal. The camera head also contains several electronic components: a preamplifier (on the CCD chip itself) to boost the signal read from the CCD, an analog-to-digital converter, and circuits for controlling CCD readout.

frame CCD, so we base our discussion of CCD operation on this design of chip.) Since the image is focused directly on the surface of the CCD, there is a point-for-point correspondence between the pixels representing the image on the chip and pixels on the computer monitor where the picture is displayed and viewed. After an exposure, a timed sequence of voltage potentials moves across the strips on the CCD surface causing all of the electron charge packets stored in the pixels in the parallel register to be transferred one row at a time toward a single row of pixels along one edge of the chip called the *serial register,* from which they are moved one pixel at a time to an *on-chip preamplifier* and the ADC (Fig. 17.6). After the serial register is emptied, the parallel register is advanced by one row to refill the serial register, the process repeating until the entire parallel register is emptied. The function of the on-chip preamplifier is to magnify the signal and transmit it as a variable voltage for a short distance along a video cable to an ADC, which converts the signal into the 0 and 1 binary code of the computer. For a 12-bit camera, the assignment of each pixel ranges from 0 to 4095 steps (12-bit imaging gives $2^{12} = 4096$ possible gray levels). Each step is called an *analog-to-digital unit* (ADU).

To fully appreciate the sophistication of the technology, let us review the sequence of events involved in taking a picture with a full-frame CCD camera:

- The camera shutter opens and pixels accumulate photoelectrons.
- The shutter closes, and pixels are moved one row at a time off the parallel register by voltages applied to the strips on the CCD in a pattern and at a rate determined

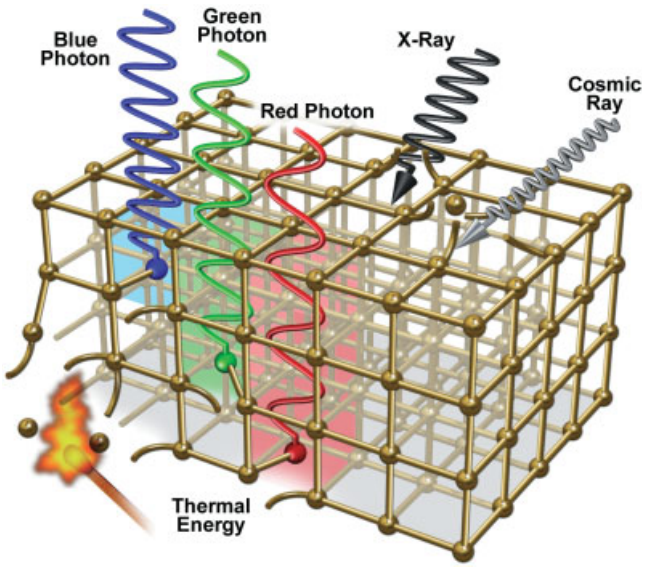

Figure 17.4

Silicon as a photon-sensitive substrate in a CCD imager. The sketch shows the effect of incident photons of various wavelengths on the silicon matrix of a CCD. Incident photons interact with the silicon, breaking covalent bonds between the silicon atoms and generating electrons and electron-deficient sites called electron holes. A voltage potential applied across the CCD holds the accumulating photoelectrons in the silicon matrix until they are read off from the chip and digitized. Red photons penetrate deeper into the matrix than green photons, followed by blue photons, accounting for the relative insensitivity of silicon to blue light. High-energy x-rays and cosmic rays disrupt many bonds and generate large saturating signals. Typically, there are a few cosmic ray hits on the CCD surface per minute. Thermal energy, represented by the match, also disrupts bonds and generates electrons (thermal noise) that cannot be distinguished from photoelectron counts; however, the problem can be reduced significantly by cooling the CCD to very low temperatures. After the electron charge packets are read off from the CCD surface, the structure of the silicon matrix is restored, and the CCD is ready for another exposure.

by timers or clocks in the camera electronics. Each row at the end of the parallel register is transferred to a special row of pixels called the serial register.

- Pixels are transferred one pixel at a time down the serial register to an on-chip preamplifier. The amplifier boosts the electron signal and generates an analog voltage output.
- An A/D converter assigns a digital code for each pixel depending on the amplitude of the signal (0–4095 for a 12-bit system).
- Pixel values are stored in a frame buffer in the computer.
- The process repeats until all 1000+ rows of pixels of the parallel register are emptied.
- For a 1-megapixel CCD chip processed at 2 bytes/pixel, 2 Mb are stored in the computer; the image is displayed in an 8-bit (256 gray level) format on the monitor.

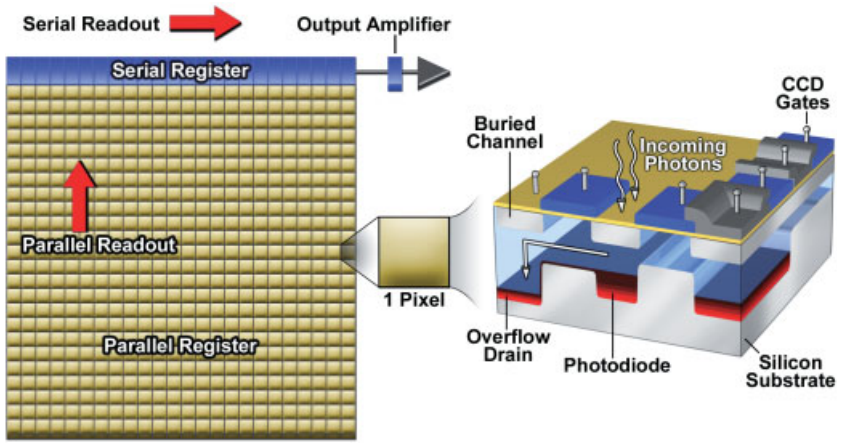

Figure 17.5

Surface design of a full-frame CCD and architecture of a photodiode. (Left) The majority of the surface area is occupied by an imaging area known as the parallel register, an array of thousands of pixels that are arranged in rows and columns with respect to the output edge of the chip near the serial register. The serial register (blue) is composed of a single row of pixels and contains the same number of pixels as the row at the output edge of the parallel register. Photoelectron counts contained in the pixels are transferred serially, from pixel to pixel, until they reach an amplifier (output amplifier), which sends an amplified voltage signal to a nearby ADC. (Right) Cutaway diagram of a single photodiode showing CCD gates, buried channels, and the overflow drain for removing blooming charge. To reveal internal structures, surface layers of the pixel are not shown.

- The CCD chip is cleared (reread without digitization) to remove residual electrons prior to the next exposure.
- The total time for readout and display is ~0.5 second for a megapixel camera operating at 5 MHz.

Considering the large number of operations, it is remarkable that greater than a million pixels can be transferred across the chip, assigned a grayscale value ranging from 0 to 4095, and stored in a frame buffer in the computer in just a few seconds! The accuracy of transfer of electron packets over thousands of pixels is also nearly error-free. The quantitative nature of a digital CCD image and the relationship between analog images observed in the microscope and digital images captured by a digital camera are shown in Figure 17.7.

Another important feature in the camera head is its cooling mechanism. As described below, CCD images are degraded by electron noises, the most serious of which are due to heat and the electronic readout of the camera. *Thermal noise* refers to the generation of electrons from the kinetic vibrations of silicon atoms in the CCD substrate. Thermal electrons cannot be distinguished from photoelectrons and so contribute noise to the image. Cooling is essential for all scientific grade CCD cameras, the benefit being about a 10-fold reduction in the number of thermoelectrons for every 20°C decrease in temperature. Thermal noise can be reduced significantly by *cooling* the CCD down to –20°C or lower using a stack of 2–3 *Peltier thermoelectric cooling*

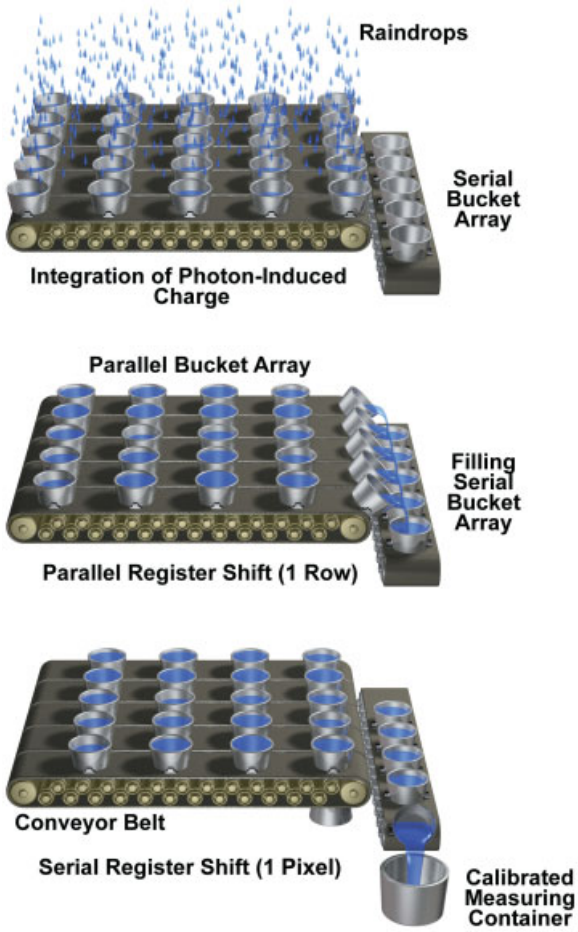

Figure 17.6

Sketch showing the concept of serial readout of a CCD. Pixels comprising the parallel and serial registers of a CCD are represented as buckets containing varying amounts of signal (water) being transported on two conveyor belts operating in stepwise fashion. When the serial register is empty, the row of buckets at the edge of the parallel register transfers its contents to the single row of empty buckets on a serial register, which moves its single row of buckets to a measuring station (the amplifier and ADC) at the end of the conveyor.

devices. In the presence of current, a Peltier bimetallic strip becomes cold on one side and hot on the other. The cold surface is mounted so that it is in direct physical contact with the CCD, while the heat on the other surface is removed by a fan or backed by a circulating liquid cooling system. Astronomical cameras used for hour-long exposures are cooled with liquid nitrogen. For biological specimens, acceptable images can be obtained from exposures lasting a second or less on CCD cameras cooled to 0–10°C, but for higher quality, lower noise images, deeper cooling to –25°C or lower is required. We will deal with the noise components in a CCD image later in the chapter.

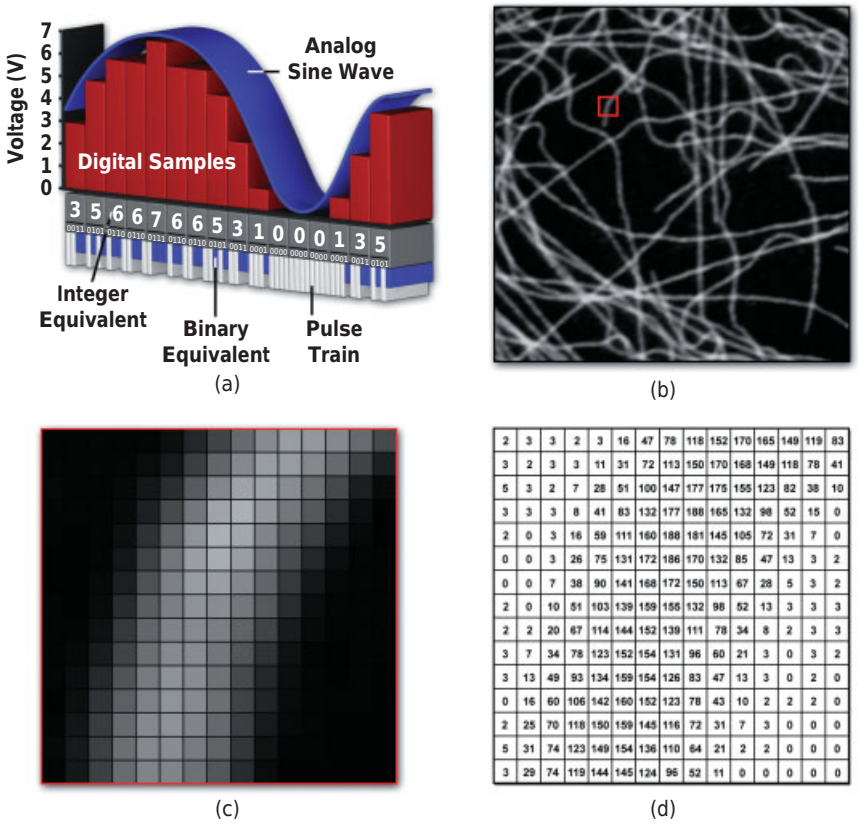

Figure 17.7

Conversion of the analog image to a computer-readable digital format must be done before being processed or displayed by a computer. This process applies to the digital conversion of any image formed by any optical device. (a) The process is illustrated showing the conversion of an analog sine wave into discrete digital values. In reality, the image exists only as a large serial array of data values having *x*,*y* coordinates that can be interpreted by a computer to produce a digital representation of the original scene. (b) Fluorescence image of human *alpha*-tubulin labeled with enhanced green fluorescent protein (EGFP) in live HeLa cells. (c) Sampling of a small portion of the original image (red box in panel b). (d) The analog image is digitized in the camera's analog-to-digital converter to transform the continuous analog output intensity values into a sequence of discrete integers representing the individual brightness values in the binary code interpreted by computers.

CCD DESIGNS

CCD imagers come in three basic designs, which are shown in Figure 17.8 and described as follows:

- *Full-frame CCD.* In this design, whose readout procedure was described in the preceding section, every pixel of the CCD surface contributes to the image (Fig. 17.8a). Exposures are usually controlled by an electromechanical shutter,

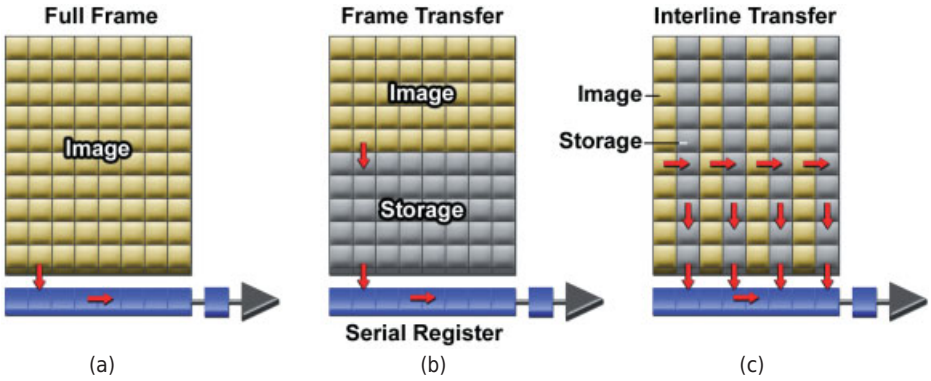

Figure 17.8

Types of CCD designs. (a) Full-frame CCD. (b) Frame-transfer CCD. (c) Interline-transfer CCD.

since the imaging surface must be protected from incident light during readout of the CCD. This was the original design used for biological imaging. Full frame CCDs are used when high dynamic range is required and time resolution is on the order of a second or longer, as in astronomy, and for large format imaging, such as macro-recording of chemiluminescence. The fastest frame rates in so-called subarray mode are ~10–50 fps and are limited by the electromechanical shutter.

- *Frame-transfer CCD.* Cameras with frame-transfer CCDs are fast because exposure and readout occur simultaneously. One-half of an elongated rectangular CCD chip is masked by an opaque cover (an aluminum coating on one half of the surface of the CCD), which is used as a storage buffer (Fig. 17.8b). After an exposure, all of the pixels in the image half of the chip are transferred to pixels on the storage side in 1 ms; the storage array is read out while the image array is being exposed for the next picture. No camera shutter is needed because the time required for transfer from the imaging area to the masked area (~1 ms) is only a fraction of the time needed for an exposure. A disadvantage is that only one-half of the chip can be used for imaging. Cameras of this type are chosen for monitoring rapid kinetic processes and where it is important to maintain high spatial resolution, dynamic range, and accurate exposure as in astronomy and dye ratio imaging.
- *Interline transfer CCD.* Interline CCDs contain columns of pixels used for imaging that alternate with columns of masked storage-transfer pixels, resulting in a pattern of stripes across the CCD (Fig. 17.8c). Interline transfer CCDs were initially used in camcorders and video cameras and became popular for biological research for the same reasons: fast time-lapse readout at 25–30 fps and the lack of a requirement for an electromechanical shutter. After an exposure, all of the pixels in the imaging columns are initially transferred to pixels in adjacent masked storage columns in ~1 μs; the storage array is then read out while the imaging array is being exposed for the next picture. A shutter is not needed, because the shift of electron counts by one pixel is so fast.

Note: Interline CCD Imagers: The Design of Choice for Biomedical Imaging

Because of their speed and sensitivity and lack of requirement for a shutter, interline CCD imagers have become a popular choice for biological imaging. Microlenses on the CCD surface straddle pairs of masked and imaging pixels so that photons that would ordinarily be blocked by the masked pixels are delivered to the imaging pixel area. Thus, by using small pixels and microlenses, the spatial resolution and light collecting efficiency are similar to those of a full frame CCD. Microlens technology also permits extending the wavelength sensitivity into the blue and UV portions of the spectrum, making the interline CCD highly desirable for applications involving short wavelengths, including UV light. The most recent interline chips also incorporate nonabsorbing materials in the circuit structures on the surface of the chip, boosting the QE to close to 80% for red light, close to the level of back-thinned CCD designs.

Since the size of imaging pixels on an interline CCD is smaller than those on a full frame CCD, the full well capacity in photoelectrons is reduced to 15,000–18,000 e^-. Ordinarily, this would result in a reduced dynamic range for the camera, but camera read noise has been reduced to as low as three to five electrons, so that true 12-bit dynamic range is possible. Electronic improvements have also resulted in increased speed of image acquisition, so that 12-bit megapixel images can be acquired at up to 30 MHz or even faster rates.

BACK-THINNED SENSORS

Front-illuminated CCD and CMOS chips are designed so that photons enter the front or imaging surface of a silicon chip, passing through partially transparent strips of conducting materials on the surface that define the pixel circuitry and control the readout of the potential wells after each exposure. The designs of three front-illuminated CCDs were described above. In front-illuminated designs, photons must pass through partially absorbing strips that define gates and microchannel stops, resulting in an overall QE of 40–60%. The backing and mechanical support for the CCD is usually a 500-μm thick slab of silicon.

In *back-illuminated sensors*, the silicon wafer is thinned down to 10–100 μm by grinding, polishing, and acid etching, and the rear surface is activated by application of a special coating, giving >90% QE and improved sensitivity to blue and UV wavelengths (Fig. 17.9). Charges generated from photons entering the rear surface are captured and stored in the same potential wells at the front surface of the chip. Because charges must migrate over longer distances in the silicon matrix to reach the potential wells, the accuracy of targeting to the correct pixel is somewhat reduced, and partly because of these constraints, back-thinned CCDs have higher read noise and are made with greater pixel dimensions (13–23 μm). Despite the difficulty of manufacture and relatively high cost, back-thinned CCDs offer excellent QE, which is useful in low light applications, and the large pixel format allows accumulation of large photon signals and provides potentially high (16-bit) dynamic range.

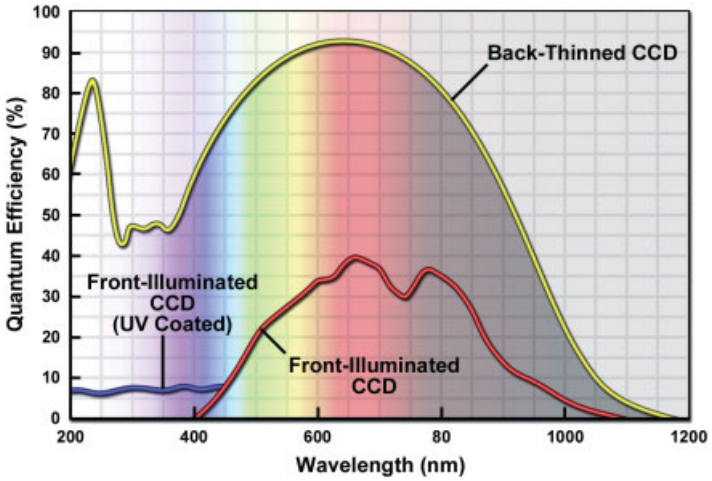

Figure 17.9

Quantum efficiency and wavelength sensitivity of front- and back-illuminated CCD devices. Plot shows quantum efficiency versus wavelength.

EMCCD CAMERAS: HIGH PERFORMANCE DESIGN FOR GREATEST SENSITIVITY

An *EMCCD or electron-multiplying CCD* is a back-thinned CCD that has been modified by the addition of ~500 pixels to the readout register to allow stepwise amplification of the photoelectron count. Increasing the signal by a process of pixel amplification before readout greatly improves detection efficiency and signal-to-noise (S/N) ratio. As described above, standard CCDs transfer photoelectrons serially over hundreds or thousands of pixels at high fidelity and provide imaging at high dynamic range. This mechanism works well for bright signals, but not as well for dim ones with counts of ~300 photoelectrons or less. The problem is the amplifier noise, which has a relatively high baseline and swamps out dim signals, making it difficult to read them accurately.

EMCCDs are based on back-thinned, frame-transfer CCD designs and use the principle of on-chip electron magnification gain to generate images based on low numbers of photoelectrons. Electron parcels are transferred down the amplification register at a slightly higher voltage than during pixel transfer in the parallel register, producing additional secondary electrons by a process of *impact ionization* (Fig. 17.10). The amount of signal amplification is small, usually <2% at each pixel, but when multiplied over ~500 pixels, a single electron can be greatly amplified, in this example by some 20,000-fold. Because signals are now much larger, there is no need to amplify the voltage as much at the readout amplifier. The noise from impact ionization is proportional to the number of electrons being transferred, but because this noise is much less than the noise of the readout amplifier of a conventional CCD (even when accumulated over many pixels), low electron counts can be amplified and digitized more accurately than on a conventional CCD. Since an amplifier noise of 5–10 e^- is applied to signals with thousands of amplified counts, the contribution of read noise to the signal is negligible. Other noises, such as dark current and clock-induced charge, are also greatly attenuated. The high signal and low noise allow true 16-bit imaging (65,500

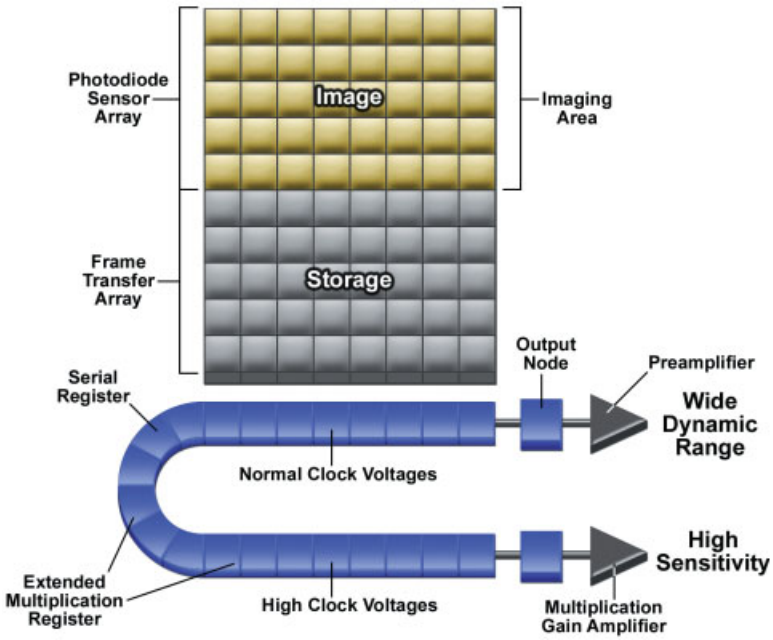

Figure 17.10
Design of an electron-multiplying CCD sensor.

gray levels) on some cameras. On earlier cameras, there was a problem with a decrease in gain due to ageing (QE degradation), but this has been minimized on the newest designs. As a result of the control of the signal and associated electronic noises, it is "easy" for EMCCD cameras cooled to –60°C and having a readout noise of 5 e^- to image single GFP molecules with an exposure time of 50 ms using an EM gain of 200–300× and a laser power density of 1–2 kW/cm^2.

EMCCD cameras are known for providing *high sensitivity at fast frame rates*—a significant advantage for low light imaging. Using such a camera, one can work in low-light conditions and acquire images that otherwise would be impossible to obtain with a standard CCD camera. Using EM gain, one can also greatly reduce the exposure time to minimize problems of photobleaching and prolong cell viability. An example of the improvement in image quality under low light conditions is shown in Figure 17.11. Three applications that especially benefit from EMCCD imaging are single molecule fluorescence microscopy, spinning disk confocal imaging, and spectral imaging. Electron magnification produces high S/N images from the low intensity fluorescence signals that are inherent to these technologies.

SCIENTIFIC CMOS: THE NEXT GENERATION OF SCIENTIFIC IMAGERS

CCD cameras are presently the detector of choice for scientific imaging because of their high sensitivity and low noise. Recently, however, *CMOS* imagers—the type of sensor found in cell phones, consumer cameras, scanners, and other imaging products—are also being used for high performance scientific imaging. CMOS imagers are unique

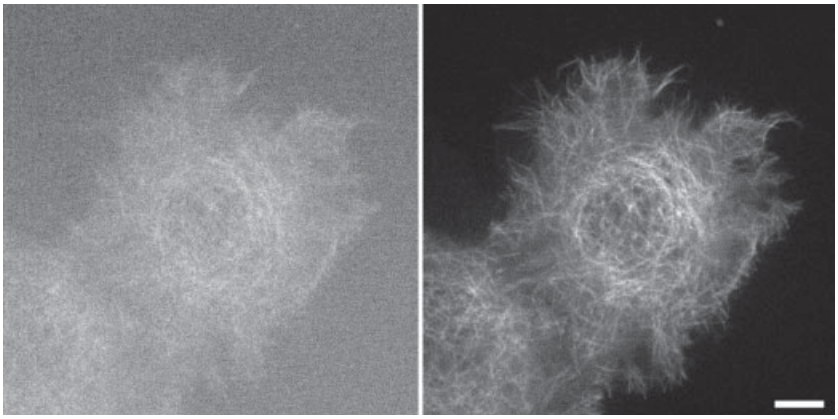

(a) (b)

Figure 17.11

Low light-level imaging of the microtubule-associated protein, tau, fused to green fluorescent protein. In panel a, the extended multiplication register on the EMCCD was turned off to simulate imaging with a standard cooled scientific CCD. (b) Turning on the EM gain to a setting of 50% dramatically reduces noise and enhances visibility and definition of dim structures. Bar = 10 μm.

in having multiple transistors associated with each pixel site that amplify pixel signals during readout. The inherent advantages for imaging are near ideal design for signal handling, very low noise (readout noise ~1 e^-), and low power consumption. Because pixels are read out in parallel, they are also very fast. These features extend the dynamic range of CMOS chips (16-bit even for 6.5-μm pixel imagers) and allow high frame rates (100 fps full frame, for a 5 megapixel chip). This means that compared to a CCD camera at the same exposure time, the CMOS camera gives better dynamic range, and potentially better S/N ratio and image clarity; alternatively, the same image quality as a CCD can be obtained with a much shorter exposure time, a convenience in live-cell imaging or when imaging dyes that are easily photobleached.

In terms of design, CMOS differs from CCD in the pixel structure and readout mechanism. CMOS imagers have pixel-resident transistors that allow each pixel's photon count to be preamplified and read out separately (Fig. 17.12). This contrasts with the CCD design that uses serial readout and a single output amplifier to read out all of the pixels on the chip. A comparison of the two designs is shown in Figure 17.12. In the past, there were difficulties in obtaining high QE and uniform behavior for the millions of transistors on a CMOS chip, but the use of microlenses and improvements in manufacturing have largely removed these difficulties.

CAMERA VARIABLES AFFECTING CCD READOUT AND IMAGE QUALITY

Readout Rate

Fast readout rates are needed for applications requiring high temporal resolution. At very high readout rates approaching the video rate of 30 fps, the image appears live and does not flicker on the computer monitor, and with addition of subarray readout

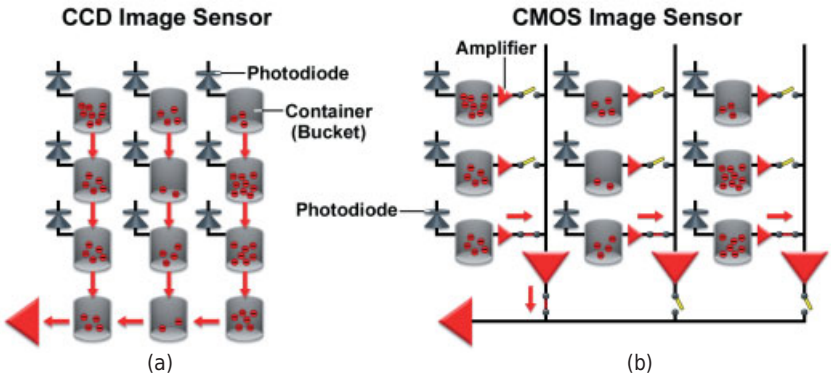

Figure 17.12

A comparison of CCD (a) and CMOS (b) image sensor design. Red arrows highlight pathways for photoelectron flow, while red triangles indicate amplifiers. Note that the CCD contains a single amplifier, whereas each pixel and each column has an amplifier in the CMOS design. Also note that rows in the parallel register are read simultaneously in the CCD image sensor, but that each individual photodiode in the CMOS sensor is controlled by a separate switch. When the switch is closed (lower left-hand photodiode in panel b), photoelectrons flow into the amplifier.

and binning, acquisition at rates of hundreds of frames per second is possible. Most scientific CCD cameras can be adjusted to operate at different readout rates ranging from 1 to 20 MHz, the processing speed of the ADC and camera electronics (1 MHz = 10^6 byte processing operations/s). However, high readout speeds increase the level of noise in the image.

Various noise components are always present in the pixels comprising an electronic image, among which readout noise is one of the major sources. Accordingly, low intensity images with low pixel values should be read out at slower rates to reduce noise and maintain an acceptable S/N ratio and image quality.

Subarray Readout

It is possible to define a small subset of pixels on the CCD (a *subarray*) corresponding to only a portion of the full image area for acquisition and display on the monitor. The subarray is defined by entering the boundaries of the region in the acquisition software or by defining the *region of interest* (*ROI*) with a mouse on the computer screen. Subarray readout is fast because the unwanted pixels are not processed by the ADC and are discarded. Image files, particularly image sequences of time-lapse acquisitions, are also correspondingly smaller and more manageable.

Binning

Binning is the combining or pooling together of photoelectrons of adjacent pixels on the CCD to form electronic superpixels (Fig. 17.13). The pooling of photoelectrons occurs in the serial register of the CCD during readout. A *superpixel*, that is, 2×2

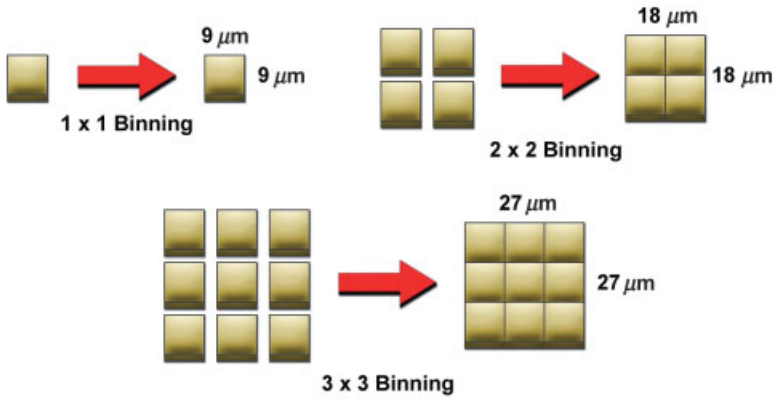

Figure 17.13

The process of binning. Photoelectrons contained in the unit pixel elements of the CCD are combined during CCD readout to form electronic "superpixels." Binning is set by the user in software and is controlled by the timing pulses that drive the pixel parcels during the time of readout in the serial register on the CCD. Since photoelectrons are pooled, camera exposures can be shortened in proportion to the number of pixels included in a superpixel. Binning also reduces the image file size on the computer and allows more rapid frame rates, but spatial resolution is reduced compared with that available in an unbinned image.

pixels, contains the combined photoelectron content of 4 physical pixels but is processed by the camera and amplifier as a single pixel. Binning reduces spatial resolution, but offers the following advantages:

- Faster acquisition of image sequences (if the rate of acquisition is limited by camera processing speed)
- Smaller size of image files on the computer
- Shorter exposure time required to obtain the same image brightness (a major benefit for live-cell imaging)
- Improved S/N ratio for the same exposure time

Gain

In digital imaging, increasing the electronic gain reduces the number of photoelectrons that are assigned per gray level, allowing a given signal to fill a larger range of gray levels (Fig. 17.14). For example, for a gain setting of 10 electrons per gray level, a 1000-electron signal corresponds to 100 gray levels. If the gain is increased fourfold, there are now 2.5 electrons per gray level, and 4000 gray levels are obtained. Note the difference between gain adjustment with a digital CCD camera and gain adjustment using a PMT or a vidicon tube, where the signal voltage is amplified by multiplication by a constant factor. By convention, the number of electrons/ADU for 1× gain is usually defined as the saturating number of electrons per pixel divided by the full range of the digitizer. Gain is usually applied when there are a limited number of photons, and it is desirable to utilize a large number of gray levels. The disadvantage of increasing the gain is a corresponding decrease in the accuracy of digitization; at high gain, the noise

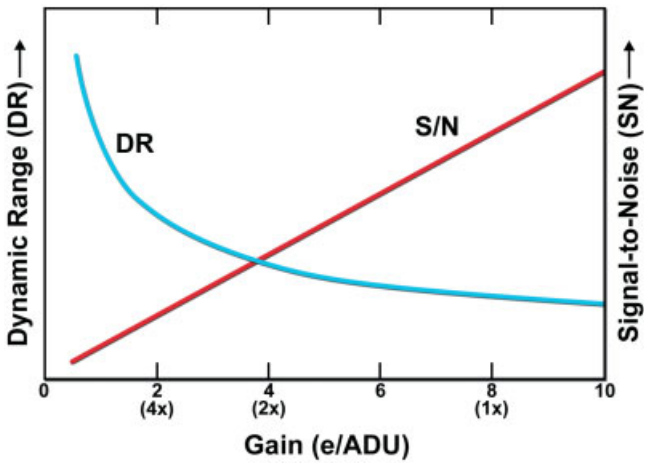

Figure 17.14

The effect of gain on dynamic range and signal-to-noise ratio. The *x*-axis shows the number of electrons corresponding to different gain settings (parentheses). For example, for a gain factor of 1, 2, and 4×, the number of electrons/ADU is typically 8, 4, and 2 electrons/ADU, respectively.

from inaccurate digitization can cause images to look grainy. There is a limit to how much gain can be applied, because at very high gain, image quality deteriorates. Nevertheless, by increasing the gain, the exposure time can be reduced while retaining a large number of grey levels. For images exposed to give a constant number of accumulated electrons, increasing the gain causes the dynamic range (number of gray level steps) to increase exponentially, while causing the S/N ratio, the measure of signal clarity, to decrease.

SIX TERMS DEFINE IMAGING PERFORMANCE

Image quality can be described in terms of four quantifiable criteria: resolution of time (sampling rate), resolution of space (ability to capture fine details without seeing pixels), resolution of light intensity (number of graylevel steps or dynamic range), and S/N ratio (clarity and visibility of object signals in the image). As we will see, it frequently occurs that not all four criteria can be optimized simultaneously in a single image or image sequence. For example, to obtain a timed sequence of a live fluorescent specimen, it may be necessary to reduce the total exposure time to avoid photobleaching and phototoxicity. This can be accomplished by exposing the specimen less often (loss of temporal resolution), binning the image (loss of spatial resolution), and/or by applying a high gain (reduction in S/N ratio). Alternatively, to maximize dynamic range in a single image requiring a short exposure time, you could apply binning or increase the gain. The ability to perform digital imaging efficiently and knowledgeably requires that the user become completely familiar with these terms and gain experience in the art of balancing camera acquisition parameters in order to optimize criteria of high priority. Although mentioned in previous chapters, we will now examine these terms in greater detail and in the context of using a digital CCD camera. This topic is also addressed in Chapters 16 and 18.

Temporal Resolution

Interline CCD cameras provide high temporal resolution at close to video rates. The latest interline cameras can image at 12-bit depth, full frame, at approximately 10 fps. With binning or subarray options selected, rates of several hundred frames per second can be obtained. Scientific CMOS cameras often feature frame rates up to 100 fps at full frame with high dynamic range.

Spatial Resolution and Image Dimensions

The spatial resolution of a CCD can be excellent and is determined by the physical size of the pixels on the detector (Fig. 17.15). Generally, pixels in cameras used for biological imaging are usually smaller than developed silver grains in typical camera film (10 μm). Even with two- to three-fold magnification on a high resolution inkjet printer, the pixels comprising the picture are essentially invisible. With such small detector elements, CCD cameras usually meet the Nyquist criterion for image sampling in preserving the diffraction-limited resolution of the objective, thus avoiding pixelation and aliasing (see section on aliasing and the Nyquist criterion below). For example, for a CCD chip with 6.45-μm pixels, there are ~4 pixels per diffraction spot radius produced by a 100×, 1.3 NA objective (0.25 μm × 100 magnifications ÷ 6.45 μm/pixel = 3.9 pixels/radius). This is double the Nyquist limit (2 pixels per unit resolution distance), so spatial resolution is very good, and the diffraction-limited resolution of the objective is maintained.

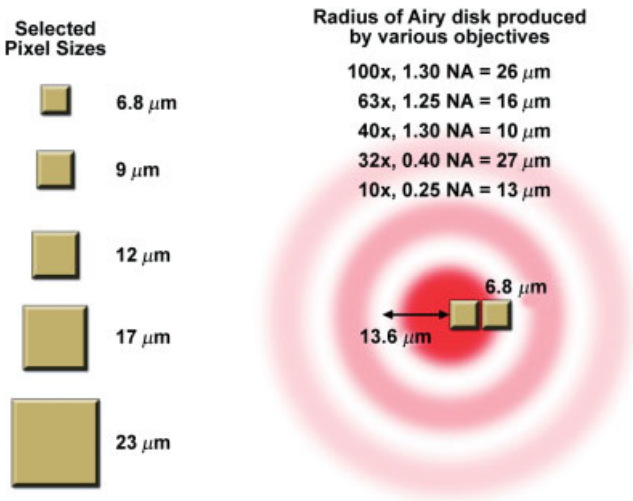

Figure 17.15

Comparison of pixel dimensions to diffraction spot size. Left: The pixel sizes of various CCD imagers are indicated in micrometers. Right: The diameter of the diffraction spot (Airy disk) produced by various objectives as it would appear on the surface of a CCD. According to the Nyquist sampling theorem, preservation of the spatial resolution of the optics requires that a diffraction disk radius be covered by a minimum of 2 adjacent pixels on the CCD. For a 40×, 1.3 NA lens, the diffraction spot radius = 40(0.61 × 0.546)/1.3 = 10 μm, so the coverage provided by a CCD with 6.8-μm pixels is just barely adequate. However, the same CCD provides excellent sampling for a 100×, 1.3 NA lens with spot radius = 100 (0.61 × 0.545)/1.3 = 26 μm, even under conditions of 2 × 2 binning (6.8 × 2 = 13.6 μm).

Even with binning at 2 × 2, the Nyquist sampling criterion is very nearly satisfied. The reader should refer to Figure 17.15, which compares CCD pixel dimensions with diffraction spot radii made by different objectives. Give this matter serious attention when selecting a CCD camera. The figure shows that 10-μm pixels are ideal for imaging with high magnification oil immersion lenses as would typically be encountered in fluorescence microscopy. The number of pixels along the length and width dimensions of the CCD is also important when considering the quality and size of a print made with a dye sublimation printer. A megapixel CCD with 1000 pixels along one edge of the CCD gives a 3.3-in print when printed at 300 pixels per inch. Pixelation in the image is not observed for printer magnifications under 2–3× (10 in on a side), which is fine for most imaging applications.

Quantum Efficiency and Spectral Range

Quantum efficiency refers to the efficiency of photon-to-electron conversion in the CCD, whereas spectral range refers to the wavelengths that can be detected. Standard front-illuminated CCDs have a peak QE of 40–50%, although new transparent materials on the surface of the chip for controlling pixel readout extend this to 60% for visible wavelengths ranging from 400 to 1100 nm with peak sensitivity at 550–800 nm (Fig. 17.16). With back-thinned CCDs (see below), QE can be greater than 90%. With special coatings on the CCD, it is possible to extend the range of spectral sensitivity from 120 to >1100 nm. Sometimes, it is important to increase the sensitivity of signal detection and improve the S/N ratio in other ways, such as by decreasing the background signal, increasing the object signal, or by selecting more efficient fluorescent dyes.

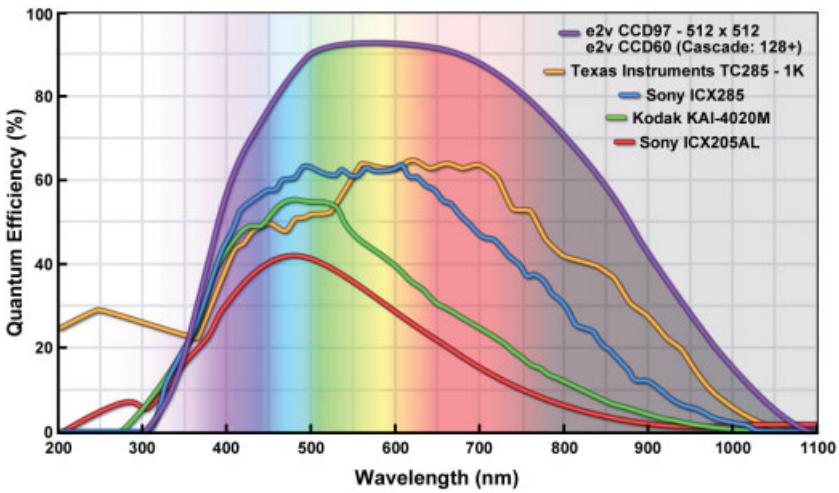

Figure 17.16

Wavelength sensitivity of some popular CCD devices. Sony ICX205AL (red) is an interline CCD; Kodak KAI-4020M (green) is an interline CCD with enhanced transmission microlenses; Sony ICX285 (blue) is a sensitive electron–hole accumulation diode sensor; Texas Instruments TC285 (orange) is an EMCCD that uses impact ionization to increase sensitivity; e2v CCD97 (purple) is a back-illuminated, frame-transfer CCD.

Noise

Digital images are affected by two principal noise sources. One of these is from the specimen itself and is called the *photon* or *shot noise*, a statistical uncertainty that is always observed when discrete quanta, such as photons, are measured within a finite time or space. Another source of noise is the readout noise from the camera. The principal readout noise comes from the amplification of pixel photoelectron counts in the on-chip amplifier where electron counts induce a voltage, which is then carried to the camera's analog-to-digital converter (ADC). There are other electronic noises from the ADC, quantitation, and application of voltage offset, and others, but the on-chip amplifier noise is the greatest. Manufacturers report this noise as the *readout noise* and give the value in electrons. Another important camera noise is the *thermal noise* from the CCD. As already described, thermal noise refers to the generation of electrons from the kinetic vibrations of silicon atoms in the CCD substrate and can be reduced to a very small value by thermoelectric cooling of the CCD. The amplitudes of the principal noises present in a CCD image are summarized in Table 17.1. Noise plays a major role in the determination of image quality as defined by the S/N ratio, which is discussed below.

Dynamic Range

The number of resolvable steps of light intensity, described as gray-level steps ranging from black to white, is called the dynamic range (DR). DR is used to describe the potential number of gray-level steps capable of being recorded by a camera and is usually calculated as the ratio of the maximum signal electrons at saturation (the full well capacity of a pixel) to the readout noise of the camera (generally 3–5 electrons). The calculation is always based on the numbers of electrons. For an interline CCD chip with a full well capacity of 15,000 e^-/pixel and a readout noise of 3 e^-, the potential DR is 5000 : 1. Since the full well capacity depends on pixel size (holding capacity is ~1000 $e^-/\mu m^2$), CCD imagers with large pixels usually have a higher dynamic range. For example, a full frame CCD with 24 μm^2 pixels, a 570,000 e^- full well capacity, and 9 e^- read noise has a DR = 65,000. The read noise of a camera is important in determining the dynamic range as well. Due to continual improvements in reducing readout noise (down to 3–5 e^- and lower for cameras used in biological laboratories), even interline cameras with small 4.5 μm pixels can have a DR ~4000.

To realize the potential dynamic range of a CCD camera, the camera must be equipped with an appropriate *digitizer*, also called an analog-to-digital converter (ADC) or digital processor. Digitizers are described in terms of their *bit depth*. Since a computer bit can only be in one of two possible states (0 or 1), the bit depth is described

TABLE 17.1 Principal Noise Sources in a CCD Image

Noise Type	Value	Source
Photon or shot noise	√ of signal e^-	Inherent noise in a photon signal
Readout (preamp) noise	~5 e^-	Preamplifier, other electronics
Thermal noise	~0.001 e^-/s	Atomic vibration in the silicon matrix

as 2^X number of steps. Therefore, 8-, 10-, 12-, 14-, and 16-bit processors can encode 2^8 and so on steps or a maximum of 256, 1024, 4096, 16,384, or 65,536 gray levels. A manufacturer would typically fit a camera with a DR ~4000 with a 12-bit processor to best match the DR of the imaging system.

On some 12-bit interline cameras, the calculated dynamic range is about 2000, so the use of a 12-bit ADC would seem to be more than is required. However, some cameras make full use of the 12-bit digitization by including a ½ X gain setting. This option is included because CCD chips are designed such that the pixels of the serial register hold twice as many photoelectrons as pixels in the parallel register. Thus, when a camera is operated with 2×2 binning, a common mode of operation for routine microscopy, 12-bit imaging at high quality can be obtained.

It is now quite common to see cameras fitted with processors having a much higher digitizing capacity than the inherent DR of the camera. If the read noise is designated as 1× electronic gain (the conventional assignment for gain), there are potentially a large number of unused intensity levels when the bit depth of the processor exceeds the dynamic range of the camera. To fill these extra levels, manufacturers apply a (hidden) 2–4× gain to boost the signal to utilize the gray levels of the processor, but as we have seen, this operation increases the noise in the image. Therefore, by noting the full well capacity of the pixel and read noise of the camera, the dynamic range of different cameras can always be calculated and compared.

In comparison with high bit CCD cameras, display devices, such as computer monitors and dye-sublimation printers, use only 8-bit processing (256 gray levels). In fact, the dynamic range of communications media, such as TV/video, pictures in newsprint, and even of the eye is a meager 5–7 bits, depending on the image and illumination conditions. If the visual requirements for printers and monitors are so low, why are high bit imaging systems necessary or even desirable? High bit depth (DR) is required:

- For purposes of accurate quantitation of light intensities, for example, for examining ratiometric or kinetic imaging data; the larger the number of gray levels, the more accurately the observed intensity can be described.
- To perform multiple image processing operations without degrading the image; because of mathematical round-off errors during processing, images with more gray levels can tolerate a greater level of mathematical manipulation.
- For selecting and working with a portion of an image for display, where the ROI covers only a narrow portion of the dynamic range of the full image. For a ROI including just 2% of the full dynamic range, this would be 82 levels for a 12-bit system but only 5 levels for an 8-bit system. If the five gray levels were now stretched to fill the 256 levels for an 8-bit monitor or print, the image would look pixelated, with noticeable steps or contour lines.

Signal-to-Noise Ratio

Signal-to-noise ratio is used to describe the photometric accuracy of a specimen's signal. In qualitative terms, we use S/N ratios to describe the clarity and visibility of objects in an image. S/N ratio is calculated as the specimen signal (total signal minus contributing background signal) divided by the noise of the surrounding background (standard deviation of the background signal). When used to describe the imaging

performance of a CCD camera, S/N is calculated in terms of a single pixel, and the calculation is always based on the number of electrons comprising the signal and the noise. The importance of S/N is easily appreciated when we examine a dim, grainy image, where the amplitude of the specimen signal is small and the read noise of the camera is a principal noise component in the image. In a side-by-side comparison of the imaging performance of two cameras with read noises differing by a factor of 2, the difference is clear: The camera with the lower read noise produces the clearer image. The effect of high camera noise can also be observed on the computer monitor or on a print in half-saturated, moderately exposed images. S/N characteristics are more significant for those using a CCD camera as a photometer to monitor changes in light intensity, such as in fluorescence experiments involving FRAP, FRET, or ratio imaging of fluorescent dyes. In this case, plots of light intensity over time are smoother and more accurate when image sequences exhibit high S/N values. We will examine S/N theory and its applications in greater detail in Chapter 18.

ALIASING

Aliasing is the phenomenon whereby the periodic structures in an object are not faithfully represented in the object image, but instead by a false period that can be mistaken for being real. The false period is often referred to as a Moiré pattern (Fig. 17.17). Aliasing (from the Latin *alius*, meaning another, other, or different) is an imaging artifact and is a property inherent to all detectors with periodic structure such as pixels in CCD cameras. We commonly observe aliasing on television. This occurs when there is insufficient magnification produced by the camera lens so that images of periodic structures (pinstripes in an announcer's shirt, bricks in the wall of a house, or seats in an empty stadium) show false banding patterns. Under these conditions, the images of these objects exhibit false patterns of wide bands. Aliasing is frequently seen in digital imaging, particularly in specimens with period structure such as diatoms or striated muscle.

Aliasing has its origins in signal sampling theory and can be described mathematically. If the image of a specimen with periodic structure (a sine wave target or the

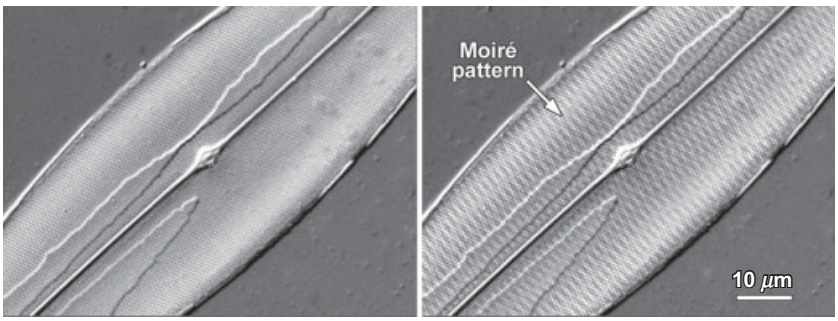

(a) (b)

Figure 17.17

Aliasing in digital microscopy. (a) A diatom imaged using differential interference contrast (DIC) optics (see Chapter 10) captures details of knobbed structures on the frustule. (b) Improperly sampled image showing a Moiré pattern artifact. Bar = 10 μm.

periodic pattern of pores in a diatom) is reconstructed from sample points that occur at a much higher frequency than detail in the specimen, it is possible to reconstruct and display an accurate image of the specimen. However, at the point where the *sampling frequency is less than twice the specimen frequency*, a condition called *undersampling*, it is no longer possible to present the signal accurately, and a false period (aliasing) is observed. Below this sampling limit, the display of periodic elements in the image actually increases as the sampling frequency becomes further reduced. The factor of 2 requirement for oversampling to avoid aliasing is called the *Nyquist limit* (see Castleman, 1993 and Inoué and Spring 1997 for theory and details). The Nyquist sampling criterion is frequently encountered in microscopy, including in confocal imaging, when choosing pixel resolution for an image and selecting the step size for preparing z-stacks for 3D imaging. The approach is straightforward: determine the spatial resolution (radius of the Airy disk) of the optics, and then select a sampling period that is 2.0–2.3× smaller than this value. For example, for preparing a *z*-stack with a 10×/0.3 NA objective, the resolution on the *z*-axis is $z = n\lambda/\mathrm{NA}^2$ or about 6 μm (see depth of field), so the required step size is 3 μm or less.

COLOR CAMERAS

Many investigators choose to use color to represent the visual appearance of specimens seen in the microscope. Although there are some technical difficulties in displaying color in prints, the increase in information in a color image can be very significant. Some common color applications include fluorescence microscopy, stained tissue sections in histology and pathology, and horse radish peroxidase (HRP) and beta-galactosidase labeling in specimens viewed by brightfield or DIC microscopy.

A CCD device by itself is not color sensitive, so the acquisition of color images requires that red, green, and blue wavelengths be isolated with filters, acquired separately by the CCD and then joined together to create a composite color picture. These requirements impose additional constraints that limit the resolution of space, time, and light intensity. Therefore, depending on the particular design and solution, color cameras tend to be slower, have reduced spatial resolution and dynamic range, and produce noisier images than grayscale cameras. The designs and solutions for providing color information vary considerably:

- *External color filters or color liquid crystal device.* A motorized filter wheel rotates separate red, green, and blue filters into the light path at the location of the lamp or in front of the camera. The camera acquires separate images for each color. The full spatial resolution of the chip is maintained using this arrangement, but the speed of acquisition and display is reduced. To increase speed, a liquid crystal tunable filter can be used. These filters are transparent, have no moving parts, and display RGB colors in very rapid sequence.
- *Three-chip design.* The camera contains a beam-splitting prism that directs the image to three separate CCD devices each masked by a color filter. The spatial resolution of the CCD is maintained, and the frame rate (important for rapid sequences and for video output) can be very fast, because acquisition is simultaneous for each color channel; however, light intensity delivered to each detector is considerably reduced. Compared with a single chip grayscale camera exposed for a comparable amount of time, the color image is nearly 10-fold dimmer. Gain can

be applied to brighten the color image but at the expense of reduced S/N ratio and increased graininess.

- *Color microlenses and moveable Bayer color mask*. CCDs can be manufactured with red, green, and blue microlenses applied in a specific pattern on individual pixels on the chip. These cameras are fast, and pixels are illuminated at greater intensity than in the three-chip design, but spatial resolution is reduced. Another solution for individual pixel masking features an array of red, green, and blue microlenses (a Bayer color mask) that moves rapidly and in a square pattern immediately over the surface of the CCD. Each pixel is responsible for providing RGB color information, so maximum spatial resolution is obtained. This camera is ideal for brightfield color photography of histological specimens.

Exercise: Evaluating the Performance of a CCD Camera

The purpose of this exercise is to prepare you for selecting a digital CCD camera for use in your laboratory. Prepare a summary report addressing the questions, and be sure to indicate the name of the camera and its manufacturer. Conclude the report by indicating the strengths and weaknesses of the camera with respect to the intended application, and indicate if you would recommend this system for purchase by your own lab.

Consider your needs and requirements

- Indicate the principal modes of light microscopy now in use in your laboratory.
- Make a list of the key resolution parameters: spatial resolution, time resolution, dynamic range, and S/N, and indicate the relative importance of each for your application. Keep these in mind while choosing a camera.

Spatial resolution (important for maintaining optical resolution)

- What CCD is mounted in the camera? What are the pixel dimensions?
- Indicate the magnification of the objective you typically use, and then calculate the radius (μm) of the diffraction disk in the image plane produced by this lens at 550 nm. Do the pixel dimensions on the CCD meet the Nyquist limit for preserving spatial resolution? If not, how would you solve this problem?
- Indicate the binning modes available (2×2, 3×3, 4×4, etc.). Remember that binning reduces spatial resolution, but reduces the exposure time and helps protect live cell preparations.
- Indicate the width and height of a full-frame image (in pixels). Calculate the image size of a print made using a 1200 dpi printer.

Camera sensitivity and noise (important for dim and/or photon-sensitive specimens)

- What is the range of wavelength sensitivity? Does the CCD contain an enhanced coating for UV or IR wavelengths? What is the QE at 550 nm?

- What is the saturation value (full well capacity) of a pixel in electrons?
- What is the read noise per pixel (in electrons) of the camera? Determine the mean value of a bias frame to establish the contribution from bias plus read noise.
- Calculate the percent contribution of the bias signal in an image signal that reaches saturation.
- What is the operating temperature of the CCD, and what is the contribution of thermal noise? For quantitative applications, thermal noise (and read noise) should be minimal. The noise levels are less important when acquiring images to prepare prints, especially if specimens are bright.

Dynamic range (important for maintaining image details and measuring light intensity)

- Calculate the dynamic range (maximum number of gray levels) from the full well saturation level and the camera read noise (values are in electrons).
- Note the bit depth of the digitizer (8, 10, 12, and 14 bits). This value is sometimes assigned to the camera as a whole.
- Is the bit depth of the digitizer a good match for the camera's dynamic range? The fact that the digitizer may be oversized does not condemn a camera, but one should be aware of (and calculate!) the compensating gain factor applied by the company to allow the camera to use all of the gray-level values. This factor is often overlooked, but is important when evaluating and comparing the performance of different cameras. Remember that high gain settings (fewer electrons/ADU) give grainier images.

Temporal resolution (important for documenting steps in rapid kinetic events)

- What is the minimum time required for the camera to acquire and display a full frame, unbinned image? A one-quarter frame binned 2×2? To do this, use a stopwatch and adjust the software for the acquisition of 10 frames in time-lapse mode, with a minimum time interval (1 ms) between the frames.

Image quality (qualitative and quantitative aspects)

- Histogram-stretch a feature spanning a limited number of pixel values and examine the quality of the displayed image in terms of noise and graininess.
- After histogram adjustment, print the image and examine its quality.
- Prepare a plot showing the ADUs of a row of pixels through an object. Examine the pixel fluctuations across a uniform feature and confirm that they are minimal.
- Determine the S/N ratio (see the text and exercise in the following chapter). This is the most important test that can be performed to judge image quality.

It is imperative to perform this test for a camera that is to be used for sensitive quantitative imaging.

Image acquisition/processing/analysis software

Because the convenience of using a camera is largely determined by the computer platform and software, it is very important to examine the acquisition-–processing–analysis software. The software used to demonstrate a camera may not be the most convenient. Whatever the selection, the software must have an extension called a camera driver, which is required to operate a particular camera.

- Is the image acquisition menu convenient and easy to use, and does it control the basic parameters of exposure time, binning, and gain?
- Is basic image processing available (histogram adjustment, gamma scaling, contrast, and sharpening adjustments) and easy to use?
- Is basic image analysis available (segmentation, data extraction, particle counts, and measurement of shapes and geometric parameters) and easy to use?
- Does the software allow you to write customized scripts that might be needed for special automated acquisition–processing–analysis operations?
- Can images be saved in TIFF, PICT, and other universal file formats so they can be imported into other programs like Photoshop for further processing and printing?

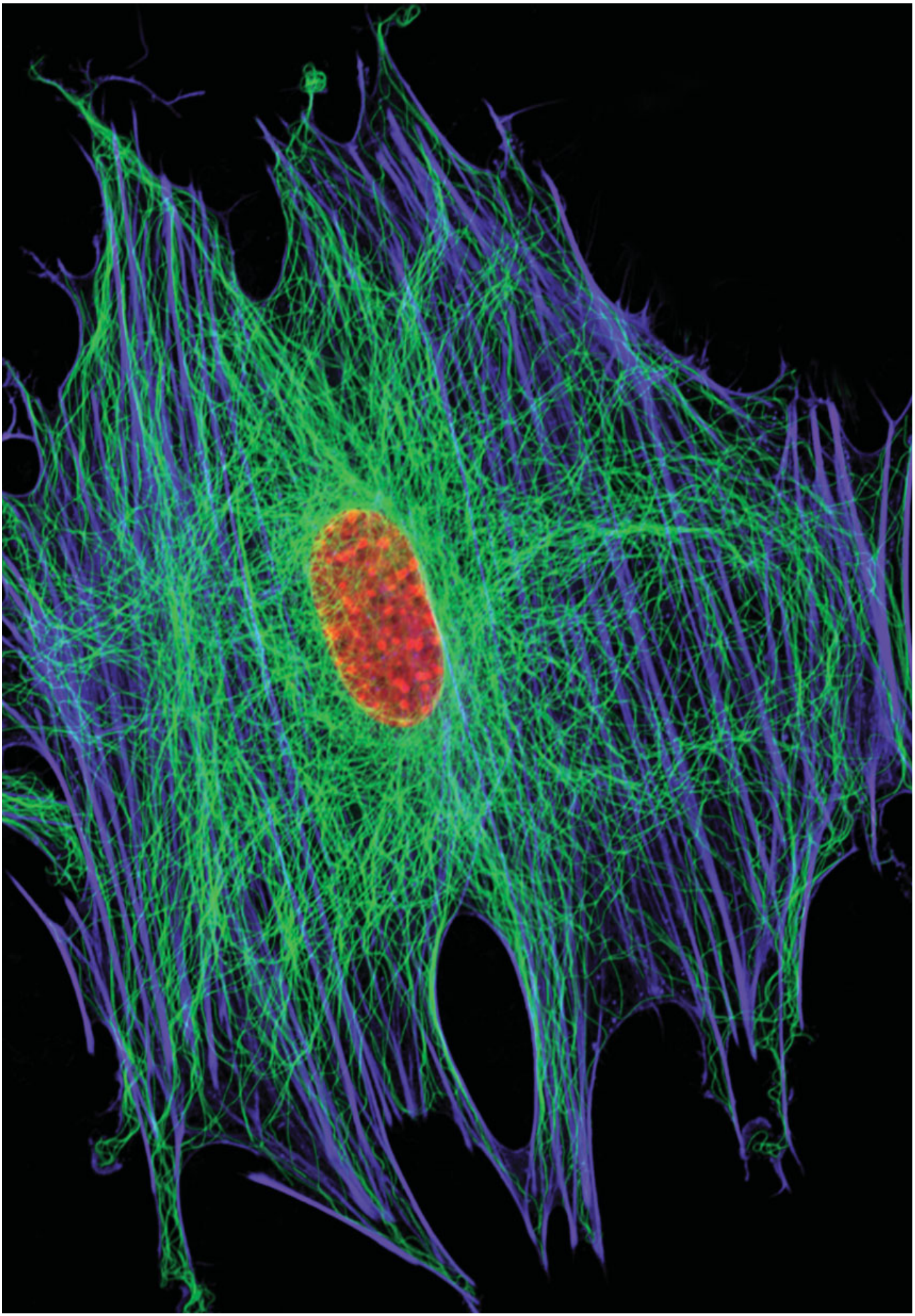

CHAPTER
18

DIGITAL IMAGE PROCESSING

OVERVIEW

Taking pictures with a digital camera requires training and experience, but this is just the first step in obtaining a properly acquired and corrected image. Image processing is used for two purposes: (1) It is required to establish photometric accuracy so that pixel values in the image display the true values of light intensity. (2) It is also an essential tool for optimizing an image for scientific publication. In preparing an image for display or printing, it is essential that the image represent the specimen as objectively as possible, and, with few exceptions, this means including all of the information (intensity values) contained in the specimen image. Because it is a matter of utmost importance, we discuss basic image processing operations and techniques in this chapter and guidelines for preparing images for scientific publication. You should distinguish between the following terms: *image processing*, which refers to the digital manipulation of pixel values in the image, and *image analysis*, which encompasses counting and measuring operations performed on objects and features in the image. Many commercial software programs for camera control and image acquisition perform these functions. Image analysis, including measurements of morphological features, the use of grids in stereology, image segmentation, and other important topics are not covered in this book. Interested readers should refer to excellent texts by Russ (2011) and Gonzalez and Woods (2007). In this chapter, we review four operations that are essential for understanding and using image processing:

- Adjusting the *image histogram* to change brightness and contrast.
- Performing *flat-field correction* to establish photometric accuracy.

Immunofluorescence image of a cell containing actin filaments, microtubules, and DNA.

Fundamentals of Light Microscopy and Electronic Imaging, Second Edition.
Douglas B. Murphy and Michael W. Davidson.

- Applying *spatial filters* for image enhancement.
- Using *signal-to-noise* (*S/N) ratio* calculations to determine confidence limits of observations.

In processing images, proceed through the following steps, performing each only as necessary:

1. Save and duplicate the raw image file; use the duplicate for processing; the original is always available as a reference in case you make a mistake.
2. Flat-field correct the image to restore photometric accuracy of pixel values. As a bonus, this procedure removes artifacts from microscope optics, the illuminator, and the camera.
3. Adjust brightness and contrast with histogram stretching (setting the levels). This is important for displaying all of the meaningful content of the image.
4. Adjust the gamma (γ) to allow exponential scaling for showing bright and dim features in the same image.
5. Apply a median filter or blurring filter to reduce speckles and noise.
6. Apply the unsharp mask or other sharpening filters to increase the visibility of details.

PRELIMINARIES: IMAGE DISPLAY AND DATA TYPES

Software programs display images on the computer monitor with the help of a *lookup table* or *LUT*, a conversion function that changes pixel input values into gray-level output values ranging from 0 to 255, the 8-bit display range of a typical monitor. Manipulation of the LUT changes the brightness and contrast of the image and is required for the display and printing of most microscope images. In most software programs, adjusting the LUT only changes how the image is displayed; it does not alter the values of pixels in the image file. When an adjusted image is saved, the LUT settings are appended as *metadata* to the image file, but the pixel values remain unchanged. Metadata is a part of the image file that is used to store information about the image, including camera settings and microscope configuration.

Some software programs show the LUT function superimposed over the *image histogram*, a display revealing the number of all of the individual pixel values comprising the image. This presentation is helpful in determining optimal LUT settings. The default settings of the LUT usually assign the lowest pixel value an output value of 0 (black) and the highest pixel value an output value of 255 (white), with intermediate values receiving output values corresponding to shades of gray. This method of display guarantees that all acquired images will be displayed with visible gray values on the monitor, but the operation can be deceiving, because images taken at different exposure times can look nearly the same, even though their pixel values may be different. However, as will be discussed later, images acquired with longer exposure times have improved quality (better S/N ratio). The default LUT function is usually linear, but one can also select exponential, logarithmic, black–white inverted, and other display options.

Data types used for processing are organized in units of bytes (8 bits/byte), and are utilized according to the number of gray levels in an image and the number of gray

levels used in image processing. The names, size, and purpose of some data types commonly encountered in microscope imaging are as follows:

- Byte files contain 8 bits (1 computer byte), giving 2^8 or 256 gray-level steps per pixel. Although byte format is used for display and printing, large format data types do not have to be saved in byte format in order to be printed. Conversion to byte format should only be performed on duplicated image files so that high-resolution intensity values in the original image are not lost.
- Short integer and unsigned 16-bit data types contain 16 bits/pixel or 65,536 steps. Images from 10- and 12-bit charge-coupled device (CCD) cameras are accommodated well by these data types.
- Long integer format contains 32 bits (4.3×10^9 steps) and is used in some programs to preserve internal precision during processing.
- Floating point format with 32 bits/pixel is used to preserve a high level of arithmetic accuracy during image processing. This data type uses scientific notation, with 23 bits assigned to the mantissa, 8-bits to the exponent, and 1 bit for plus or minus, giving steps that range from 20×10^{38} to 20×10^{-38}.

Thus, an image captured by a 12-bit camera is typically contained in a 2-byte (16-bit) data type. This size is convenient because the extra bits allow for greater numeric accuracy during image processing. Be aware that changing the data type to a lower format, such as byte or 8-bit (256 gray levels), permanently reduces the resolution of gray levels and eliminates the flexibility for further processing of the image. *Once a data type is converted to a lower level, the original pixel values are permanently altered and cannot be recovered.* However, in some image processing software programs, conversions to a lower size format, such as 8-bit, might be required for certain processing operations. Most programs allow one to save image files in a variety of different data types. Finally, the data types used for processing should not be confused with common file formats, such as TIFF, PNG, PIC, JPEG, BMP, GIF, and so on, commonly used for storage of files in a compressed format, import of files into other programs or transmission to other computers.

HISTOGRAM ADJUSTMENT

Nearly all images require adjustments to the LUT, or alternatively, to the image histogram in order to optimize brightness, contrast, and image visibility. Image processing programs vary in their implementation of how this is performed. In some programs, such as Photoshop (Adobe), adjusting the histogram (the *Levels* command) changes the values of pixels in the image file. In Photoshop, original gray-level values are lost once a file is saved, and cannot be recovered. When a histogram-adjusted file is reopened, a new histogram appears, reflecting the changes made in the previous *Levels* command, not the data in the original image file. In most acquisition and processing programs for microscopes, adjusting the LUT changes the appearance of the displayed image, but does not alter pixel values in the image file. When a LUT-adjusted file is reopened, all of the original pixel values are displayed in a window showing the original histogram overlaid with the existing LUT function curve. Because it is not known if a file might become damaged during processing, it is important to maintain a backup of the original

image file and to understand how individual programs operate before applying brightness/contrast or other adjustments.

The histogram is an invaluable tool that allows for examining the range and relative distribution of pixel values at a glance and for adjustment of the output display of the image on the monitor. An *image histogram* is a plot showing input pixel values on the *x*-axis versus the number or relative number (frequency) of pixels for any given value of *x* on the *y*-axis (Fig. 18.1). The numeric range of input values on the *x*-axis usually corresponds to the bit depth of the acquired image (0–255 for 8-bit images, 0–4095 for 12-bit images, etc.). For teaching purposes, Figure 18.1 and the following figures show

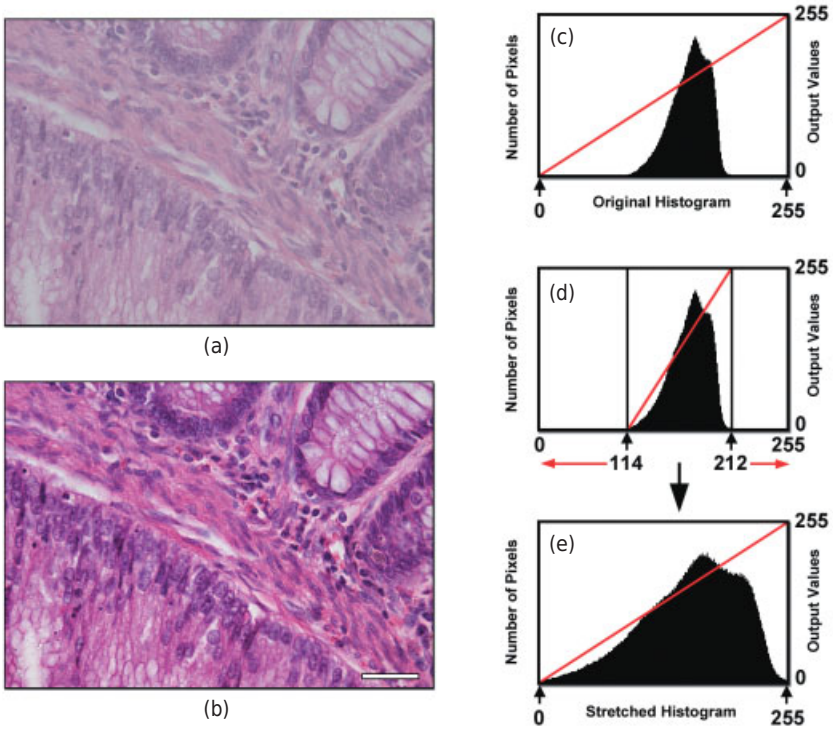

Figure 18.1

Stretching the image histogram to improve contrast. (a) Image display of human intestinal tissue stained with eosin and hematoxylin before adjustment. (b) Image display after adjustment. (c)–(e) The *y*-axis (left) shows the number of pixels of value *x* in the histograms, and the *y*-axis (right) shows the output values given by the LUT, while the *x*-axis shows the original pixel values acquired in the image. When shown on a full 8-bit scale ranging from 0 to 255, the image has low contrast (a). After histogram stretching, contrast is increased (b). In this case, the white set was adjusted to 212 and the black set to 114 (d), causing values above and below these values to be shown as white and black. Stretching allows image pixels to span all 256 gray levels, ranging from black (0) to white (255) on the monitor. In software programs, such as Photoshop, histogram adjustment resets the range of input pixel values (e). Histograms for color images (actually a composite of individual histograms from the red, green, and blue channels) can be adjusted as a unit as shown in the figure, or color channels can be adjusted individually. Bar = 100 μm.

the image histogram overlaid with the LUT function. As an image processing tool, the interactive LUT or interactive histogram allows you to increase or decrease the white-set and black-set values or change the value corresponding to mid-level gray. The handles at the ends of the function line are moved to define the white and black set points. Moving the handles (shown as arrows beneath the x-axis) to new locations on the histogram changes the brightness and contrast of the image (Fig. 18.1). To increase contrast, the handles are moved closer together. All pixels with values greater than the white set point are displayed as white, and all values lower than the black set point are displayed as black. All intermediate values are assigned a gray-level value according to their distribution along the LUT display function. Moving the handles closer together to increase image contrast is called *histogram stretching*, because the act of selecting new black and white set points for a middle range of gray values effectively stretches the desired portion, from black to white. In effect, the user has now defined a new LUT that the computer uses for displaying the image. To brighten or darken an image, the white and dark set handles are moved, respectively, to the left or to the right.

Before making any adjustments, the user should first become familiar with the image by determining the pixel values and locations on the image histogram corresponding to various regions in the specimen, including shadows (or the dark background in the case of fluorescence images), bright features (called *highlights*), and other important features of intermediate intensity. This is done by moving the cursor over different regions of the image and reading the corresponding numeric values from a statistics or status window. Knowledge of the intensities of different specimen features and their position in the histogram will allow the user to act more judiciously and conservatively in selecting the black and white set points to be used in histogram stretching. This is also a good time to check the image for indications of *clipping*, the appearance of saturated white or underexposed black areas in the image. Clipping must be avoided, both during acquisition and during processing. With this knowledge in mind, the operator then sets the handles on the histogram. An objective and conservative approach is to include all of the pixel values representing the specimen within the upper and lower set points. It is useful to remember that human vision cannot distinguish all of the 256 grayscale values that might be present in an 8-bit image, let alone an image with a deeper bit depth. Therefore, as the situation demands, you are justified in altering the display by histogram stretching to see internal details. Guidelines on the use of histogram stretching are presented in later in this chapter.

There are several ways of displaying the image histogram. The standard or regular histogram has already been described and is shown in Figure 18.2a. A *logarithmic histogram* shows the input pixel value (x-axis) versus the number of pixels having that value on a log scale on the y-axis. This type of display is useful when it is necessary to see and consider pixel values that comprise just a minority of the image and exhibit a strong response to histogram stretching (Fig. 18.2b). Logarithmic histograms should not be confused with a logarithmic LUT, which uses logarithmic scaling to display the image itself.

Another useful histogram display is the *integrated* or *cumulative histogram,* which can be convenient for adjusting the contrast and brightness of certain images (Fig. 18.2c). This histogram display is more useful for phase contrast, differential interference contrast (DIC), and brightfield images that tend to have light backgrounds than it is for dark fluorescence images, which typically include a wide range of intensities. In this histogram, the x-axis shows the input pixel values, while the y-axis shows the cumulative number of all pixels having a value of x and lower on the x-axis. For

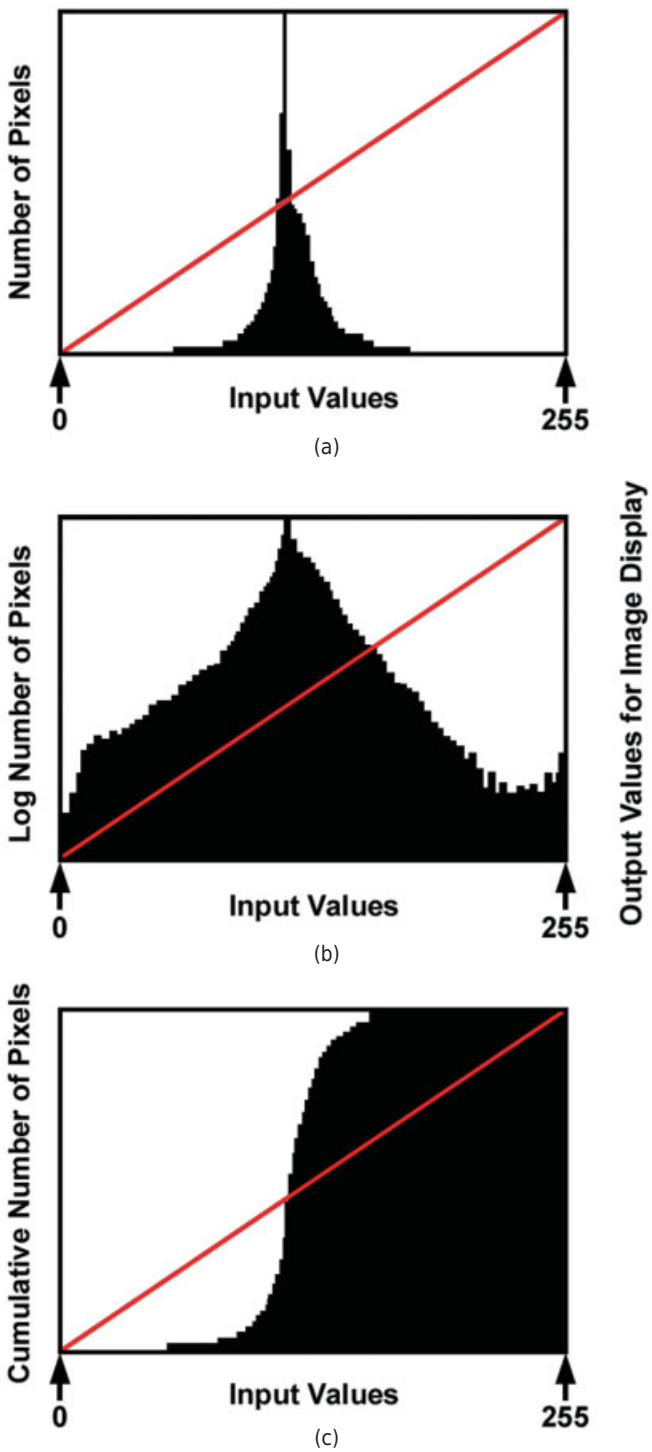

Figure 18.2

Three kinds of histogram displays. (a) The regular histogram is shown as a plot of input pixel value (*x*-axis) versus the number of pixels of value *x* in the histogram. The LUT function is shown here as a line superimposed on top of the histogram. (b) Semi-log plot shows the input pixel value (*x*-axis) versus the number of pixels having an input value of *x* on a log scale (*y*-axis). (c) Cumulative histogram showing input pixel value on the *x*-axis versus the cumulative number of pixels having an input value of *x* or lower on the *y*-axis.

relatively bright images (DIC and phase contrast microscopy), the max–min handles (white set/black set handles) are usually moved so that they define a line that is tangent to the rapidly rising slope of the histogram.

ADJUSTING GAMMA (γ) TO CREATE EXPONENTIAL LUTS

As mentioned above, LUT display functions can be linear, logarithmic, exponential, or in the case of Adobe Photoshop software, even arbitrarily curvilinear as set by the operator. Linear functions (in 8-bit format) have the form:

$$\text{Displayed Value} = 255\ (\text{Data Value} - \text{Min})/(\text{Max} - \text{Min}),$$

and are commonly used for adjusting the image display. However, linear functions present difficulties when the goal is to include *all* of the pixel values contained in the image. In some cases, such as fluorescence images, dim fluorescent features appear dark gray and seem to be lost. No linear LUT setting seems to show the full range of data satisfactorily or in the way we see the image when looking in the microscope. Partly, this is because a CCD camera is a linear detector of light intensities, whereas the eye gives a logarithmic response, allowing us to see bright objects and dim, low amplitude objects in the same visual scene. Exponential functions more closely match the nonlinear response of the eye or camera film and are created using a function with variable exponent gamma (γ) such that:

$$\text{Displayed Value} = [(\text{Normalized Value} - \text{Min})/(\text{Max} - \text{Min})]^{\gamma}.$$

With γ settings <1, low pixel values are boosted relative to high values and appear a medium gray in the image; this adjustment also reduces the contrast between bright features and the darker background. A γ setting of 0.7 approximates the response of the eye, allowing the image to more closely resemble the view we perceive when looking in the microscope. Conversely, γ values >1 depress dark and medium gray pixel values and increase the contrast of bright features. The effect of adjusting γ on the image display is shown in Figure 18.3. In Photoshop, a slider in the Levels toolbox used to define the midpoint of gray values performs an identical function. Photoshop gives you the choice of reading off a γ value corresponding to the slider's location or entering a numerical value of your own choosing for γ.

FLAT-FIELD CORRECTION

A single image prior to processing and adjustments is called a *raw image*. In many cases, raw images are suitable for printing directly, perhaps after first making some minor adjustments in brightness and contrast with the histogram. However, a raw image contains two significant kinds of noises that make it unsuitable for quantitative purposes: First, the image contains the bias signal and noise counts that increase pixel values beyond their true photometric values, which can cause significant errors in measuring the amplitudes of object features. Second, a raw image may contain numerous artifacts from the camera and microscope optical system (distortions due to detector irregularities, dust and scratches on lens surfaces, and uneven illumination) that appear

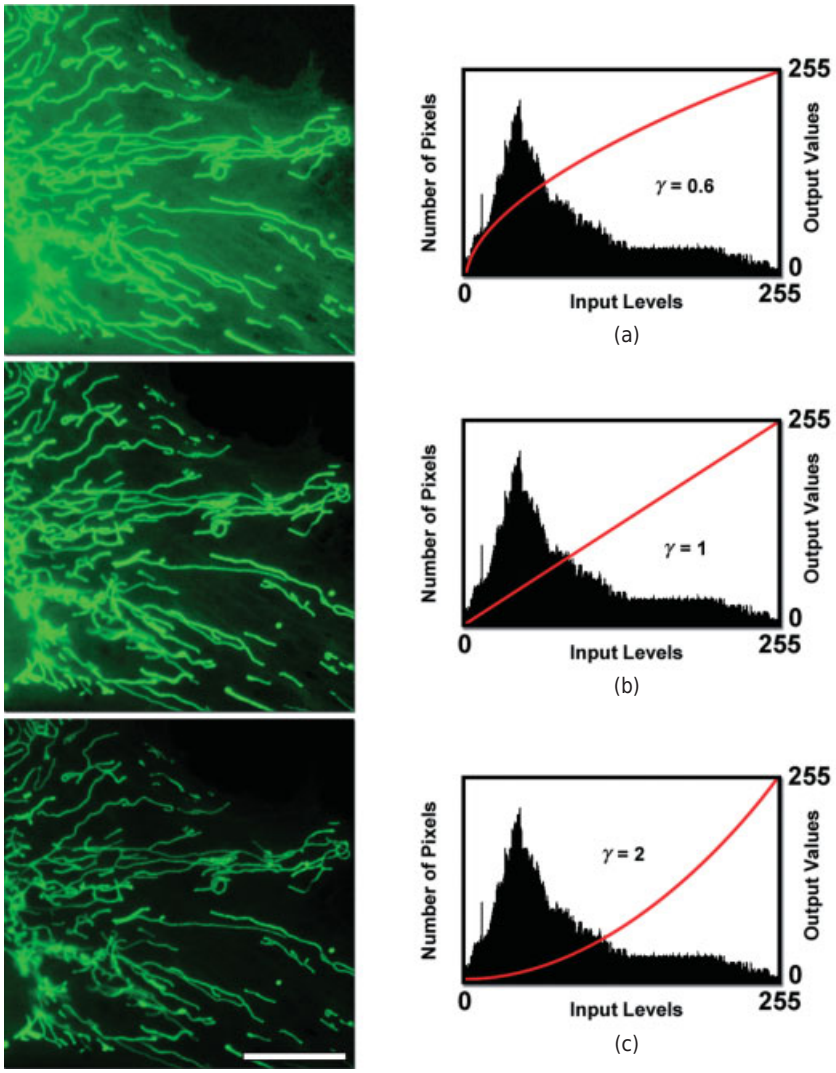

Figure 18.3

Gamma (γ) correction for differential enhancement of light and dark features. (a) Values of $\gamma < 1$ differentially enhance dark pixels in the image, causing them to look brighter, while reducing the contrast between dark and bright features in the image. (b) Values of $\gamma = 1$ are the default display setting. (c) γ-values >1 differentially suppress the dark features, accentuate bright features, and increase their contrast in the image. Contrast adjustments with γ allow you to use the entire range of pixels representing the specimen; this is distinct from contrast adjustment by histogram stretching. Bar = 10 μm.

as dark shadows and specks in the image and alter the true pixel values. These artifacts are particularly visible in images with bright, uniform backgrounds (phase contrast, DIC) and in fluorescence images with medium gray or bright backgrounds. In order to restore photometric accuracy and remove the defects, the raw image must be adjusted by an operation known as *flat-field correction* (Gilliland, 1992; Howell 1992; Marty 2007). Only corrected images are suitable for measuring light amplitudes. Although

flat-field correction is not required to display or print an image, it is very effective in removing disfiguring faults, so the procedure is widely used for cosmetic purposes as well. As shown in Figure 18.4 and described here, the correction procedure requires three frames:

- A *raw frame* contains the image signal plus signals from optical defects and electronic and thermal noises.
- A *flat-field frame* is the image of a smooth featureless field without the specimen, and, if possible, is made at the same focal point as the raw frame. Flat frames should be bright and utilize the full dynamic range of the camera in order to minimize the noise in the final corrected image. If both the raw and flat-field frames are dim and noisy, the final processed frame will be very noisy indeed. This situation is particularly relevant to fluorescence imaging. Therefore, the exposure time for a flat-field frame might be longer than that used for producing the raw image itself. To reduce noise in this frame, a master flat-field frame should be prepared based on the average of 9–16 successive images captured under the same conditions. In fluorescence microscopy, the flat-field frame can be the image of a uniform field of a fluorescent dye. This can be prepared by streaking a drop of fluorescein-conjugated protein or dextran across the surface of a coverslip, allowing it to dry, and then preparing a permanent reference slide using a drop of ProLong or SlowFade (Life Technologies) or other antifade reagent. Although prepared for a certain dye, such as fluorescein, the flat-field frame is valid for a number of different filter sets and is useful for days until such time that the light source has been refocused or changed, after which a new master flat-field frame should be prepared. Several filter companies, such as Chroma Technology Corp., market autofluorescent plastic slides in colors ranging from blue to red, which are useful for flat-field correction.
- A *dark frame* contains the bias signal plus the electronic and thermal noise components that are present in the image. Bias counts are from the positive voltage applied to the CCD as required for its operation; electronic noises include the components contributing to the readout noise of the camera; thermal noise is due to the kinetic vibration of silicon atoms in the chip. At full and one-quarter saturation of a scientific grade CCD camera, the bias count and noises may contribute roughly 5 and 20% of the apparent pixel amplitude, respectively, and must be subtracted from the flat-field frame and the raw frame to restore photometrically accurate pixel values. Dark frames are prepared using the same exposure time as the raw image, but without opening the shutter. Since dark frames have low signals, a master dark frame should be prepared by averaging 9–16 dark frames together.

The equation for flat-field correction is:

$$\text{Corrected Image} = M[(\text{Raw}) - (\text{Dark})]/[(\text{Flat}) - (\text{Dark})],$$

where M is the mean pixel value in the raw image. The multiplication by M simply keeps the intensity of the corrected image similar to that of the original raw image. In applying the correction, the order in which the operations are performed is important. The dark frame must be subtracted from the raw and flat frames first, followed by the

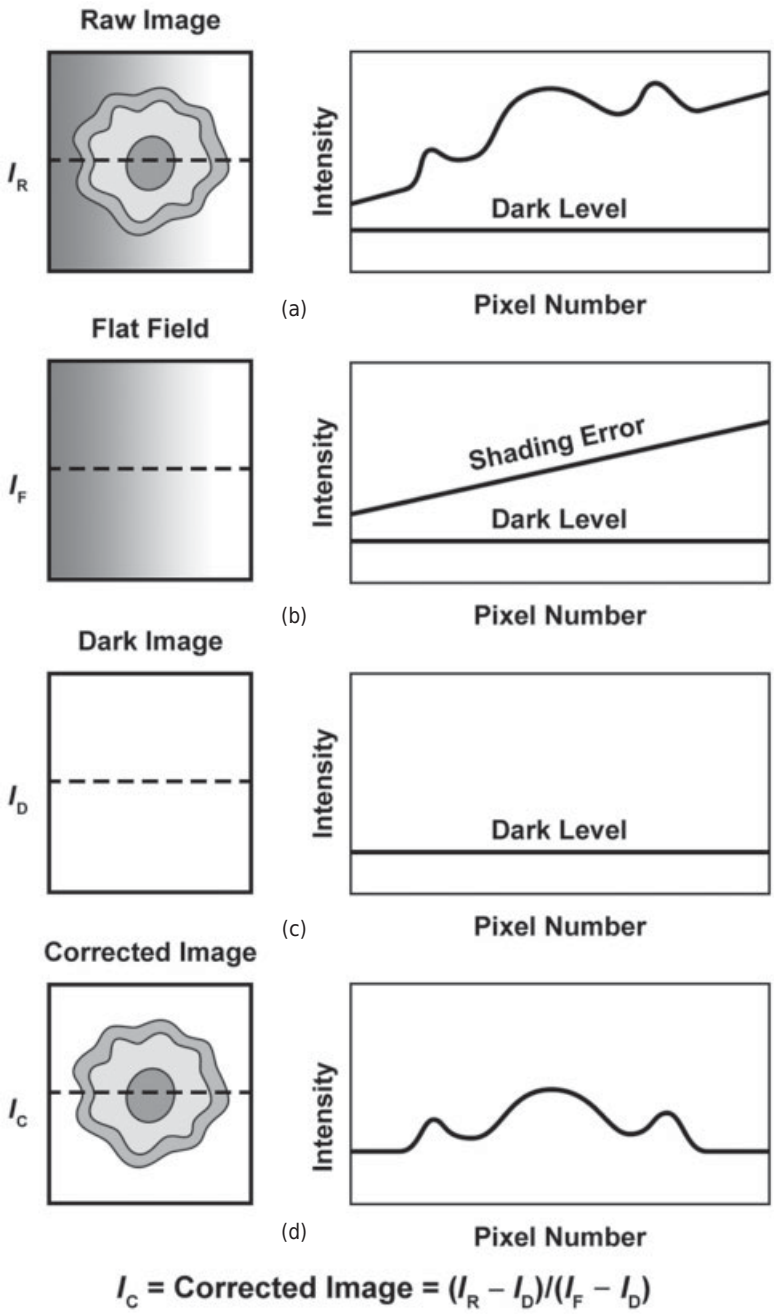

Figure 18.4

Sketch showing the strategy for performing the flat-field correction of a raw image. The pairs of figures show the image and an intensity plot (dotted line) across its diameter. (a) The raw image shows a central object with shading error across the background; the intensity profile shows the irregular profile of the object, an overall slope due to shading error, and an overall boost in the signal due to the dark level. (b) The flat-field image is from a featureless background region in the specimen. (c) The dark image, a uniform, blank frame, contains the bias and read noise of the camera. (d) The correction equation is applied as follows: The dark image is subtracted from both the raw and flat images before dividing the corrected raw image by the corrected flat image. The final corrected image is shown with uneven illumination and dark-level contribution removed. The final image is usually multiplied by a factor (M), the mean pixel value in the raw image, to brighten the image as a convenience for viewing.

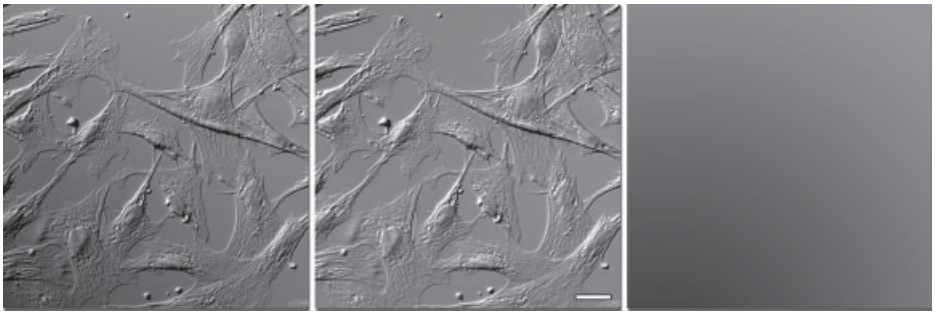

(a) (b) (c)

Figure 18.5

Example of raw and flat-field corrected CCD images. (a) Raw image. (b) Corrected image. (c) Flat-field frame. Notice that optical faults from uneven illumination are removed. The specimen is a culture of living Indian Muntjac cells imaged with DIC optics. Bar = 20 μm.

division of the dark-subtracted raw frame by the dark-subtracted flat frame. The correction is performed in floating point data type to preserve numeric accuracy. To be seen optimally, the brightness and contrast of the corrected image may need to be adjusted. The visual effect of flat-field correction can look similar to that obtained by background subtraction, but performing the correction by division is more accurate. This is because light amplitudes in an image result from a multiplicative process (luminous flux multiplied by exposure time). Once corrected, the relative amplitudes of objects in the image will be photometrically accurate. Surprisingly, the corrected image lacks the optical defects that were present in the raw image. An example of a flat-field corrected image is shown in Figure 18.5. Practice in performing this correction is included as an exercise at the end of this chapter.

IMAGE PROCESSING WITH FILTERS

Filtering is used to sharpen or blur an image by *convolution,* an operation that uses the weighted intensity of neighboring pixels in the original image to compute new pixel values in a new filtered image. A matrix kernel of numbers (the *convolution matrix*) is multiplied against each pixel covered by the kernel, the products are summed, and the resulting pixel value placed in a new image. Only original pixel values are used to compute the new pixel values in the processed image. The *kernel* or *mask* can have different sizes and cover a variable number of pixels such as 1×3, 3×3, 4×4, and so forth. Note that the sum of the numbers in the kernel always adds up to 1. As a result, the magnitude of the new computed pixel value is similar to the group of pixels covered by the kernel in the original image. After a pixel value has been computed, the kernel moves to the next pixel in the original image, and the process is repeated until all of the pixels have been read, after which the new image is displayed on the screen (Fig. 18.6). For a megapixel image, the process can take several seconds. Linear filters are used for smoothing, sharpening, and edge enhancement. The filters menu in the image processing software usually provides several kernel choices for any given operation. These filters are sensitive, so there can be some difficulty is controlling the amount

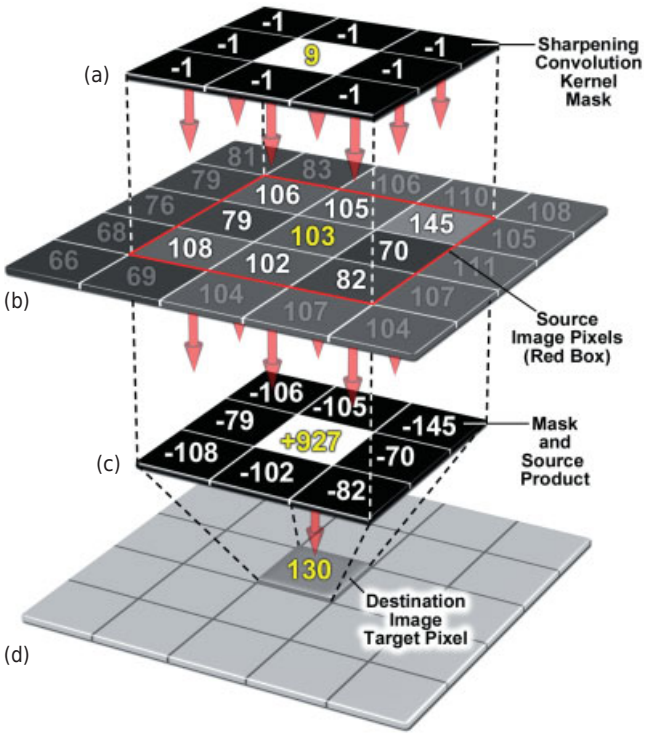

Figure 18.6

The operation of a convolution matrix in a sharpening filter. The matrix in this example has numeric values covering a 3 × 3 pixel area (a). A kernel or mask containing these values is multiplied against the values of 9 pixels covered by the mask in the original image (red box) (b), a process called convolution. The resulting nine products (c) are summed to obtain a value that is assigned to the central pixel location (yellow number) in the new filtered image (d). The kernel then moves by 1 pixel to calculate the next pixel value, and the process repeats until all of the pixels in the original image have been recalculated. Notice the values in the convolution matrix used for sharpening. The central value is emphasized (matrix value 9) relative to the eight surrounding values. The sum of the values in the matrix is 1.

of filtering, with some filters giving overfiltration, and others producing only a minimal effect. Therefore, most image processing programs also allow you to create your own convolution matrix, in case the menu selections are inappropriate. With practice, you will learn to select a particular filter based on the intensity gradients and size dimensions of the detail needing adjustment in the image.

Lowpass Filter for Blurring

This filter removes high spatial frequency details, such as sharply defined intensity transitions at the edges of objects in the image (Fig. 18.7a). It blurs by partially leveling the values of pixels in a small pixel neighborhood. A low-pass filter has the effect of passing or minimally altering low-spatial-frequency components (large features in the image), hence its designation as a lowpass filter and can make cosmetic improvement to grainy, low S/N images but at the expense of reduced resolution.

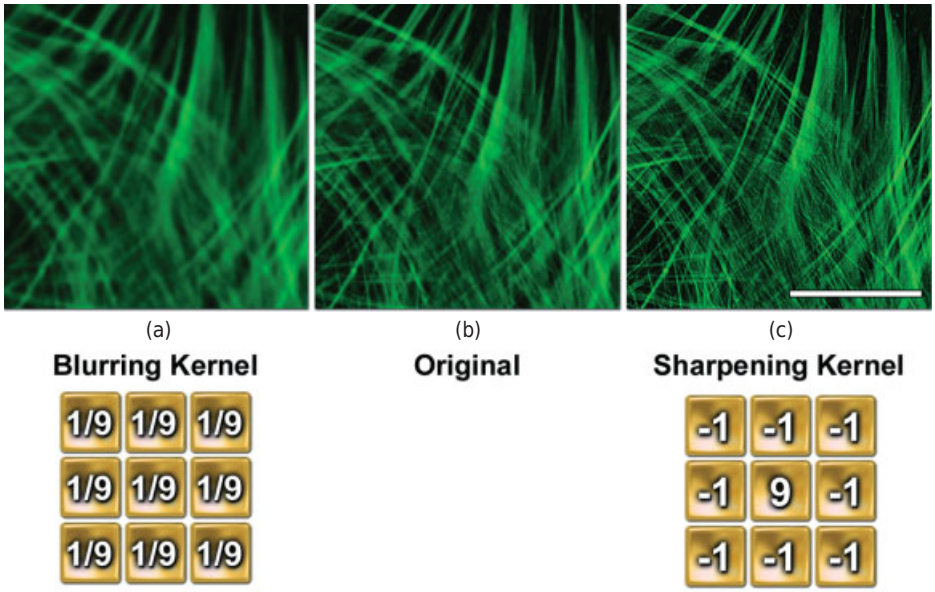

Figure 18.7

Convolution filters for blurring and sharpening. The figure shows the effects of applying blurring and sharpening filters and the corresponding convolution kernels that were used. (a) Blurred. (b) Original. (c) Sharpened. The specimen is a culture of Indian Muntjac deer skin fibroblast cells labeled with Alexa Fluor 488 conjugated to phalloidin to highlight the filamentous actin network. Alexa Fluor dyes are available from Life Technologies. Bar = 10 μm.

Highpass Filter for Sharpening

High-pass filtering differentially emphasizes fine details in an image and is an effective way to sharpen soft, low-contrast features in an image. The effect of sharpening and the pattern of a strong sharpening kernel are shown in Figure 18.7c. Unfortunately, this filter also emphasizes noise and can make an image look grainy.

Median Filter

The median filter reduces noise and smoothes out pixel values with respect to the values of neighboring pixels (Fig. 18.8). It is very effective at removing noise, faulty pixels, and fine scratches. A median filter can be more effective than a low-pass filter in reducing noise. Like all linear filters, a median filter uses a kernel or cluster of pixels (the dimensions determined by the operator) that moves in linear fashion, pixel by pixel and row by row across all of the pixels in the image. For this filter, there is no convolution matrix as such. At each successive pixel location, the original pixel values covered by the kernel are rank ordered according to magnitude, and the median value is then determined and assigned to the central pixel location in a new filtered image. In the following example using a kernel size of 3×3, the central noisy pixel with a value 20 in the original image becomes 7 in the new filtered image:

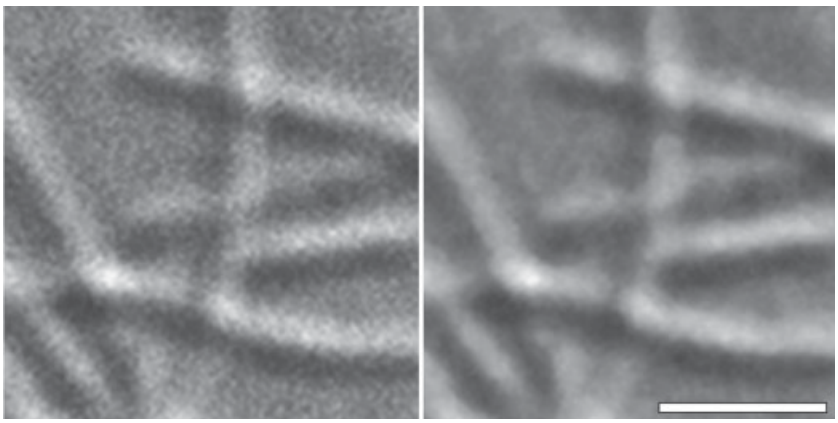

(a) (b)

Figure 18.8
Median filter for removing noise. Highly magnified CCD image of a field of microtubules in DIC microscopy. (a) The original image was acquired at the full 12-bit dynamic range of the camera, but looks grainy after histogram stretching due to photon noise. (b) The same image after applying a median filter with a 3×3 pixel kernel shows that much of the graininess has been removed. The S/N ratio of the original could have been improved by averaging a number of like frames at the time of acquisition. Bar = 300 nm.

Pixel values covered by 3×3 kernel in the original image	**Rank order of pixels**	**Median pixel value assigned to central pixel in new image**
6 6 4 5 20 7 7 8 9	4, 5, 6, 6, 7, 7, 8, 9, 20	7

Histogram Equalization

Most image processing programs have an "equalize contrast" function that reassigns pixel values so that each gray level is represented by the same number of pixels. The process, called *histogram equalization* or histogram leveling, yields a histogram that contains no peaks and has a flat, horizontal profile. In leveling, pixel values are reassigned so that each gray level is given the same number of pixels, while the rank order of the pixel values in the original picture is preserved as much as possible. This operation is used to enhance contrast in very low contrast (flat) images where most of the pixels have close to the same value, and where conventional methods of histogram stretching are ineffective. Equalization is an extreme measure to rescue images with low-amplitude gradients, which can look nearly featureless. The effect of histogram equalization is often dramatic.

Unsharp Masking

This popular image processing procedure does an excellent job of enhancing fine details in an image. Unsharp masking is well known to photographers and astronomers who

originally used the method as a darkroom technique to enhance faint details in photographic prints. In photography, a blurred, reverse-contrast negative (or unsharp mask) is made of the original negative. The two negatives are sandwiched together in perfect registration in the enlarger and a print is made. To perform this operation on a computer, an unsharp mask is produced by blurring and reducing the amplitude of the original image; the unsharp mask is then subtracted from the original to produce a sharpened image. Extended, uniform regions are rendered a medium gray, whereas regions with sharp gradients in amplitude appear as brighter or darker intensities. The principle of unsharp masking is shown in Figure 18.9, and an example of a microscope image processed by this method is shown in Figure 18.10. If the program you are using does not perform unsharp masking, you can perform this operation manually using the following steps:

- Prepare a copy of the original and blur it with a conservative blurring filter. Images with fine details (high spatial frequencies) require more conservative blurring than images containing big blocky objects (low spatial frequencies).
- Subtract 50–95% of the amplitude of the blurred image from 100% of the original using an image math function in the program. The higher the percentage that is subtracted, the greater the sharpening effect.

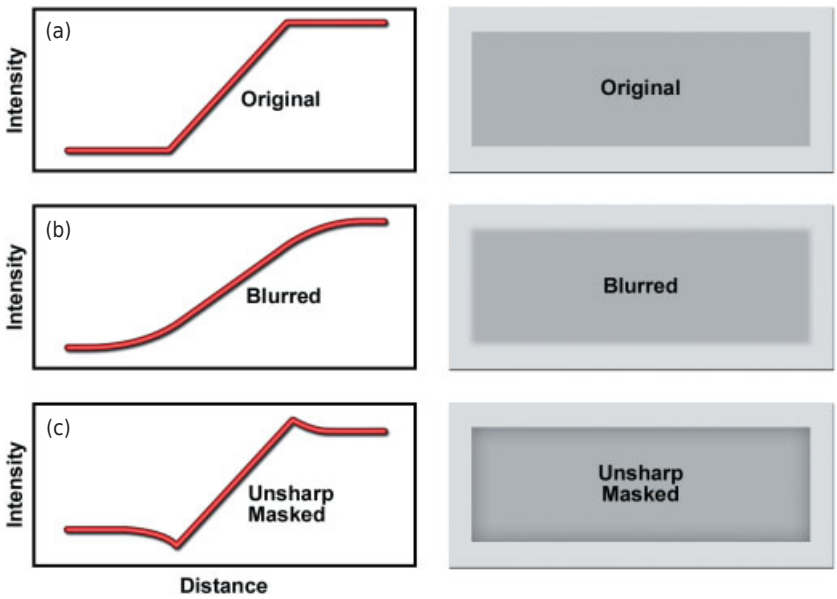

Figure 18.9

The strategy of unsharp mask filtering for image enhancement. Three intensity plots (left) show a boundary between two regions of different light intensity as depicted by the edge of the grayscale rectangles (right). (a) The original image profile. (b) A blurred version of the original. (c) An unsharp mask-corrected version prepared by subtracting 50% of the blurred profile from the original profile. Notice that the small negative and positive spikes in the unsharp mask plot are seen as bright and dark edges in the bottom drawing. The amount of sharpening depends on the amount of blurring, the amount of amplitude reduction created by subtraction of the blurred image, and the amount of subsequent histogram stretching.

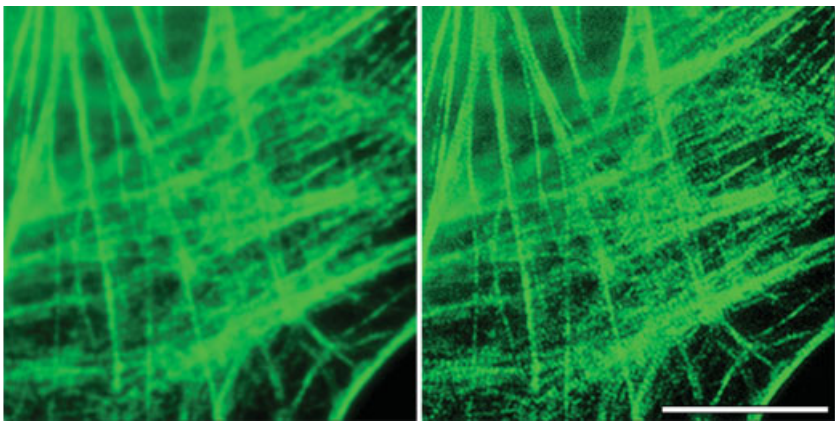

(a) (b)

Figure 18.10

Unsharp masking emphasizes object details. The figure shows the effect of unsharp masking on a pseudocolored (green) image of HeLa cells expressing a fusion of mEmerald (a high-performance EGFP derivative) to human myosin IIA. (a) Bright fluorescence of the myosin IIA filaments in the original image hides the periodic striations typically seen in motile cells. (b) Unsharp masking enhances details and differentially emphasizes faint structures. Bar = 10 μm.

- Using histogram stretching, adjust the brightness and contrast in the difference image.

Fast Fourier Transform (FFT) Filtering

This sophisticated filtering operation selectively diminishes or enhances low or high spatial frequencies (extended vs. finely detailed structures) in the specimen image. FFT is a valuable operation to consider, because it reinforces concepts described in previous chapters on the location of high and low spatial frequency information in the diffraction plane, which is located in the objective rear aperture in the microscope. The effect is similar to that of the blurring and sharpening filters already described, but can be made to be much more specific due to an operation called spatial frequency filtering (Fig. 18.11). When an image is transformed into the so-called frequency domain through an FFT command, the information is represented in two plots (images), one containing a distribution of magnitudes (amplitudes) and the other a distribution of phases. The relation of the image to its Fourier transform is analogous to the relation of images in the image plane and diffraction plane (rear aperture of the objective) of the microscope. To review these concepts, refer to Chapters 5 and 15. The FFT operation is performed in a high-resolution data type, such as floating point. Usually, only the amplitude (or magnitude) plot is used for display and manipulation. Most image processing programs display the amplitude or power spectrum with a log rather than a linear scale, since the transform is otherwise too dark to see anything. Depending on the program, histogram stretching and γ scaling can be applied to improve visibility of the amplitude plot without affecting the data. In a Fourier transform:

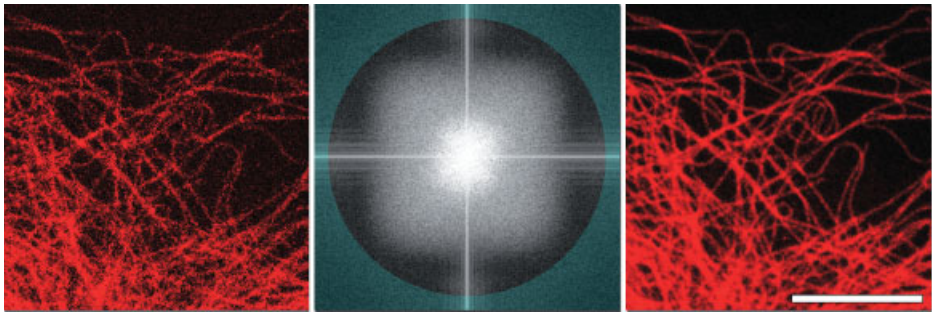

(a) (b) (c)

Figure 18.11

Fast Fourier transform is used for processing in the spatial frequency domain. (a) The original fluorescence image of microtubule filaments labeled with Alexa Fluor 568 (pseudocolored red) is grainy. (b) Fourier transform of panel a. (c) The same image after processing the Fourier transform using the cyan mask in panel b to eliminate high spatial frequency information. The procedure reduces the graininess but does not alter the coarse structure of the filaments. Bar = 5 μm.

- Frequency information is represented at different distances from the central point in the magnitude image, such that information from large structural features (low spatial frequencies) is found near the center of the image, and information from small features (high spatial frequencies) is located at some distance away from the center.
- Amplitudes seen along one axis in the magnitude plot are represented in the image on an axis shifted by 90°.
- The amplitude at each location in the magnitude plot is proportional to the amount of information at that frequency and orientation in the image.

On the computer, one performs a FFT transformation and obtains a pair of amplitude and phase plots. The next step is to apply an occluding spatial frequency mask over one of the plots (the amplitude plot) to select low, midrange, or high spatial frequencies and block out unwanted frequencies. The masked plots are then used to produce an *inverse transform*: an image that is recreated based on frequencies not occluded by the mask. Both the magnitude and phase plots are required for this operation. Processing images in the frequency domain is useful for:

- Removing noise that occurs at specific frequencies (electrical interference and raster scan lines).
- Enhancing or removing periodic structural features of the object.
- Identifying spatial frequencies of defined structures in an image.
- Determining the periodicity and/or orientation of indistinct features that are difficult to see in the object image.
- Detecting optical aberrations, such as astigmatism.
- Applying convolution kernels to the magnitude plot for sharpening or blurring.

SIGNAL-TO-NOISE RATIO

Signal-to-noise ratio represents the ratio of a signal to the surrounding background noise from which the signal must be distinguished. It is the universally accepted parameter for describing image quality. As we shall see, S/N also has statistical meaning because it describes the confidence level (α-value) at which a feature having a specific intensity can be distinguished from the background. In qualitative terms, S/N values are used to describe the visibility of an object in an image. For reference, Figure 18.12 shows a test pattern of gray squares whose visibility is shown to vary depending on S/N. Everyone using a scientific-grade camera for quantitative purposes should understand the meaning of S/N, be able to calculate it, and be familiar with its use. Using S/N theory, you can:

- Provide a quantitative description of image quality. S/N is the accepted parameter for describing the visibility and clarity of an object in an image and for comparing the quality of images amongst themselves.
- Determine the probability that a faint signal is distinct from the background. This might occur if you were comparing changes in the fluorescence intensity in response to an experimental condition and wanted to determine if a change in fluorescence was statistically significant.
- Calculate the minimum exposure time required to obtain a signal within a certain confidence level. Your goal is to obtain smooth kinetic data to within 10% precision to accurately determine the halftime of fluorescence recovery from an image sequence; however, it is also important to keep the exposure time to a minimum to avoid photodamage. Cosmetically attractive images require long exposures that can kill a living cell but are not necessary for quantitative work. S/N can be used to determine the minimum exposure time required to give an image passing the required criteria.

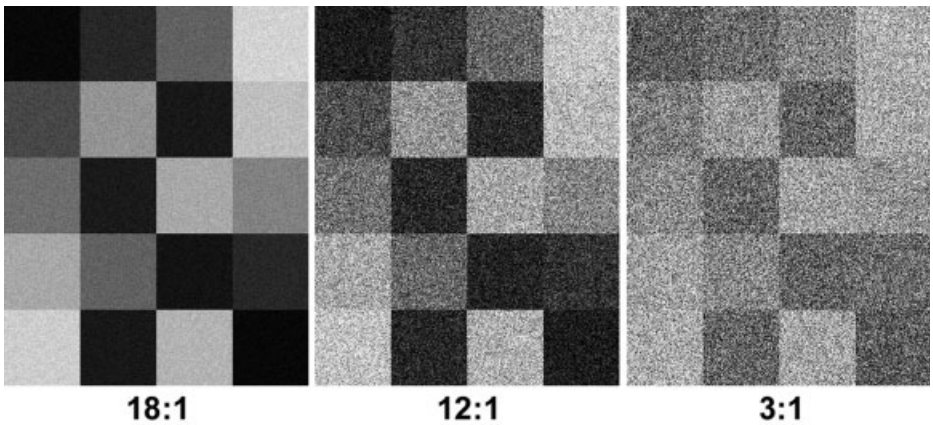

Figure 18.12
Effect of S/N ratio on the visibility of a test pattern. A checkerboard test pattern with squares of varying intensity is shown at different S/N ratios. At S/N ratios below 3, transitions between certain adjacent gray-level steps are difficult to see.

- Evaluate camera performance, which is important when selecting a camera for purchase.

Excellent descriptions of the application of S/N theory to quantitative image analysis have been presented by several authors, including Christenson (2005), Russ (2011), Sheppard et al. (2006), and Murray et al. (2007). The earlier literature also contains excellent articles by Newberry (1991), Gilliland (1992), and Howell (1992).

Definition of S/N Ratio

It is easy to determine the S/N of an object in a digital image, but before we do, we will first examine the definition of S/N and its component terms. Formally, the S/N ratio is obtained by dividing the sum of components contributing to the signal by the square root of the sums of the variances of the various noise components. If the noises are independent of each other, they are added in quadrature ($N_1^2 + N_2^2 + N_3^2 \ldots$), and the noise is shown as the square root of this term:

$$\mathrm{S/N} = (S_1 + S_2 + S_3 \ldots)/\sqrt{(N_1^2 + N_2^2 + N_3^2 \ldots)}.$$

In digital microscopy, the principal signal components are the photoelectrons corresponding to the object and underlying background, and bias and thermal signals; the principal noises are the photon noises of these signals (see below), and the camera readout noise (for which there are several independent sources; see Chapter 17). We will recognize this general form of the equation in descriptions of practical solutions. Two additional points should be noted: (1) the statistics of photon counting are based on the number of photons converted to electrons by the detector, and correspondingly, S/N is always calculated in electrons (never in terms of analog-to-digital units, which are the numeric values assigned to pixels in digital images). The electron equivalent of an ADU is given as ADU x gain, where gain is the number of electrons per digital unit. (2) S/N statistics can be applied on a per pixel basis for describing equipment performance, or to a group of pixels when describing an extended feature in an image.

Photon Noise

Because the number of photons recorded by the camera over a discrete interval of time and space is stochastic, the accumulation of photoelectrons is described by a Poisson distribution. If the photon signal is large, as it is for most microscope images, the principal noise is *photon noise* (also called the *shot noise*), which is described as the standard deviation of the signal amplitude in photoelectrons. For a Poisson distribution, the standard deviation (and therefore the photon noise) is simply the square root of the signal. Thus, for a fluorescence microscope signal of 10,000 electrons, the photon noise = ✓10,000 = 100 electrons. The fact that the photon noise is the square root of the signal explains why S/N must be calculated in terms of electrons, not in ADUs. Several additional points are worth noting:

- An image is considered to be *photon-limited* if the photon noise of the specimen signal is greater than the camera read noise. For a CCD camera with 15 e^- read

noise, this occurs when the corrected photon count from the specimen reaches ~225 e^- (~20 ADU/pixel), since at this level the photon noise is $\checkmark 225$ or 15 e^-, the read noise of the camera. Because microscope images are relatively bright, most images are usually photon limited, and the following discussion is based on this assumption.

- Under photon-limited conditions, the S/N ratio increases as the square root of the exposure time or the square root of the number of frames. Thus, increasing the exposure time by 4 or averaging four similar frames increases the S/N ratio twofold. The poor S/N of a dim image can be greatly improved by simply increasing the exposure time. For this reason, images should be acquired so that the brightest features in the image approach the saturation level of the camera (see Chapter 17). This relationship also explains why the S/N of confocal images can sometimes be dramatically improved by averaging replicate scans.
- For microscope images where the visibility of an *extended specimen* is of interest, the S/N ratio can be calculated based on dozens or even hundreds of pixels and not on a per pixel basis. In this case, a feature covering a large patch of pixels can have an S/N value that is hundreds of times larger than the S/N of an individual pixel. Formulas for determining the S/N of extended objects are given in this chapter.

S/N and the Precision of Numeric Values

One valuable benefit of S/N analysis is that one can state the confidence limits (in units of standard deviations) that a signal stands out from the noise of the background. This calculation is possible because the S/N ratio is the ratio of the object signal to the standard deviation of the background signal and because standard deviations are directly related to α-values and percent confidence. Consider an image with a specimen signal of 100 electrons and a noise of $\checkmark 100 = 10$ e^-, giving an S/N ratio of 10. The inverse of this value, N/S = 0.1, is called the *relative error*—that is, the fractional component of the signal that is noise. For our example, we would say that noise is 0.1 or 10% of the signal. Since photon noise is the same as the standard deviation (SD) of the photon signal, we can say that fluctuations in the signal greater than 10% can be detected at a confidence level of 68% (1 SD). Extending this further, by multiplying by 2 for two standard deviations, we would say that fluctuations in the signal >20% are detected at the 95% confidence level (2 SD), and so on. Another way of interpreting this is to say that given a relative error of 0.1, we can say we detect a signal at 10% precision, or that our ability to measure the signal precisely is no better than 10%. The ability to set confidence limits has profound implications, because it allows the investigator to calculate in advance how many electrons (and therefore how many ADUs and what exposure time) are required to visualize fluctuations of a certain percent at a specified confidence level.

In summary, given S/N = 10, taking $(1/S/N) \times 2\ SD \times 100 = 20\%$, we say that fluctuations >20% are detected at the 95% confidence level.

Correlation of S/N Ratio with Image Quality

The relationships between S/N, percent fluctuations detected at 95% confidence, and image quality are given in Table 18.1. A specimen image with S/N = 10–20 is poor and

TABLE 18.1 S/N Value and Image Quality[a]

S/N ratio	% Fluctuations at 95% Confidence	Visual Image Quality
3	67	Visual limit of detection
10	20	Coarse and grainy, barely acceptable
20	10	Fine grain very obvious
30	7	
40	5	Okay to good
50	4	
100	2	Excellent
200	1	
400	0.5	
2000	0.1	
20,000	0.01	

[a] Values for S/N are given on a per pixel basis.

Table 18.2 Effect of Background Signal on S/N[a]

Total Signal (e^-/pixel)	Background/Total %				
	10	25	50%	75	90
43	24	20	13	7	3
171	79	65	44	22	11
685	206	171	114	48	29
2675	447	372	249	123	50
10,700	921	768	512	256	102
42,800	1857	1547	1031	576	206

[a] S/N values are shown for various combinations of signal strength and percent of signal contributed by the background. S/N values were calculated for a 100-pixel object and a CCD with a capacity of 42,800 e^-/pixel using Newberry's equation.

grainy looking, whereas the appearance of the same specimen at S/N > 100 is good to excellent.

Effect of the Background Signal on S/N

In microscopy, the background signal can be large, sometimes >90% of the total signal representing an object. Figure 11.12 in Chapter 11 demonstrates the significance of the background signal in an immunofluorescence image. *In most cases, photon noise from the background is the major source of noise, not the read noise of the camera*. Thus, the S/N equation includes a term for the background noise as will be recognized in the following sections. As seen in Table 18.2, a high background signal reduces the S/N considerably.

Quick Estimate of the S/N Ratio of a Single Object Pixel in a Digital Image

The following procedure yields good approximate values of S/N for most images of moderate to bright magnitude where the noise is photon limited. The measurement gives S/N for a single specimen pixel. You will need to look up the electron gain (photoelectrons/ADU) in the camera's operating manual, because the calculation must be performed in units of electrons, not ADUs. Since the camera's gain varies depending on MHz operating speed of the camera, be sure to pick the gain that was used at the time of image acquisition. Figure 18.13 demonstrates the concept of this approach.

- Perform flat-field correction to obtain an accurate image. Alternatively, acquire a dark frame, then determine the average ADU value of the frame, and use an image math function in software to subtract this value from all of the pixels in the raw image (see flat-field correction previously discussed).
- Determine the ADU value of a specimen pixel. Since the specimen signal is usually the sum of specimen and underlying background counts, the background must be subtracted from the total to obtain the specific object counts (ADUs). The specimen signal S in electrons is described:

$$\mathrm{S} = \text{specimen-specific ADUs} \times \text{electron gain}.$$

- Use the region of interest (ROI) tool to select a group of several hundred background pixels, and use the *Analyze Statistics* function to determine the standard deviation of the background sample mean in ADUs. The photon noise N of the background is given as:

$$N = \sqrt{(\mathrm{SD}^2 \times \text{gain})}.$$

- Calculate S/N.

Newberry's Analytical Equation for S/N

The following S/N equation should be used when it is necessary to obtain an accurate determination of S/N. This equation should only be applied to flat-field corrected images. See Newberry (1991) for details. The analysis equation reads:

$$\mathrm{S/N} = \frac{\sqrt{C_o}}{\sqrt{(1/g) + (n\sigma^2 / C_o) + (n\sigma^2 / pC_o)}},$$

where

C_o = total object counts in ADU where $C_{specimen} = C_{total} - C_{background}$;
$\sqrt{C_o}$ = object noise in ADU;
n = number of pixels in measured object area;
p = number of pixels in measured background area;
σ^2 = variance of background pixels as $(SD)^2$ in ADU; and
g = gain (electrons/ADU).

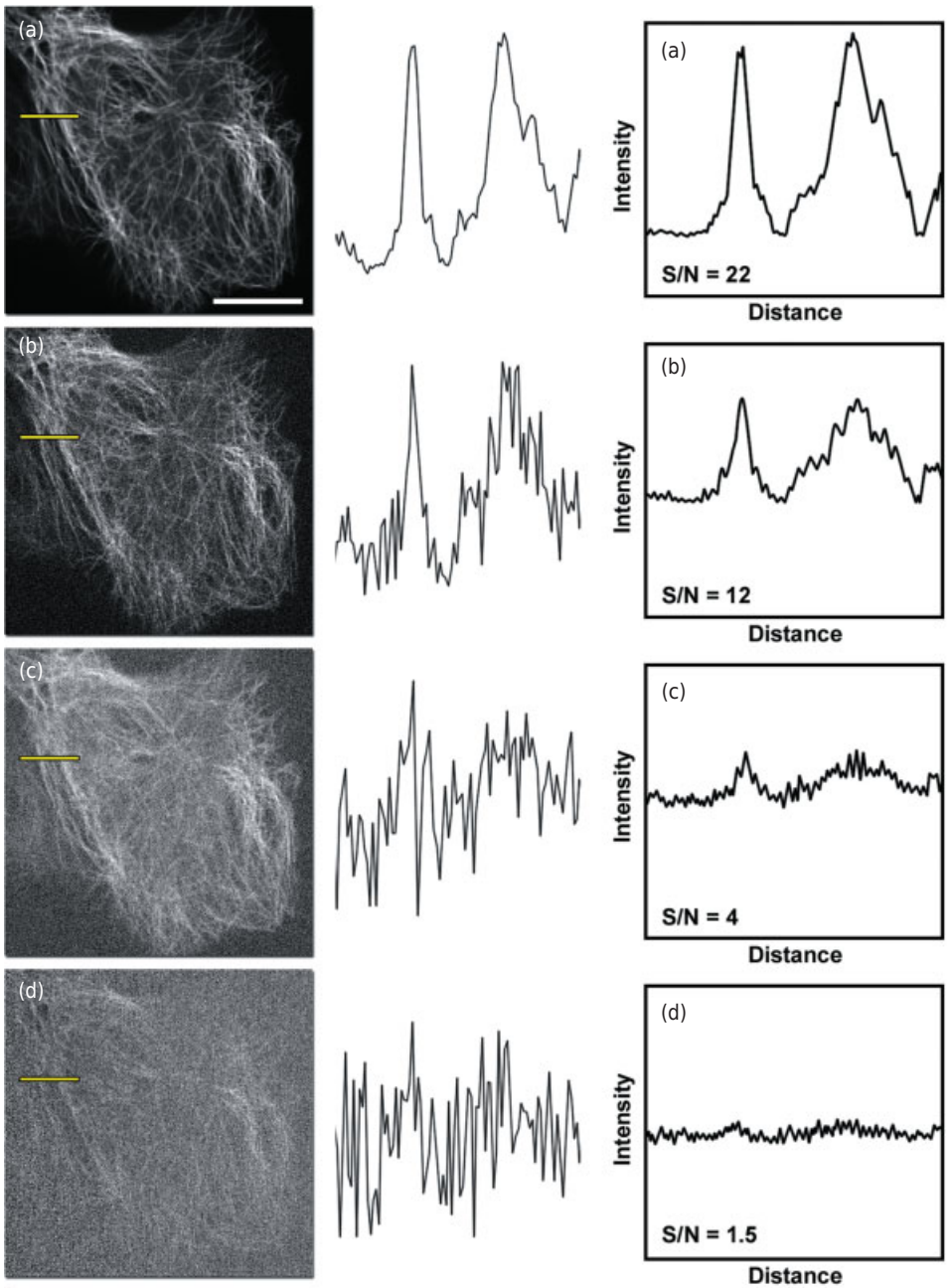

Figure 18.13

Demonstration of the S/N ratio. The CCD images in panels a–d depict microtubules labeled with fluorescent antibodies to tubulin captured at different S/N ratios. The yellow bar in each panel covers a row of pixels, whose values are shown in the intensity profile to the right of the corresponding image (center column). On a per pixel basis, S/N is the ratio of the amplitude of the object signal to the standard deviation of the surrounding background. Analog-to-digital units (ADUs) must be converted to electrons using the appropriate gain factor before calculating the S/N ratio in the graphs presented on the right-hand side of the figure. The pixel values are shown full scale, 0–4095. Bar = 20 μm.

The C_o and $\sigma^2_{(background)}$ measurements are taken from selected specimen and adjacent background ROIs using the *measure ROI* command in the analysis software. The units are in ADU with the correction for electrons appearing as gain in the denominator. The background variance is the calculated statistical variance of the pixel sample (the square of the standard deviation) and is obtained from the *measure ROI* command; it is not the Poissonian mean that was discussed earlier under photon shot noise. For convenience, set up these equations and related tables of variables in a spreadsheet.

THE USE OF COLOR

Color in Prints and Electronic Displays

The eye is extremely sensitive to color. Therefore, assigning a color to a fluorescent probe is an excellent way to represent two or more different signals in the same image. Because we perceive the visual world in color and perceive color when looking in the microscope, the presence of color makes prints and monitor displays appear natural and attractive. As a result, in fluorescence imaging involving multiple fluorophores, a common approach is to assign a monochrome color channel to each grayscale fluorescence image and display the information in a composite color print. Thus, color allows us to view multiple channels simultaneously and is especially effective in demonstrating the colocalization of two or more signals.

To preserve the dynamic range of original pixel values, color images should be handled and stored in as high level a data structure as is practical and feasible. This is particularly important when image files are submitted directly for publication. Thus, data type is as important for color images as it is for grayscale image files. Previously, color was limited to 8–12 bits per color channel, but because of improvements in computer speed and storage space, recent versions of image-processing software, such as Photoshop, can now support 16 bits per color channel. While monitors and printers are still limited at 8-bit resolution, color image files can be handled and stored in data types with much higher bit depth. At the present time, however, many programs still require conversion to 8 bits for displaying and storing 24-bit color images.

Despite the advantages of using color and the improvements in handling and storing color images at high resolution, displaying multiple color signals in a single image presents a unique set of problems:

- Brightness and visual dynamic range, the range of light intensities, and the amount of detail that is perceived by the eye when examining a picture (either a print or a computer monitor), are potentially much greater in a grayscale image than in a color image.
- Some colors are perceived as being much brighter than others owing to differences in the quantum efficiency of the eye at different wavelengths (see Chapter 2), a fact that can bias image displays.

On monitors and on prints, conversion to color can reduce brightness and visibility. While color can increase information content in an image by including multiple channels of color-encoded information, color can also reduce the brightness and visual dynamic range of light intensities perceived by the eye compared with the same image

presented in full grayscale range. Thus, on a monitor or on a print, color images appear darker because they have reduced light intensities. The reduction in intensity in going from grayscale to monochrome color is explained in the following way. On luminous color displays, such as monitors and LCD projectors, distinct red, green, and blue pixels contained in the screen are excited to create the colors of the visual spectrum. For displaying white, the electron guns excite the three color phosphors at maximum, and the eye perceives the RGB pixel cluster as white. However, for a monochrome red image, the excitation of green and blue pixels is minimized, so the visual intensity of saturated red features drops to about a third of the intensity of the same feature shown as white in a grayscale image. Therefore, for red monochrome color in an illuminated display, the brightness and visual dynamic range of the image are greatly reduced.

In color printing, red, green, and blue inks (RGB mode) or cyan, magenta, yellow and black inks (CMYK mode) are printed as dots on a sheet of paper. For saturating red color, inks are applied with the result that only red is reflected from the page to the eye, while all other wavelengths are absorbed and are not reflected. So, again, for a monochrome red image, saturated features reflect only a fraction of the light that is capable of being reflected by white in a grayscale print.

Blue (indigo blue at 400–450 nm) is a particularly difficult color to display (particularly when shown against a black background) owing to the 40- to 100-fold reduced sensitivity of the eye to blue (430 nm) compared with its peak sensitivity to green at 550 nm. In color prints, blue chromosomes or nuclei against a dark background are often disappointing, because little can be perceived or resolved. A much preferred strategy, particularly for known, defined structures, such as chromosomes or nuclei, is to use cyan (a blue-green color) for the blue color channel. For two-fluorophore specimens, the image display can be made brighter by choosing green and red colors to which the eye is very sensitive and avoiding blue altogether. To increase the intensity of green-red images, you can change the color palette to show green as yellow-green and red as orange-red, since both red and green pixels are used to show each of these two colors. This raises the value of the saturated orange-red pixel by about 30–50% compared with the value for saturated red alone. Overlap of the two colors still produces yellow, the same as if we had used only pure red and green. The main point is that the intensity of a saturated feature in a grayscale picture is significantly brighter and easier to see than the intensity of the same saturated feature in a color image. For a three-panel figure showing each of two fluorophores separately and combined together, an effective strategy is to show the separate fluorophores in grayscale, reserving color for just the combined image.

Use of Pseudocolor to Display Colocalization of Molecular Signals

A common goal in fluorescence microscopy is to determine if two fluorescent signals are coincident in the same structure. For complex patterns, the use of a combined pseudocolor display is very useful. Two color channels are selected (red and green) so that regions of overlap appear yellow. Other pairings, such as blue and green, giving cyan, and blue and red, giving magenta, may also be used, but are much less effective because of the reduced sensitivity of the eye to blue. During planning for image acquisition and display, it is best to adopt a standard that is easy to define and understand,

namely, combine images having the same dynamic range for each fluorescent signal. In the case of confocal microscopy, this practice actually matches the procedure recommended for image acquisition. Once combined, overlapping bright red and green signals give an unambiguous bright yellow signal. Remember that dark yellow hues, such as colocalized dim objects and backgrounds with equal red and green contributions, look brown. Optimize the gain and offset separately for each fluorescence signal (background = 0, saturation = 255) so that each fluorophore is displayed using a full 0–255 grayscale range (objective, easy to do, and easy to explain and describe to others). The images are then processed if necessary and merged. This is a conventional way to acquire and display multicolor images; however, because each signal is acquired to fill the grayscale range, this method does not allow you to determine the relative amplitudes of the two signals in the original specimen, only the relative signal strength within a given color channel.

In a perfectly aligned fluorescence imaging system, a point source in the specimen is perfectly registered, pixel for pixel, by different filter sets at the image plane in the camera. However, inadequate color correction of the objective or poorly aligned filters can cause misregistration of fluorescence signals during color merging. This artifact is recognizable by the uniform displacement of signals. In images with complex patterns and a mixture of bright and dim signals, misregistration can go undetected, leading you to conclude that signal distribution in a structure is distinct or partially overlapping. Therefore, during a color merge operation, in order to obtain good registration, it is important to be able to freely move the color layers with respect to each other, an operation called *panning*. The ability to align through panning requires the presence of coincident reference points (prominent features in the object) in each color layer. If multiply stained reference points do not exist, it may be useful to add multifluorescent beads to the specimen, at a dilution giving just a few beads per field of view, prior to mounting with a coverslip. For critical applications, there is another solution: use a single multifluorescence filter cube with multiple-bandpass dichromatic mirror and emission filter together with different fluorophore-specific exciter filters so that the same dichromatic mirror is used for all of the fluorescence signals; this configuration is used in confocal microscopes and other widefield fluorescence microscopes where color alignment is critical.

More problematic is the case where the microscopist's acquisition and processing methods are uneven. Inaccurate interpretations regarding colocalization in merged color images can result from improper gain and offset settings of the camera during acquisition or from extreme histogram stretching during image processing. This is depicted in a sketch in Figure 18.14. It is important to follow the procedures outlined in this book; otherwise, a too high black-level setting may produce distinct segments of separate colors that under conditions of lower black-level setting and reduced contrast are observed to be contained in the same structures. For critical applications, ratio imaging methods can be used to distinguish between signals that are colocalized versus signals that are only partially overlapping.

Image processing is often essential for preparing digital images for display where you want the image to look good, and for publication where you want an accurate record. When these goals conflict, as they frequently do, we might ask if there are image-processing standards to guide us in making key decisions. Unfortunately for the microscope community, there is no recognized set of standards, and the usual course is for individuals to create solutions on their own. While many image-processing operations available in popular software packages, such as NIH Image or Photoshop,

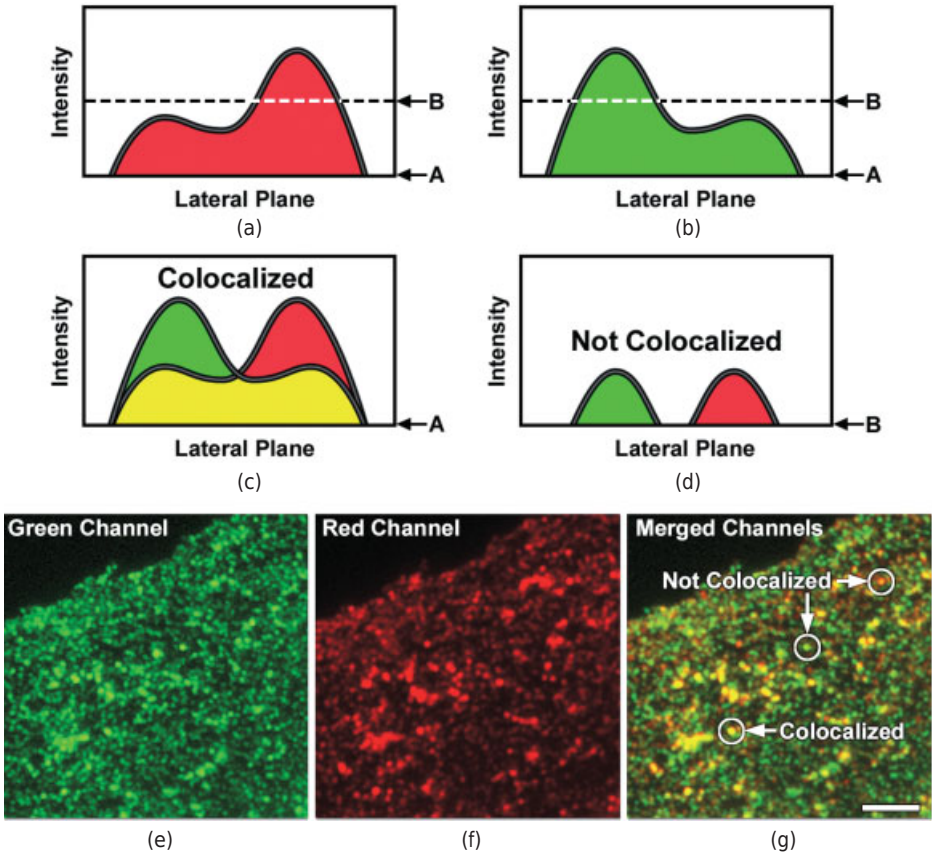

Figure 18.14

Colocalization of two fluorescent signals. (a) Cartoon of a red fluorescent signal showing intensity versus spatial distribution. (b) Cartoon of a green fluorescent signal. (c–d) Overlay of the two signals from panels a and b. The signals represented by the solid and dotted patterns are interpreted to be partially colocalized or have distinct distributions depending on the offset applied to the image. (c) Overlaid solid and dotted images using the offset at position A. (d) Overlaid solid and dotted images using the higher offset setting at position B. (e) Data from fluorescence colocalization experiment showing a fusion of mEmerald (a green fluorescent protein) fused to caveolin (pseudocolored green). (f) Same viewfield as panel e, but showing anticaveolin antibody labeled with Alexa Fluor 568 (pseudocolored red). (g) Colocalization overlay of panels e and f showing areas with colocalization and no colocalization. Bar = 2 μm.

can be performed in a photographer's darkroom, they are more easily performed digitally on a computer, tempting us to overprocess images. As an example, Figure 18.15 is processed in ways that give different interpretations regarding the intracellular distribution of a fluorescent protein. Recognizing the need to present the image in a nonarbitrary way, it would be useful to consider if image processing guidelines are feasible and if they would help assure that images remain faithful portrayals of their objects. In the authors' opinion, the answer to these questions is yes. However, experts agree that attaining this goal is difficult because guidelines are constraining and inherently

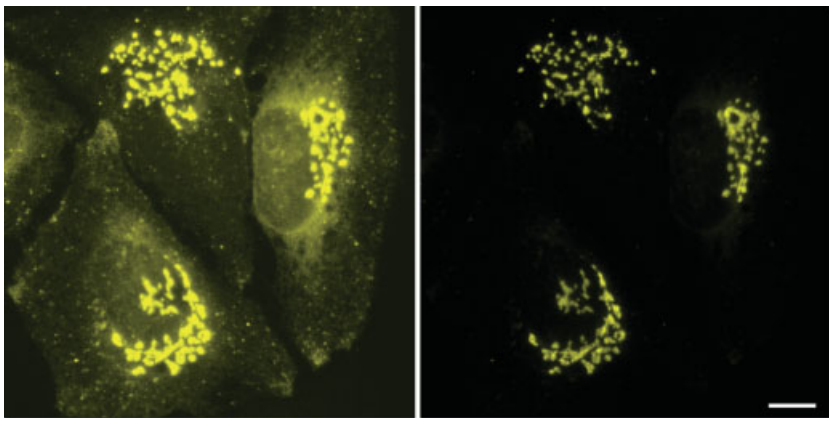

(a) (b)

Figure 18.15

Two interpretations of a specimen's structure resulting from selective manipulation of tools used for image processing. The specimen is a fusion of a Golgi complex targeting signal to an orange-yellow fluorescent protein (Kusabira Orange) expressed in HeLa cells. Bar = 10 μm.

subjective. No single set of guidelines would be appropriate for all images, and guidelines are to some extent arbitrary. Nevertheless, as electronic imaging and image processing become indispensable in the laboratory, guidelines would help standardize the way in which we present scientific images. It should be pointed out that the main focus of this chapter deals with the processing of fluorescence microscope images, a category that poses unique problems in the display of intensity, contrast, and the use of color. However, in many places, the guidelines are relevant to images obtained by other forms of light microscopy. We begin by examining the significance and history of processing in presenting microscope images.

IMAGES AS RESEARCH DATA AND REQUIREMENTS FOR SCIENTIFIC PUBLICATION

Image Processing: One Variable Out of Many Affecting the Appearance of the Microscope Image

Consider the large number of factors that affect the quality and appearance of a fluorescence microscope image:

- Microscope optics introducing distortions to an image if not properly employed.
- Environmental conditions affecting the morphology of cells in culture and during handling.
- Fixatives causing some morphological distortion, high autofluorescence, and differential extraction of components.
- Labeling is too heavy, uneven or unbalanced, or inappropriate choice of labels.

- Different filter sets giving varying views of fluorescent signals.
- Photobleaching of fluorescent dyes and proteins.
- Uneven illumination.
- Visual perception not matching the linear response of a CCD camera.
- Instrumental distortions (fixed bias pattern noise and electrical interference).
- Variation in parameters for image acquisition (gain, offset, and dynamic range).
- Image processing operations.

Any of these factors can affect the appearance of the object, sometimes in profound ways that selectively emphasize certain features and bias our interpretation of nature. So why single out image processing, the last item on the list, as a major concern? In large measure, it is because the other sources of image variability share in common the fact that they are defined by physical and chemical parameters. These parameters are generally understood, or if they are variable, can be described by procedures written into the materials and methods section of the research paper. The situation regarding image processing is, at present, much less defined. Just as we follow accepted procedures in preserving, labeling, and photographing cells, we should also consider what standards are appropriate for image processing. With time, procedures for processing scientific images will become standardized, and image processing will be less of a concern. For now, however, it deserves attention.

The Need for Image Processing

Although the goal in scientific imaging is to minimize image processing and standardize operations, experience tells us that moderate to extreme image processing can be an invaluable agent in scientific discovery. Contrast enhancement of minute cellular structures, the processing of Fourier transforms in crystallography, and contrast manipulations to medical x-rays and astronomical images are all examples of this. In some cases, little can be seen without significant processing of the original image. Nevertheless, for the typical microscope image, processing should be conservative, and features that are difficult to see should not be selectively enhanced without specific explanation. Scientific journals hold the position that artifacts such as dust spots and fluorescent precipitates should not be selectively cut and removed with tools such as the Photoshop clone-stamp and dodge-burn features. Images are no different from any other form of scientific data, and repeatability and confirmation of observations are essential. If there is only one image showing some type of information, then it is not wise to trust it. But if the same feature shows up repeatedly, then it might be considered valid even if it is difficult to observe. In such situations, image processing might be the only way to display image details and describe an observation to others.

Processing Standards May Vary, Depending on Their Use

Images used as data in scientific publications are distinct from the cover images of scientific journals or the enhanced images used to highlight scientific presentations and

those entered into imaging competitions. These categories of images are important, but serve different purposes and are prepared using different standards. Ideally, figures of scientific merit must represent a specimen objectively and completely. *The fundamental tenet of scientific publishing—that the reader should be able to repeat observations based on the details given in the article—should be the goal*. The editorial boards of scientific journals actively promote image processing guidelines, and the reader is referred to several useful articles by Rossner and O'Donnell (2004), Rossner and Yamada (2004), and Cromey (2010). Images on journal covers serve a different purpose. Here the rules are relaxed, and artistic manipulation of the image may be important to emphasize a particular feature, although the cover legend should usually acknowledge this point. Experience in bioimaging suggests it is best to act conservatively. You will have the confidence that you have prepared an objective record based on defined parameters for acquisition and processing.

Record Keeping during Image Acquisition and Processing

Good image processing begins with keeping good records.

- *Save raw and processed image files separately.* Before processing an image, make a copy of the original raw image for processing, and save the processed image as a separate file. When preparing figures for publication, keep notes about the processing steps applied to each image. Try to standardize your operations so that each image is treated similarly. Remember that it will be necessary to include details on image processing in the paper so that readers will know what you have done.
- *Keep record sheets of imaging sessions in the research notebook*. Prepare an entry describing your acquisition parameters for each experiment. For general microscopy, the sheet might include objective magnification, NA and type, and the illuminator and filters used (fluorescence filter set, ND, IR- and UV-blocking filters, and others). For confocal images that do not contain metadata, notes on the pinhole size, scan rate, black level and gain settings, frame averaging, as well as step size in a *z*-series are important. It also helps to add notes about the level of protein expression, labeling efficiency and signal strength, balance of fluorophores, photobleaching rate, and other observations pertinent to each exposure. One set of notes is usually adequate for each session involving the same preparation, but if settings change significantly during a session, you should write them down and indicate the image to which they pertain. It is easy to use a microscope casually without taking notes, but the value of the images will be limited, and you are more likely to repeat errors and waste time.
- *Keep folders and directories of all computer image files so that they can be easily reviewed and examined.* All image files should be stored in logical order in appropriately named directories. Try to imagine how difficult it will be to find a specific image file 6–12 months after it has been stored, and name the file as well as its storage directory accordingly. Keep all related image files together in a common directory and make sure to back up this data onto an external hard drive, RAID array, or computer tape storage. It is also a good idea to record the name of the image file and its parent directory in your notebook.

Guidelines for Image Acquisition and Processing

The following guidelines are listed in the order of their occurrence from specimen preparation to processing:

- *Give priority to the quality of the specimen preparation.* If the visual image does not measure up, it is always far better to prepare a new and improved specimen in the lab rather than to compensate for a poor image by image processing. For example, if fluorescence labeling is nonspecific or if there is considerable bleedthrough (unwanted signal in an image from another fluorophore), processing the image can be difficult and should not be encouraged. This is a particular concern when the goal is to determine if two signals are colocalized.
- *Optimize image acquisition with the microscope/camera system.* For fluorescence microscopy, this means proper adjustment of the microscope, illuminator, and filters for the best visible image, as well as full dynamic range and proper gain and offset camera settings for the best acquired image. Of all the things affecting image quality, specimen preparation and image acquisition are the most important. All too often the offset and gain settings of the camera, and, later, the histogram settings on the computer, are used without being aware of their consequences during subsequent image processing. There is little that even an experienced computer operator can do with an undersaturated, low-bit image.
- *Retain image resolution and metadata.* Remember that the print medium requires a high number of dots per square inch, such as 300 dpi. Images submitted at 72 dpi as taken from a PowerPoint presentation are not suitable. Accidental downconversion of the spatial resolution is quite common, so when working from a program like PowerPoint, which is used to display images on a monitor or projection screen, first save the image as a PDF file without compression, and then convert into TIFF format in a program like Photoshop. For purposes of sharing and publication of image files, images can now be sent between parties using OME-XML or OME-TIFF. These are special file formats for preserving resolution and metadata, and were defined by the Open Microscopy Environment consortium (http://www.openmicroscopy.org). For really large files, the *Journal of Cell Biology* has introduced a special browser-based application that greatly facilitates viewing of large and multidimensional image data (http://jcb-dataviewer.rupress.org).
- *Display all of the specimen information in the image histogram.* Before beginning processing, examine the pixel values of objects and background in the image. If you are aware of where the information is from the start, the danger of losing information by adjusting the histogram will be reduced. Also, check that the image does not show evidence of clipping at white and black values, a sign that an image has not been acquired or processed correctly. As a general rule, include all of the image data contained in the original image histogram and display it using the full range of grayscale values from 0 to 255 using histogram stretching. For example, in a brightfield image where the information might occupy a fraction of the grayscale range, one

should bring in the white and black set sliders to encompass the values contained in the histogram display. If contrast needs to be improved, it is generally acceptable to eliminate signals corresponding to the top and bottom 1% of the data values (do not exceed this by more than 0.5%). Beyond that, you should consider using γ scaling. These operations are described earlier in this chapter. If bright, saturating features (dead cells, precipitates) appear in the image, it is legitimate to determine the value of the brightest features in the cell of interest, and stretch the image histogram based on the revised range of pixel values.

If regions of an image other than the principle specimen show dim fluorescence, include them within the image histogram, because it is likely that there will be similar intensities in the object of interest. If you exclude the unwanted intensities from the histogram by stretching the histogram, the image might look posterized, leaving extensive black (or white) areas. This is one of the most frequent errors made in image processing. It is rarely justifiable to remove visible features of the image by adjusting the histogram just to make the picture look better. This is especially true when you expect to see a signal in "unwanted" places because of the biology of the system or based on the properties of immunofluorescence labeling (Figure 18.15).

- *Apply global processing operations conservatively.* For routine image processing, limit yourself to 5–10% of the estimated maximum capacity of image enhancement filters, such as γ scaling, sharpening and blurring filters, and unsharp mask operations. Fortunately, there are objective criteria for thinking about this. For example, in using γ scaling on a dark fluorescence image, it is useful to remember that a γ factor of 0.7 closely matches the logarithmic response of the eye; under bright-light conditions, contrast thresholds for adjacent objects that are barely visible versus readily distinguishable are approximately 3 and 30%, respectively. The best test for whether an image has been overprocessed is to compare the processed image, side by side, with the original unprocessed image or with the real view in the microscope. *Image processing operations should be reported in the methods section of a research article or in the figure legend so that the reader understands how the image was manipulated*.
- *Avoid using extreme black and white values in the image during printing.* Typically, the dark background around a cell in an immunofluorescence image should not be set to 0. Because halftone cells blur during printing, publishers recommend that the grayscale in submitted images not extend to true black or white. The lowest value (black) should be set to ~12% above 0 (30 units on an 8-bit scale), and the highest value should be set to ~8% below 255 (235 on an 8-bit scale). The precise value depends on the kind of paper on which the image is to be published. For high-quality paper in a journal, the bottom cut-off is about 10%; for newsprint, the value is about 20%. So for newsprint, pixels with values of ~50 ($256 \times 20\%$) and below will all appear black, even though they are easily visible on the computer screen. If you follow this guideline, dark gray values will not become swallowed up by black, and light gray values will not disappear and come out looking white.

- *Display highly manipulated features as an inset or separate figure.* Ordinarily, cellular features should not be differentially enhanced or diminished (dodge and burn operations in Photoshop) unless their very visibility is at stake. It is better to show the whole cell normally, with highly manipulated features included as an inset or as a separate picture and with processing details explained in the accompanying legend. If a montage is created from parts of different images, indicate this by placing lines separating the component parts. Do not present the montage as if it was a single acquired image and typical of what could be seen in the microscope.

A Checklist for Evaluating Image Quality

The following are criteria we might use in evaluating the quality of a scientific image. They contain the principles we have described along the way for specimen preparation, optical adjustments, and image acquisition, processing, and presentation.

- Fixation and labeling:
  - absence of fixation artifacts;
  - fluorophore intensities are adequate;
  - absence of bleedthrough and nonspecific signals; and
  - control experiments are negative.
- The acquired image:
  - proper optical zoom or magnification to preserve the required degree of optical resolution;
  - the full range of grayscale values is utilized;
  - camera gain (and offset) are appropriate; and
  - careful notes on the microscope optics and camera acquisition parameters.
- Image processing:
  - image studied to match pixel values with locations on the image histogram;
  - histogram white and black sets include all of the data in the image;
  - no or minimal black and white saturated areas in the image;
  - conservative use of gamma scaling and sharpening filters; and
  - insets and explanations made separately for emphasized features requiring extreme image processing.
- Use of color:
  - single fluorophores shown in grayscale format; and
  - for colocalization of different fluorophores, minimum and maximum values of color channels properly adjusted on the image histogram for display of multiple fluorophores in a montage, grayscale used for single channels, and color used for combined multichannel image.

The check list and guidelines presented in this chapter will allow new microscopists to use image processing knowledgeably and appropriately, provided they carefully follow the outlined steps. Although processing needs vary depending on the application and the particular image, at a minimum, this chapter will help direct discussion on what processing operations should be performed. When a reader of your article can understand and reproduce an observation in his or her own laboratory, you will know that you have mastered the essentials of image processing and many fundamentals of light microscopy and electronic imaging.

Exercise: Flat-Field Correction and Determination of S/N Ratio

In this exercise, you are to correct a raw image by flat fielding, extract numeric values from a structure in the image, and determine the S/N ratio. You will need access to Adobe Photoshop software on a computer. Although this manipulation is somewhat awkward in Photoshop (PS), the exercise will make you think about what you are doing and reinforce the processing operations. Prepare raw, flat, and dark images with a CCD camera, convert them to 8-bit data type (byte), and save them in TIFF format on the hard drive. In some cases, a supervisor may choose to do this for you. A flat-field correction is obtained by performing the following steps:

$$\text{Corrected image} = M \times [(R - D)/(F - D)].$$

a. Subtract the dark frame from the raw frame ($R - D$).

   In PS: Image/Calculations: Source 1 = raw; source 2 = dark; blending = difference; opacity = 100%; result = new; channel = new; save the new image.

b. Subtract the dark frame from the flat frame ($F - D$).

   In PS: same as above and save the image.

c. Determine the average pixel value M in the corrected flat frame ($F - D$).

   In PS: Image/histogram: record the mean value from data table.

d. Divide the corrected raw image frame by the corrected flat field frame $(R - D)/(F - D)$.

   In PS: you cannot divide images in PS, so take the inverse of the corrected flat frame and multiply it by the corrected raw frame. Use the menus: Image/Map/Invert, and save the inverted flat corrected image. Then use Image/Calculations to do the multiplication.

e. Multiply each pixel element in the image from step d by M.

   In PS: prepare a new image that contains only the value of M. *Make a copy of the raw image. Then go to Image/Adjust/Levels, and in the bottom scale bar, move the upper and lower pointers to the value of* M *determined in step c. The image will look a uniform gray. Name and save the image.*

Using Image/Calculations multiply the divided image from step d by the average image M.

That's it. Now touch up the contrast of the flat field-corrected image. Select *Image/Adjust* and then *Brightness/Contrast.*

1. Print the raw image and the corrected images together on the same page on a color printer.
2. Now calculate the S/N of an object in the image.
   a. Determine the average pixel value of the object (actually the object plus background together).

      In PS: Use the ROI tool to draw a rectangle around the object; use Image/Histogram to obtain the mean value of the ROI. Convert to electrons by multiplying by the gain.

   b. Determine the mean and standard deviation of the pixel value in the surrounding background area.

      In PS: use the ROI tool to draw a rectangle around a patch of background area. Then use Image/Histogram to determine the mean and standard deviation of the ROI. Convert to electrons by multiplying by the gain.

   c. Subtract the two means to determine the specific value of the signal (*S*) electrons.
   d. Divide the signal *S* by the noise *N*, the standard deviation of the background. The result is the S/N ratio calculated per object pixel in the image. Show your work.
3. For this object, fluctuations in the background of what percent can be distinguished at a 95% confidence level? Show your work.
4. Name two methods that could be used to improve the S/N ratio of the object.

APPENDIX

A

ANSWER KEY TO EXERCISES

CHAPTER 1

(2) For pancreatic acinar cells, cell diameter ~10 μm, nucleus diameter ~5 μm; secretory granule ~1 μm. (3) The field stop diaphragm is used to limit the area of illumination in the specimen to protect the specimen and reduce the amount of scattered light reaching the eye or detector. Opening the diaphragm too far causes unnecessary exposure and reduces contrast; closing the diaphragm too far masks the field of view. Neither operation changes the intensity of light in the image to a significant extent. The condenser diaphragm likewise has an optimum setting, typically allowing transmission through 70% of the rear aperture of the objective. A Bertrand lens (centering telescope) is required to make the adjustment. If opened too far, excess light fogs the image; if stopped down, contrast is improved, but spatial resolution is compromised. The 70% position offers a good compromise between image contrast and resolution. Reduction of image brightness should be made by reducing the voltage of the power supply or by inserting a neutral density filter in the optical path.

CHAPTER 2

(1) The principal complementary color pairs are red-cyan; yellow-blue; green-magenta.

Fundamentals of Light Microscopy and Electronic Imaging, Second Edition.
Douglas B. Murphy and Michael W. Davidson.

CHAPTER 4

(1) No, the object is located slightly outside the focal length of the objective. To produce a magnified real image, the object is located between 1 and 2 focal lengths. (2) No, the intermediate image is located slightly inside the focal length of the ocular as is required to form a magnified virtual image. (3) The eye-brain system perceives a magnified virtual image because the linear extensions of rays, focused on the retina by the ocular and eye lens, appear to converge in a virtual image plane located about 25 cm in front of the eye. The ray diagram in Figure 1.3 helps clarify the role of perspective in perceiving a virtual image.

CHAPTER 6

For a 40× 0.65 NA dry lens and 546-nm green light, striae or pore spacings of 0.5 μm are barely resolved. Only *Gyrosigma*, *Navicula*, and *Stauroneis* are clearly resolved. *Nitzschia* and *Pleurosigma* are barely resolved. (3) The spatial resolution is given as $d = 0.61\lambda/\text{NA} = (0.61 \times 0.546)/0.65 = 0.51$ μm (5) The diffraction patterns preserve the orthogonal and hexagonal arrangements of striae and pores seen in the normal (orthoscopic) viewing mode of the microscope. The narrowest spacings in the object correspond to the widest spacings in the diffraction patterns. (6) Lowest resolution with red light and restricted aperture; best resolution with blue light and open aperture. For demonstration of the effect of condenser aperture size on resolution, try *Gyrosigma*, *Navicula*, or *Stauroneis* with a 20× lens in green light; alternatively, examine *Gyrosigma*, *Stauroneis*, *Nitzschia*, or *Pleurosigma* with a 40× lens in red light. (7) If a 100× oil lens is used without oil, the NA corresponds to about 1, and *Pleurosigma* is barely resolved. With oil immersion, definition and resolution are both dramatically improved and pores are evident.

CHAPTER 7

The molarity of hemoglobin is calculated: g/L BSA at 50% match point × 1/64,000 mol/g = mol/L. The concentration of hemoglobin in erythrocytes is approximately 4–5 mM. This is 2500 times the molarity of tubulin and 250,000 times the concentration of aldolase. (4) The range of phase densities is partly due to real differences in hemoglobin content. The ratio of blood volume to BSA solution volume should be very small and the solution should be mixed very well. Cells could be fractionated on a density gradient and the hemoglobin content of cells in various fractions determined quantitatively.

CHAPTER 9

(3) For the slow axis of the waveplate running NW–SE between crossed polarizers and a magenta-colored background: starch grains, NE–SW quadrants yellow. SE–NW quadrants blue; bordered pits, NE–SW quadrants blue, SE–NW quadrants yellow. (4) Carbon bond alignments in amylose chains are arranged radially as in a pincushion; the carbon

bond alignments in lignin molecules in wood pits are arranged tangentially, like the layers of an onion.

CHAPTER 13

(1) Removing a neutral density filter or increasing laser power provides more fluorescent light, allowing one to reduce the gain setting or scan at a faster rate; opening the pinhole diaphragm increases the thickness of the optical section in the specimen; increasing the gain on the PMT makes the image look grainy; decreasing the offset on the PMT can make the image look flat and washed out; reducing the scan speed increases the rate of photobleaching; increasing the zoom factor improves spatial resolution but increases the rate of photobleaching. (2) The relationship between pinhole size and the thickness of an optical section is nonlinear, being greater at small pinhole diameters. (3) Generally, the phenomenon of bleed-through is that long-wavelength fluorochromes bleed into filter sets for short-wavelength fluorochromes. For this to occur, excitation of short-wavelength fluorochromes must also excite a longer-wavelength fluorochrome; some of the emission of the longer-wavelength dye must also be able to pass through the filter set for the short-wavelength fluorochrome.

CHAPTER 16

(1) Rhodamine bleeds through the fluorescein filter set, and fluorescein bleeds through the DAPI filter set. (2) Rhodamine is stimulated by the 490-nm excitation wavelength for fluorescein. Since a long-pass emission filter for fluorescein transmits red light, the fluorescence emission of rhodamine is also transmitted by this set. A bandpass emission filter for fluorescein is much more selective but still transmits a portion of rhodamine fluorescence. (3) The fluorescein set with narrow bandpass filter is not completely effective in transmitting fluorescein-specific fluorescence. Rhodamine is weakly excited by the band of wavelengths at 490 nm used to excite fluorescein, and its emission spectrum overlaps the region of peak fluorescence by fluorescein, so it is unavoidable that some rhodamine fluorescence is transmitted by the fluorescein-narrow set. (4) A fluorescein set with long-pass emission filter is useful when fluorescein is the only label, fluorescence emission is weak, and it is desirable to transmit the maximum amount of emitted fluorescent light. (5) To reduce bleed-through, reduce the amount of rhodamine label or use an illuminator such as a xenon arc lamp that does not stimulate rhodamine 10 times the amount it does fluorescein (as is the case for a mercury arc lamp). A better long-term strategy may be to use a different dye, such as Texas Red, with longer excitation and emission wavelengths and a filter set optimized for Texas Red.

APPENDIX

B

MATERIALS FOR DEMONSTRATIONS AND EXERCISES

CHAPTER 1: CALIBRATION OF MAGNIFICATION

Materials

Pancreas slides, H&E stain (Carolina Biological Supply), immersion oil

Lens tissue and cleaner

Eyepiece reticules (Klarmann Rulings)

Stage micrometers (Klarmann Rulings)

CHAPTER 2: COMPLEMENTARY COLORS

Materials

3 focusable projector lamps

Red, green, blue gelatin filters, colored glass filters, or interference filters (Edmund Scientific)

Aluminum foil masks with 1-cm hole in mounting for projection slide

Optical bench with filter holders (Edmund Scientific)

Holographic diffraction grating (Edmund Scientific)

2 × 2-in IR cut filter (hot mirror) (Edmund Scientific)

2 × 2-in opaque mounting with 0.5- to 1.0-mm diameter slit

Fundamentals of Light Microscopy and Electronic Imaging, Second Edition.
Douglas B. Murphy and Michael W. Davidson.

Yellow and blue food coloring
2 one-liter beakers
Light box
Extension cords
Quartz-halogen or xenon light source (xenon is better) and power supply
4- to 6-in handheld magnifying glass
Spectroscope (Learning Technologies)
Sheet of cardboard, white on one surface
Scissors
1- to 2-in test objects (paper or plastic sheet) of saturated red, green, and blue colors

CHAPTER 3: SPECTRA OF COMMON LIGHT SOURCES

Materials

Optical bench
Narrow slit
IR blocking filter
Holographic grating
100-W quartz halogen microscope lamp
100-W mercury arc microscope lamp
100-W xenon microscope lamp
Hand-held spectroscopes (Learning Technologies)
Aluminum foil
Razor blades
Scissors

CHAPTER 4: OPTICAL BENCH MICROSCOPE, LENS ABERRATIONS

Materials

Optical bench with lens holders and screen
50-mm lens, two 200-mm lenses for optical bench
Quartz-halogen microscope lamp and power supply
Lens tissue or microscope slide, marking pen, adhesive tape
Aluminum foil
Fine-gauge syringe needle
Scissors
Adhesive tape

CHAPTER 5: DIFFRACTION IMAGES IN REAR FOCAL PLANE OF OBJECTIVE

Materials

- 3-mW HeNe laser or laser pointer
- Aluminum foil
- Fine-gauge syringe needles
- 20 × 30-cm glass baking dish
- Small container of milk
- Pasteur pipette and rubber bulb
- EM grid, 400 mesh
- Microscope slide
- Adhesive tape
- Optical bench with lens and specimen holders
- Demonstration lenses, 50- and 100-mm focal length
- Transparent diffraction gratings, various spacings (Edmund Scientific)
- Transparent holographic grating
- Aperture mask, 0.5- to 1-mm slit width, made from the edges of two razor blades or 2- to 3-mm diameter hole in a square of aluminum foil
- IR blocking filter or IR hot mirror
- Tape measure
- Stage micrometer and eyepiece reticule
- Compact disk (CD)
- Bird feather
- Handheld calculators

CHAPTER 6: RESOLUTION OF STRIAE IN DIATOMS

Materials

- Immersion oil, lens cleaner, lens tissue
- Diatom test plates (Carolina Biological Supply)
- Diatom exhibition mounts (Carolina Biological Supply)
- Red, green, and blue glass filters or interference filters (Edmund Scientific)

CHAPTER 7: PHASE CONTRAST MICROSCOPY

Materials

- Box Pasteur pipettes
- Rubber bulbs

Kimwipes or laboratory wiping tissue
70% Ethanol
Gauze wipes for cleaning finger tip
Adhesive bandages
Lancets
Microscope slides and no. 1.5 coverslips
Container for used lancets

Notes on Preparing Stock Solution of Serum Albumin

1. Dialyze 50 mL of 30% (wt/vol) bovine serum albumin (Sigma liquid stock A 7284) against 2 L distilled water to remove 158 mM NaCI. Change water after 1–2 hours, then continue overnight with 2 L water containing 30-mL ion exchange resin (BioRad AG 501-X8 mixed-bed resin) on a stirring box at 4°C.
2. Transfer the albumin to a lyophilizer jar, freeze in liquid nitrogen or dry ice/ethanol bath with swirling, and lyophilize overnight until dry.
3. Resuspend the dry albumin powder in 25 mL distilled water. Break up clumps of albumin periodically during the day. It takes several hours to resuspend the albumin. The solution may need to be centrifuged to remove bubbles and foam using a benchtop centrifuge.
4. Determine the protein concentration by reading absorbance at 280 nm in a UV spectrophotometer. Dilute the stock 1 : 1000 in water before reading. Use care in performing the dilution, since the BSA stock is extremely thick and concentrated. The $0D_{280}$ of a 1 mg/mL solution is 0.66. The concentration of the stock will be ≥400 mM.
5. Prepare the following five solutions as indicated. The final total solute concentration in each tube will be 326 mOsm. All solutions contain added sodium chloride to maintain the erythrocytes. NaCl is added to give the same value of osmolarity for each tube, but albumin contributes 95–98% of the refractive index, the balance being due to the salt, which we will ignore. (If albumin is prepared at other concentrations, the following values will be useful: from tables, the osmolarity equivalent of 100 mg/mL BSA = 13.793 mM NaCI, and 9.463 g/L NaC1 = 326 mOsm.)

mg/mL BSA	**grams NaCl/L**
200	7.863
250	7.463
300	7.063
350	6.663
400	6.263

References: Barer et al. (1953) and James and Dessens (1962).

CHAPTER 8: POLARIZED LIGHT

Materials

2 dichroic sheet polarizers
Light box or overhead projector
Microscope slide
Sheet of cellophane (not plastic food wrap)
Calcite crystals

CHAPTER 9: POLARIZATION MICROSCOPY

Materials

2 dichroic polarizer sheets
Light box or overhead projector
Sheet of cellophane
Cellophane tape
Red-I plate (A.-plate)
Dichroic sheet polarizers, 2 × 4-cm strips, with one edge parallel to transmission axis of polarizer
Red-I plates; 2 × 4-cm strips, with edges parallel to the axes of the refractive index ellipsoid of the plate (see instructions for cutting strips)
Corn starch, a few grains of starch mounted on a slide under a coverslip with a drop of glycerol
Leaf of *Amaryllis* or *Dieffenbachia*, a drop of plant cell sap mounted on a slide under a coverslip
Onion skin, a thin sliver mounted on a slide in a drop of water under a coverslip
Preparation of squashed *Drosophila* thorax, mounted on slide in drop of water under a coverslip
Stained section of pinewood, *Pinus strobus*, radial section (Carolina Biological Supply)
Stained section of buttercup root, *Ranunculus* (Carolina Biological Supply)
Stained section of striated muscle, H&E (Carolina Biological Supply)
Razor blades for cutting materials
Pasteur pipettes and rubber bulbs

Preparation of Red-1 Plates for Student Microscopes

On a light box, rotate two dichroic sheet polarizers to obtain extinction. Between the polars, insert the red-1 plate that is to be cut into 2 × 4-cm strips for the student microscopes. With the polars crossed and held in a fixed position, rotate the red-I plate until the bright interference color is observed. The axes of the refractive index ellipsoid of the plate are now oriented at 45° with respect to the transmission axes of the crossed

polars. Attach a strip of cellophane tape to a microscope slide and insert the slide between the crossed polars. The long axis of the tape is parallel to the long axis of the refractive index ellipsoid (= slow axis of the wavefront ellipsoid) and will serve as a reference. Rotate the microscope slide through 360°. At two positions, the tape will look bright yellow, and at two positions rotated by 90° with respect to the first, the tape will look pale yellow. In between these two axes, the tape will have the same red color as the red-1 plate by itself. The orientation of the tape giving the bright yellow color marks the high refractive index axis of the red-I plate. Mark this axis on the red-I plate as a short line with a marker pen. The red-I plate can now be cut into strips with a paper cutter carefully so that one edge of the strips is perfectly parallel to the axis drawn on the plate. Blacken this edge with the marker pen and draw an ellipsoid at a corner of the plate with its short axis parallel to the blackened edge.

CHAPTER 10: DIC MICROSCOPY

Materials

24 coverslips of cultured cells
Serum-free MEM culture medium supplemented with 10 mM HEPES, pH 7.2
Filter paper
Petroleum jelly
Paper wipes (Kimwipes)
Lens cleaner, water, immersion oil
Pasteur pipettes and rubber bulbs
Plastic beakers for discarded medium
Fine forceps

CHAPTER 11: FLUORESCENCE MICROSCOPY

Materials

Chlorophyll extract
Fluorescein solution, 10-mg fluorescein in 1 L water
Long-wave UV lamp (blacklight)
Light box
Spectrometers
Cardboard sheet with 1-cm wide slit
Optical bench
IR cut filter
Holographic diffraction grating
1-mm slit aperture
Xenon arc lamp and power supply

Preparation of Chlorophyll

Place two cups of fresh spinach and 1 L isobutyl alcohol in a glass food blender and homogenize until the leaf tissue is thoroughly dispersed. Filter the solution through several layers of cheesecloth. The same procedure can be used to prepare extracts of other tissues (50 g).

CHAPTER 16: LIVE CELL IMAGING

Materials

24 coverslips of cultured cells
Serum-free MEM culture medium supplemented with 10 mM HEPES, pH 7.2
Filter paper
Petroleum jelly
Paper wipes (Kimwipes)
Lens cleaner, water, immersion oil
Pasteur pipettes and rubber bulbs
Plastic beakers for discarded dyes and medium
Fine forceps
Delipidated BSA (Sigma A-6003)

Stock Solutions of Fluorescent Dyes

Ethidium bromide, 10 mg/mL in water
JC-1 dye, 10 mg/mL in DMSO
$DiOC_6$, 5 mg/mL in DMSO
BODIPY-ceramide, 1 mM in ethanol
MitoTracker red
LysoTracker green
BODIPY-phalloidin, 3 μM in DMSO
DAPI, 5 mg/mL in water

APPENDIX

C

SOURCES OF MATERIALS FOR DEMONSTRATIONS AND EXERCISES

Carolina Biological Supply Co., Inc., Burlington, NC, tel. 800-334-5551
Microscope slides, histological preparations:
Skeletal muscle, H1310
Bordered pits, pine wood, long section, B520
Ranunculus root, cross section, B520
Diatom test plate, 8 forms, whole mount, P7-B25D
Pancreas, monkey, H&E, 98-9652

Edmund Scientific Company, Inc., Barrington, NJ, tel. 800-728-3299
Sheet of transmission diffraction grating, 600 lines/in
Sheet of transmission diffraction grating, 23,000 lines/in
Holographic diffraction grating, 3600 lines/mm
Calcite crystals
Red HeNe laser, 0.8 mW, Uniphase class IIIa laser, K61-337
Hot mirror, 50 × 50 mm, reflects IR, K43-452
BG-38 Schott IR-blocking filter, 50 × 50 mm, K46-434
KG1 Schott IR-blocking filter, 50 × 50 mm, Y45-649
GG-420 Schott UV-blocking filter, 50 × 50 mm, K46-427
Red, green, blue gelatin filters (Kodak Wratten filters 25, 58, 47B), 75 × 75 mm
Polarizing film, tech spec quality, 8.5 × 15-in sheet, K45-668
Polarizer pack, demo kit
Lens cleaner, K53-881

Klarmann Rulings, Inc., Manchester, NH, tel. 800-252-2401
Eyepiece micrometer, 0.01-cm divisions
Stage micrometer, 0.01-mm divisions

Fundamentals of Light Microscopy and Electronic Imaging, Second Edition.
Douglas B. Murphy and Michael W. Davidson.

Learning Technologies, Inc., Cambridge, MA, tel. 800-537-8703
Plastic hand-held spectrometer, PS-14
Holographic diffraction grating, 750 lines/mm, PS-08-A, 9 × 5-in sheet

3M/Optical Systems Division, Norwood, MA, tel. 781-386-6264
Full-wave plate retarders
Dichroic polarizing film

GLOSSARY

Aberrations of a lens. Faults in lens design that cause optical performance to deviate from that of an ideal lens. Aberrations are usually attributed to materials composing the lens and the spherical curvatures of lens surfaces. Lens aberrations include chromatic and spherical aberration, astigmatism, coma, distortion, and field curvature.

Absorbance (optical density). In spectroscopy, the amount of light absorption by a substance in solution and defined as $A = \log_{10}(I_0/I)$, where I_0/I is the transmittance, the ratio of incident and transmitted light intensities. Absorbance is determined by the wavelength, pathlength, and concentration of the substance.

Acceptor-photobleaching FRET. A strategy for measuring fluorescence resonance energy transfer in which the acceptor molecule is photobleached to prevent energy transfer from the donor. Upon donor excitation, acceptor fluorescence decreases while donor fluorescence increases. See *Dequenching of donor fluorescence.*

Achromat. A lens corrected for chromatic aberration at two wavelengths (red and blue) and for spherical aberration (green).

Acousto-optical tunable filter (AOTF). A device, based on sound waves, to control the wavelength or intensity of light delivered from a laser or other light source to a specimen. Sound waves induced in a transparent quartz block set up a standing wave with alternating domains of high and low refractive index, allowing the block to act as a diffraction grating and to deflect an incident beam of light. The period of the grating is changed by altering the frequency of sound waves delivered to the block.

Acridine orange. A chromophore containing the acridine nucleus, which binds to DNA and RNA to produce a strong, but very broad fluorescence emission band in the green to red wavelength region. Acridine orange is excited by blue-green laser light (488 nm) or by ultraviolet, violet, and blue interference filters coupled to an arc-discharge lamp (mercury or xenon). The fluorophore is an excellent candidate

Fundamentals of Light Microscopy and Electronic Imaging, Second Edition.
Douglas B. Murphy and Michael W. Davidson.

for displaying many cellular structures, but is not useful for multiprobe staining because of the broad emission spectrum.

ADC. See *Analog-to-digital converter (ADC)*.

ADU. See *Analog-to-digital unit (ADU)*.

AFIC. See *Automated fluorescence image cytometry (AFIC)*.

Airy disk. The central diffraction spot in the focused image of a point source of light. Diffraction at the front aperture of the lens disturbs the incident wavefront, causing the diffraction pattern. The Airy disk diameter is determined by the wavelength of light and the angular diameter of the lens as seen from the image plane.

Alexa Fluor dyes. Synthetic fluorescent dyes, trademarked by Molecular Probes, that are useful for labeling antibodies, nucleic acids, and as general probes for proteins, cytoskeletal elements, lipids, and general neuroscience. The excitation and emission spectra for Alexa Fluor dyes span higher wavelength portions of the ultraviolet region and the entire visible light spectrum, even stretching into the near infrared frequencies. Alexa Fluor dyes have absorption spectral maxima that are matched to common laser lines and mercury arc discharge lamps. In general, Alexa Fluor dyes are noted for their high stability and resistance to photobleaching.

Aliasing. In microscopy, the false pattern of spacings that is observed when periodic detail in an object is recorded by an electronic imager, which itself has periodic sampling units (pixels and raster lines), and when the number of samples per specimen period is less than 2. Aliasing artifacts often give rise to *Moiré patterns*. Aliasing is avoided by adjusting the magnification high enough so that two or more imaging elements cover a unit period of resolution in the object. See also *Nyquist criterion*.

Amplitude. The magnitude of the electric field vector of an electromagnetic wave. Amplitude is distinguished from intensity (irradiance), a measure of the amount of light energy or photon flux, which in visual perception is proportional to amplitude squared.

Amplitude object. Objects that absorb light and reduce amplitude as opposed to those that shift the phase of light (phase objects) as the basis for image formation.

Amplitude of an electromagnetic wave. The magnitude of the electric field vector of an electromagnetic wave. Amplitude is distinguished from intensity (irradiance), a measure of the amount of light energy or photon flux, which in visual perception is proportional to amplitude squared.

Analog signal. A signal that is continuously variable—for example, the variable voltage signal sent from a photomultiplier tube to a digitizer in a confocal microscope. Analog signals are distinct from digital signals, which are composed of a stream of discrete numeric values in binary computer code.

Analog-to-digital converter (ADC). A device for converting an analog electrical signal into the digital code of the computer. A 12-bit converter in the circuit board of a CCD camera uses an ADC to convert the camera's signal into one of 4096 possible digital values for processing and display on a computer. ADC circuits in a CCD camera are noted for their high processing rate and low noise.

Analog-to-digital unit (ADU). In digital imaging, the numeric value assigned to represent the amplitude of a photon signal. The conversion factor used in making the assignment—for example, 10 photoelectrons/ADU—is related to the gain factor.

Analyzer. A linear polarizer used to analyze or determine the plane of vibration of an incident ray of polarized light. Analyzers are used in conjunction with polarizers in light microscopy.

Angle of incidence. In reflection, the angle subtended by an incident beam and a line perpendicular to the surface at the point of incidence.

Angle of reflection. In reflection, the angle subtended by a reflected beam and a line perpendicular to the surface at the point of incidence.

Angular aperture. See *Aperture angle*.

Anisotropic. In describing the optical properties of an object or propagation medium, having dissimilar properties in different directions, such as variations in refractive index along different directions of propagation of light in anisotropic crystals.

Annulus. In phase contrast microscopy, the transparent ring at the front aperture of the condenser that provides illumination of the specimen.

AOTF. See *Acousto-optical tunable filter (AOTF)*.

Aperture angle. The angle subtended by the edges of a lens as seen from a point in the specimen plane or in the image plane. Aperture angle is included in the expression for numerical aperture ($NA = n\sin\theta$), where n is the refractive index and θ is one-half of the full aperture angle. See also *Numerical aperture (NA)*.

Aperture plane. In a microscope adjusted for Koehler illumination, the set of conjugate focal planes located at the light source, the front aperture of the condenser, the rear aperture of the objective, and the iris of the eye. Adjustable aperture diaphragms and fixed aperture stops at these locations are used to limit stray light and determine the numerical aperture, and hence the spatial resolution, of the instrument.

Apochromat. A lens especially designed to correct for chromatic aberration at three or four wavelengths (red, green, blue, and ultraviolet) and at two or more wavelengths (green and red) for spherical aberration. The high degree of color correction makes apochromat objectives suitable for fluorescence microscopy and stained histological specimens in brightfield microscopy.

Astigmatism. An off-axis optical aberration of spherical lenses whereby rays from an off-axis object passing through the lens along horizontal and vertical axes are focused as a short streak at two different focal planes. The streaks appear as ellipses drawn out in horizontal and vertical directions at either side of best focus, where the point image is a small disk. Off-axis astigmatism increases with increasing displacement of the object from the optical axis. Astigmatism is also caused by asymmetric lens curvature due to mistakes in manufacture or improper mounting of a lens in its barrel.

Attenuation (blocking) level. Reduction or suppression of a light signal before it is detected in an optical system. Attenuation, also referred to as modulation or blocking of light intensity, can be accomplished with neutral density filters or an acousto-optic tunable filter (AOTF) in confocal microscopy. Attenuation is also a term used by filter manufacturers to indicate the out-of-band exclusion level of light by interference filters.

Autofluorescence (primary fluorescence). Nonspecific fluorescence signal due to endogenous metabolites (flavins, nucleotides, vitamins, etc.), as well as constituents in culture medium, immersion oil, optical coatings, and glass in optical components and lenses. In live-cell imaging, autofluorescence is greatest when cells are examined with blue and ultraviolet excitation wavelengths.

Automated fluorescence image cytometry (AFIC). The application of fluorescent probes coupled with computerized microscopy systems (reflected light fluorescence microscope, low light level camera, and computer) to enable the high-speed automatic screening of stained specimens with reliable and accurate detection of almost all cells. Disease markers in clinical specimens can be monitored with this technique through the use of specific and sensitive fluorophores attached to antibodies or

nucleic acids. Selective excitation of the target fluorophore produces images with high signal-to-noise ratios that further increase the sensitivity of detection.

Average transmission. In filter nomenclature, average transmission refers to the average level of light transmitted in a particular wavelength region (the useful transmission band) rather than over the entire spectrum. In a standard bandpass filter, the average transmission region spans the full width at half maximum (FWHM) of the transmission band. In longpass and shortpass filters, the term indicates the wavelength region transmitted past the cut-on and cut-off wavelengths, respectively.

Azimuth angle. A term used to describe the orientation of an object in a plane, such as the specimen plane of the microscope. On a graph with polar coordinates marked off in 360°, the angle subtended between a fixed reference (designated 0°) and a vector rotated about the origin.

Back aperture of the objective. See *Objective rear aperture*.

Background. Detectable light (noise) that is not part of the specimen signal in bright-field illumination or part of the emission signal from a fluorescent probe in fluorescence microscopy. Sources of background noise include crosstalk between excitation and emission filters, light leaking from pinhole artifacts in excitation and emission filters, bleeding of fluorophores in mounting medium, nonspecific fluorophore staining, electronic noise in digital camera systems, and autofluorescence.

Background subtraction. An operation in electronic imaging whereby an image of the featureless background or the average pixel value near an object is subtracted from the image of the specimen to remove background signal, as well as patterns of irregular illumination and other optical faults, such as scratches and dust.

Background wave. See *Surround wave*.

Back-thinned CCD. A CCD device thinned by etching the back surface so that the chip can be inverted and its back surface used for photon capture. The light efficiency of back thinned CCDs is 95% or greater.

BaLM. Bleaching/blinking assisted localization microscopy. In BaLM, the specimen is photobleached while capturing an image stream. Subtracting each image in the stack from the previous and following images enables single-molecule localization analysis. BaLM works with any fluorophore.

Bandpass filter. A filter that transmits a defined region (or band) of wavelengths while attenuating light having wavelengths both shorter and longer than the passband. The central wavelength of the transmitted band is known as the center wavelength (commonly abbreviated CWL). The effective bandwidth is indicated by the full width at half maximum (FWHM) transmission, which is alternatively referred to as the half bandwidth (HBW). Bandpass filters are commonly employed as excitation, and less often, as barrier filters in fluorescence microscopy.

Barrier (emission) filter. See *Emission filter*.

Beamsplitter. An optical device for dividing an incident beam of light into two or more beams. A prism beamsplitter in the trinocular head of a microscope directs the imaging beam to the eyepieces and to the camera simultaneously. A polarizing beamsplitter made of a crystalline birefringent material is used to produce linearly polarized light. A dichromatic mirror beamsplitter reflects excitation wavelengths while transmitting long-wavelength fluorescence emission.

Bertrand lens (phase telescope, centering telescope). A built-in telescope lens located behind the rear aperture of the objective. When rotated into the optical path, the rear aperture and diffraction plane are seen, and other planes that are conjugate to it, while looking in the oculars of the microscope. This lens is used for adjusting

the aperture of the condenser diaphragm and for centering the phase annulus in phase contrast microscopy.

Bias noise. One of the noise components contained in a raw CCD image. Bias noise is calculated as the square root of the bias signal, and is considered in determining the S/N ratio of images.

Bias retardation. In polarization microscopy, the alteration of optical path differences between O and E rays, made by adjusting a compensator. Bias retardation is introduced by the operator to change the contrast of an object or is introduced in order to measure the relative retardation Γ of the O and E wavefronts of birefringent objects. In DIC microscopy, bias retardation is introduced using a Wollaston or Nomarski prism to optimize image contrast.

Bias signal. In digital CCD cameras, the signal resulting from the application of a bias voltage across the CCD chip, a condition required to store and read the pixels on the chip, as no imaging pixel is allowed to have a negative value. The bias signal must be subtracted from the total image signal in order to obtain a photometrically accurate image signal.

Binning. In CCD microscopy, the command given in software to combine the signal content of multiple adjacent pixels. Because the total number of photon counts required to reach saturation remains the same, binning reduces the exposure time required to reach a certain signal value by a factor equal to the number of binned pixels. However, because there are overall fewer pixels in a binned picture covering a given area, binning also increases pixel size and reduces the spatial resolution.

Bioluminescence. An oxidative process resulting in the release of energy as light emission—for example, firefly luminescence, which requires an enzyme, luciferase, to catalyze a reaction between the substrate luciferin and molecular oxygen in the presence of ATP.

Bioluminescence resonance energy transfer (BRET). The technique, similar to FRET, is based on energy transfer from sea pansy luciferase to a fluorescent protein moiety in a fusion protein. A proprietary coelenterazine derivative, DeepBlueC™, is used to generate the BRET signal.

Birefringence. The double refraction of light in transparent, molecularly ordered materials caused by the existence of orientation-dependent differences in refractive index. Also refers to the refractive index difference experienced by a transmitted ray through such a material. Incident beams of light on a birefringent specimen are split into O and E rays that can recombine after emergence from the object, giving linearly, elliptically, or circularly polarized light.

Bit. In computer language, a binary digit 1 or 0. An 8-bit image therefore has 2^8 or 256 gray level steps, while a 12-bit image contains 2^{12} or 4096 steps.

Bleedthrough or crossover. In fluorescence microscopy, the transmission of unwanted wavelengths through a filter designed to block them. Bleedthrough or crossover occurs when a filter's design does not allow complete destructive interference of unwanted wavelengths, when the angle of incident rays on the filter is oblique, when the transmission and emission spectra of fluorescent dyes overlap, and for other reasons.

Blocking level. See *Attenuation level*.

Blooming. An artifact in imaging using silicon detectors like CCD devices, where the photoelectrons in saturated pixels spill over into neighboring pixels, particularly pixels within the same column, causing visible streaks in the image.

BRET. See *Bioluminescence resonance energy transfer*.

Brewster's angle. The unique angle formed by an incident ray and the perpendicular to a reflective dielectric substance, such as water or glass (the transmitting medium), at which the reflected ray is totally linearly polarized. Brewster's angle θ is given as $\tan\theta = n_i/n_t$, where n_i, and n_t are the refractive indices of the medium of the incident beam and the transmitting medium, respectively.

Brightfield microscopy. A mode of optics employing the basic components of objective and condenser lenses for the examination of amplitude objects, such as stained histological specimens.

Brightness. A qualitative expression for the intensity of light.

Byte. In computer language, a unit of information containing 8 bits.

Caged fluorophores. A caged fluorophore is covalently linked to an inactivating moiety (usually an organic structure), but can be photolytically released (uncaging) by a pulse of light. Caged fluorophores are useful for photoactivation experiments in living cells to track dynamic events.

CALI. See *Chromophore-assisted laser inactivation (CALI).*

Cameleons. Chimeric fluorescent proteins containing calmodulin used to observe intracellular calcium concentration by FRET microscopy. Most cameleons are based on FRET between cyan and yellow fluorescent proteins and their high-performance derivatives.

Camera control unit (CCU) or camera electronics unit (CEU). The main external electronics control unit of an electronic imaging system.

CARS. See *Coherent anti-Stokes Raman scattering (CARS) microscopy.*

CCD. See *Charge-coupled device (CCD).*

CEU. See *Camera control unit (CCU).*

Charge-coupled device (CCD). A slab of silicon semiconductor that is divided into an array of pixels that function as photodiodes in a light-sensitive photodetector. In the presence of an applied voltage and incident light, the pixels generate and store "photoelectrons" (alternatively, electron holes) resulting from the disruption of silicon bonds from incident photons. The number of stored "photoelectrons" determines the amplitude of pixel signals in the displayed image.

Chromatic aberration. A common aberration of lenses, whereby light waves of different wavelength are brought to focus at different locations along the optical axis. In the typical case of a simple thin lens, the focal length is shorter for blue wavelengths than it is for red ones.

Chromophore. A naturally occurring or synthetic pigment with characteristic optical absorption or fluorescence, usually containing a combination of alternating single and double bonds or a high degree of cyclic aromatic or heterocyclic conjugation. Chromophore also refers to the cluster of atoms responsible for absorption and fluorescence, such as the parts of amino acid residues responsible for fluorescence in fluorescent proteins like GFP.

Chromophore-assisted laser inactivation (CALI). In CALI, fluorescent proteins and synthetic dyes are used to generate substantial levels of reactive oxygen species upon absorption of light. The reactive species perturb biological function, which can be monitored spatially and temporally.

Circularly polarized light. A form of polarized light whereby the E vector of the wave rotates about the axis of propagation of the wave, thus sweeping out a spiral. If the wave could be viewed end-on, the movement of the E vector would appear to trace the form of a circle.

CLSM. See *Confocal laser scanning microscope (CLSM).*

CMOS detector. A silicon area-array detector (complementary-metal-oxide-semiconductor) with pixels arranged in rows and columns, where each pixel has its own readout amplifier. Additional amplifiers for columns and whole block areas of the chip surface provide rapid readout rates (100 full fps). The large full well capacity of each pixel and low readout noise provide greater sensitivity and dynamic range.

CMYK. A popular format for color printing, whereby colors are reproduced using four different inks: cyan, magenta, yellow, and black.

Coherent anti-Stokes Raman scattering (CARS) microscopy. An imaging technique based on the vibrational properties of the target molecule and not requiring illumination by ultraviolet or visible light. In practice, IR laser pulses are focused onto the specimen with a microscope objective and scanned in a raster. At the proper harmonic frequency, wavelengths scattered by the specimen are used to form an image.

Coherent light. A beam of light defined by waves vibrating in the same phase, although not necessarily in the same plane of vibration. To maintain the same phase over long distances, coherent waves must be monochromatic (have the same wavelength). Laser light is monochromatic, linearly polarized, and highly coherent.

Cold mirror. A specialized dichromatic interference filter that reflects the entire visible light spectrum (the nonheat-generating portion of the spectrum), while efficiently transmitting infrared wavelengths.

Collector lens. A focusable lens of the illuminator capable of collecting light over a wide area and directing it toward the specimen. In Koehler illumination, the collector lens is used to focus a magnified real image of the filament or arc of the bulb in the front aperture of the condenser.

Collimated beam. A beam in which rays proceed in the same direction and follow trajectories that are parallel to one another. Collimated light need not be monochromatic, polarized, or coherent.

Colored-glass filter. A slab of glass containing colloids or metals that absorb certain wavelengths while freely transmitting others. In microscopy, colored-glass filters are commonly employed in fluorescence filter sets and as effective blockers of UV and IR light.

Coma. An off-axis aberration of lenses, whereby rays from an off-axis point passing through the edge of the lens are focused closer to the optical axis than are rays that pass through the center of the lens, causing a point object to look like a comet with the tail extending toward the periphery of the field. Coma is the most prominent off-axis aberration. For lenses having the same focal length, coma is greater for lenses with wider apertures.

Compensator. In polarization microscopy, a birefringent slab that is positioned between the polarizer and analyzer and can be tilted or rotated. This action varies the optical path difference between the O and E rays emergent from a birefringent object and is performed to make quantitative measurements of relative O and E wave retardations, or for qualitative purposes in changing image contrast and brightness.

Composite view (projection view). In confocal microscopy, an image created by adding together multiple optical sections acquired along the *z*-axis. Frequently, the range of light intensities is selected by the operator. The images of three-dimensional objects, although blurry in conventional wide-field fluorescence mode, are often remarkably clear in confocal composite view.

Compound light microscope. An optical instrument that forms a magnified image of an object through a two-step series of magnifications: The objective forms a

magnified real image of the object, and the eyepiece forms a magnified virtual image of the real image made by the objective. This basic design forms the basis of all modern light microscopes.

Condenser annulus. In phase contrast and darkfield microscopy, a transparent annulus in an opaque black disk located in the front aperture of the condenser that serves as the source for illuminating the specimen.

Condenser lens. A lens assembly located near the specimen and specimen stage that collects light from the illuminator and focuses it on the specimen. Proper optical performance requires that the condenser be highly corrected to minimize chromatic and spherical aberration.

Cone cell photoreceptors. Retinal cells responsible for color vision and visual acuity. See also *Fovea*.

Confocal laser scanning microscope (CLSM). A mode of light microscopy whereby a focused laser beam scans the specimen in a raster and the return emitted fluorescent light or reflected light signal passes through a pinhole aperture in front of a photomultiplier tube and is displayed in pixels on a computer monitor. The dimensions of the pixel display depend on the sampling rate of the electronics and the dimensions of the raster. A variable pinhole aperture, located in a plane confocal with the specimen, rejects out-of-focus signals and allows for optical sectioning.

Conjugate focal planes. In optics, a plane P' that is conjugate to a given focal plane P, where all points on P are imaged at P'. In light microscopy, two sets of field and aperture planes whose precise geometrical positioning in the microscope is assured by adjusting the focus of the objective, condenser, and lamp collector lenses as required for Koehler illumination. The two sets of focal planes are conjugate with each other but not with the focal planes belonging to the other set; as a consequence, looking from one focal plane along the optical axis simultaneously reveals the images of the other conjugate focal planes.

Constructive interference. In wave optics and image formation, the condition where the summation of the E vectors of the constituent waves results in an amplitude greater than that of the constituents. For interference to occur, a component of one wave must vibrate in the plane of the other.

Contrast. Optical contrast is the perceived difference in the brightness (intensity or irradiance) between an object and its surround, and is usually given as the ratio of the light intensity of an object I_o to the light intensity of the object's background I_b, thus: $C = (I_o - I_b)/I_b$, or alternatively as $C = (I_o - I_b)/(I_o + I_b)$.

Contrast threshold. The minimal contrast required for visual detection. The contrast threshold is strongly dependent on the angular size, shape, and brightness of the specimen, the brightness of the viewing environment, the region of the retina used for detection, and other factors. For extended objects, the contrast threshold is usually given as 2–3% in bright light and 30–100% or even greater in dim light.

Convolution. In image processing, the procedure of combining the values of image pixels with a 3×3, 5×5, and so on, matrix of numbers through a defined function for purposes of image sharpening and blurring. The processing values in the convolution matrix or kernel are applied to each image pixel and to neighboring pixels covered by the mask in order to calculate new pixel values in a processed image that takes into account the values of neighboring pixels.

Critical angle, θ_c. In total internal reflection, the angle subtended by the incident beam and a line perpendicular to the reflecting surface at the point of incidence at which

the beam travels along the interface and does not enter the second medium. At angles greater than θ_c, beams are reflected away from the reflecting surface.

Crossover. See *Bleedthrough*.

Crosstalk. A term that describes the minimum attenuation (blocking) level over a specified range of two filters stacked back-to-back in a series. The degree of filter crosstalk should be seriously considered when matching excitation and emission filters for fluorescence filter sets. Dichromatic mirrors are often included in crosstalk evaluation of fluorescence filter combinations. Reduction or elimination of crosstalk improves contrast of multiply stained specimens.

Curvature of field. An aberration of a lens that causes the focal plane to be curved instead of flat.

Cyanine dyes. A family of reactive cyanine dyes—Cy2, Cy3, Cy5, and Cy7 and others—were originally developed for fluorescence imaging by Alan Waggoner (Carnegie Mellon University) and are presently marketed by GE Healthcare, Jackson ImmunoResearch, and other companies. These dyes contain two partially saturated indole nitrogen heterocyclic units separated by a polyalkene bridge of varying length. The cyanine dyes have reasonably narrow excitation and emission spectra, and compared with fluorescein and rhodamine, have improved water solubility, photostability, quantum yield, and a decreased sensitivity to pH. The excitation spectra are distributed such that commonly used laser lines and arc-lamp emission lines can be used for their excitation. Dyes Cy5, Cy5.5, and Cy7 are frequently used as near-infrared labels. While invisible to the eye, infrared fluorescence is seen well by most CCD cameras, making these dyes valuable for multifluorescence labeling.

Dark count and dark noise. In electronic cameras, the photon-independent signal in an image. The major constituents of the dark count are the bias signal, thermal noise, and camera read noises from the detector and processing circuits. The dark count must be subtracted from a raw image in order to obtain a corrected image based solely on photon-dependent counts. The dark noise is defined as the square root of the dark count and remains a part of the corrected image. The dark count is determined by acquiring an image (a dark frame) without opening the camera shutter.

Darkfield microscopy. A mode of light microscopy in which 0th order undeviated light is excluded from the objective and image formation is based solely on the interference of waves of diffracted light. Typically, darkfield images are obtained by illuminating the specimen with a transparent annulus in an otherwise opaque mask at the condenser front aperture. A relatively small NA objective is used so that undeviated light does not enter the objective, allowing only diffracted waves to enter the objective and form an image.

Dark frame. In image processing, a picture containing the dark count (thermal and bias counts) and showing a featureless, low amplitude background that is used to prepare a flat field-corrected image of the object. A dark frame is prepared using the same exposure time as for the raw image but without opening the shutter.

Deconvolution fluorescence microscopy. A method that applies computer deconvolution algorithms to a through-focus stack of images along the *z*-axis to enhance photon signals specific for a given image plane or multiple focal planes in an image stack. A stepper motor attached to the microscope focus drive guarantees image acquisition at regular intervals through the specimen. In typical applications, deconvolution methods are used to deblur and remove out-of-focus light from a particular focal plane of interest. In more sophisticated applications, image frames of an entire stack

can be deconvolved to allow clear views of a specimen displayed in projection view or in 3D viewing mode.

Depth of field. The thickness of the optical slice through a specimen that is in focus in the real intermediate image. The thickness measurement is dependent on geometric and wave-optical parameters. For a high NA objective, the thickness of the optical slice in the specimen Z is given approximately as $Z = n\lambda/\mathrm{NA}^2$, where n is the refractive index of the medium between the lens and the object, λ is the wavelength of light in air, and NA is the numerical aperture.

Depth of focus. The thickness of the image at the real intermediate image plane in the microscope. Like depth of field, the focus thickness depends on geometric and wave-optical parameters. The depth of focus is given approximately as $[1000\, M_{\mathrm{objective}}/(7\, NA \times M_{\mathrm{total}})] + [\lambda M^2_{\mathrm{objective}}/2\mathrm{NA}^2_{\mathrm{objective}}]$, where M is magnification, λ is wavelength, and NA is the numerical aperture.

Dequenching of donor fluorescence. In FRET imaging, the procedure known as "acceptor photobleaching" that reduces acceptor fluorescence, thus dequenching the donor and causing it to fluoresce. See *Acceptor photobleaching FRET.*

Descanning. In confocal microscopy, the optical design of allowing the fluorescent light emitted at the specimen upon excitation by the scanning laser spot to retrace its path back through the objective and scanner mirrors to the dichromatic mirror. With descanning, the fluorescent image spot at the detector pinhole remains steady and does not wobble.

de Sénarmont method of compensation. In polarization and DIC microscopy, the use of a fixed quarter-waveplate retarder together with a rotating analyzer as a method for measuring optical path differences (relative retardations) between 0 and E rays and for introducing compensating retardation to adjust image contrast. Retardations of $\lambda/20$ to 1λ can be measured with an accuracy of ±0.15 nm.

Destructive interference. In wave optics and image formation, the condition where the summation of the E vectors of constituent waves results in an amplitude less than that of the constituents. For interference to occur, a component of one wave must vibrate in the plane of the other.

Dichroic mirror. See *Dichromatic beamsplitter.*

Dichroism. The property exhibited by linear polarizing films and certain naturally occurring minerals, whereby incident wavelengths are differentially absorbed, causing the object to appear in two different colors depending on the angle of view and the orientation of incident waves. The phenomenon reflects the difference between the absorption curves for chromophores oriented in different directions in the dichroic object.

Dichromatic beamsplitter (dichroic mirror). An interference filter/mirror combination commonly used in fluorescence microscopy filter sets to produce a sharply defined transition between transmitted and reflected wavelengths. When inclined at a 45° angle with respect to the incident illumination and emission light beams, the dichromatic mirror usually reflects short excitation wavelengths through a 90° angle onto the specimen and transmits longer emitted fluorescence wavelengths straight through to the eyepieces and detector system. Dichromatic mirrors fabricated with interference thin films for fluorescence microscopy are capable of reflecting 90% or more of the excitation light while simultaneously transmitting approximately 90% of the emission band. The dichromatic mirror is usually the central element of three filters (excitation, barrier, and dichromatic mirror) contained within a fluorescence filter optical block.

DIC microscopy. See *Differential interference contrast (DIC) microscopy*.

DIC prism. See *Wollaston prism*.

Dielectric constant. A parameter describing the electrical permittivity of a material (the degree to which a material is permeated by the electric field in which it is immersed). Substances with low electrical conductivity (and low permittivity), such as glass, plastic, and water, are called insulators or dielectrics. The dielectric constant ε is related to the refractive index n such that $n = \sqrt{\varepsilon}$.

Differential interference contrast (DIC) microscopy. A mode of light microscopy employing dual-beam interference optics that transforms local gradients in optical path length in an object into regions of contrast in the object image. Also referred to as Nomarski optics after Georges Nomarski. The specimen is illuminated by myriad pairs of closely spaced coherent rays that are generated by a crystalline beamsplitter called a Wollaston prism. Members of a ray pair experience different optical path lengths if they traverse a gradient in refractive index in a phase object. Optical path differences become translated into amplitude differences (contrast) upon interference in the image plane. DIC images have a distinctive relief-like, shadow-cast appearance.

Diffracted wave. In phase contrast and other modes of interference microscopy, waves that become deviated from the path of 0th order (background) waves at the object. Diffracted waves can he shown to be retarded in phase by ~ ¼ wavelength from the background wave by vector analysis. Diffracted waves combine with background waves through interference in the image plane to generate resultant particle (P) waves of altered amplitude that are perceived by the eye. See also *Particle wave and Surround wave*.

Diffraction. The bending or breaking up of light that occurs when waves interact with objects, much in the way that waves of water bend around the edge of a log or jetty. Light waves that become scattered upon interacting with an object (diffracted waves) follow paths that deviate from the direction followed by waves that do not interact with the specimen (nondiffracted or undeviated waves).

Diffraction grating. A transparent or reflective substrate containing an array of parallel lines having the form of alternating grooves and ridges with spacings close to the wavelength of light. Light that is reflected by or transmitted through such a grating becomes strongly diffracted. Depending on the geometry of illumination and wavelength, a grating can generate color spectra and patterns of diffraction spots.

Diffraction plane. One of the aperture planes of the light microscope containing the focused diffraction image of the object. Under conditions of Koehler illumination, the diffraction plane is located at or near the rear focal plane of the objective.

Diffusion coefficient, *D*. A characteristic hydrodynamic property of molecules, usually defined for standard physical conditions in water, which is used to calculate the rate of diffusion and speed of movement of molecules in a medium such as water or cytoplasm.

Digital image processor. In video imaging, a signal processing device that converts analog video signals to digital format for rapid image processing operations, such as frame averaging, background subtraction, and contrast adjustment.

Digitizer. See *Analog-to-digital converter (ADC)*.

Dipole–dipole interactions. Dipoles are molecules with positively and negatively charged poles separated by a small distance. The attraction between two poles of opposite charge promotes close molecular associations between fluorophore labels and is essential for the phenomenon of fluorescence resonance energy transfer (FRET) in fluorescence microscopy.

Distortion. An aberration of lenses, where the magnification factor describing an image varies continuously between the central and peripheral portions of the image. Depending on whether the magnification is greater at the center or at the periphery, the distortion can be of the barrel or the pincushion type, respectively.

Double refraction. In polarization optics, the splitting of light into distinct O and E rays in a birefringent material. When a birefringent crystal of calcite is placed on a page of printed words, the effects of double refraction are clearly observed as an overlapping, double image of the text. See *Birefringence*.

DR. See *Dynamic range (DR)*.

dSTORM. Direct STORM is a method of single molecule localization that allows one to use photoswitchable fluorophores such as Cy5 and Alexa Fluor 647 individually without having to use coupled methods of cyanine switching. dSTORM requires oxygen depletion and a reducing environment produced by thiols.

Dwell time. In confocal microscopy, the length of time that the scanning laser beam remains at a unit of space corresponding to a single pixel in the image. In a laser scanning microscope, dwell time is typically 0.1–1.0 μs or more. Long dwell times increase the rate of photobleaching and decrease the viability of living cells.

DyLight dyes. These are sulfonated coumarin, rhodamine, xanthene (fluorescein), and cyanine derivatives with high quantum yield and enhanced photostability that give very bright fluorescence compared with standard rhodamine and fluorescein family members. Sulfonation makes the dyes negatively charged and hydrophilic. These dyes were developed/marketed by Diomics/Thermo Fisher (DyLight). The dyes are available with reactive functional groups for conjugation to proteins and antibodies, including reactive succinimidyl-ester and maleimide groups.

Dynamic range (DR). The term describing the resolution of light intensity, the number of steps in light amplitude in an image that can be resolved by an imaging device. This number can range from several hundred to a thousand for video and low-end CCD cameras to greater than 65,000 for the 16-bit CCD cameras used in astronomy. For CCD cameras, the DR is defined as the full well capacity of a pixel (the number of photoelectrons at saturation) divided by the camera's read noise.

EGFP. See *Enhanced green fluorescent protein*.

Electronic state. The overall configuration of electrons in an atom or molecule, which in turn determines the distribution of negative charge (electrons) in the molecule and the molecular geometry. Any given molecule can exist in one of several electronic states, depending upon the total electron energy and on the symmetry of the electron spins in the orbitals. At room temperature, the majority of molecules exist in the electronic state with the least energy (the ground state). When the molecule absorbs a photon, electrons are excited to higher energy states (excited states).

Elliptically polarized light. A form of polarized light whereby the E vector of a polarized wave rotates about the axis of propagation of the wave, thus sweeping out a right- or left-handed spiral. If you could view the wave end-on, the movement of the E vector would appear to trace the form of an ellipse.

EMCCD. Electron-multiplying CCDs feature a 500-pixel extension of the serial register that is operated under variable voltage to allow for photoelectron amplification through a process of impact ionization. The increased gain per pixel is generally < 2%, but typically provides up to 20,000-fold gain overall. High quality images of dim specimens can be obtained because of the low overall read noise of the system. EMCCD cameras are useful in live-cell imaging.

Emission filter. In fluorescence microscopy, the final element in a fluorescence filter cube, which transmits fluorescence emission wavelengths while blocking residual excitation wavelengths. Commonly called a barrier filter. Emission filters are colored glass or interference filters and have the transmission properties of a bandpass or longpass filter.

Emission spectrum. The band (spectrum) of wavelengths emitted by an atom or molecule (fluorophore) after it has been excited by a photon of light or energy from another radiation source. After the fluorophore has emitted a photon, it returns to the ground-level energy state and is ready for another cycle of excitation and emission. Typically, the fluorescence emission spectrum is shifted to longer wavelengths than the stimulating excitation spectrum (in effect, the average wavelength of emission is longer than the average wavelength of excitation). In addition, the wavelength range and intensity profile of the fluorescence emission spectrum is generally independent of the excitation wavelength.

Enhanced green fluorescent protein (EGFP). A mutated version of GFP that is brighter, more photostable, and does not photoswitch under normal imaging conditions. EGFP has largely replaced the native GFP protein in fluorescence microscopy imaging application. See *Green fluorescent protein (GFP)*.

Environmental chamber. In live-cell imaging, a space around the specimen stage contained by an acrylic box or even a plastic bag in which environmental factors of temperature, CO_2 concentration, and humidity are controlled by external equipment.

Epi-illumination (reflected light). A common method of illumination in fluorescence microscopy, where the illuminator is placed on the same side of the specimen as the objective, and the objective performs a dual role as both a condenser and an objective. A dichromatic mirror is placed in the light path to reflect excitatory light from the lamp toward the specimen and transmit emitted fluorescent wavelengths to the eye or camera. The microscope component containing the illuminator, optics, aperture stops, and filter revolver is called an epi-illuminator.

E ray. See *Extraordinary ray (E ray)*.

Evanescent wave. Under conditions of total internal reflection, a standing wave of excitation light that penetrates for a short distance into the low refractive index medium and whose intensity diminishes exponentially with increasing distance from the reflection surface. When used for excitation in fluorescence microscopy (a technique known as total internal reflection; TIRF), only molecules within about 100 nm of the surface become excited.

Excitation (exciter) filter. In fluorescence microscopy, the first element in a fluorescence filter cube and the filter that produces the exciting band of wavelengths from a broadband light source such as a mercury or xenon arc lamp. Commonly, the excitation filter is a high-quality bandpass interference filter.

Excitation spectrum. The spectrum of wavelengths, usually spanning the ultraviolet and visible light spectrum, which is capable of exciting a fluorochrome (atom or molecule) to exhibit fluorescence. Excitation spectra are generated by scanning through the absorption spectrum of a fluorochrome or fluorophore while monitoring the emission at a single (peak) wavelength. In a manner similar to the absorption spectrum, the excitation is broadened due to vibrational and rotational relaxation (internal conversion) of excited molecules. Absorption and excitation spectra are distinct but often overlap, sometimes to the extent that they are nearly indistinguishable.

Exciter filter. See *Excitation filter*.

Extinction and extinction factor. In polarization optics, the blockage of light transmission through an analyzer. This condition occurs when the vibrational plane of the E vector of a linearly polarized beam is oriented perpendicularly with respect to the transmission axis of the analyzer. If two Polaroid filters are held so that their transmission axes are crossed, extinction is said to occur when the magnitude of light transmission drops to a sharp minimum. The extinction factor is the ratio of amplitudes of transmitted light obtained when (a) the E vector of a linearly polarized beam and the transmission axis of the analyzer are parallel (maximum transmission) and (b) they are crossed (extinction).

Extraordinary ray (E ray). Also termed a wavefront or ray, the extraordinary component of linearly polarized light that is transmitted through a birefringent medium traveling with a velocity that varies with the direction of transmission. The extraordinary wave is oriented parallel to the optical axis of a quartz wedge as it travels through a Wollaston or Nomarski prism. An extraordinary wavefront emanating from an imaginary point source in a birefringent medium can be described as the surface of a three-dimensional ellipsoid.

Eyepiece (ocular). The second magnifying lens of the microscope used to focus a real magnified image on the retina of the real intermediate image produced by the objective. The added magnification provided by the eyepiece increases the angular magnification of the virtual image perceived by the eye. The typical range of eyepiece magnifications is 5–25×.

Eyepiece telescope. See *Bertrand lens*.

Fast axis. In polarization optics, the long axis of the wavefront ellipsoid, a construction used to describe the surface of an emergent wavefront from a point source of light in a birefringent material. The fast axis indicates the direction of low refractive index in the specimen. See also *Refractive index ellipsoid*.

Fast Fourier transform (FFT). A filtering operation in the frequency domain used to selectively diminish or enhance low or high spatial frequencies (extended vs. fine detailed structures) in the object image. In generating a transform, image details are separated into sinusoidal frequency components to create a map of spatial frequencies. The transform can be covered with a mask to enhance or diminish spatial frequencies of interest. Reversing the procedure produces an image (the inverse transform) in which the contrast of spatial details is modified.

FCS. See *Fluorescence correlation spectroscopy (FCS)*.

FFT. See *Fast Fourier transform (FFT)*.

Field diaphragm. A variable diaphragm located in or near the aperture plane of the light source that is used to reduce the amount of stray light in the object image. Since the edge of the diaphragm is conjugate with the object plane under conditions of Koehler illumination, the field diaphragm is used as an aid in centering and focusing the condenser lens.

Field planes. That set of conjugate focal planes representing the field diaphragm, the object or specimen, the real intermediate image in the eyepiece diaphragm, and the retina.

Filter slope. The slope of an optical filter is a measure of the filter profile in the transition region between blocking and transmission. In general, the slope of a filter is defined by the wavelength at which the filter exhibits a specified blocking level and the rate of change in this region. Two filters can have the same cut-on or cut-off wavelengths, but still have different blocking levels and slopes. Very sharp slopes

transmit a narrow bandwidth of wavelengths in the cut-off or cut-on region, while shallow slopes have large bandwidths.

FISH. See *Fluorescence* in situ *hybridization (FISH)*.

FLAP. See *Fluorescence localization after photobleaching (FLAP)*.

Flat-field correction. In image processing, the procedure used to obtain a photometrically accurate image from a raw image. A so-called dark frame containing bias and thermal counts is subtracted from the raw image and from a "flat" or "background" image. The dark-subtracted raw image is then divided by the dark-subtracted flat-field image to produce the corrected image. With operation, all optical faults are removed. The photometric relation of pixel values to photoelectron count is also lost during division, although the relative amplitudes of pixel values within an image are retained. See also *Dark frame and Flat field frame*.

Flat-field frame. In image processing, a picture of featureless background that is used to prepare a flat-field-corrected image of the object. A flat-field frame is obtained by photographing a featureless region, close to and in the same focal plane as the object.

FLIM. See *Fluorescence lifetime imaging microscopy (FLIM)*.

FLIP. See *Fluorescence loss in photobleaching (FLIP)*.

Fluorescence. The process by which a suitable atom or molecule, which is transiently excited by absorption of external radiation at the proper energy level (usually ultraviolet or visible light), releases the absorbed energy as a photon having a wavelength longer than the absorbed energy. In fluorescence, an electron promoted into a singlet state of the excited orbital is paired (or the opposite spin) with respect to a second electron in the ground-state orbital. As a result, the return of the electron to the ground state is spin-allowed and occurs rapidly with the accompanying emission of a photon. The fluorescence excitation and emission processes usually occur in less than a nanosecond.

Fluorescence anisotropy. A term referring to the photoselective excitation of fluorophores due to the transient alignment of the absorption dipole moment with the electric vector of incoming photons. Similar to excitation, fluorescence emission by the excited fluorophore occurs in a plane oriented parallel to the emission dipole moment. The transition (dipole) moments for excitation and emission have a defined orientation with respect to the molecular axes of the dye molecule, and are separated from each other by an angle. During the excited state lifetime, rotation of the fluorophore will depolarize its emission with respect to the excitation vector, resulting in a mechanism with which to measure the rigidity (viscosity) of the environment containing the fluorophore. Fluorescence anisotropy is defined as the ratio of the difference between the emission intensity parallel to the polarized electric vector of the exciting light and the intensity perpendicular to the vector, divided by the total intensity.

Fluorescence correlation spectroscopy (FCS). Used primarily with laser scanning confocal or multiphoton microscopy, fluorescence correlation spectroscopy is a technique designed to determine molecular dynamics in volumes containing only one or a few molecules, yielding information about chemical reaction rates, diffusion coefficients, molecular weights, flow rates, and aggregation. In FCS, a small volume (approximately one femtoliter) is irradiated with a focused laser beam to record spontaneous fluorescence intensity fluctuations arising from the number or quantum yield of the molecules occupying the volume as a function of time. Relatively small fluorophores diffuse rapidly through the illuminated volume to generate short, randomized bursts of intensity. In contrast, larger complexes (fluorophores bound to

macromolecules) move more slowly and produce a longer, more sustained time-dependent fluorescence intensity pattern.

Fluorescence and DIC combination microscopy. Fluorescence and differential interference contrast (DIC) can be coupled to image much of the fine detail in living cells while simultaneously observing the distribution of added fluorophores. Because DIC requires a polarization arrangement and transmitted light, fluorescence and DIC images must be captured separately. The resulting images are then combined (overlaid) to spatially map fluorescence intensity as a function of cellular architecture. In some cases, the fluorescence microscope dichromatic mirror can be employed to act as a polarizer (the analyzer) to enable simultaneous imaging in both modes.

Fluorescence filter set. Usually housed in cube-shaped optical blocks, fluorescence filter sets are composed of an excitation filter, an emission (barrier) filter, and a dichromatic mirror. The filter block is positioned in the vertical illuminator, above the objective, so that incident illumination can be directed through the excitation filter and reflected from the surface of the dichromatic mirror onto the specimen. The fluorescence emitted by the specimen is gathered by the objective and transmitted through the dichromatic mirror to the eyepieces or detector system. Fluorescence filter sets are matched with respect to bandpass regions for the various filter combinations to minimize crosstalk between the filters and maximize recorded fluorescence intensity.

Fluorescence *in situ* hybridization (FISH). The fluorescence FISH technique is based on hybridization between target sequences of chromosomal DNA with fluorescently labeled single-stranded complementary sequences (termed cDNA) to ascertain the location of specific genetic sequences. In a method referred to as direct FISH, fluorophores are coupled directly to the complementary nucleic acid probe to enable the probe-target hybrid complexes to be visualized with a fluorescence microscope. Indirect FISH involves binding of a fluorescently labeled antibody to the complementary probe after hybridization in order to amplify the fluorescence signal and expand the number of fluorophores available for multiple labeling experiments.

Fluorescence lifetime. The characteristic time that a molecule remains in an excited state prior to returning to the ground state. During the excited state lifetime, the fluorophore can undergo conformational changes, as well as interact with its local environment. The fluorescence lifetime is defined as the time in which the initial fluorescence intensity of a fluorophore decays to $1/e$ (approximately 37%) of the initial intensity. This quantity is the inverse of the rate constant of the fluorescence decay from the excited state to the ground state.

Fluorescence lifetime imaging microscopy (FLIM). A sophisticated technique that enables simultaneous recording of both the fluorescence lifetime and the spatial location of fluorophores throughout every location in the image. The methodology provides a mechanism to investigate environmental parameters, such as pH, ion concentration, solvent polarity, and oxygen tension in single living cells, presenting the data in a spatial and temporal array. FLIM measurements of the nanosecond excited state lifetime are independent of localized fluorophore concentration, photobleaching artifacts, and path length (specimen thickness), but are sensitive to excited state reactions, such as resonance energy transfer.

Fluorescence localization after photobleaching (FLAP). A derivative of FRAP where the molecular target being studied is labeled with two different fluorophores (usually fluorescent proteins) that can be imaged independently at the same time. One of the fluorophores is photobleached in a selected ROI, while the other

fluorophore can be observed as localized by the targeting protein. The FLAP image is calculated by subtracting the photobleached signal from that of the unbleached fluorophore.

Fluorescence loss in photobleaching (FLIP). In a technique related to FRAP, a defined region of fluorescence within a living cell is subjected to repeated photobleaching by illumination with intense irradiation. Over a measured time period, this action will result in complete loss of fluorescence signal throughout the cell if all of the fluorophores are able to diffuse into the region that is being photobleached. By calculating the rate at which fluorescence is extinguished from the entire cell, the diffusional mobility of the target fluorophore can be determined.

Fluorescence microscopy. A popular clinical and research technique in optical microscopy that relies on excitation of fluorescent molecules with a specific wavelength region to produce an image generated by the secondary fluorescence emission at longer wavelengths. Modern fluorescence microscopes are equipped with reflected light illuminators that incorporate neutral density filters and a specialized combination of interference filters to segregate incident illumination from the detected fluorescence emission. Widefield fluorescence microscopy uses the full aperture of the objective and an extended light source, such as an arc lamp, to form an image.

Fluorescence and phase contrast combination microscopy. Traditional phase contrast optics can be coupled with fluorescence microscopy to observe the spatial distribution of fluorophores in living and fixed cells and map the emission intensity to specific structures and organelles. Because the phase contrast technique requires transmitted light illumination that is modified with a ring-shaped aperture (condenser annulus) and detected with a spatial filter (phase plate) positioned in the objective rear focal plane, viewfields must be captured independently from fluorescence in order to obtain the best contrast. The resulting images are then combined (overlaid) to spatially map fluorescence intensity as a function of cellular architecture. Some manufacturers offer low density phase plates that enable simultaneous imaging of live cells in phase contrast and fluorescence.

Fluorescence photobleaching and recovery (FPR). See *fluorescence recovery after photobleaching (FRAP)*.

Fluorescence recovery after photobleaching (FRAP). In FRAP, a very small, selected region is subjected to intense illumination, usually with a laser, to produce photobleaching of fluorophores in the region within a few milliseconds. After the photobleaching pulse, the rate and extent of fluorescence recovery are monitored as a function of time to determine the kinetics of recovery. FRAP can also be used to measure the diffusion coefficients of molecules.

Fluorescence resonance energy transfer (FRET). Also known as Förster resonance energy transfer. In microscopy, the term refers to the transfer of energy from one fluorophore (the donor) to another chromophore (the acceptor) in close proximity through a mechanism of dipole-dipole coupling. There is no emission of radiation in the process. The efficiency of energy transfer depends strongly on intermolecular distance, molecular orientation, and spectral overlap among other factors. FRET provides information about the binding and interaction between macromolecules. FRET microscopy is performed using either steady-state or time-resolved techniques, but time-resolved FRET imaging has the advantage of more accurately mapping the donor-acceptor distance. A standard fluorescence microscope equipped with the proper excitation and emission filters and a sensitive digital camera can be utilized to perform FRET imaging.

Fluorescence speckle microscopy (FSM). A technique compatible with widefield and confocal microscopy that employs a very low concentration of fluorescent labeled subunits to reduce fluorescence away from the focal plane, and thus improve visibility of labeled structures and their dynamics in thick regions of living cells. This is accomplished by labeling only a small fraction of the entire structure of interest. Fluorescence speckle microscopy has been very useful for defining the movement and polymerization kinetics of cytoskeletal elements, such as actin and microtubules, in live cells.

Fluorescent biosensor. A chimeric protein composed of a functional domain (protease, calcium or metal binding protein, pH, etc.) and a fluorescent indicator, usually a fluorescent protein. The fluorescence of the indicator changes upon a conformational change in the function domain.

Fluorite (semiapochromat) lens. Objectives made of fluorite or CaF_2, a highly transparent material of low color dispersion. The excellent color correction afforded by simple fluorite elements accounts for their alternative designation as semiapochromats. The maximum numerical aperture is usually limited at 1.3.

Fluorochrome. A dye or molecule capable of exhibiting fluorescence. Fluorochromes (also termed fluorescent molecules, probes, or fluorescent dyes) are usually polynuclear heterocyclic organic molecules containing carbon, nitrogen, sulfur, and/or oxygen with delocalized electron systems and reactive moieties that enable the compounds to be attached to a biological species.

Fluorophore. The specific region or structural domain of a molecule capable of exhibiting fluorescence. Fluorophores are divided into two general classes, intrinsic and extrinsic. Intrinsic fluorophores are those that occur naturally in biological structures and other materials. Extrinsic fluorophores are added to a specimen that does not display the desired spectral (fluorescent) properties. In many cases, a fluorophore is composed of a smaller aromatic molecule (fluorochrome) attached through a chemical reaction or by absorption to a larger macromolecule. Typical examples include acridine orange intercalated between successive DNA base pairs, the fluorescein moiety in a conjugated protein or antibody, and the tetrapyrrole ring system in chlorophyll.

F-number. See *Focal ratio.*

Focal length. The distance along the optical axis between the principal plane of a lens and its focal plane. For a simple converging (positive) lens illuminated by an infinitely distant point source of light, the image of the point lies precisely one focal length away from the principal plane.

Focal ratio (f-number). The ratio of the focal length of a lens to the diameter of its aperture.

Förster distance, R_o. In FRET microscopy, the intermolecular distance in nanometers that can be computed between fluorescently tagged proteins or macromolecules. R_o is directly related to the FRET efficiency (E) and is influenced by relative molecule orientation and the refractive index of the medium, as well as factors pertaining to the fluorescence and spectral overlap of the particular system under study.

Fovea. A 0.2- to 0.3-mm diameter spot in the center of the macula on the retina that defines the optical axis of the eye and contains a high concentration of cone cell photoreceptors for color vision and visual acuity in bright light conditions.

Frame accumulation. In electronic imaging, the method of adding together a number of image frames to create a brighter image with improved signal-to-noise ratio.

Frame averaging (Kalman averaging). In electronic imaging, the method of averaging a number of raw image frames to reduce noise and improve the signal-to-noise

ratio. The signal-to-noise ratio varies as the square root of the number of frames averaged.

Frame grabber board. In electronic imaging, the computer board that determines the frame memory, a remote access memory for storing the pixel values comprising an image. Grabbing is the process of acquiring and storing an image into a frame buffer.

Frame-transfer CCD. A CCD whose pixel array is divided into two equal halves. One section is uncovered and contains active photosites; the other area is masked with a light-shielding metal film and acts as a storage site. This design of CCD speeds image capture, because readout of the storage site and acquisition at the image site occur simultaneously and because the camera can work without a shutter.

Franck–Condon principle. A fundamental concept governing the fluorescence phenomenon based on the fact that molecular nuclei are stationary during electronic transitions (represented by vertical lines in a Franck–Condon or Jablonski diagram). Electronic transitions from the ground state to a higher energy excited state occur in such a short time frame (measured in femtoseconds) that the nuclei do not have sufficient time to vibrate. As a result, the only electronic transitions from the ground state to the excited that can occur are those where the probabilities of the electron position in the ground and excited states maximally overlap.

FRAP. See *Fluorescence recovery after photobleaching (FRAP).*

Free radical. A reactive chemical species having an unpaired electron, which is generated by molecular excitation in the presence of light. Free radicals engage in cycles of oxidation that damage fluorophores and molecules, such as proteins, lipids and DNA, which are essential to cell function. Free radical formation is controlled by reducing oxygen concentration and/or providing free radical scavengers.

Frequency domain. In imaging, spatial features can be converted into frequencies that are composed of a number of sine wave frequency components and represented in separate but correlated plots of magnitude and phase. Image processing in the frequency domain allows selective manipulation of coarse, medium, or fine features throughout the image and is the basis of structured illumination microscopy. See *SIM*.

Frequency of vibration. The number of periods measured in per unit time or unit distance of an electromagnetic wave.

FRET. See *Fluorescence resonance energy transfer (FRET).*

FSM. See *Fluorescence speckle microscopy (FSM).*

Full-frame CCD camera. A CCD design in which all of the pixels in the so-called parallel register function as active photosites. Full-frame CCDs have a high dynamic range because all of the pixel area is used for photon capture and storage.

Full wave plate. In polarization optics, a birefringent plate (retarder) capable of introducing an optical path length difference between O and E rays equivalent to a full wavelength of light. Since the unique wavelength emerges with a linearly polarized waveform, positioning the plate diagonally between two crossed polars under conditions of white light illumination extinguishes the linearly polarized wavelength, resulting in the visual perception of an interference color. A first-order red plate shows a first-order red interference color because 551 nm green wavelengths have been removed.

Full width at half maximum (FWHM). A parameter describing the spectral range of transmitted wavelengths of a bandpass filter. The cut-on and cut-off boundaries are defined as the wavelengths giving 50% of maximum transmittance of the filter. A

FWHM of 20 indicates that the transmitted bandwidth spans 20 nm. Also called the half bandwidth (HBW).

FWHM. See *Full width at half maximum (FWHM)*.

GaAsP photomultiplier detector. A PMT used in confocal microscopes and other microscopes with a photocathode containing a coating of gallium-arsenide-phosphide, which is very light sensitive and is used for imaging dim specimens. GaAsP detectors are susceptible to damage by bright light, and their sensitivity decreases over time.

Gain. In electronic imaging, the amplification factor applied to an input signal to adjust the amplitude of the signal output. In confocal imaging with PMTs, an input voltage signal might be multiplied by a positive gain factor to increase the voltage of the signal output and hence the brightness of the signal on the TV. In digital CCD microscopy, 1× gain is defined as the number of photoelectrons assigned per ADU; 2× gain is one-half the number of photoelectrons/ADU, etc.

Galvanometer scanner. In point-scanning laser confocal microscopes, the device responsible for moving a mirror attached to a rotating post that scans a focused laser beam (a point) over the specimen in a raster pattern. Galvanometers are transducers that can produce rapid rotary deflections in response to a current.

Gamma (γ). The exponent in the mathematical expression relating an output signal to its corresponding input signal for a camera, monitor, or other display device. In image processing, changing gamma increases or decreases the contrast between high and low pixel values according to the function, displayed value = [(normalized value − min)/(max − min)]$^{\gamma}$. For $\gamma = 1$, the relationship between signal strength and display intensity is linear.

GFP. See *Green fluorescent protein (GFP)*.

Green fluorescent protein (GFP). A fluorescent 28 kDa protein from the jellyfish *Aequorea victoria*, which is commonly used as a fluorescent marker to determine the location, concentration, and dynamics of a protein of interest in cells and tissues. The excitation and emission maxima of enhanced GFP (EGFP) occur at 488 and 507 nm, respectively. The DNA sequence of GFP can be ligated to the DNA encoding a protein of interest to produce a recombinant chimera capable of protein expression in the cells of interest. Cells transfected with the modified DNA subsequently express fluorescent chimeric proteins *in situ*.

Ground state depletion (GSD) microscopy. Ground state depletion is a method of exciting fluorophores with light so that they enter a darkened state that is long relative to rapid microscope imaging operations. In superresolution imaging, GSD is used to shape the point spread function (PSF) using certain fluorophores.

Ground state depletion with individual molecule return microscopy (GSDIM). A form of single-molecule localization imaging that employs ground state depletion of fluorophores by shelving the molecules in a dark state as the method to turn molecules on and off.

GSD. *See Ground state depletion (GSD) microscopy.*

GSDIM. *See Ground state depletion with individual molecule return microscopy (GSDIM).*

Half bandwidth (HBW). In describing the transmission band of a filter, the full width of a bandpass at one-half of the peak height. See *Full width at half maximum (FWHM)*.

Halo. In phase contrast microscopy, characteristic contrast patterns of light or dark gradients flanking the edges of objects in a phase contrast image. Halos are caused

by the phase contrast optical design that requires that the image of the condenser annulus and objective phase plate annulus have slightly different dimensions in the rear focal plane of the objective.

High-pass filter. In image processing, a filter that transmits high spatial frequencies and blocks low spatial frequencies. After filtering, edges and fine details are strongly enhanced, whereas large extended features are made less distinct.

Histogram equalization or histogram leveling. In image processing, an operation that reassigns pixel values so that each step of the grayscale is represented by an approximately equal number of pixels. In equalization, the cumulative histogram distribution is scaled to map the entire range of the grayscale, the rank order of the original pixel values being maintained as closely as possible. This operation is used to increase the contrast of flat images in which the pixel values differ by only a small amount compared with the potential grayscale range of the image.

Histogram stretching. In image processing, the operation for image display whereby a subset of gray-level values is stretched from black to white. The effect of this operation is to increase the contrast of the selected range of gray levels.

HMC. Hoffman modulation contrast. See *Modulation contrast microscopy (MCM)*.

Hot mirror. A specialized dichromatic interference filter that reflects infrared wavelengths while transmitting shorter wavelengths of visible light. By transmitting visible light wavelengths while reflecting infrared, hot mirrors can also serve as a dichromatic beamsplitter for specialized applications in fluorescence microscopy.

Huygens' principle. A geometrical method used to show the successive locations occupied by an advancing wavefront. An initial source or wavefront is treated as a point source or a collection of point sources of light, each of which emits a spherical wave known as a Huygens' wavelet. The surface of an imaginary envelope encompassing an entire group of wavelet profiles describes the location of the wavefront at a later time, *t*. Huygens' principle is commonly used to describe the distribution of light energy in multiple interacting wavefronts as occurs during diffraction and interference.

iFRAP or inverse FRAP. iFRAP is a variation of the photobleaching technique, FRAP, similar to FLIP. Instead of photobleaching the region of interest directly, the inverse region is photobleached before examining fluorescence recovery kinetics.

Image analysis. Any number of measurement operations of objects contained in an image, including particle counts; geometrical measurements of length, width, area, centroid location, and so forth; intensity measurements; contour measurements; stereology; and many other operations.

Image distance and object distance. With respect to the principal planes of a lens, the image-to-lens and object-to-lens distances, as described by the lens equation in geometrical optics. See also *Lens equation*.

Image histogram. A frequency histogram of pixel values comprising an image, with pixel values shown on the *x*-axis and the frequency of occurrence on the *y*-axis. The histogram allows one to see the relative contributions of dark, gray, and bright pixels in an image at a glance and is useful for adjusting image brightness and contrast.

Image processing. The adjustment of an image's pixel values for purposes of image correction and measurement (flat-field correction) or display (adjustment of image brightness and contrast).

Immobile fraction. In FRAP, the fraction of fluorescence that is not restored during fluorescence recovery.

Immunofluorescence microscopy. A mode of fluorescence microscopy in which a certain molecular species in a specimen is labeled with a specific fluorescent antibody. Fluorescence emission from excited antibodies is collected by the objective to form an image of the specimen. Antibodies can be made fluorescent by labeling them directly with a fluorescent dye (direct immunofluorescence) or with a second fluorescent antibody that recognizes epitopes on the primary antibody (indirect immunofluorescence).

Incandescent lamp. A bulb containing an inert gas and metal (usually tungsten) filament that emits photons as the filament becomes excited during passage of electric current. The spectrum of visible wavelengths emitted by the filament shifts to increasingly shorter wavelengths as the amount of excitation is increased. The output of incandescent lamps is very high at red and infrared wavelengths.

Incubator microscope. A specially designed instrument for time-lapse imaging of living cells in which a microscope with illuminators and motorized stage is integrated with a tissue culture incubator. Adjustments for environmental and microscope control are all made outside the box to minimize thermal focus drift. Confocal incubator microscopes are also available.

Index ellipsoid. See *Refractive index ellipsoid*.

Infinity corrected optics. The latest optical design for microscope objectives in which the specimen is placed at the focal length of the lens. Used by itself, the image rays emerge from the lens parallel to the optical axis, and the image plane is located at infinity. In practice, a tube lens or Telan lens located in the body of the microscope acts together with the objective to form an image in the real intermediate image (eyepiece) plane. This optical design relaxes constraints on the manufacture of the objective itself and allows for placement of bulky accessory equipment, such as fluorescence filter cubes in the space between the objective and the tube lens.

Integrated histogram. A modified form of an image histogram in which the *x*-axis indicates the pixel value and the *y*-axis indicates the cumulative number of pixels having a value of *x* and lower on the *x*-axis. The edge of the histogram defines a display function from which one can determine the rate of change in light intensity at any value of *x* along the grayscale. Integrated histograms are useful for determining the gray-level midpoint and for determining if LUTs should be linear, exponential, and so on.

Intensifier silicon-intensifier target (ISIT) camera. A video camera tube used for low-light imaging applications. An ISIT tube is essentially a SIT tube modified by the addition of an image intensifier coupled by fiber optics as a first stage of light amplification.

Intensity of light. Qualitatively, the brightness or flux density of light energy perceived by the eye. By universal agreement, the term intensity, meaning the flow of energy per unit area per unit time, is being replaced by the word irradiance, a radiometric term indicating the average energy (photon flux) per unit area per unit time, or watts/meter^2. As a term describing the strength of light, intensity is proportional to the square of the amplitude of an electromagnetic wave.

Interference. The sum of two or more interacting electromagnetic waves. Two waves can interfere only if a component of the E vector of one wave vibrates in the plane of the other wave. Resultant waves with amplitudes greater or less than the constituent waves are said to represent constructive and destructive interference, respectively.

Interference color. The color that results from the removal of a band of visible wavelengths from a source of white light.

Interference filter. A filter made from alternating layers of different dielectric materials or layers of a dielectric material and thin metal film that transmits a specific band of wavelengths. The spacings between the layers of one-quarter or one-half wavelength allow constructive interference and reinforce propagation through the filter of a particular wavelength (λ). All other wavelengths give destructive interference and are absorbed or reflected and do not propagate through the filter.

Interline transfer CCD. A CCD design having alternate columns of pixels that function as exposed photosites and masked storage sites. During operation, the masked pixels are read out and digitized while exposed sites simultaneously capture photoelectrons. This double-duty action speeds up camera operation. Newer interline CCDs contain microlenses that cover storage- and photosite-pixel pairs to increase light-gathering efficiency. Upon completion of an exposure, the transfer of signal charges from a photosite pixel to an adjacent storage pixel is so fast that a camera shutter is not required.

Intermolecular FRET. Fluorescence resonance energy transfer between two separate molecules, where each molecule bears a distinct fluorophore.

Intramolecular FRET. Fluorescence resonance energy transfer between two fluorophores that are attached to separate regions of the same molecule.

Intrinsic lifetime. Defined as the lifetime of the excited state in the absence of any processes that compete for deactivation of excited state electrons, the intrinsic lifetime is measured as the inverse of the rate constant for the decay of fluorescence. In practice, the measured lifetime of a fluorophore is a combination of the intrinsic fluorescence lifetime and the nonfluorescent processes (quenching, nonradiative relaxation, etc.) that lead to relaxation of the excited state. The measured lifetime is always less than the intrinsic lifetime and is an indicator of the quantum yield.

Inverse transform. In image processing, the image created by a Fourier transform operation used primarily to blur and sharpen images. A Fourier transform appears similar to a diffraction pattern and represents spatial details as spatial frequencies. After applying a mask to select low or high spatial frequency information, the transform is converted back into an image (the inverse transform). Spatial frequency masking with a Fourier transform gives results similar to blurring and sharpening convolution filters, but can give a more even result.

Ion arc lamp. Lamps containing an ionized gas or plasma between two electrodes that radiates visible wavelengths when excited by an electric current. Arc lamps used in light microscopy usually contain mercury vapor or xenon gas.

Irradiance of light. The radiometrically correct term for light intensity. Irradiance is the radiant flux incident per surface unit area and is given as watts/meter^2. Irradiance is a measure of the concentration of power.

ISIT camera. See *Intensifier silicon-intensifier target (ISIT) camera*.

Isosbestic point. An isosbestic point is commonly observed when the excitation or emission spectra of a fluorophore undergoing a chemical or physical reaction in equilibrium are recorded as a function of the concentration of each species. A curve of emission versus wavelength (or frequency) for such a mixture will often intersect at one or more points (wavelengths), termed the isosbestic points. The effect may also appear in the spectra for a set of two or more unrelated, noninteracting fluorophores having the same total concentration. In a single chemical species, the isosbestic points will appear at all wavelengths in which the molar extinction coefficients are equal. As an example, the excitation spectrum of the fluorophore fura-2 displays an isosbestic point at 362 nm when a dilute solution is titrated with calcium.

Isotropic. In describing the optical properties of an object or propagation medium, having identical properties in all different directions.

Jablonski diagram. A diagram showing the electronic states occupied by an excited electron in an atom or molecule. Energy levels within an electronic state are shown vertically as a series of ladder-like steps, whereas transitions between states are shown as parallel structures.

Kalman averaging. See *Frame averaging*.

Kernel. See *Convolution*.

Koehler illumination. The principal method for illuminating specimens in the light microscope, whereby a collector lens near the light source is used to focus an image of the light source in the front aperture of the condenser. The microscope condenser is focused to position the conjugate image of the light source in the rear focal plane (diffraction plane) of the objective. The method provides bright, even illumination across the diameter of the specimen.

LCTF. See *Liquid crystal tunable filter (LCTF).*

Lens equation. In geometrical optics, the equation $1/f = 1/a + 1/b$ describing the relationship between the object distance a and the image distance b for a lens of focal length f.

Light microscope. A microscope employing light as an analytic probe and optics based on glass lenses to produce a magnified image of an object specimen.

Linear filters in image processing. Operations such as convolution performed in the spatial domain with a convolution kernel that is multiplied against the pixels in an image to affect changes in sharpening of edges, reducing noise, blurring, correcting for irregularities in illumination, and so on.

Linearly polarized light. A beam of light in which the E vectors of the constituent waves vibrate in planes that are mutually parallel. Linearly polarized light need not be coherent or monochromatic.

Linear unmixing. A computational process, related to deconvolution, which uses the spectra from two or more spectrally overlapping fluorophores as though it were a point-spread function of fixed location to separate or unmix the component signals. Knowing the spectra of two separate dyes, the spectrum of a dye mixture can be analyzed to calculate the amount of each dye separately. When performed pixel by pixel on a complex specimen, two dye-specific images can be created.

Liquid crystal tunable filter (LCTF). An electronically controlled device that gives color filtration of light while providing a clear aperture for optical microscopy. These filters operate through a series of waveplates that are composed of a layer of birefringent material paired with a liquid crystal layer and sandwiched between two linear polarizers. The birefringence of the liquid crystal layer is fine-tuned by varying the voltage applied to transparent conductive coatings adjacent to the layer. Polarized light entering the filter undergoes a wavelength-dependent rotation by the waveplate, which is attenuated and converted into an amplitude variation by the analyzer (a second polarizer) giving output of a specific color or wavelength band. LCTFs are designed to control filtering parameters by varying the birefringence of the liquid crystal and employing multiple waveplates in series.

Live-cell imaging chamber. Chambers for imaging live cells under static conditions or under conditions of perfusion of the culture medium. The simplest chambers are glass microscope slide or coverslip substrates containing an array of plastic chambers that are sterile and suitable for growing cells in a culture chamber and examining cells live on the microscope.

Longpass (LP) filter. An optical interference or colored glass filter that attenuates shorter wavelengths and transmits (passes) longer wavelengths over the active range of the target spectrum (ultraviolet, visible, or infrared). Longpass filters, which can have a very sharp slope (referred to as edge filters), are described by the cut-on wavelength at 50% of peak transmission. In fluorescence microscopy, longpass filters are frequently utilized in dichromatic mirrors and barrier (emission) filters. Use of the older term of highpass to describe longpass filters is now discouraged because it more accurately refers to frequency rather than wavelength.

Long working distance lens. An objective having a working distance many times greater than that of a conventional objective of the same magnification. A long working distance lens is sometimes easier to employ and focus, can look deeper into transparent specimens, and allows the operator greater working space for placing micropipettes or other equipment in the vicinity of the object. However, the NA and resolution are less than those for conventional lenses of comparable magnification.

Lookup table (LUT). In image processing, a mathematical function that converts input values of the signal into output values for display.

LP filter. See *Longpass filter.*

Lumen. A unit of luminous flux equal to the flux through a unit solid angle (steradian) from a uniform point source of 1 candle intensity.

Luminescence. The emission of light from any substance (usually a molecule or atom) that occurs from an electronically excited state generated either by a physical (light absorption), mechanical, or chemical mechanism. Luminescence is formally divided into two categories, fluorescence and phosphorescence, depending upon the electronic configuration of the excited state and the emission pathway. The generation of luminescence can occur through excitation by ultraviolet or visible light photons (photoluminescence), an electron beam (cathodoluminescence), through application of heat (thermoluminescence), chemical energy (chemiluminescence), a biochemical enzyme-driven reaction (bioluminescence), or by energy from a mechanical action (triboluminescence), such as friction.

LUT. See *Lookup table (LUT)*.

Lux. A unit of illumination equal to 1 lumen per square meter.

Magnitude. See *Amplitude of an electromagnetic wave*.

Median filter. In image processing, a nonlinear filter for blurring and removing graininess. The filter uses a kernel or mask that is applied to each pixel in the original image to calculate the median value of a group of pixels covered by the kernel. The median values computed at each pixel location are assigned to the corresponding pixel locations in the new filtered image.

Metadata. Parameters of acquisition such as magnification, filters, exposure time, scan rate, pinhole size, and so on, which are included in a header at the front of an image file. The operator can access the acquisition parameters at a later time in software, or the software itself might utilize parameters for further steps in image processing.

Microchannel plate. A device for amplifying the photoelectron signal in Gen II (and higher-generation) image intensifiers. The plate consists of a compact array of capillary tubes with metalized walls. Photoelectrons from the intensifier target are accelerated onto the plate where they undergo multiple collision and electron amplification events with the tube wall, which results in a large electron cascade and amplification of the original photon signal.

Mirror image rule. The fluorescence emission spectrum of a molecule is usually a mirror image of the excitation spectrum when plotted as a function of relative

intensity versus wave number (as opposed to wavelength). This phenomenon occurs because the probability of an excited electron returning to a particular ground state vibrational energy level is related to the degree of similarity between the vibrational and rotational energy states in the ground state versus those present in the excited state. In effect, the most likely return pathway for the excitation transition of an electron from the 0th vibrational ground state to the second vibrational level in the first excited state is from the 0th vibrational level in the excited state to the second vibrational level in the ground state (excitation from $S(0) = 0$ to $S(1) = 2$, followed by emission from $S(1) = 0$ to $S(0) = 2$).

mCherry fluorescent protein. A red fluorescent protein commonly used in combination with EGFP for two-color imaging in fluorescence microscopy. mCherry has absorption and emission peaks at 586 and 610 nm, respectively, and is one of the most photostable red-emitting fluorescent proteins.

Mobile fraction. In FRAP, the fraction of fluorescence that is restored during fluorescence recovery.

Modulation contrast microscopy (MCM). A mode of light microscope optics in which a transparent phase object is made visible by providing unilateral oblique illumination and employing a mask in the rear aperture of the objective that blocks one sideband of diffracted light and partially attenuates the 0th order undeviated rays. In both MCM and DIC optics, brightly illuminated and shadowed edges in the three-dimensional relief-like image correspond to optical path gradients (phase gradients) in the specimen. Although resolution and detection sensitivity are somewhat reduced compared with DIC, the MCM system produces superior images at low magnifications, allows optical sectioning, and permits examination of cells on birefringent plastic dishes.

Modulation transfer function (MTF). A function showing percent modulation in contrast versus spatial frequency. MTF is used to describe the change in contrast between input signals and output signals for optical and electronic signal-handling devices. To obtain the MTF for an optical system, a test pattern of alternating black and white bars can be used, whose amplitudes are shown as sinusoidal curves and whose interline spacing changes from large to small across the diameter of the pattern. At large spacings where the contrast is maximal, the percent modulation is 1; at the limit of spatial resolution for a device, the so-called cutoff frequency, the percent modulation drops to 0.

Moiré patterns. Interference patterns that occur when two grids are overlaid at an angle or when overlapping grids have different mesh sizes. Moiré patterns are associated with aliasing in digital imaging and are purposely generated in microscopy by superimposing a structured sinusoidal illumination pattern on the specimen.

Mobile fraction. In FRAP, the fraction of fluorescence that is restored during fluorescence recovery.

Molar extinction coefficient, ε. In photometry, the factor used to convert units of absorbance into units of molar concentration for a variety of chemical substances. ε is given as the absorbance for a 1 M concentration and a 1-cm path length at a reference wavelength, usually the wavelength giving maximum absorbance in its absorption spectrum.

Molecular cross-section, σ. In the nonlinear process of two-photon excitation, molecular absorption is described in terms of the probability of molecular excitation in the electric field of light. The term σ includes the product of the areas of two excitation photons times the length of time within which a molecule simultaneously absorbs the two photons and enters an excited state and so has the units cm^4 s/photon.

Monochromatic. In theory, light composed of just one wavelength, but in practice, light that is composed of a narrow band of wavelengths. Owing to Heisenberg's uncertainty principle, true monochromatic light does not exist in nature. Even the monochromatic emission from a laser or an excited atomic source has a measurable bandwidth. Therefore, while the light produced by a narrow bandpass interference filter is called monochromatic, this is just an approximation.

MTF. See *Modulation transfer function (MTF)*.

Multi-immersion objective. An objective whose spherical aberration is corrected for use at different temperatures or in media of various refractive indices, including water, glycerin, and oil. A focusable lens element is adjusted by rotating a focus ring on the barrel of the objective.

Multiphoton microscopy. See *Two-photon microscopy*.

Multiple fluorescence filter set. A filter set designed for simultaneous viewing or photography of multiple (two, three, or four) fluorescent signals. The transmission profile of each filter in the set contains multiple peaks and troughs for the reflection and transmission of the appropriate excitation and emission wavelengths as in a conventional single-fluorophore filter set. Because of constraints on the widths of bandwidths, the steepness of transmission profiles, and the inability to reject certain wavelengths, the performance is somewhat less than that of individual filter sets for specific fluorophores.

NA. See *Numerical aperture (NA)*.

ND filter. See *Neutral density filter*.

Negative colors. Colors resulting from the removal of a certain band of visible wavelengths. Thus, white light minus blue gives the negative color yellow, because simultaneous stimulation of red and green cone cells results in this color perception. Similarly, the mixture of cyan pigment (absorbs red wavelengths) and yellow pigment (absorbs blue wavelengths) gives green, because green is the only reflected wavelength in the pigment mixture.

Negative lens. A lens that diverges a beam of parallel incident rays. A simple negative lens is thinner in the middle than at the periphery and has at least one concave surface. It does not form a real image, and when held in front of the eye, it reduces or demagnifies.

Negative phase contrast. In phase contrast optics, the term applies to systems employing a negative phase plate that retards the background 0th order light by $\lambda/4$ relative to the diffracted waves. Since the diffracted light from an object is retarded $\sim\lambda/4$ relative to the phase of the incident light at the specimen, the total amount of phase shift between background and diffracted waves is 0, and interference is constructive, causing objects to appear bright against a gray background.

Neutral density (ND) filter. A light-attenuating filter that reduces equally the amplitudes of all wavelengths across the visible spectrum passing through. The glass substrate contains light-absorbing colloids or is coated on one surface with a thin metal film to reduce transmission. Neutral density filters are labeled according to their absorbance or fractional transmission.

Nipkow disk. In confocal microscopy, a thin opaque disk with thousands of minute pinholes, which when rotated at high speed provides parallel scanning of the specimen with thousands of minute diffraction-limited spots. The return fluorescence emission is refocused at the same pinhole in the disk, which provides the same function in rejecting out-of-focus light as does a single pinhole in a conventional confocal microscope. Nipkow disk confocal microscopes produce a real image that

can be inspected visually or recorded on a high-resolution CCD camera, whereas images of single-spot scanning microscopes are reconstructed from signals from a PMT and are displayed on a computer monitor.

Noise. The sources causing degradation of a signal in electronic imaging. Noises have origins in the photon signal itself (photon, Poisson, or shot noise), the detector (read noise, amplification noise, bias noise, thermal noise, and others) and digitization (digitization noise). Accounting for noises is important for image restoration and calculations of the signal-to-noise ratio.

Nomarski prism. Similar in construction to a Wollaston prism, the Nomarski beam-splitter prism design incorporates a specially cut quartz wedge having the optical axis oriented obliquely to the flat face of the lower prism wedge element. The angle of the optical axis dictates where the interference plane of the prism is located (usually at some point on the exterior of the prism). Nomarski prisms are used for splitting and recombining beams of light in DIC microscopy.

Nondescanned detectors. In sensitive point scanning techniques, such as two-photon microscopy, the fluorescence emission signal is often diverted to detectors by a dichromatic mirror located between the objective and the scanning mirrors. Measuring the signal before descanning it increases sensitivity.

Numerical aperture (NA). The parameter describing the angular aperture of objective and condenser lenses. NA is defined as $n\sin\theta$, where n is the refractive index of the medium between the object and the lens, and θ, the angle of light collection, is the apparent half-angle subtended by the front aperture of the lens as seen from a point in the specimen plane.

Nyquist criterion. With respect to preservation of spatial resolution in electronic imaging, the requirement that a resolution unit (the spacing between adjacent features in a specimen) be registered by at least two contiguous sampling units (pixels, raster lines) of the detector in order to be represented correctly in the image. Thus, an object consisting of a pattern of alternating black and white lines will be represented faithfully by a detector capable of providing two or more image samples per black and white line.

Object distance. See *Image distance.*

Objective. The image-forming lens of the microscope responsible for forming the real intermediate image located in the front apertures of the eyepieces.

Objective heater. In live-cell imaging, the objective acts as a heat sink that cools the specimen when applied to a 37° coverslip, potentially causing coverslip flex and focus drift. To help minimize these problems, the objective can be heated with a thermoelectric heating collar or a closed circulatory loop with temperature-regulated fluid.

Objective rear aperture. An aperture plane of the light microscope located at the rear focal plane of the objective, frequently at or near the rear lens element, and the site of formation of a diffraction image of the specimen. The aperture is often defined physically by an aperture mask or diaphragm made of plastic with an opening suitable for transmitting the light bundle of the lens but no more. Optical devices, such as phase plates, DIC prisms, and aperture masks, used in forms of interference microscopy are located at or near this location.

Ocular. See *Eyepiece.*

Offset. In electronic imaging, the electronic adjustment that is made to set the black level in the image. Adjusting the offset adds a voltage of positive or negative sign sufficient to give the desired feature or background a display intensity of 0.

Optic (optical) axis. In an aligned optical system, a straight line joining the centers of curvature of lens surfaces contained in the system. In polarized light optics, the path followed by the ordinary or O ray in a birefringent material.

Optical density. See *Absorbance.*

Optical (molecular) highlighters. A unique group of fluorescent proteins that can be spectrally altered by irradiation at specific wavelengths (usually with a laser). Protein chromophores that can be activated to initiate fluorescence emission from a quiescent state (a process known as photoactivation), or are capable of being optically converted from one fluorescence emission bandwidth to another (photoconversion), enable the direct and controlled highlighting of distinct molecular pools within a cell.

Optical path length. In wave optics, a measure of the time or distance (measured in wavelengths) defining the path taken by a wave between two points. Optical path length is defined as $n \times t$, where n is the refractive index and t indicates the thickness or geometrical distance. A complex optical path composed of multiple domains of different refractive index and thickness is given as $\Sigma = n_1t_1 + n_2t_2 + \ldots n_it_i$.

Optical path length difference. The difference in the optical path lengths of two waves that experience refractive index domains of different value and thickness. In interference optics, differences in optical path length determine the relative phase shift and thus the degree of interference between 0th order and higher order diffracted waves that have their origins in a point in the object.

Optovar. A built-in magnification booster lens that can be rotated into the optical path to further increase the magnification provided by the objective by a small amount.

O ray. See *Ordinary ray (O ray).*

Ordinary ray (O ray). In polarization optics, the member of a ray (wave) pair that obeys normal laws of refraction and whose velocity remains constant in different directions during transmission through a birefringent medium. See also *Extraordinary ray.*

PALM. Acronym for photoactivated localization microscopy, a superresolution technique that relies on single-molecule imaging to obtain highly precise locations (to a resolution of 10–40 nm) of molecules in an image. In practice, sparse molecular subsets of a labeled structure are photoactivated and imaged until they photoswitch off or photobleach. The position of each single molecule is then recorded and a new subset is photoactivated. The procedure is repeated hundreds or thousands of times until a complete image is built up representing a high-resolution image of the structure.

PALMIRA. A single-molecule localization method based on photon activated localization microscopy with independently running acquisition. In this mode, the digital camera runs at high speed, without synchronization to the activation laser or the switching cycles of the fluorescent probes. The method works using photoswitchable fluorophores and increases acquisition speed up to 100-fold.

Panning. In electronic imaging, the movement of the camera to bring into view portions of an object field that cannot be included in a single image frame; in image processing, the relative displacement of one image over another for purposes of alignment.

Paraboloid condenser. A high numerical aperture condenser for darkfield microscopy having a reflective surface that is a segment of a paraboloid. The steeply pitched illumination cone produced by the condenser is suitable for darkfield examination with high-power oil immersion objectives.

Parallel register. In CCD cameras, the extended array of imaging (and storage) pixels of the imaging area of a CCD device. Columns of pixels in the parallel register deliver their charge packets (photoelectrons) to a separate serial register from which the image signal is read and digitized by the camera electronics.

Parfocal. The property of having the same distance between the specimen and the objective turret of the microscope. With parfocal lenses, one can focus an object with one objective and then switch to another higher or lower magnification objective without having to readjust the focus dial of the microscope.

Particle wave. In phase contrast and other modes of interference microscopy, the wave (P wave) that results from interference between diffracted and surround waves in the image plane, and whose amplitude is different from that of the surrounding background, allowing it to be perceived by the eye. See also *Diffracted wave and Surround wave*.

Peltier thermoelectric cooling. A compact bimetallic strip that becomes hot on one surface and cold on the other during the application of a current. Peltier devices are commonly used in CCD cameras where it is necessary to quickly and efficiently cool the CCD 50–60°C below ambient temperature in a compact space.

Phase. Relative position in a cyclical or wave motion. Since one wavelength is described as 2π radians or 360°, the phase of a wave is given in radians or degrees or fractions of a wavelength.

Phase (centering) telescope. See *Bertrand lens*.

Phase contrast microscopy. A form of interference microscopy that transforms differences in optical path in an object to differences in amplitude in the image, making transparent phase objects appear as though they had been stained. Surround and diffracted rays from the specimen occupy different locations in the diffraction plane at the rear aperture of the objective where their phases are differentially manipulated in order to generate a contrast image. Two special pieces of equipment are required: a condenser annulus and a modified objective containing a phase plate. Because the method is dependent on diffraction and scattering, phase contrast optics differentially enhance the visibility of small particles, filaments, and the edges of extended objects. The technique allows for examination of fine details in transparent specimens, such as live cells.

Phase difference. The phase angle by which one periodic disturbance or wavefront lags behind or precedes another in time or space. Phase differences are usually described in terms of fractions or multiples of a wavelength.

Phase gradient. In interference microscopy, the gradient of phase shifts in an image corresponding to optical path differences in the object.

Phase object. Objects that shift the phase of light as opposed to those that absorb light (amplitude objects) as the basis for image formation. See also *Amplitude object*.

Phase plate. In phase contrast microscopy, a transparent plate with a semitransparent raised or depressed circular annulus located at the rear focal plane of a phase contrast objective. The annulus reduces the amplitude of background (0th order) waves and advances or retards the phase of the 0th order component relative to diffracted waves. Its action is responsible for the phase contrast interference image.

Phase specimen. Specimens that shift the phase of light waves traveling through without affecting the amplitude. Many phase specimens are completely or partially transparent, and are ideal candidates for imaging with phase contrast and DIC microscopy techniques.

Phosphorescence. The emission of light (photons) from an excited triplet state where the electron in the excited orbital has the same spin orientation as its partner in the ground state. Because a triplet state transition to the ground state is forbidden by the rules of quantum mechanics, the phosphorescence emission rate is much slower (measured in milliseconds to seconds) than that observed for fluorescence emission. In general, phosphorescence is not usually observed in solution, which includes most chemical and biochemical environments, at room temperature.

Photoactivation. Genetically encoded fluorescent proteins or synthetic fluorophores that generally display little or no initial fluorescence under excitation at the imaging wavelength, but dramatically increase their fluorescence intensity after activation by irradiation at a different (usually lower) wavelength. Among the proteins that demonstrate photoactivation, a green fluorescent protein variant, termed PA-GFP, has been the most widely studied.

Photobleaching. The diminution of fluorescence emission due to the chemical modification of a fluorophore upon continued exposure to excitation wavelengths. Photon-induced damage resulting in photobleaching is largely due to the generation of free oxygen radicals that attack and permanently destroy the light-emitting properties of the fluorophore. The rate of photobleaching can be reduced by including antifree radical reagents, such as ascorbate, or by reducing the concentration of oxygen in the mounting medium. Bleaching is usually irreversible.

Photoconversion. The change in the emission spectrum that can occur for certain fluorophores following excitation with short wavelength light. Examples of GFP variants that exhibit photoconversion are Eos, which shifts from green to red emission following excitation with 405 nm light, and Dronpa, a photoswitchable protein whose emission can be switched between a bright fluorescent state and a dark non-fluorescent state.

Photodiode. A semiconductor device, such as a CCD, for detecting and measuring light by means of its conversion into an electric current. Incident photons generate charge carriers (electrons and electron holes) in the CCD matrix that support the conduction of a current in the presence of an applied voltage.

Photoelectron. In digital imaging, the electron resulting from the impact of a photon from the imaging system with the silicon matrix of an imaging CCD chip, and which remains stored at a pixel site until readout.

Photomultiplier tube (PMT). An electrical device for amplifying photon signals. Photons striking a target at the face of the PMT liberate free electrons, which are accelerated onto a dynode that in turn liberates a shower of electrons. By arranging several dynodes in a series, a large amplification of the original photon is achieved, which is then transmitted to other signal-processing circuits. PMTs amplify photon signals but do not form an image as does an image intensifier.

Photon-limited. In image processing, a signal is said to be photon limited when the photon noise is greater than the electronic noises associated with the camera (bias, thermal, and read noises).

Photon noise (shot noise, Poisson noise). In image processing, the noise associated with the photon signal itself. Since the accumulation of photons per unit area or time is random (Poissonian) by nature, the photon signal is typically described as the mean of a collection of measurements, and the noise is described as the square root of the photon signal. Since the signal is based on "photoelectron counts," the photon noise is calculated in terms of electrons, not in the digitized signal units (analog-to-digital units or ADUs) used by the computer.

Photopic vision. The mode of vision based on cone cell photoreceptors in the retina that provides visual acuity and color perception under bright light conditions.

Photoswitching. The switching between *on* and *off* states of fluorescence by a fluorophore induced by illumination.

Phototoxicity. Damage to a living specimen mostly due to free radicals resulting from excessive exposure to high intensity illumination. The level of phototoxicity generally increases with decreasing wavelength, but the potentially numerous mechanisms behind the phenomenon are poorly understood. Most living cells display an enhanced level of phototoxicity when simultaneously exposed to synthetic fluorophores that target specific subcellular locations, such as the nucleus, mitochondria, Golgi apparatus, or endoplasmic reticulum.

Pinhole aperture. In confocal microscopy, the variable diaphragm (0.01–0.10 mm in diameter) in the real intermediate image plane that is adjusted to receive the focused spot of fluorescent light that is emitted by an excited laser-scanned spot in a fluorescent specimen. A photomultiplier tube located behind the pinhole generates an electrical signal that is proportional to the number of photons passing through the pinhole.

Pixel. A "picture element" in electronic cameras. In confocal microscopes, pixels correspond to the photon signal received and digitized per unit of sampling time during laser scanning. In CCD cameras, pixels are square or rectangular areas of silicon substrate that are delimited by conducting strips on the CCD surface.

Plane parallel. In wave optics, the term applies to waves vibrating in a plane that is parallel to some reference plane, but not necessarily in the reference plane itself. See also *Linearly polarized light*.

PMT. See *Photomultiplier tube (PMT)*.

Point-scanning. In microscopy, the technique of moving a focused laser beam as a single point over the surface of a specimen in a raster pattern. Single-point scanning is distinct from other scanning methods that scan the specimen simultaneously with a parallel array of hundreds or thousands of points, or scan with a line.

Point-spread function. The response of a diffraction limited optical system, such as a microscope objective, in imaging a point source of light. Because the optical system does not faithfully reproduce the image of a point, but rather generates a blurred extended diffraction image, the point-spread function is a measure of image degradation.

Polar. The common term applied to a sheet of linear polarizing film (dichroic filter or Polaroid filter) and particularly to its use as a polarizer or analyzer in producing and analyzing polarized light.

Polarizability. In polarization optics, a property describing the strength of interaction of light with molecules in a manner that depends on the orientation of atomic bonds. Light waves interact more strongly with molecules when their E vectors are oriented parallel to the axis defining light-deformable (polarizable) covalent bonds, such as the axes of long-chain hydrocarbon polymers like polyvinyl alcohol, cellulose, and collagen. This geometry is supported when an incident light ray is perpendicular to the long axis of the polymer. Interaction of light with molecules along their polarizable axis retards wave propagation and accounts for the direction-dependent variability in their refractive index, a property known as birefringence.

Polarization cross. In polarization microscopy, the appearance of a dark upright cross in the rear aperture of the objective under conditions of extinction with two crossed polars. Ideally, the rear aperture is uniformly dark under this condition, but the

depolarization of light by the curved lens surfaces of the condenser and objective causes brightening in four quadrants and hence the appearance of a cross.

Polarization microscopy. A mode of light microscopy based on the unique ability of polarized light to interact with polarizable bonds of ordered molecules in a direction-sensitive manner. Perturbations to waves of polarized light from aligned molecules in an object result in phase retardations between sampling beams, which in turn allow interference-dependent changes in amplitude in the image plane. Typically, the microscope contains a polarizer and analyzer, and a retardation plate or compensator. Image formation depends critically on the existence of ordered molecular arrangements and a property known as double refraction or birefringence.

Polarized light. Light waves whose E vectors vibrate in plane-parallel orientation at any point along the axis of propagation. Polarized light can be linearly polarized (vibrations at all locations are plane parallel) or elliptically or circularly polarized (vibration axis varies depending on location along the propagation axis). Polarized light need not be monochromatic or coherent.

Polarizer. A device that receives random light and transmits linearly polarized light. In microscopy, polarizers are made from sheets of oriented dichroic molecules (Polaroid filter) or from slabs of birefringent crystalline materials.

Polaroid sheet. A sheet of aligned long-chain polyvinyl alcohol molecules impregnated with aligned microcrystals of polyiodide. The E vectors of incident waves vibrating along the axis parallel to the crystal axes are absorbed and removed, resulting in the transmission of waves that are linearly polarized.

Polychroic beamsplitter. See *Polychromatic mirror*.

Polychromatic mirror (polychroic beamsplitter). A specialized mirror or beamsplitter, sometimes called a multiple dichroic, which is designed to transmit multiple bandpass regions of fluorescence emission from the specimen, while reflecting other defined wavelength regions that correspond to the excitation bands. Polychromatic mirrors are a critical member of multiband fluorescence filter combinations tailored to eliminate registration shifts when imaging several probes in a single specimen. The most complex polychromatic mirrors can reflect three or more excitation bands and transmit at least three emission bands.

Positive colors. Colors that result from mixing different wavelengths of light. The equal mixture of red and green wavelengths results in the perception of yellow, a positive color.

Positive lens. A lens that converges a beam of parallel incident rays into a focal point. A simple positive lens is thicker in the middle than at the periphery, and has at least one convex surface. A positive lens forms a real image and enlarges or magnifies when held in front of the eye.

Positive phase contrast. In phase contrast optics, the term applies to systems employing a positive phase plate that advances the background wave by $\lambda/4$ relative to the diffracted wave. Since the diffracted light from an object is retarded ~ $\lambda/4$ relative to the phase of the incident light, the total phase shift between background and diffracted waves is $\lambda/2$ and interference is destructive, causing objects to appear dark against a gray background.

Primary fluorescence. See *Autofluorescence*.

Principal plane. For a simple thin lens, the plane within the lens and perpendicular to the optical axis from which the focal length is determined. Thick simple lenses have two principal planes separated by an intervening distance. Complex compound lenses may have multiple principal planes.

Processed image. A raw image after it has been subjected to image processing.

Progressive scan cameras. A reference to video cameras and camcorders with interline CCD detectors. The designation "progressive scan" indicates that the entire image signal is read off the chip at one time and that images are displayed as a series of complete frames without interleaving as in the case of conventional broadcast video signals.

Projection view. See *Composite view*.

Pseudocolor. All detectors, even color cameras, are effectively grayscale imagers. Pseudocolor is the name of the convention for displaying different bands of wavelengths in different colors, for example, DAPI (blue), FITC (green), and TRITC (red).

QE. See *Quantum efficiency*.

Quantum efficiency (QE). Quantum efficiency is a measure of the effectiveness of an image sensor (such as CCD, PMT, film, etc.), and is described as the percent of incident photons on a sensor that generates an electron–hole pair. A QE of 1 means the detector is 100% efficient. Quantum efficiency varies as a function of the incident wavelength and composition of the detector surface. Most manufacturers provide plots of imager quantum efficiency versus wavelength for comparison purposes.

Quantum yield. A quantitative measure of fluorescence emission efficiency, the quantum yield of a fluorochrome or fluorophore is expressed as the ratio of the number of photons emitted to the number of photons absorbed. In other words, the quantum yield represents the probability that a given excited fluorochrome will produce an emitted (fluorescence) photon. Quantum yields range between a value of 0 and 1, and fluorescent molecules commonly employed as probes in microscopy have quantum yields ranging from very low (0.05 or less) to almost unity. In general, a high quantum yield is desirable in most imaging applications. The quantum yield of a given fluorophore varies, sometimes to large extremes, with environmental factors, such as pH, concentration, and solvent polarity.

Quenching. The reduction in fluorescence emission by a fluorophore due to environmental conditions (solvent type, pH, and ionic strength) or to a locally high concentration of fluorophores that reduces the efficiency of fluorescence emission.

Raster. A zigzag pattern of straight line segments, driven by oscillators, used to scan a point source over the area covered by a specimen or an image.

Raw image or raw frame. In image processing, the name of an image prior to any modifications or processing.

Rayleigh criterion for spatial resolution. The criterion commonly used to define spatial resolution in a lens-based imaging device. Two point sources of light are considered to be just barely resolved when the diffraction spot image of one point lies in the first-order minimum of the diffraction pattern of the second point. In microscopy, the resolution limit d is defined, $d = 1.22\ \lambda/(\mathrm{NA}_{\mathrm{objective}} + \mathrm{NA}_{\mathrm{condenser}})$, where λ is the wavelength of light and NA is the numerical aperture of the objective and of the condenser.

Readout noise or read noise. In digital imaging, read noise refers to the noise background in an image due to the reading of the image and therefore the CCD noise associated with the transfer of charge packets between pixels, preamplifier noise, and the digitizer noise from the analog-to-digital converter. For scientific CCD cameras, the read noise is usually 2–20 electrons/pixel.

Readout rate. The rate in frames per second required for pixel transfer, digitization, and storage or display of an image.

Real image. An image that can be viewed when projected on a screen or recorded on a piece of film.

Real intermediate image. The real image focused by the combination of objective and tube lens in the oculars (eyepieces) of the microscope.

Red fluorescent protein (RFP). Originally, a fluorescent protein from a sea anemone of the genus *Discosoma* used as a fluorescent marker to determine the location, concentration, and dynamics of a protein of interest in cells and tissues. RFP is now a common generic name for any fluorescent protein emitting the red spectral region.

Reflected-light. See *Epi-illumination*.

Refraction. The change in direction of propagation (bending) experienced by a beam of light that passes from a medium of one refractive index into another medium of different refractive index when the direction of propagation is not perpendicular to the interface of the second medium.

Refractive index ellipsoid and wavefront ellipsoid. An ellipsoid is the figure of revolution of an ellipse. When rotated about its major axis, the surface of the ellipsoid is used to describe the surface wavefront locations of E waves propagating outward from a central point through a birefringent material. The same kind of figure is used to describe the orientation and magnitude of the two extreme refractive index values that exist in birefringent uniaxial crystals and ordered biological materials.

Region of interest (ROI). In image processing, the subset of pixels defining the "active region" of an image, determined by defining x and y coordinates or by drawing with a mouse over the image. The ability to define an ROI is useful during image processing and when saving a part of an image as a new image.

Relative error. The reciprocal of the signal-to-noise ratio and therefore the ratio of the noise to the signal.

Relative retardation. In polarization optics, the relative shift in phase between two waves expressed in fractions of a wavelength.

Relay lens. An intermediate magnifying lens in an imaging system placed between the objective and the real intermediate image. In video, so-called TV lenses increase the magnification of the image projected on the camera two- to eightfold.

RESOLFT. Reversible saturable (or switchable) optical fluorescence transitions (RESOLFT) is the term applied by Stephan Hell and coworkers to the property of fluorescent dyes that is essential for several forms of superresolution microscopy, including STED, SSIM, and GSD.

Resolving power. See *Spatial resolution*.

Resonant scanner. A special scanning mechanism used for high-speed imaging in forms of point scanning microscopy. Resonant scanners operate at a unique vibrational frequency or resonance at which they give stable scanning performance (30 fps for a 512×512 image), which is several times faster than a linear galvanometer scanner.

Retardation plate. In polarization optics, a birefringent plate positioned between the polarizer and analyzer that introduces a relative retardation between the O and E rays in addition to that produced by a birefringent object to change image contrast or render path differences in color. When used in a device to measure the amount of relative retardation in the object, the plate is called a compensator. See also *Compensator*.

RFP. See *Red fluorescent protein (RFP)*.

RGB (red, green, and blue). A mode of color image display that is based on the red-green-blue tricolor stimulus system for the visual perception of color. Commonly used in television, computer monitors, and other image display devices.

Rod cell photoreceptors. Retinal cells located outside the fovea and in the periphery of the retina responsible for vision in dim light. Rod cell vision, or scotopic or night vision, is absent of color.

ROI. See *Region of interest*.

Saturated structured illumination microscopy (SSIM). A nonlinear form of structured illumination microscopy (SIM) that uses photoswitchable probes and/or very high laser powers to saturate the excited state. The result is sharpening of the structured illumination pattern to allow higher spatial frequencies to be resolved.

Scotopic vision. Night vision based on rod cell photoreceptors. See *Rod cell photoreceptors*.

Second harmonic generation (SHG). Harmonic generation occurs when an optical excitation event involving two or more photons at a particular frequency results in cooperative emission at multiple harmonics (primarily, the second and third) without absorption of the photons. Generation of the harmonic frequencies at the specimen is a nonlinear scattering process yielding an emitted photon wavelength that is twice the frequency or half the wavelength (for second harmonic generation) of the incident illumination. The forward scattered light is highly coherent. Transparent specimens that lack molecular symmetry are ideal candidates for harmonic generation techniques. Unlike the situation with linear scattering, changing the excitation illumination wavelength produces a corresponding change in the scattered wavelength.

Semiapochromat lens. See *Fluorite lens*.

Serial register. In CCD cameras, a single row of pixels that receives charge packets from all of the adjacent columns of pixels in the parallel register. The serial register transmits the charge packets pixel by pixel to the on-chip preamplifier and analog-to-digital converter until the register is emptied.

Shade-off. In phase contrast microscopy, the gradient in light intensity that is observed from the edge to the center of extended phase objects of uniform thickness and refractive index. In central regions of uniform objects where diffraction is minimal, the corresponding amplitude in the image can approach that of the background.

Shear. A term used in DIC microscopy for the angular splitting of coaxial orthogonal wavefronts resulting in a spatial separation defined by a specific angle (the shear angle). Shear occurs at the refractive index junction between cemented quartz wedges in a Wollaston prism or at the glass–air interface in the lower quartz wedge in a Nomarski prism.

Shear angle. The specific angle defined by angular separation of paraxial orthogonal wavefronts as they become displaced and spatially separated in a Wollaston or Nomarski prism.

Shear axis. In DIC microscopy, the axis of displacement of the O and E rays caused by the DIC prisms. In a DIC image, the axis is identified as the line connecting the bright and dark shaded edges of refractile objects.

Shear distance. Displaced orthogonal ordinary and extraordinary wavefronts are separated by a spatial separation length, the shear distance, derived from the geometrical constraints of the Wollaston or Nomarski prism housed in the microscope condenser. The shear distance ranges between 0.1 and 1.5 μm, a linear range that is designed to be slightly smaller than (or in some cases equal to) the lateral resolution of the objective.

SHG. See *Second harmonic generation (SHG)*.

Shortpass (SP) filter. An optical interference or colored glass filter that attenuates longer wavelengths and transmits (passes) shorter wavelengths over the active range

of the target spectrum (usually the ultraviolet and visible region). Shortpass filters, which can have a very sharp slope (referred to as *edge* filters), are described by the cut-off wavelength at 50% of peak transmission. In fluorescence microscopy, shortpass filters are frequently employed in dichromatic mirrors and excitation filters. Use of the older term of *lowpass* to describe shortpass filters is now discouraged because it more accurately refers to frequency rather than wavelength.

Shot noise. See *Photon noise*.

Signal-to-noise (S/N) ratio. The ratio of the signal of an object to the noise of the surrounding background, where noise is the square root of the sum of the variances of contributing noise components. In the case that noise is photon limited and background noise may be approximated by the square root of the background signal, S/N gives the number of standard deviations that distinguish the object signal from the mean signal of the background.

Sign of birefringence. In polarization optics, a reference to the sign of birefringence b, where $b = n_e - n_o$. For the case that the refractive index describing the trajectory of the E ray is greater than that describing the trajectory taken by the O ray, the sign of birefringence of the material is positive.

Silicon-intensifier target (SIT) camera. A video camera tube for imaging under low light conditions. The camera tube contains a photocathode that accelerates photoelectrons onto a silicon diode target plate, which greatly amplifies the signal. A scanning electron beam neutralizes the target while generating a beam current containing the signal.

SIM. See *Structured illumination microscopy.*

Simple lens. A lens consisting of a single lens element and distinct from a compound lens having multiple lens elements.

Singlet excited state. In light microscopy, molecules can absorb a photon and enter a higher energy state, the singlet excited state, where an electron pair occupies two orbitals and the electrons retain opposite spins. Molecules in the singlet state are unstable and return to the ground state by a number of mechanisms, including through fluorescence, the release of a longer wavelength photon.

SIT camera. See *Silicon-intensifier target (SIT) camera*.

Slow axis. In polarization optics, the short axis of the wavefront ellipsoid, a construction used to describe the surface of an emergent wavefront from a point source of light in a birefringent material. The slow axis indicates the direction of high refractive index in the specimen. See also *Refractive index ellipsoid*.

Slow-scan CCD camera. Another designation for a full-frame CCD design. The time required for the serial readout of the parallel register of the CCD is slow compared with the time to read an interline CCD of comparable size and dimensions.

Snell's law. The law of refraction describing the bending of light at the interface of two media of different refractive index and relating the refractive index and velocity of light in those media to the angles of incidence and refraction.

S/N ratio. See *Signal-to-noise (S/N) ratio*.

SP filter. See *Shortpass filter.*

Spatial filter. A filter that selectively manipulates a location in an image such as an aperture in a field plane of a microscope or a sharpening or blurring filter in image processing.

Spatial frequency. The reciprocal of the distance between two objects (periods/distance).

Spatial frequency filter. A filter that selectively manipulates a location in the diffraction plane in a microscope (aperture plane masks in modulation contrast microscopy) or a mask applied to Fourier transforms to manipulate low and high spatial frequency information in image processing.

Spatial resolution. The resolution of component features in an image. In optical systems, resolution is directly proportional to the wavelength and inversely proportional to the angular aperture. The practical limits on wavelength and angular aperture determine the limit of spatial resolution, which is approximately one-half the wavelength of light.

Spectral imaging. An advanced fluorescence microscopy technique that utilizes hardware (usually incorporated into a confocal detector unit) to separate the emitted light from multiple fluorophores into separate identifiable spectral components. Linear unmixing is the accompanying computational process, related to deconvolution, which uses the spectrum from each fluorophore as though it were a point-spread function of fixed location to separate or unmix the component signals. The technique is a powerful analytical tool that can be used to discriminate distinct fluorophores, even those with highly overlapping spectral profiles.

Spectral range. The range of wavelengths, or bandwidth, under consideration.

Spectroscope. A device for determining the wavelength of a certain emission line, bandwidth, or color. A diffraction grating is positioned between the eye and a narrow slit, and the eye-slit axis is directed at a target light source. The grating produces a spectrum of the constituent wavelengths admitted by the slit, and the spectrum is superimposed on a scale indicating the wavelength.

Spherical aberration. A lens aberration typical of lenses with spherical surfaces that causes paraxial rays incident on the center and periphery of a lens to be focused at different locations in the image plane. The degree of aberration increases with the decreasing focal ratio of the lens. This aberration can be corrected by using aspherical surfaces in simple lenses and by using symmetric doublet lenses and overcorrecting some elements in microscope objectives.

Spinning disk confocal microscope. A method of parallel scanning featuring a spinning disk with arrays of pinholes or slits that are focused to points or lines of light that sweep over the specimen at high speed. High spin rates (1000–10,000 rpm) allow image acquisition at rates up to 100–200 fps. The fluorescence detector is usually a CCD camera. The advantages of repeated low light stimulation are reduced rates of photobleaching of fluorophores and prolonged cell viability.

SSIM. See *Saturated structured illumination microscopy (SSIM)*.

Steady-state fluorescence. Encompassing all imaging and measurements performed with constant illumination and observation, steady-state fluorescence is the most common type of fluorescence. The specimen is illuminated with a continuous beam of filtered light, and the fluorescence intensity or emission spectrum is recorded with a detector. A majority of specimens observed in fluorescence microscopy reach a steady state immediately upon being exposed to excitation illumination.

STED. See *Stimulated emission depletion microscopy (STED)*.

Stepper motor. A motor whose drive shaft does not rotate continuously, but advances in discrete intervals or steps.

Stimulated emission depletion microscopy (STED). Stimulated emission depletion microscopy is a method of point-spread function engineering that uses co-linear laser sources to produce scanning point sources that are 50 nm or less in diameter. The technique relies on inhibiting fluorescence of excited molecules at the periphery of

a laser-scanning focal spot using synchronized laser pulses for excitation of fluorophores and spatially coordinated donut-shaped STED pulses to deplete emission. Resulting fluorescence is inhibited at the periphery of the spot, but not in the center, thus dramatically reducing the fluorescence spot size (i.e., point-spread function) with a concomitant increase in spatial resolution.

Stokes shift. The wavelength difference between excitation and emission maxima in the respective spectra of a fluorescent molecule, named in honor of George G. Stokes, who first observed the phenomenon in 1852 while studying at Cambridge University. This value varies widely—approximately 20 nm for fluorescein, but over 200 nm for porphyrins. The Stokes shift is of great utility in fluorescence microscopy because it indicates the feasibility of isolating excitation and emission wavelengths using interference filters.

STORM. Acronym for stochastic optical reconstruction microscopy, which together with PALM and other methods, represents a form of single-molecule localization microscopy. The method uses photoswitchable light and dark states of fluorescent dyes, which allow the microscopist to acquire hundreds or thousands of images in series, determine the centroids of the central diffraction spots corresponding to single fluorescent molecules, and assigning them as points in a single image frame that is built up over time. See *PALM*.

Structured illumination microscopy (SIM). A technique for improving spatial resolution that relies on projecting a sinusoidal illumination pattern onto the microscope specimen plane to extract high spatial frequency information and obtain images that are beyond the conventional limit of resolution. In SIM, the patterned illumination is translated over the specimen at specific increments and rotation angles while images are acquired. The raw images are treated mathematically in reciprocal space to reconstruct an optical section or superresolution image.

Structured illumination microscopy for optical sectioning. A method of optical sectioning by which illumination in the pattern of a grid is translated in increments over the specimen at each *z*-location in an image stack. The images at each *z* lane are processed to generate high contrast optical sections similar to those obtained using a confocal microscope.

Subarray readout. An option for image acquisition with a CCD camera whereby a portion of the total available imaging area of the CCD is selected as the active area. Selection of the subarray region is made in the image acquisition software. In subarray readout mode, the acquisition rate is fast, and images take up less storage space on the hard drive.

Superresolution. In electronic imaging, the increase in spatial resolution made possible by adjusting the gain and offset of a camera. In confocal microscopy, superresolution is obtained by constricting the confocal pinhole to about one-quarter of the Airy disk diameter. The term superresolution is also used to describe high resolution imaging techniques, such as STED, PALM, STORM, and SIM, which produce images with resolution below the classical diffraction limit described by the Abbé equation.

Surface flatness (filters). A term widely applied in optics, surface flatness is a measure of the surface deviation from a perfect plane in an optical element. In fluorescence filters designed for optical microscopy, surface flatness is measured in fractions or multiples of a visible light wavelength corresponding to green (550 nm), red-orange (630 nm), or using the center wavelength of a specific bandpass filter. When a plane wavefront is reflected from the surface of a mirror or filter, the actual wavefront

distortion is twice the value of the surface flatness. In dichromatic mirrors, the surface flatness is determined by the wavefront distortion of light reflected from the front (reflecting) surface.

Surround wave (background wave). In phase contrast and other modes of interference microscopy, waves that traverse an object but do not interact with it. Surround waves are not deviated by the object and do not become altered in phase. For purposes of describing diffraction and interference, such waves are called the 0th order component. Surround (S) waves combine with diffracted (D) waves through interference in the image plane to generate resultant particle (P) waves of altered amplitude that are perceived by the eye. See also *Diffracted wave* and *Particle wave*.

Sweptfield confocal microscopy. A method of parallel confocal scanning implemented by Prairie Technologies and marketed by Nikon that uses two conjugate pinhole plates and galvanometer scanning. Each plate has patterns of pinholes and slits of various sizes that are selected by the user. The excitation plate generates parallel patterns of point sources that scan the specimen. The fluorescence is descanned by the mirrors and is returned to a second identical plate that functions as the pinhole aperture for generating a confocal image. The detector is an area detector such as a CCD camera.

Synthetic probes. Small organic molecules with fluorescent properties such as the fluorescein, rhodamine, and cyanine families of dyes.

System MTF. A function describing the percent modulation (percent reduction in the peak to trough amplitude difference for a signal) of a signal resulting from transit through a series of signal-handling devices. For a cascaded series of devices, the system MTF for a given frequency f is the product of the values of percent modulation for each individual component in the system so that % modulation of the system = $a\% \times b\% \times c\% \ldots$

Telan lens. See *Tube lens*.

TEM_{00} mode. Transverse electromagnetic mode of a beam of light, such as a laser, such that the shape of a cross (transverse) section of the focused laser beam is a disk with a Gaussian distribution of light intensity.

TEM_{01*} mode. Transverse electromagnetic mode of a beam of light, such as a laser, such that the shape of a cross (transverse) section of the focused laser beam is a ring rather than a disk.

Thermal noise. In CCD imaging, the noise of the thermal signal in an image caused by the kinetic vibration of silicon atoms in the matrix of a CCD device. Thermal noise is considerably reduced by cooling the CCD to temperatures below –20°C. Low-light-level cameras used in astronomy are sometimes cooled to the temperature of liquid nitrogen to effectively eliminate thermal noise.

Thin-film interference coating. The main component of interference filters, these coatings are fabricated by applying alternating layers of several dielectric materials or successive layers of a dielectric material and a thin metal film. The spacings between dielectric layers (or between a dielectric and metal layer) are limited to either one-quarter or one-half of an optical wavelength to allow constructive interference and reinforce propagation of light through the filter at a specific wavelength. All other wavelengths produce destructive interference and are absorbed or reflected, but do not pass through the filter. Each layer of the interference coating is colorless, but reflections created at the multiple interfaces between layers combine through interference to selectively reflect some wavelengths and transmit others, rendering the filter with an apparent color.

Thin lens. A lens whose thickness is small compared with its focal length. A line through the center of the lens (a plane representing the two coincident principal planes of the lens) provides a reasonably accurate reference plane for refraction and object and lens distance measurements. Lenses are assumed to be thin when demonstrating the principles of graphical ray tracing.

Time-resolved fluorescence. Employed for measuring intensity or anisotropic decays, time-resolved fluorescence measurements rely on exposing the specimen to a short pulse of light, where the pulse width is typically shorter than the decay time of the fluorophore. The intensity decay of fluorescence emission is usually recorded with a high-speed detection system that permits the intensity or anisotropy to be measured on a nanosecond time scale.

TIRFM. See *Total internal reflection fluorescence microscopy (TIRFM).*

Total internal reflection fluorescence microscopy (TIRFM). A technique designed to probe objects lying within 100 nm of the coverslip surface, including isolated molecules and structures near cell surfaces. In practice, an incident laser beam is brought to the reflective interface at an angle greater than the critical angle. The incident beam is deflected by total internal reflection and an evanescent wave is set up on the coverslip surface that vanishes exponentially into the aqueous medium but provides a 100-nm zone within which fluorescence can be excited and observed. The thin observation zone and absence of background fluorescence provide high contrast for sensitive fluorescence imaging, even imaging of single fluorescent molecules.

Transient transfection. In live-cell imaging, the technique of expressing exogenous fusion proteins in tissue culture cells. Bacterial plasmids bearing DNA sequences for a chimeric protein that includes the protein of interest fused to a fluorescent protein are made and introduced into cells by techniques that disrupt the cell membrane and allow uptake of the plasmids into the cell cytoplasm. After intracellular transport into the nucleus and transcription, fluorescent fusion proteins appear in the cell.

Transillumination. A mode of microscope illumination in which the light source and objective are on opposite sides of the specimen so that illuminating beams pass through the specimen.

Transmitted wavefront distortion (TWD). The degree of distortion introduced into a plane wavefront when it is transmitted through an optical element. Transmitted wavefront distortion is measured in fractions or multiples of a wavelength (usually 550 or 630 nm). Distortion of the transmitted wavefront arises from surface flatness variations along the outer surfaces of the optical element, as well as from internal discontinuities and inhomogeneity of refractive index.

Triplet excited state. In light microscopy, molecules that absorb a photon can enter an excited energy state, one of which is the triplet excited state, where an electron pair occupies two orbitals and have the same spin. Molecules in the triplet excited state are chemically reactive and can damage other molecules and are themselves subject to photo-oxidation. Molecules in the triplet state can return to the ground state, including through phosphorescence, the release of a longer wavelength photon.

Tube lens (Telan lens). An auxiliary lens in the body of the microscope, which in conjunction with an infinity-focus objective forms the real intermediate image. In Zeiss and Leica microscopes, the Telan lens corrects for lateral chromatic aberration, which lessens constraints on the manufacture of the objectives.

TWD. See *Transmitted wavefront distortion (TWD)*.

Two-photon and (multiphoton) microscopy. A method of scanning microscopy where the energy of a pulsed infrared laser is adjusted to allow frequency doubling or tripling at the point of beam focus in the specimen. Fluorophores in the specimen are simultaneously excited by two or three photons to produce excited state transitions that are equivalent to single-photon fluorescence. For example, two and three photon excitation at 900 nm is equivalent to excitation by higher energy photons of 450 and 300 nm, respectively. Multiphoton microscopy enables deep penetration into thick tissues and eliminates the need for a pinhole aperture because fluorescence emission is restricted to a single focal plane.

Uniaxial crystal. A birefringent crystal characterized by having a single optical axis.

Unsharp masking. An image sharpening procedure, in which a blurred version of the original image (called an unsharp mask) is subtracted from the original to generate a difference image in which fine structural features are emphasized. Edges in the difference image are sharpened, but the contrast between bright and faint objects is reduced.

VALAP. A 1:1:1 mixture of Vaseline, lanolin, and paraffin, used to seal coverslip-based observation chambers and eliminate evaporation of the culture medium.

Vibration-isolation table. A sturdy table with dampened microscope platform that attenuates vibrations from surrounding sources that may interfere with cell manipulation and imaging.

Video electron tube. An electron tube that functions as a video pickup tube for recording an image for subsequent display on television. The tube contains a photosensitive target, magnetic coils for deflecting an electron beam in a raster over the target, and electronics for generating an analog voltage signal from an electric current generated during scanning of the target.

Video-enhanced contrast microscopy. In video microscopy, a method of image enhancement (contrast enhancement) in which the offset and gain positions of the camera and/or image processor are adjusted close together to include the gray-level values of an object of interest. As a result, the object image is displayed at very high contrast, making visible features that can be difficult to distinguish when the image is displayed at a larger dynamic range. See *Histogram stretching*.

Virtual image. An image that can be perceived by the eye or imaged by a converging lens, but that cannot be focused on screen or recorded on film as can be done for a real image. The image perceived by the eye when looking in a microscope is a virtual image.

Volume rendering. A technique using algorithms to create a computer visualization of three-dimensional images from arbitrary angles without any intermediate conversion of the data set to represent surface geometry. In laser scanning confocal microscopy, volume rendering is usually conducted on optical section stacks gathered from fluorescent specimens to produce a semi-realistic model of the specimen in three dimensions.

Voxel. A volumetric pixel with *x*, *y*, and *z* dimensions. With a confocal microscope, *x* and *y* dimensions are determined by the pixel format and scan speed of the raster, while *z* is determined by the step size along the optical axis. In widefield microscopes with CCD cameras, *x* and *y* dimensions have fixed pixel dimensions on the surface of the CCD made variable by binning, while *z* is the step size along the optical axis. The basic spatial element in 3D images composed of multiple optical slices is always described in voxels.

Wavefront ellipsoid. See *Refractive index ellipsoid*.

Wavelength. The distance of one beat cycle of an electromagnetic wave. Also, the distance between two successive points at which the phase is the same on a periodic wave. The wavelength of light is designated λ, and is given in nanometers.

Wollaston prism. In interference microscopy, a beamsplitter made of two wedge-shaped slabs of birefringent crystal, such as quartz. In differential interference contrast (DIC) microscopy, specimens are probed by pairs of closely spaced rays of linearly polarized light that are generated by a Wollaston prism acting as a beamsplitter. An important feature of the prism is its interference plane, which lies inside the prism (outside the prism in the case of modified Wollaston prism designs).

Working distance. The space between the front lens surface of the objective and the coverslip. Lenses with high NAs typically have short working distances (60–100 μm). Lenses with longer working distances can bring to focus details deep within a specimen.

Zone-of-action effect. See *Shade-off*.

Zoom factor. In confocal microscopy, an electronically set magnification factor that is used to provide modest adjustments in magnification and to optimize spatial resolution. Since the spatial interval of sampling is small at higher zoom settings, higher zoom increases the spatial resolution. However, since the same laser energy is delivered in a raster of smaller footprint, increasing the zoom factor also increases the rate of photobleaching.

***Z*-stack.** A stack of adjacent optical slices which together form a 3D image of a specimen.

MICROSCOPY WEB RESOURCES

MICROSCOPY EDUCATION

Andor Learning Center (http://www.andor.com/learning/)

Featured on the Andor Technology website, offers information on confocal microscopy, digital imaging, and applications.

C & L Instruments (http://www.fluorescence.com)

Contains a tutorials section with information on fluorescence microscopes and interference filters.

Carl Zeiss Microscopy Online Campus (http://zeiss-campus.magnet.fsu.edu)

Sponsored by ZEISS, this educational site contains interactive tutorials and review articles on the fundamentals of microscopy, as well as leading-edge technologies. Included are image galleries and an extensive reference library.

Hamamatsu Learning Center (http://learn.hamamatsu.com)

Targeted at education in digital imaging, this site is sponsored by Hamamatsu Photonics. Included are review articles, interactive tutorials, and image galleries.

Leica Science Lab (http://www.leica-microsystems.com/science-lab/)

A scientific and educational portal for microscopy and histology that offers topics ranging from the basics to specific application know-how. This site is sponsored and hosted by Leica Microsystems.

Life Technologies (http://www.invitrogen.com/site/us/en/home/support/Tutorials.html)

The technical resources section of this site features a series of Flash video tutorials on fluorescence-based techniques.

Microbus (http://www.microscope-microscope.org)

Basic information on microscopes, imaging, and microscopy applications. Includes image gallery and links.

Fundamentals of Light Microscopy and Electronic Imaging, Second Edition.
Douglas B. Murphy and Michael W. Davidson.

Micrographia (http://www.micrographia.com)

Aimed at students and teachers of fresh water biology, this site features articles, tutorials, applications, and specimen galleries.

Microscopy.info (http://www.microscopy.info)

Information site on microscopes and microscopy techniques featuring news articles, a microscope buyers' guide, and a comprehensive microscopy web resource guide.

Microscopy-UK (http://www.microscopy-uk.org.uk/)

Resources for enthusiast microscopists, students, and anyone interested in microscopy. Collection of freely contributed articles, images, and videos.

Modern Microscopy (http://www.modernmicroscopy.com)

A free web journal for the professional microscopist featuring articles and a series of tutorials on research techniques.

Molecular Expressions (http://microscopy.fsu.edu)

Sponsored by Florida State University, Molecular Expressions is perhaps the most comprehensive microscopy educational site on the Internet. The site contains review articles, interactive tutorials, image galleries, K-12 optics projects, and discussions of topics in general cell biology.

Nikon MicroscopyU (http://www.microscopyu.com)

Education site sponsored by Nikon USA, Inc. that features review articles, interactive Java and Flash tutorials, digital still and video galleries, references, and the annual Nikon Small World competition.

Olympus Microscopy Resource Center (http://olympusmicro.com)

A site sponsored by Olympus America Inc. that covers a wide range of topics in optical microscopy, including basic concepts, the physics of light and color, specialized techniques, digital imaging, fluorescence, and confocal. Also features image and video galleries.

MICROSCOPE MANUFACTURERS

Carl Zeiss Microscopy (http://www.zeiss.de/microscopy)

Features information about ZEISS confocal, widefield, and stereo microscopes, software, cameras, industrial products, and accessories.

Dino-Lite (http://www.dino-lite.com/)

Digital handheld microscopes and accessories for education, hobby, industrial, medical, and law enforcement purposes.

Jenoptik (http://www.jenoptik.com/en_home)

Offers optical components, including lens systems, optoelectronic modules, digital microscope cameras, and optical systems.

Leica Microsystems (http://www.leica-microsystems.com)

Products for microscopy and histology, including confocal, stereo, digital pathology, software, cameras, and staining accessories.

Meiji Techno (http://www.meijitechno.com/)

Manufacturer of optical microscopes and accessories in Japan. Product lines extend into industrial, laboratory, and higher education markets.

Motic Microscopes (http://www.motic.com)

A Chinese manufacturer of economical clinical, industrial, and educational microscopes for those with a tight budget (many Motic products are not useful for research purposes).

Nikon Instruments: Microscopes and Imaging Systems (http://www.nikoninstruments.com)

Products featured: Microscopes, measuring systems, semiconductor instruments, digital pathology, cameras, software, optics, and accessories.

Olympus Corporation of the Americas Inc. (http://www.olympusamerica.com)

Information about cameras, medical and surgical products, industrial products, and life science and imaging systems (microscopes).

SCIENTIFIC DIGITAL CAMERA MANUFACTURERS

Andor Technology (http://www.andor.com)

Products include low light imaging cameras (EMCCDs), scientific CMOS cameras, microscope systems, and time-resolved cameras.

Apogee Imaging Systems (http://www.ccd.com)

High performance CCD cameras for astronomy, microscopy, and spectroscopy. The website also features CCD University, containing information about how digital cameras work.

Cooke/PCO (http://www.pco-tech.com)

Featuring a large array of camera products, Cooke offers scientific CMOS cameras, intensified cameras, sensitive cameras, high-speed cameras, software, and accessories.

Dage-MTI (http://www.dagemti.com)

Offering a wide spectrum of camera solutions, Dage-MTI also markets software, monitors, and other accessories.

Hamamatsu Photonics (http://sales.hamamatsu.com)

One of the world's largest manufacturers of detectors, Hamamatsu products include sCMOS, EMCCD, and cooled scientific CCD cameras systems. The company also offers complete microscope systems, accessories, and software.

Optronics (http://www.optronics.com)

The company offers digital cameras for microscopy, along with imaging devices for biomedical and industrial applications.

Roper Scientific (http://www.roperscientific.com)

A family of camera companies that includes Photometrics, Princeton Instruments, QImaging, and Media Cybernetics. Products include high-end camera systems and software. A nice series of review articles on CCD operation can be found at www.photometrics.com/learningzone.

FLUORESCENCE FILTERS

Chroma Technology Corporation (http://www.chroma.com)

One of the pioneers in filter technology, Chroma offers a wide range of high performance filters for microscopy, light sources, and fluorescent samples.

Omega Optical (http://www.omegafilters.com)

Featuring "Curvomatic," an online filter spectra database, the Omega website contains information on filters for microscopy, astronomy, and industrial applications.

Semrock (http://www.semrock.com)

This company introduced ion-beam sputtering technology that revolutionized the filter industry for light microscopy. Semrock filters feature sharp edges and high transmission.

FLUORESCENT DYES AND PROTEINS

Addgene (http://www.addgene.org/)

Nonprofit plasmid repository dedicated to helping academic scientists around the world share high-quality plasmids.

Amaxa Biosystems (http://www.lonzabio.com/)

Offers a range of products designed for efficient transfection and electroporation of mammalian cell lines, including the pmaxFP line of fluorescent protein vectors.

ATTO-TEC GmbH (http://www.atto-tec.com)

Manufacturer of the ATTO series of synthetic dyes, marketed as conjugates, reactive dyes, and labeled phospholipids.

BD Biosciences Pharmingen (http://www.bdbiosciences.com/home.jsp)

Markets mammalian, nematode, and insect expression vectors containing blue, green, and yellow fluorescent protein sequences.

Biostatus Limited (http://www.biostatus.com)

Maker of DRAQ5, a novel far-red fluorescent DNA dye that can be used in living cells in combination with other common fluorophores, especially GFP fusions and FITC-tags.

Biotium (http://www.biotium.com)

Developed CF™ dyes, a series of highly water-soluble fluorescent dyes spanning the visible and near-infrared spectrum for labeling biomolecules.

BioVision (http://www.biovision.com)

Develops and offers a wide variety of products including fluorescent proteins, assay kits, antibodies and other research tools.

Clontech Laboratories (http://www.clontech.com/)

Development, production, and marketing of a wide spectrum of biological products, including their Living Colors lineup of fluorescent protein vectors.

DNA2.0 (http://www.dna20.com/)

Provider of synthetic genes, the company's DNA-2-Go program enables researchers to obtain custom gene synthesis of specific DNA sequences in the database.

Evrogen (http://www.evrogen.com/)

Provides products for molecular and cellular biological investigations, including a lineup of fluorescent protein and optical highlighter vectors ranging in color from cyan to the far red.

GE-Healthcare (http://www.gelifesciences.com)

Products include Amersham CyDye™ Fluors, versatile fluorophores for use in a broad range of applications.

Genomics (http://www.genomics.agilent.com/)

The fluorescent protein vectors are bundled into the company's Vitality product line, which includes hrGFP II, a humanized green fluorescent protein derived from *Renilla reniformis*.

Jackson ImmunoResearch Laboratories, Inc. (http://www.jacksonimmuno.com)

Products include secondary antibodies (H + L), Fab_2 fragment, and Fab fragment conjugates to cyanine and Alexa Fluor dyes. Unlabeled antibodies and sera are also available.

KPL, Inc. (http://www.kpl.com)

KPL offers a range of affinity purified antibodies coupled to DyLight dyes for sensitive fluorescent detection. They also market over 600 reagents and complete assay kits.

Life Technologies—Molecular Probes (http://www.invitrogen.com/site/us/en/home/brands/Molecular-Probes.html)

Molecular Probes offers a wide range of synthetic fluorophores, reactive dyes, conjugated antibodies, fluorescent proteins, and cell assays. Original source of Alexa Fluor dyes and QDot quantum dot products.

LUX Biotechnology (http://luxassure.com/web/)

The company has three product ranges that include whole organism screening, scientific reference devices, and a wide variety of novel luminescence and fluorescence research reagents.

MBL International (http://www.mblintl.com/)

Offers a wide variety of agents for research in cellular biology including their CoralHue lineup of fluorescent protein and optical highlighter vectors.

NanoLight Technology (http://www.nanolight.com/)

Focusing on broad based applications of marine bioluminescence. Products include reagent luciferins, recombinant bioluminescent proteins, photoproteins, and fluorescent proteins.

Nature Technology Corporation (http://www.natx.com/)

Technology-based molecular biology and gene therapy company, providing vector and DNA vaccine development, as well as highly purified plasmid DNA production and recombinant protein manufacturing services.

Perkin Elmer (http://www.perkinelmer.com/)

A leading provider of products for drug discovery, genetic engineering, and chemical analysis. The company distributed GFP2 (squared) vectors, which are human codon-optimized derivatives of the original *Aequorea victoria* jellyfish GFP.

Promega (http://www.promega.com/)

Markets the Monster Green fluorescent protein, which is packaged in a mammalian expression vector (hMGFP) derived from the Great Star coral, *Montastraea cavernosa*.

Thermo-Fisher Scientific (http://www.thermoscientific.com)

Distributor for the subsidiary, Pierce Protein Research Products, manufacturers of DyLight synthetic dyes. The company offers a wide selection of products including reagents, proteins, antibodies, and assay kits.

SPECTRAL VIEWERS FOR FLUORESCENT DYES AND FILTERS

Curvomatic (http://www.omegafilters.com/Products/Curvomatic)

Flash-based spectral tool from Omega Optical.

DyLight Fluor Spectra (http://www.piercenet.com/Objects/View.cfm?type=Page&ID=FCC04663-63D6-4F6D-94F6-13A07031FC67)

Thermo Scientific/ Pierce Protein Research Products page for spectra of the DyLight family of dyes.

Filter Assistant (http://www.micro-shop.zeiss.com/?p=us&f=f)

Spectral viewer for dyes and filters, featuring an interactive database provided by ZEISS.

Fluorescence SpectraViewer (http://www.invitrogen.com/site/us/en/home/support/Research-Tools/Fluorescence-SpectraViewer.html)

A tool to examine multiple fluorophore spectra from Life Technologies.

Spectral Traces for Fluorescent Dyes (http://www.mcb.arizona.edu/IPC/spectra_page.htm)

Prepared by the department of Molecular Cell Biology, University of Arizona.

Two-Photon Cross-Sections Of Fluorescent Dyes (http://www.drbio.cornell.edu/cross_sections.html)

An atlas of two-photon cross sections prepared by the Developmental Resource for Biophysical Imaging Optoelectronics.

SOFTWARE FOR ACQUISITION, PROCESSING, AND ANALYSIS

Auto-Montage (http://www.syncroscopy.com/syncroscopy/)

A software solution that works with any optical microscope to automatically capture in-focus regions from a range of focal planes and combine them into a single, fully focused, high resolution image.

AutoQuant Imaging (http://www.mediacy.com/)

Produces deconvolution and visualization tools without point spread function acquisition, fully blind deconvolution, quantitative analysis of deconvolved images, and 3-D microscopy and visualization.

Clemex Technologies (http://www.clemex.com/)

Provides digital imaging solutions for the acquisition, archiving, and analysis of images used in quality control and research laboratories.

Huygens Software (http://www.svi.nl/)

Offers deconvolution and volume rendering software that enables the restoration of wide-field and confocal 2D, 3D, and 4D images.

Image J (http://rsbweb.nih.gov/ij/)

Public domain software that is used for image analysis and processing that works with all operating systems: Mac, Linux and Windows. Fiji is an Open Source image processing package based on ImageJ.

Imaris (http://www.bitplane.com/)

Imaging software that provides the necessary functionality for data visualization, analysis, segmentation, and interpretation of 3D and 4D microscopy data sets, and allows visualization of original and derived data objects in a real time interactive manner.

MetaMorph (http://www.moleculardevices.com/)

A modular platform that allows automated microscope acquisition, device control, and image analysis.

Micromanager (http://www.micro-manager.org)

Open source software for controlling automated microscopes. The software works on Windows, Mac, and Linux operating systems and includes ImageJ for image processing.

Mirametrics (http://www.mirametrics.com)

Software for scientific image processing, analysis, and visualization. This site has a Tech Notes page with many helpful papers and bulletins.

Neurolucida (http://www.mbfbioscience.com/neurolucida/)

Software for performing 3D brain mapping, neuron tracing, anatomical mapping, and morphometry.

NIS-Elements (http://www.nikoninstruments.com/)

Combines automated intelligence to microscopes, cameras, components and peripherals with powerful archiving, analysis, visualization, and archiving tools.

Northern Eclipse (http://www.empix.com/)

Image analysis software with morphometry, densitometry, CCD camera control, image filtering, animation, 3D reconstruction, fluorescent overlays, image histograms, DDE, and equalization.

Probe3d (http://www.gennano.com/)

Software package for computer-programmed microscope image acquisition, 3D image rendering, enhancement, and analysis.

SimplePCI (http://www.cimaging.net/)

A high performance imaging software system developed by Hamamatsu that contains acquisition, microscope control, and analysis routines.

Slidebook (http://www.slidebook.com/)

Features a robust set of standard tools for device control, data collection, and analysis, as well as providing many specialized expansion modules that include photo manipulation, FRET, ratio imaging, and particle tracking.

Soft Imaging System (http://www.soft-imaging.com/)

Products include: image analysis software and hardware for machine vision, image processing, medical imaging, biometric, and metallographic applications.

softWoRx (http://www.appliedprecision.com/)

Products include measurement, analysis, and process-control systems for semiconductor testing, assembly, and packaging. Software is also available for researchers involved in cell microscopy, genomics, and proteomics.

TILLvisION (http://www.till-photonics.de)

Image analysis package designed to facilitate fluorescent microscopy through advanced image acquisition, live analysis of the images, and a full spectrum of processing, enhancement, and correction tools.

Vaa3D (http://www.vaa3d.org/)

Vaa3D is an Open Source, cross-platform 3D/4D/5D image visualization and analysis system for biological images and surface objects.

Vision (http://www.impuls-imaging.com/)

Offers commercially supported Image Processing and Analysis solutions that fully exploit the capabilities of Microsoft Windows through software development kits that can be used to create dedicated image processing solutions.

Volocity (http://www.perkinelmer.com/)

Image analysis software that has the capabilities to acquire, visualize, analyze, and publish 3D and 4D data from a wide range of microscopy, widefield, and high content screening systems.

Zen (http://www.zeiss.com)

Zen software saves acquisition parameters, so that settings such as laser intensity, beam path configuration and scanning parameters can be recreated instantly. Optional packages include Topography and StichArt.

MICROSCOPY SOCIETIES

American Microscopical Society (http://amicros.org/)

An international society of biologists organized to encourage the use of microscopy in research and teaching. The society conducts annual meetings on research, organizes workshops, and publishes the journal *Invertebrate Biology*.

European Microscopy Society (http://www.eurmicsoc.org/)

Aims to promote the use and the quality of advanced microscopy in all its aspects in Europe, with particular reference to developments in instrumentation and methodology and novel applications of all types of microscopy.

International Federation of Societies for Microscopy (http://www.ifsm.uconn.edu/)

IFSM aims to contribute to the advancement of microscopy in all its aspects. It comprises microscopy societies from all around the world.

Microanalysis Society (http://www.microbeamanalysis.org/)

MAS aims to advance and disseminate knowledge concerning the principles, instrumentation, and applications of microanalysis. The society holds annual meetings, workshops, seminars, and publishes the journal *Microscopy & Microanalysis*.

Microscopical Society of Canada (http://msc.rsvs.ulaval.ca/)

Activities of the MSC embrace all forms of microscopy, and membership is drawn from scientists in both materials and biological sciences.

Microscopy Society of America (http://www.microscopy.org/)

A nonprofit organization dedicated to the promotion and advancement of techniques and applications of microscopy and microanalysis in all relevant scientific disciplines.

Quekett Microscopical Club (http://www.quekett.org.uk/)

Organization for anyone interested in the microscope and microscopy, with an international membership of both amateur and professional microscopists that aims to promote the understanding and use of all aspects of the microscope.

Royal Microscopical Society (http://www.rms.org.uk/)

One of the oldest and most respected societies for the advancement of microscopy, the RMS serves the needs of its members in the academic and industrial communities, promoting both theory and practical application.

Society for Ultrastructural Pathology (http://www.ultrapath.org/)

An international association of electron microscopists. The Society fosters the application of electron microscopy in the diagnosis and research of human diseases.

MICROSCOPY COURSES AND WORKSHOPS

Advanced Course in Laser Scanning Microscopy (http://www.zeiss.de/courses)

Held in Jena, Germany (in English) at the Carl Zeiss Center for Microscopy. A range of courses is offered in basic microscopy, fluorescence techniques, laser scanning confocal microscopy, and fluorescence correlation spectroscopy.

Advanced Optical Microscopy Course (http://www.events.embo.org/11-optical-microscopy)

Advanced course in microscope imaging in Plymouth, England, that includes experience in imaging around experiments.

Analytical and Quantitative Light Microscopy (http://www.mbl.edu/education/courses/special_topics/aqlm.html)

Offered biannually by the Marine Biological Laboratory at Woods Hole, Massachusetts, the AQLM is a comprehensive course in light microscopy for researchers in biology, medicine, and material sciences.

Cellular Imaging and Confocal Techniques (http://kiwas.ki.se/katalog/katalog/kurser)

This 2-week course in Stockholm, Sweden, is directed towards graduate students undertaking or planning projects involving cellular imaging techniques, including confocal microscopy.

Cold Spring Harbor Laboratory Meetings and Courses (http://meetings.cshl.edu/)

Annual course held at Cold Spring Harbor Laboratory, Cold Spring Harbor, NY. Their offerings often include courses related to confocal and fluorescence microscopy, live-cell imaging, and other topics of interest to microscopists.

Confocal Light Microscopy: Fundamentals and Biological Applications (http://wwwmc.bio.uva.nl/cam/courses.htm)

The Center for Advanced Microscopy of the Swammerdam Institute for Life Sciences, Amsterdam, Netherlands, organizes an annual course covering fluorescence and confocal microscopy in addition to a variety of topics in digital imaging, sample preparation, and live cell microscopy.

European Molecular Biology Laboratory Courses (http://www.embl.de/training/)

Topics include transmission and fluorescence microscopy, confocal microscopy, multiphoton microscopy, image processing, and 2D/3D time-lapse microscopy. Basic and advanced courses are taught. Check website for current courses offered.

Fluorescence Lifetime and Spectral Imaging in the Biological Sciences (http://www.uthscsa.edu/csb/)

Department of Cellular and Structural Biology at the University of Texas Health Science Center. The course material focuses on sophisticated lifetime imaging (FLIM) and resonance energy transfer (FRET) fluorescence techniques in biological systems.

Focus on Microscopy (http://www.focusonmicroscopy.org/)

The continuation of a yearly conference series (in Singapore) presenting the latest innovations in optical microscopy and their application in biology, medicine, and the material sciences.

FRET Microscopy Workshop (http://www.kcci.virginia.edu/workshop)

Advanced lecture/laboratory course on fluorescence resonance energy transfer microscopy with emphasis on detectors and instrumentation, especially three-cube fluorescence, confocal, two-photon, and fluorescence lifetime microscopy. The course is held annually at the University of Virginia

Leica Advanced Microscopy Course (http://www.leica-microsystems.com/products/confocal-microscopes/)

Held annually in Heidelberg, Germany, and the National Institutes of Health (NIH) in Washington DC, USA. Topics include digital imaging, confocal microscopy, advanced fluorescence techniques, laser micro dissection, and tissue specimen preparation.

Microscopy/Marketing and Education (MME) Courses (http://www.microscopyeducation.com/)

The MME organizes specialized courses in fluorescence imaging and optical microscopy, including in-house training tailored to a specific laboratory or institute.

Microscopy and Microanalysis (http://www.microscopy.org/)

An annual event cosponsored by the Microscopy Society of America, typically includes short courses, symposia, tutorials, exhibitions, poster sessions, and special events covering a wide array of subject matter.

Monash Micro Imaging Courses (http://www.microimaging.monash.org/training.html)

Monash University, Melbourne, Australia offers basic light microscopy, fluorescence, and confocal microscopy short courses.

Optical Microscopy and Imaging in the Biomedical Sciences (http://www.mbl.edu/education/courses/special_topics/om.html)

Annual course held at the Marine Biological Laboratory (MBL), Woods Hole, MA covering basic principles of microscopy, contrast-enhancing techniques, fluorescence, confocal and multiphoton microscopy, digital imaging, and fluorescent probes.

Quantitative Fluorescence Microscopy (http://www.mdibl.org/courses/Quantitative_Fluorescent_Microscopy/159/)

This 1-week, intensive microscopy course in Bar Harbor, Maine, covers all aspects of the technology, from the principals of fluorescence imaging to multidimensional imaging in living cells.

Sydney Key Center Courses in Microscopy (http://sydney.edu.au/acmm/)

The University of Sydney conducts regular training courses that cover a wide variety of topics including light microscopy, confocal microscopy, specimen preparation, stereology, and image analysis.

3D Microscopy of Living Cells (http://www.3dcourse.ubc.ca/)

Sponsored by the Brain Research Institute and the Departments of Pharmacology and Physiology at the University of British Columbia, this course includes basic microscopy through confocal, multiphoton, and STED microscopy.

LIGHT SOURCES, SHUTTERS, AND FILTER WHEELS

Applied Scientific Instrumentation (http://www.asiimaging.com/)

Among the products offered are illuminators and laser systems, shutters and controllers, and a high-speed filter wheel assembly.

C & L Instruments (http://www.fluorescence.com/)

In addition to numerous innovative instruments and accessories for fluorescence applications, C & L offers interference filters, illumination sources, filter wheels, and detectors.

Cairn Research (http://www.cairn-research.co.uk/)

Offers a variety of illumination products including arc light and LED light sources, laser illumination, filter changers, and the unique Optoscan monochromator.

Conix Research (http://www.conixresearch.com/)

Manufacturer of motorized stages, filter cube sliders, filter wheels, microscope accessories, and custom electronic and mechanical devices.

Ludl (http://www.ludl.com/)

Provider of leading-edge microscope automation including motorized stages, programmable filter wheels, nano positioning, and slide handler systems.

Melles Griot (http://www.cvimellesgriot.com/)

Produces a line of electromechanical shutters that feature a reliable, multiblade shutter mechanism to guarantee high operational speed and nearly 100% light extinction.

Prior (http://www.prior.com/)

Products include illumination systems. They also offer a range of light sources designed for use in stereo microscopy, including cold light sources, with power and accessories.

Sutter (http://www.sutter.com/)

Offers a wide range of products, including filter wheels, controllers, shutters, microinjection systems, and illumination sources.

Thorlabs (http://www.thorlabs.com/)

Offers an entire line of photonics products including filter mounts, shutters, emitters, sources, and controllers. Many of their standard components are compatible with microscopes produced by Leica, Olympus, Nikon, and Zeiss.

LIVE-CELL IMAGING

Andor Technology (http://www.andor.com/)

Develops and manufactures products for scientific imaging and spectroscopy. The BioImaging Division offers a family of hardware and software especially designed for live cell confocal experiments.

ATCC Global Bioresource Center (http://www.atcc.org/)

A global, nonprofit resource center that provides biological products, technical services, and educational programs to organizations around the world.

Cell Centered Database (http://ccdb.ucsd.edu/)

Promotes data sharing among scientists interested in cellular and subcellular anatomy and in developing computer algorithms for three-dimensional reconstruction and modeling of such data.

Northwestern University Cell Imaging Facility (http://www.feinberg.northwestern.edu/cif/)

Featured is information on upcoming cell imaging workshops, descriptions of hardware and software, recommended reading, and technical tips on immunofluorescence, tissue samples, emission crosstalk, and other pertinent topics.

Plant Cell Imaging (Carnegie Institution of Washington) (http://deepgreen.stanford.edu/)

Provides detailed information regarding the use of laser scanning confocal microscopy to visualize live plant cells. Features articles, descriptions of protocols and experiments, numerous sample images and videos, and links to related sites.

Salmon Lab Homepage (http://labs.bio.unc.edu/Salmon/)

Includes wide-ranging information on live cell protocols. Related web links and a collection of live cell videos created in the lab are also featured.

***Science* Magazine Special Issue: Biological Imaging** (http://www.sciencemag.org/content/300/5616)

The April 2003 special issue of ***Science*** magazine offers a plethora of information about live-cell imaging. Covered are the latest techniques in the field, development, and usage of fluorescent protein markers.

Spector Lab Homepage (http://spectorlab.cshl.edu/)

Stunning live cell images and videos, a research summary, and protocols for immunofluorescence, *in situ* hybridization, and a variety of other laboratory activities are provided.

Web Atlas of Cellular Structures Using Light and Confocal Microscopy (http://itg.beckman.illinois.edu/technology_development/web_atlas/)

Education resource for those interested in cytology. It has an extensive collection of images, as well as technical information, reports on specimen preparation, microscopy methods, and tissue culture.

MICROSCOPY JOURNALS

Bulletin of the Microscopical Society of Canada (http://msc.rsvs.ulaval.ca/)

This bulletin includes reviews on current topics in microscopy, regular columns on transmission electron microscopy, scanning electron microscopy, light microscopy, and so on.

Journal of Advanced Microscopy Research (http://www.aspbs.com/jamr/)

A multidisciplinary, peer-reviewed journal that provides a forum for rapid dissemination of important research developments in the fields of high-resolution microscopy techniques, as well as their applications in all areas of science, engineering, and medicine.

Journal of Biomedical Optics (http://spie.org/)

Publishes peer-reviewed articles on the use of modern optical technology for improved health care and biomedical research.

Journal of Microscopy (http://onlinelibrary.wiley.com/journal/10.1111/(ISSN)1365-2818)

A peer-reviewed scientific journal on all aspects of microscopy, spatially resolved spectroscopy, compositional mapping, and image analysis.

Micron (http://www.journals.elsevier.com/micron/)

Micron aims to serve as an interdisciplinary forum for all work that involves new applications of microscopy or where microscopy plays a central role.

The Microscope Journal (http://www.mcri.org/)

Covering a variety of industries, this publication emphasizes new advances in microscope design, new accessories, new techniques, and unique applications.

Microscopy and Analysis (http://www.microscopy-analysis.com)

This site features access to tutorials, webinars, literature, and other educational content in the areas of optical, electron, and scanning probe microscopy.

Microscopy and Microanalysis (http://journals.cambridge.org/action/displayJournal?jid=MAM)

Publishes original research articles in the fields of microscopy, imaging, and compositional analysis.

Microscopy Research and Technique (http://www.wiley.com/WileyCDA/WileyTitle/productCd-JEMT.html)

Publishes articles on all aspects of advanced microscopy in the biological, clinical, chemical, and materials sciences.

Microscopy Today (http://www.microscopy-today.com/)

Editorial coverage spans all microscopy methods, including light microscopy, scanning probe microscopy, electron microscopy, ion-beam techniques, and a wide range of microanalytical methods.

Modern Microscopy (http://www.modernmicroscopy.com/)

Free web journal. Articles are contributed from the microscopy community and reviewed by experts in various microscopy specialties.

RECOMMENDED READING

Bell, S. and Morris, K. (2010). *An Introduction to Microscopy*. CRC Press/Taylor and Francis Group, Boca Raton, FL.

Born, M. and Wolf, E. (1999). *Principles of Optics: Electromagnetic Theory of Propagation, Interference and Diffraction of Light*, 7th ed. Cambridge University Press, Cambridge, UK.

Chalfie, M. and Kain, S. R. (2006). *Green Fluorescent Protein: Properties, Applications, and Protocols*, 2nd ed. Wiley-Interscience, New York.

Diaspro, A. (2002). *Confocal and Two-Photon Microscopy: Foundations, Applications, and Advances*. Wiley-Liss, New York.

Freshney, R. I. (2010). *Culture of Animal Cells: A Manual of Basic Technique and Specialized Applications*, 6th ed. Wiley-Blackwell, New York.

Goldman, R. D., Swedlow, J. R., and Spector, D. L. (2010). *Live Cell Imaging: A Laboratory Manual*, 2nd ed. Cold Spring Harbor Laboratory Press, Cold Spring Harbor, NY.

Gonzalez, R. C. and Woods, R. E. (2007). *Digital Image Processing*, 3rd ed. Prentice Hall/Pearson Education, Inc., Upper Saddle River, NJ

Hecht, E. (2001). *Optics*, 4th ed. Addison Wesley Longman, Boston.

Hibbs, A. R. (2004). *Confocal Microscopy for Biologists*. Kluwer Academic/Plenum Publishers, New York.

Holst, G. C. (1998). *CCD Arrays, Cameras, and Displays (SPIE—The International Society for Optical Engineering*. JCD Publishing, Winter Park, FL.

Inoué, S. and Spring, K. R. (1997). *Video Microscopy: The Fundamentals*, 2nd ed. Plenum Press, New York.

Johnson, I. and Spence, M. T. Z. (2010). *Molecular Probes Handbook: A Guide to Fluorescent Probes and Labeling Technologies*, 11th ed. Life Technologies, Inc., Eugene, OR.

Lacey, A. J. (1999). *Light Microscopy in Biology: A Practical Approach*, 2nd ed. Oxford University Press, New York.

Lakowicz, J. R. (2006). *Principles of Fluorescence Spectroscopy*, 2nd ed. Kluwer Academic/Plenum Publishers, New York.

Matsumoto, B. (2002). *Methods in Cell Biology, Volume 70: Cell Biological Applications of Confocal Microscopy*, 2nd ed. Academic Press, New York.

Fundamentals of Light Microscopy and Electronic Imaging, Second Edition.
Douglas B. Murphy and Michael W. Davidson.

Mertz, J. (2010). *Introduction to Optical Microscopy*. Roberts and Company Publishers, Greenwood Village, CO.

Pawley, J. B. (2006). *Handbook of Biological Confocal Microscopy*, 3rd ed. Springer Science, New York.

Periasamy, A. (2001). *Methods in Cellular Imaging*. Oxford University Press, New York.

Periasamy, A. and Day, R. N. (2005). *Molecular Imaging: FRET Microscopy and Spectroscopy*. Oxford University Press, New York.

Pluta, M. (1988). *Advanced Light Microscopy, Volume 1: Principles and Basic Properties*. Elsevier Science Publishers, B.V., Amsterdam.

Pluta, M. (1989). *Advanced Light Microscopy, Volume 2: Specialized Methods*. Elsevier Science Publishers, B.V., Amsterdam.

Pluta, M. (1993). *Advanced Light Microscopy, Volume 3: Measuring Techniques*. Elsevier Science Publishers, B.V., Amsterdam.

Price, R. L. and Jerome, W. G. (2011). *Basic Confocal Microscopy*. Springer Science+Business Media, LLC., New York.

Rietdorf, J. (2005). *Advances in Biochemical Engineering/Technology, Volume 95: Microscopy Techniques*. Springer-Verlag, Berlin, Germany.

Rost, F. and Oldfield, R. (2000). *Photography with a Microscope*. Cambridge University Press, Cambridge, UK.

Russ, J. C. (2011). *The Image Processing Handbook*, 6th ed. CRC Press/Taylor and Francis Group, Boca Raton, FL.

Selvin, P. R. and Ha, T. (2008). *Single-Molecule Techniques: A Laboratory Manual*. Cold Spring Harbor Laboratory Press, Cold Spring Harbor, NY.

Shotton, D. (1993). *Electronic Light Microscopy: Techniques in Modern Biomedical Microscopy*. Wiley-Liss, New York.

Slayter, E. M. (1970). *Optical Methods in Biology*. John Wiley and Sons, New York.

Slayter, E. M. and Slayter, H. S. (1992). *Light and Electron Microscopy*. Cambridge University Press, New York.

Sluder, G. and Wolf, D. E. (2007). *Methods in Cell Biology, Volume 81: Digital Microscopy*, 3rd ed. Academic Press/Elsevier, New York.

Török, P. and Kao, F. J. (2007). *Springer Series in Optical Sciences, Volume 87: Optical Imaging and Microscopy: Techniques and Advanced Systems*, 2nd ed. Springer Science+Business Media, LLC., New York.

Wang, X. F. and Herman, B. (1996). *Chemical Analysis, Volume 137: Fluorescence Imaging Spectroscopy and Microscopy*. Wiley-Interscience, New York.

Yuste, R., Lanni, F., and Konnerth, A. (2000). *Imaging Neurons: A Laboratory Manual*. Cold Spring Harbor Laboratory Press, Cold Spring Harbor, NY.

REFERENCES

Agard, D. A., Hiraoka, Y., Shaw, P., and Sedat, J. W. (1989). Fluorescence microscopy in three dimensions. *Methods in Cell Biology* **30**, 353–377.

Aitken, C. E., Marshall, R. A., and Puglisi, J. D. (2008). An oxygen scavenging system for improvement of dye stability in single-molecule fluorescence experiments. *Biophysical Journal* **94**, 1826–1835.

Albeanu, D. F., Soucy, E., Sato, T. F., Meister, M., and Murthy, V. N. (2008). LED arrays as cost effective and efficient light sources for widefield microscopy. *PLoS ONE* **3**, e2146.

Allen, R. D. (1985). New observations on cell architecture and dynamics by video-enhanced contrast optical microscopy. *Annual Review of Biophysics and Biophysical Chemistry* **14**, 265–290.

Allen, R. D., David, G. B., and Nomarski, G. (1969). The Zeiss-Nomarski differential interference equipment for transmitted-light microscopy. *Zeitschrift für Wissenschaftliche Mikroskopie und Mikroskopische Technik* **69**, 193–221.

Axelrod, D., Koppel, D. E., Schlessinger, J., Elson, E., and Webb, W. W. (1976). Mobility measurement by analysis of fluorescence photobleaching recovery kinetics. *Biophysical Journal* **16**, 1055–1069.

Axelrod, D., Burghardt, T. P., and Thompson, N. L. (1984). Total internal reflection fluorescence. *Annual Review of Biophysics and Bioengineering* **13**, 247–268.

Barer, R., Ross, K. F. A., and Tkaczyk, S. (1953). Refractometry of living cells. *Nature* **171**, 720–724.

Beacher, J. (2008). LEDs for fluorescence microscopy. *Biophotonics International* **15**, 34–37.

Bennett, A. H., Jupnik, H., Osterberg, H., and Richards, O. W. (2011). *Phase Microscopy: Principles and Applications*. Nabu Press, Charleston, SC, Reprint of the original book published in 1951.

Berek, V. M. (1927). Grundlagen der Tiefenwahrnehmung im Mikroskopie. *Marburg Sitzungsber, Berlin* **62**, 189–223.

Betzig, E., Patterson, G. H., Sougrat, R., Lindwasser, O. W., Olenych, S., Bonifacino, J. S., Davidson, M. W., Lippincott-Schwartz, J., and Hess, H. F. (2006). Imaging intracellular fluorescent proteins at nanometer resolution. *Science* **313**, 1642–1645.

Fundamentals of Light Microscopy and Electronic Imaging, Second Edition.
Douglas B. Murphy and Michael W. Davidson.

Biggs, D. S. C. (2010). A practical guide to deconvolution of fluorescence microscope imagery. *Microscopy Today* **18**, 10–14.

Biteen, J. S., Thompson, M. A., Tselentis, N. K., Bowman, G. R., Shapiro, L., and Moerner, W. E. (2008). Super-resolution imaging in live *Caulobacter crescentus* cells using photoswitchable EYFP. *Nature Methods* **5**, 947–949.

Bossi, M., Fölling, J., Dyba, M., Westphal, V., and Hell, S. W. (2006). Breaking the diffraction resolution barrier in far-field microscopy by molecular optical bistability. *New Journal of Physics* **8**, 275–280.

Brenner, M. (1994). Imaging dynamic events in living tissue using water immersion objectives. *American Laboratory,* April, pp. 14–19.

Bretschneider, S., Eggeling, C., and Hell, S. W. (2007). Breaking the diffraction barrier in fluorescence microscopy by optical shelving. *Physical Review Letters* **98**, 218103.

Buil, C. (1991). *CCD Astronomy: Construction and Use of an Astronomical CCD Camera*. Willmann-Bell, Inc., Richmond, VA.

Burnette, D. T., Sengupta, P., Dai, Y., Lippincott-Schwartz, J., and Kachar, B. (2011). Bleaching/blinking assisted localization microscopy for superresolution imaging using standard fluorescent molecules. *Proceedings of the National Academy of Sciences U S A* **108**, 21081–21086.

Campagnola, P. J., Millard, A. C., Terasaki, M., Hoppe, P. E., Malone, C. J., and Mohler, W. A. (2002). Three-dimensional high-resolution second-harmonic generation imaging of endogenous structural proteins in biological tissues. *Biophysical Journal* **81**, 493–508.

Castleman, K. R. (1993). Resolution and sampling requirements for digital image processing, analysis, and display. In: D. Shotton, ed. *Electronic Light Microscopy: Techniques in Modern Biomedical Microscopy*. Wiley-Liss, Inc., New York, pp. 71–94.

Chen, Y., Mills, J. D., and Periasamy, A. (2003). Protein localization in living cells and tissues using FRET and FLIM. *Differentiation* **71**, 528–541.

Christenson, M. (2005). The application of scientific-grade CCD cameras to biological imaging. In: R. Yuste, F. Lanni, and A. Konnerth, eds. *Imaging in Neuroscience and Development*. Cold Spring Harbor Laboratory Press, Cold Spring Harbor, NY, pp. 6.1–6.14.

Chung, E., Kim, D., Cui, Y., Kim, Y. H., and So, P. T. C. (2007). Two-dimensional standing wave total internal reflection fluorescence microscopy: superresolution imaging of single molecular and biological specimens. *Biophysical Journal* **93**, 1747–1757.

Clegg, R. M. (1996). Fluorescence resonance energy transfer (FRET). In: X. F. Wang and B. Herman, eds. *Fluorescence Imaging and Spectroscopy*. Wiley-Interscience, New York, pp. 179–252.

Coons, A., Creech, H. J., and Jones, R. N. (1941). Immunological properties of an antibody containing a fluorescent group. *Proceedings of the Society for Experimental Biology and Medicine* **47**, 200–202.

Cromey, D. W. (2010). Avoiding twisted pixels: ethical guidelines for the appropriate use and manipulation of scientific digital images. *Science and Engineering Ethics* **16**, 639–667.

Denk, W. and Svoboda, K. (1997). Photon upmanship: why multiphoton imaging is more than a gimmick. *Neuron* **18**, 351–357.

Denk, W., Strickler, J. H., and Webb, W. W. (1990). Two-photon laser scanning fluorescence microscopy. *Science* **248**, 73–76.

Dyba, M., Jakobs, S., and Hell, S. W. (2003). Immunofluorescence stimulated emission depletion microscopy. *Nature Biotechnology* **21**, 1303–1304.

Edidin, M. (1994). Fluorescence photobleaching and recovery, FPR, in the analysis of membrane structure and dynamics. In: S. Damjanovich, M. Edidin, J. Szollosi, and L. Tron, eds. *Mobility and Proximity in Biological Membranes*. CRC Press, Boca Raton, FL, pp. 109–136.

Eggeling, C., Ringemann, C., Medda, R., Schwarzmann, G., Sandhoff, K., Polyakova, S., Belov, V., Hein, B., von Middendorff, C., Schönle, A., and Hell, S. W. (2009). Direct observation of the nanoscale dynamics of membrane lipids in a living cell. *Nature* **457**, 1159–1162.

Egner, A., Geisler, C., von Middendorff, C., Bock, H., Wenzel, D., Medda, R., Andresen, M., Stiel, A. C., Jakobs, S., Eggeling, C., Schönle, A., and Hell, S. W. (2007). Fluorescence

nanoscopy in whole cells by asynchronous localization of photoswitching emitters. *Biophysical Journal* **93**, 3285–3290.

Elangovan, M., Wallrabe, H., Chen, Y., Day, R. N., Barroso, M., and Periasamy, A. (2003). Characterization of one- and two-photon excitation fluorescence resonance energy transfer microscopy. *Methods* **29**, 58–73.

Ellenberg, J. and Lippincott-Schwartz, J. (1999). Dynamics and mobility of nuclear envelope proteins in interphase and mitotic cells revealed by green fluorescent protein chimeras. *Methods* **19**, 362–372.

Ellis, G. W. (1978). Advances in visualization of mitosis in vivo. In: E. Dirksen, D. Prescott, and C. E. Fox, eds. *Cell Reproduction: In Honor of Daniel Mazia. ICN-UCLA Symposia on Molecular and Cellular Biology*. Academic Press, New York, pp. 465–476.

Erdogan, T. (2011). Optical filters for wavelength selection in fluorescence instrumentation. *Current Protocols in Cytometry Unit* 2.4.

Erickson, M. G., Alseikhan, B. A., Peterson, B. Z., and Yue, D. T. (2001). Preassociation of calmodulin with voltage-gated Ca(2+) channels revealed by FRET in single living cells. *Neuron* **31**, 973–985.

Falk, D., Brill, D., and Stork, D. (1986). *Seeing the Light: Optics in Nature, Photography, Color, Vision, and Holography*. John Wiley and Sons, Inc., New York.

Focht, D. C. (1998). Observation of live cells in the light microscope. In: D. L. Spector, R. D. Goldman, and L. A. Leinwand, eds. *Cells: A Laboratory Manual*. Cold Spring Harbor Laboratory Press, Cold Spring Harbor, NY, pp. 75.1–75.13.

Fölling, J., Bossi, M., Bock, H., Medda, R., Wurm, C. A., Hein, B., Jakobs, S., Eggeling, C., and Hell, S. W. (2008). Fluorescence nanoscopy by ground-state depletion and single-molecule return. *Nature Methods* **5**, 943–945.

Françon, M. (1961). *Progress in Microscopy*. Row-Peterson Publishing, Evanston, IL.

Franken, P. A., Hill, A. E., Peters, C. W., and Weinreich, G. (1961). Generation of optical harmonics. *Physical Review Letters* **7**, 118–119.

Freshney, R. I. (2010). *Culture of Animal Cells: A Manual of Basic Technique and Specialized Applications*, 6th ed. Wiley-Blackwell, New York.

Freund, I., Deutsch, M., and Sprecher, A. (1986). Optical second-harmonic microscopy, crossed-beam summation, and single-angle scattering in rat-tail tendon. *Biophysical Journal* **50**, 693–712.

Frohn, J. T., Knapp, H. F., and Stemmer, A. (2000). True optical resolution beyond the Rayleigh limit achieved by standing wave illumination. *Proceedings of the National Academy of Sciences U S A* **97**, 7232–7236.

Funatsu, T., Harada, Y., Tokunaga, M., Saito, K., and Yanagida, T. (1994). Imaging of single fluorescent molecules and individual ATP turnovers by single myosin molecules in aqueous solution. *Nature* **374**, 555–559.

Galbraith, W. and David, G. B. (1976). An aid to understanding differential interference contrast microscopy: computer simulation. *Journal of Microscopy* **108**, 147–176.

Gall, J. G. (1967). The light microscope as an optical diffractometer. *Journal of Cell Science* **2**, 163–168.

Gastou, P. and Comandon, J. (1909). L'ultramicroscope et son role essentiel dans le diagnostic de la syphilis. *Journal la Médecine France* **4**.

Gilliland, R. L. (1992). Details of noise sources and reduction processes. In: S. B. Howell, ed. *Astronomical CCD Observing and Reduction Techniques*, Vol. 23, Astronomical Society of the Pacific Conference Series, Astronomical Society of the Pacific, San Francisco, pp. 68–89.

Goldman, R. D., Swedlow, J. R., and Spector, D. L. (2010). *Live Cell Imaging: A Laboratory Manual*, 2nd ed. Cold Spring Harbor Laboratory Press, Cold Spring Harbor, NY.

Gonzalez, R. C. and Woods, R. E. (2007). *Digital Image Processing*, 3rd ed. Prentice Hall/Pearson Education, Inc., Upper Saddle River, NJ.

Gordon, G. W., Berry, G., Liang, X. H., Levine, B., and Herman, B. (1998). Quantitative fluorescence resonance energy transfer measurements using fluorescence microscopy. *Biophysical Journal* **74**, 2702–2713.

Gustafsson, M. G. L. (2000). Surpassing the lateral resolution limit by a factor of two using structured illumination microscopy. *Journal of Microscopy* **198**, 82–87.

Gustafsson, M. G. L. (2005). Nonlinear structured-illumination microscopy: wide-field fluorescence imaging with theoretically unlimited resolution. *Proceedings of the National Academy of Sciences (USA)* **102**, 13081–13085.

Hecht, E. (2001). *Optics*, 4th ed. Addison Wesley Longman, Boston.

Heilemann, M., van de Linde, S., Schüttpelz, M., Kasper, R., Seefeldt, B., Mukherjee, A., Tinnefeld, P., and Sauer, M. (2008). Subdiffraction-resolution fluorescence imaging with conventional fluorescent probes. *Angewandte Chemie, International Edition* **47**, 6172–6176.

Heintzmann, R. (2006). Structured illumination methods. In: J. B. Pawley, ed. 3rd ed. *Handbook of Biological Confocal Microscopy*. Springer Science+Business Media, LLC, New York, pp. 265–279.

Heintzmann, R. and Jovin, T. M. (2002). Saturated patterned excitation microscopy—a concept for optical resolution improvement. *Journal of the Optical Society of America A* **19**, 1599–1609.

Hell, S. W. and Kroug, M. (1995). Ground-state-depletion fluorescence microscopy: a concept for breaking the diffraction resolution limit. *Applied Physics B* **60**, 495–497.

Hell, S. W. and Wichmann, J. (1994). Breaking the diffraction resolution limit by stimulated emission: stimulated-emission-depletion fluorescence microscopy. *Optics Letters* **19**, 780–782.

Hess, S. T., Girirajan, T. P. K., and Mason, M. D. (2006). Ultra-high resolution imaging by fluorescence photoactivation localization microscopy. *Biophysical Journal* **91**, 4258–4272.

Hiraoka, Y., Sedat, J. W., and Agard, D. A. (1987). The use of a charge-coupled device for quantitative optical microscopy of biological structures. *Science* **238**, 36–41.

Hoffman, R. (1977). The modulation contrast microscope: principles and performance. *Journal of Microscopy* **110**, 205–222.

Hoffman, R. and Gross, L. (1975). Modulation contrast microscopy. *Applied Optics* **14**, 1169–1176.

Hofmann, M., Eggeling, C., Jakobs, S., and Hell, S. W. (2005). Breaking the diffraction barrier in fluorescence microscopy at lowlight intensities by using reversibly photoswitchable proteins. *Proceedings of the National Academy of Sciences U S A* **102**, 17565–17569.

Holst, G. C. (1998). *CCD Arrays, Cameras, and Displays*. SPIE—The International Society for Optical Engineering—JCD Publishing, Winter Park, FL.

Holtmaat, A. and Svoboda, K. (2009). Experience-dependent structural synaptic plasticity in the mammalian brain. *Nature Reviews. Neuroscience* **10**, 647–658.

Howell, S. B. (1992). Introduction to differential time-series astronomical photometry using charge-coupled devices. In: S. B. Howell, ed. *Astronomical CCD Observing and Reduction Techniques*, Vol. 23. Astronomical Society of the Pacific Conference Series, Astronomical Society of the Pacific, San Francisco, pp. 105–129.

Inoué, S. (1989). Imaging of unresolved objects, superresolution, and precision of distance measurement with video microscopy. *Methods in Cell Biology* **30**, 85–112.

Inoué, S. (2006). Foundations of confocal scanned imaging in light microscopy. In: J. B. Pawley, ed. *Handbook of Biological Confocal Microscopy*, 3rd ed. Springer Science+Business Media, LLC, New York, pp. 1–19.

Inoué, S. and Inoué, T. (2000). Direct-view high-speed confocal scanner—the CSU-10. In: B. Matsumoto, ed. *Cell Biological Applications of Confocal Microscopy*, 2nd ed. Academic Press, New York, pp. 88–128.

Inoué, S. and Oldenbourg, R. (1998). Microtubule dynamics in mitotic spindle displayed by polarized light microscopy. *Molecular Biology of the Cell* **9**, 1603–1607.

Inoué, S. and Spring, K. R. (1997). *Video Microscopy: The Fundamentals*, 2nd ed. Plenum Press, New York.

Ishii, Y. and Yanagida, T. (2000). Single molecule detection in life science. *Single Molecules* **1**, S5–S16.

James, J. and Dessens, H. (1962). Immersion-refractometric observations on the solid concentration of erythrocytes. *Journal of Cellular Physiology* **60**, 235–241.

James, J. and Tanke, H. J. (1991). *Biomedical Light Microscopy*. Kluwer Academic Publishers, Boston.

Jares-Erijman, E. A. and Jovin, T. M. (2003). FRET imaging. *Nature Biotechnology* **21**, 1387–1395.

Johnson, I. and Spence, M. T. Z. (2010). *Molecular Probes Handbook: A Guide to Fluorescent Probes and Labeling Technologies*, 11th ed. Life Technologies, Inc., Eugene, OR.

Khodjakov, A. and Rieder, C. L. (2006). Imaging the division process in living tissue culture cells. *Methods* **38**, 2–16.

Klar, T. A., Jakobs, S., Dyba, M., Egner, A., and Hell, S. W. (2000). Fluorescence microscopy with diffraction resolution barrier broken by stimulated emission. *Proceedings of the National Academy of Sciences U S A* **97**, 8206–8210.

Kner, P., Chhun, B. B., Griffis, E. R., Winoto, L., and Gustafsson, M. G. L. (2009). Super-resolution microscopy of live cells by structured illumination. *Nature Methods* **6**, 339–342.

Koehler, A. (1893). A new system of illumination for photomicrographic purposes. *Zeitschrift für Wissenschaftliche Mikroskopie* **10**, 433–440. Translated to English in *Royal Microscopical Society—Koehler Illumination Centenary,* 1994.

Lakowicz, J. R. (2006). *Principles of Fluorescence Spectroscopy*, 2nd ed. Kluwer Academic/Plenum Publishers, New York.

Lang, W. (1968). Nomarski differential-interference contrast microscopy. I. Fundamentals and experimental designs. *ZEISS Information* **70**, 114–120.

Lang, W. (1969). Nomarski differential-interference contrast microscopy. II. Formation of the interference image. *ZEISS Information* **71**, 12–16.

Lang, W. (1970). Nomarski differential-interference contrast system. *American Laboratory,* April, pp. 45–51.

Lang, W. (1971a). Nomarski differential-interference contrast microscopy. III. Comparison with phase contrast. *ZEISS Information* **76**, 69–76.

Lang, W. (1971b). Nomarski differential-interference contrast microscopy. IV. Applications. *ZEISS Information* **77/78**, 22–26.

Lemmer, P., Gunkel, M., Weiland, Y., Müller, P., Baddeley, D., Kaufmann, R., Urich, A., Eipel, H., Amberger, R., Hausmann, M., and Cremer, C. (2009). Using conventional fluorescent markers for far-field fluorescence localization nanoscopy allows resolution in the 10-nm range. *Journal of Microscopy* **235**, 163–171.

Lippincott-Schwartz, J., Snapp, E., and Kenworthy, A. (2001). Studying protein dynamics in living cells. *Nature Reviews Molecular Cell Biology* **2**, 444–456.

Marty, G. D. (2007). Blank-field correction for achieving a uniform white background in bright-field digital photomicrographs. *BioTechniques* **42**, 716–720.

McNally, J. G., Karpova, T., Cooper, J., and Conchello, J. A. (1999). Three-dimensional imaging by deconvolution microscopy. *Methods* **19**, 373–385.

Mertz, J. (2004). Nonlinear microscopy: new techniques and applications. *Current Opinion in Neurobiology* **14**, 610–616.

Minnaert, M. (1954). *The Nature of Light and Color in the Open Air*. Dover Publications, New York.

Miyawaki, A., Llopis, J., Heim, R., McCaffery, J. M., Adams, J. A., Ikura, M., and Tsien, R. Y. (1997). Fluorescent indicators for Ca^{2+} based on green fluorescent proteins and calmodulin. *Nature* **388**, 882–887.

Murray, J. M., Appleton, P. L., Swedlow, J. R., and Waters, J. C. (2007). Evaluating performance in three-dimensional fluorescence microscopy. *Journal of Microscopy* **228**, 390–405.

Nakar, D., Malul, A., Feuermann, D., and Gordon, J. M. (2008). Radiometric characterization of ultrahigh radiance xenon short-arc discharge lamps. *Applied Optics* **47**, 224–229.

Nathans, J. (1984). In the eye of the beholder: visual pigments and inherited variation in human vision. *Cell* **78**, 357–360.

Neil, M. A. A., Juškaitis, R., and Wilson, T. (1997). Method of obtaining optical sectioning using structured light in a conventional microscope. *Optics Letters* **22**, 1905–1907.

Newberry, M. V. (1991). Signal-to-noise considerations for sky-subtracted data. *Publications of the Astronomical Society of the Pacific* **103**, 122–130.

Nolte, A., Pawley, J. B., and Höring, L. (2006). Non-laser light sources for three-dimensional microscopy. In: J. B. Pawley, ed. *Handbook of Biological Confocal Microscopy*, 3rd ed. Springer Science+Business Media, LLC, New York, pp. 126–144.

Oldenbourg, R. (1996). A new view on polarization microscopy. *Nature* **381**, 811–812.

Oldenbourg, R. (1999). Polarized light microscopy of spindles. *Methods in Cell Biology* **61**, 175–208.

Oldenbourg, R., Terada, H., Tiberio, R., and Inoue, S. (1993). Image sharpness and contrast transfer in coherent confocal microscopy. *Journal of Microscopy* **172**, 31–39.

OSRAM (1999). *Mercury Short Arc Lamps HBO for Microlithography*.

OSRAM (2000). *Tungsten Halogen Low Voltage Lamps Photo Optics*.

Padawer, J. (1968). The Nomarski interference-contrast microscope. An experimental basis for image interpretation. *Journal of the Royal Microscopical Society* **88**, 305–349.

Pawley, J. B. (2006). *Handbook of Biological Confocal Microscopy*, 3rd ed. Springer Science, New York.

Pierce, D. W. and Vale, R. D. (1999). Single-molecule fluorescence detection of green fluorescent protein and application to single-protein dynamics. *Methods in Cell Biology* **58**, 49–73.

Ploem, J. S. (1967). The use of a vertical illuminator with interchangeable dielectric mirrors for fluorescence microscopy with incident light. *Zeitschrift für Wissenschaftliche Mikroskopie* **68**, 129–142.

Pluta, M. (1988). *Advanced Light Microscopy, Volume 1: Principles and Basic Properties*. Elsevier Science Publishers, B.V., Amsterdam.

Pluta, M. (1989). *Advanced Light Microscopy, Volume 2: Specialized Methods*. Elsevier Science Publishers, B.V., Amsterdam.

Pluta, M. (1993). *Advanced Light Microscopy, Volume 3: Measuring Techniques*. Elsevier Science Publishers, B.V., Amsterdam.

Reichman, J. (2000). *Handbook of Optical Filters for Fluorescence Microscopy*. Chroma Technology Corp., Brattleboro, VT.

Rossner, M. and O'Donnell, R. (2004). The *JCB* will let your data shine in RGB. *Journal of Cell Biology* **164**, 11–13.

Rossner, M. and Yamada, K. M. (2004). What's in a picture? The temptation of image manipulation. *Journal of Cell Biology* **166**, 11–15.

Roux, P., Muenter, S., Frischknecht, F., Herbomel, P., and Shorte, S. (2004). Focusing light on infection in four dimensions. *Cellular Microbiology* **6**, 333–343.

Russ, J. C. (2011). *The Image Processing Handbook*, 6th ed. CRC Press/Taylor and Francis Group, Boca Raton, FL.

Rust, M. J., Bates, M., and Zhuang, X. (2006). Sub-diffraction-limit imaging by stochastic optical reconstruction microscopy (STORM). *Nature Methods* **3**, 793–795.

Shao, L., Isaac, B., Uzawa, S., Agard, D. A., Sedat, J. W., and Gustafsson, M. G. L. (2008). I^5S: wide-field light microscopy with 100-nm-scale resolution in three dimensions. *Biophysical Journal* **94**, 4971–4983.

Shao, L., Kner, P., Rego, E. H., and Gustafsson, M. G. L. (2011). Super-resolution 3D microscopy of live whole cells using structured illumination. *Nature Methods* **8**, 1044–1046.

Sheppard, C. J. R., Gan, X., Gu, M., and Roy, M. (2006). Signal-to-noise ratio in confocal instruments. In: J. B. Pawley, ed. *Handbook of Biological Confocal Microscopy*, 3rd ed. Springer Science, New York, pp. 442–452.

Shotton, D. (1993). *Electronic Light Microscopy: Techniques in Modern Biomedical Microscopy*. Wiley-Liss, Inc., New York.

Slayter, E. M. (1970). *Optical Methods in Biology*. John Wiley and Sons, New York.

Slayter, E. M. and Slayter, H. S. (1992). *Light and Electron Microscopy*. Cambridge University Press, New York.

Snapp, E. L. (2009). Fluorescent proteins: a cell biologist's user guide. *Trends in Cell Biology* **16**, 649–655.

Spencer, M. (1982). *Fundamentals of Light Microscopy*. Cambridge University Press, New York.

Strong, J. D. (1958). *Concepts of Classical Optics*. W. H. Freeman and Company, San Francisco.

Sullivan, K. F. and Kay, S. A. (1999). *Methods in Cell Biology, Volume 58, Green Fluorescent Proteins*. Academic Press, New York.

Svoboda, K. and Yasuda, R. (2006). Principles of two-photon excitation microscopy and its applications to neuroscience. *Neuron* **50**, 823–839.

Tardy, Y., McGrath, J. L., Hartwig, J. H., and Dewey, C. F. (1995). Interpreting photoactivated fluorescence microscopy measurements of steady-state actin dynamics. *Biophysical Journal* **69**, 1674–1682.

Texereau, J. (1963). *How to Make a Telescope*. Doubleday, Garden City, NY.

Thomson, L. A. and Hageage, G. J. (1975). Evaluation of excitation light sources for incident immunofluorescence microscopy. *Applied Microbiology* **30**, 616–624.

Tsay, T. T. and Jacobson, K. A. (1991). Spatial Fourier analysis of video photobleaching measurements. *Biophysical Journal* **60**, 360–368.

Tsien, R. Y. (2009). Constructing and exploring the fluorescent protein paintbox (Nobel Lecture). *Angewandte Chemie International Edition* **48**, 5612–5626.

Tsien, R. Y., Ernst, L., and Waggoner, A. (2006). Fluorophores for confocal microscopy: photophysics and photochemistry. In: J. B. Pawley, ed. *Handbook of Biological Confocal Microscopy*, 3rd ed. Springer Science+Business Media, LLC, New York, pp. 338–352.

Wadsworth, P. and Salmon, E. D. (1986). Analysis of the treadmilling model during metaphase of mitosis using fluorescence redistribution after photobleaching. *Journal of Cell Biology* **102**, 1032–1038.

Wallace, W., Schaefer, L. H., and Swedlow, J. R. (2001). A workingperson's guide to deconvolution in light microscopy. *BioTechniques* **31**, 1076–1097.

Wang, E., Babbey, C. M., and Dunn, K. W. (2005). Performance comparison between the high-speed Yokogawa spinning disc confocal system and single-point scanning confocal systems. *Journal of Microscopy* **218**, 148–159.

Webb, R. H. (2006). Bibliography of confocal microscopy. In: J. B. Pawley, ed. *Handbook of Biological Confocal Microscopy*, 3rd ed. Springer Science+Business Media, LLC, New York, pp. 889–899.

Wharmby, D. O. (1997). Electrode-less lamps. In: J. R. Coaten and A. M. Marsden, eds. *Lamps and Lighting*, 4th ed. Wiley and Sons, New York, pp. 216–226.

White, J. G., Amos, W. B., and Fordham, M. (1987). An evaluation of confocal versus conventional imaging of biological structures by fluorescence light microscopy. *Journal of Cell Biology* **105**, 41–48.

Wilhelm, S., Gröbler, B., and Heinz, H. (2010). *Confocal Laser Scanning Microscopy*. Carl Zeiss MicroImaging GmbH, Jena, Germany.

Williams, R. M., Zipfel, W. R., and Webb, W. W. (2005). Interpreting second-harmonic generation images of collagen I fibrils. *Biophysical Journal* **88**, 1377–1386.

Willig, K. I., Rizzoli, S. O., Westphal, V., Jahn, R., and Hell, S. W. (2006). STED microscopy reveals that synaptotagmin remains clustered after synaptic vesicle exocytosis. *Nature* **440**, 935–939.

Wood, E. A. (1964). *Crystals and Light: An Introduction to Optical Crystallography*, 2nd ed. D. Van Nostrand Company, Inc., Princeton, NY.

Yildiz, A., Forkey, J. N., McKinney, S. A., Ha, T., Goldman, Y. E., and Selvin, P. R. (2003). Myosin V walks hand-over-hand: single fluorophore imaging with 1.5-nm localization. *Science* **300**, 2061–2065.

Zernike, F. (1955). How I discovered phase contrast. *Science* **121**, 345–349.

Zipfel, W. R., Williams, R. M., and Webb, W. W. (2003). Nonlinear magic: multiphoton microscopy in the biosciences. *Nature Biotechnology* **21**, 1369–1377.

Zucker, R. M. and Price, O. (2001). Evaluation of confocal microscopy system performance. *Cytometry* **44**, 273–294.

INDEX

Fundamentals of Light Microscopy and Electronic Imaging, Second Edition.
Douglas B. Murphy and Michael W. Davidson.